

## 8 WCOBRA/TRAC REACTOR KINETICS AND DECAY HEAT MODELS

### 8-1 INTRODUCTION

The heat sources during a postulated LOCA are important in determining the cladding heatup. It is important, therefore, to include all possible heat sources in an accurate way such that the PCT calculated from an analysis model is realistic without having an unnecessary penalty.

The primary heat sources during a LOCA are fission product decay heat, fission heat, actinide decay heat, stored energy, and cladding chemical reaction. The objective of this section is to summarize the models related to the first three heat sources, which have been programmed in the code WCOBRA/TRAC. The cladding chemical reaction was described in Section 7. The models described in this section are identical to the approved models which have been documented in Hochreiter et al. (1988).

The variables of each equation presented in this section are defined after each equation. The nomenclature of this section is independent of the nomenclature of the rest of this report.

### 8-2 DECAY HEAT SOURCE

**Model Basis** In general, the time-dependent decay activity for a given nuclide can be solved by the following relationship:

$$\begin{aligned} \frac{d}{dt} DH^i &= \alpha_i (\Sigma_F \varphi) - \Gamma_i DH^i + \varphi \sum_{j=1}^n DH^j \sigma_a^j A(i,j) \\ &+ \sum_{j=1}^n \Gamma_j DH^j D(i,j) \end{aligned} \quad (8-1)$$

where:

- $DH^i$  = the decay activity of the i-th decay heat pseudo-nuclide,
- $\alpha_i$  = the yield fraction of the i-th decay heat pseudo-nuclide directly from fission,
- $\Sigma_F$  = the macroscopic fission cross section,
- $\Sigma_F \varphi$  = the fission rate of the reactor of interest,
- $\Gamma_i$  = the decay constant of the i-th decay heat pseudo-nuclide,
- $\varphi$  = the neutron flux in the reactor of interest,

- $\sigma_a^j$  = the microscopic absorption cross section of the j-th nuclide,  
 $A(i,j)$  = the probability that absorption in the j-th isotope will produce the i-th isotope, and  
 $D(i,j)$  = the probability that decay of the j-th nuclide will produce the i-th nuclide.

Equation 8-1 is numerically exact for the decay heat problem. However, the direct solution of Equation 8-1 involves 250 to 350 cross-coupled equations.

To simplify the preceding equation, three assumptions have been used to implement a generalized decay heat source consistent with ANSI/ANS 5.1-1971 Draft (1971) and ANSI/ANS 5.1-1979 (1978). The first two are:

- $A(i,j) = 0$
- $D(i,j) = 0$

That is, the contributions from the absorption in the j-th isotope and decay of the j-th isotope which will produce the i-th isotope are much less significant than the direct production,  $(\alpha_i \sum_f \phi)$ , and decay,  $(\Gamma_i DH^i)$ , except for very few nuclides in very high flux reactors. The third assumption is:

- Grouping of nuclides of similar time constants into a single pseudo-nuclide with the weighted average energy yield of all the nuclides involved.

The above assumption yields fewer equations to be solved with negligible loss in accuracy when the nuclide groups are chosen appropriately.

The final form of Equation 8-1 with the above assumptions is

$$\frac{d}{dt} DH^i = \alpha_i (\sum_f \phi) - \Gamma_i DH^i \quad (8-2)$$

Table 8-1 lists the standard data of  $\alpha_i$  and  $\Gamma_i$  from the ANSI/ANS 5.1-1979 model for U-235, Pu-239 thermal fission, and U-238 fast fission.

The ANSI/ANS 5.1-1979 standard data are represented in an exponential form (MeV/fission):

$$DH(t, T) = \sum_{n=1}^3 w_n(BU, \epsilon) \left[ \sum_{i=1}^{23} \frac{\alpha_i}{\Gamma_i} e^{-\Gamma_i t} (1 - e^{-\Gamma_i T}) \right]_n \quad (8-3)$$

where:

- $t$  = time after shutdown (sec),  
 $T$  = irradiation time (sec), and,  
 $w_n (BU, \epsilon)$  = fission fraction of the  $n$ -th fissile isotope as a function of burnup ( $BU$ ) and initial enrichment ( $\epsilon$ ),  
 $n=1$ : U-235 Thermal Fission  
 $n=2$ : Pu-239 Thermal Fission  
 $n=3$ : U-238 Fast Fission.

Equation 8-3 is the general solution of Equation 8-2 for a constant fission rate for an irradiation time  $T$  followed by a zero fission rate for time  $t$ . WCOBRA/TRAC solves Equation 8-2 as the generalized differential equation representation of Equation 8-3 for U-235 and Pu-239<sup>(2)</sup> thermal fission as well as U-238 fast fission. The energy yield constants are weighted by the appropriate fission rate fractions,  $w_n (BU, \epsilon)$ , as a function of initial enrichment and burnup within WCOBRA/TRAC.

The fission rate weighting was obtained from detailed physics evaluation of PWR fuel lattice designs. Figure 8-1 illustrates the U-235 thermal fission rate weighting obtained from these evaluations. Similarly, Figures 8-2 and 8-3 illustrate the Pu-239 thermal fission and U-238 fast fission weightings, respectively. The U-235 fission rate fraction presented in Figure 8-1 was evaluated as directed by ANSI/ANS 5.1-1979, as all fissions that are not U-238 or Pu-239.

The decay heat model within WCOBRA/TRAC has been benchmarked against the ANSI/ANS 5.1-1979 Standard. Table 8-2 presents the results of decay heat solved by Equation 8-2 in WCOBRA/TRAC and the standard form (Equation 8-3) for U-235 only. The difference between the two approaches is negligible. Similar comparisons exist for Pu-239 and U-238. WCOBRA/TRAC solves for the composite decay heat of the reactor of interest using the fission rate fractions derived from specific physics calculations for the fuel lattice design.

As for the ANSI/ANS 5.1-1971 model, the standard formulation is a piece-wise power fit over ranges of time from 0.1 seconds to  $2 \times 10^8$  seconds (Table 8-3). The standard data have been refitted and incorporated in WCOBRA/TRAC in the same form as Equation 8-3, except only 11 groups instead of 69 groups of pseudo-nuclides were used.

Table 8-3 lists the fitted values of  $\alpha_i$  and  $\Gamma_i$  of the ANSI/ANS 5.1-1971 model. It can be seen in Table 8-4 that the exponential form with the fitted coefficients generates results which deviate from the standard power form by about one percent.

### 8-3 FISSION HEAT

**Model Basis** The fission heat is treated using a point kinetics model. The derivation of the final form of the point kinetics model can be found in various nuclear reactor analysis textbooks, such as Henry (1975) and Glasstone and Sesonske (1967). The most familiar form of the point kinetics model is

$$\frac{dn}{dt} = \frac{\rho(t) - \bar{\beta}}{\ell^*} n(t) + \sum_{i=1}^6 \lambda_i C_i + S_e \quad (8-4)$$

and

$$\frac{dC_i}{dt} = \frac{\beta_i n(t)}{\ell^*} - \lambda_i C_i \quad (8-5)$$

where:

- $n$  = neutron density,
- $\rho$  = reactivity,  $(k-1)/k$ ,
- $\beta_i$  = the  $i$ -th group delayed neutron precursor yield fraction,
- $\bar{\beta} = \sum_{i=1}^6 \beta_i$ ,
- $\ell^*$  = effective neutron lifetime,
- $\lambda_i$  = the  $i$ -th delayed neutron precursor time constant,
- $C_i$  = the  $i$ -th delayed neutron precursor concentration, and,
- $S_e$  = external source strength.

The assumptions in deriving Equations 8-4 and 8-5 are the time and space separability of the neutron density and six groups of delayed neutrons.

Once the neutron density  $n(t)$  is solved from the point kinetics model, the fission power can be obtained by the equation

$$FH(t) = v n(t) \kappa \Sigma_F \quad (8-6)$$

where:

- $v$  = neutron velocity,
- $\kappa$  = prompt energy release per fission, and,
- $\Sigma_F$  = macroscopic fission cross section.



The macroscopic fission cross section is a neutron energy dependent parameter. The moderator density affects the thermalization of neutrons. Therefore, the fission interaction frequency ( $\nu\kappa\Sigma_f$ ) should be a function of moderator density. The moderator of a typical PWR is the primary loop coolant. During a LOCA, the coolant density will undergo a rapid change. Therefore, to assume  $\nu\kappa\Sigma_f$  is a constant throughout the transient would be overly conservative (lower coolant density should result in harder neutron energy spectrum, hence lower thermal fission rate). A water-density-dependent form of fission interaction frequency ( $\nu\kappa\Sigma_f$ ) has been incorporated in WCOBRA/TRAC, which is

$$\nu\kappa\Sigma_f(\rho_t) = A_0 + \sum_{n=1}^6 A_n \rho_t^n \quad (8-7)^{(1)}$$

where:

$\rho_t$  = water density.

The seven coefficients ( $A_0 - A_6$ ) are obtained by space/energy calculations for the fuel assembly of interest.

A series of detailed space/energy calculations have been performed for a typical fresh assembly to quantitatively evaluate fission rate per unit neutron density for water densities that occur during the LOCA transient. Table 8-5 lists the values of the 7 coefficients, and Figure 8-4 shows the calculated density dependence of  $\kappa\Sigma_f$ , which is normalized to the value at  $\rho_t = 0.7 \text{ g/cm}^3$ . [

] <sup>ac</sup>. Therefore, the modification of the fission frequency ( $\nu\kappa\Sigma_f$ ) should be considered. This quantity, as with all other plant and reactor specific data, is modelled in WCOBRA/TRAC using input appropriate to the specific plant and reactor design being considered.

WCOBRA/TRAC explicitly models the burnup and initial enrichment dependence of kinetics data, i.e., groupwise delayed neutron fractions, groupwise delayed neutron time constants, prompt neutron lifetime, prompt energy release per fission, and total energy release per fission. Figure 8-5 presents the effective delayed neutron fraction as a function of burnup and initial enrichment. Figure 8-6 presents the prompt neutron lifetime as a function of initial enrichment and burnup. Figures 8-7 and 8-8 present the prompt and total energy release per fission as a function of initial enrichment and burnup, respectively. Figures 8-9 through 8-14 illustrate the groups 1 through 6 delayed neutron time constants as a function of initial enrichment and burnup. The data presented in Figures 8-5 through 8-14 were generated for typical Westinghouse fuel lattice designs.

#### 8-4 ACTINIDE DECAY HEAT SOURCE<sup>(2)</sup>

**Model Basis** The time dependent actinide heat source due to the buildup and decay of U-239 and Np-239 is a relatively simple problem. The basic equations for U-239 and Np-239 are given below as Equations 8-8 and 8-9, respectively.

$$\frac{dU}{dt} = \bar{R}(BU, \epsilon)(v\Sigma_{fn}(t)) - \lambda_u U(t) \quad (8-8)$$

$$\frac{dNp}{dt} = \lambda_u U(t) - \lambda_n Np(t) \quad (8-9)$$

where:

- $U(t)$  = time-dependent U-239 concentration,
- $\bar{R}(BU, \epsilon)$  = U-238 capture to fission ratio, function of initial enrichment  $\epsilon$ , and burnup ( $BU$ ),
- $v\Sigma_{fn}(t)$  = time-dependent fission rate,
- $\lambda_u$  = U-239 decay constant,
- $Np(t)$  = time-dependent Np-239 concentration, and,
- $\lambda_n$  = Np-239 decay constant.

It is much more convenient to express the decay equations in terms of instantaneous decay power. Recall that decay power is simply the product of concentration, decay constant and energy release per decay as shown in Equations 8-10 and 8-11 for U-239 and Np-239, respectively:

$$P_u = q_u \lambda_u U(t) \quad (8-10)$$

$$P_n = q_n \lambda_n Np(t) \quad (8-11)$$

where:

- $P_u$  = time dependent decay power due to U-239 decay,
- $q_u$  = energy release per U-239 decay,
- $P_n$  = time dependent decay power due to Np-239 decay and,
- $q_n$  = energy release per Np-239 decay.

Equations 8-8 through 8-11 can now be combined into a form suitable for implementation as Equations 8-12 and 8-13 below:

$$\frac{dP_u}{dt} = \bar{R}\alpha_u(v\Sigma_f n(t)) - \lambda_u P_u \quad (8-12)$$

$$\frac{dP_n}{dt} = \frac{\lambda_u P_u(t)\alpha_n}{\alpha_u} - \lambda_n P_n \quad (8-13)$$

where:

$\alpha_u = q_u \lambda_u$ , decay power yield per capture (MeV/sec/capture) for U-239, and  
 $\alpha_n = q_n \lambda_n$ , decay power yield per capture (MeV/sec/capture) for Np-239.

[ ]<sup>a,c</sup>. With this assumption, the initial conditions for U-239 and Np-239 are described by Equations 8-14 and 8-15, respectively: [

] <sup>a,c</sup> (8-15)

The values of constants required for explicit actinide representation were taken from ANSI/ANS 5.1-1979 and are presented in Table 8-6. The U-238 capture to fission ratio,  $\bar{R}$ , is a function of fuel lattice design, initial enrichment, and burnup. Figure 8-15 presents  $\bar{R}$  for a typical PWR fuel lattice design. ENDF-B/V data were used in PWR core depletion calculations to determine variations in  $\bar{R}$  with burnup and enrichment.

[ ]<sup>a,c</sup> (8-16)<sup>(3)</sup>

where:

$\kappa_f$  = total energy release per fission.

## 8-5 SPACE DEPENDENT HEAT SOURCE MODEL

**Model Basis** WCOBRA/TRAC models the space dependent composition and initial condition dimensions of the decay heat source. This model is based upon the space/time separability assumptions of the point reactor kinetics solutions as well as the input composition and initial condition description. WCOBRA/TRAC models decay heat using channel average compositions. Initial condition concentrations are input based on conservative irradiation history evaluations. Channel average compositions are realistic representations of decay heat in limiting elevations.

The basic space independent equations derived in Sections 8-1 and 8-2, are repeated below:

$$\frac{dn}{dt} = \frac{\rho(t) - \bar{\beta}}{\ell^*} n(t) + \sum_{i=1}^6 \lambda_i C_i(t) + S_e \quad (8-4)$$

$$\frac{dC_i}{dt} = \frac{n(t)\beta_i}{\ell^*} - \lambda_i C_i \quad (8-5)$$

$$\frac{d DH^j}{dt} = v \Sigma_f(t) n(t) \alpha_j - \Gamma_j DH^j \quad (8-2)$$

$$P(t) = FH(t) + \sum_j DH^j + AH(t) \quad (8-17)$$

$$FH(t) = \kappa v \Sigma_f(t) n(t) \quad (8-18)$$

where:

- $P(t)$  = time-dependent heat source,
- $n(t)$  = time-dependent neutron density,
- $\rho(t)$  = time-dependent reactivity defined as  $(k-1)/k$ ,
- $\ell^*$  = prompt neutron lifetime,
- $\bar{\beta}$  = effective delay neutron fraction,
- $\lambda_i$  = time constant for the i-th delayed neutron group
- $S_e$  = external source strength,
- $v \Sigma_f(t)$  = time dependent interaction frequency for fission,
- $\beta_i$  = effective delayed neutron fraction for the i-th group,

- $DH^j$  = energy release rate of the j-th decay heat pseudo-nuclide,  
 $\alpha_j$  = energy yield of the j-th decay heat pseudo nuclide,  
 $\Gamma_j$  = time constant of the j-th decay heat pseudo nuclide,  
 $\kappa$  = prompt energy release per fission,  
 $FH(t)$  = time dependent fission heat, and  
 $AH(t)$  = time dependent actinide heat.

Assuming space/time separability, Equation 8-17 can be expressed with a general time-independent space dependence for each basic heat source as Equation 8-19 below:

$$P_i(z,t) = F_i(z)FH(t) + \sum_j D_i^j(z)DH^j(t) + A_i(z)AH(t) \quad (8-19)$$

where:

- $P_i(z,t)$  = the heat-source as a function of elevation and time in the i-th xy channel,  
 $F_i(z)$  = the elevation dependence of fission heat for the i-th xy channel,  
 $D_i^j(z)$  = the elevation dependence of the j-th decay heat pseudo-nuclide for the i-th xy channel,  
 and  
 $A_i(z)$  = the elevation dependence of actinide heat for the i-th xy channel.

] <sup>a,c</sup>

The decay heat source is most conveniently expressed in terms of the [

] <sup>a,c</sup> (8-21)

where:

[ ] <sup>a,c</sup>.

Equation 8-21 is now solved for  $D_i^j(z)$  as Equation 8-22 below: [

] <sup>a,c</sup> (8-22)

The space/time dependent heat source can now be expressed in terms of the fission distribution and the initial power by substituting Equation 8-22 into Equation 8-19 as Equation 8-23 below: [

] <sup>a,c</sup> (8-23)

Equation 8-23 can be further simplified by defining the [   
 ] <sup>a,c</sup> as defined in Equation 8-24 below: [

] <sup>a,c</sup> (8-24)

Equation 8-24 is now solved for the initial condition for [   
 ] <sup>a,c</sup> as Equation 8-25 below: [

] <sup>a,c</sup> (8-25)

Equation 8-25 is now substituted into Equation 8-23 to give the final form of the space/time dependent heat source as Equation 8-26 below: [

] <sup>a,c</sup> (8-26)

The remaining task is to provide initial conditions for Equations 8-4, 8-5, and 8-2 in terms of Equation 8-26. The first of these conditions is that the input power peaking  $FT_i(z)$  be normalized to a reactor average value of unity. This relation is expressed for  $FT_i(z)$  as Equation 8-27 below:

$$\frac{\sum_i \int_z FT_i(z) V_i(z) dz}{\sum_i \int_z V_i(z) dz} = 1.0, \quad (8-27)$$

where  $V_i(z)$  is the volume of the  $i$ -th channel at elevation  $z$ . The second initial condition is that the initial reactor power,  $P_{TH}$ , be given by Equation 8-28 below:

$$P_{TH} = \sum_i \int_z V_i(z) P_i(z, 0) dz \quad (8-28)$$

The initial conditions of Equations 8-4, 8-5, and 8-2 can now be solved in terms of  $P_{TH}$ . First, it is necessary to derive the relations for  $P_i(z, 0)$  as Equation 8-29 below (from Equations 8-26 and 8-20): [

$$]^{a.c} \quad (8-29)$$

Substituting Equation 8-25 into Equation 8-29 yields a statement of initial condition in terms of [  $]^{a.c}$  as Equation 8-30: [

$$]^{a.c} \quad (8-30)$$

Finally, Equation 8-30 can be integrated over the entire reactor as specified in Equation 8-28, and [  $]^{a.c}$  as shown in Equation 8-31 below: [

$$]^{a.c} \quad (8-31)$$

Now, solve for the initial neutron density  $n(0)$  by substituting Equation 8-18 into Equation 8-31 to yield the initial conditions in terms of initial total power  $P_{TH}$  as Equation 8-32 below: [

$$]^{a.c} \quad (8-32)$$

Recall Equation 8-24 defines that [

$$]^{a.c} \quad (8-33)$$

where the two power distributions,  $D_i(z)$  and  $F_i(z)$ , are normalized to a reactor average value of unity.

Equation 8-22 is now substituted into Equation 8-33 to yield an expression for  $AVFR^j$  in terms of the fission peaking as Equation 8-34: [

] <sup>a,c</sup> (8-34a)

and [

] <sup>a,c</sup> (8-34b)

All that remains to be done is to solve for  $F_i(z)$  in terms of  $FT_i(z)$ . Recall that Equation 8-27 requires that  $FT_i(z)$  be normalized such that  $P_i(z, 0)$  is given by Equation 8-35 below:

$$P_i(z, 0) = P_{AV}(0) FT_i(z), \quad (8-35)$$

where:

$$P_{AV}(0) = \frac{P_{TH}}{\sum_i \int_z V_i(z) dz} \quad (8-36)$$

Substituting Equation 8-30 into Equation 8-35 and rearranging gives Equation 8-37 below: [

] <sup>a,c</sup> (8-37)

## 8-6 ENERGY DEPOSITION MODELLING

### 8-6-1 Introduction

WCOBRA/TRAC models the energy sources within the reactor fuel in three distinct categories. These categories are prompt fission, fission product decay, and actinide nuclide decay. The specific details of the energy source modelling can be found in (Hochreiter et al., 1988). The distribution of energy sources is, however, of no interest to the thermal and hydraulic modelling of deposition resulting from the various



distributed energy sources. The specific details of the methodology by which the spatial distribution of the energy sources is transformed into the spatial distribution of energy deposition are the subject of the following discussion.

The energy from fission events appears in varying forms with large differences in spatial transport characteristics. Table 8-7 illustrates a typical breakdown of the energy released due to a fission event and the relative spatial transport length of the component. The degree to which a radiation source will propagate through a medium is strongly related to whether the radiation is expressed as a charged particle (e.g., fission fragment or beta particle), an uncharged particle (e.g., neutron), or a photon, (e.g., gamma-ray). Charged particles emitted from within a nuclear fuel material are, from a practical viewpoint, unable to penetrate the confines of the fuel rod and, therefore, deposit essentially all of their energy within the fuel rod as heat. As illustrated in Table 8-7, the vast majority of the total energy released due to a fission event is expressed as the kinetic energy of the fission products. The fission fragments are emitted as highly charged particles essentially instantaneously after the fission event and are deposited almost exclusively within the fuel pin in which they are generated. The beta particle energy from both the decay of fission fragments and the transmutation of the actinide activation products are also charged particles which are, like the fission fragments, deposited almost exclusively within the fuel pin in which they are generated. The beta particle energy is released as a result of the radioactive decay process, which is not directly related to the fission rate; rather it is related to the concentration of the various radio-nuclides which compose the source. WCOBRA/TRAC explicitly models the spatial distribution and temporal relationships which describe all heat sources and deposits the energy from non-penetrating radiation sources [ ]<sup>a,c</sup>. The fraction of the total heat source which is deposited in this manner is independent of coolant conditions and ranges from [ ]<sup>a,c</sup> during steady state operation to [ ]<sup>a,c</sup>.

The balance of the energy released as a result of the fission event is expressed as uncharged particles, i.e., neutrons and gamma photon energy. These penetrating radiation sources, due to their lack of charged particles, easily escape the confines of the fuel rod and deposit their energy [ ]<sup>a,c</sup>.

The deposition of the energy contained within these sources is quite important to the consequences of the LOCA transient since [ ]<sup>a,c</sup> of the decay power released during the LOCA transient is expressed as penetrating radiation. WCOBRA/TRAC models the spatial deposition of spatially varying penetrating radiation sources using a generalized energy deposition model, GEDM. The GEDM is [ ]<sup>a,c</sup> and relies on input to describe the energy deposition as a function of [ ]<sup>a,c</sup>. The formulation of the GEDM and the methodology for the generation of the model input follows. Illustrative examples are presented for a typical application. The application of the GEDM is restricted only to the [ ]<sup>a,c</sup>.

## 8-6-2 Generalized Energy Deposition Model

### Generalized Energy Deposition Model (GEDM) Derivation

**Model Basis** The WCOBRA/TRAC GEDM utilizes the linear superposition of distribution sources to compute the spatial distribution of deposited energy due to a generalized distributed source. The energy deposition, modelled as either heat flux or volumetric, is based upon the results of detailed particle transport calculations which form the basis of the GEDM input. The WCOBRA/TRAC GEDM utilizes the relationship illustrated in Equation 8-38 below to account for the energy deposition as heat flux at the point of interest due to generalized penetrating and non-penetrating radiation source spatial distribution(s). [

]<sup>a,c</sup> (8-38)

where:

[

]<sup>a,c</sup>

The WCOBRA/TRAC GEDM utilizes the relationship in Equation 8-39 below to account for the energy deposition as volumetric coolant heating at the point of interest due to generalized penetrating and non-penetrating radiation source spatial distribution(s). [

]<sup>a,c</sup> (8-39)

where: [

]<sup>a,c</sup>

The GEDM transfer matrices  $\Gamma_{ij}''$  and  $\phi_{ij}''$  represent [ ]<sup>a,c</sup>,  
 respectively. As stated above, the theoretical basis behind the GEDM transfer matrices is the  
 [ ]

[ ]<sup>a,c</sup>. The GEDM transfer matrix elements are derived from [ ]

[ ]<sup>a,c</sup>. Equation 8-40 below describes  
 the derivation of the GEDM [ ]<sup>a,c</sup> transfer matrix elements  $\Gamma_{ij}''$ . [ ]

[ ]<sup>a,c</sup> (8-40)

where:

[ ]<sup>a,c</sup>

Equation 8-41 below describes the derivation of the GEDM [ ]<sup>a,c</sup> transfer matrix elements  
 $\phi_{ij}''$ . [ ]

[ ]<sup>a,c</sup> (8-41)

where:

[ ]<sup>a,c</sup>

The numeric values of  $(1 - \beta_n)$  have been derived from the [ ]  
 [ ]<sup>a,c</sup>. Typical values for  $\beta_n$  are given in Table 8-8.

## Generalized Energy Deposition Model (GEDM) Transfer Matrix Generation

The GEDM transfer matrix elements are the product of a [

] <sup>a,c</sup>.

[

chosen because it can [ ] <sup>a,c</sup>. The GEDM [ ] <sup>a,c</sup> methodology was  
matrices have been found to be independent of [ ] <sup>a,c</sup>. The GEDM transfer

] <sup>a,c</sup>.

[

] <sup>a,c</sup>. The following discussion will present a sample set of GEDM [ ] <sup>a,c</sup>  
calculations that have been performed using the Westinghouse 15x15 fuel design. The  
methodology described below applies generically to all other fuel designs.

The current model for [

] <sup>a,c</sup>.

## Gamma Transfer Matrix Generation Methodology

A series of [ ] <sup>a,c</sup> calculations were performed for a typical 15x15 OFA fuel  
design at typical plant conditions. The purpose of these calculations was to quantify, in a generalized  
fashion, the relative distribution of gamma energy as [ ] <sup>a,c</sup> throughout the  
reactor, parameterized as a function of [ ] <sup>a,c</sup>. DOT (Disney et al., 1970) was used as

the dimensional particle transport code for the examples presented in this report. The methodology presented within this report does not rely on the use of DOT, but rather on [

] <sup>a,c</sup>.

The dimensional problem was modelled as a [

] <sup>a,c</sup>.

The basic methodology employed in the generation of GEDM transfer matrix elements is the use of a [

] <sup>a,c</sup>.

Nuclear particle cross sections were taken from the familiar SAILOR (1985) and BUGLE-80 (1980) library, developed at the Oak Ridge National Laboratory as part of the Radiation Shielding Information Center (RSIC). [

] <sup>a,c</sup>.

Gamma kerma factors were taken from the BUGLE-80 library and used as [ <sup>a,c</sup>. The SAILOR/BUGLE-80 cross-section libraries are described in ORNL RSIC reports DLC-76 and DLC-75, respectively. The SAILOR basic multigroup cross sections were [

] <sup>a,c</sup>. The Kerma data used in the development of the [ <sup>a,c</sup> are presented in Table 8-11 and illustrated in Figure 8-20.

The final results of the [

] <sup>a,c</sup>.

The results of these calculations were then used to calculate the GEDM transfer matrix elements as shown in Equations 8-40 and 8-41 for [ <sup>a,c</sup> respectively. The results of this evaluation for the 15x15 fuel design are presented in Table 8-12.

The data presented in Table 8-12 quantifies the [

] <sup>a,c</sup>. A sample evaluation of the spatial energy deposition distributed using the data from Table 8-12 is presented in Figure 8-21 as the [

] <sup>a,c</sup>,

respectively. Figure 8-22 illustrates the [

] <sup>a,c</sup>, respectively. These figures clearly illustrate the dependence of heat flux deposition on [ <sup>a,c</sup>.

## Application of Generalized Energy Deposition Model (GEDM) within WCOBRA/TRAC

The data presented in Table 8-12 can be used directly in WCOBRA/TRAC provided that the [

] <sup>a,c</sup>.

[

] <sup>a,c</sup> can be found in Table 8-13 and demonstrates that the

[

] <sup>a,c</sup>.

The relationship used to apply [

] <sup>a,c</sup>. [

] <sup>a,c</sup> (8-42c)

where:

- $\Gamma_{ij}$  = problem specific transfer element,
- $V_i$  = problem specific channel volume,
- $\Gamma_{ij}^{ref}$  = reference transfer element, and
- $V_{ij}^{ref}$  = reference channel volume.

The relationship used to apply [

]<sup>a,c</sup>. [

]<sup>a,c</sup> (8-43c)

where:

- $\phi_{ij}$  = problem specific transfer element,
- $V_i$  = problem specific channel volume,
- $\phi_{ij}^{ref}$  = reference transfer element, and
- $V_j^{ref}$  = reference channel volume.

As discussed above, WCOBRA/TRAC currently models [

]<sup>a,c</sup>.



## 8-7 DECAY HEAT UNCERTAINTY EVALUATION

Decay heat uncertainty has been modelled in WCOBRA/TRAC through the use of pseudo-isotope energy yield,  $\alpha_i$ , augmentation factors. The values of the augmentation factors are presented in Table 8-14. The values in Table 8-14 were generated using a least squares fit to the uncertainty data provided in ANSI/ANS 5.1-1979, and provide a conservative representation of the standard's quoted uncertainties. Figures 8-23 to 8-25 illustrate the fit deviation in both energy and decay heat versus cooling time. Figures 8-26 to 8-28 compare the predicted decay heat with uncertainties to the standard decay heat plus  $2\sigma$  uncertainties.<sup>(4)</sup>

## 8-8 REACTOR POINT KINETICS VALIDATION

The WCOBRA/TRAC heat source model is a fully integrated model containing a total of [

]<sup>a,c</sup>. The decay heat model validation was presented previously in Tables 8-2 and 8-4 against the ANSI/ANS 5.1 1979 and 1971 decay heat standards, respectively. WCOBRA/TRAC shows excellent agreement with the decay heat standard data.

The point kinetics model within WCOBRA/TRAC has been validated on a [ ]<sup>a,c</sup> for two basic test problems. The first test problem is the time-dependent solution of a step reactivity input. Figures 8-29 through 8-31 illustrate the WCOBRA/TRAC point kinetics solution of reactor period for a step reactivity insertion of  $+3.0 \times 10^{-3}$ ,  $+1.5 \times 10^{-3}$ , and  $-3.0 \times 10^{-2} \Delta K$  in the absence of external feedback mechanisms, respectively. The WCOBRA/TRAC kinetics model stabilizes at a constant asymptotic reactor period after a short period of time. The asymptotic reactor period for a step reactivity insertion can be solved for analytically using the familiar Inhour Equation below:

$$\rho = \frac{\ell^*}{T} + \sum_{i=1}^6 \frac{\beta_i}{1 + \lambda_i T} \quad (8-44)$$

where T is the asymptotic reactor period.

Table 8-15 presents the calculated and theoretical asymptotic reactor period for these step insertions. WCOBRA/TRAC shows excellent agreement against this theoretical validation test.

[

]<sup>a,c</sup>.

[

 $J^{ac}$ .

## 8-9 JUSTIFICATION OF SIMPLIFICATIONS AND ASSUMPTIONS

### 8-9-1 Actinide Decay Power

ANSI/ANS 5.1-1979 directs the user to evaluate the impact of other actinide isotopes. As stated previously, WCOBRA/TRAC explicitly models the decay power due to U-239 and Np-239 with the

[

 $J^{ac}$ .

Detailed calculations have been performed to evaluate the impact of the total actinide heat source. Table 8-16 presents the basic physical data for the [

 $J^{ac(5)}$ 

### 8-9-2 WCOBRA/TRAC Fission Energy Accounting

WCOBRA/TRAC explicitly accounts for the energy deposition due to fission by five basic mechanisms. Direct fission energy deposition due to fission fragments, prompt gamma reactions, and prompt beta reactions are a direct and immediate result of a fission event. These components, as well as the neutron slowing down deposition and structural material radiative capture mechanisms, are included explicitly in the prompt energy release per fission as illustrated in Figure 8-7. The basic physics data used to generate Figure 8-7 as a function of burnup and initial enrichment is based upon ENDF-B/V as utilized at Westinghouse for standard reactor design. Table 8-17 presents the prompt fission energy release,

radiative capture release, and average fission neutron energy utilized in the evaluation of the composite prompt energy release per fission. Thus, WCOBRA/TRAC complies with the standard's requirement to evaluate the energy release per fission including radiative capture in structural components.

### 8-9-3 Decay Heat Absorption Effects

ANSI/ANS 5.1-1979 directs the user that the basic decay heat data supplied within the standard is uncorrected for neutron capture effects. The standard supplies a means of correction for neutron capture as a function of irradiation time, shutdown time, and integrated fissions per initial fissile atom as shown in Equation 8-45 below:

$$G(t) = 1.0 + (3.24E-06 + 5.23E-10t)T^{0.4}\psi \quad (8-45)$$

where:

- $t$  = time after shutdown in seconds, ( $t < 10,000$  sec)
- $T$  = irradiation time in seconds, ( $T < 1.2614E+08$  sec)
- $\psi$  = fissions per initial fissile atom, ( $\psi < 3.0$ )

Integrated fissions per initial fissile atom have been evaluated for PWR fuel lattice designs, as illustrated in Figure 8-34, as a function [

]<sup>a,c</sup>. Thus, WCOBRA/TRAC conservatively accounts for neutron capture effects in the decay heat model as required by the standard.

## 8-10 GENERALIZED ENERGY DEPOSITION MODEL (GEDM) VALIDATION

The GEDM has been validated in two separate manners for application within WCOBRA/TRAC. The first validation calculation was performed to validate the [

]<sup>a,c</sup>

[

] <sup>a,c</sup>.

The final validation of the GEDM and input generation methodology was the comparison of the GEDM

[

] <sup>a,c</sup>. The results of this comparison are

given in Table 8-18. It is apparent from the [

] <sup>a,c</sup>.

## 8-11 INTERFACE BETWEEN NEUTRONICS AND THERMAL-HYDRAULICS MODELS

Figure 8-35 shows the calculation block diagram for WCOBRA/TRAC. The neutronics part of the calculation is performed by a subroutine within WCOBRA/TRAC called LUCIFER (Hochreiter et al., 1988). There are two options available for the neutronics calculations in terms of the reactivity feedback to LUCIFER. <sup>(6)</sup> The first option is the user supplied reactivity table. With this option, LUCIFER is essentially a stand alone code for calculating the power history associated with the reactivity table. The second option is the internal feedback option. The core average fuel temperature and coolant density calculated in WCOBRA/TRAC are fed back to LUCIFER for the reactivity calculation and the associated power history calculation. The calculated power history is then supplied to WCOBRA/TRAC as the heat source in the thermal-hydraulics calculations.

## 8-12 REACTOR KINETICS, DECAY HEAT, AND INTERFACE MODELS AS CODED

WCOBRA/TRAC solves the reactor kinetics, decay heat, and actinide decay heat models with a system of first-order ordinary differential equations of the form  $y' = f(x,y)$  or  $Ay' = f(x,y)$  with initial conditions, where  $A$  is a matrix of order  $N$ . The solution method is the backward differentiation formula (up to order 6), also called Gear's stiff method (1971). Because the basic formula is implicit, an algebraic system of equations must be solved at each step. The matrix in this system has the form  $L = A + \eta J$ , where  $\eta$  is a small number and  $J$  is the Jacobian.

The FORTRAN coding in WCOBRA/TRAC is consistent with the models described in this section.

## 8-13 REACTOR KINETICS, DECAY HEAT, AND INTERFACE MODELS SCALING CONSIDERATIONS

The models described in this section are scale independent.

## 8-14 CONCLUSIONS

The models and derivations described in this section have been reviewed and checked. It is concluded that the models are correct. The coding in WCOBRA/TRAC is found to be consistent with the models described in this section.

## 8-15 REFERENCES

ANSI/ANS 5.1-1971 Draft, 1971, "Proposed ANS Standard Decay Energy Release Rates Following Shutdown of Uranium Fueled Thermal Reactors," American Nuclear Society.

ANSI/ANS 5.1-1979, 1978, "Decay Heat in Light Water Reactors," American Nuclear Society.

BUGLE-80 Gamma Cross Sections, 1980, ORNL RSIC DLC-76.

Disney, R. K., et al., 1970, "Nuclear Rocket Shielding Methods, Modification, Updating, and Input Preparation," Volume 5, Two Dimensional Discrete Ordinates Transport Techniques, WANL-PR-(LL)-034, Westinghouse Astro Nuclear Laboratory.

DOT2W, "A Two-Dimensional Discrete Ordinates Computer Program," ORNL/RSIC CCC-89. Contributed by Westinghouse Advanced Reactors Division, Madison, PA, USA.

Gear, C. W., 1971, Numerical Initial-Value Problems in Ordinary Differential Equations, Prentice-Hall, Englewood Cliffs, New Jersey.

Glasstone, S. and Sesonske, A., 1967, Nuclear Reactor Engineering, Van Nostrand, New York.

Henry, A. F., 1975, Nuclear Reactor Analysis, The MIT Press, Cambridge, Mass. and London England.

Hochreiter, L. E., et al., 1988, "Westinghouse Large Break LOCA Best Estimate Methodology, Volume 1: Model Description and Validation, Addendum 2: Revised Appendix B: Heat Source Models," WCAP-10924-P-A, Revision 1.

SAILOR Gamma Cross Sections, 1985, ORNL RSIC DLC-75.

## **8-16 RAI LISTING**

1. RAII-227 (refers to WCAP-12945, Rev. 1, page 8-12; now page 8-5)
2. RAII-228 (refers to WCAP-12945, Rev. 1, page 8-7; now page 8-3)
3. RAII-229
4. RAII-230
5. RAII-231 (refers to WCAP-12945, Rev. 1, page 8-45; now page 8-22)
6. RAII-232
7. RAII-1, item pp

**Table 8-1**      **ANSI/ANS 5.1-1979**  
**Decay Heat Standard Data for U-235 Thermal Fission**

Group	$\alpha_i$ (MeV/f.sec)	$\Gamma_i$ (sec <sup>-1</sup> )
1	6.5057E-01*	2.2138E+01
2	5.1264E-01	5.1587E-01
3	2.4384E-01	1.9594E-01
4	1.3850E-01	1.0314E-01
5	5.5440E-02	3.3656E-02
6	2.2225E-02	1.1681E-02
7	3.3088E-03	3.5870E-03
8	9.3015E-04	1.3930E-03
9	8.0943E-04	6.2630E-04
10	1.9567E-04	1.8906E-04
11	3.2535E-05	5.4988E-05
12	7.5595E-06	2.0958E-05
13	2.5232E-06	1.0010E-05
14	4.9948E-07	2.5438E-06
15	1.8531E-07	6.6361E-07
16	2.6608E-08	1.2290E-07
17	2.2398E-09	2.7213E-08
18	8.1641E-12	4.3714E-09
19	8.7797E-11	7.5780E-10
20	2.5131E-14	2.4786E-10
21	3.2176E-16	2.2384E-13
22	4.5038E-17	2.4600E-14
23	7.4791E-17	1.5699E-14

\*read as 6.5057 x 10<sup>-1</sup>

**Table 8-1**      **ANSI/ANS 5.1-1979**  
**(cont)**        **Decay Heat Standard Data for Pu-239 Thermal Fission**

Group	$\alpha_i$ (MeV/f.sec)	$\Gamma_i$ (sec <sup>-1</sup> )
1	2.083E-01*	1.002E+01
2	3.853E-01	6.433E-01
3	2.213E-01	2.186E-01
4	9.460E-02	1.004E-01
5	3.531E-02	3.728E-02
6	2.292E-02	1.435E-02
7	3.946E-03	4.549E-03
8	1.317E-03	1.328E-03
9	7.052E-04	5.356E-04
10	1.432E-04	1.730E-04
11	1.765E-05	4.881E-05
12	7.347E-06	2.006E-05
13	1.747E-06	8.319E-06
14	5.481E-07	2.358E-06
15	1.671E-07	6.450E-07
16	2.112E-08	1.278E-07
17	2.996E-09	2.466E-08
18	5.703E-11	9.378E-09
19	5.703E-11 <sup>(7)</sup>	7.450E-10
20	4.138E-14	2.426E-10
21	1.088E-15	2.210E-13
22	2.454E-17	2.640E-14
23	7.557E-17	1.380E-14

\*read as 2.083 x 10<sup>-1</sup>



**Table 8-1**      **ANSI/ANS 5.1-1979**  
**(cont)**        **Decay Heat Standard Data for U-238 Fast Fission**

Group	$\alpha_i$ (MeV/f.sec)	$\Gamma_i$ (sec <sup>-1</sup> )
1	1.2311E+0*	3.2881E+0
2	1.1486E+0	9.3805E-1
3	7.0701E-1	3.7073E-1
4	2.5209E-1	1.1118E-1
5	7.1870E-2	3.6143E-2
6	2.8291E-2	1.3272E-2
7	6.8382E-3	5.0133E-3
8	1.2322E-3	1.3655E-3
9	6.8409E-4	5.5158E-4
10	1.6975E-4	1.7873E-4
11	2.4182E-5	4.9032E-5
12	6.6356E-6	1.7058E-5
13	1.0075E-6	7.0465E-6
14	4.9894E-7	2.3190E-6
15	1.6352E-7	6.4480E-7
16	2.3355E-8	1.2649E-7
17	2.8094E-9	2.5548E-8
18	3.6236E-11	8.4782E-9
19	5.7030E-11	7.5130E-10
20	4.4963E-14	2.4188E-10
21	3.6654E-16	2.2739E-13
22	5.6293E-17	9.0536E-14
23	7.1602E-17	5.6098E-15

\*read as 1.2311 x 10<sup>0</sup>

<b>Table 8-2      ANSI/ANS 5.1-1979</b> <b>Decay Heat Model Comparison for Infinite Radiation of U-235</b>			
<b>Time After Trip (sec.)</b>	<b>WCOBRA/TRAC (MeV/fission)</b>	<b>Standard (MeV/Fission)</b>	<b><math>\Delta\%</math></b>
0	13.1825	13.183	- 0.003
1	12.3190	12.318	+ 0.008
10	9.5002	9.500	+ 0.007
20	8.4616	8.461	+ 0.003
40	7.4674	7.465	+ 0.036
100	6.2039	6.204	- 0.002
200	5.3744	5.374	+ 0.0002
400	4.6751	4.673	+ 0.04
1000	3.8013	3.801	0.0

<b>ANSI/ANS 5.1-1979</b> <b>Decay Heat Model Comparison for 10<sup>6</sup> Second Irradiation of U-235</b> <b>From Zero Concentration</b>			
<b>Time After Trip (sec.)</b>	<b>WCOBRA/TRAC (MeV/fission)</b>	<b>Standard (MeV/Fission)</b>	<b><math>\Delta\%</math></b>
0	12.626	12.626	0.000
1	11.761	11.761	0.000
10	8.944	8.943	+ 0.015
20	7.907	7.905	+ 0.020
40	6.909	6.908	+ 0.012
100	5.648	5.647	+0.014
200	4.820	4.818	+ 0.034
400	4.118	4.117	+ 0.013
1000	3.245	3.245	0.000

**Table 8-3      ANSI/ANS 5.1-1971**  
**Decay Heat Standard Data for U-235 Thermal Fission**

**Standard Formulation**

$$\frac{DH(t)}{DH_{\infty}} = At^B, \text{ where,}$$

t(sec)	A*	B
$0.1 \leq t < 10$	0.07236	-0.0639
$10 \leq t < 150$	0.09192	-0.181
$150 \leq t < 4 \times 10^6$	0.156	-0.283
$4 \times 10^6 \leq t \leq 2 \times 10^8$	0.3192	-0.335
<b>EXPONENTIAL REPRESENTATION**</b>		
	$\alpha_i$	$\Gamma_i$
1	6.587E+00***	2.658E+00
2	1.490E-01	4.619E-01
3	2.730E-01	6.069E-02
4	2.173E-02	5.593E-03
5	1.961E-03	6.872E-04
6	1.025E-04	6.734E-05
7	4.923E-06	6.413E-06
8	2.679E-07	6.155E-07
9	1.452E-08	8.288E-08
10	1.893E-09	1.923E-08
11	1.633E-10	1.214E-09

\* Includes 20% required Appendix K uncertainty.

\*\* Assumes 200 MeV/fission total recoverable energy

\*\*\* Read as  $6.587 \times 10^0$

Table 8-4    ANSI/ANS 5.1-1971 Decay Heat Standard for U-235 Thermal Fission			
Time After Trip	WCOBRA/TRAC (MeV/fission)	Standard (MeV/fission)	$\Delta\%$
0.1	16.549	16.766	-1.29
1	14.458	14.472	-0.094
10	12.095	12.118	-0.186
20	10.757	10.689	+0.632
40	9.409	9.429	-0.213
100	8.018	7.964	+0.675
200	6.869	6.899	-0.446
400	5.674	5.725	-0.888
1000	4.479	4.417	+1.39

**Table 8-5 Typical Normalized Interaction Frequency Fit Data**

[	
	] <sup>ac</sup>

**Table 8-6 Actinide Heat Source Data**

Isotope	q(MeV)	$\alpha$ (MeV/Sec/Capture)	$\lambda$ (Sec <sup>-1</sup> )
U-239	0.474	2.32834E-4	4.91E-4
Np-239	0.419	1.42879E-6	3.41E-6

<b>Table 8-7 Typical Radiation Source Timing, Strength, and Range</b>				
<b>WCOBRA/TRAC Energy Category</b>	<b>Radiation Type</b>	<b>Timing</b>	<b>Energy (MeV)</b>	<b>Range</b>
Fission <sup>a</sup>	Fragments	Prompt	161.0	Very Short
Fission	Direct Gamma	Prompt	5.0	Long
Fission <sup>b</sup>	Capture Gamma	Prompt	~5.0	Long
Fission	Neutron	Prompt	5.0	Medium
Fission	Neutron	Delayed	0.04	Medium
Fission Fragment <sup>c</sup> Decay	Gamma	Delayed	6.5	Long
Fission Fragment Decay	Beta	Delayed	6.5	Short
Actinide Decay	Gamma	Delayed	0.4	Long
Actinide Decay	Beta	Delayed	0.4	Short

- a. Typical prompt fission energy source taken from "Nuclear Heat Transport," M. M. El-Wakil, American Nuclear Society, 1978.
- b. Typical BOL capture gamma energy source.
- c. Typical BOL decay heat source representative of ANSI/ANS 5.1-1979.

<b>Table 8-8 Typical Values for Redistribution Fraction Values</b>		
<b>I</b>		
		<b>J<sup>LC</sup></b>

**Table 8-9 Neutron Heating Transfer Model**

[		
		]. <sup>c</sup>

].<sup>c</sup>

[illegible]



**Table 8-11 BUGLE-80 Gamma Kerma Data<sup>a</sup>**[illegible]

I

**J<sup>a.c</sup>**

**Table 8-12 Typical 15x15 GEDM Gamma Transfer Matrix**

I						



J<sup>ac</sup>

Table 8-13 [ ] <sup>ac</sup>						
[ ]						



] <sup>ac</sup>

Table 8-14 Decay Group Uncertainty Factors Per One Sigma (%)			
Decay Group	U-235	Pu-239	U-238
1	20.00	30.00	12.00
2	18.00	25.00	14.00
3	3.90	7.00	19.50
4	3.10	4.60	19.80
5	2.60	4.20	20.20
6	2.25	3.90	11.20
7	1.95	3.80	6.80
8	1.85	4.00	5.70
9	1.75	4.00	5.50
10	1.70	4.20	5.30
11	1.65	4.50	5.10
12	1.65	4.50	5.00
13	1.80	4.90	4.70
14	2.00	5.00	3.80
15	2.00	5.00	3.40
16	2.00	5.00	3.60
17	2.00	5.00	3.90
18	2.00	5.00	4.70
19	2.00	5.00	5.00
20	2.00	5.00	5.00
21	2.00	5.00	5.00
22	2.00	5.00	5.00
23	2.00	5.00	5.00

Note: Above table quotes percent uncertainty by group for one-sigma uncertainty values from ANSI/ANS 5.1-1979. Two sigma values can be obtained by doubling the table values above.

**Table 8-15 Point Reactor Kinetics Validation**

<u>W</u> COBRA/TRAC		Inhour Solution <sup>2</sup>	
$\Delta\rho$ (pcm)	T(sec) <sup>1</sup>	$\Delta\rho$ (pcm)	T(sec)
-30000	-80.707	-30027.1	-80.77
+300	+9.147	+300.002	+9.147
+150	+34.14	+150.001	+34.14

1. Observed asymptotic period
2. Data for each solution given below

Group	Beta	Lambda
1	3.5410E-04*	3.00
2	1.0104E-03	1.13
3	2.9479E-03	0.301
4	1.4271E-03	0.111
5	1.5313E-03	0.0305
6	2.2920E-04	0.0124

$\ell^* = 16.06 \mu\text{s}$ ,  $\bar{\beta} = 0.0075$

\*Read as  $3.541 \times 10^{-4}$





Table 8-18 [ ] <sup>a,c</sup>								
[ ]								

] <sup>a,c</sup>



a.c

**Figure 8-1. U-235 Fission Fraction**

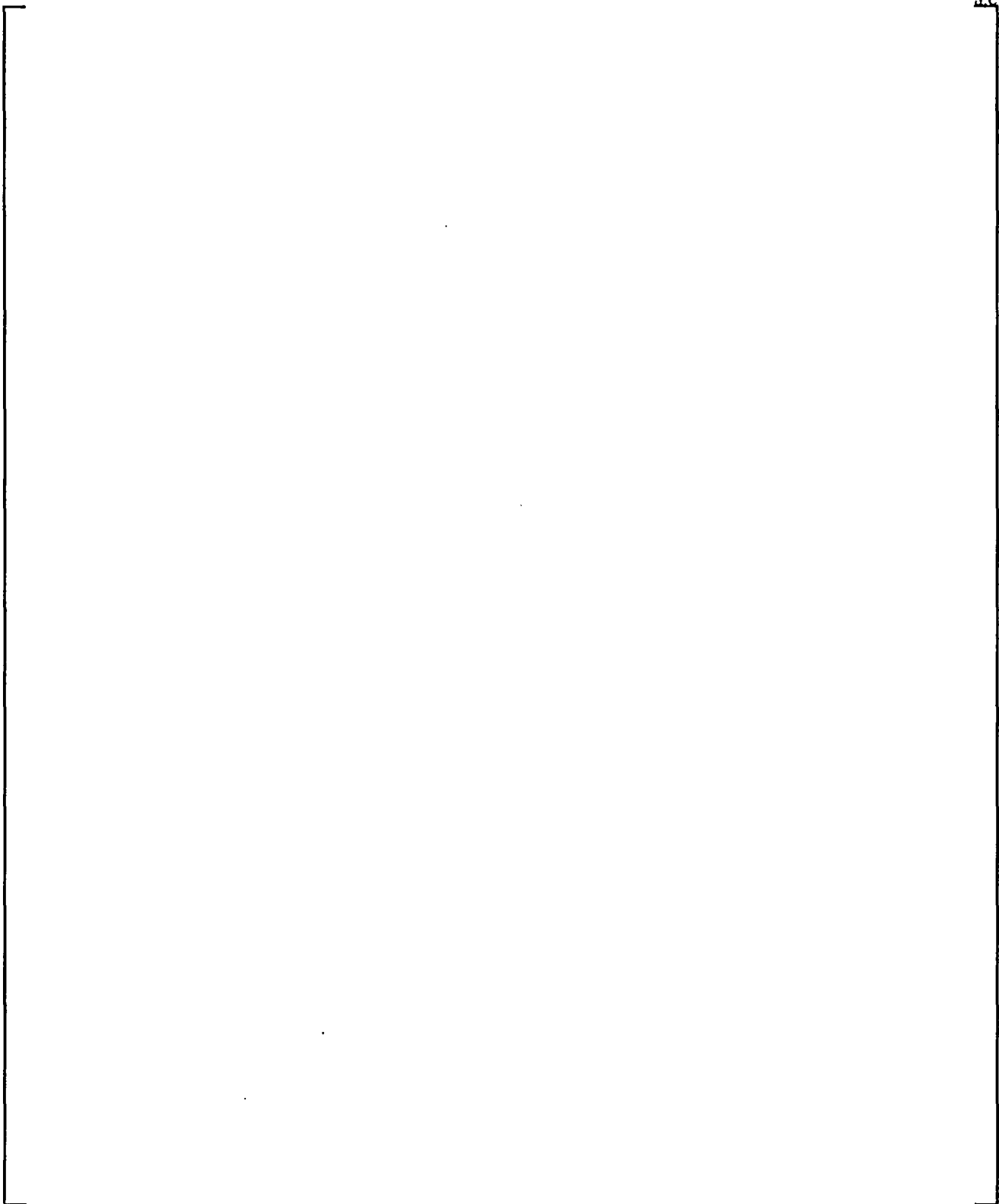


**Figure 8-2. Pu-239 Fission Fraction**

a.c

Figure 8-3. U-238 Fission Fraction

a.c

**Figure 8-4.     Calculated Normalized Macroscopic Cross Sections versus Core Average Water Density**

a.c

Figure 8-5.  $\bar{\beta}$  vs. Burnup at Various Enrichments

a.c.

**Figure 8-6. Prompt Neutron Lifetime**

a.c

**Figure 8-7. Prompt Energy Release**

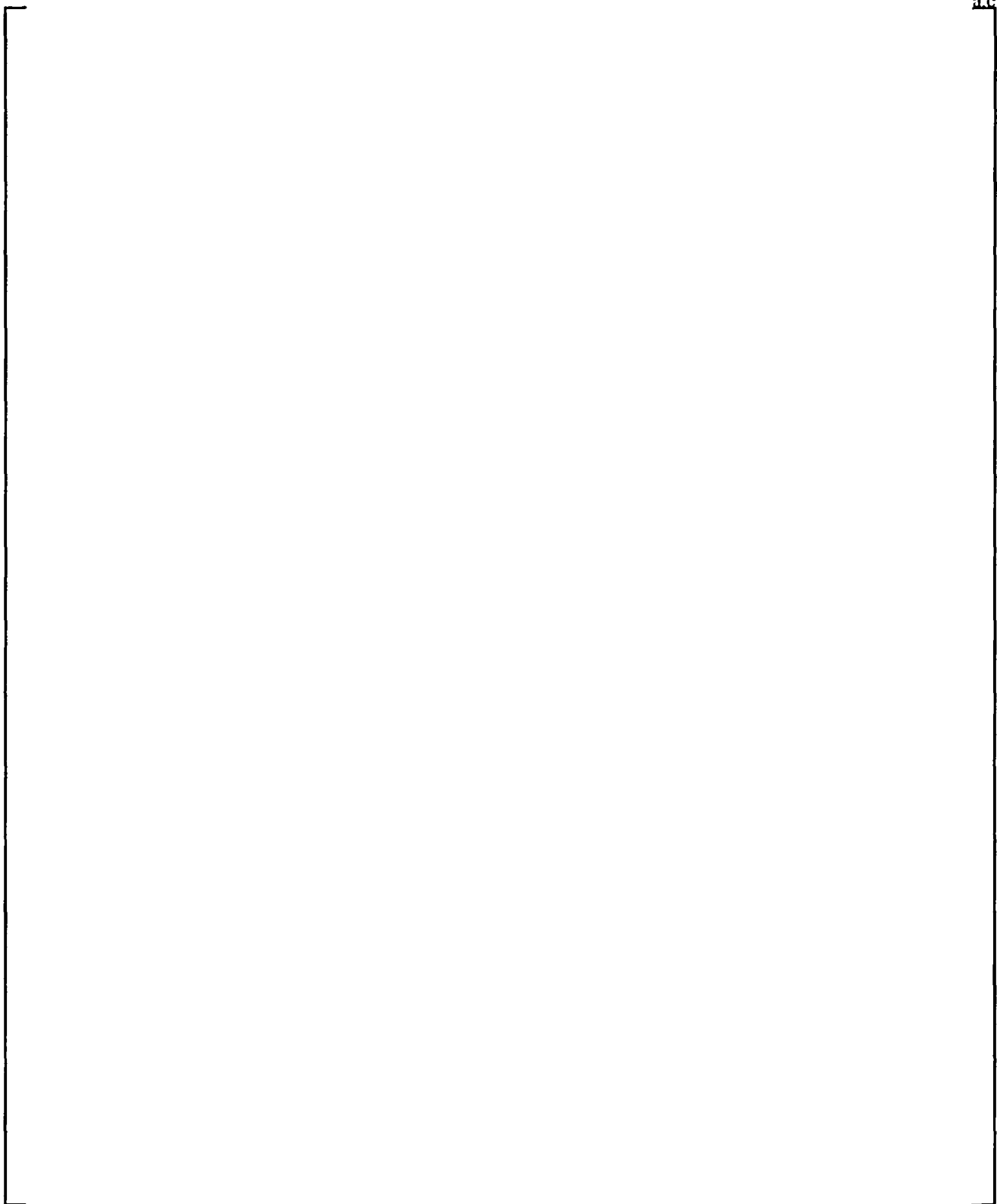


**Figure 8-8. Total Energy Release**



a.c

**Figure 8-9. Delayed Group I Lambda**

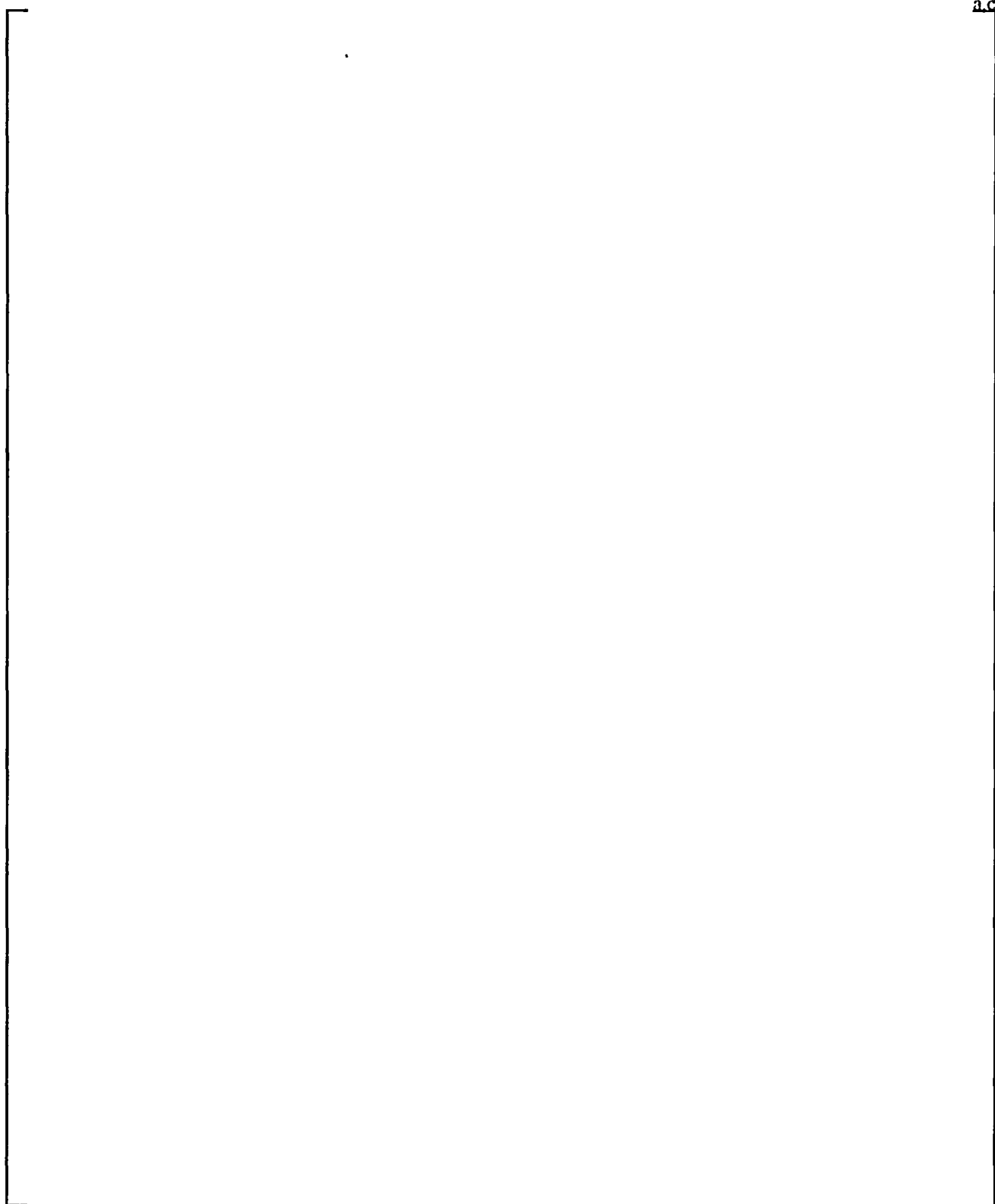


**Figure 8-10. Delayed Group II Lambda**

a.c

**Figure 8-11. Delayed Group III Lambda**

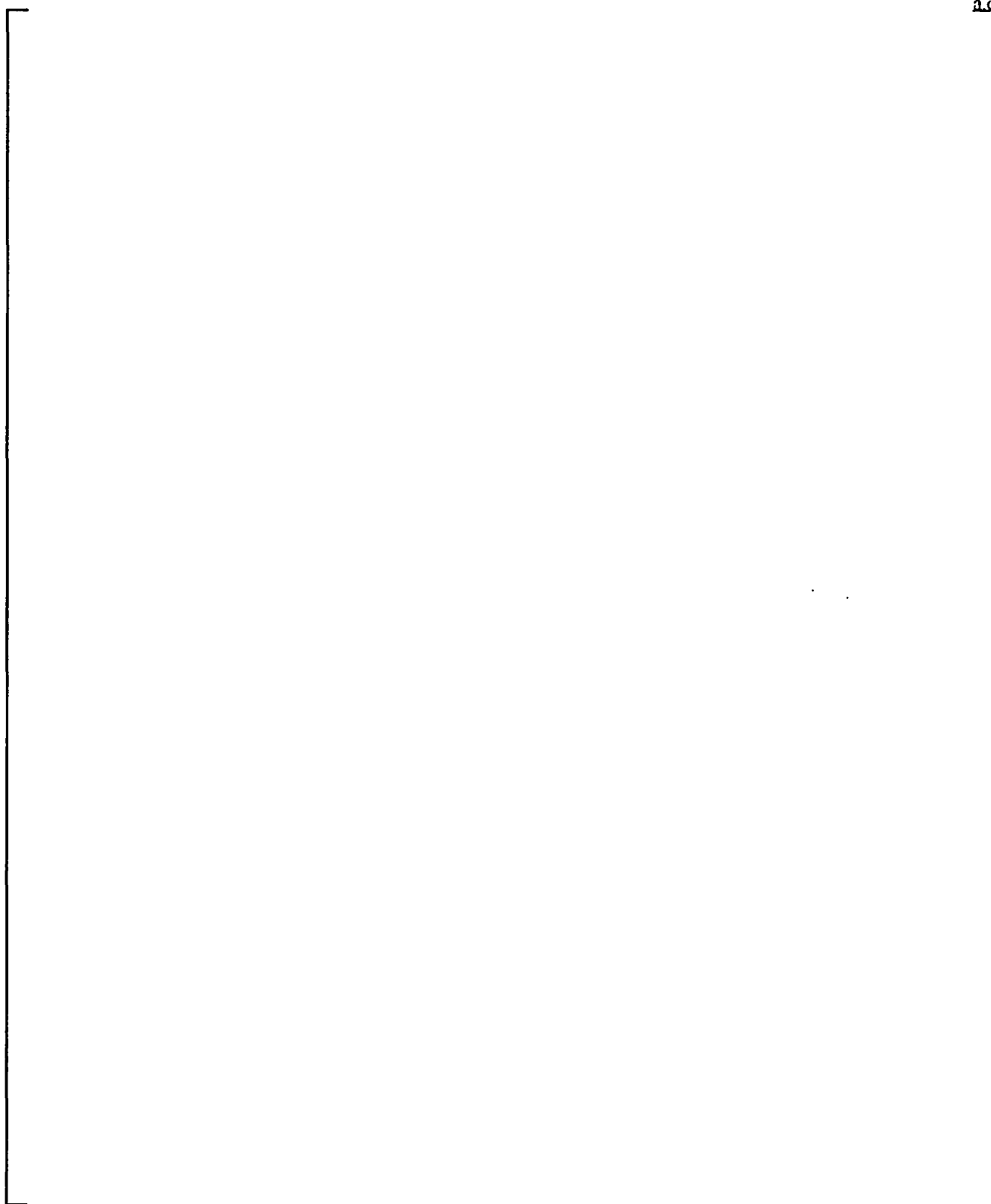


**Figure 8-12. Delayed Group IV Lambda**

a.c

**Figure 8-13. Delayed Group V Lambda**

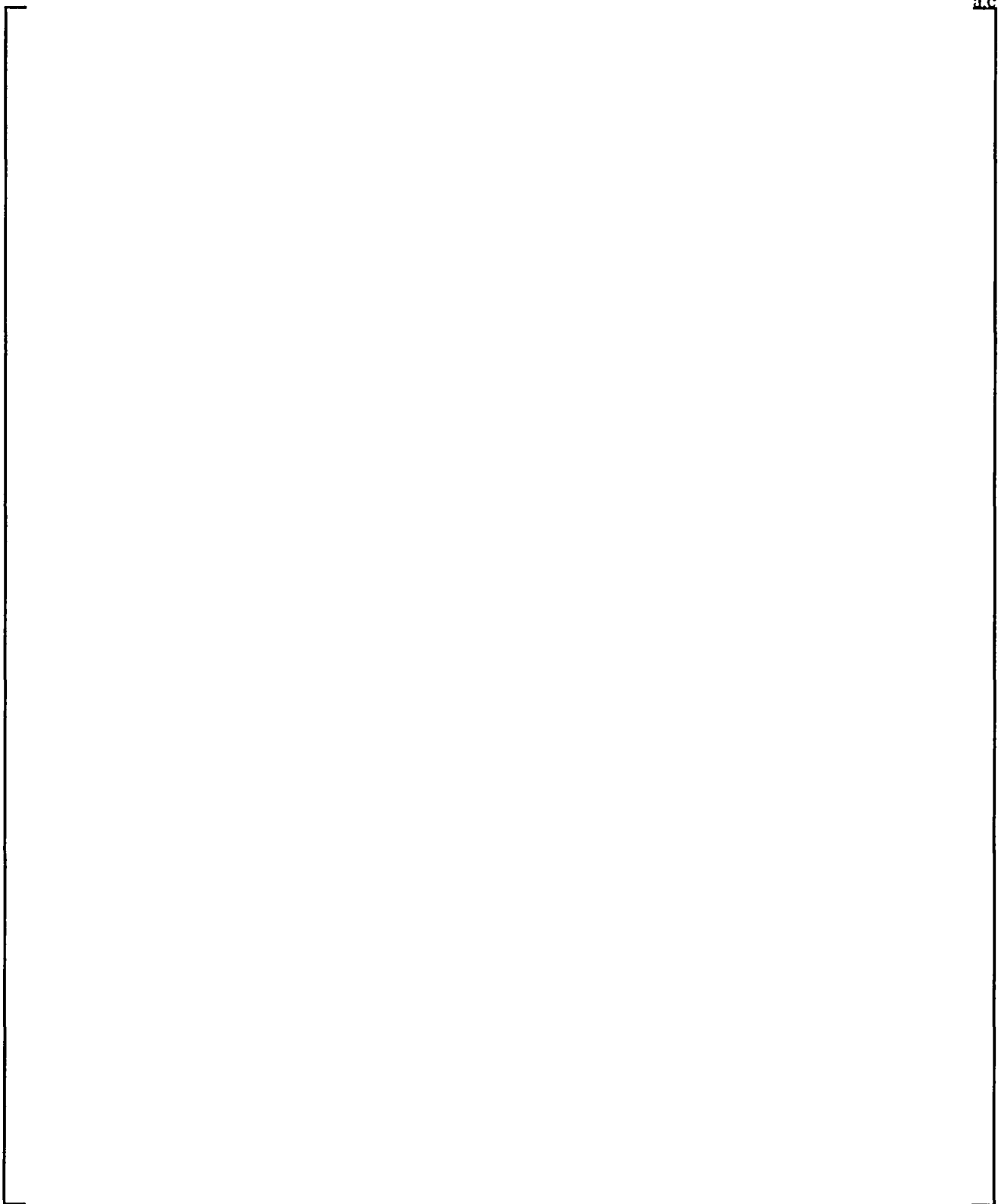


**Figure 8-14. Delayed Group VI Lambda**

a.c

**Figure 8-15. U-238 Capture/Fission Ratio as a Function of Initial Enrichment and Burnup**

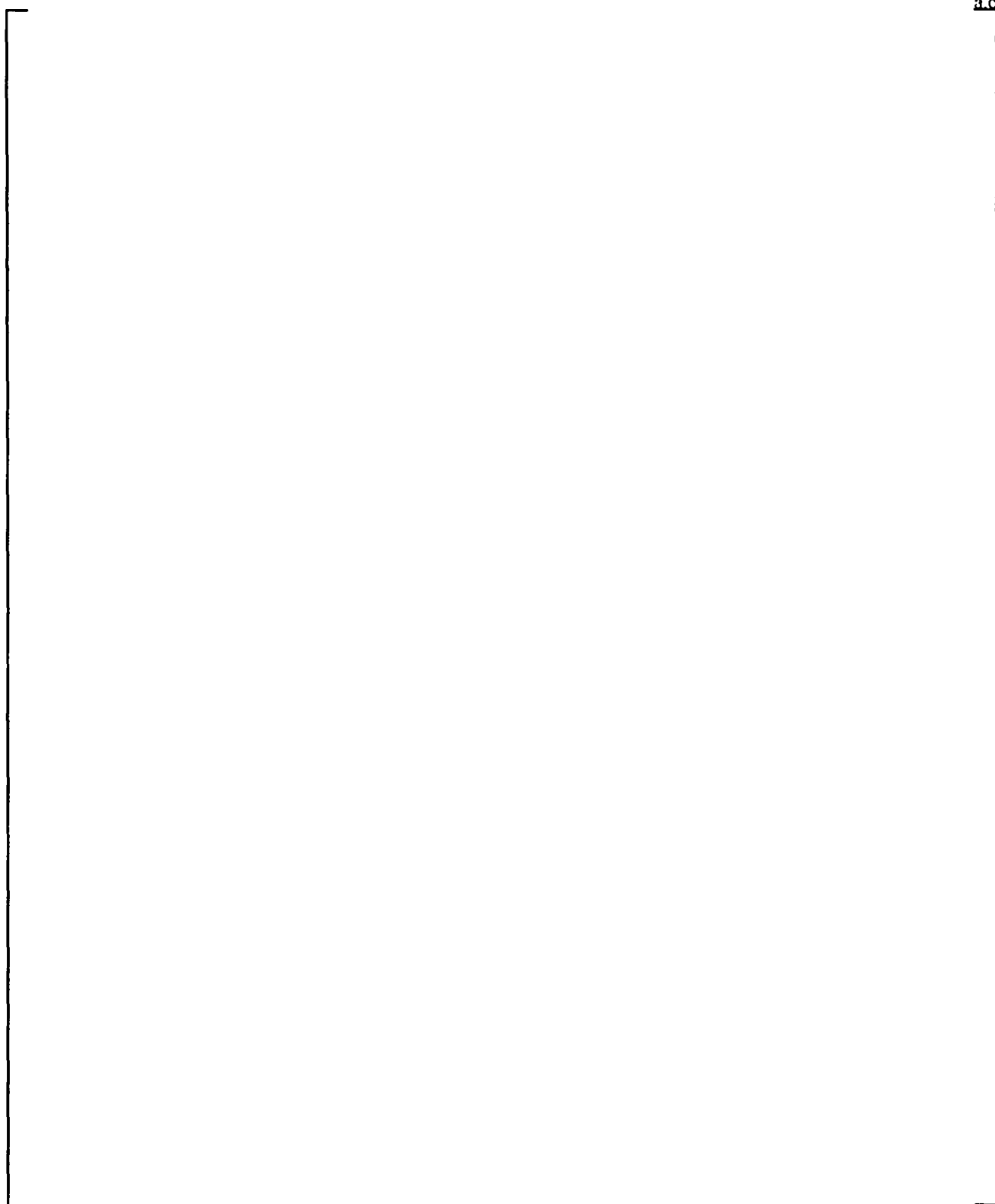


**Figure 8-16. 15x15 Material Composition Assignment Layout**



a.c

**Figure 8-17. 15x15 Core Balance Fixed Source Distribution**

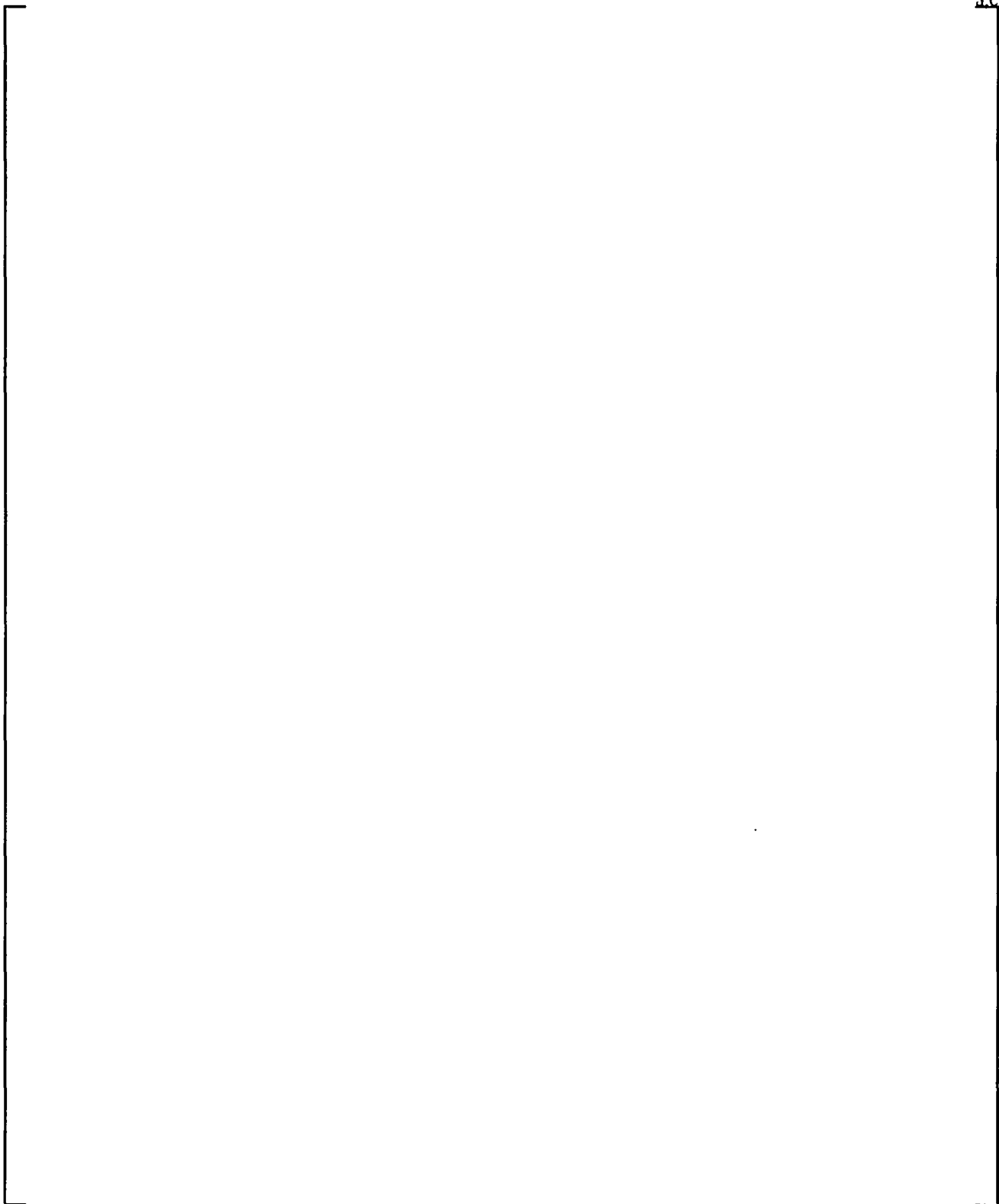


**Figure 8-18. 15x15 Hot Assembly Fixed Source Distribution**

a.c

**Figure 8-19. 15x15 Hot Rod Fixed Source Distribution**

**Figure 8-20. Gamma Kerma Cross Section Energy Dependence**

a.c

**Figure 8-21. Typical Heat Flux Deposition Fractions versus Coolant Density**

**Figure 8-22. Typical Heat Flux Deposition Fractions versus Coolant Density**

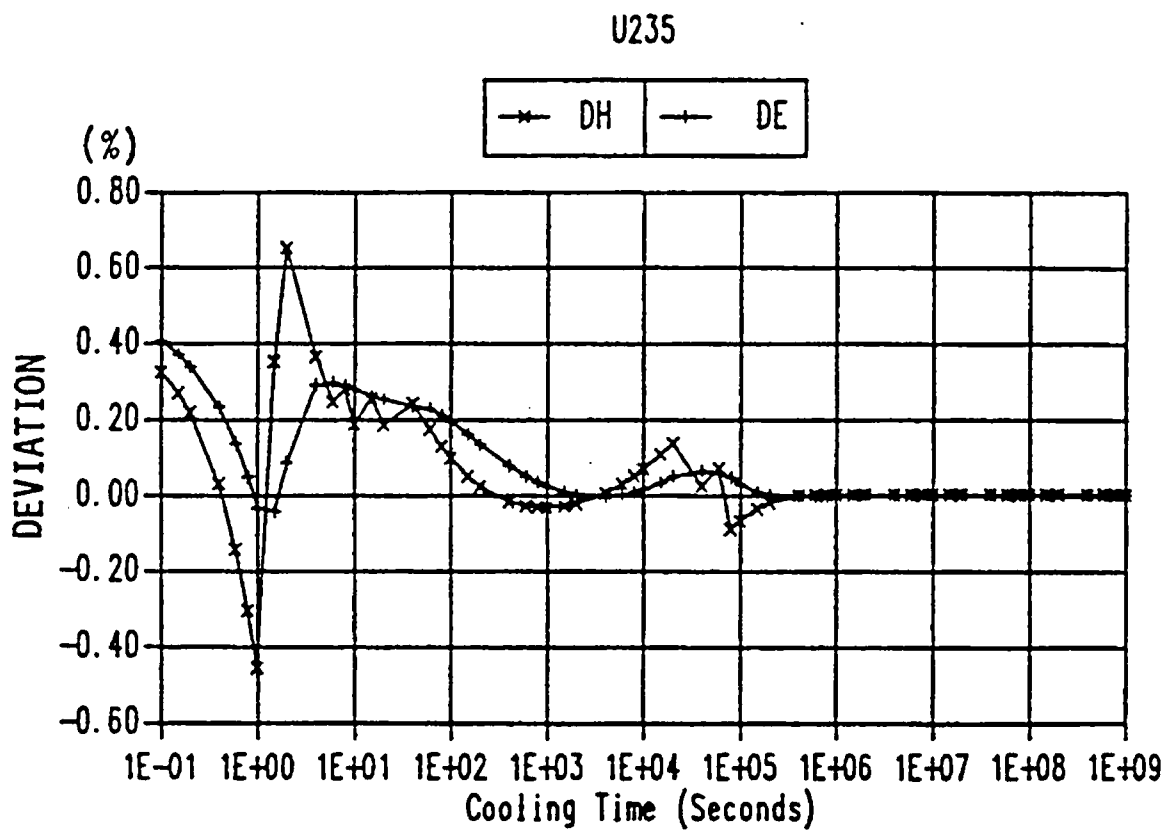


Figure 8-23. Percent Fit Deviations for U-235 ANSI/ANS 5.1 - 1979 Plus Two Sigma

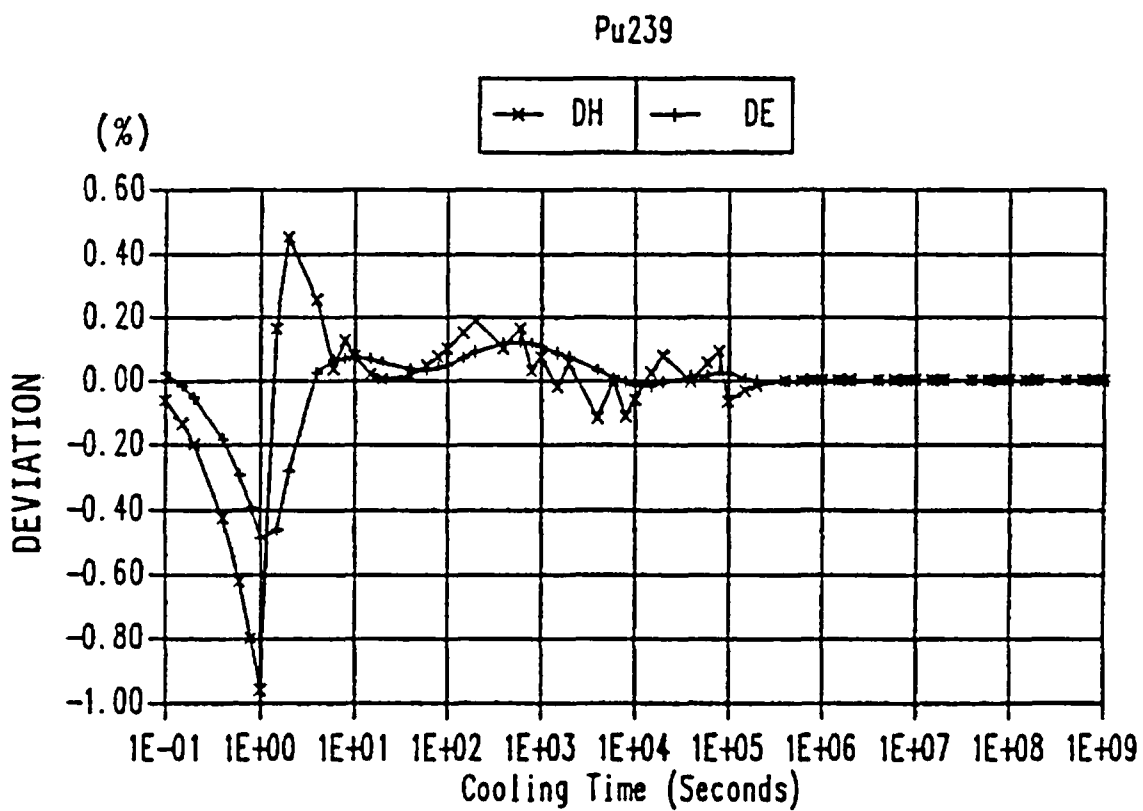


Figure 8-24. Percent Fit Deviations for Pu-239 ANSI/ANS 5.1 - 1979 Plus Two Sigma



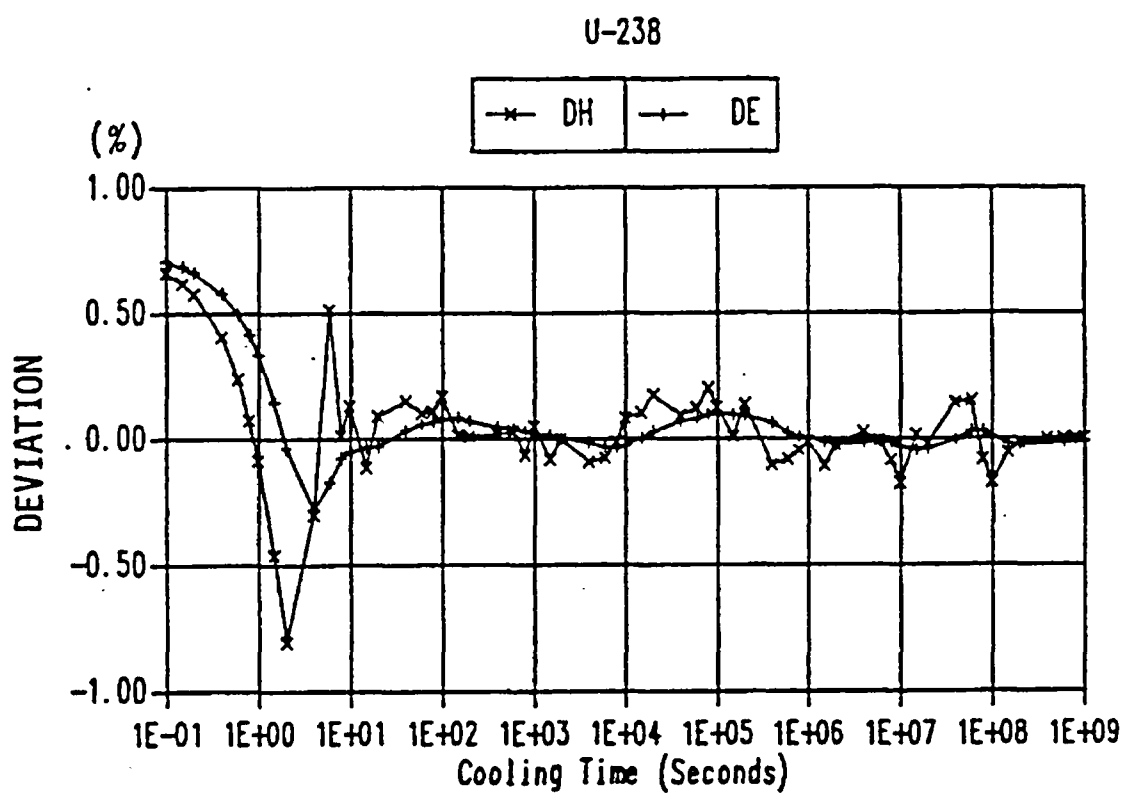


Figure 8-25. Percent Fit Deviations for U-238 ANSI/ANS 5.1 - 1979 Plus Two Sigma

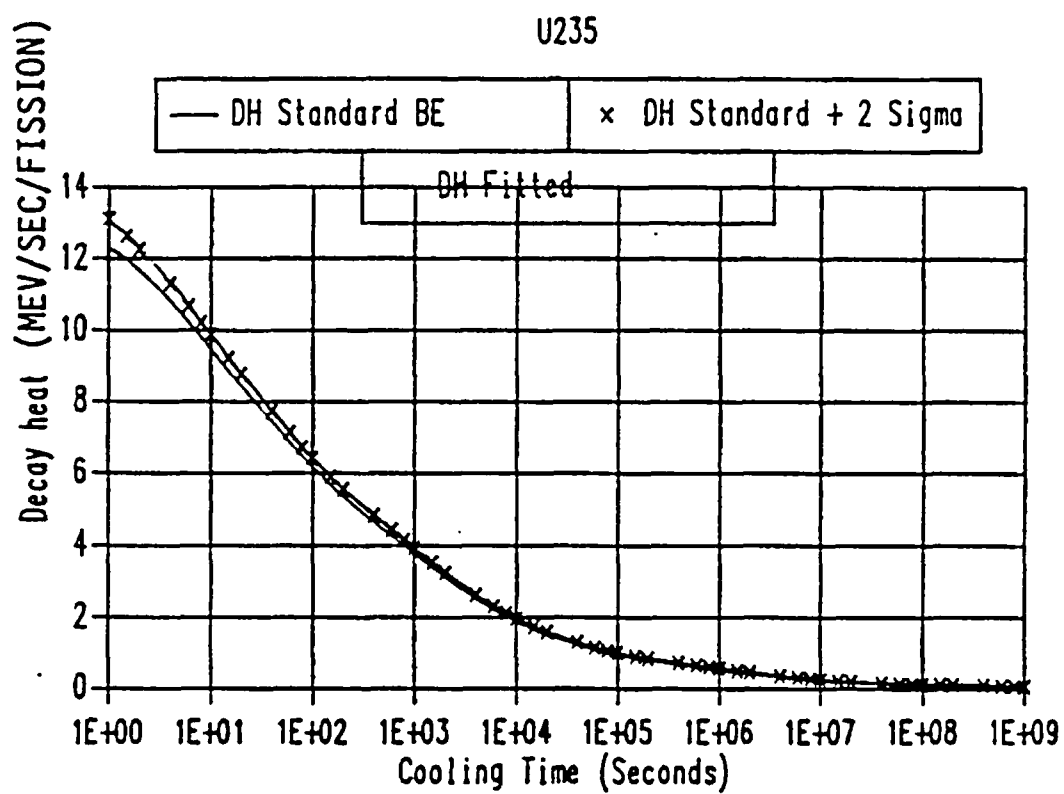


Figure 8-26. U-235 ANSI/ANS 5.1 - 1979 Decay Heat Standard vs. Fitted Results

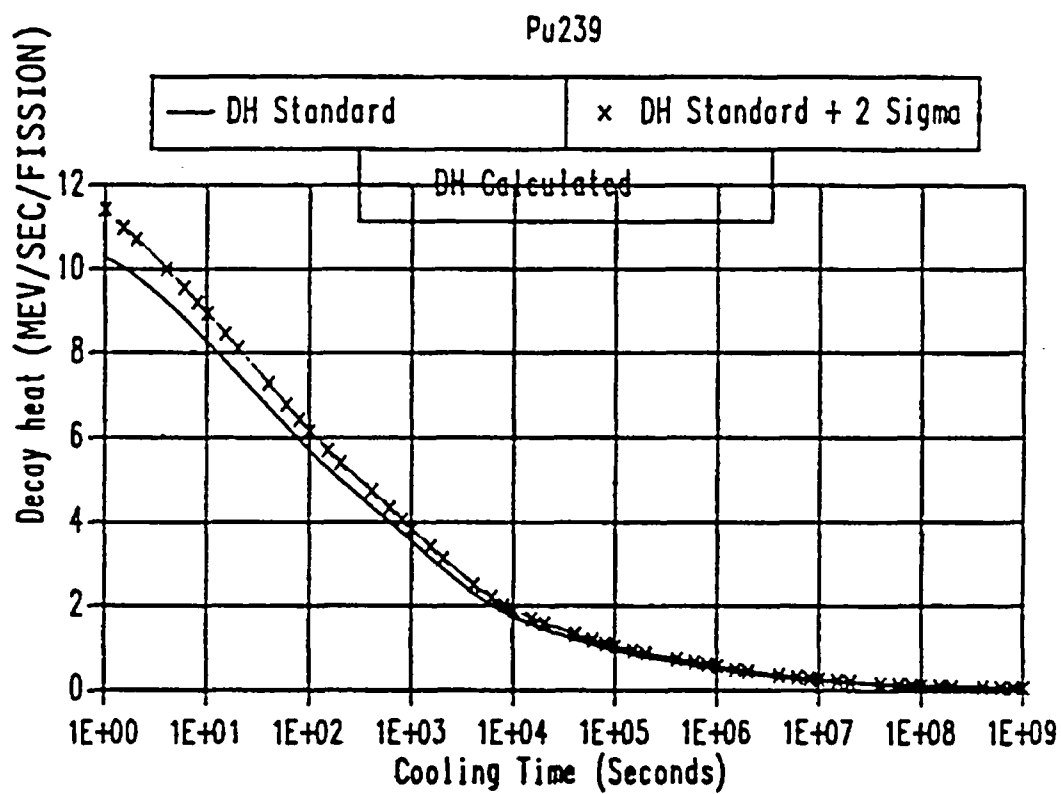


Figure 8-27. Pu-239 ANSI/ANS 5.1 - 1979 Decay Heat Standard vs. Fitted Results

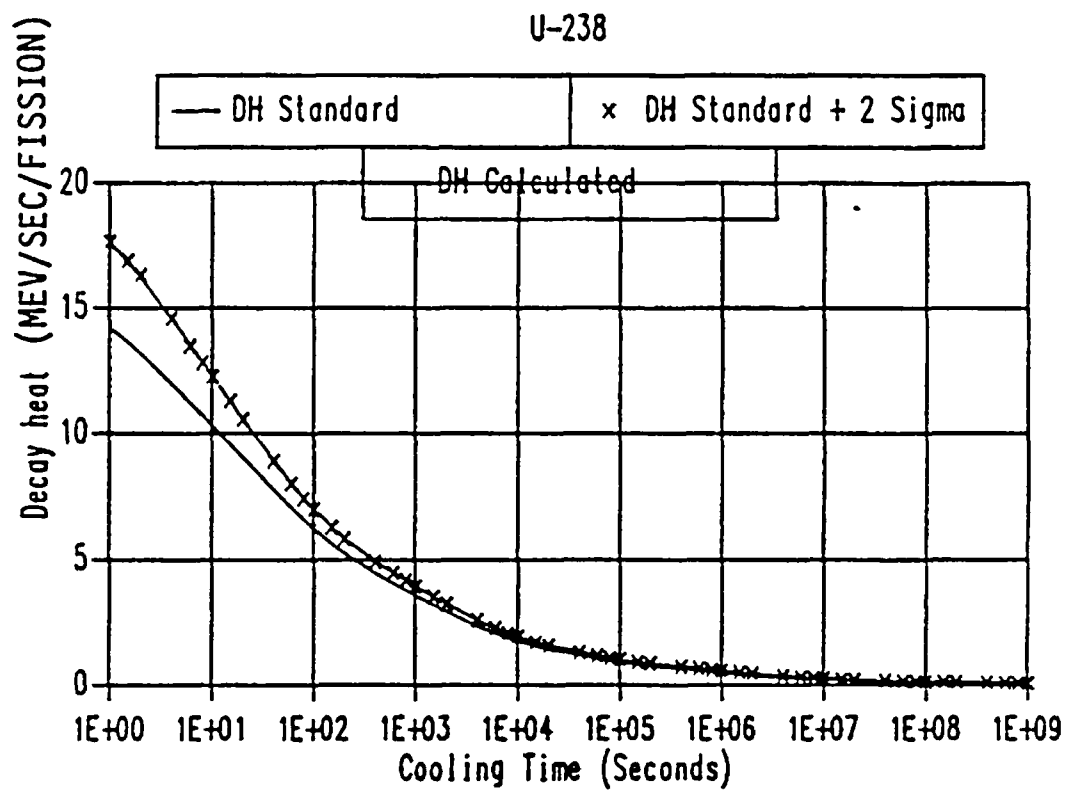


Figure 8-28. U-238 ANSI/ANS 5.1 - 1979 Decay Heat Standard vs. Fitted Results

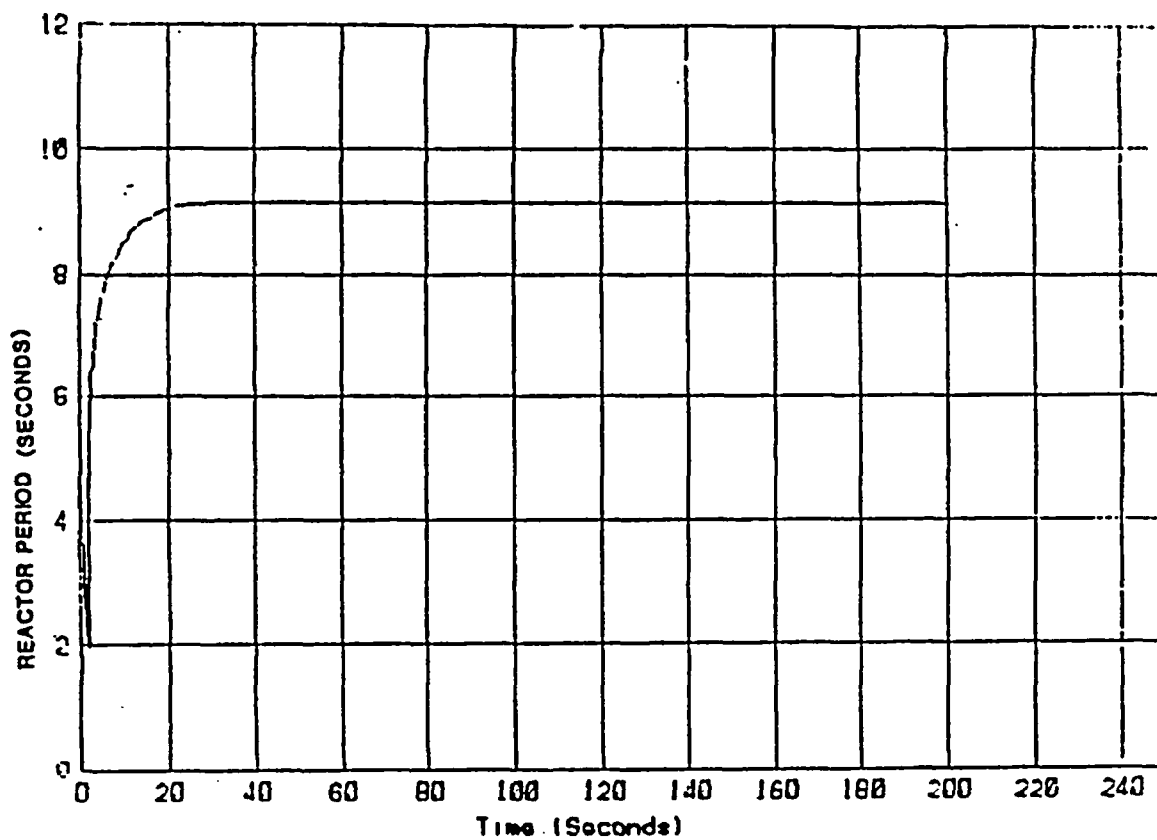


Figure 8-29. Time Dependent Reactor Period for + 0.003  $\Delta K$  Reactivity Insertion versus Time After Insertion

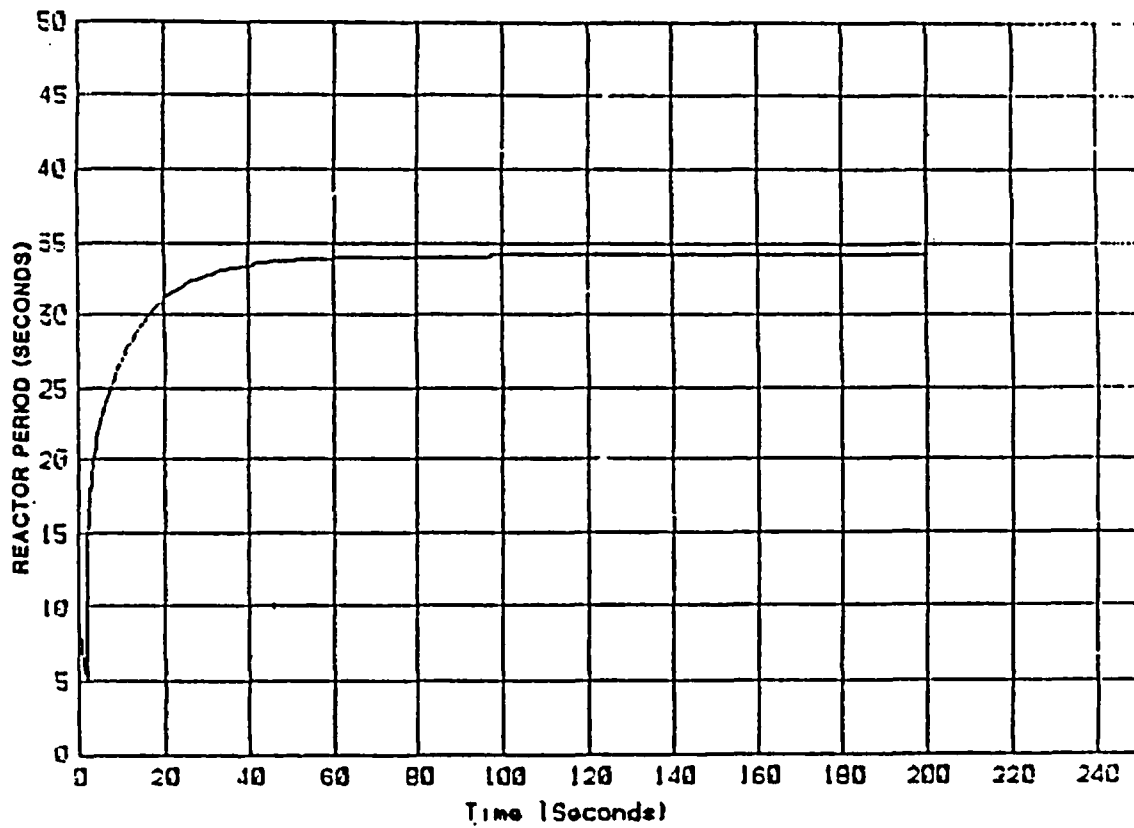


Figure 8-30. Time Dependent Reactor Period for + 0.0015  $\Delta K$  Reactivity Insertion versus Time After Insertion

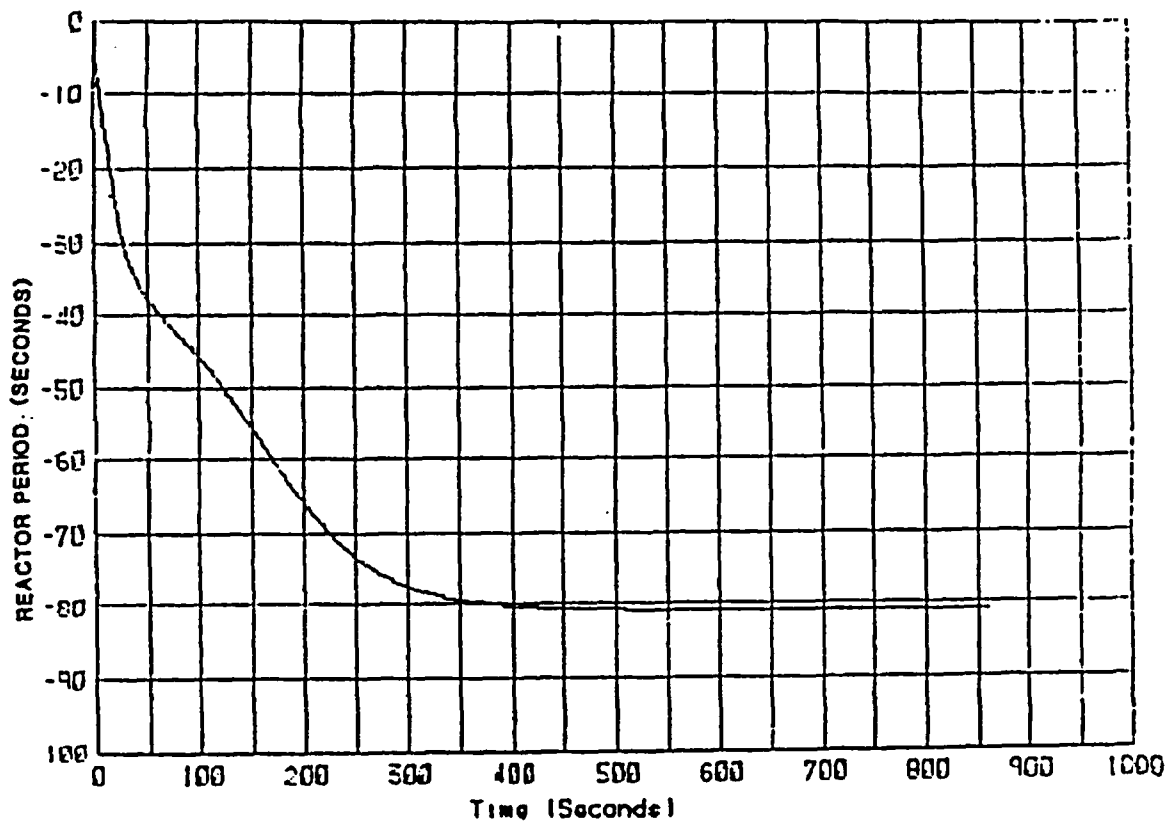
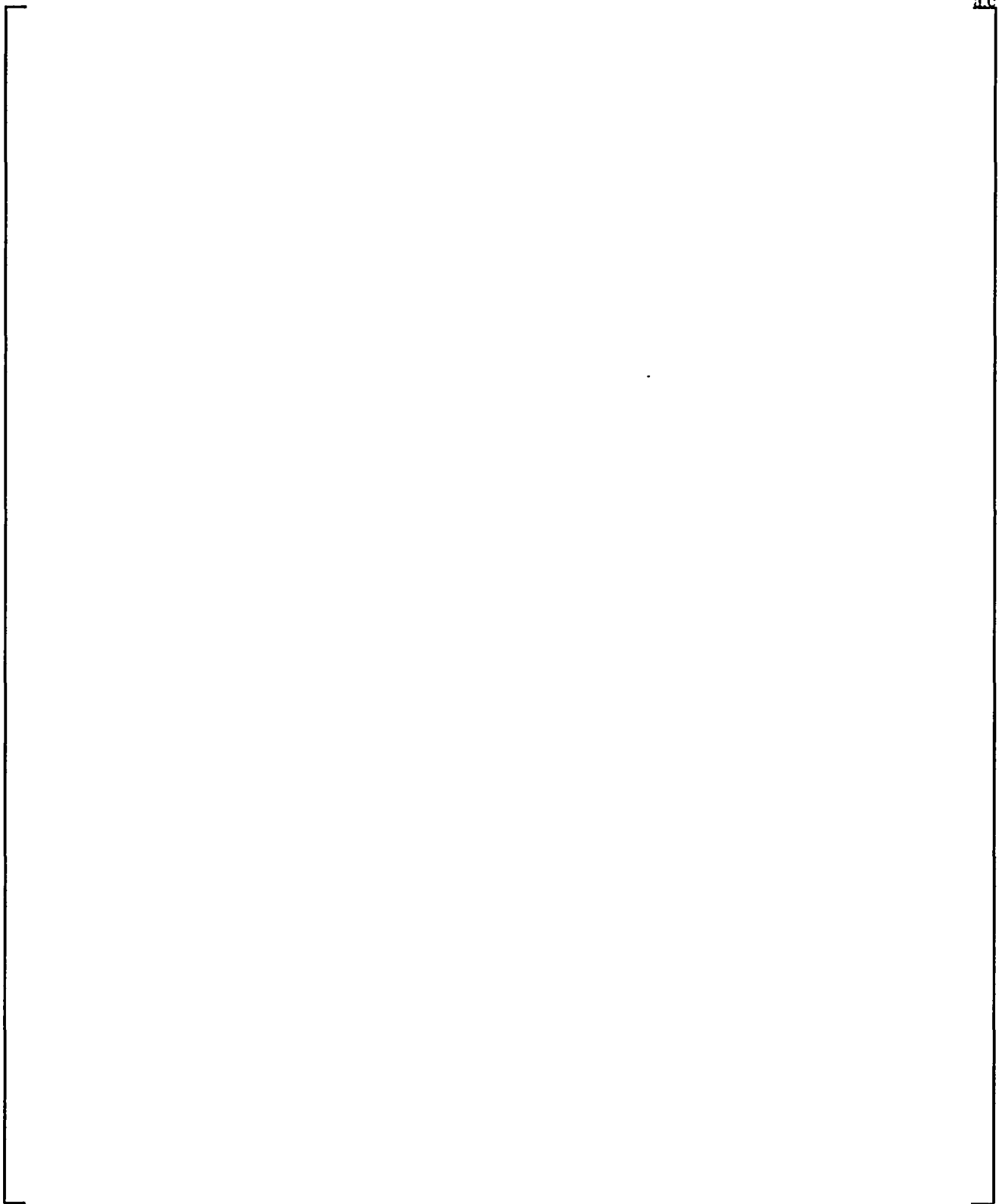


Figure 8-31. Time Dependent Reactor Period for - 0.030  $\Delta K$  Reactivity Insertion versus Time After Insertion



**Figure 8-32. Total Actinide Decay Power versus Burnup and Initial Enrichment**



a.c

**Figure 8-33. Actinide Decay Power versus Burnup and Initial Enrichment**

a.c

**Figure 8-34. Capture Correction versus Burnup and Initial Enrichment**

### OPTIONS IN WCOBRA/TRAC FOR NEUTRONICS CALCULATIONS

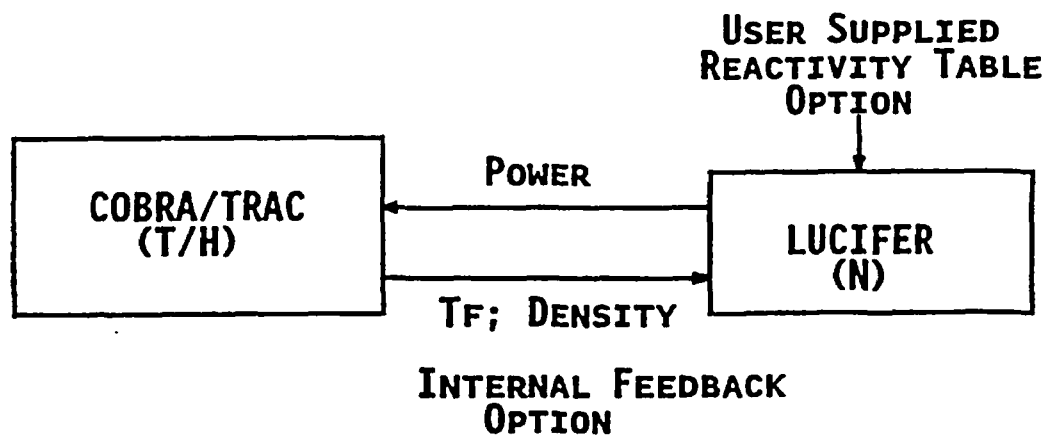


Figure 8-35. WCOBRA/TRAC Calculation Block Diagram

## 9 WCOBRA/TRAC ONE-DIMENSIONAL COMPONENT MODELS

### 9-1 INTRODUCTION

The one-dimensional components in WCOBRA/TRAC are modules derived from TRAC-PD2 to model the reactor primary system. These components provide models for accumulators, pressurizers, pipes, tees, pumps, steam generators, and valves. In addition, there are two modules that provide boundary conditions for parts of the system not modelled, consisting of either a pressure sink/source or a flow boundary.

The conservation equations used for the one-dimensional components are discussed in Section 2-4. The following sections will describe the features of each of the one-dimensional components and elaborate on their unique characteristics. Many of the modules are virtually unchanged from their original TRAC-PD2 versions, so many of the descriptions are the same as those given by Liles et al. (1981).

### 9-2 PIPE COMPONENT

**Model Basis** The PIPE component is used to model one-dimensional thermal-hydraulic flow in a duct or pipe. A PIPE can be used alone in a problem or can connect other components together to model a system. Area changes, wall heat sources and heat transfer across the inner and outer wall surfaces can be modelled in the PIPE component.

Figure 9-1 shows a typical noding diagram for a PIPE containing a venturi and an abrupt area change. The numbers within the PIPE indicate cell numbers, and those above it are cell boundary numbers. The geometry is specified by providing a volume and length for each cell and a flow area and hydraulic diameter at each cell boundary. The junction variables JUN1 and JUN2 provide reference numbers for connecting this PIPE to other components.

Wall friction losses and form losses associated with bends, orifices, etc. are set where required at the appropriate node boundaries. Five options are available to determine the wall friction losses based on a variety of flow configurations and correlations. These options are described in Section 4-7.

Wall heat transfer from the inner and outer surfaces of the PIPE may be calculated as well as heat generation within the wall. The calculation of critical heat flux may be determined by the Biasi et al. (1967) correlation. Section 6-3 describes the selection of heat transfer coefficients in the one-dimensional components. The wall material properties are selected from stainless steel (304, 316, and 347), carbon steel A508, or Inconel 600.

The PIPE component includes an option that allows the user to simulate the effect of a non-condensable gas on the condensation rate. This option is used to simulate the suppression of the condensation rates in

the PIPE caused by nitrogen injection from the accumulator or from ingestion of air from the containment. Application of the condensation suppression factor to the interfacial heat transfer coefficients is described in Section 5-3-5.

The numerical solution method used for the PIPE component is specified by the user. The semi-implicit method is adopted due to its increased computational efficiency. In components which can expect high flow velocities, the fully implicit solution method is used to avoid the restriction set by the low Courant limit. The junctions of the one-dimensional components are always solved semi-implicitly.

**Model As Coded** No special models or correlations are applied in a PIPE component. The conservation equations are solved as described in Section 2, with the closure relations discussed in Sections 3 through 8, referring to one-dimensional components. The thermodynamic and material properties are described in Section 10. During the execution of a problem, the solution procedure is controlled by subroutines PIPE1, PIPE2, and PIPE3. At the beginning of each time step, PIPE1 calls subroutine SLIP to obtain relative velocities, and subroutine FWALL for wall friction and irrecoverable loss coefficients to determine the interfacial drag coefficients and calculate the relative phase velocities. Subroutine HPIPE is then called to determine the wall heat transfer coefficients. During the timestep iteration, PIPE2 calls DF1D, which is the controlling routine for the hydrodynamics solution.

DF1D calls DF1DS or DF1DI depending on whether the semi-implicit or implicit solution scheme has been chosen. In these routines the interfacial mass and heat transfer, condensation suppression, and in the case of DF1DS, water packing logic are applied or calculated. The controlling routine PF1CHK is called if the critical flow model has been selected. After a timestep is successfully completed, PIPE3 calls CYLHT and FPROP to determine the wall temperatures and calculate the new fluid properties, respectively. The boundary arrays are again updated for the converged solution. If the time step fails to converge, the calculation is backed up to the previous time step values, and a new time step, half the size of the old one, is tried.

### 9-3 TEE COMPONENT

**Model Basis** The TEE component models the thermal-hydraulics of three piping branches, two of which lie along a common line with the third entering at some angle  $\beta$  from the main axis of the other two. The code basically treats a TEE component as two PIPES, as indicated in Figure 9-2. The angle  $\beta$  is from the low-numbered end of PIPE 1 to PIPE 2. The low-numbered end of PIPE 2 always connects to PIPE 1. The straight PIPE segment is numbered from cell 1 to NCELL1, with the connection to PIPE 2 at cell JCELL. The branch PIPE segment is numbered from the cell immediately adjacent to JCELL, beginning with cell 1 and ending with cell NCELL2.

The connection to PIPE 1 from PIPE 2 is treated with mass, momentum, and energy source terms. For PIPE 2 the conditions in cell JCELL of PIPE 1 form the inlet boundary conditions. The mass and energy terms associated with the side branch flow are added to the governing mass and energy equations representing the main branch flow. The losses at the junction are modelled in terms of the momentum

change resulting from the combining or dividing flow. For the combining case an additional momentum source term is added to the main branch momentum equations. This term represents the momentum source or sink associated with the secondary flow in relation to the main branch flow. The time differencing and iteration procedures guarantee conservation of scalar quantities within a convergence tolerance. The levels of implicitness for the finite-difference equations applied to PIPE 1 and PIPE 2 can be specified independently using the input variables IHYD1 and IHYD2. Since the junction between PIPE 1 and PIPE 2 is always treated semi-implicitly, the velocity at that point is always included in the computation of the time step stability limit. Phase separation at the junction is calculated if the flag ISEP is set to one. Phase separation is computed if the void fraction in the junction cell JCELL exceeds the user-specified value ALSEP.

**Model as Coded** Since the TEE is modelled as two connected PIPEs, the PIPE model description in Section 9-2 should be consulted for additional information. The calculational sequence for a TEE includes separate calculations of the primary and secondary sides. For the junction momentum source, an additional source term is calculated in subroutine ETEE and is incorporated in the momentum equation in DF1DS or DF1DI depending on the solution option chosen. This source term is set to zero when the TEE is a dividing tee.

## 9-4 PUMP COMPONENT

**Model Basis** The pump model employed in WCOBRA/TRAC describes the interaction of the system fluid with a centrifugal pump. The model calculates the pressure differential across the pump and its angular velocity as a function of the fluid flowrate and the fluid properties. The model is designed to treat any centrifugal pump and can include two-phase effects.

$$\frac{U_{1.5} - U_{1.5}^n}{\Delta t} = \frac{(P_1 - P_2)}{\rho_{1.5}^n \Delta x} - C^n - g_z - \frac{f U_{1.5}^n |U_{1.5}^n|}{D_h} + \Omega \quad (9-1)$$

The pump model is represented by a one-dimensional component with N cells, where N must be greater than 1. A typical nodding diagram for the pump component is shown in Figure 9-3. The pump momentum is modelled as a source  $\Omega$  that is included between cells 1 and 2. The source is positive for normal operation with the pressure rise occurring from cell 1 to cell 2, so it is necessary to number the cells so that the cell number increases in the normal flow direction.

The pump model is identical to the one-dimensional pipe model except that a momentum source is included in the mixture momentum equation written between cells 1 and 2:

where  $U$  is the mixture velocity,  $P$  is the pressure,  $C$  represents the convective terms,  $g_z$  is the gravity term,  $f$  is the friction factor,  $\rho$  is the fluid density,  $\Delta x$  is the cell length,  $D_h$  is the hydraulic diameter, the subscript 1.5 refers to the average value between cell 1 and cell 2, and the superscript  $n$  indicates that the parameter was evaluated at the previous timestep. Parameters without a superscript are the updated, new time values. The source term  $\Omega$  is taken to be:

$$\Omega = \frac{\Delta P_{pump}}{\rho_{1.5}^n \Delta X} + C^n + g_z + \frac{f}{D_h} U_{1.5}^n |U_{1.5}^n| \quad (9-2)$$

where  $\Delta P_{pump}$  is the pressure rise across the pump evaluated from the pump characteristic curves. With this definition of the momentum source, the steady-state solution of Equation 9-1 is  $P_2 - P_1 = \Delta P_{pump}$ . The model for  $\Delta P_{pump}$  is described next.

### The Pump Characteristic Curves - The Homologous Curves

It has been well known that for single-phase flow the characteristics of a pump can be quite accurately obtained from those of a geometrically similar scale-model using the similarity laws. Following these laws, the head and the torque of the pump can be represented in nondimensional forms which are independent of the scale of the pump model. The approach used to establish the so-called homologous curves is one of the methods that has utilized the similarity laws to nondimensionalize the variables involved in pump operations. In this approach, four homologous curve segments (one curve segment represents a family of curves) are established. These curves describe in a compact manner all the operating states of the pump. The following definitions are employed in the subsequent development:

- $H$  = pump head =  $\Delta P_{pump} / \rho$
- $\rho$  = fluid density at pump inlet
- $Q$  = volumetric flow rate through pump
- $\omega$  = pump impeller angular speed
- $T$  = pump hydraulic torque

To allow one set of curves to be used for a variety of pumps, the following normalized quantities are used:

- $v = Q/Q_R$
- $\alpha_N = \omega/\omega_R$
- $h = H/H_R$
- $\beta = (T/T_R)/(\rho_R/\rho)$

where the subscript  $R$  denotes the rated conditions. Use of the pump similarity relations (Olson, 1974a) shows that

$$\frac{h}{\alpha_N^2} = f\left(\frac{v}{\alpha_N}\right) \quad (9-3)$$

and

$$\frac{\beta}{\alpha_N^2} = f\left(\frac{v}{\alpha_N}\right) \quad (9-4)$$

for

$$\left| \frac{v}{\alpha_N} \right| \leq 1 ,$$

and

$$\frac{h}{v^2} = f\left(\frac{\alpha_N}{v}\right) \quad (9-5)$$

and

$$\frac{\beta}{v^2} = f\left(\frac{\alpha_N}{v}\right) \quad (9-6)$$

for

$$\left| \frac{\alpha_N}{v} \right| \leq 1$$

Table 9-1 shows the resulting four segments of the homologous head and torque curves that represent the complete pump operational characteristics.



### Pump Single-Phase Head and Torque Homologous Curves

Figures 9-4 and 9-6 show typical single-phase homologous head and torque characteristic curves for Westinghouse designed pumps.

### Pump Fully-Degraded Head and Torque Homologous Curves

A basic assumption of the WCOBRA/TRAC pump model is that the same type of scaling laws, which are applied under single-phase conditions, can also be applied under two-phase conditions. It is assumed that there exists a condition at an intermediate range of void fractions in which the pump head and torque can be described by a set of homologous curves, similar to the single-phase curves. A typical set of curves is illustrated in Figures 9-5 and 9-7.

### The Head and Torque Multipliers

To provide for a transition from single- to two-phase conditions, the following correlations are used:

$$H_* = H_1 - M(\alpha) (H_1 - H_2) \quad (9-7)^{(1)}$$

and

$$T_* = T_1 - N(\alpha) (T_1 - T_2) \quad (9-8)^{(1)}$$

where

$M$  = head multiplier

$N$  = torque multiplier

$\alpha$  = donor-cell vapor void fraction at pump inlet

and the subscript 1 denotes the single-phase value, the subscript 2 denotes the two-phase value, both calculated from the homologous curves, and the subscript \* denotes the derived value for a given two-phase condition.

### Pump Impeller Speed

The angular speed of the pump impeller is calculated from the equation

$$I \frac{d\omega}{dt} = T_M - (T_* + T_{FR} + T_E) \quad (9-9)$$

where

- $I$  = moment of inertia of the pump rotor assembly
- $T_M$  = torque supplied by motor (after trip,  $T_M = 0.0$ )
- $T_{FR}$  = total friction torque (including all mechanical, bearing friction and windage loss)
- $T_E$  = electric torque (caused by induced voltage after trip)

The total friction torque is (Bordelon et al., 1974) [

]<sup>a,c</sup> (9-10)

where

[  
]<sup>a,c</sup>

for the 93A pump, and is assumed to apply to other pumps of similar design. The pump hydraulic torque ( $T_h$ ) is evaluated from the homologous curves and Equation 9-8 as a function of the fluid density and flow rate as well as pump angular velocity.

### Pump Options and Limitations

The wall heat transfer, wall friction, CHF calculation and implicit hydrodynamics options for the PUMP module are the same as for the PIPE module. In addition, the following options are specified: pump type, motor action, reverse speed option, two-phase option, and pump curve option.

If the pump motor is energized, its angular velocity is assumed to be the constant value specified. If the motor is not energized, a pump coastdown calculation is performed using the specified initial pump speed.

There are two pump options available. For pump option 1 (IPMPTY = 1) the pump speed variation is specified by input. The pump is initially energized at a constant speed specified by input (OMEGA). The pump motor may be tripped by a TRIP signal. If a pump trip has occurred, the pump speed is taken from a table of pump speed versus time-after-trip (array SPTBL).

Pump option 2 (IPMPTY = 2) is similar to option 1 except that the pump speed is calculated from Equation 9-9 after a trip has occurred rather than from an input table. The electric torque  $T_E$  is assumed to be zero. The relationships between the various pump input parameters as well as the algorithm for the pump speed calculation are shown in Table 9-2. The value entered for IPMPTR is the TRIP identification number for pump trip initiation and NPMPTX is the number of pairs of points in the pump speed table (SPTBL). If IPMPTR = 0, the pump will maintain a constant speed.

If the reverse speed option is specified ( $IRP = 1$ ), the pump can rotate in both the forward and reverse directions. If reverse speed is not allowed ( $IRP = 0$ ), the pump will rotate in the forward direction only. For this case, if a negative speed is calculated (after trip with option 2), the speed will be set to zero.

If the two-phase option is turned on ( $IPM = 1$ ), the degraded pump head and torque will be calculated from Equations 9-7 and 9-8. If the two-phase option is turned off ( $IPM = 0$ ), only the single-phase head and torque homologous curves will be used.

The user may either specify pump homologous curves in the input or use the built-in pump curves. The built-in pump curves are for the MOD-1 Semiscale system pump and are based on the data of Olson (1974a, b) and Loomis (1974). For other types of PWR pumps their corresponding homologous curves and multiplier values would be specified. Since these homologous curves are dimensionless, they can be used to describe a variety of pumps by specifying as input the rated values for density, head, torque, flow, and angular velocity.

There are several restrictions and limitations in the current version of the pump component. Since there is no pump motor torque-versus-speed model, the pump speed is assumed at the input value if the motor is energized. The pump momentum source must be located between cells 1 and 2 of the pump model. Finally, the head degradation multiplier  $M(\alpha)$  and the torque degradation multiplier  $N(\alpha)$  are assumed to apply to all operating states of the pump.

The PUMP module input consists of the same geometric and hydrodynamic data and initial conditions that are required for the PIPE module. In addition, information specific to the PUMP is required. The speed table (SPTBL) as well as the homologous pump curve arrays must be input.

**Model as Coded** For the new timestep, Equation 9-9 is evaluated explicitly:

$$\omega = \omega^n + \left( \frac{d\omega}{dt} \right)^n \Delta t \quad (9-11)$$

The momentum source for a pump cell is evaluated once each timestep, and the source is applied only during the explicit pass in subroutine DF1DI or subroutine DF1DS. The mixture velocity and mixture density from the donor component (i.e., conditions at the upstream boundary of the pump component) are used to establish the volumetric flowrate through the pump. Standard curve fitting techniques are then used to compute the pump head. The pump source evaluation is performed by subroutine PUMPSR.

**Scaling Considerations** During blowdown and reflood periods, reactor coolant pumps will be under two-phase flow conditions, and both the pump head and the pump torque will be degraded. Although the physical mechanisms responsible for the performance degradation in two-phase flows are not well understood, analysis of tests on pumps (Kamath and Swift, 1982) revealed that "scaling down the size of the pump while maintaining the same design specific speed produces very similar performance characteristics both in single and two-phase flows." The study also indicated that effects due to size and operating speed were not discernible within the range of test conditions and within experimental

uncertainties. The system pressure, however, appeared to affect the rate of degradation even for the same pump. Similar results were also observed in the scaled-pump experimental tests conducted by KWU (Kostner and Seeburger, 1983). These test results suggest that uncertainties due to scaling distortion from the pump are small compared to other contributors. The effect of scaling and other uncertainties is minimized in the WCOBRA/TRAC model by using data from a 1/3-scale model similar in design to the Westinghouse pump (Snyder and Grigsby, 1982).

**Conclusions** The pump model is constructed by combining the experimentally-established pump characteristic correlations and the WCOBRA/TRAC PIPE module based on a one-dimensional drift-flux formulation. The frictional torque correlation was also experimentally established. The pump model can handle all single- and two-phase operations (with or without phase separation) and provide accurate speed, flow, and head predictions during the transient (including coastdown). The options of the model provide the users with the flexibility to model a variety of system operating conditions. The WCOBRA/TRAC pump model has been assessed against LOFT L2-5 test data (Bayless et al., 1982) with satisfactory results. The model can be utilized to simulate any PWR pump for which the homologous characteristic curves have been adequately established.

## 9-5 STEAM GENERATOR COMPONENT (STGEN)

**Model Basis** In a PWR, the steam generators transfer energy from the primary coolant loop to the secondary coolant to produce steam. The STGEN module can model either "U-tube" or "once-through" steam generators; the basic operation is similar for both types. Primary coolant enters an inlet plenum, flows through a tube bank in which the primary coolant exchanges heat with a secondary coolant that flows over the exterior of the tube bank, and finally discharges into an outlet plenum. Figure 9-8 provides typical noding diagrams for U-tube and once-through steam generators. In both cases the tube bank is represented by a single effective tube that has heat transfer characteristics of the entire tube bank.

**Model as Coded** The number of fluid mesh cells is specified by NCELL1 on the primary side and by NCELL2 on the secondary side. There are some constraints imposed on the possible values for (NCELL1, NCELL2) combinations. For a once-through type, it is required that  $NCELL2 = NCELL1 - 2$ . For a U-tube type, it is assumed that there is a one-to-one correspondence between two active primary cells and one active secondary cell (Figure 9-8). Thus for the fluid cells on the secondary side to reach the U-tube bundle top, it is required that  $NCELL2 \geq (NCELL1 - 2)/2$ . The secondary-side cells that are greater than  $(NCELL1 - 2)/2$  are treated adiabatically and are used to model possible area changes and volumes above the tube bank. In Figure 9-8, these are cells 6 through 8 on the secondary side. There is an inlet plenum (cell 1) and outlet plenum (last cell) on the primary side; these two cells are assumed adiabatic.

The steam generator, primary-side, and secondary-side hydrodynamics are treated separately. Coupling between the two sides is achieved through wall heat transfer, which is modelled in a semi-implicit fashion. The calculational sequence for a steam generator is identical to that for a PIPE (component) except that it is performed twice, once for the primary side and once for the secondary side. It is possible

to connect the secondary-side junctions to any TRAC component, but the most common arrangement is to connect the inlet to a FILL, specifying the secondary-side fluid inlet conditions and flow rate, and to a BREAK at the discharge, specifying the steam-generator secondary discharge pressure.

The cylindrical heat conduction equation for a typical tube is solved as described in Section 7-7. There must be at least one wall temperature node, but three are suggested, placing one at each tube surface and one at the tube wall center. The tube material is selected from the material options given in Section 10-5. Wall friction correlations and additional frictional losses for the primary and secondary sides can be specified as described in Section 4-7. Either fully implicit or semi-implicit hydrodynamics may be selected for the steam generator component.

## 9-6 PRESSURIZER COMPONENT (PRIZER)

**Model Basis** The pressurizer in a PWR is used to control the primary coolant system operating pressure and accommodate any change in the coolant volume during normal operation. It consists of a pressure vessel connected to one of the hot legs by a surge line. Approximately half of the vessel is filled with water, which is pressurized by saturated steam above it. The pressure is maintained at the operating setpoint value by a system of heaters and sprays which regulate the energy input to the water.

**Model as Coded** The pressurizer is simulated by the PRIZER component. It can connect only to another one-dimensional component, and its nodes are numbered, 1 to NCELL, from the top (closed end) to the junction at the bottom as shown in Figure 9-9. The PRIZER component is treated in most respects as a PIPE; however, the drift velocities are not obtained from the slip routine, but are specified in subroutine PRIZR1, which imposes a sharp liquid/vapor interface during the pressurizer discharge. This is done by setting the relative velocity to a large value, [

$$]^{ac} \quad (9-12)^{(2)}$$

The negative sign is included to be consistent with the sign conventions used in the code.

The controlling action of the heater/spray can be simulated in the PRIZER component. The heater/spray model is available as an input option and is used as a system pressure controller. If this option is used, the setpoint pressure and the pressure deviation DPMAX at which the heaters deliver their maximum power QHEAT are input. The calculated heater power is directly proportional to the difference between PSET and P(1), the pressure in node 1.

$$Q_{pressurizer} = QHEAT(PSET - P(1))/DPMAX$$

This power ( $Q_{pressurizer}$ ) is limited to  $\pm QHEAT$  and is distributed to each node as a function of the node liquid fraction to total pressurizer liquid fraction. Power is not added if the collapsed liquid level

falls below the input height ZHTR. The collapsed liquid level within the PRIZER component is given by the following equation:

$$z = V_t/A \quad (9-13)$$

where

$$V_t = \sum_{i=1}^{NCELLS} (1 - \alpha_i) V_i \quad (9-14)$$

and  $V_i$  and  $V_t$  are the volume of the node  $i$  and the total volume of liquid in the pressurizer, respectively.  $A$  is the maximum flow area of nodes 1 and 2.

## 9-7 VALVE COMPONENT

**Model Basis** The VALVE component is used to simulate the controlling action of a valve fitting. It comprises at least two fluid nodes. The flow area and hydraulic diameter at a given node boundary are used as the controlling parameters to model the valve operation. In all other respects, the VALVE component is identical to the PIPE component.

**Model as Coded** The noding scheme is shown in Figure 9-10. Node IVPS defines the node boundary where the valve action is modelled. Five options are provided to describe the valve operation (Table 9-3). Options 1 through 4 open or close the valve with a trip. The action can be instantaneous or a function of time. Option 5 models a check valve with the open or closed condition determined by a pressure differential between the specified nodes (IVPS and IVPS-1) and a set point. For this option the valve opening and closing is damped to prevent pressure oscillations.

## 9-8 ACCUMULATOR COMPONENT (ACCUM)

An accumulator is a pressure vessel partially filled with water and pressurized with nitrogen gas. The accumulator is isolated from the primary coolant system (RCS) by a check valve. If reactor coolant pressure falls below accumulator pressure, the check valve opens and the accumulator water is forced into the RCS. This flow continues until the accumulator is empty, after which the nitrogen cover gas is discharged.

During a LOCA transient, the accumulators of a PWR will deliver ECC water to the cold legs. The accumulator injection period may be divided into two time intervals:

Phase A:  $t_{ACC} \leq t \leq t_o$

Phase B:  $t_o \leq t \leq t_c$

where  $t_{ACC}$  is the time when the accumulator starts to deliver ECC water (typically 10 seconds),  $t_o$  is the time when the accumulator is empty of water (typically 40 seconds),  $t_e$  is the time when the pressure in the accumulator is in equilibrium with that of the intact cold leg (ICL), and no more flow issues from the accumulator (typically 60 seconds).

During phase A, only water enters the ICL. The nitrogen in the accumulator continues to expand in volume as the pressure in the accumulator decreases. The nitrogen cools as it expands. During this phase, accumulator water begins to fill the reactor vessel downcomer, lower plenum, and core. Meanwhile, the reactor pressure falls to near the containment pressure. During phase B a water/nitrogen mixture, and finally only the-nitrogen gas, enters the ICL. Because of the width of the tank, the water-nitrogen interface is likely to be well-defined. Consequently, the time during which a water-nitrogen mixture flows from the tank is expected to be small. The nitrogen flow passes through the downcomer of the vessel and exhausts to the containment at the broken cold leg (BCL).

The expanding nitrogen from the accumulator will significantly increase the volumetric flow in the ICL, displacing the steam originally in the ICL. Because nitrogen is an inert gas, condensation is reduced.

As the nitrogen flows into the vessel and out the break, the ICL and the upper portion of the downcomer may be pressurized due to the presence of the nitrogen flow. This increase in pressure may affect the cooling flow entering or leaving the core. The way in which these phenomena are simulated in WCOBRA/TRAC is described below.

**Accumulator Model Basis (Phase A)** The accumulator component is simulated in the ACCUM module in WCOBRA/TRAC. This component can only be connected at one junction to other WCOBRA/TRAC components. This connection is the highest number cell, and it is assumed that cell 1 is closed, as shown in the typical noding diagram in Figure 9-11. It is also assumed that the accumulator is not connected to a nitrogen pressure source. Therefore, the nitrogen pressure results from the expansion of the initial gas volume.

The following additional assumptions are made for the ACCUM component during Phase A:

1. The vapor phase in the accumulator is an ideal gas with the properties of nitrogen.
2. The relative velocity between the vapor and liquid is set to a large value to create a sharp interface between the liquid and vapor. This assumption is made because the relatively large diameter of the tank leads to low fluid velocities and rapid phase separation.
3. The mixture properties at the last accumulator cell are controlled such that only pure liquid is discharged. This assumption is also a result of the expected sharp interface between liquid and vapor.

4. The wall friction factor for each accumulator tank cell is set to a constant value of 0.005. The accumulator is expected to represent a negligible portion of the overall resistance to flow.
5. The accumulator tank walls are assumed to be adiabatic. Heat transfer from the accumulator walls is not expected to be significant, due to the small surface area per unit volume.

**Nitrogen Discharge Model Basis (Phase B)** During the accumulator water injection period, a nitrogen gas field is assumed to exist in the accumulator, while steam is assumed everywhere else in WCOBRA/TRAC. While the nitrogen field can be extended (as an input option) to all other WCOBRA/TRAC components, a combined nitrogen-steam-water model is not available. To simulate the nitrogen discharge, the subcooled vapor model in WCOBRA/TRAC is used to provide similar pressure/flow characteristics to those obtained from a nitrogen model. In this model, the normal hydrodynamics package is used. However, the following additional assumptions are made:

1. Phase B is assumed to begin when the water level in the accumulator tank falls below [ ]<sup>ac</sup> (the basis for this value is described in Section 16-2-5 of WCAP-12945-P-A (Bajorek et al., 1998)). At this point, a mixture of water and nitrogen is assumed to flow out of the tank.
2. During Phase B, heat transfer between liquid and vapor is suppressed in regions of the RCS expected to contain significant amounts of nitrogen. This is assumed to occur as long as the accumulator pressure remains significantly above the RCS pressure (implying significant flow of nitrogen).

The region over which the condensation suppression is assumed to occur is shown in Figure 9-12 and consists of the accumulator and line, the intact cold leg, the upper downcomer region, and the broken cold leg on the vessel side. The nitrogen influence is assumed to be limited to this region as discussed below.

At the time nitrogen begins to inject, the lower plenum and downcomer are full of water, and the core has begun to reflood. Any steam generated in the core will flow up the core and out through the loops and upper head vent paths. In addition, the high downcomer water level provides a driving force for this flow. It is therefore unlikely that accumulator nitrogen flow will cause reverse flow in the loop or upper head. If it does, this flow would have to be sustained for a substantial period of time before the nitrogen will reach the upper plenum.

In the reactor vessel, the accumulator water isolates the nitrogen from the core. The region of influence is assumed to extend to a point in the downcomer level with the bottom of the core. If the downcomer is full above this level, no steam will be available for condensation and the condensation suppression will make no difference.



3. During Phase B, the behavior of the nitrogen can be simulated using the subcooled vapor models in the code.

This assumption was checked by comparing two simple models of the accumulator, one in which the entire process takes place with nitrogen, and one where the nitrogen model is replaced during Phase B with a model using the one-dimensional component subcooled vapor equations.<sup>(3)</sup> In the nitrogen model, the pressure/temperature/density relationships are for a perfect gas.

The simple models were used to predict pressure and flow, using a linear ramp for the pressure at the accumulator exit and representative accumulator dimensions.

**Accumulator and Nitrogen Model as Coded** The procedures for data input, initialization of arrays, advancement of time-dependent variables, and editing are similar to those given for a PIPE component. The hydrodynamics are treated using the one-dimensional, semi-implicit drift-flux routine DFIDS.

No metal heat transfer is permitted for the accumulator. In addition, the following special coding is employed for each of the phases. During Phase A:

1. Nitrogen properties are calculated in subroutine THERMO. The gas constant used is  $287.12 \text{ Pa m}^3/\text{kg } ^\circ\text{K}$  ( $53.4 \text{ ft lb}_f/\text{lb}_m ^\circ\text{R}$ ), which is consistent with standard values found in handbooks.
2. The liquid vapor interface is sharply defined by setting the relative velocity to a large value. This is set in ACCUM1 and is [

]<sup>a,c</sup> (9-15)

The negative sign is included to be consistent with the sign conventions used in the code.

3. The discharge at accumulator exit during Phase A is limited to liquid only by setting the component boundary array elements representing the void fraction to zero. This is done in subroutine ACCUMBD.
4. Accumulator wall friction is set to 0.005 in ACCUM1. User specified friction factors, input via the parameter FRIC, may be added to this value.

The end of Phase A is determined by the collapsed liquid level. The collapsed liquid level is calculated in subroutine ACCMIX by computing the total liquid volume in the accumulator tank and then determining the height of this volume at the bottom of the tank. This collapsed level is used to signal that the accumulator is nearly empty. The signal is set when the collapsed level falls below [        ]<sup>a,c</sup>. The time when this occurs is  $t_o$ , and the code moves to Phase B.

For Phase B (simulated nitrogen injection), additional special coding is required as described below.

1. In the accumulator, [ ] <sup>ac</sup> as  
described in Section 5-3.
2. The steam properties for [ ] <sup>ac</sup>.
3. Discharge from the accumulator becomes two-phase.

**Scaling Considerations** The model was tested in simulations of the accumulator in the LOFT test facility, and against data obtained from in-plant tests. A description of this test simulation as it applies to the accumulator model is given in Section 16-2 of WCAP-12945-P-A.

**Conclusions** The basic assumptions which are made in the application of this model to the PWR and which introduce uncertainty into the calculation are:

1. The condensation is assumed to be suppressed in the intact cold legs, upper downcomer, and broken nozzle until all nitrogen has been exhausted from the accumulator and swept from the systems.
2. The nitrogen vapor properties are approximated by subcooled vapor flow.

Conclusions regarding uncertainties due to noncondensable gases and accumulator nitrogen effects are summarized in Section 25-8 of WCAP-12945-P-A.

## 9-9 BREAK AND FILL COMPONENTS

These models differ from other components in that they do not model any system component per se, and no hydrodynamic or heat transfer calculations are performed for them. In all other respects, they are treated as any other component, with the same input, initialization, and identification procedures.

A BREAK component is used to impose a pressure boundary condition adjacent to the one-dimensional component with which it connects (Figure 9-13). The boundary conditions specified by the BREAK are pressure, mixture temperature and node void fraction, all of which may be time dependent. Care is required when setting the mixture temperature and void fraction values, as these are used to determine the properties of the fluid if the flow is calculated to be in the reverse direction, i.e., into the system from the BREAK. In the normal mode of operation, where the fluid flows out through the BREAK, the mixture temperature and void fraction do not affect the calculation.

The FILL component is used to impose a velocity boundary condition at the junction between the FILL and the adjoining one-dimensional component (Figure 9-14). The boundary velocity may be specified by one of the five different input options. The options define the velocity as a constant, or as a function of time or pressure, or as a constant until a trip signal is reached, then again as a function of time or pressure. The fluid properties within the FILL node are determined from the user input values of void fraction, mixture temperature, and pressure.

## 9-10 REFERENCES

- Bajorek, S. M., et al., 1998, "Code Qualification Document for Best Estimate LOCA Analysis," WCAP-12945-P-A, Volume 1, Revision 2, and Volumes 2 through 5, Revision 1, and WCAP-14747 (Non-Proprietary).
- Bayless, P. D., et al., 1982, "Experimental Data Report for LOFT Large-Break Loss-of-Coolant Experiment L2-5," NUREG/CR-2826, EGG-2210.
- Biasi, L., et al., 1967, "Studies on Burnout, Part 3: A New Correlation for Round Ducts and Uniform Heating and Its Comparison with World Data," Energia Nucleare, Vol. 14, pp. 530-536.
- Bordelon, F. M., et al., 1974, "SATAN VI Program: Comprehensive Space-Time Dependent Analysis of Loss-of-Coolant," WCAP-8302.
- Kamath, P. S. and Swift, W. J., 1982, "Two-Phase Performance of Scale Models of a Primary Coolant Pump," EPRI NP-2578, Final Report.
- Kostner, W. and Seeburger, G. J., 1983, "Pump Behaviour and Its Impact on a Loss of Coolant Accident in a Pressurized Water Reactor," Nuclear Technology, Vol. 60.
- Liles, D. R., et al., 1981, "TRAC-PD2, An Advanced Best Estimate Computer Program for Pressurized Water Reactor Loss-of-Coolant Accident Analysis," NUREG/CR-2054.
- Loomis, G. G., 1974, "Intact Loop Pump Performance During the Semiscale MOD-1 Isothermal Test Series," Aerojet Nuclear Company, Report-1240.
- Olson, D. J., 1974a, "Single- and Two-Phase Performance Characteristics of the MOD-1 Semiscale Pump Under Steady-State and Transient Fluid Conditions," Aerojet Nuclear Company, Report ANCR-1165.
- Olson, D. J., 1974b, "Experimental Data Report for Single- and Two-phase Steady-State Test of the 1 Loop MOD-1 Semiscale System Pump," Aerojet Nuclear Company, Report ANCR-1150.
- Snyder, P. H., and Grigsby, J. M., 1982, "EVA Project on Two-Phase Reactor Coolant Pump Performance - Data Analysis and Model," Vol. 1-3, WCAP-10109.

**9-11 RAI LISTING**

1. RAI1-233
2. RAI1-234
3. RAIS-21

Table 9-1 The Four Segments of Pump Homologous Curves				
Curve Segment	Homologous Head	Homologous Torque	Variable Range	Operating Condition
1	$h/\alpha_N^2$	$\beta/\alpha_N^2$	$ v/\alpha_N  \leq 1$	$\omega > 0$
2	$h/v^2$	$\beta/v^2$	$ v/\alpha_N  > 1$	$Q > 0$
3	$h/v^2$	$\beta/v^2$	$ v/\alpha_N  > 1$	$Q < 0$

Note: A fourth segment may also be input for negative pump rotation ( $\omega < 0$ ). This condition will not occur in Westinghouse PWR's due to locking devices on the pumps.

<b>Table 9-2 Pump Control Input Parameter</b>				
<b>IPMPTY Pump Option</b>	<b>IMPPTR Pump Trip I.D.</b>	<b>NPMPTX (SPTBL) Pair of Points</b>	<b>Pump Speed Speed Table</b>	<b>Algorithm</b>
1	x = pump trip desired	x	x	OMEGA before trip
	0 = no pump trip	0		SPTBL after trip
2	x = pump trip desired	x		OMEGA before trip
	0 = no pump trip	0		Code calculated after trip

**Table 9-3 Valve Control Options**

1. Valve is normally open and is closed instantly on a trip signal.

Controlling logic is as follows:

Before trip,

$$A_{(valve)} = AVLVE$$

$$D_{h(valve)} = HVLVE$$

After trip,

$$A_{(valve)} = 0.0$$

$$VM = 1.E-10$$

$$VR = 0.0$$

where,

AVLVE equals completely open valve area

HVLVE equals completely open valve hydraulic diameter

VM equals mixture velocity of phases

VR equals relative velocity of phases

2. Valve is normally closed and is opened instantly on a trip signal.

Controlling logic is as follows:

Before trip,

$$A_{(valve)} = 0.0$$

$$VM = 1.E-10$$

$$VR = 0.0$$

After trip,

$$A_{(valve)} = AVLVE$$

$$D_{h(valve)} = HVLVE$$

3. Valve is normally open and is closed on a trip signal according to a time-dependent valve table.

Controlling logic is as follows:

Before trip,

$$A_{(valve)} = AVLVE$$

$$D_{h(valve)} = HVLVE$$

After trip,

$$A_{(valve)} = AVLVE * SCALE$$

$$D_{h(valve)} = HVLVE * SCALE$$

where SCALE equals the linear interpolated multiplier from the user input forcing factor versus time table. If SCALE equals 0.0,

$$VM = 1.E-10$$

$$VR = 0.0$$

**Table 9-3      Valve Control Options**  
(cont)

4. Valve is normally closed and is opened on a trip signal according to a time-dependent valve table. Controlling logic is as follows:

Before trip,

$$\begin{aligned} A_{(valve)} &= 0.0 \\ VM &= 1.E-10 \\ VR &= 0.0 \end{aligned}$$

After trip,

$$\begin{aligned} A_{(valve)} &= AVLVE * SCALE \\ D_{h(valve)} &= HVLVE * SCALE \end{aligned}$$

where,

SCALE has the same definition as given above.

5. Check valve is controlled by a static pressure gradient. If IVPG = 1, then  $DP = P(IVPS - 1) - P(IVPS)$ ; if IVPG = 2 then  $DP = P(IVPS) - P(IVPS-1)$

If  $DP + PVS \geq 0$ , the valve opens.

If  $DP + PVS < 0$ , the valve closes.

For this option the valve opening and closing action is damped according to the following equations.

Opening,

$$\begin{aligned} A_{(valve)} &= A_{(valve)} * 0.99 + 0.01 * AVLVE \\ D_{h(valve)} &= D_{h(valve)} * 0.99 + 1.0E-5 \end{aligned}$$

The above equations are applied at each timestep until the opening or closing action has been completed.



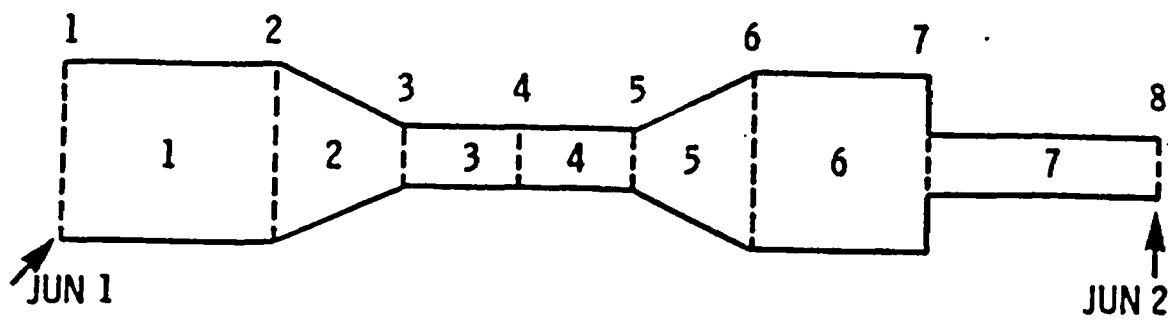


Figure 9-1. PIPE Component Noding

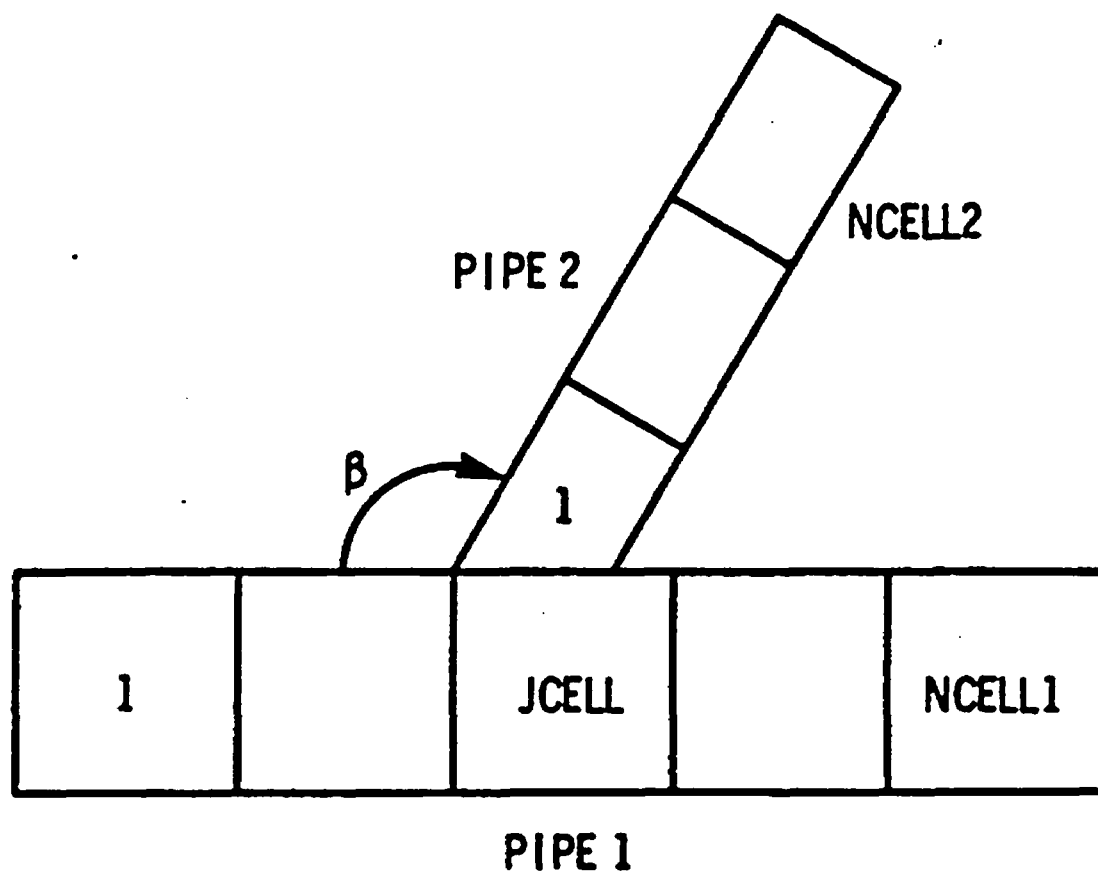


Figure 9-2. TEE Component Noding

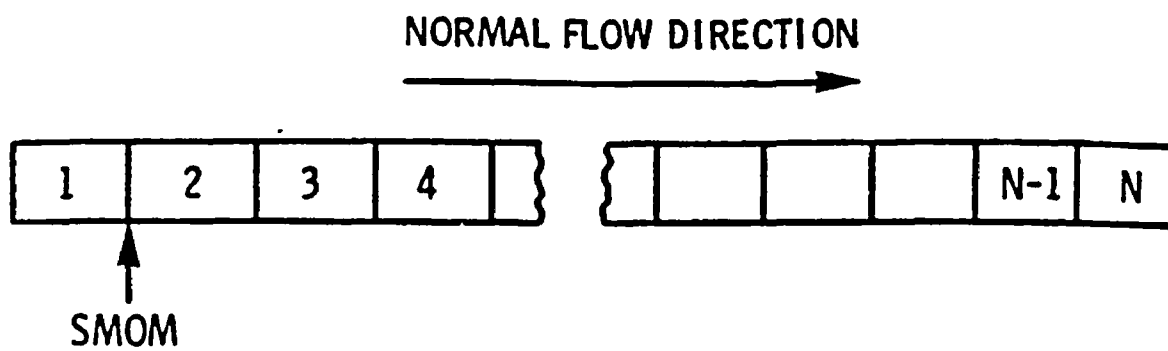


Figure 9-3. PUMP Noding Diagram

a,c

**Figure 9-4. 93A Pump Single-Phase Homologous Head Curves**

a,c

**Figure 9-5. 93A Pump Two-Phase Homologous Head Curves**

**Figure 9-6. 93A Pump Single-Phase Homologous Torque Curves**

a,c

**Figure 9-7. 93A Pump Two-Phase Homologous Torque Curves**

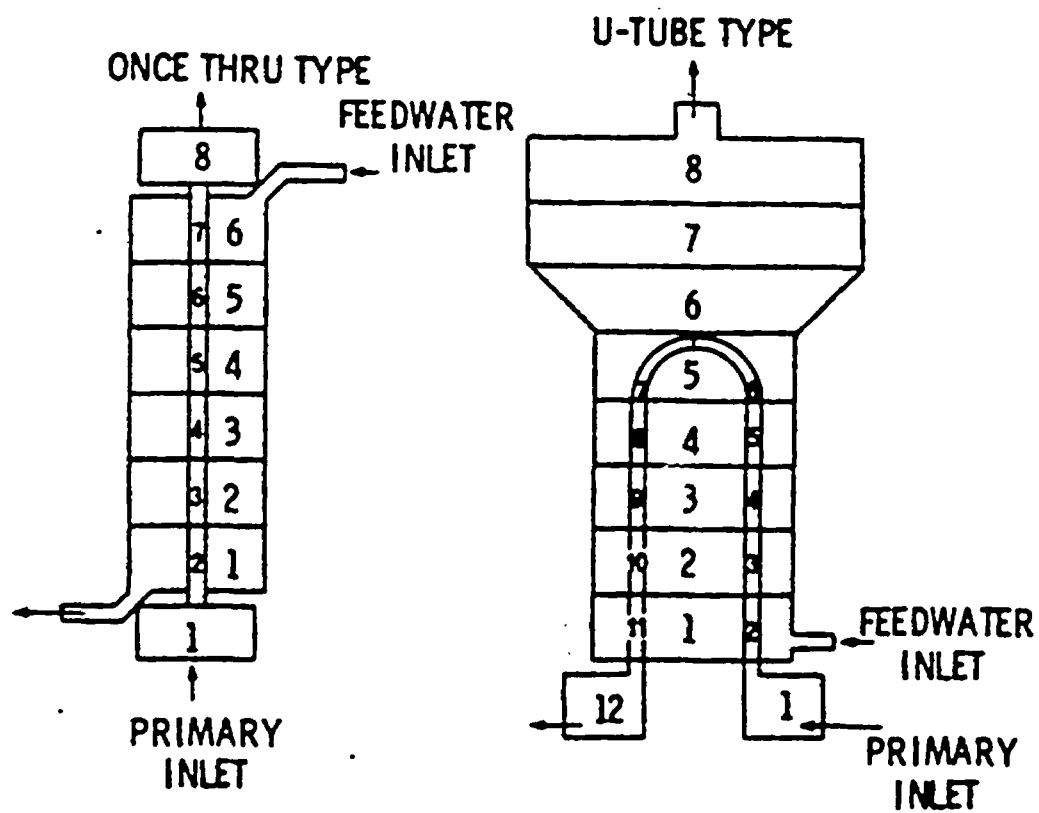


Figure 9-8. Steam Generator Noding Diagram



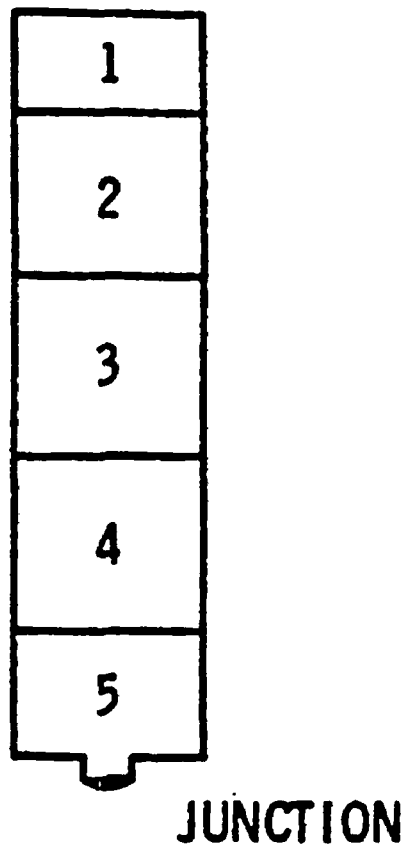


Figure 9-9. Pressurizer (PRIZER) Component Noding

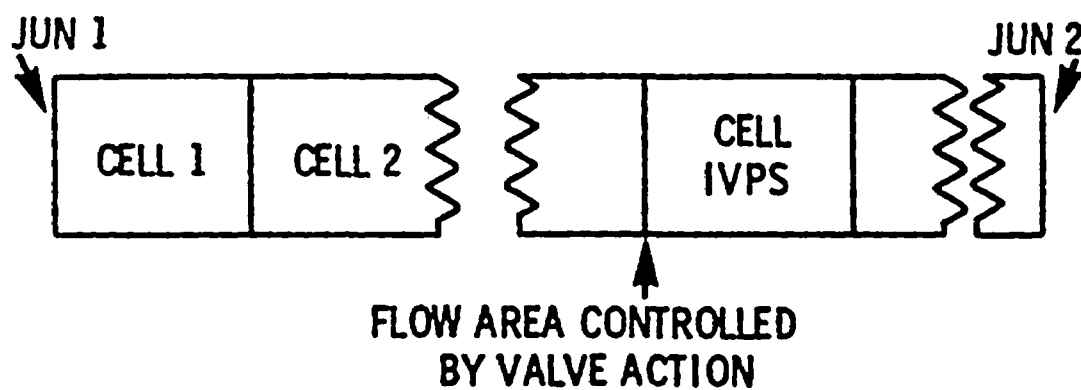


Figure 9-10. VALVE Component Noding

a,c

**Figure 9-11. Accumulator Noding Diagram**

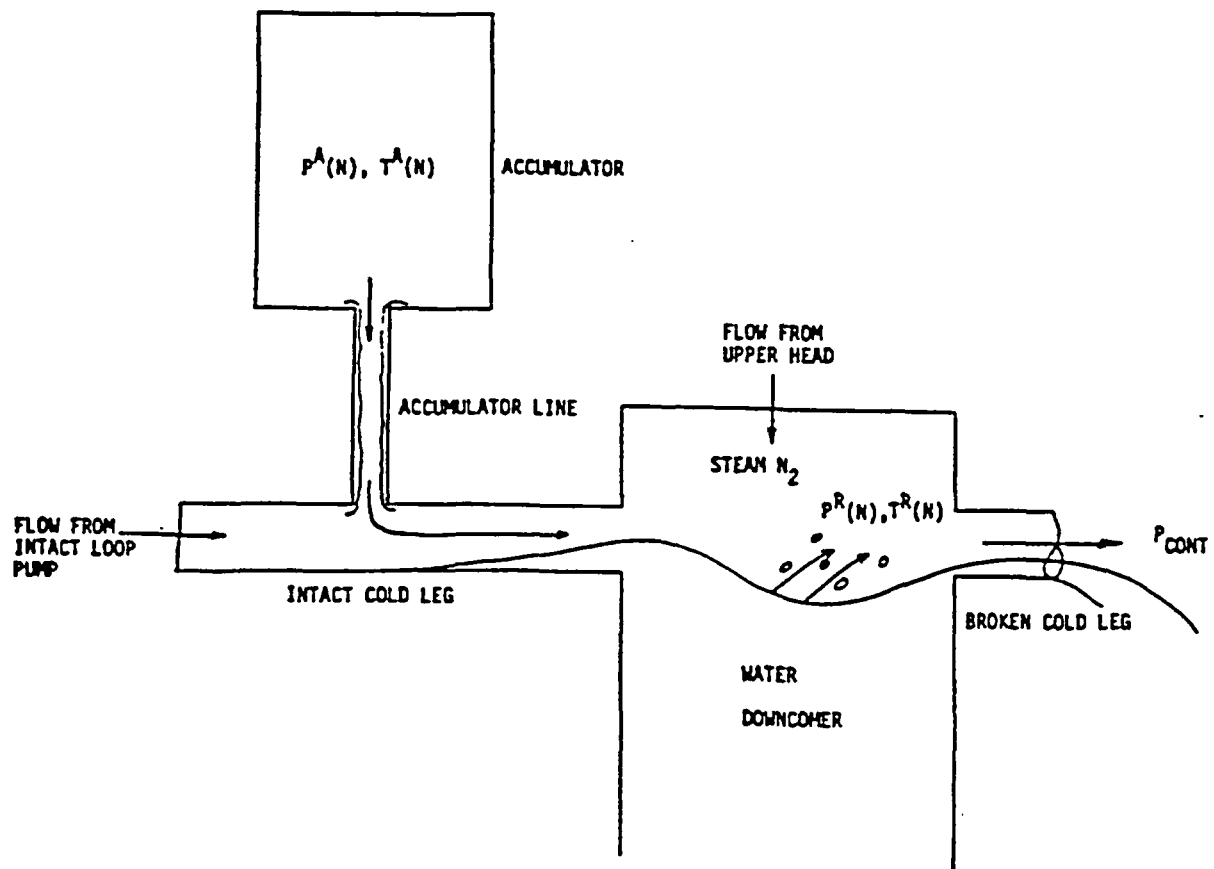


Figure 9-12. Condensation Suppression Region for Accumulator/Nitrogen Model

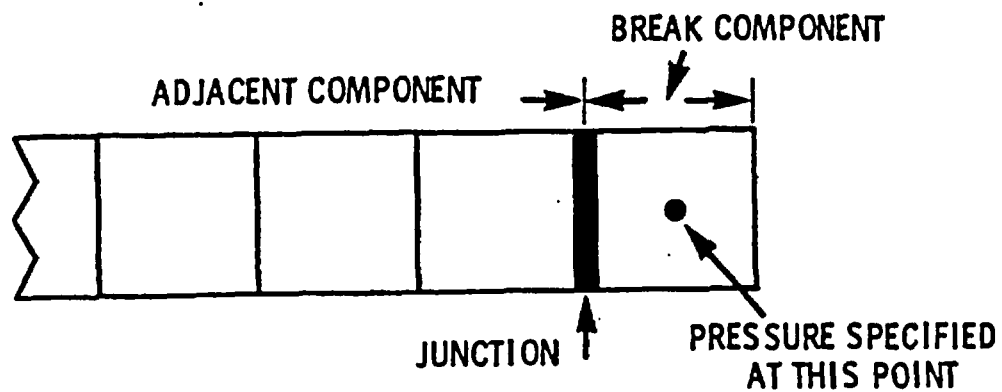


Figure 9-13. Pressure Boundary Condition Using BREAK Component

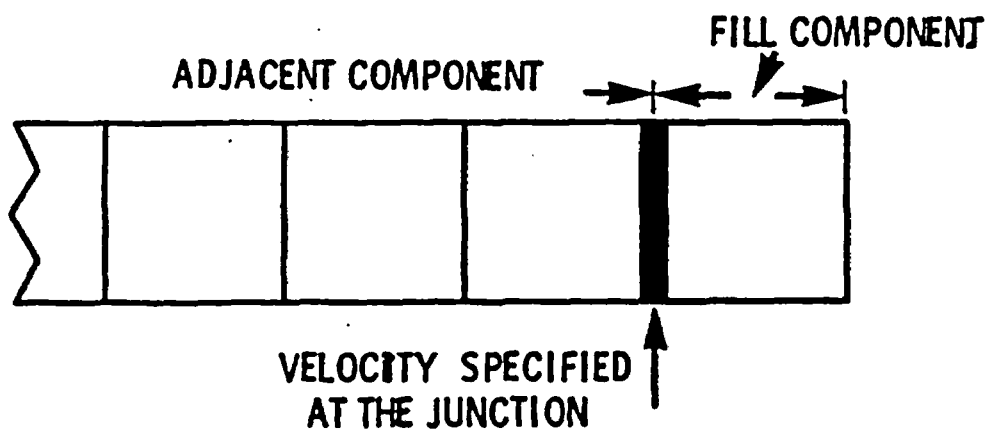


Figure 9-14. Velocity Boundary Condition Using FILL Component

## 10 THERMOPHYSICAL PROPERTIES

### 10-1 INTRODUCTION

WCOBRA/TRAC includes a set of functional routines and individual correlations to calculate the thermal properties of water, air, nuclear rods and several common structural materials. This section describes the manner in which the thermal properties are calculated for the vessel and one-dimensional components. Section 10-2 describes calculation of the thermodynamic properties of water. Section 10-3 describes the WCOBRA/TRAC calculation of air thermal properties. Section 10-4 describes the thermal properties of materials used in nuclear fuel rods including mixed oxide fuel, clad materials, and fuel rod gap gases. WCOBRA/TRAC can also calculate the thermal properties of several common PWR structural materials such as stainless steel. These calculations are described in Section 10-5.

### 10-2 THERMOPHYSICAL PROPERTIES OF WATER

#### 10-2-1 Vessel Component Water Properties

The thermal-hydraulic calculations performed by the WCOBRA/TRAC vessel component frequently require the thermal conductivity, specific heat, viscosity, Prandtl number, and surface tension for water as functions of the fluid pressure and specific enthalpy. This section describes the thermodynamic property calculations performed by WCOBRA/TRAC for saturated, superheated, and subcooled fluid conditions.

##### 10-2-1-1 Saturated Fluid Properties

**Model Basis** The saturated liquid and saturated vapor enthalpies are calculated as functions of the pressure. Values for the saturation temperature, densities of saturated liquid and vapor, thermal conductivities and viscosities of saturated liquid and vapor, saturated liquid specific heat, and the surface tension are interpolated from tables indexed by saturated liquid enthalpy. The saturated liquid and saturated vapor specific enthalpies are determined from polynomial representations of the saturation curve. This representation provides close agreement with ASME Steam Tables (1968) and the NBS/NRC Steam Tables (Haar, Gallagher, and Kell, 1984). The tables of values at saturation for the other properties (conductivities, viscosities, etc.) are also in close agreement with the standard tables.

The saturation enthalpies are calculated in Btu/lbm as functions of pressure based on expressions developed for EPRI (McFadden et al., 1980).

The polynomial expansions for saturated liquid enthalpy are

$$H_f(P) = \sum_{n=1}^9 A_n [\ln(P)]^{n-1} \quad (10-1)$$

if  $P < 2529.9$  psia and

$$H_f(P) = \sum_{n=1}^9 A_n [(3208.2 - P)^{0.41}]^{n-1} \quad (10-2)$$

for  $2529.9 \leq P < 3208.0$  psia.

The constants  $A_n$  for Equations 10-1 and 10-2 are shown in Table 10-1.

The saturated vapor enthalpy is calculated using

$$H_g(P) = \sum_{n=1}^5 B_n [\ln(P)]^{n-1} + \sum_{n=6}^8 B_n [\ln(P)]^{n+3} \quad (10-3)$$

if  $0.1 \leq P < 1467.6$  psia, by

$$H_g(P) = \sum_{n=1}^9 B_n [\ln(P)]^{n-1} \quad (10-4)$$

if  $1467.6 \leq P < 2586.0$  psia and by

$$H_g(P) = \sum_{n=1}^9 B_n [(3208.2 - P)^{0.41}]^{n-1} \quad (10-5)$$

if  $2586.0 \leq P < 3208.0$  psia.

The constants  $B_n$  for Equations 10-3 through 10-5 are listed in Table 10-2.

These expressions are compared to values from the ASME Steam Tables (1968, 1983) in Figures 10-1 and 10-2.

Table 10-3 lists values of the saturation temperature, density, viscosity, thermal conductivity, specific heat, and surface tension that are used to represent the saturation curve for those properties. The saturation curves defined by these tables are compared to values from the standard tables in Figures 10-3 through 10-11.

**Model as Coded** For a known pressure  $P$  the saturated liquid enthalpy is calculated using either Equation 10-1 or 10-2 in subroutine SAT. From that calculated value of saturated liquid enthalpy, the other properties are determined in subroutine PROP by linearly interpolating between the 90 values listed in Table 10-3.

**Scale Considerations** Calculation of saturated water thermophysical properties is not dependent on scale.

**Conclusions** The WCOBRA/TRAC vessel component calculates saturated liquid and saturated vapor enthalpies as functions of pressure using polynomial representations, and then uses the saturated liquid enthalpy to determine the other thermal properties by linear interpolation. All of the saturated properties agree very closely with values found in the standardized Steam Tables.

## 10-2-1-2 Properties of Superheated Vapor

### Model Basis

**Vapor Enthalpy** The enthalpy of superheated vapor as a function of pressure and temperature is calculated by the expression developed by Keenan and Keys (1936):

$$H_v = 0.43 \left[ 0.10129 \left( F_0 P + \frac{F_1}{2} P^2 + \frac{F_3}{4} P^4 + \frac{F_{12}}{13} P^{13} \right) + F^1 \right] \quad (10-6)$$

where,  $F_0$ ,  $F_1$ ,  $F_3$ , and  $F_{12}$  are defined by

$$F_k = \frac{\partial}{\partial \tau} (B_k \tau), \quad k = 0, 1, 3, 12 \quad (10-7)$$

The coefficients  $B_k$  are defined as:

$$\tau = 1/T \quad (10-8)$$

$$B_0 = 1.89 - 2641.62 \tau \cdot 10^{80870\tau^2} \quad (10-9)$$

$$B_1 = B_0^2 (82.546 \tau^2 - 1.6246(10)^5 \tau^3) \quad (10-10)$$

$$B_3 = B_0^4 (0.21828 \tau^3 - 1.2697(10)^5 \tau^5) \quad (10-11)$$

$$B_{12} = -B_0^{13} (3.635(10)^{-4} \tau^{12} - 6.768(10)^{64} \tau^{36}) \quad (10-12)$$



and  $F^1$  is given by

$$F^1 = 2502.36 + \int_{273.16}^T (1.472 + 0.00075566T + \frac{47.8365}{T})dT \quad (10-13)$$

In Equations 10-6 through 10-13,  $T$  is in °K,  $P$  is in atmospheres, and  $H_v$  is in J/g.

**Vapor Temperature** Values for superheated vapor temperature as a function of pressure and enthalpy are calculated using an iterative method described by McClintock and Silvestri (1936). Estimates for  $T$  and  $C_p$  are computed from the expressions

$$T = A_1 + A_2H_v + A_3H_v^2 + A_4H_v^3 + A_5P + A_6P^2 + A_7P^3 + P(A_8H_v + A_9H_v^2 + A_{10}H_v^3) \quad (10-14)$$

$$1/C_p = B_1 + B_2H + B_3H^2 + B_4H^3 + B_5\ln P + B_6(\ln P)^2 + B_7(\ln P)^3 + (\ln P)(B_8H + B_9H^2 + B_{10}H^3) \quad (10-15)$$

where  $T$  is in °F,  $P$  is in psia,  $H_v$  is in Btu/lbm, and  $C_p$  is in Btu/lbm-°F. The constants  $A_n$  and  $B_n$  depend on the range of pressure and enthalpy as shown in Table 10-4.

The estimated temperature is then used to approximate the enthalpy as

$$H_v^1(P, T) = f(P, T) \quad (10-16)$$

where the function  $f(P, T)$  is described by Equations 10-6 through 10-13. A temperature correction is calculated as

$$\Delta T = \frac{1}{C_p} (H_v - H_v^1) \quad (10-17)$$

and a new estimated temperature is defined as

$$T^1 = T + \Delta T \quad (10-18)$$

A new enthalpy is calculated and the iteration is continued until

$$|\Delta T| < 1.0^\circ F$$

$$\text{or } |H_v - H_v^1| < 0.5 \text{ Btu/lbm}$$

**Vapor Density** The vapor specific volume is calculated as a function of pressure and enthalpy using equations from Keenan and Keys (1936):

$$v_v = \frac{1}{P_v} = E_1 + E_2 P + \frac{E_3}{P} + E_4 H_v + E_5 P H_v + E_6 \frac{H_v}{P} \quad (10-19)$$

where  $P$  is in psia,  $H_v$  is in Btu/lbm, and  $v$  is in ft<sup>3</sup>/lbm. The constants for these equations are

$$E_1 = -0.81735849\text{E-}03$$

$$E_2 = 0.12378514\text{E-}04$$

$$E_3 = -0.10339904\text{E+}04$$

$$E_4 = -0.62941689\text{E-}05$$

$$E_5 = -0.872921608\text{E-}08$$

$$E_6 = 0.12460225\text{E+}01$$

**Vapor Thermal Conductivity** The thermal conductivity for superheated vapor is calculated as a function of temperature and density using equations given in the ASME Steam Tables (1968). The expression for thermal conductivity is:

$$k_v = k_1 + (103.51 + 0.4198 T - 2.771(10)^{-5} T^2) \rho_v + 2.1482(10)^{14} \frac{\rho_v^2}{T^{4.2}} \quad (10-20)$$

where:

$$k_1 = 17.6 + 5.87(10)^{-2} T + 1.04(10)^{-4} T^2 - 4.51(10)^{-8} T^3 \quad (10-21)$$

In Equations 10-20 and 10-21,  $T$  is in °C,  $\rho_v$  is in g/cm<sup>3</sup>, and  $k_v$  is in mW/m-°K.

**Vapor Viscosity** The viscosity for superheated vapor is calculated as a function of temperature and density using equations given in the ASME Steam Tables (1968).

The viscosity is given by

$$\mu_v = \begin{cases} \mu_1 - \rho(1858 - 5.9T), & \text{if } T < 340^\circ\text{C} \\ \mu_1 + 353\rho + 676.5\rho^2 + 102.1\rho^3, & \text{if } T > 365^\circ\text{C} \end{cases} \quad (10-22)$$

$$\mu_1 = 0.407T + 80.4 \quad (10-23)$$

For values of  $T$  between  $340^\circ\text{C}$  and  $365^\circ\text{C}$  the viscosity is interpolated between the values given by the two expressions in Equation 10-22. In Equations 10-22 and 10-23 temperature is in  $^\circ\text{C}$ , density is in  $\text{g}/\text{cm}^3$ , and viscosity is in micropoise.

Values of superheated vapor enthalpy, temperature, density, thermal conductivity, and viscosity defined by the foregoing expressions are compared with the ASME tables (1968, 1983) and the National Bureau of Standards/National Research Council tables (Haar, Gallagher, and Kell, 1984) in Figures 10-12 through 10-16.

**Model as Coded** The properties for superheated vapor represented by Equations 10-6 through 10-23 are coded as described above without modification in subroutines HGAS, TGAS, VOLVAP, and TRANSP. Properties are not calculated if  $P < 0.1$  psia or if  $P > 3208.0$  psia, in which cases an error message is printed and execution is terminated.

In the calculation of vapor temperature as a function of pressure and enthalpy, Equations 10-14 through 10-18 describe an iterative method. A maximum of 10 iterations are permitted.

**Scaling Considerations** The equations and methods used to calculate the properties for superheated vapor are independent of scale.

## Conclusions

The WCOBRA/TRAC vessel component calculates superheated vapor enthalpy as a function of temperature and pressure, density as a function of pressure and enthalpy, and thermal conductivity as a function of temperature and density, using generalized polynomials. Temperature as a function of pressure and enthalpy is found iteratively using the enthalpy function. All of these properties agree closely with values found in standard steam tables.

### 10-2-1-3 Subcooled Liquid Properties

**Model Basis** Subcooled liquid specific volume is calculated using the equation

$$v_t = \exp \left[ \sum_{i=1}^5 \left( \sum_{j=1}^3 C_{cxij} P^{j-1} \right) H_t^{i-1} \right] \quad (10-24)$$

where  $H_l$  is in Btu/lbm,  $P$  is in psia, and the values of the coefficients  $C_{cxij}$  are given in Table 10-5.

The liquid temperature at enthalpy ( $H_l$ ) is assumed to be equal to the saturation temperature at  $H_l$ . The properties  $C_p$ ,  $k$ , and  $\mu$  for subcooled liquid at temperature  $T$  are assumed to be equal to the saturated liquid properties at  $T$ . These properties are only weakly dependent on pressure in the low to moderate pressure range.

The liquid Prandtl number is calculated as

$$Pr_l = \frac{\mu_f C_{pf}}{k_f} \quad (10-25)$$

**Model as Coded** The equation for subcooled liquid specific volume is programmed as shown in subroutine VOLLIQ. Other subcooled liquid properties are determined by linear interpolation of the saturation properties listed in Table 10-3. The liquid enthalpy is used as the index to determine the appropriate location in the table in which to perform the interpolation.

**Scaling Considerations** The method in which subcooled liquid properties are determined is scale independent.

**Conclusions** Subcooled liquid properties are estimated to be equal to the properties of saturated liquid corresponding to the liquid temperature. Since these properties are only weakly dependent on pressure, only a negligible error is introduced into the calculation.

## 10-2-2 One-Dimensional Component Water Properties

The thermodynamic and transport properties used in the WCOBRA/TRAC one-dimensional (1D) components are based on polynomial fits to steam table data for water, and on ideal gas behavior for air. The fits for transport properties were obtained from Coffman and Lynn (1966).

### 10-2-2-1 Saturated Fluid Properties

#### Model Basis

**Saturation Temperature and Pressure** Saturation temperature as a function of pressure, and saturation pressure as a function of temperature, are calculated using expressions recommended by Rivard and Torrey (1975). These are

$$P_{sat} = 10^5 \left( \frac{T_{sat} - 255.2}{117.8} \right)^{\frac{1}{0.223}} \quad (10-26)$$

and

$$T_{sat} = 117.8(10^{-5}P_{sat})^{0.223} + 255.2 \quad (10-27)$$

The derivative of saturation temperature with respect to pressure is given by

$$\frac{dT_{sat}}{dP_{sat}} = \frac{0.223(T_{sat} - 255.2)}{P_{sat}} \quad (10-28)$$

**Saturated Vapor Internal Energy and Enthalpy** Two main pressure regions are used in the calculation of water vapor internal energy and enthalpy. The low pressure range is  $P < 2.0 \times 10^6$  Pa and the high pressure range is  $2.0 \times 10^6 \text{ Pa} \leq P$ , where  $P$  is the pressure and  $T_{sat}$  is its corresponding saturation temperature.

**Low Pressure Region:** The internal energy of saturated vapor and its derivative with respect to pressure are

$$e_g = AVE(1) + BVE(1)T_1 \quad (10-29)$$

$$\frac{de_g}{dP} = -BVE(1) T_1^2 \quad (10-30)$$

where:

$$T_1 = 1/(P + 3.403E5) \quad (10-31)$$

**High Pressure Region:**

$$e_g = AVE(2) + BVE(2) P + CVE(2) P^2 \quad (10-32)$$

$$\frac{de_g}{dP} = BVE(2) + 2 CVE(2) P \quad (10-33)$$

The values of the constants  $AVE(i)$ ,  $BVE(i)$ , and  $CVE(i)$  are listed in Table 10-6.

All pressures: The ratio of specific heats, saturated vapor enthalpy, and derivatives with respect to pressure are calculated from:

$$\gamma_g = AVG(i) + BVG(i) P + CVG(i) P^2 \quad (10-34)$$

$$\frac{d\gamma_g}{dP} = BVG(i) + 2 CVG(i) P \quad (10-35)$$

$$H_g = \gamma_g e_g \quad (10-36)$$

$$\frac{dH_g}{dP} = \gamma_g \frac{de_g}{dP} \quad (10-37)$$

The values of the constants  $AVG(i)$ ,  $BVG(i)$ , and  $CVG(i)$  are listed in Table 10-7.

**Saturated Liquid Internal Energy and Enthalpy** A series of polynomials in  $T_{sat}$  is used to calculate the internal energy of saturated liquid and its derivative with respect to saturation temperature. These are given by:

$$e_f = ALE(i) + BLE(i) T_{sat} + CLE(i) T_{sat}^2 + DLE(i) T_{sat}^3 + ELE(i) T_{sat}^4 \quad (10-38)$$

and

$$\frac{de_f}{dT_{sat}} = BLE(i) + 2 CLE(i) T_{sat} + 3 DLE(i) T_{sat}^2 + 4 ELE(i) T_{sat}^3 \quad (10-39)$$

where:

$$\begin{aligned} i = 1 & \text{ for } T_{sat} < 548.15 \text{ K,} \\ i = 2 & \text{ for } 548.15 \leq T_{sat} < 611.15 \text{ K,} \\ i = 3 & \text{ for } 611.15 \leq T_{sat} \end{aligned}$$

Table 10-8 lists the constants  $ALE(i)$ ,  $BLE(i)$ ,  $CLE(i)$ ,  $DLE(i)$ , and  $ELE(i)$  for the given temperature ranges.

Saturated liquid enthalpy is calculated using the definition

$$H_f = e_f + \frac{P}{\rho_f} \quad (10-40)$$

and its derivative by

$$\frac{dH_f}{dP} = \frac{de_f}{dT_{sat}} \frac{dT_{sat}}{dP} + \frac{1}{\rho_f} - \frac{P}{\rho_f^2} \left[ \left( \frac{\partial \rho_f}{\partial P} \right)_{T_{sat}} + \left( \frac{\partial \rho_f}{\partial T_{sat}} \right)_P \frac{dT_{sat}}{dP} \right] \quad (10-41)$$

where  $e_f$  and its derivative are evaluated as shown earlier, and where  $\rho_f = \rho_f(P, T_{sat})$  and its derivatives are evaluated using the equations in Section 10-2-2-4 with  $T_t$  equal to  $T_{sat}$ .

**Saturated Vapor Specific Heat Capacity** The heat capacity of saturated steam at constant pressure is also calculated using a polynomial representation in  $T_{sat}$ . The saturated vapor specific heat and its derivative are given by

$$C_{pg} = ACP \Theta_r^{-2} + BCP \Theta_r^{-1} + CCP + DCP \Theta_r + ECP \Theta_r^2 \quad (10-42)$$

$$\frac{dC_{pg}}{dP} = \left[ 2ACP \Theta_r^{-3} + BCP \Theta_r^{-2} - DCP - 2ECP \Theta_r \right] T_{cr} \frac{dT_{sat}}{dP} \quad (10-43)$$

where:

$$\Theta_r = 1 - T_{sat} / T_{crit}$$

$$T_{crit} = 647.3 \text{ K}$$

and

$$ACP = 8.349824$$

$$BCP = 349.519444$$

$$CCP = 2996.018036$$

$$DCP = -8448.077393$$

$$ECP = 9700.016602$$

**Model as Coded** Subroutine THERMO supplies thermodynamic properties for WCOBRA/TRAC one-dimensional components. The input variables are the pressure and the liquid- and vapor-phase

temperatures. The output variables include the saturation temperature, saturated liquid, and saturated vapor enthalpies corresponding to the pressure, and their derivatives with respect to pressure. These variables also include the internal energies and densities of the liquid and vapor phases, and their partial derivatives with respect to pressure (at constant temperature) and with respect to temperature (at constant pressure).

THERMO supplies thermodynamic properties valid for temperatures and pressures within the following ranges:

$$280 \text{ K} \leq T_f \leq 697 \text{ K}$$

and

$$1000 \text{ Pa} \leq P \leq 19.0 \times 10^6 \text{ Pa}.$$

If THERMO is provided with a temperature outside this range, the calculation stops. Given a pressure outside this range, it adjusts the data to the corresponding limit and issues a warning message.

Subroutine RHOLIQ calculates liquid densities and density derivatives used in THERMO.

Saturation pressure, and phasic densities and enthalpies as calculated are compared with NBS/NRC tables (Haar, Gallagher, and Kell, 1984) in Figures 10-17 through 10-21.

**Scaling Considerations** Not applicable.

**Conclusions** The saturation conditions for the WCOBRA/TRAC one-dimensional components are calculated using polynomial expressions that provide a close approximation to the Steam Table values. The error introduced by the WCOBRA/TRAC routines is small and is not considered a major contributor to the overall code calculational uncertainty.

#### 10-2-2-2 Properties of Superheated Vapor

**Model Basis** Specific Heat at Constant Pressure The constant pressure specific heat of steam at temperature  $T_v$  is approximated as

$$C_{pv} = \left( \frac{\partial h_v}{\partial T_v} \right)_P = \frac{C_{pv,ideal}}{2} \left[ 1 + \frac{T_v}{(T_v^2 - \beta)^{1/2}} \right], \quad (10-44)$$



where:

$$\beta = T_{sat}^2 \left[ 1 - \frac{1}{\left( \frac{2 C_{pg}}{C_{pv, ideal}} - 1 \right)^2} \right] \quad (10-45)$$

The term  $C_{pg}$  is calculated as defined in Equation 10-42 and  $C_{pv, ideal}$  is defined by ideal gas behavior, such that

$$C_{pv, ideal} = \frac{R_v \gamma_{ideal}}{\gamma_{ideal} - 1} \quad (10-46)$$

where  $R_v$  is the gas constant for steam (461.7 J/kg-K) and  $\gamma_{ideal} = 1.3$  is the ratio of ideal specific heats for steam.

**Internal Energy** The internal energy is obtained by integrating the expression for  $C_{pv}$  along a line of constant pressure  $P$ . Integrating Equation 10-44 gives

$$h_v = h_g + \frac{C_{pv, ideal}}{2} \left[ (T_v - T_{sat}) + (T_v^2 - \beta)^{1/2} - \frac{T_{sat}}{\left( \frac{2 C_{pg}}{C_{pv, ideal}} - 1 \right)} \right] \quad (10-47)$$

The internal energy of vapor is therefore

$$e_v = e_g + \frac{C_{pv, ideal}}{2} \left[ (T_v - T_{sat}) + (T_v^2 - \beta)^{1/2} - \frac{T_{sat}}{\left( \frac{2 C_{pg}}{C_{pv, ideal}} - 1 \right)} \right] - P \left( \frac{1}{\rho_v} - \frac{1}{\rho_g} \right) \quad (10-48)$$

The definitions of enthalpy and internal energy allow the density of the water vapor to be written such that

$$\begin{aligned} \rho_v &= \frac{P}{h_v - e_v} = \frac{P}{\left[ h_g + C_{pv, ideal} (T_v - T_{sat}) \right] - \left[ e_g + C_{vv, ideal} (T_v - T_{sat}) \right]} \\ &= \frac{P}{(h_g - e_g) + (\gamma_{ideal} - 1) (e_v - e_g)} \end{aligned} \quad (10-49)$$

Substitution of  $p_v$  and  $p_g$ , as defined by the preceding equation, into the equation for the internal energy of the vapor, gives

$$e_v = e_g + \frac{C_{vv,ideal}}{2} \left[ (T_v - T_{sat}) + (T_v^2 - \beta)^{1/2} - \frac{T_{sat}}{\left(2 \frac{C_{pg}}{C_{pv,ideal}} - 1\right)} \right] \quad (10-50)$$

where  $C_{vv,ideal}$  is the constant volume specific heat for steam as defined by ideal gas behavior given by

$$C_{vv,ideal} = \frac{R_v}{\gamma_{ideal} - 1} \quad (10-51)$$

The partial derivatives are given by

$$\left( \frac{\partial e_v}{\partial T_v} \right)_p = \frac{C_{vv,ideal}}{\left( 1 - \frac{\beta}{\kappa^2} \right)} \quad (10-52)$$

$$\left( \frac{\partial e_v}{\partial p} \right)_{T_v} = - \frac{1}{2} \left( \frac{\partial e_v}{\partial T_g} \right)_p \left[ \left( 1 - \frac{\beta}{\kappa^2} \right) \kappa'_p + \frac{1}{\kappa} \frac{d\beta}{dp} \right] \quad (10-53)$$

where:

$$\kappa = \frac{2}{C_{vv,ideal}} (e_v - e_g) + T_{sat} \left[ 1 + \frac{1}{\frac{2C_{pg}}{C_{pv,ideal}} - 1} \right] \quad (10-54)$$

and

$$\kappa_P' = \left( \frac{\partial \kappa}{\partial P} \right)_{T_v} = - \frac{2}{C_{vv,ideal}} \frac{de_g}{dP} + \left[ 1 + \frac{1}{\left( \frac{2C_{pg}}{C_{pv,ideal}} - 1 \right)} \right] \frac{dT_{sat}}{dP} \quad (10-55)$$

$$- \frac{2}{C_{pv,ideal}} \left[ \frac{T_{sat}}{\left( \frac{2C_{pg}}{C_{pv,ideal}} - 1 \right)^2} \right] \frac{dC_{pg}}{dP}$$

and

$$\frac{d\beta}{dP} = \frac{2}{T_{sat}} \left\{ \beta \frac{dT_{sat}}{dP} + \frac{2}{C_{pv,ideal}} \left[ \frac{T_{sat}}{\left( \frac{2C_{pg}}{C_{pv,ideal}} - 1 \right)} \right]^3 \frac{dC_{pg}}{dP} \right\} \quad (10-56)$$

**Superheated Vapor Density** The vapor density is calculated as

$$\rho_v = \frac{P}{(\gamma_g - 1) e_g + (\gamma_{ideal} - 1) (e_v - e_g)} \quad (10-57)$$

Therefore, the partial derivatives are calculated by

$$\left( \frac{\partial \rho_v}{\partial T_v} \right)_P = - \left( \frac{\partial e_v}{\partial T_v} \right)_P \left[ \frac{(\gamma_{ideal} - 1) \rho_v}{(\gamma_g - 1) e_g + (\gamma_{ideal} - 1) (e_v - e_g)} \right] \quad (10-58)$$

and

$$\left( \frac{\partial \rho_v}{\partial P} \right)_{T_v} = \left\{ 1 - \rho_v \left[ e_g \frac{d\gamma_g}{dP} + (\gamma_g - \gamma_{ideal}) \frac{de_g}{dP} \right] \right. \quad (10-59)$$

$$\left. \left[ \frac{1}{(\gamma_g - 1) e_g + (\gamma_{ideal} - 1) (e_v - e_g)} \right] \right\} + \left( \frac{\partial \rho_v}{\partial e_v} \right)_P \left( \frac{\partial e_v}{\partial P} \right)_{T_v}$$

where:

$$\left( \frac{\partial \rho_v}{\partial e_v} \right)_P = - \frac{(\gamma_{ideal} - 1) \rho_v}{(\gamma_g - 1) e_g + (\gamma_{ideal} - 1)(e_v - e_g)} \quad (10-60)$$

**Enthalpy** The enthalpy of superheated vapor is calculated using the definition of enthalpy,

$$h_v = e_v + \frac{P}{\rho_v} \quad (10-61)$$

where  $e_v$  is calculated from Equation 10-50, and  $\rho_v$  is calculated using Equation 10-57.

**Model as Coded** Thermodynamic properties for superheated water vapor are calculated in subroutine THERMO as described in this section. For superheated vapor, however, minimum and maximum limits are placed on the calculated values of the density and its partial derivatives. In low pressure regions where the above equations may predict a negative density, and near the critical point, it is necessary to impose the following limits on the density ratio

$$0 < \frac{\rho_v}{\rho_t} \leq 0.9 \quad (10-62)$$

to avoid singularities when calculating certain parameters. If the calculated value of  $\rho_v$  is outside these bounds, the vapor density and its derivatives are superseded by

$$\rho_v = 0.9 \rho_t \quad (10-63)$$

$$\left( \frac{\partial \rho_v}{\partial T_v} \right)_P = 0.9 \left( \frac{\partial \rho_t}{\partial T_t} \right)_P \quad (10-64)$$

$$\left( \frac{\partial \rho_v}{\partial P} \right)_{T_v} = 0.9 \left( \frac{\partial \rho_t}{\partial P} \right)_{T_t} \quad (10-65)$$

**Scaling Considerations** Not applicable.

**Conclusions** The thermodynamic properties for superheated vapor in WCOBRA/TRAC one-dimensional components are calculated from thermodynamic first principles. The calculated values are in good agreement with those found in the Steam Tables. The error introduced by the

WCOBRA/TRAC routines is small and thus is not considered a major contributor to the overall code calculational uncertainty.

### 10-2-2-3 Subcooled Vapor Properties

**Model Basis** WCOBRA/TRAC calculates internal energy, density, and enthalpy in one-dimensional components in the following manner when the vapor is subcooled.

**Internal Energy** The internal energy and its derivatives for subcooled vapor are calculated as

$$e_v = e_g + (T_v - T_{sat}) \frac{C_{pg}}{\gamma_{ideal}} \quad (10-66)$$

$$\left( \frac{\partial e_v}{\partial T_v} \right)_P = \frac{C_{pg}}{\gamma_{ideal}} \quad (10-67)$$

$$\left( \frac{\partial e_v}{\partial P} \right)_{T_v} = \frac{de_g}{dP} + \left( \frac{e_v - e_g}{C_{pg}} \right) \frac{dC_{pg}}{dP} - \left( \frac{\partial e_v}{\partial T_v} \right)_P \frac{dT_{sat}}{dP} \quad (10-68)$$

where  $T_{sat}$  is the saturation temperature corresponding to the vapor pressure ( $P_v$ ).

The subcooled vapor density is calculated using Equation 10-57. If this value falls outside of the range

$$0 < \rho_v < 0.9\rho_t$$

then the internal energy and its derivatives are recalculated and used in subsequent density recalculations. A new value of constant-pressure specific heat for vapor at the saturation condition is estimated:

$$C_{pg} = 958.75 \left( 1 - \frac{T_{sat}}{T_{crit}} \right)^{-0.8566} \quad (10-69)$$

and its derivative is

$$\frac{dC_{pg}}{dP} = (958.75) (0.8566) \left( 1 - \frac{T_{sat}}{T_{crit}} \right)^{-1.8566} \frac{1}{T_{crit}} \frac{dT_{sat}}{dP} \quad (10-70)$$

Vapor internal energy and its derivatives are

$$e_v = e_g + (T_v - T_{sat}) C_{pg} \gamma_{ideal} \quad (10-71)$$

$$\left( \frac{\partial e_v}{\partial T_v} \right)_P = C_{pg} \gamma_{ideal} \quad (10-72)$$

$$\left( \frac{\partial e_v}{\partial P} \right)_{T_v} = \frac{de_g}{dP} + \frac{(e_v - e_g)}{C_{pg}} \frac{dC_{pg}}{dP} - \left( \frac{\partial e_v}{\partial T_v} \right)_P \frac{dT_{sat}}{dP} \quad (10-73)$$

**Density** Subcooled vapor density and its derivatives are determined using the same method of calculation as in the case of superheated vapor, as described in Section 10-2-2-2.

If the subcooled vapor density calculated with Equation 10-57 falls outside the range

$$0 < \rho_v < 0.9 \rho_t$$

then the vapor internal energy is recalculated using Equations 10-69 through 10-73 and the density and its derivatives are recalculated:

$$\rho_v = P / ((\gamma_g - 1) e_v) \quad (10-74)$$

$$\left( \frac{\partial \rho_v}{\partial T_v} \right)_P = \frac{-\rho_v}{e_v} \left( \frac{\partial e_v}{\partial T_v} \right)_P \quad (10-75)$$

$$\left( \frac{\partial \rho_v}{\partial P} \right)_{T_v} = \frac{\rho_v}{P} \left[ 1 - \frac{P}{(\gamma_g - 1)} \frac{d\gamma_g}{dP} - \frac{P}{e_v} \left( \frac{\partial e_v}{\partial P} \right)_{T_v} \right] \quad (10-76)$$

**Enthalpy** The enthalpy of subcooled vapor is calculated using the definition of enthalpy,

$$h_v = e_v + \frac{P}{\rho_v} \quad (10-77)$$

where  $e_v$  is calculated from Equation 10-66 or 10-71, and  $\rho_v$  is calculated using Equation 10-57 or 10-74.

**Model as Coded** The thermodynamic properties for subcooled vapor are calculated directly as described in this section, in subroutine THERMO. The enthalpy is calculated in subroutine FPROP.

**Scaling Considerations** Not applicable.

**Conclusions** The thermodynamic properties for subcooled vapor in WCOBRA/TRAC one-dimensional components are calculated in a manner consistent with calculations for superheated vapor, which are derived from thermodynamic first principles. Subcooled vapor occurs only infrequently during a LOCA transient. As such, the error introduced by WCOBRA/TRAC subcooled vapor property calculations is assumed minor and is not considered a contributor to the code uncertainty.

#### 10-2-2-4 Subcooled Liquid Properties

##### Model Basis

**Internal Energy** For a liquid at a subcooled temperature  $T_l$  and pressure  $P$  the liquid internal energy associated with that state is calculated starting with the internal energy of the saturated liquid state described by  $T_l$  and  $P_{sat}(T_l)$ , which is the saturation pressure corresponding to  $T_l$ , and adding an additional term which represents the change in internal energy from the state  $(T_l, P_{sat}(T_l))$  to the state  $(T_l, P)$ . That is,

$$e_l(T_l, P) = e_f(T_l) + \theta_1(P, T_l) \quad (10-78)$$

The additional term  $\theta_1$ , which represents the change in energy required to move along the isotherm at  $T_l$  between two different pressure values, namely  $P_{sat}(T_l)$  and  $P$ , is represented as

$$\theta_1 = (P - P_{sat}(T_l)) \left( \frac{\partial e_l}{\partial P} \right)_{T_l} \quad (10-79)$$

where:

$$P_{sat}(T_l) = (10^5) \left[ \frac{T_l - 255.2}{117.8} \right]^{1/0.223} \quad (10-80)$$

The partial derivative with respect to pressure of the internal energy is

$$\left( \frac{\partial e_l}{\partial P} \right)_{T_l} = C_{K0} + C_{K2} P_{sat}(T_l) \quad (10-81)$$

where:

$$C_{K0} = -8.33544 \times 10^{-4}$$

$$C_{K2} = -2.24745 \times 10^{-17}$$

Therefore the partial derivative with respect to  $T_t$  of the internal energy increment is calculated as

$$\left( \frac{\partial \theta_1}{\partial T_t} \right)_P = \frac{-C_{K0} - C_{K2} [2 P_{sat}(T_t)P - 3 P_{sat}(T_t)^2]}{\frac{(117.8)(0.223)}{10^5} \left[ \frac{P_{sat}(T_t)}{10^5} \right]^{-0.767}} \quad (10-82)$$

and the derivative of internal energy is

$$\left( \frac{\partial e_t}{\partial T_t} \right)_P = \frac{de_f}{dT_{sat}} + \left( \frac{\partial \theta_1}{\partial T_t} \right)_P \quad (10-83)$$

The saturated liquid internal energy and its derivative with respect to temperature are determined over three temperature domains as was previously described (Equations 10-38 and 10-39).

**Density** Liquid density is also calculated over three temperature domains. Defining  $P_{BAR} = (10^{-5})P$  and  $T_{tc} = T_t - 273.15$ , density and its derivatives are as follows.

For  $T_t > 525.15$ :

$$\rho_t = 1.43 + 1000 [C_{t1} + C_{t2} P_{BAR} + C_{t3} P_{BAR}^2 + \beta_1 T_{tc} + \beta_2 T_{tc}^2]^{-1} \quad (10-84)$$

$$\left( \frac{\partial \rho_t}{\partial P} \right)_{T_t} = -(\rho_t - 1.43)^2 (10^{-8}) [C_{t2} + 2C_{t3} P_{BAR} + T_{tc} (C_{t5} + 2C_{t6} P_{BAR}) + T_{tc}^2 (C_{t8} + 2C_{t9} P_{BAR})] \quad (10-85)$$

$$\left( \frac{\partial \rho_t}{\partial T_t} \right)_P = -(\rho_t - 1.43)^2 (10^{-3}) (\beta_1 + 2\beta_2 T_{tc}) \quad (10-86)$$



where:

$$\beta_1 = C_{t4} + C_{t5}P_{BAR} + C_{t6}P_{BAR}^2 \quad (10-87)$$

and

$$\beta_2 = C_{t7} + C_{t8}P_{BAR} + C_{t9}P_{BAR}^2 \quad (10-88)$$

For  $T_t < 521.15$ :

$$\rho_t = 1000[d_{t1} + d_{t2}P_{BAR} + d_{t3}P_{BAR}^2 + \beta_3T_{tc} + \beta_4T_{tc}^2] - 2.01 \quad (10-89)$$

$$\left(\frac{\partial \rho_t}{\partial P}\right)_{T_t} = -(\rho_t + 2.01)^2(10^{-8})[d_{t2} + 2d_{t3}P_{BAR} + T_{tc}(d_{t5} + 2d_{t6}P_{BAR}) + T_{tc}^2(d_{t8} + 2d_{t9}P_{BAR})] \quad (10-90)$$

$$\left(\frac{\partial \rho_t}{\partial T_t}\right)_P = -(\rho_t + 2.01)^2(10^{-3})(\beta_3 + 2\beta_4T_{tc}) \quad (10-91)$$

where:

$$\beta_3 = d_{t4} + d_{t5}P_{BAR} + d_{t6}P_{BAR}^2 \quad (10-92)$$

and

$$\beta_4 = d_{t7} + d_{t8}P_{BAR} + d_{t9}P_{BAR}^2 \quad (10-93)$$

For  $521.15 \leq T_t \leq 525.15$  a linear interpolation of the above two ranges is used. Representing the values from Equations 10-84 through 10-88 by  $\rho_{ta}$  and those from Equations 10-89 through 10-93 by  $\rho_{tb}$ , then

$$\rho_t = F_b\rho_{tb} + F_a\rho_{ta} \quad (10-94)$$

$$\frac{\partial \rho_t}{\partial P} = F_b \frac{\partial \rho_{tb}}{\partial P} + F_a \frac{\partial \rho_{ta}}{\partial P} \quad (10-95)$$

$$\frac{\partial \rho_t}{\partial T_t} = F_b \frac{\partial \rho_{tb}}{\partial T_t} + F_a \frac{\partial \rho_{ta}}{\partial T_t} + \frac{\rho_{ta} - \rho_{tb}}{4.0} \quad (10-96)$$

where:

$$F_a = (T_t - 521.15)/4 \quad (10-97)$$

$$F_b = 1 - F_a \quad (10-98)$$

The coefficients used in Equations 10-84 through 10-93 are:

$C_{t1} = 2.25262$	$d_{t1} = 1.00213623$
$C_{t2} = 0.014859$	$d_{t2} = -5.632785E-05$
$C_{t3} = -7.15488E-05$	$d_{t3} = -8.971304E-09$
$C_{t4} = -0.0104588$	$d_{t4} = -2.28287459E-05$
$C_{t5} = -1.02962E-04$	$d_{t5} = 4.76596787E-07$
$C_{t6} = 5.09135E-07$	$d_{t6} = 5.021318E-10$
$C_{t7} = 2.59266E-05$	$d_{t7} = 4.10115658E-06$
$C_{t8} = 1.7241E-07$	$d_{t8} = -3.803989E-09$
$C_{t9} = -8.98419E-10$	$d_{t9} = -1.42199752E-12$

**Model as Coded** The thermodynamic properties for subcooled liquid are calculated in subroutine THERMO as described in the previous paragraphs. For subcooled liquid, however, the density and its derivatives are corrected to reflect a residual void fraction. The correction is shown below.

In the following, the liquid values calculated in the previous section are denoted by a tilde (~).

For  $P \geq 0.4 \times 10^6 \text{ Pa}$

$$\rho_t = \left(1 - \frac{1000}{P}\right) \bar{\rho}_t \quad (10-99)$$

and

$$\left(\frac{\partial \rho_t}{\partial T_t}\right)_P = \left(1 - \frac{1000}{P}\right) \left(\frac{\partial \bar{\rho}_t}{\partial T_t}\right)_P \quad (10-100)$$

$$\left( \frac{\partial \rho_t}{\partial P} \right)_{T_t} = \left( 1 - \frac{1000}{P} \right) \left( \frac{\partial \tilde{\rho}_t}{\partial P} \right)_{T_t} + \frac{1000 \rho_t}{P^2} \quad (10-101)$$

For  $P < 0.4 \times 10^6 \text{ Pa}$

$$\rho_t = (0.995 + 6.25 \times 10^{-9} P) \tilde{\rho}_t \quad (10-102)$$

and,

$$\left( \frac{\partial \rho_t}{\partial T_t} \right)_P = (0.995 + 6.25 \times 10^{-9} P) \left( \frac{\partial \tilde{\rho}_t}{\partial T_t} \right)_P \quad (10-103)$$

$$\left( \frac{\partial \rho_t}{\partial P} \right)_{T_t} = (0.995 + 6.25 \times 10^{-9} P) \left( \frac{\partial \tilde{\rho}_t}{\partial P} \right)_{T_t} + 6.25 \times 10^{-9} \tilde{\rho}_t \quad (10-104)$$

**Scaling Considerations** Not applicable.

**Conclusions** The TRAC-PD2 subcooled water thermodynamic property routines used in WCOBRA/TRAC for one dimensional components have been compared by Rivard and Torrey (1975) with steam table data. The agreement is good in the region for  $373 \text{ K} < T_t < 523 \text{ K}$  and  $0.4178 \times 10^6 \text{ J/Kg} < e_t < 1.0808 \times 10^6 \text{ J/Kg}$ . Comparison with the WATER package (Coffman and Lynn, 1966) over a wider range also showed good agreement except for very extreme cases not expected in a PWR LOCA.

### 10-2-2-5 Transport Properties

**Model Basis** This section describes the WCOBRA/TRAC calculations performed to obtain the specific heat, fluid viscosity, thermal conductivity, and surface tension for one-dimensional components. The equations used for these quantities are polynomial fits to data.

**Specific Heat** The constant pressure specific heat for liquid water is given in  $\text{J/kg}^\circ\text{K}$  as a function of enthalpy and pressure by

$$C_{pt} = \{H_t [H_t (D_{ot} + D_{1t} P) + (C_{ot} + C_{1t} P)] + B_{ot} + B_{1t} P\}^{-1} \quad (10-105)$$

For vapor, the constant pressure specific heat is given by:

$$C_{pv} = C_{1v} + C_{2v}T_v + \frac{C_{3v}P}{(C_{5v}T_v - C_{6v})^{2.4}} + \frac{C_{4v}P^3}{(C_{5v}T_v - C_{6v})^9} \quad (10-106)$$

where the coefficients of Equations 10-105 and 10-106 are listed in Table 10-9.

**Liquid Viscosity** Calculation of liquid viscosity is divided into three different ranges based on the liquid enthalpy.

For  $H_t \leq 0.276 \times 10^6$  J/kg, liquid viscosity in N-s/m<sup>2</sup>

$$\mu_t = \{A_{0t} + A_{1t}\chi + A_{2t}\chi^2 + A_{3t}\chi^3 + A_{4t}\chi^4\} - [B_{0t} + B_{1t}\eta + B_{2t}\eta^2 + B_{3t}\eta^3] (P - P_o) \quad (10-107)$$

where:

$$\chi = (H_t - c_{0n}) H_o \quad (10-108)$$

and

$$\eta = (H_t - e_{c0n}) e_{h0} \quad (10-109)$$

For  $0.276 \times 10^6$  J/kg  $< H_t \leq 0.394 \times 10^6$  J/kg the liquid viscosity is,

$$\mu_t = [E_{0t} + E_{1t}H_t + E_{2t}H_t^2 + E_{3t}H_t^3] + [F_{0t} + F_{1t}H_t + F_{2t}H_t^2 + F_{3t}H_t^3] (P - P_o) \quad (10-110)$$

and for  $H_t > 0.394 \times 10^6$  J/kg

$$\mu_t = [D_{0t} + D_{1t}z + D_{2t}z^2 + D_{3t}z^3 + D_{4t}z^4] \quad (10-111)$$

$$z = (H_t - c_n) H_{oo} \quad (10-112)$$

The coefficients for the liquid viscosity equations are found in Table 10-10.

**Vapor Viscosity** Calculation of the viscosity of vapor is divided into three different temperature ranges. The ranges and expressions used for vapor viscosity are:

For  $T_v < 280 \text{ K}$ ,

$$\mu_v = 17.08 \times 10^{-6} + 5.927 \times 10^{-8}(T_v - 273.15) - 8.14 \times 10^{-11}(T_v - 273.15)^2 \quad (10-113a)$$

For  $280 \text{ K} \leq T_v \leq 573.15 \text{ K}$ ,

$$\mu_v = [B_{1v}(T_v - 273.15) + C_{1v}] - \rho_v [D_{1v} - E_{1v}(T_v - 273.15)] \quad (10-113b)$$

For  $573.15 \text{ K} < T_v < 648.15 \text{ K}$ ,

$$\begin{aligned} \mu_v = & B_{1v}(T_v - 273.15) + C_{1v} + \rho_v [F_{0v} - F_{1v}(T_v - 273.15) \\ & + F_{2v}(T_v - 273.15)^2 + F_{3v}(T_v - 273.15)^3] \\ & + \rho_v [G_{0v} + G_{1v}(T_v - 273.15) + G_{2v}(T_v - 273.15)^2] \\ & + G_{3v}(T_v - 273.15)^3 \left[ A_{0v} + A_{1v}\rho_v + A_{2v}\rho_v^2 \right] \end{aligned} \quad (10-114)$$

and for  $T_v \geq 648.15 \text{ K}$ ,

$$\mu_v = B_{1v}(T_v - 273.15) + C_{1v} + \rho_v [A_{0v} + A_{1v}\rho_v + A_{2v}\rho_v^2] \quad (10-115)$$

The coefficients for Equations 10-113 through 10-115 are listed in Table 10-11.

**Liquid Thermal Conductivity** The liquid thermal conductivity is given  $W/m-K$  by

$$k_l = A_{t0} + A_{t1}\chi_\kappa + A_{t2}\chi_\kappa^2 + A_{t3}\chi_\kappa^3 \quad (10-116)$$

where:

$$\chi_\kappa = \frac{H_l}{A_{t4}} \quad (10-117)$$

### Vapor Thermal Conductivity

If  $280.0 \text{ K} \leq T_v$

$$k_v = \chi_1 + \rho_v \left[ \chi_2 + \frac{A_{v4} \rho_v}{(T_v - 273.15)^{4.2}} \right] \quad (10-118)$$

where:

$$\chi_1 = A_{v0} + A_{v1}(T_v - 273.15) + A_{v2}(T_v - 273.15)^2 + A_{v3}(T_v - 273.15)^3 \quad (10-119)$$

and

$$\chi_2 = B_{v0} + B_{v1}(T_v - 273.15) + B_{v2}(T_v - 273.15)^2 \quad (10-120)$$

The coefficients used in Equations 10-116 through 10-120 are listed in Table 10-12.

If  $T_v < 280.0 \text{ K}$ , the vapor conductivity is

$$k_v = 0.0228 \quad (10-121)$$

**Surface Tension** The surface tension is calculated in N/m as,

$$\sigma = \left( a_2 + \frac{a_1}{1 + 0.83\theta} \right) \theta^2 + a_3 \theta^3 + a_4 \theta^4 + a_5 \theta^5 \quad (10-122)$$

where:

$$\theta = 647.3 - T_{sat} \quad (10-123)$$

The coefficients for Equation 10-122 are given in Table 10-13.

**Model as Coded** Subroutine FPROP is used to obtain transport properties for liquid and vapor water. The input variables for this subroutine are the saturation temperature corresponding to the total pressure, the internal energies, densities, and temperatures of the liquid and vapor phases and the total pressure. The output transport variables include the constant pressure specific heats, viscosities, and thermal conductivities of the liquid and gas phases, and the surface tension of the liquid.

The transport property calls are function calls within the FPROP subroutine. Function CPLL calculates the constant pressure specific heat of the liquid, while function CPVV1 determines the value of the constant pressure specific heat of the vapor. Function THCL evaluates the liquid thermal conductivity, and function THCV calculates the steam thermal conductivity. Similarly, functions VISCL and VISCV determine viscosity values. Finally, function SIGMA calculates the surface tension.

The equations shown are coded directly. Sample curves of liquid and vapor specific heat, viscosity, thermal conductivity, and the surface tension calculated by these routines along the saturation line are shown in Figures 10-22 through 10-28.

In some instances, upper and lower limits are maintained on the calculated values of the transport properties. These limits are summarized as follows:

**Specific Heat** The maximum permitted value for the liquid specific heat is  $C_{pt}=4.0 \times 10^4$ . If the calculation of  $C_{pt}$  by Equation 10-105 performed by function CPLL yields a value greater than this,  $C_{pt}$  is reset to  $4.0 \times 10^4$ . No limits are placed on the calculation of the vapor specific heat.

**Viscosity** The minimum permitted value of vapor viscosity is  $\mu_v=10^{-7}$ . If the calculation of  $\mu_v$  by Equations 10-113 through 10-115 yields a value less than this in function VISCV,  $\mu_v$  is reset to  $10^{-7}$ . No limits are imposed on the liquid phase viscosity.

**Thermal Conductivity** The minimum permitted value of the liquid thermal conductivity is  $k_l=0.09$ . If, in function THCL, Equation 10-116 yields a value lower than this,  $k_l$  is reset to 0.09.

The minimum permitted value for vapor thermal conductivity is  $k_v=10^{-4}$ . If Equation 10-118 in function THCV calculates a value less than  $10^{-4}$ ,  $k_v$  is reset to  $10^{-4}$ .

**Surface Tension** If  $T_{sat} > 647.3$ , the surface tension is set to  $\sigma = 0.0$ .

**Scaling Considerations** Not applicable.

**Conclusions** In NUREG/CR-2054, it was reported that the thermodynamic and transport property fits used in TRAC-PD2 were compared by Rivard and Torrey (1975) with steam table data over a wide range of parameters. The agreement is satisfactory in the saturation region and in the superheated steam region for  $1.0 \times 10^5 \text{ Pa} < P < 100.0 \times 10^5 \text{ Pa}$  and  $423.0 \text{ K} < T_v < 823.0 \text{ K}$ . The agreement also is good in the subcooled water region for  $373.0 \text{ K} < T_l < 523.0 \text{ K}$  and  $0.4178 \times 10^6 \text{ J/kg} < e_l < 1.0808 \times 10^6 \text{ J/kg}$ .

Further verification was performed by comparing the TRAC-PD2 polynomial fits with the WATER package (Coffman and Lynn, 1966) over a wider range of nonequilibrium (99 K of both superheat and subcooling) for a pressure variation of  $1.0 \times 10^5 \text{ Pa}$  to  $2.0 \times 10^7 \text{ Pa}$ . The comparisons showed good

agreement for both the thermodynamic and transport properties throughout the saturation and nonequilibrium regions except for very extreme cases, which are not expected in a PWR LOCA.

The WCOBRA/TRAC property package for one-dimensional components is identical to the TRAC-PD2 package. Therefore, for most WCOBRA/TRAC applications, the thermodynamic and transport property routines will provide realistic values over a wide range. The simplified polynomial fits provide an efficient and low-cost method compared to other approaches such as steam table interpolation.

### 10-3 THERMOPHYSICAL PROPERTIES OF AIR

#### 10-3-1 Vessel Component

**Model Basis** WCOBRA/TRAC can perform calculations for conditions in which there is air in the vessel component. This section describes the thermodynamic properties which are defined for air in the WCOBRA/TRAC vessel component.

**Enthalpy** The enthalpy of air is calculated as

$$H_{air} = C_{p,ref}(T_{air} - T_{ref}) + H_{ref} \quad (10-124)$$

where the reference values are  $T_{ref} = 40.0^\circ\text{F}$ ,  $H_{ref} = 188.49 \text{ Btu/lbm}$ , and  $C_{p,ref} = 0.249 \text{ Btu/lbm-}^\circ\text{F}$ .

**Density** The density of air is calculated from the ideal gas law with the gas constant for air assumed to be  $R_{air} = 0.37042 \text{ psi/}^\circ\text{R (lb/ft}^3\text{)}$ . Thus, the density of air is given by

$$\rho_{air} = \frac{P}{R_{air}(T_{air} + 459.6)} \quad (10-125)$$

**Gas Temperature** The air temperature is estimated from the enthalpy using the inverse of Equation 10-124.

**Specific Heat** The specific heat for air in BTU/lbm- $^\circ\text{F}$  is determined in two different temperature ranges.

If  $T_{air} \leq 600\text{K}$ ,

$$C_p = 0.244388 + A_1 T_{air} + A_2 T_{air}^2 + A_3 T_{air}^3 \quad (10-126)$$

and if  $T_{air} > 600\text{K}$ ,

$$C_p = 0.208831 + B_1 T_{air} + B_2 T_{air}^2 + B_3 T_{air}^3 \quad (10-127)$$



where the coefficients  $A_i$  and  $B_i$  are listed in Table 10-14, and  $T_{air}$  is in degrees K.

**Model as Coded** The equations used to calculate the thermodynamic properties of air, Equations 10-124 through 10-127, are coded as shown without modification. No upper or lower limits are imposed on the values calculated. Calculations are performed in Subroutines HGAS and TGAS.

**Scaling Considerations** Not applicable.

**Conclusions** The WCOBRA/TRAC vessel component can perform calculations to estimate the thermodynamic properties of air. This option, however, is not used in a LOCA analysis.

### 10-3-2 One-Dimensional Components

**Model Basis** This section describes the calculation of thermodynamic and transport properties in WCOBRA/TRAC one-dimensional components for air.

**Internal Energy** The internal energy and its derivatives for air are given by

$$e_{air} = C_{vair} T_{air} \quad (10-128)$$

$$\left( \frac{\partial e_{air}}{\partial T_{air}} \right)_p = C_{vair} \quad (10-129)$$

and

$$\left( \frac{\partial e_{air}}{\partial P} \right)_{T_{air}} = 0.0 \quad (10-130)$$

The constant volume specific heat ( $C_{vair}$ ) is

$$C_{vair} = 714.9 \text{ J/kg-K} \quad (10-131)$$

**Density** The density and its derivatives are based on the Ideal Gas Law and are given by

$$\rho_{air} = \frac{P}{R_{air} T_{air}} \quad (10-132)$$

$$\left( \frac{\partial \rho_{air}}{\partial P_{air}} \right)_{T_{air}} = \frac{1}{R_{air} T_{air}} \quad (10-133)$$

$$\left( \frac{\partial \rho_{air}}{\partial T_{air}} \right)_P = -R_{air} \rho_{air} \left( \frac{\partial \rho_{air}}{\partial P} \right)_{T_{air}} \quad (10-134)$$

where

$$R_{air} = 287.12 \text{ J/kg-K} \quad (10-135)$$

**Enthalpy** The enthalpy of air is calculated using the definition of enthalpy:

$$H_{air} = e_{air} + \frac{P}{\rho_{air}} \quad (10-136)$$

where  $e_{air}$  is determined by Equation 10-128, and  $\rho_{air}$  is given by Equation 10-132.

**Viscosity** Two different temperature ranges are used to calculate the viscosity of air.

If  $T_{air} \leq 502.15 \text{ K}$ ,

$$\mu_{air} = a_{a0} + a_{a1}(T_{air} - 273.15) + a_{a2}(T_{air} - 273.15)^2 \quad (10-137)$$

and if  $T_{air} > 502.15 \text{ K}$ ,

$$\mu_{air} = a_{b0} + a_{b1}(T_{air} - 273.15) + a_{b2}(T_{air} - 273.15)^2 \quad (10-138)$$

where the coefficients  $a_{ai}$  and  $a_{bi}$  are listed in Table 10-15.

**Thermal Conductivity** The thermal conductivity of air is assumed to be constant,

$$k_{air} = 0.0228 \text{ W/m-K} \quad (10-139)$$

**Model as Coded** The internal energy and its derivatives and the density and its derivatives for air are calculated in subroutine THERMO. Subroutine FPROP calculates the enthalpy. The transport properties viscosity and thermal conductivity are determined in subroutines VISCV and THCV, respectively.

**Scaling Considerations** Not applicable.

**Conclusions** The WCOBRA/TRAC one-dimensional components calculate thermodynamic properties for air assuming it behaves as an ideal gas. The transport properties are based on polynomial fits to data. The correlations approximately calculate properties for air at low temperatures.

## 10-4 THERMAL PROPERTIES OF NUCLEAR FUEL ROD MATERIALS

A typical nuclear fuel rod is composed of uranium-dioxide fuel pellets and a zirconium based clad material. The gap between the fuel pellets and the clad is filled with the initial backfill gas and fission gas. As part of the WCOBRA/TRAC default nuclear fuel rod model, the material properties of uranium-dioxide, Zircaloy-4, ZIRLO™, and of gas mixtures are included. This section describes the calculation of the thermal properties for these fuel rod materials.

### 10-4-1 Uranium Dioxide

**Model Basis** The material properties of uranium dioxide are based on MATPRO-9 (MacDonald et al., 1976) and on MATPRO-11, Rev. 1 (Hagman, Reymann, and Mason, 1980) calculations.

**Density** The (cold) density for uranium-dioxide is assumed to be

$$\rho_{UO_2} = 684.86 f_D \quad (10-140)$$

where  $f_D$  is the fraction of theoretical density and is input by the user. The density  $\rho_{UO_2}$  has units of lbm/ft<sup>3</sup>.

**Thermal Conductivity** The  $UO_2$  thermal conductivity is computed from the MATPRO-9 correlation instead of the more complex version in MATPRO-11 to reduce computer time. Both correlations have the same error band (0.2 W/m-°K) and give very nearly the same conductivity over the expected operating range of 500-3000° K. The thermal conductivity in Btu/hr-ft-°F is determined from

$$k_{UO_2} = \left[ \max \left( 0.0191, \frac{40.4}{(T_c + 464)} \right) + 1.216 \times 10^{-4} \exp(1.867 \times 10^{-3} T_c) \right] C \quad (10-141)$$

where  $T_c$  is the temperature in °Celsius and

$$C = (0.5779)100[1.0 - \beta(1.0 - f_D)]/(1.0 - 0.05\beta) \quad (10-142)$$

and

$$\beta = 2.58 - (5.8 \times 10^{-4}) T_c \quad (10-143)$$

**Specific Heat** The specific heat in Btu/lbm-°F for uranium dioxide is given by

$$C_{p_{UO_2}} = (2.388 \times 10^{-4}) \left\{ \frac{K_1 \theta^2 \exp(\theta/T_K)}{T_K^2 [\exp(\theta/T_K) - 1]^2} + K_2 T_K + \frac{F_{OM} K_3 E_D}{2 R T_K^2} \exp(-E_D/RT_K) \right\} \quad (10-144)$$

where  $T_K$  is the temperature in °K and

$$\begin{aligned} \theta &= \text{Einstein temperature}(535.285^\circ K) \\ R &= 8.3143 \text{ (J/mol-}^\circ K) \\ K_1 &= 296.7 \text{ (J/kg-}^\circ K) \\ K_2 &= 2.43 \times 10^{-2} \text{ (J/kg-}^\circ K^2) \\ K_3 &= 8.745 \times 10^7 \text{ (J/kg)} \\ E_D &= 1.577 \times 10^5 \text{ (J/mol)} \\ F_{OM} &= \text{oxygen/metal ratio}(2.0) \end{aligned}$$

**Model as Coded** The equations representing the density, thermal conductivity and specific heat for uranium dioxide are coded into WCOBRA/TRAC as described by Equations 10-140 through 10-144 without modification.

Calculations for uranium dioxide density are performed in Subroutine SETUP, those for thermal conductivity in subroutines SSTEMP and TEMP, and those for specific heat in Subroutines TEMP and MOVE. Values of conductivity and specific heat versus temperature are shown in Figures 10-29 and 10-30.

**Scaling Considerations** Not applicable.

**Conclusions** The WCOBRA/TRAC correlations for  $UO_2$  density, specific heat and thermal conductivity are based on MATPRO-9 and MATPRO-11. The models and correlations for these properties were used in simulations of NRU and LOFT. Therefore, the uncertainty and reliability of these models is accounted for in the overall code bias and uncertainty.

#### 10-4-2 Zircaloy-4

**Model Basis** The material properties of Zircaloy-4 are based on MATPRO-9 and MATPRO-11 calculations.

**Density** The (cold) density of Zircaloy-4 clad material is assumed to be  $\rho_{Zr} = 409.0 \text{ lbm/ft}^3$ .

**Thermal Conductivity** The thermal conductivity in Btu/hr-ft-°F for Zircaloy-4 clad is given by

$$k_{Zr} = 0.5779 \left[ 7.51 + 0.0209T_K - (1.45 \times 10^{-5})T_K^2 + (7.67 \times 10^{-9})T_K^3 \right] \quad (10-145)$$

where  $T_K$  is temperature in °Kelvin.

**Specific Heat** WCOBRA/TRAC calculates the specific heat for Zircaloy-4 by linearly interpolating between values from a built-in table. Table 10-16 lists the values used to determine the specific heat of Zircaloy-4.

**Model as Coded** The equations for the density, thermal conductivity and specific heat of Zircaloy-4 are coded into WCOBRA/TRAC as described above without modification. Density is calculated in Subroutine SETUP and HEAT, conductivity in Subroutines STEMP, TEMP, and HEAT and specific heat in Subroutines TEMP, HEAT, and MOVE. Curves of conductivity and specific heat versus temperature are shown in Figures 10-31 and 10-32.

**Scaling Considerations** Not applicable.

**Conclusions** The WCOBRA/TRAC correlations for the density, thermal conductivity, and specific heat of Zircaloy-4 are based on MATPRO-9 and MATPRO-11. These property relations were used in simulations of NRU and LOFT.

### 10-4-3 ZIRLO™

**Model Basis** The ZIRLO™ alloy developed by Westinghouse represents a modification to Zircaloy-4 which was achieved by reducing the tin and iron content, eliminating the chromium, and adding a nominal one percent niobium. Table 10-17 shows a comparison of the two alloys.

Since tin is an alpha phase stabilizer and niobium is a beta phase stabilizer, the reduction in tin and the addition of niobium result in reductions in the temperatures at which the ZIRLO™ alloy undergoes the alpha to beta phase change, relative to Zircaloy-4. Measurements performed by Westinghouse show that the ZIRLO™ alloy starts the transformation at 1023°K and ends at 1213°K.

Since the ZIRLO™ and Zircaloy-4 alloys are both about 98 percent zirconium, it should not be expected that the material properties are significantly different, except to the extent that they are affected by the differences in the phase change temperatures. Density, thermal expansion, thermal conductivity, and specific heat of both alloys have been measured by the Properties Research Laboratory using samples cut from Westinghouse production tubing (Taylor, Groot, and Larimore, 1989). Evaluation of the test results indicated that the materials are sufficiently similar that the Zircaloy-4 material properties can be used for the ZIRLO™ alloy, with the exception of the specific heat (Davidson and Nuhfer, 1990). The specific heat of the ZIRLO™ alloy is based on an adjustment to Table 10-16, which considers the difference in phase change temperatures.

**Density** The (cold) density of the ZIRLO™ cladding material is taken to be identical to that of Zircaloy-4 (409.0 lbm/ft³).

**Thermal Conductivity** The thermal conductivity of the ZIRLO™ cladding material is taken to be identical to that of Zircaloy-4, given by Equation 10-145.

**Specific Heat** The specific heat shown in Table 10-16 for Zircaloy-4 includes both the true specific heat and the alpha to beta phase heat of transformation. The specific heat for the ZIRLO™ cladding material was obtained by adjusting Table 10-15 to account for the difference in phase change temperatures, assuming both the true specific heat and the heat of transformation are the same for the two alloys. The true specific heat is taken to be equal to the total specific heat in Table 10-16 for  $T \leq 1090^\circ\text{K}$ , 0.085 Btu/lbm-°F for  $T \geq 1213^\circ\text{K}$ , and [

$$J^{ac} \quad (10-147)$$

where: [

$$J^{ac} \quad (10-148)$$

WCOBRA/TRAC calculates the specific heat for the ZIRLO™ cladding material using the resulting total specific heat values, shown in Table 10-18.

**Model as Coded** The density, thermal conductivity, and specific heat of the ZIRLO™ cladding material are coded into WCOBRA/TRAC as described above, without modification. Figure 10-33 shows a comparison of specific heat for ZIRLO™ with that of Zircaloy-4.

**Scaling Considerations** Not applicable.

**Conclusions** Comparisons of the material properties for the ZIRLO™ and Zircaloy-4 cladding materials have shown that the Zircaloy-4 relations for density and thermal conductivity can also be applied to the ZIRLO™ alloy. The difference in the phase change temperatures of the two alloys requires that different

specific heat correlations be used. The specific heat correlation for the ZIRLO™ alloy is based on an adjustment to the Zircaloy-4 correlation, which accounts for the different phase change temperature range. This correlation will be used for analyses of nuclear reactors which utilize the ZIRLO™ cladding material.

#### 10-4-4 Fuel Rod Gas Mixtures

**Model Basis** For the gas mixture in the fuel-clad gap, only the thermal conductivity is calculated. The fill gas in the WCOBRA/TRAC fuel rod model assumes that the gas is a mixture composed of helium, xenon, argon, krypton, hydrogen, and nitrogen. The thermal conductivity of the gas mixture as a function of temperature is determined, as described in MATPRO-11 Rev. 1 (Hagrman, Reymann, and Mason, 1980), from the relation

$$k_{gas} = \sum_{i=1}^N \frac{k_i}{1 + \sum_{\substack{j=1 \\ j \neq i}}^N \Psi_{ij} \frac{n_j}{n_i}} \quad (10-149)$$

where N = number of component gases, and where

$$\Psi_{ij} = \Phi_{ij} \left[ 1 + 2.41 \frac{(M_i - M_j)(M_i - 0.142M_j)}{(M_i + M_j)^2} \right] \quad (10-150)$$

and

$$\Phi_{ij} = \frac{\left[ 1 + \left( \frac{k_i}{k_j} \right)^{1/2} \left( \frac{M_i}{M_j} \right)^{1/4} \right]^2}{2^{3/2} \left( 1 + \frac{M_i}{M_j} \right)^{1/2}} \quad (10-151)$$

where:

- $M_i$  = molecular weight of gas species i
- $n_i$  = mole fraction of gas species i
- $k_i$  = thermal conductivity of gas species i

The thermal conductivities of the six component gases are evaluated in Btu/hr-ft-°F as a function of temperature from the following relations:

<u>Gas</u>	<u><math>k(\text{Btu/hr-ft-}^\circ\text{F})</math></u>	
Helium	$(1.314 \times 10^{-3}) T_{\text{gas}}^{0.668}$	(10-152)
Argon	$(1.31 \times 10^{-3}) T_{\text{gas}}^{0.701}$	(10-153)
Krypton	$(1.588 \times 10^{-5}) T_{\text{gas}}^{0.92331}$	(10-154)
Xenon	$(1.395 \times 10^{-5}) T_{\text{gas}}^{0.872}$	(10-155)
Hydrogen	$(5.834 \times 10^{-4}) T_{\text{gas}}^{0.8213}$	(10-156)
Nitrogen	$(7.35 \times 10^{-5}) T_{\text{gas}}^{0.846}$	(10-157)

where  $T_{\text{gas}}$  = gas temperature (°R).

**Model as Coded** Equations 10-149 through 10-151 for gap gas thermal conductivity are coded in WCOBRA/TRAC as described without modification in subroutine GTHCON.

**Scaling Consideration** Not applicable.

**Conclusions** Thermal conductivity for the gas mixture in the fuel-clad gap is calculated using the equations in MATPRO-11 Rev. 1 (Hagman, Reymann, and Mason, 1980).

## 10-5 THERMAL PROPERTIES OF STRUCTURAL MATERIALS

### 10-5-1 Vessel Component Structural Material Properties

**Model Basis** The density, specific heat, and thermal conductivity for structural materials within the vessel are specified by the user for a range of temperatures. Values for each material are obtained from standard references for thermal properties such as Touloukian (1967). When available, material properties provided by the material supplier are used.

**Model as Coded** Values for the material specific heat and thermal conductivity are linearly interpolated with temperature. A warning message is printed if the temperature is outside of the range supplied by the user.

**Scaling Considerations** Not applicable.



**Conclusion** Material thermal properties are supplied by the user. This permits the representation of the material properties by the actual measured values and minimizes uncertainty.

### 10-5-2 One-Dimensional Component Structural Material Properties

**Model Basis** A library of temperature-dependent material properties is incorporated in WCOBRA/TRAC for the one-dimensional components. There are five sets of material properties that make up the library. Each set supplies values for the density, thermal conductivity, specific heat, and spectral emissivity for use in heat transfer calculations. The material sets are for Types 304, 316, and 347 Stainless Steel, Medium Carbon Steel, and Inconel 600.

In the following expressions,

$$\begin{aligned}\rho &= \text{density} \left( \frac{\text{kg}}{\text{m}^3} \right) \\ C_p &= \text{specific heat} \left( \frac{\text{J}}{\text{kg-K}} \right) \\ k &= \text{thermal conductivity} \left( \frac{\text{W}}{\text{m-K}} \right) \\ T_K &= \text{temperature}(\text{K}) \\ T_F &= \text{temperature} (^\circ\text{F})\end{aligned}$$

**Stainless Steel, Type 304** The density is given by

$$\rho(T_F) = 8054.65 - 0.2595T_F \quad (10-158)$$

Specific heat is given by

$$C_p(T_F) = 426.17 + 0.43816T_F - (6.3759 \times 10^{-4})T_F^2 + (4.4803 \times 10^{-7})T_F^3 - (1.0729 \times 10^{-10})T_F^4 \quad (10-159)$$

Thermal conductivity is calculated by

$$k(T_F) = 14.79 + 0.00714T_F \quad (10-160)$$

**Stainless Steel, Type 316** Density is given by

$$\rho(T_K) = 8084.0 - 0.4209T_K - (3.894 \times 10^{-5})T_K^2 \quad (10-161)$$

Specific heat is given by Equation 10-159 and thermal conductivity is given by

$$k(T_K) = 9.248 + 0.01571T_K \quad (10-162)$$

**Stainless Steel, Type 347** The density is assumed constant at

$$\rho = 7913 \frac{\text{kg}}{\text{m}^3} \quad (10-163)$$

The specific heat is given by

$$C_p(T_F) = 502.416 + 0.0984(T_F - 240) \quad (10-164)$$

and the thermal conductivity is

$$k(T_F) = 14.1926 + (7.269 \times 10^{-3})T_F \quad (10-165)$$

**Carbon Steel** The density for carbon steel is assumed constant:

$$\rho = 7855.23 \frac{\text{kg}}{\text{m}^3} \quad (10-166)$$

The specific heat is given by

$$C_p(T_F) = 400.48 + 0.4582T_F - (6.5532 \times 10^{-4})T_F^2 + (5.3706 \times 10^{-7})T_F^3 \quad (10-167)$$

and the thermal conductivity is given by

$$k(T_F) = 48.43 - 0.011366T_F \quad (10-168)$$

**Inconel 600** The density for Inconel 600 is assumed constant,

$$\rho = 8409.45 \frac{\text{kg}}{\text{m}^3} \quad (10-169)$$

The specific heat is given by

$$C_p(T_F) = 4184 \left[ 0.1014456 + (4.378952 \times 10^{-5})T_F - (2.046138 \times 10^{-8})T_F^2 + \right. \\ \left. (3.418111 \times 10^{-11})T_F^3 - (2.060318 \times 10^{-13})T_F^4 + (3.682836 \times 10^{-16})T_F^5 - \right. \\ \left. (2.458648 \times 10^{-19})T_F^6 + (5.597571 \times 10^{-23})T_F^7 \right] \quad (10-170)$$

and thermal conductivity is given by

$$k(T_F) = 1.730 \left[ 8.011332 + (4.643719 \times 10^{-3})T_F + (1.872857 \times 10^{-6})T_F^2 - \right. \\ \left. (3.914512 \times 10^{-9})T_F^3 + (3.475513 \times 10^{-12})T_F^4 - (9.936696 \times 10^{-16})T_F^5 \right] \quad (10-171)$$

**Model as Coded** The correlations described by Equations 10-158 through 10-171 are programmed as shown without modification in subroutine MSTRCT. Curves of specific heat and thermal conductivity as functions of temperature calculated with this subroutine are shown in Figures 10-34 through 10-42.

**Scaling Considerations** Not applicable.

**Conclusions** The WCOBRA/TRAC code uses built-in correlations to calculate the thermal properties of common structural materials modeled by one dimensional components. Comparisons to data show that these correlations provide a good estimate of the properties at low temperature. Since the one-dimensional components generally remain at low temperature during a LOCA transient, use of these correlations introduces only a small uncertainty into the transient calculation.

## 10-6 CONCLUSIONS

WCOBRA/TRAC routines provide appropriate means for calculation of thermodynamic and transport properties of liquid water, steam, and air for the vessel component and for one-dimensional components. Routines to calculate properties of fuel rod materials, i.e., fuel, cladding, and gap gas, are also included. Properties of structural materials in the vessel component are interpolated from user-provided tables. For one-dimensional components, routines to calculate properties of common structural materials are included. The routines generally calculate properties in the form of equations, for example as functions of temperature and pressure, or by linear interpolation in built-in tables. These property calculations have been compared with standard references and found to agree satisfactorily over the range of conditions expected for PWR LOCA calculations. No scaling uncertainty is required for the use of these models in reactor analysis.

## 10-7 REFERENCES

ASME Steam Tables, 1968, American Society of Mechanical Engineers, 2nd Edition.

ASME Steam Tables, 1983, Thermodynamic and Transport Properties of Steam, 5th ed., The American Society of Mechanical Engineers, New York.

Coffman, W. A. and Lynn, L. L., 1966, "WATER: A Large Range Thermodynamic and Transport Water Property FORTRAN-IV Computer Program," Bettis Atomic Power Laboratory Report WAPD-TM-568.

Davidson, S. L. and Nuhfer, D. L. (Eds.), 1990, "VANTAGE+ Fuel Assembly Reference Core Report," WCAP-12610, Westinghouse Electric Corporation, Pittsburgh, Pennsylvania. [PROPRIETARY].

Haar, L., Gallagher, J. S., and Kell, G. S., 1984, NBS/NRC Steam Tables, Hemisphere Publishing Corporation, New York.

Hagman, D. L., Reymann, G. A., and Mason, R. E., 1980, "MATPRO - Version 11 (Revision 1): A Handbook of Materials Properties for Use in the Analysis of Light Water Reactor Fuel Rod Behavior," USNRC Report NUREG/CR-0497, TREE-1280, Revision 1.

Keenan, J. H. and Keyes, F. G., 1936, Thermodynamic Properties of Steam, John Wiley & Sons, New York.

MacDonald, P. E., et al., 1976, "MATPRO - Version 9: A Handbook of Materials Properties for Use in the Analysis of Light Water Reactor Fuel Rod Behavior," Idaho National Engineering Laboratories, TREE-NUREG-1005.

McClintock, R. B. and Silvestri, G. J., 1936, Formulations and Iterative Procedures for the Calculation of Properties of Steam, American Society of Mechanical Engineers.

McFadden, J. H., et al., 1980, "RETRAN-02 A Program for Transient Thermal-Hydraulic Analysis of Complex Fluid Flow Systems, Volume 1: Equations and Numbers," Report NP-850, Electric Power Research Institute, Palo Alto, California.

Rivard, W. C. and Torrey, M. D., 1975, "Numerical Calculation of Flashing from Long Pipes Using a Two-Field Model," Los Alamos Scientific Laboratory Report LA-6104-MS.

Taylor, R. E., Groot, H., and Larimore, J., 1989, "Thermophysical Properties of ZR-4 and ZIRLO," PRL-820, Properties Research Laboratory, West Lafayette, Indiana. [PROPRIETARY].

Touloukian, Y. S., 1967, Thermophysical Properties of High Temperature Materials, Thermophysical Properties Research Center, Purdue University, The Macmillan Co., New York.

**Table 10-1 Constants for Saturated Liquid Enthalpy**

$\Lambda_n$	Pressure:		
	$0.1 \leq P < 898.7$	$898.7 \leq P < 2529.9$	$2529.9 \leq 3208$
1	0.6970887859E+02	0.8408618802E+06	0.9060030436E+03
2	0.3337529994E+02	0.3637413208E+06	-0.1426813520E+02
3	0.2318240735E+01	-0.4634506669E+06	0.1522233257E+01
4	0.1840599513E+00	0.1130306339E+06	-0.6973992961E+00
5	-0.5245502294E-02	-0.4350217298E+03	0.1743091663E+00
6	0.2878007027E-02	-0.3898988188E+04	-0.2319717696E-01
7	0.1753652324E-02	0.6697399434E+03	0.1694019149E-02
8	-0.4334859620E-03	-0.4730726377E+02	-0.6454771710E-04
9	0.3325699282E-04	0.1265125057E+01	0.1003003098E-05

**Table 10-2 Constants for Saturated Vapor Enthalpy**

$B_n$	Pressure:		
	$P < 1467.6$	$1467.6 \leq P < 2586.0$	$2586.0 \leq 3208.0$
1	0.1105836875E+04	0.5918671729E+06	0.9059978254E+03
2	0.1436943768E+02	-0.2559433320E+06	0.5561957539E+01
3	0.8018288621E+00	0.3032474387E+05	0.3434189609E+01
4	0.1617232913E-01	0.4109051958E+01	-0.6406390628E+00
5	-0.1501147505E-02	0.3475066877E+00	0.5918579484E-01
6	-0.1237675562E-04	-0.3026047262E+00	-0.2725378570E-02
7	0.3004773304E-05	-0.1022018012E+02	0.5006336938E-04
8	-0.2062390734E-06	0.1591215116E+01	0.0
9	0.0	-0.6768383759E-01	0.0

$P_{sat}$ (psia)	$T_{sat}$ (°F)	$\rho_f$ (lbm/ft <sup>3</sup> )	$\rho_g$ (lbm/ft <sup>3</sup> )	$H_f$ (Btu/lbm)	$H_g$ (Btu/lbm)	$\mu_f$ (lbm/hr/ft)	$\mu_g$ (lbm/hr/ft)	$k_f$ (Btu/hr/ft/F)	$k_g$ (Btu/hr/ft/F)	$C_{pf}$ (Btu/lbm/F)	$C_{pg}$ (Btu/lbm/F)	$\sigma$ (lb/ft)
0.1	41.97	62.42	0.000	10.00	1079.83	3.61570	0.02262	0.33023	0.01002	1.00440	0.44426	0.00513
0.2	51.93	62.40	0.001	20.00	1084.18	3.06850	0.02295	0.33627	0.01022	1.00320	0.44477	0.00508
0.3	61.91	62.36	0.001	30.00	1088.55	2.64160	0.02331	0.34218	0.01041	1.00140	0.44542	0.00502
0.4	71.90	62.29	0.001	40.00	1092.92	2.30190	0.02368	0.34791	0.01062	0.99975	0.44623	0.00496
0.5	81.91	62.20	0.002	50.00	1097.28	2.02710	0.02406	0.35338	0.01083	0.99851	0.44723	0.00491
0.7	91.93	62.09	0.002	60.00	1101.62	1.80170	0.02445	0.35848	0.01105	0.99776	0.44844	0.00484
1.0	101.95	61.97	0.003	70.00	1105.94	1.61440	0.02485	0.36334	0.01128	0.99743	0.44988	0.00478
1.4	111.98	61.83	0.004	80.00	1110.23	1.45700	0.02526	0.36765	0.01152	0.99745	0.45157	0.00472
1.8	122.00	61.68	0.005	90.00	1114.49	1.32340	0.02568	0.37183	0.01177	0.99774	0.45353	0.00465
2.3	132.02	61.52	0.007	100.00	1118.70	1.20900	0.02611	0.37530	0.01203	0.99823	0.45577	0.00459
3.0	142.04	61.34	0.009	110.00	1122.86	1.11020	0.02654	0.37863	0.01230	0.99888	0.45832	0.00452
3.9	152.04	61.15	0.011	120.00	1126.97	1.02440	0.02698	0.38146	0.01258	0.99965	0.46117	0.00445
5.0	162.04	60.95	0.014	130.00	1131.04	0.94915	0.02742	0.38403	0.01287	1.00050	0.46435	0.00438
6.3	172.02	60.75	0.017	140.00	1135.03	0.88297	0.02787	0.38624	0.01318	1.00150	0.46786	0.00432
7.9	182.01	60.53	0.021	150.00	1138.98	0.82425	0.02832	0.38814	0.01349	1.00270	0.47172	0.00424
9.7	191.96	60.31	0.025	160.00	1142.85	0.77208	0.02877	0.38984	0.01381	1.00390	0.47591	0.00417
12.0	201.92	60.07	0.031	170.00	1146.66	0.72533	0.02923	0.39115	0.01415	1.00530	0.48047	0.00410
14.7	211.84	59.83	0.037	180.00	1150.39	0.68345	0.02969	0.39236	0.01449	1.00690	0.48538	0.00403
17.8	221.78	59.58	0.045	190.00	1154.05	0.64561	0.03015	0.39320	0.01486	1.00860	0.49067	0.00396
21.4	231.66	59.32	0.053	200.00	1157.62	0.61149	0.03061	0.39397	0.01523	1.01050	0.49633	0.00388
25.7	241.55	59.05	0.063	210.00	1161.12	0.58043	0.03107	0.39444	0.01561	1.01260	0.50239	0.00381
30.6	251.39	58.78	0.074	220.00	1164.50	0.55228	0.03153	0.39481	0.01601	1.01490	0.50882	0.00373
36.2	261.22	58.50	0.087	230.00	1167.79	0.52655	0.03199	0.39496	0.01642	1.01740	0.51569	0.00366

**Table 10-3 Vessel Component Saturated Water Thermal Properties**  
(cont)

$P_{sat}$ (psia)	$T_{sat}$ (°F)	$\rho_f$ (lbm/ft <sup>3</sup> )	$\rho_g$ (lbm/ft <sup>3</sup> )	$H_f$ (Btu/lbm)	$H_g$ (Btu/lbm)	$\mu_f$ (lbm/hr/ft)	$\mu_g$ (lbm/hr/ft)	$k_f$ (Btu/hr/ft/F)	$k_g$ (Btu/hr/ft/F)	$C_{pf}$ (Btu/lbm/F)	$C_{pg}$ (Btu/lbm/F)	$\sigma$ (lb/ft)
42.5	271.02	58.21	0.101	240.00	1170.98	0.50302	0.03245	0.39498	0.01684	1.02010	0.52299	0.00358
49.8	280.80	57.92	0.117	250.00	1174.05	0.48145	0.03291	0.39485	0.01727	1.02300	0.53075	0.00351
58.0	290.54	57.61	0.135	260.00	1177.01	0.46163	0.03337	0.39456	0.01772	1.02610	0.53899	0.00343
67.2	300.26	57.30	0.155	270.00	1179.84	0.44339	0.03383	0.39418	0.01817	1.02940	0.54775	0.00335
77.6	309.93	56.99	0.177	280.00	1182.54	0.42656	0.03429	0.39358	0.01864	1.03290	0.55706	0.00327
89.1	319.58	56.66	0.202	290.00	1185.10	0.41101	0.03474	0.39293	0.01912	1.03670	0.56696	0.00320
101.8	329.19	56.34	0.229	300.00	1187.53	0.39661	0.03520	0.39205	0.01962	1.04060	0.57748	0.00312
116.0	338.76	56.00	0.260	310.00	1189.82	0.38325	0.03565	0.39113	0.02012	1.04470	0.58869	0.00304
131.6	348.28	55.66	0.293	320.00	1191.95	0.37083	0.03610	0.39000	0.02064	1.04910	0.60063	0.00296
148.6	357.77	55.31	0.329	330.00	1193.94	0.35927	0.03655	0.38882	0.02116	1.05380	0.61336	0.00288
167.4	367.21	54.95	0.368	340.00	1195.77	0.34849	0.03699	0.38743	0.02170	1.05870	0.62693	0.00280
187.8	376.61	54.59	0.411	350.00	1197.44	0.33842	0.03744	0.38597	0.02225	1.06390	0.64141	0.00272
210.0	385.96	54.22	0.458	360.00	1198.96	0.32898	0.03788	0.38435	0.02281	1.06940	0.65687	0.00264
234.0	395.26	53.85	0.508	370.00	1200.30	0.32014	0.03832	0.38265	0.02338	1.07530	0.67338	0.00256
260.0	404.50	53.47	0.563	380.00	1201.48	0.31182	0.03876	0.38078	0.02396	1.08150	0.69101	0.00248
288.0	413.69	53.08	0.622	390.00	1202.49	0.30399	0.03920	0.37881	0.02455	1.08820	0.70984	0.00240
318.1	422.83	52.69	0.686	400.00	1203.32	0.29660	0.03964	0.37667	0.02516	1.09540	0.72995	0.00232
350.4	431.90	52.29	0.755	410.00	1203.97	0.28961	0.04008	0.37441	0.02578	1.10300	0.75144	0.00224
384.9	440.91	51.88	0.828	420.00	1204.44	0.28299	0.04052	0.37199	0.02642	1.11130	0.77439	0.00216
421.6	449.86	51.47	0.907	430.00	1204.71	0.27670	0.04095	0.36946	0.02707	1.12010	0.79891	0.00208
460.7	458.73	51.05	0.992	440.00	1204.79	0.27072	0.04139	0.36679	0.02773	1.12970	0.82510	0.00200
502.1	467.53	50.62	1.082	450.00	1204.67	0.26501	0.04183	0.36401	0.02841	1.13990	0.85307	0.00192

**Table 10-3 Vessel Component Saturated Water Thermal Properties**  
(cont)

$P_{sat}$ (psia)	$T_{sat}$ (°F)	$\rho_f$ (lbm/ft <sup>3</sup> )	$\rho_g$ (lbm/ft <sup>3</sup> )	$H_f$ (Btu/lbm)	$H_g$ (Btu/lbm)	$\mu_f$ (lbm/hr/ft)	$\mu_g$ (lbm/hr/ft)	$k_f$ (Btu/hr/ft/F)	$k_g$ (Btu/hr/ft/F)	$C_{pf}$ (Btu/lbm/F)	$C_{pg}$ (Btu/lbm/F)	$\sigma$ (lb/ft)
546.0	476.26	50.18	1.178	460.00	1204.34	0.25954	0.04227	0.36106	0.02912	1.15100	0.88295	0.00185
592.2	484.91	49.74	1.281	470.00	1203.79	0.25431	0.04271	0.35800	0.02984	1.16290	0.91488	0.00177
641.2	493.51	49.29	1.391	480.00	1203.02	0.24926	0.04315	0.35472	0.03059	1.17590	0.94916	0.00169
692.1	501.94	48.84	1.507	490.00	1202.04	0.24444	0.04359	0.35138	0.03136	1.18980	0.98549	0.00161
745.9	510.35	48.37	1.631	500.00	1200.81	0.23976	0.04404	0.34782	0.03218	1.20490	1.02460	0.00154
802.0	518.65	47.90	1.762	510.00	1199.35	0.23524	0.04450	0.34426	0.03300	1.22130	1.06650	0.00146
860.5	526.84	47.42	1.901	520.00	1197.64	0.23086	0.04495	0.34043	0.03390	1.23890	1.11140	0.00139
921.3	534.91	46.93	2.048	530.00	1195.69	0.22662	0.04541	0.33660	0.03480	1.25800	1.15940	0.00132
984.4	542.86	46.44	2.204	540.00	1193.50	0.22250	0.04588	0.33255	0.03581	1.27870	1.21100	0.00124
1050.0	550.72	45.93	2.368	550.00	1191.03	0.21846	0.04636	0.32846	0.03684	1.30120	1.26690	0.00117
1117.8	558.47	45.42	2.543	560.00	1188.31	0.21452	0.04685	0.32427	0.03795	1.32560	1.32710	0.00111
1187.8	566.10	44.89	2.727	570.00	1185.33	0.21067	0.04734	0.31999	0.03915	1.35220	1.39240	0.00104
1259.9	573.61	44.36	2.922	580.00	1182.08	0.20689	0.04785	0.31571	0.04038	1.38120	1.46330	0.00097
1334.0	580.98	43.82	3.127	590.00	1178.57	0.20318	0.04837	0.31134	0.04174	1.41290	1.54050	0.00091
1410.0	588.22	43.27	3.344	600.00	1174.80	0.19953	0.04891	0.30694	0.04324	1.44770	1.62510	0.00084
1487.8	595.33	42.71	3.574	610.00	1170.75	0.19594	0.04946	0.30255	0.04486	1.48590	1.71800	0.00078
1567.2	602.29	42.14	3.816	620.00	1166.42	0.19239	0.05004	0.29817	0.04663	1.52810	1.82060	0.00073
1648.2	609.11	41.56	4.072	630.00	1161.76	0.18889	0.05063	0.29382	0.04854	1.57490	1.93450	0.00067
1730.4	615.77	40.96	4.343	640.00	1156.76	0.18543	0.05125	0.28954	0.05069	1.62710	2.06150	0.00061
1813.8	622.28	40.36	4.629	650.00	1151.40	0.18200	0.05190	0.28531	0.05307	1.68570	2.20410	0.00056
1898.2	628.62	39.74	4.931	660.00	1145.66	0.17859	0.05258	0.28115	0.05565	1.75180	2.36520	0.00051
1983.9	634.84	39.11	5.253	670.00	1139.49	0.17518	0.05330	0.27709	0.05848	1.82770	2.55010	0.00046
2069.5	640.84	38.47	5.593	680.00	1132.96	0.17181	0.05405	0.27314	0.06173	1.91440	2.76120	0.00042



**Table 10-3 Vessel Component Saturated Water Thermal Properties**  
(cont)

$P_{sat}$ (psia)	$T_{sat}$ (°F)	$\rho_f$ (lbm/ft <sup>3</sup> )	$\rho_g$ (lbm/ft <sup>3</sup> )	$H_f$ (Btu/lbm)	$H_g$ (Btu/lbm)	$\mu_f$ (lbm/hr/ft)	$\mu_g$ (lbm/hr/ft)	$k_f$ (Btu/hr/ft/F)	$k_g$ (Btu/hr/ft/F)	$C_{pf}$ (Btu/lbm/F)	$C_{pg}$ (Btu/lbm/F)	$\sigma$ (lb/ft)
2155.4	646.65	37.81	5.953	690.00	1126.01	0.16845	0.05485	0.26926	0.06527	2.01490	3.00550	0.00037
2241.1	652.28	37.14	6.335	700.00	1118.63	0.16509	0.05570	0.26545	0.06919	2.13280	3.29110	0.00033
2326.3	657.69	36.46	6.740	710.00	1110.82	0.16173	0.05661	0.26186	0.07374	2.27250	3.62830	0.00029
2410.6	662.89	35.76	7.170	720.00	1102.59	0.15837	0.05758	0.25836	0.07854	2.44030	4.03110	0.00025
2494.0	667.89	35.03	7.630	730.00	1093.91	0.15497	0.05863	0.25520	0.08401	2.64650	4.52210	0.00022
2575.2	672.62	34.29	8.117	740.00	1084.90	0.15156	0.05975	0.25212	0.08983	2.90110	5.12290	0.00019
2653.8	677.08	33.53	8.635	750.00	1075.52	0.14813	0.06096	0.24935	0.09704	3.22290	5.87350	0.00016
2729.8	681.29	32.75	9.190	760.00	1065.74	0.14464	0.06228	0.24673	0.10465	3.64070	6.14500	0.00013
2801.8	685.18	31.95	9.777	770.00	1055.59	0.14113	0.06371	0.24493	0.11447	4.19150	6.14500	0.00011
2869.6	688.77	31.12	10.403	780.00	1045.00	0.13755	0.06526	0.24313	0.12429	4.94400	6.14500	0.00008
2931.9	692.01	30.27	11.066	790.00	1034.06	0.13393	0.06694	0.24418	0.13890	5.99630	6.14500	0.00007
2988.5	694.90	29.39	11.771	800.00	1022.75	0.13024	0.06878	0.24576	0.15442	6.14500	6.14500	0.00005
3038.4	697.40	28.48	12.513	810.00	1011.17	0.12649	0.07076	0.24734	0.16993	6.14500	6.14500	0.00004
3081.4	699.53	27.55	13.293	820.00	999.32	0.12268	0.07291	0.25288	0.19158	6.14500	6.14500	0.00002
3116.7	701.26	26.60	14.101	830.00	987.40	0.11885	0.07520	0.26470	0.22270	6.14500	6.14500	0.00002
3144.7	702.62	25.63	14.927	840.00	975.50	0.11500	0.07761	0.29237	0.27220	6.14500	6.14500	0.00001
3165.7	703.63	24.65	15.750	850.00	963.98	0.11119	0.08008	0.81017	0.80644	6.14500	6.14500	0.00000
3180.5	704.34	23.68	16.541	860.00	953.38	0.10744	0.08253	2.55507	2.55265	6.14500	6.14500	0.00000
3190.3	704.81	22.72	17.243	870.00	944.22	0.10382	0.08475	4.29997	4.29886	6.14500	6.14500	0.00000
3196.0	705.08	21.78	17.759	880.00	937.47	0.10034	0.08642	10.00000	10.00000	6.14500	6.14500	0.00000
3198.3	705.19	20.87	17.987	890.00	934.25	0.09704	0.08717	50.00000	50.00000	6.14500	6.14500	0.00000
3206.4	705.39	20.16	19.244	900.00	917.46	0.09704	0.08717	100.00000	100.00000	6.14500	6.14500	0.00000

Table 10-4 Superheated Vapor Temperature Constants		
Term	$P \leq 1000$ psia or $P > 1000$ psia and $h \geq 1280$ Btu/lbm	$P > 1000$ psia and $H_v < 1280$ Btu/lbm
$A_1$	-1.0659659E+04	-4.5298646E+03
$A_2$	2.0110905E+01	1.5358850E+01
$A_3$	-1.250954E-02	-1.5655537E-02
$A_4$	2.8274992E-06	5.2687849E-06
$A_5$	4.9815820	4.4185386E-01
$A_6$	-7.7618225E-06	-9.1654905E-06
$A_7$	2.4391612E-10	2.7549766E-10
$A_8$	-9.8147341E-03	-1.1541553E-03
$A_9$	6.5824890E-06	1.2384560E-06
$A_{10}$	-1.4749938E-09	-4.1724604E-10
$B_1$	-2.8557816	1.2659960E+02
$B_2$	1.3250230E-02	-2.5611614E-01
$B_3$	-1.0521514E-05	2.2270593E-04
$B_4$	2.5007955E-09	-5.9928922E-08
$B_5$	-3.4620214	-2.1818030E+01
$B_6$	-3.6261637E-02	1.3424036
$B_7$	7.3529479E-04	-4.9110372E-02
$B_8$	5.7703098E-03	2.7966370E-02
$B_9$	-2.9972073E-06	-2.4665012E-05
$B_{10}$	5.2037300E-10	6.7723080E-09

Table 10-5 Subcooled Water Density Constants					
$C_{cxy}$					
$i=$	1	2	3	4	5
$j=1$	-0.413450E1	0.13252E-4	0.15812E-5	-0.21959E-8	0.21683E-11
$j=2$	-0.59428E-5	0.63377E-7	-0.39974E-9	0.69391E-12	-0.36159E-15
$j=3$	0.15681E-8	-0.40711E-10	0.25401E-12	-0.52372E-15	0.32503E-18

Table 10-6 Saturated Steam Internal Energy Constants				
$i$	$P$	$AVE(i)$	$BVE(i)$	$CVE(i)$
1	$\leq 2E+6$	2.619410618E+6	-4.995E+10	--
2	$> 2E+6$	2.5896E+6	6.350E-3	-1.0582E-9

Table 10-7 Saturated Steam Enthalpy Constants				
$i$	$P$	$AVG(i)$	$BVG(i)$	$CVG(i)$
1	$\leq 2E+6$	1.06655448	1.02E-8	-2.548E-15
2	$> 2E+6$	1.0764	3.625E-10	-9.063E-17

**Table 10-8 Saturated Liquid Internal Energy Constants**

<i>i</i>	<i>ALE(i)</i>	<i>BLE(i)</i>	<i>CLE(i)</i>	<i>DLE(i)</i>	<i>ELE(i)</i>
1	1.75880E+4	3.7402E+3	4.02435	-0.0157294	3.1301E-5
2	6.18527E+6	-8.14547E+4	4.46598E+2	-1.04116	9.26022E-4
3	2.283789029E+9	-2.62215677E+7	1.12948667E+5	-2.16233985E+2	0.155283438

**Table 10-9 Constants for Specific Heat**

$B_{0f} = 2.394907 \times 10^{-4}$	$B_{1f} = -5.196250 \times 10^{-13}$	$C_{1f} = 1.68835968 \times 10^3$
$C_{0f} = 1.193203 \times 10^{-11}$	$C_{1f} = 2.412704 \times 10^{-18}$	$C_{2f} = 0.6029856$
$D_{0f} = -3.944067 \times 10^{-17}$	$D_{1f} = -1.680771 \times 10^{-24}$	$C_{3f} = 4.820979623 \times 10^2$
		$C_{4f} = 2.95317905 \times 10^7$
		$C_{5f} = 1.8$
		$C_{6f} = 4.60 \times 10^2$

Table 10-10 Liquid Viscosity Constants	
$A_{0t} = 1.299470299 \times 10^{-3}$ $A_{1t} = -9.264032108 \times 10^{-4}$ $A_{2t} = 3.81047061 \times 10^{-4}$ $A_{3t} = -8.219444458 \times 10^{-5}$ $A_{4t} = 7.022437984 \times 10^{-6}$	$B_{0t} = -6.5959 \times 10^{-12}$ $B_{1t} = 6.763 \times 10^{-12}$ $B_{2t} = -2.88825 \times 10^{-12}$ $B_{3t} = 4.4525 \times 10^{-13}$
$D_{0t} = 3.026032306 \times 10^{-4}$ $D_{1t} = -1.836606896 \times 10^{-4}$ $D_{2t} = 7.567075775 \times 10^{-5}$ $D_{3t} = -1.647878879 \times 10^{-5}$ $D_{4t} = 1.416457633 \times 10^{-6}$	$E_{0t} = 1.4526052612 \times 10^{-3}$ $E_{1t} = -6.9880084985 \times 10^{-9}$ $E_{2t} = 1.5210230334 \times 10^{-14}$ $E_{3t} = -1.2303194946 \times 10^{-20}$
$F_{0t} = -3.8063507533 \times 10^{-11}$ $F_{1t} = 3.9285207677 \times 10^{-16}$ $F_{2t} = -1.2585799292 \times 10^{-21}$ $F_{3t} = 1.2860180788 \times 10^{-27}$	$H_o = 8.581289699 \times 10^{-6}$ $c_{on} = 4.265884 \times 10^4$ $P_o = 6.894575293 \times 10^5$
$H_{oo} = 3.892077365 \times 10^{-6}$ $e_{on} = 5.53588 \times 10^4$	$e_{ho} = 6.484503981 \times 10^{-6}$ $c_n = 4.014676 \times 10^5$

**Table 10-11 Vapor Viscosity Constants**

$A_{0v} = 3.53 \times 10^{-8}$ $A_{1v} = 6.765 \times 10^{-11}$ $A_{2v} = 1.021 \times 10^{-14}$	$B_{1v} = 0.407 \times 10^{-7}$ $C_{1v} = 8.04 \times 10^{-6}$ $D_{1v} = 1.858 \times 10^{-7}$ $E_{1v} = 5.9 \times 10^{-10}$
$F_{0v} = -0.2885 \times 10^{-5}$ $F_{1v} = 0.2427 \times 10^{-7}$ $F_{2v} = -0.6789333333 \times 10^{-10}$ $F_{3v} = 0.6317037037 \times 10^{-13}$	$G_{0v} = 0.176 \times 10^3$ $G_{1v} = -1.6$ $G_{2v} = 0.0048$ $G_{3v} = -0.47407407407 \times 10^{-5}$

**Table 10-12 Liquid and Vapor Thermal Conductivity Constants**

$A_{t0} = 0.573738622$ $A_{t1} = 0.2536103551$ $A_{t2} = -0.145468269$ $A_{t3} = 0.01387472485$ $A_{t4} = 5.815 \times 10^5$	$A_{v0} = 1.76 \times 10^{-2}$ $A_{v1} = 5.87 \times 10^{-5}$ $A_{v2} = 1.04 \times 10^{-7}$ $A_{v3} = -4.51 \times 10^{-11}$ $A_{v4} = 2.1482 \times 10^5$	$B_{v0} = 1.0351 \times 10^{-4}$ $B_{v1} = 0.4198 \times 10^{-6}$ $B_{v2} = -2.771 \times 10^{-11}$
--	---	---

**Table 10-13 Surface Tension Constants**

$a_1 = 1.160936807E-04$ $a_2 = 1.12140468E-06$ $a_3 = -5.752805180E-09$ $a_4 = 1.286274650E-11$ $a_5 = -1.149719290E-14$
--

**Table 10-14** Constants for Specific Heat of Air

$i$	$A_i$	$B_i$
1	-4.20419E-05	7.71027E-05
2	9.61128E-08	-8.56726E-09
3	-1.16383E-11	-4.75772E-12

**Table 10-15** Constants for Viscosity of Air

$i$	$a_{ai}$	$a_{bi}$
0	$1.708 \times 10^{-5}$	$1.735 \times 10^{-5}$
1	$5.927 \times 10^{-8}$	$4.193 \times 10^{-8}$
2	$-8.14 \times 10^{-11}$	$-1.09 \times 10^{-11}$

**Table 10-16**    **Specific Heat of Zircaloy-4**

<b>T(°K)</b>	<b>C<sub>p</sub> (Btu/lbm - °F)</b>
300.0	0.0671
400.0	0.0721
640.0	0.0790
1090.0	0.0896
1093.0	0.1199
1113.0	0.1409
1133.0	0.1469
1153.0	0.1717
1173.0	0.1949
1193.0	0.1839
1213.0	0.1478
1233.0	0.1120
1248.0	0.0850
>1248.0	0.0850





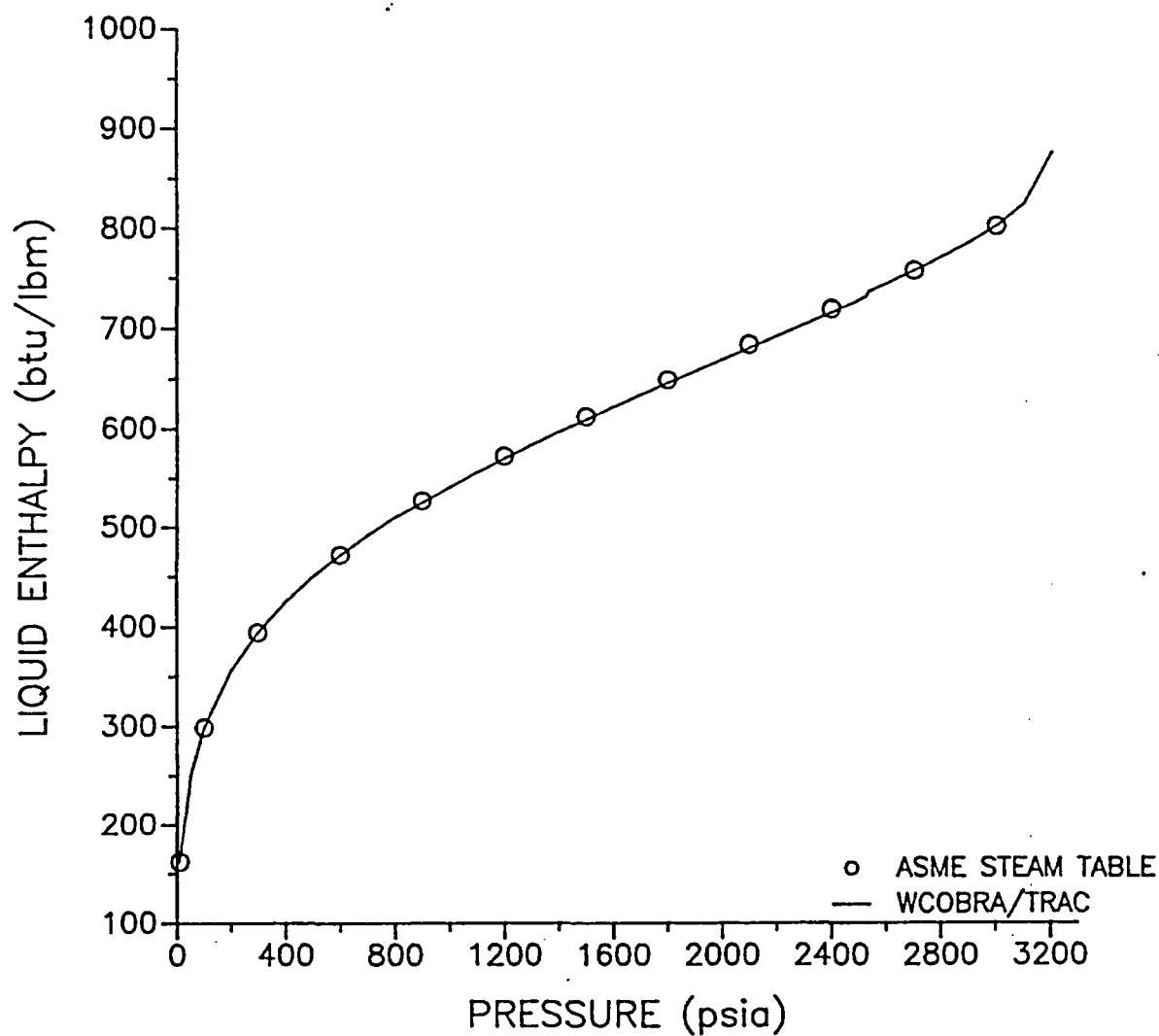


Figure 10-1. WCOBRA/TRAC Vessel Component Saturated Liquid Enthalpy Function

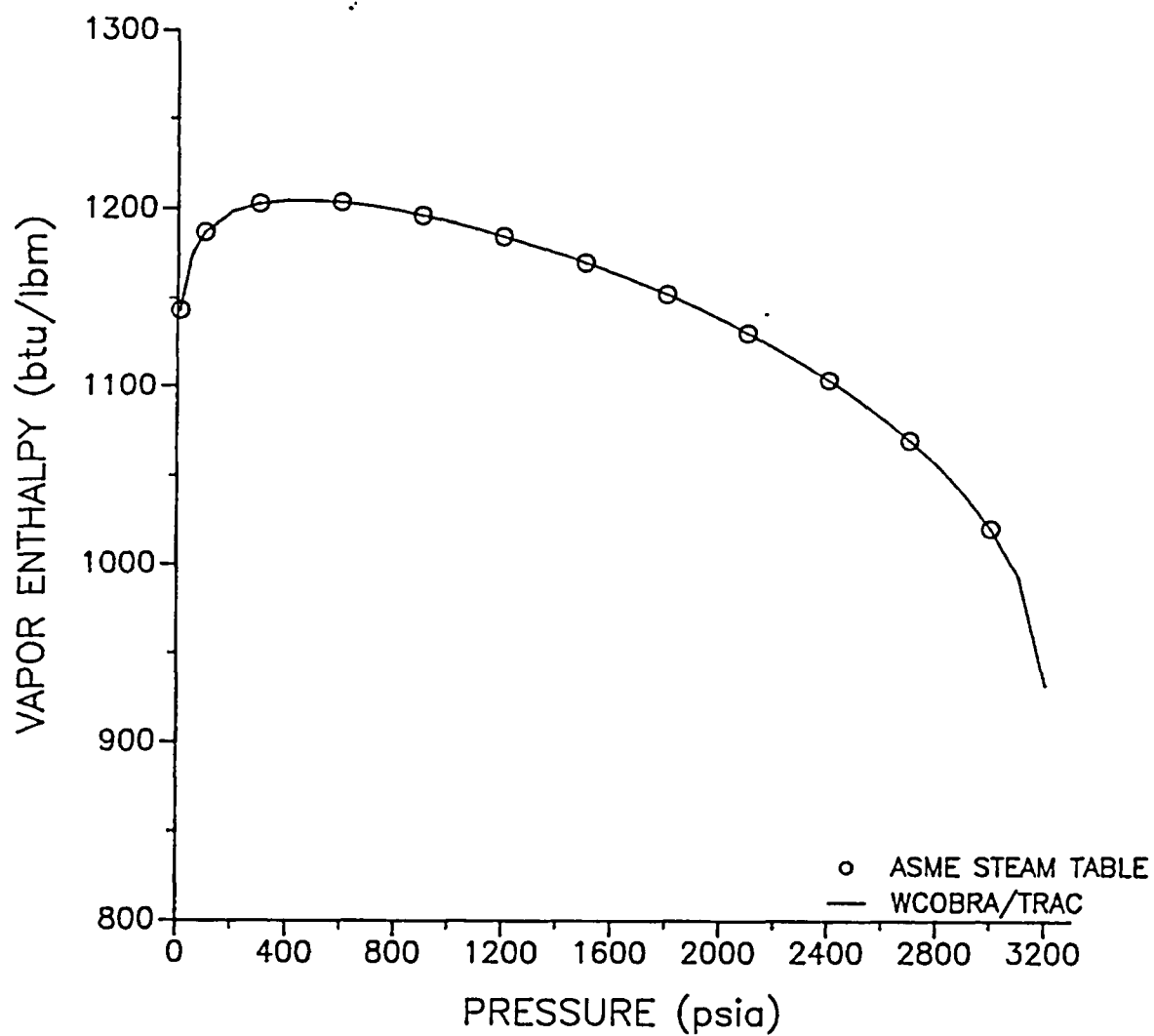


Figure 10-2. WCOBRA/TRAC Vessel Component Saturated Vapor Enthalpy Function

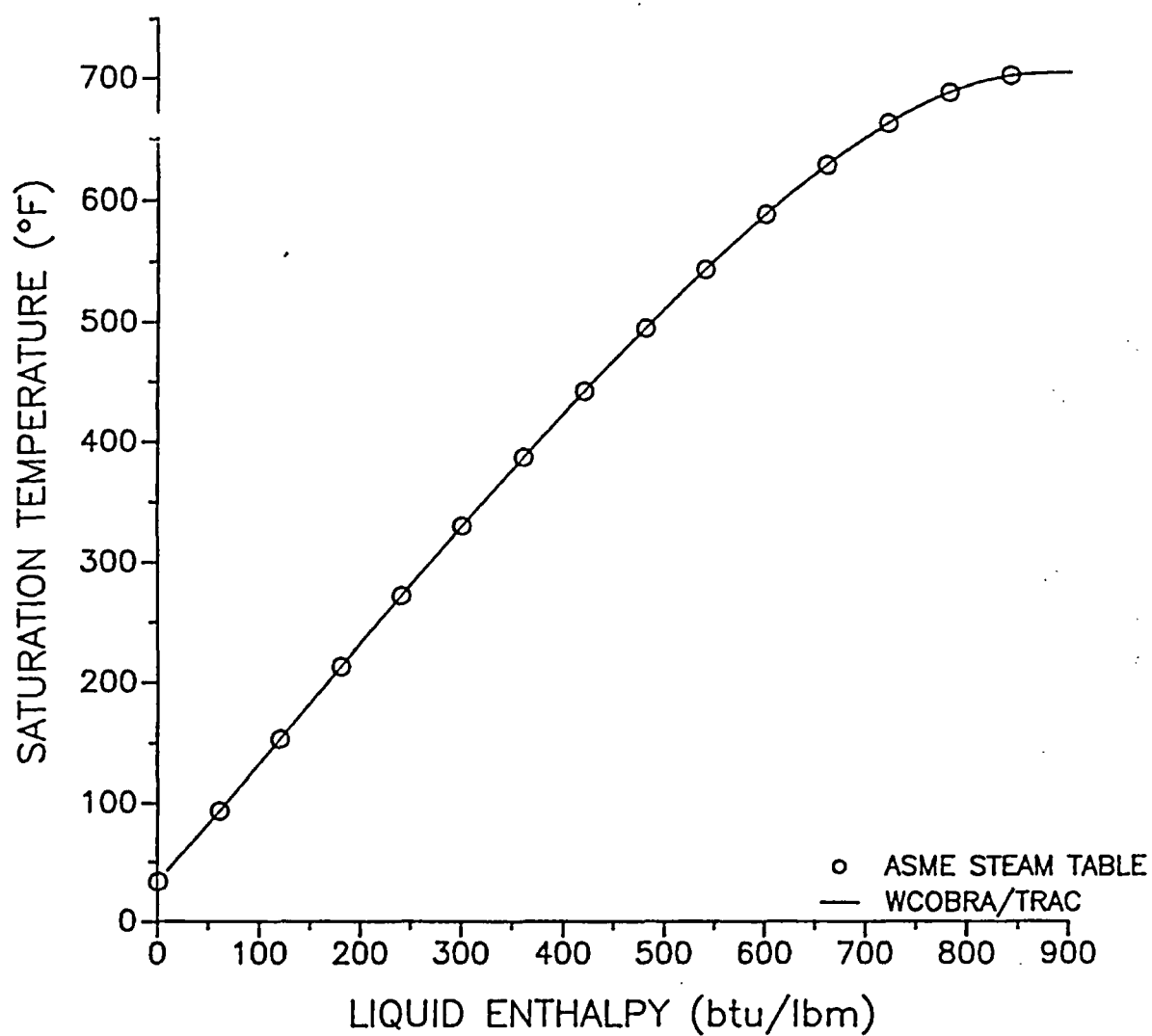


Figure 10-3. WCOBRA/TRAC Vessel Component Saturation Temperature

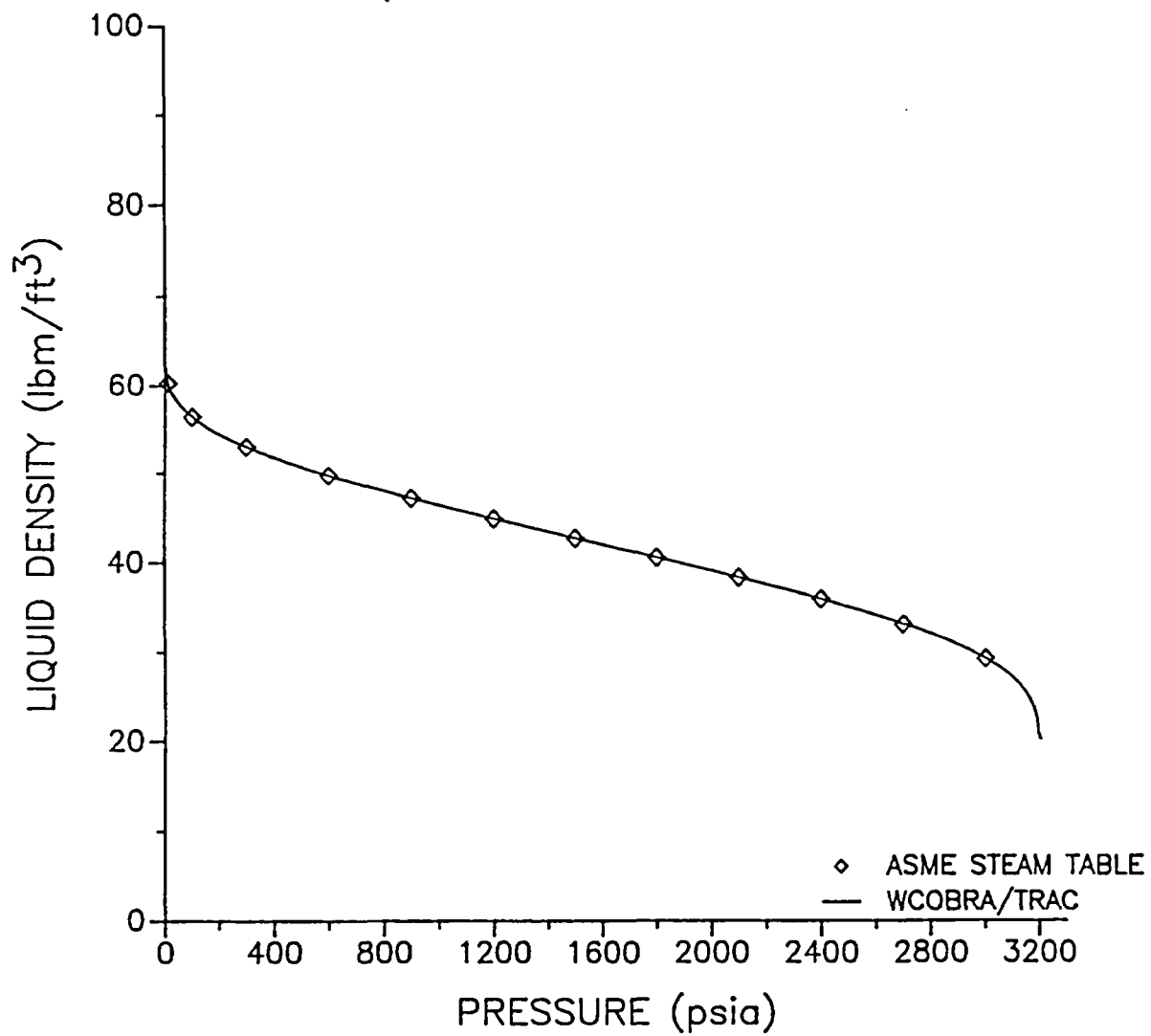


Figure 10-4. WCOBRA/TRAC Vessel Component Saturated Liquid Density

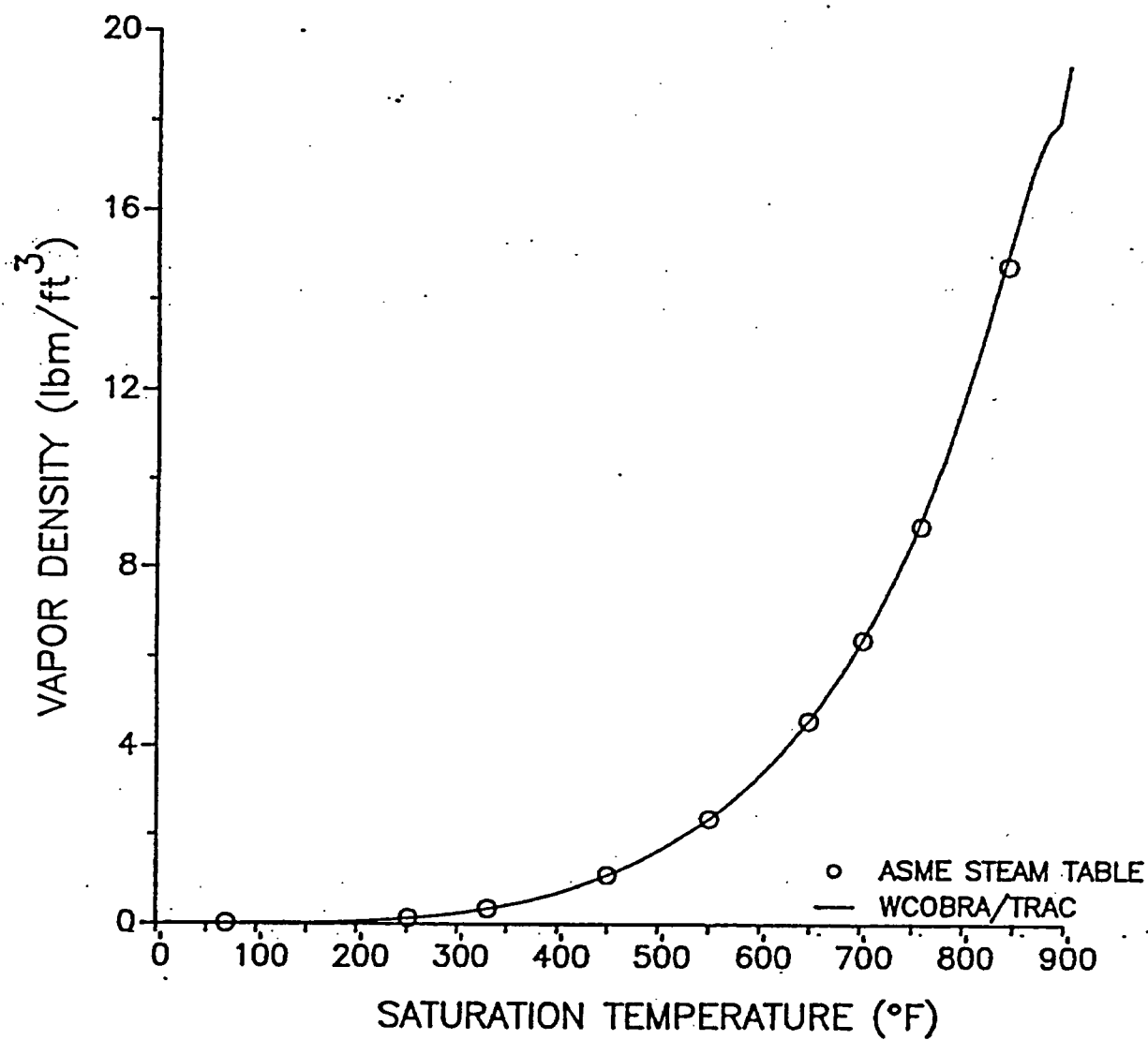


Figure 10-5. WCOBRA/TRAC Vessel Component Saturated Vapor Density

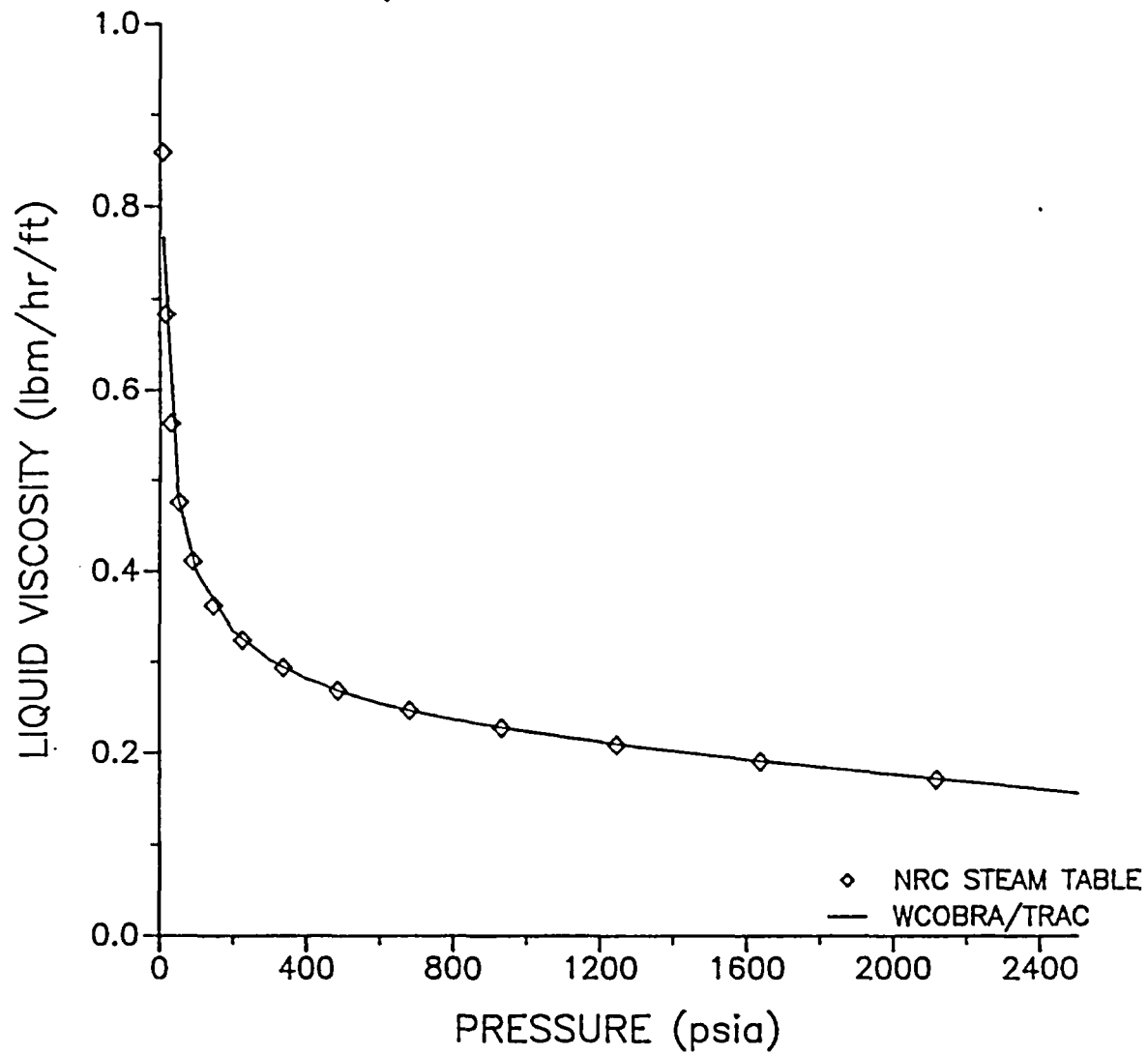


Figure 10-6. WCOBRA/TRAC Vessel Component Saturated Liquid Viscosity

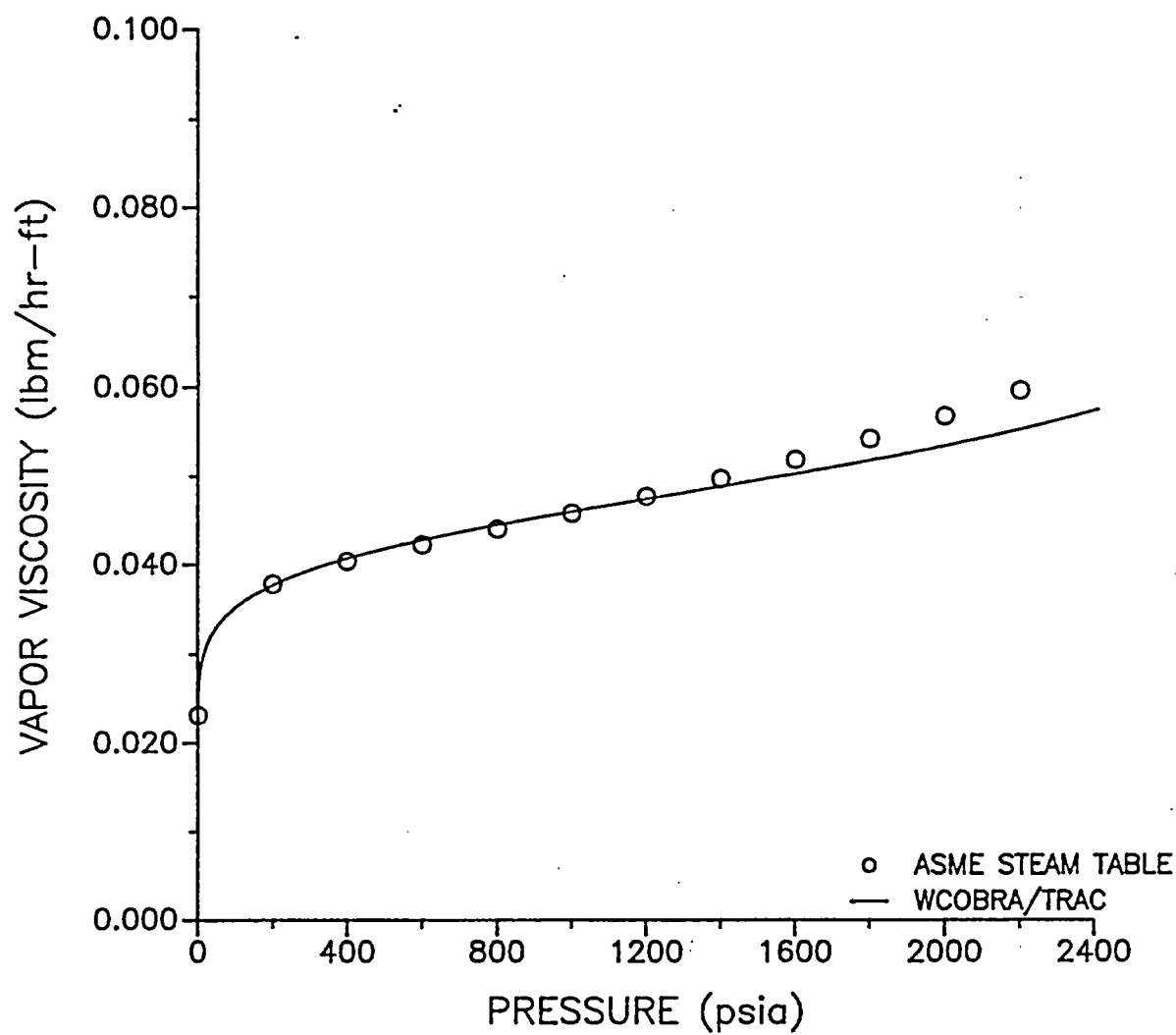


Figure 10-7. WCOBRA/TRAC Vessel Component Saturated Vapor Viscosity



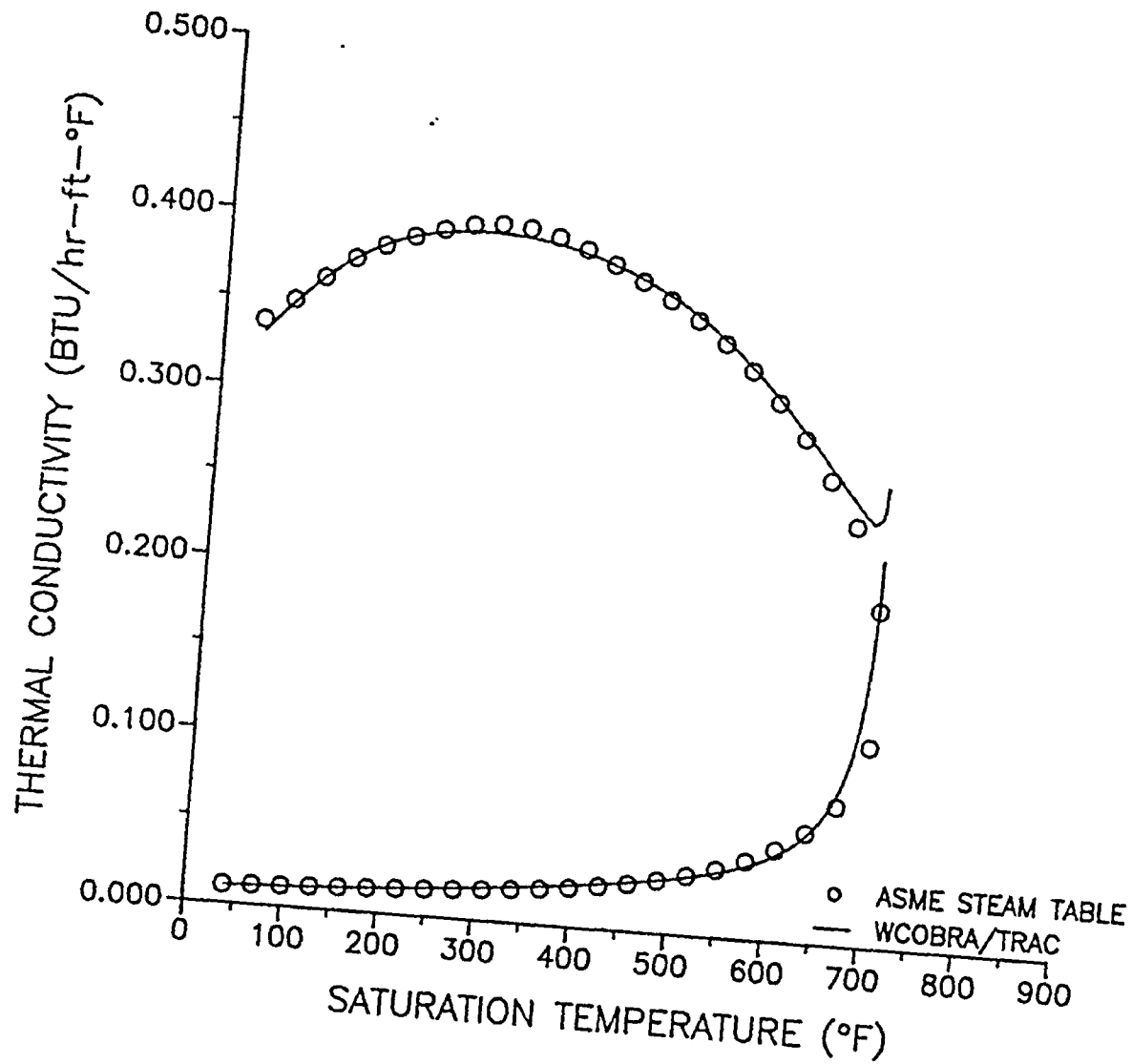


Figure 10-8. WCOBRA/TRAC Vessel Component Saturated Liquid and Vapor Thermal Conductivity

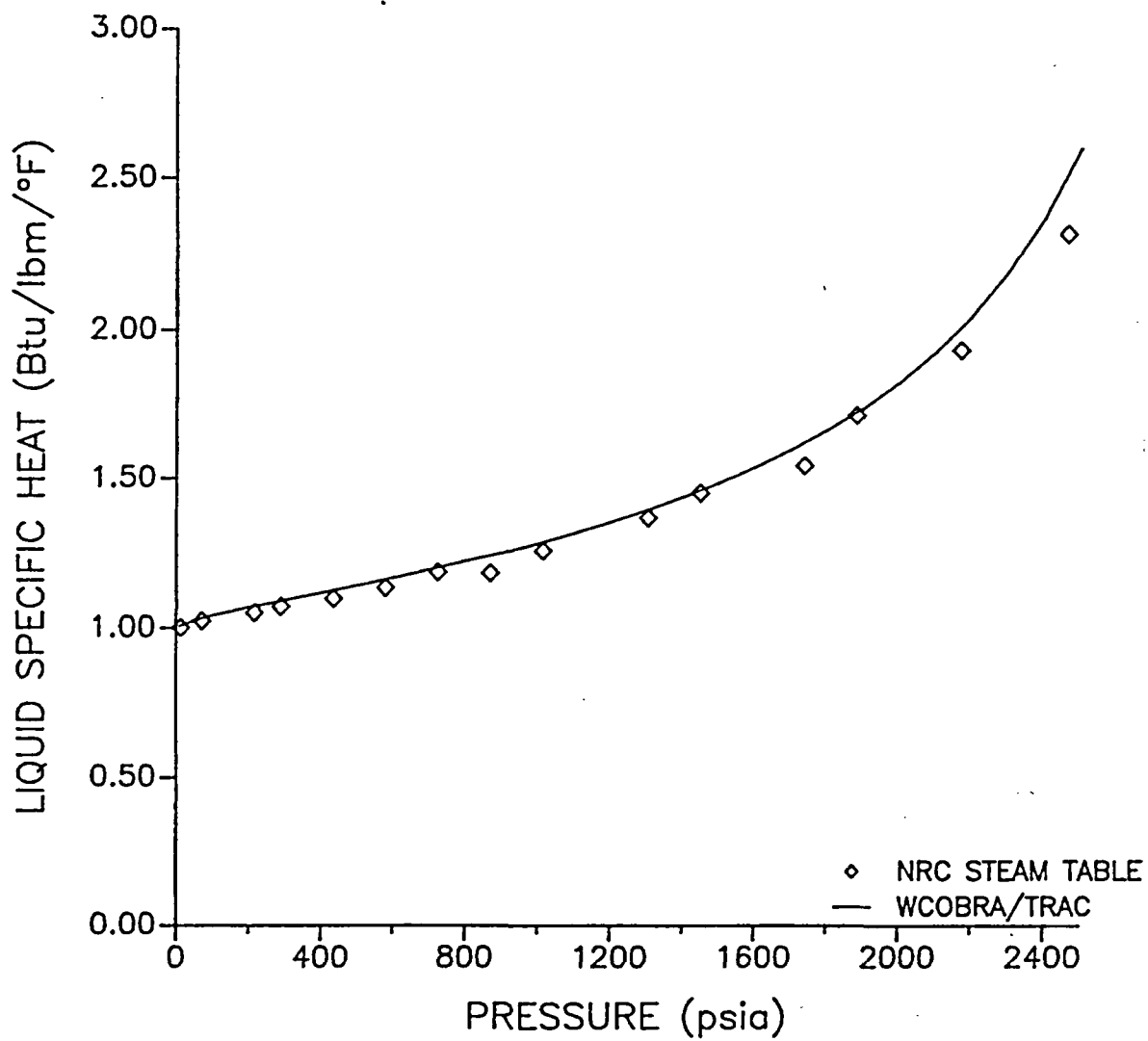


Figure 10-9. WCOBRA/TRAC Vessel Component Saturated Liquid Specific Heat

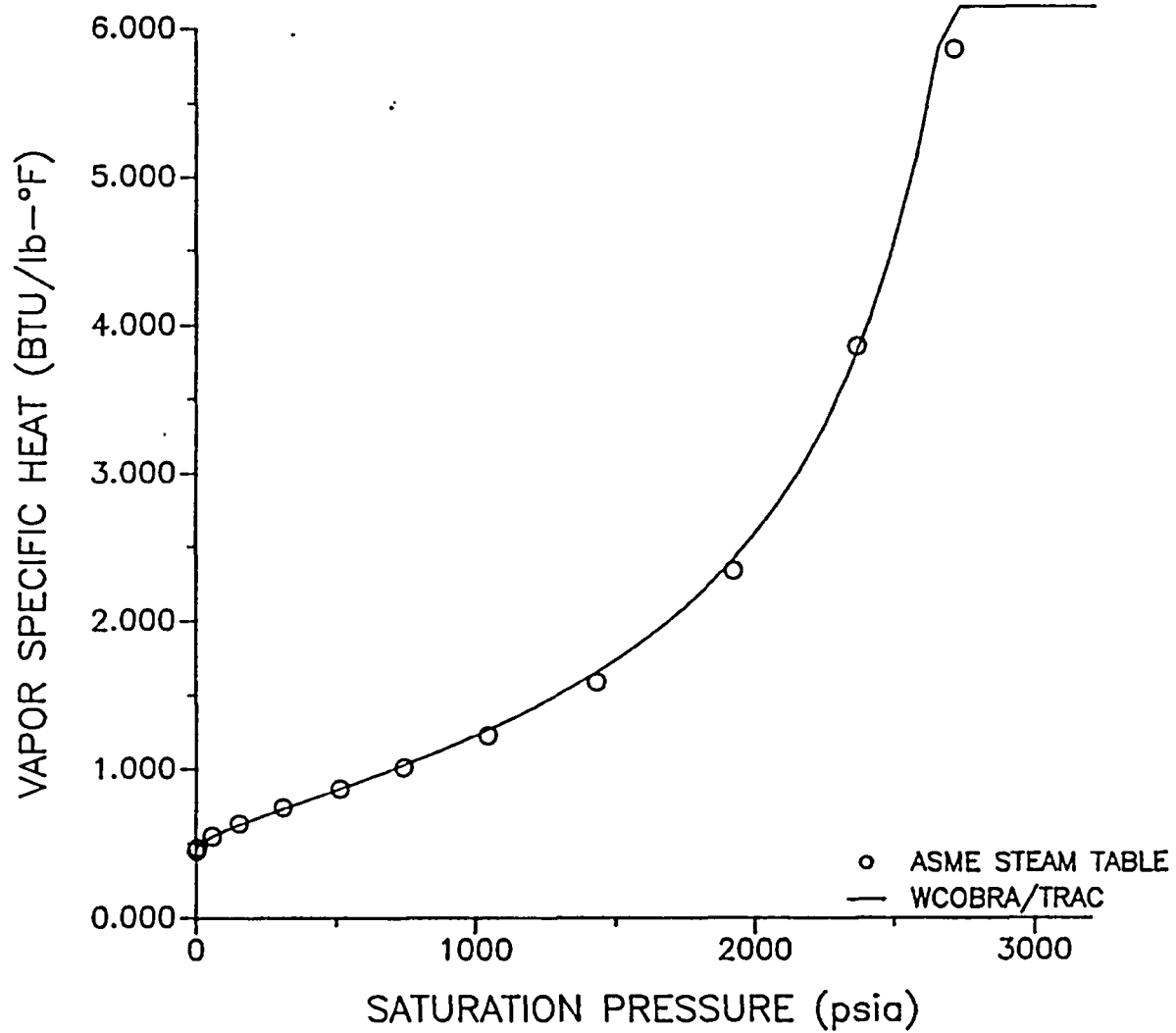


Figure 10-10. WCOBRA/TRAC Vessel Component Saturated Vapor Specific Heat

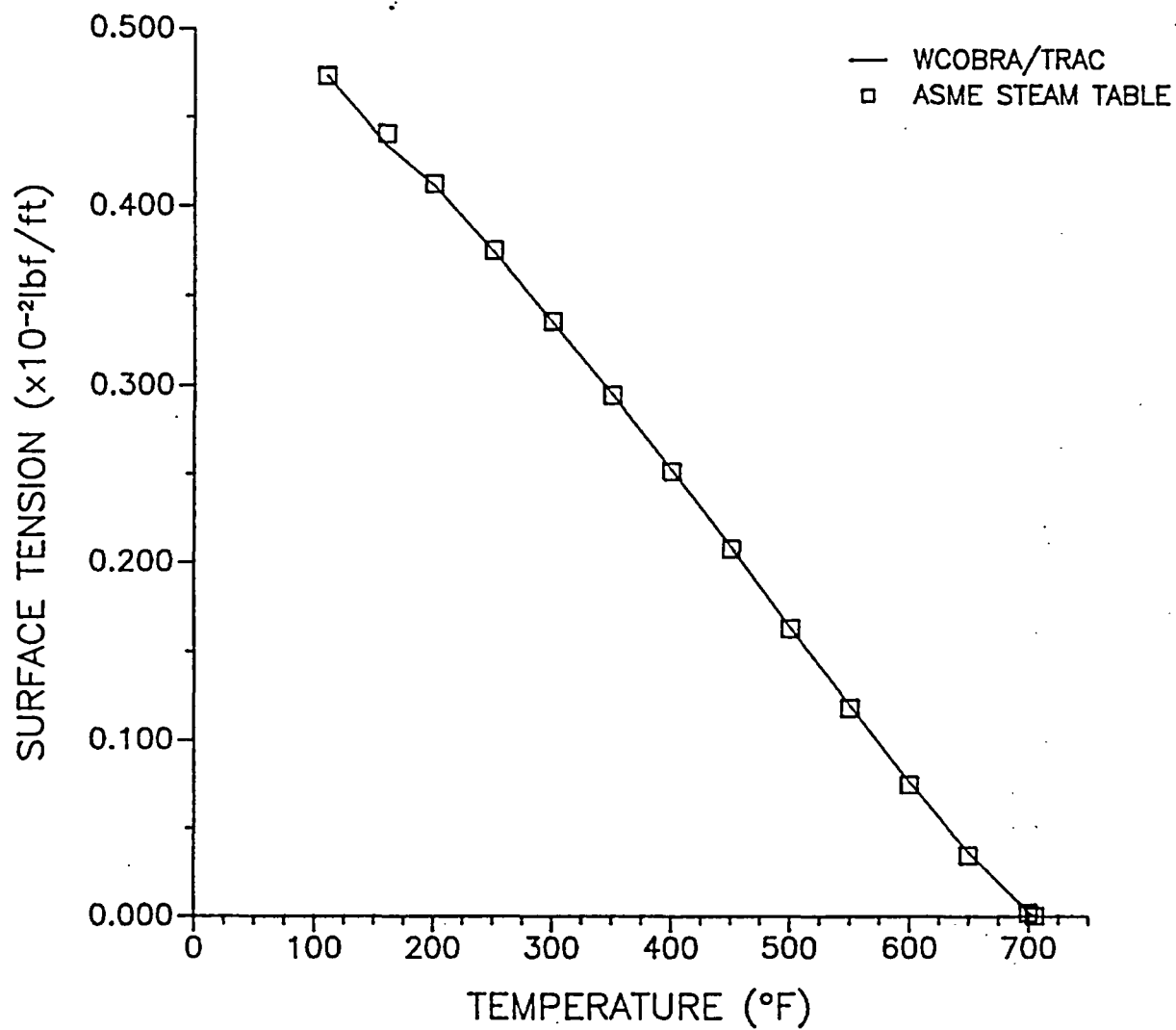


Figure 10-11. WCOBRA/TRAC Vessel Component Saturated Liquid Surface Tension

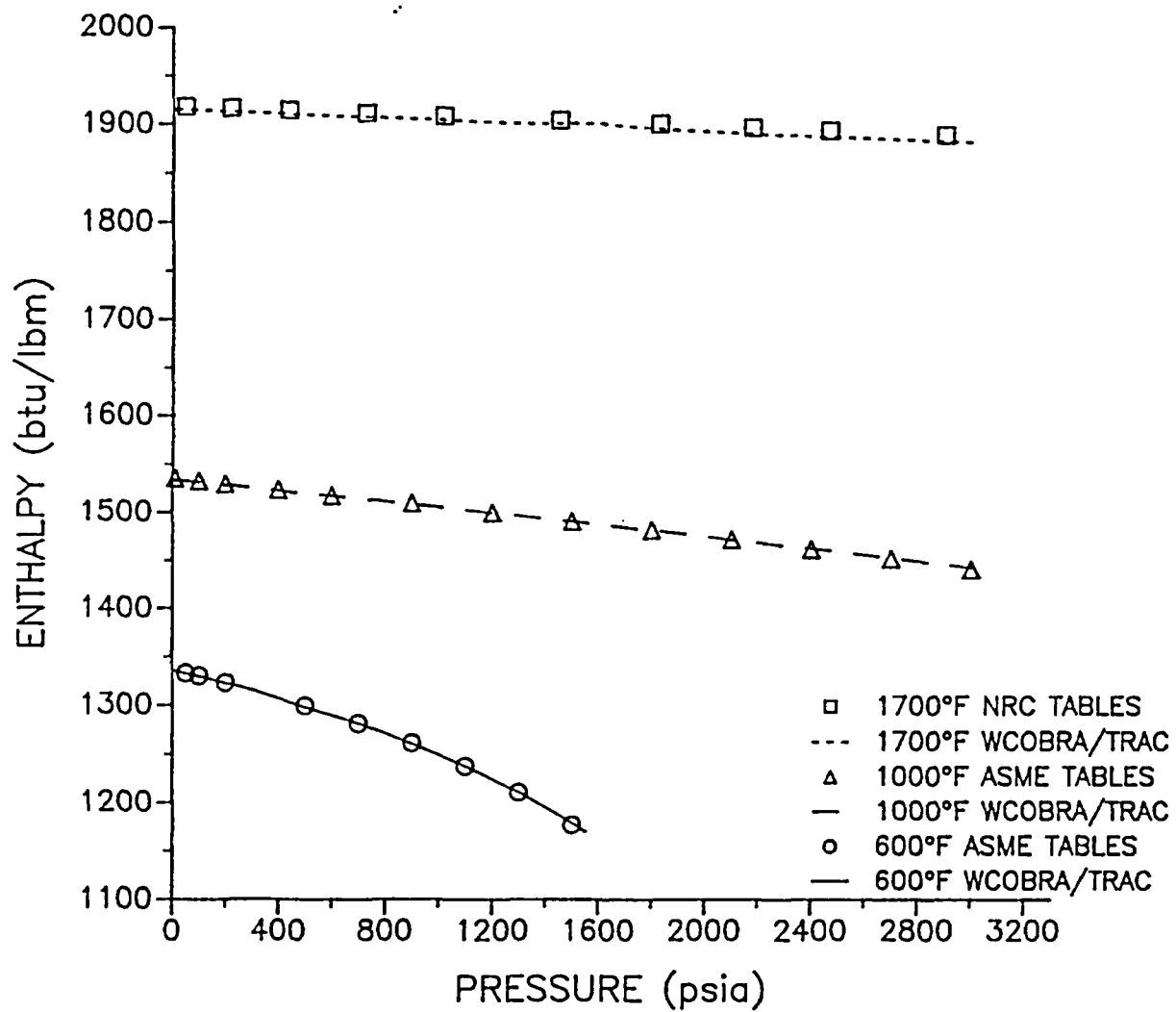


Figure 10-12. WCOBRA/TRAC Vessel Component Superheated Vapor Enthalpy

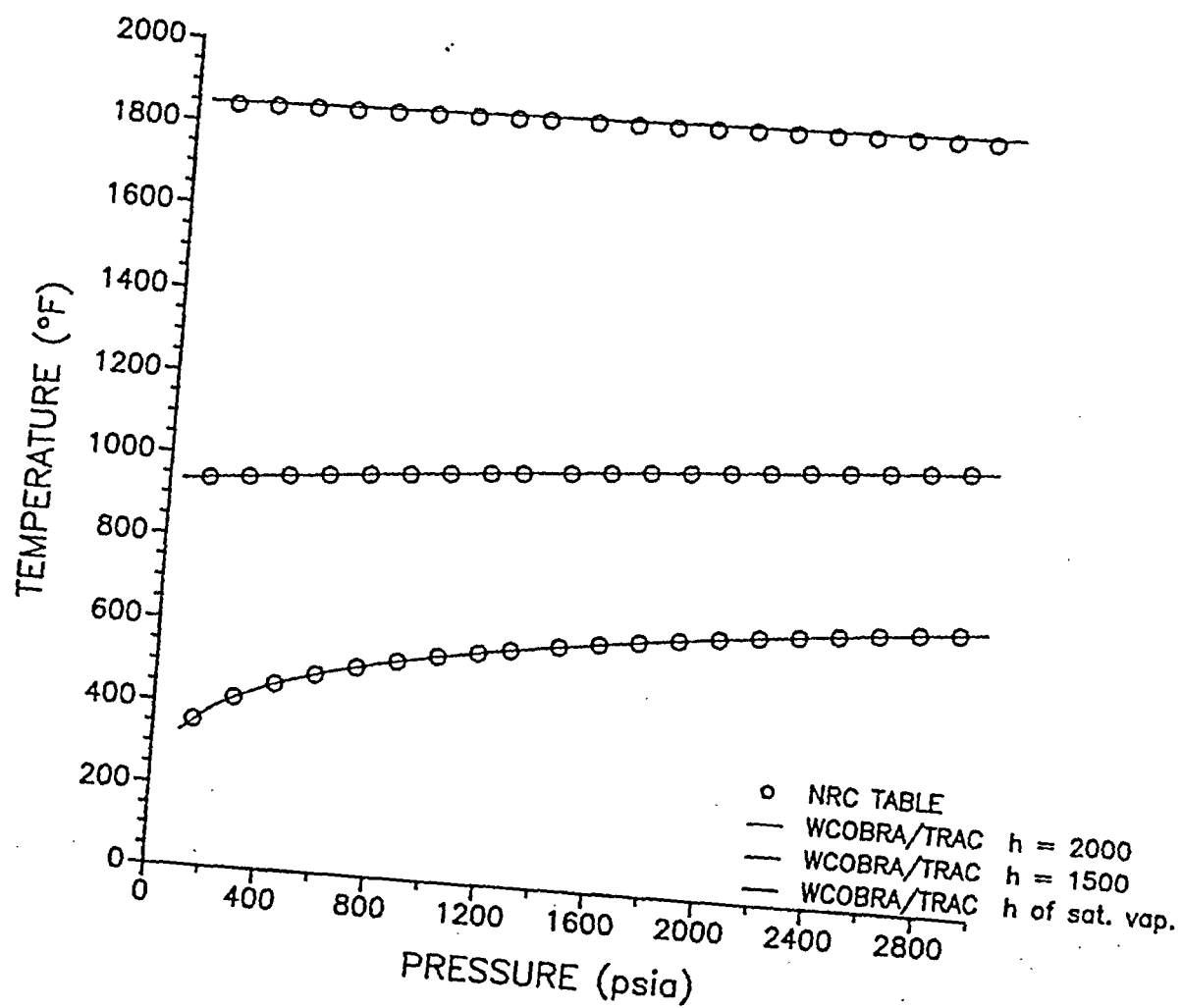


Figure 10-13. WCOBRA/TRAC Vessel Component Superheated Vapor Temperature

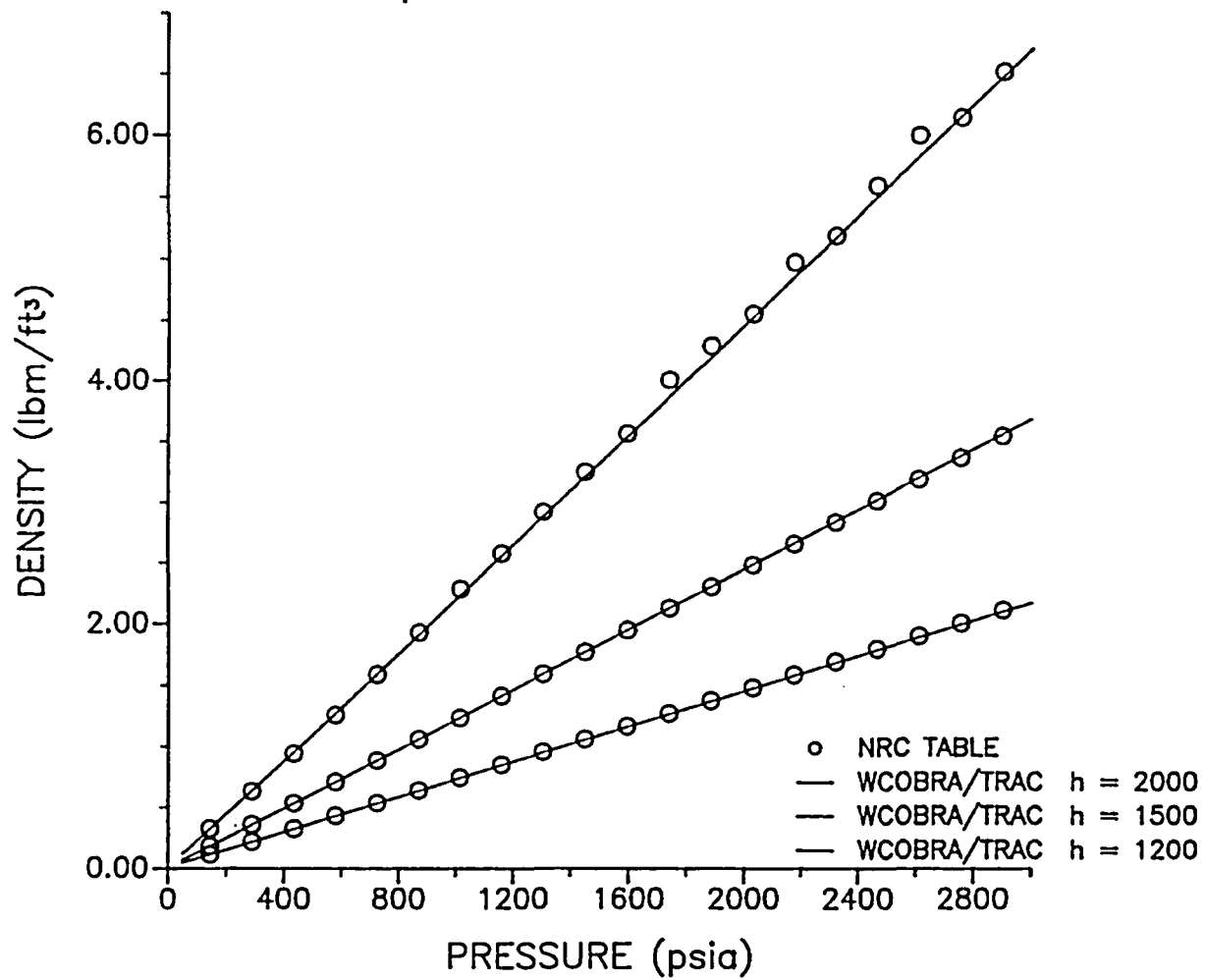


Figure 10-14. WCOBRA/TRAC Vessel Component Superheated Vapor Density

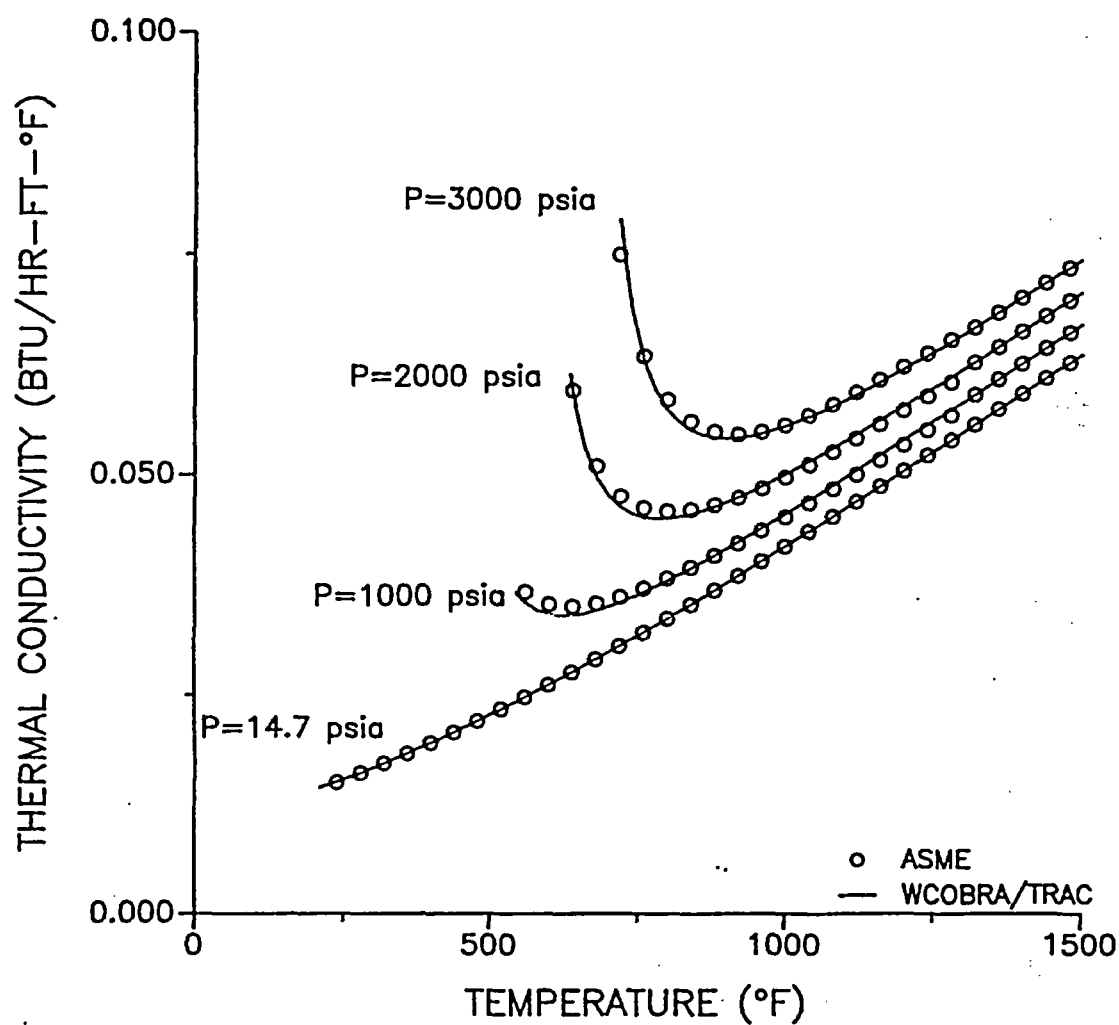


Figure 10-15. WCOBRA/TRAC Vessel Component Superheated Vapor Thermal Conductivity



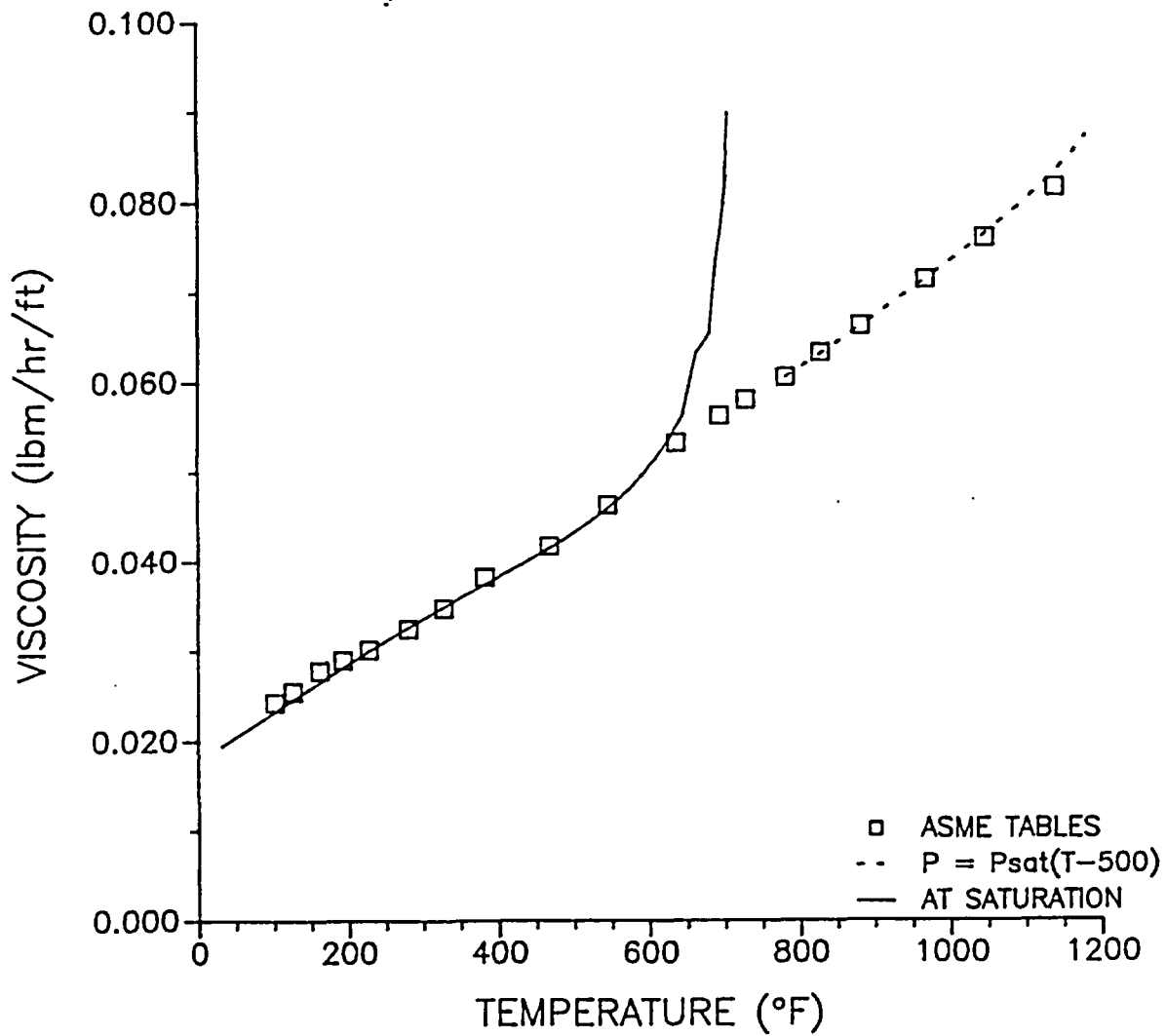


Figure 10-16. WCOBRA/TRAC Vessel Component Superheated Vapor Viscosity

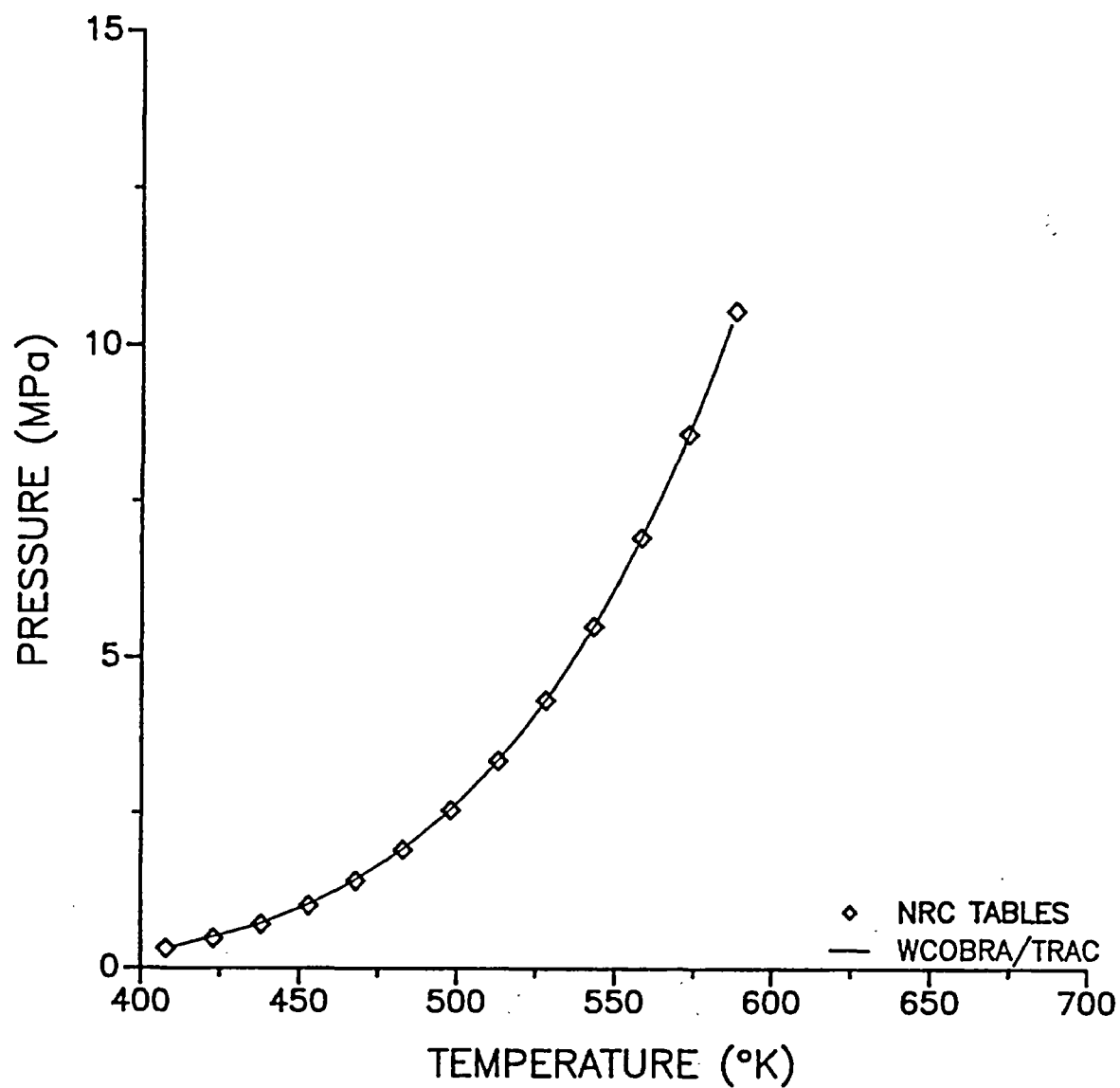


Figure 10-17. WCOBRA/TRAC 1-D Component Saturation Pressure

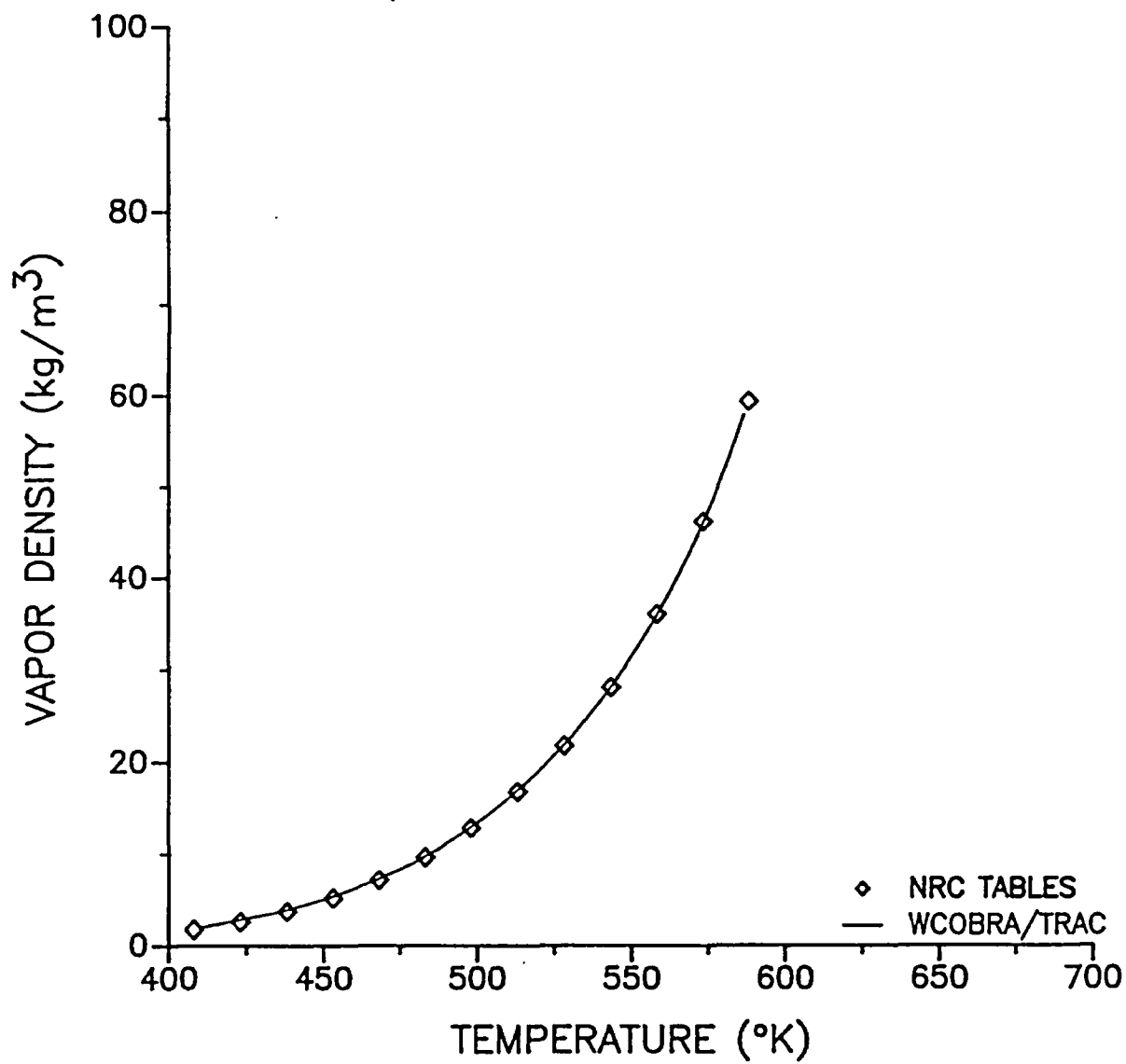


Figure 10-18. WCOBRA/TRAC 1-D Component Saturated Vapor Density

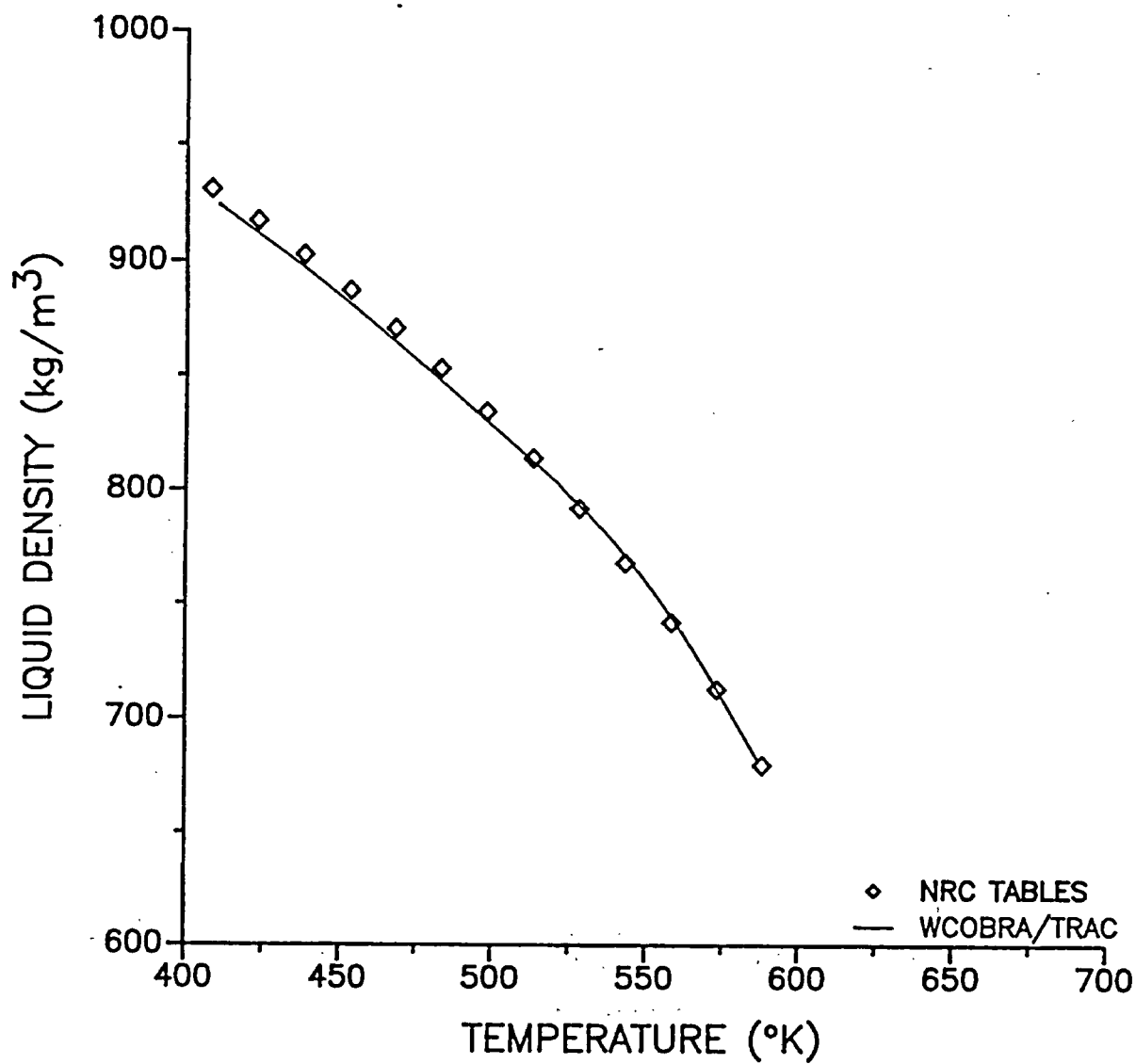


Figure 10-19. WCOBRA/TRAC 1-D Component Saturated Liquid Density

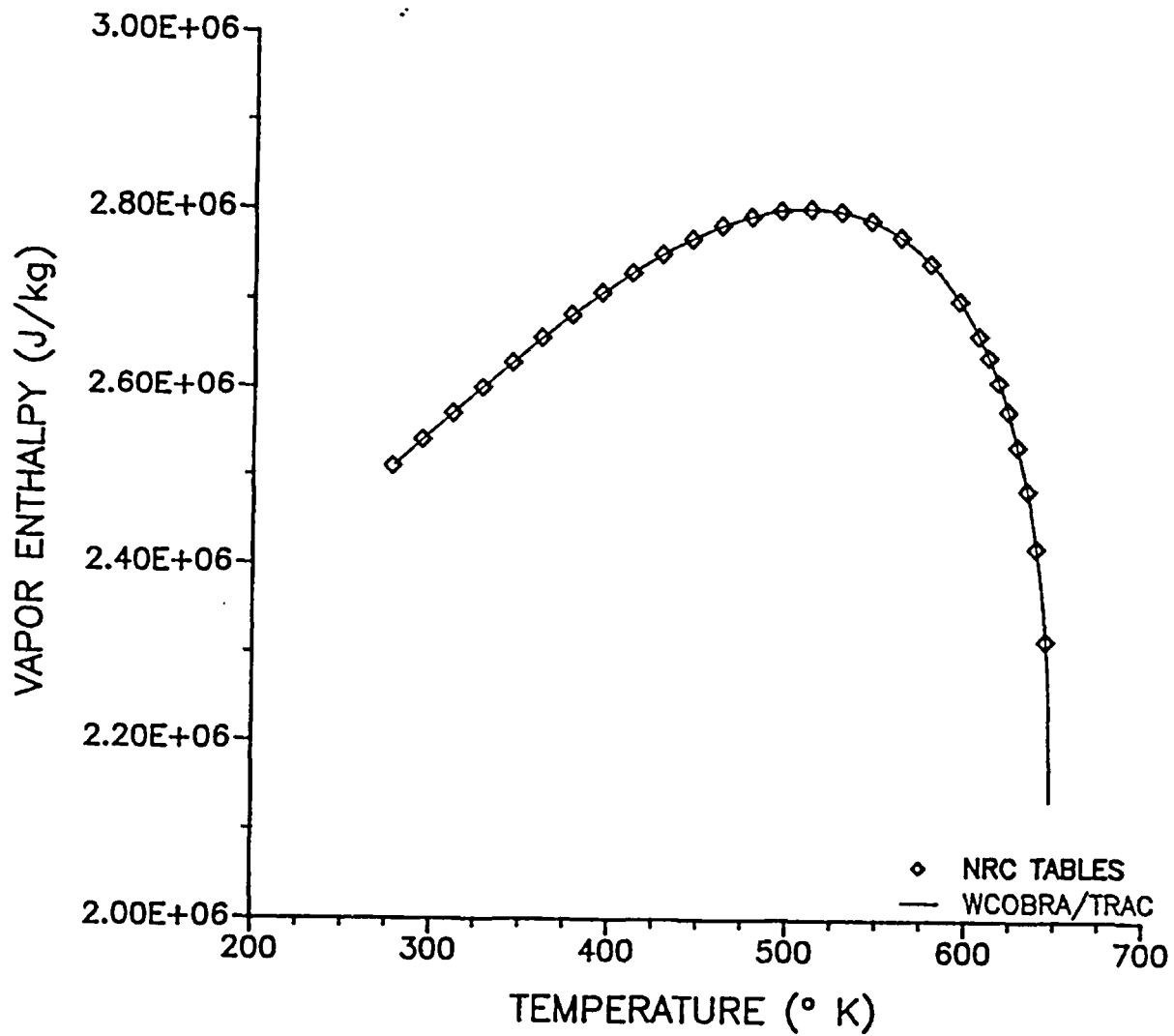


Figure 10-20. WCOBRA/TRAC 1-D Component Saturated Vapor Enthalpy

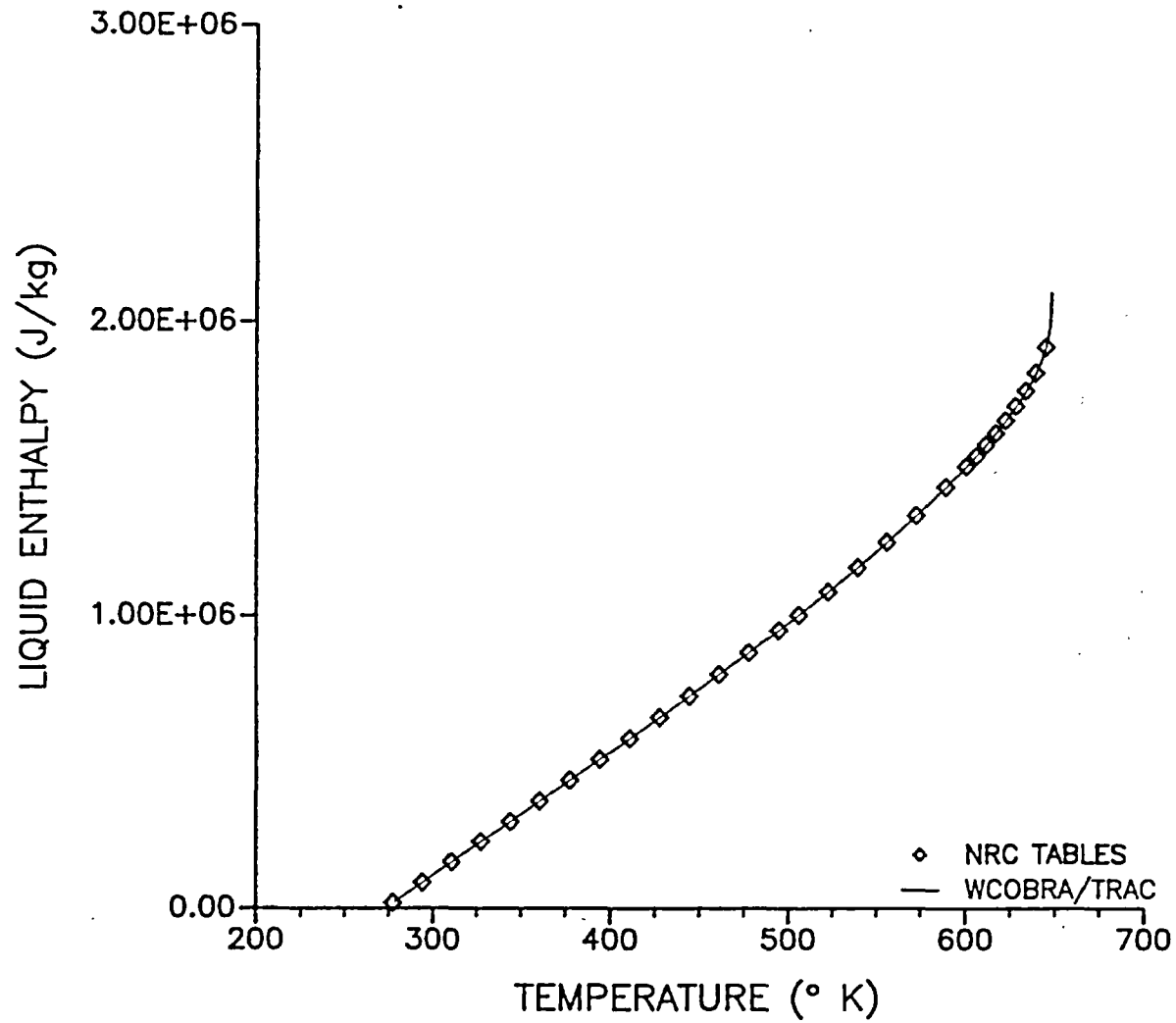


Figure 10-21. WCOBRA/TRAC 1-D Component Saturated Liquid Enthalpy

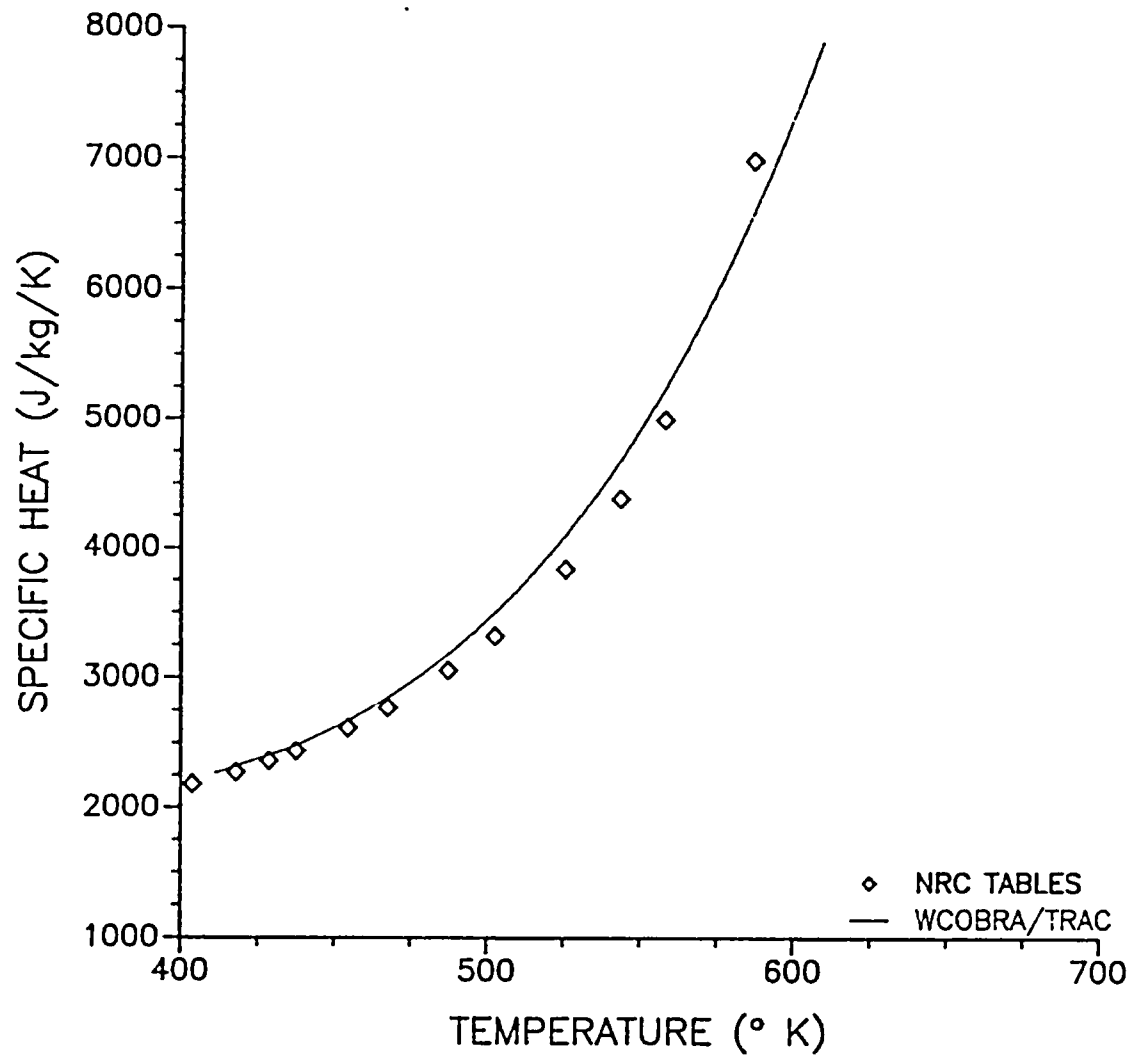


Figure 10-22. WCOBRA/TRAC 1-D Component Saturated Vapor Specific Heat

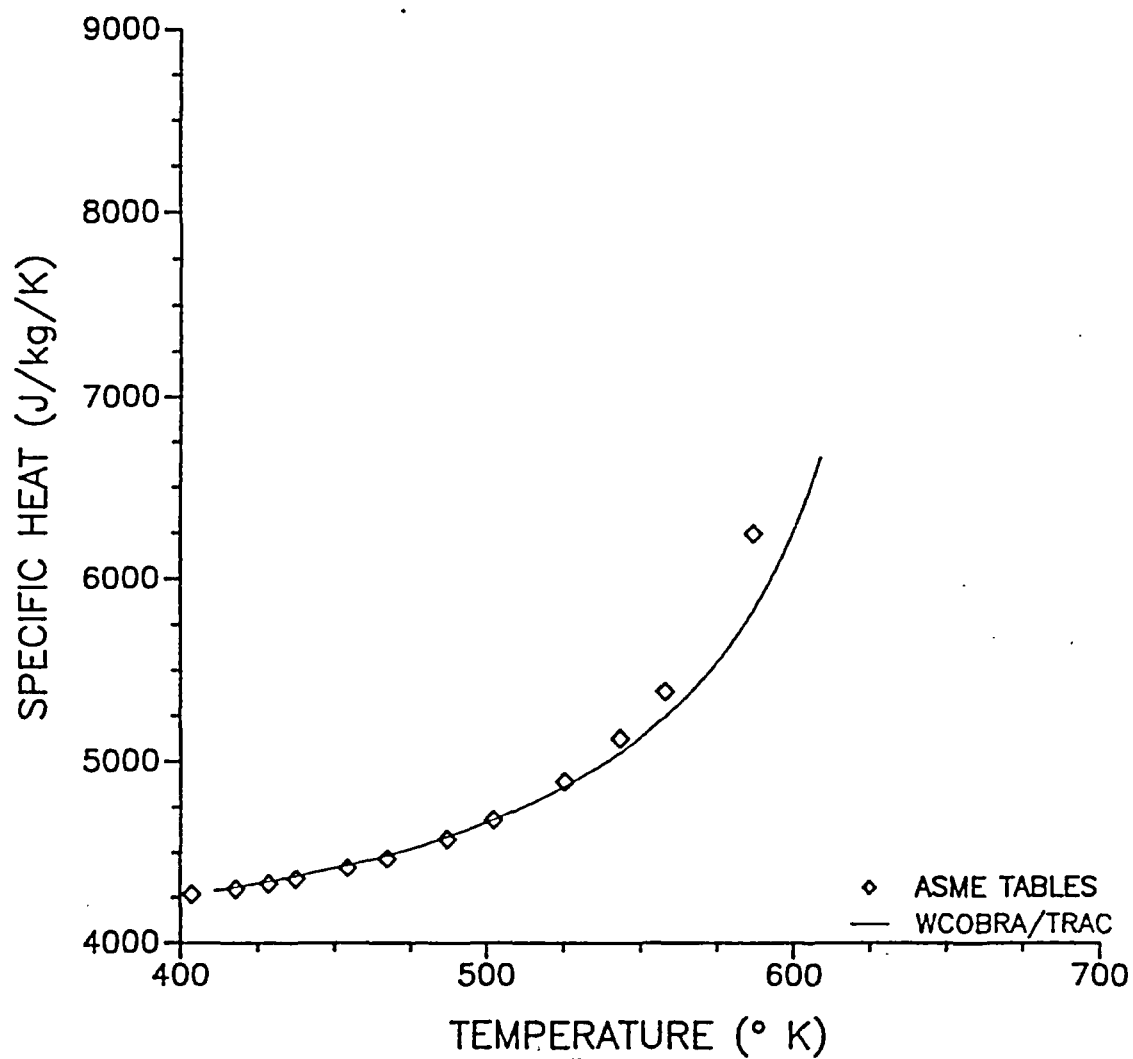


Figure 10-23. WCOBRA/TRAC 1-D Component Saturated Liquid Specific Heat



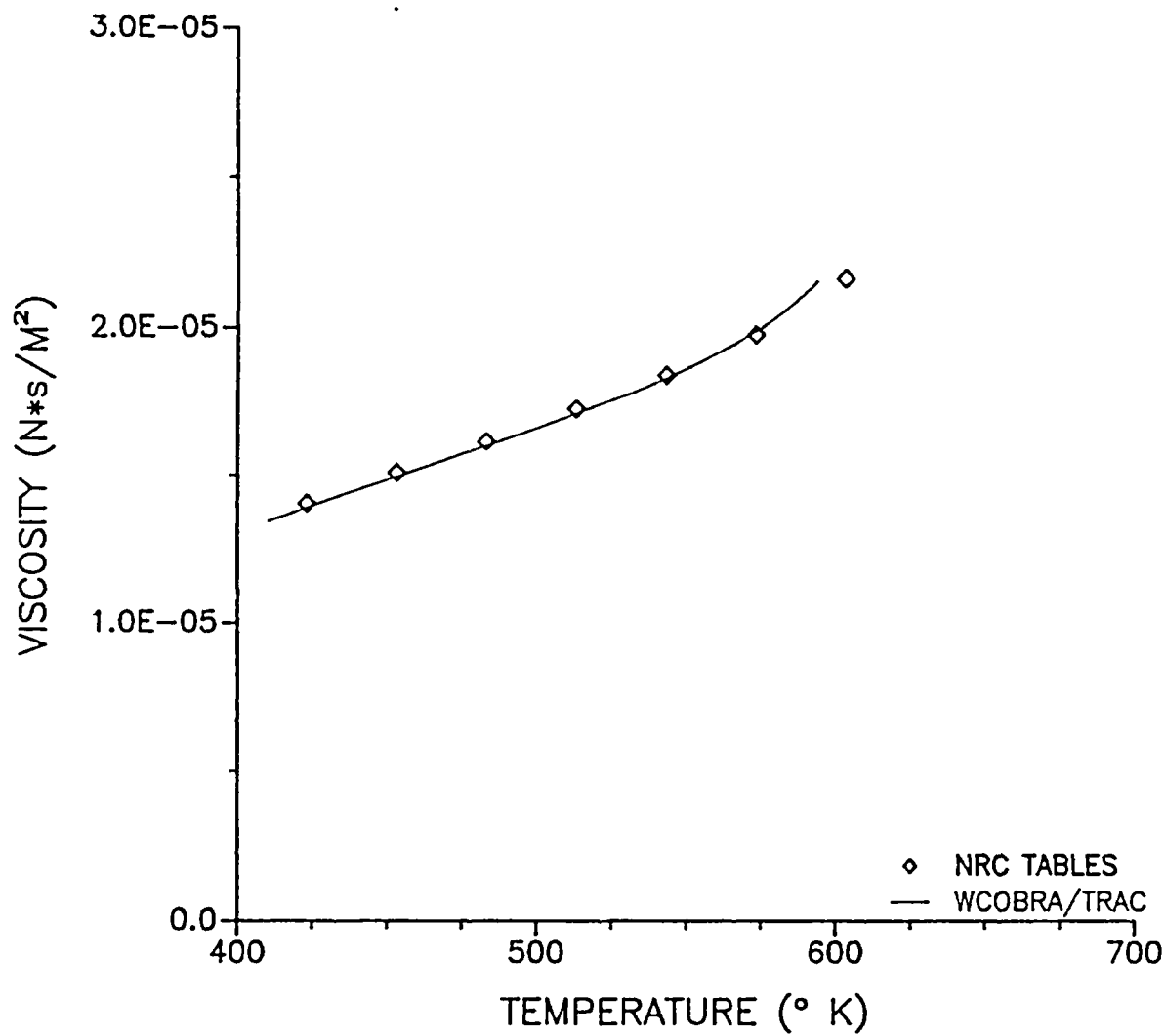


Figure 10-24. WCOBRA/TRAC 1-D Component Saturated Vapor Viscosity

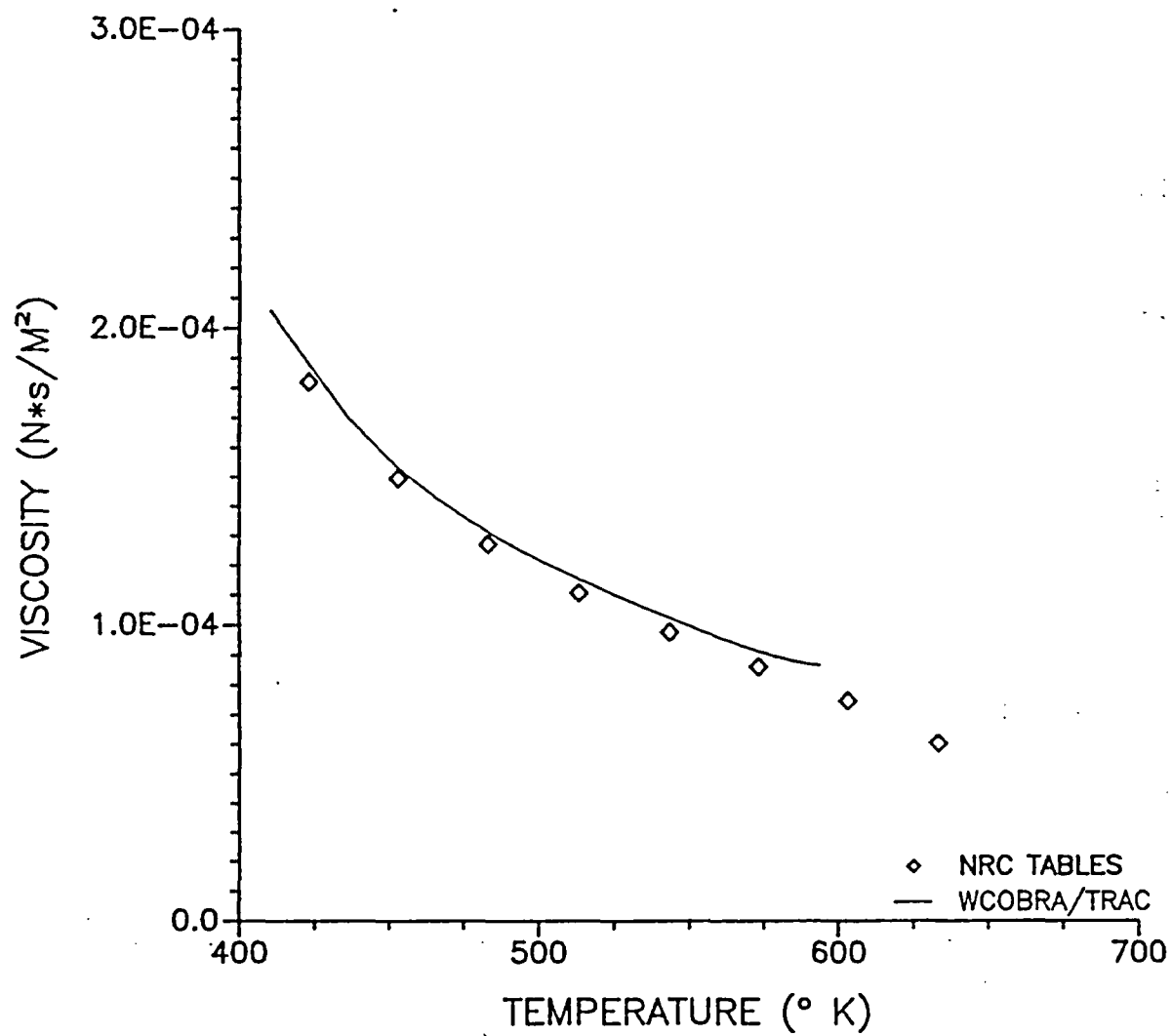


Figure 10-25. WCOBRA/TRAC 1-D Component Saturated Liquid Viscosity

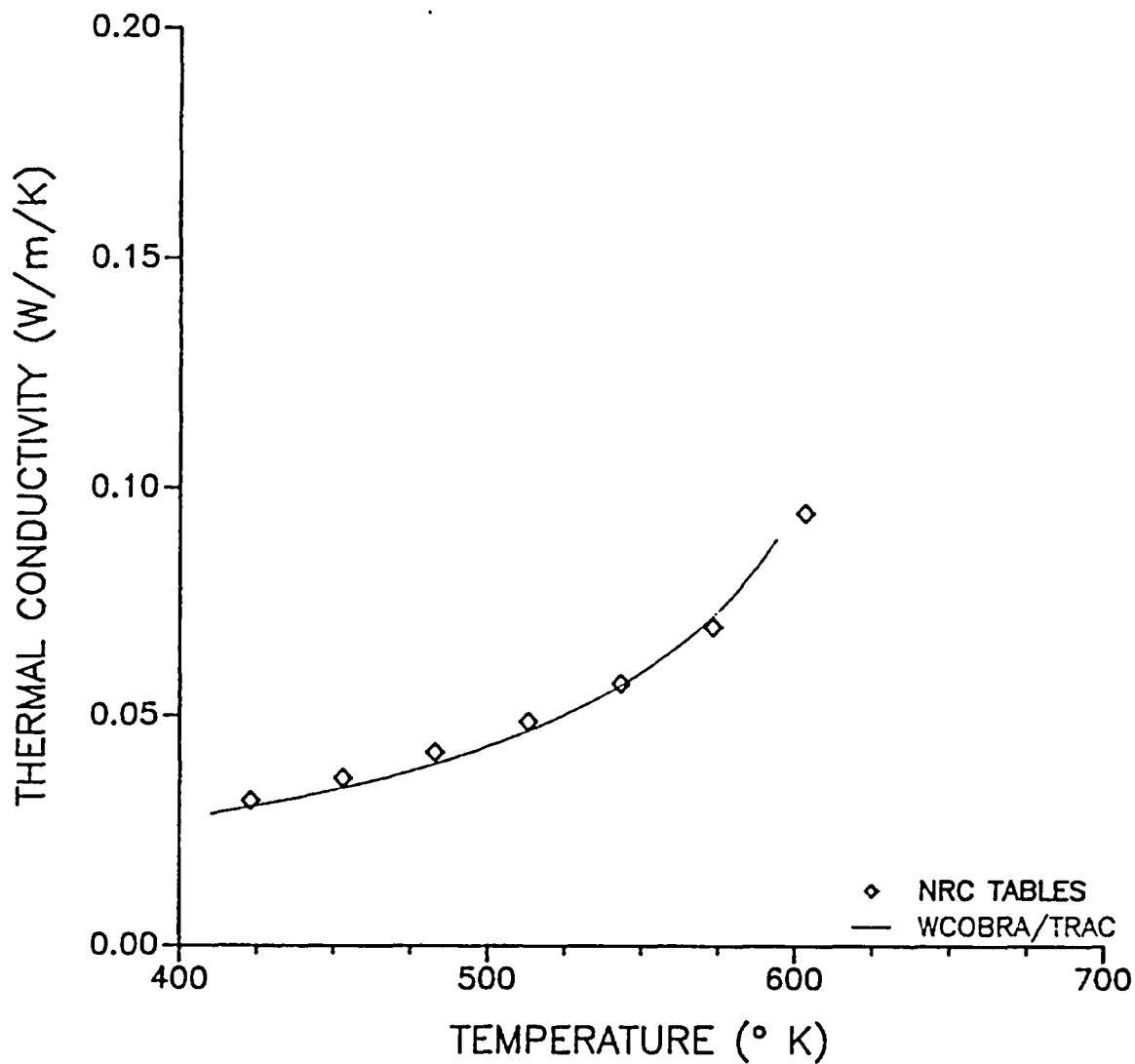


Figure 10-26. WCOBRA/TRAC 1-D Component Saturated Vapor Thermal Conductivity

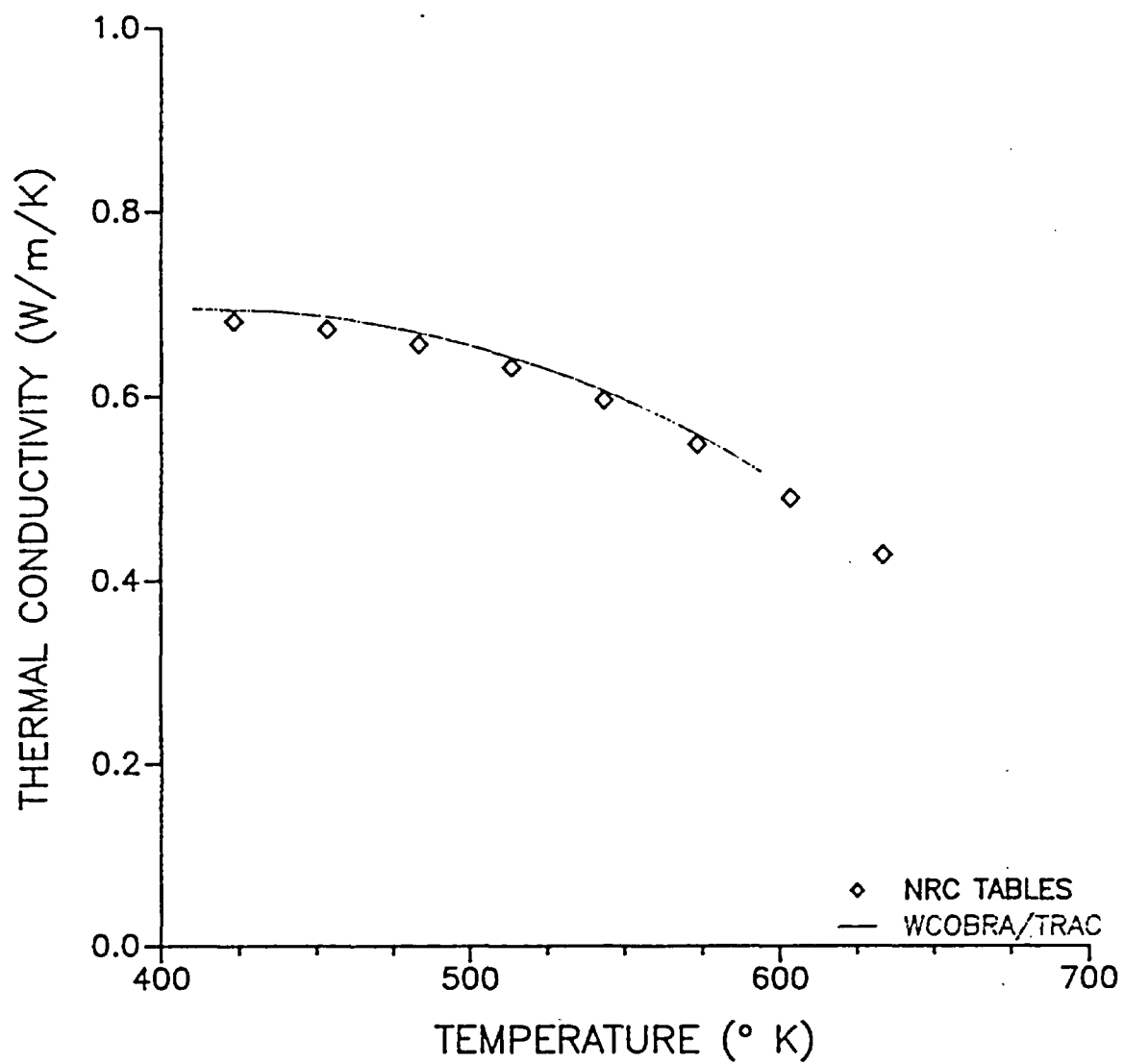


Figure 10-27. WCOBRA/TRAC 1-D Component Saturated Liquid Thermal Conductivity

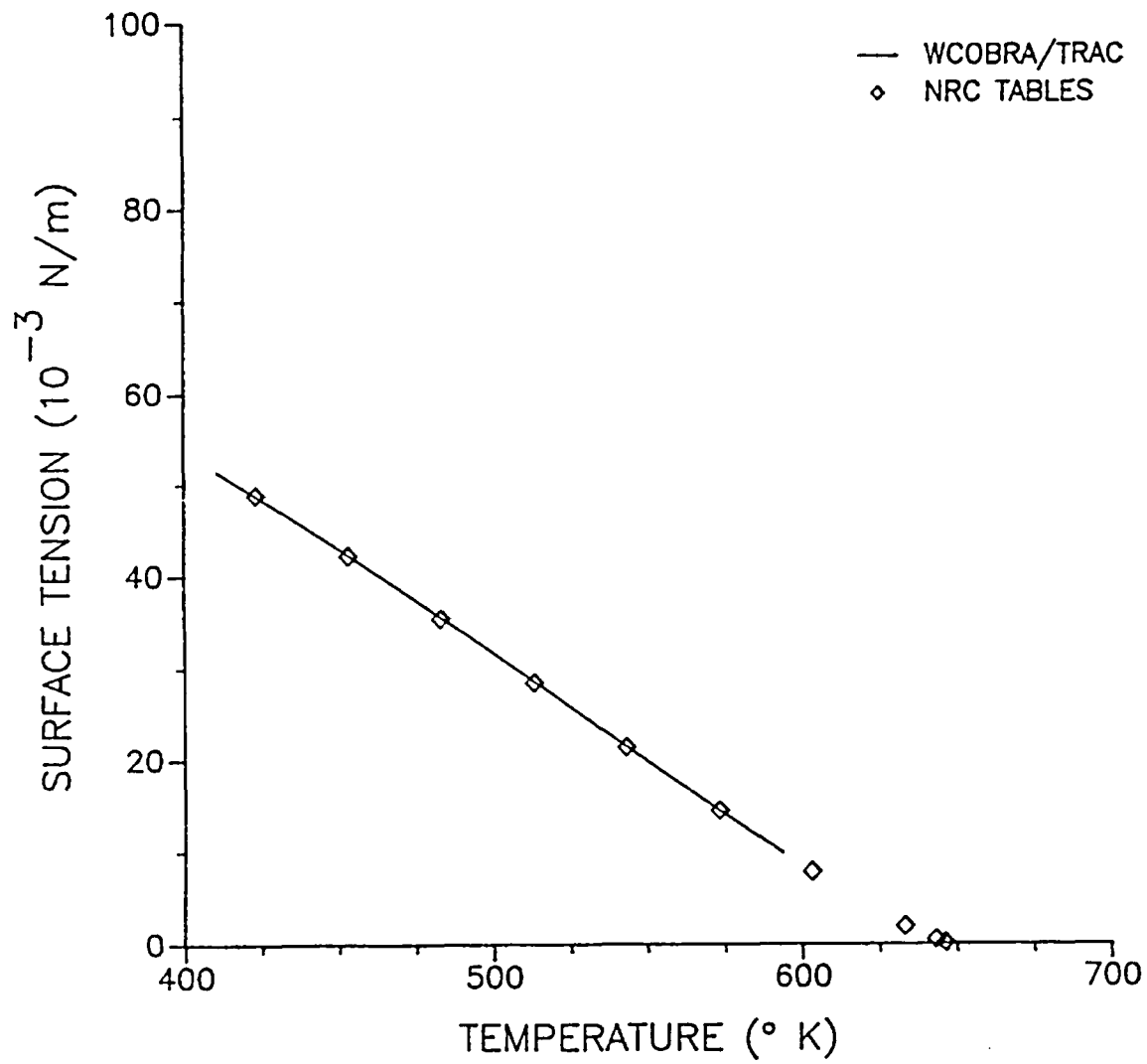


Figure 10-28. WCOBRA/TRAC 1-D Component Surface Tension

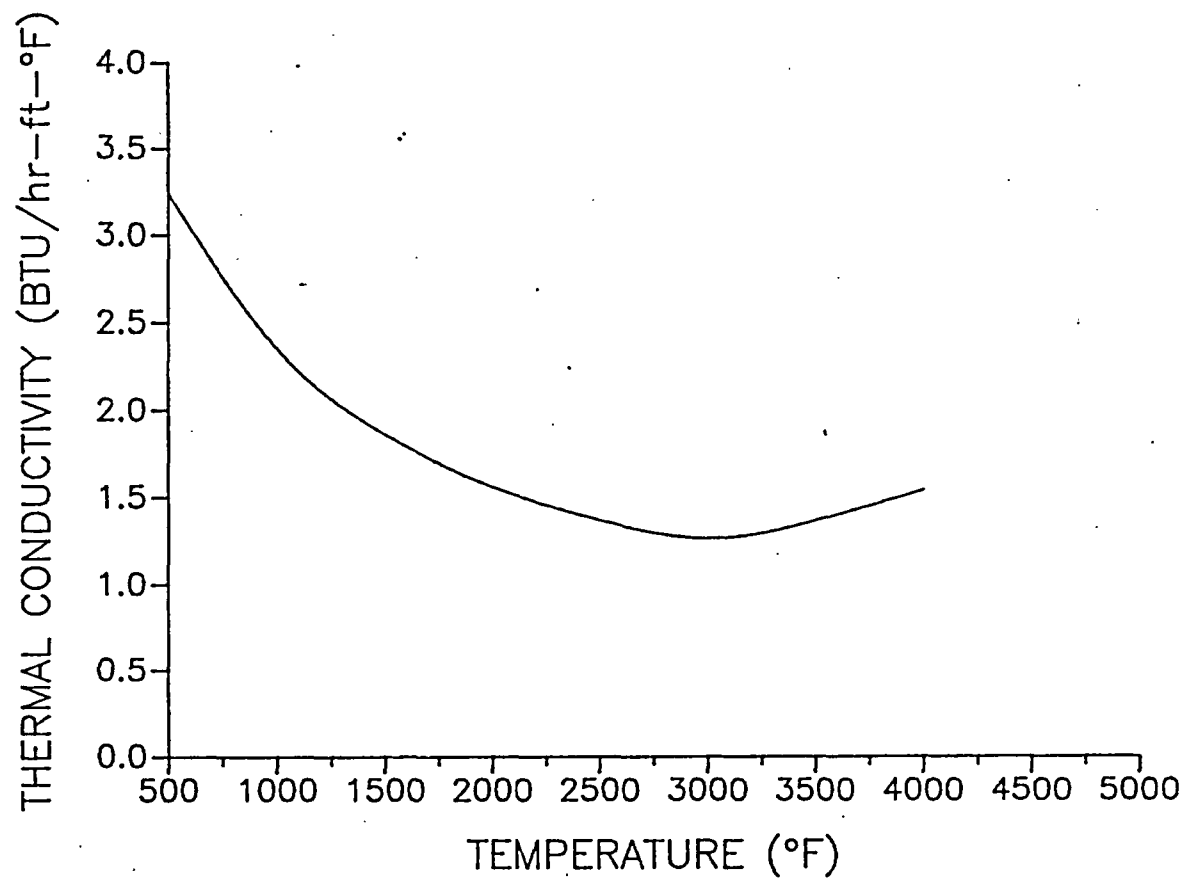


Figure 10-29. WCOBRA/TRAC UO<sub>2</sub> Thermal Conductivity (95% of Theoretical Density)

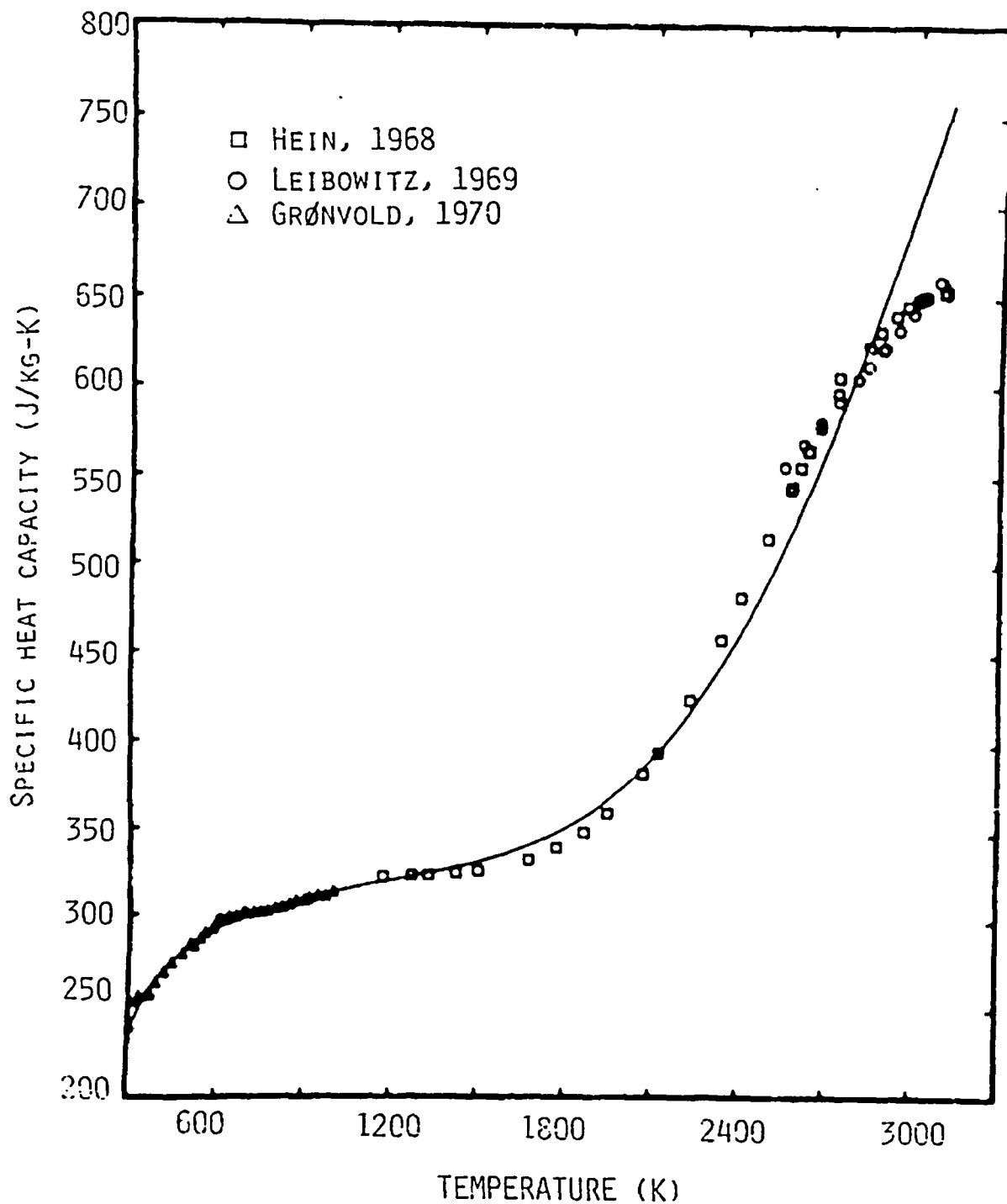


Figure 10-30. WCOBRA/TRAC  $\text{UO}_2$  Specific Heat

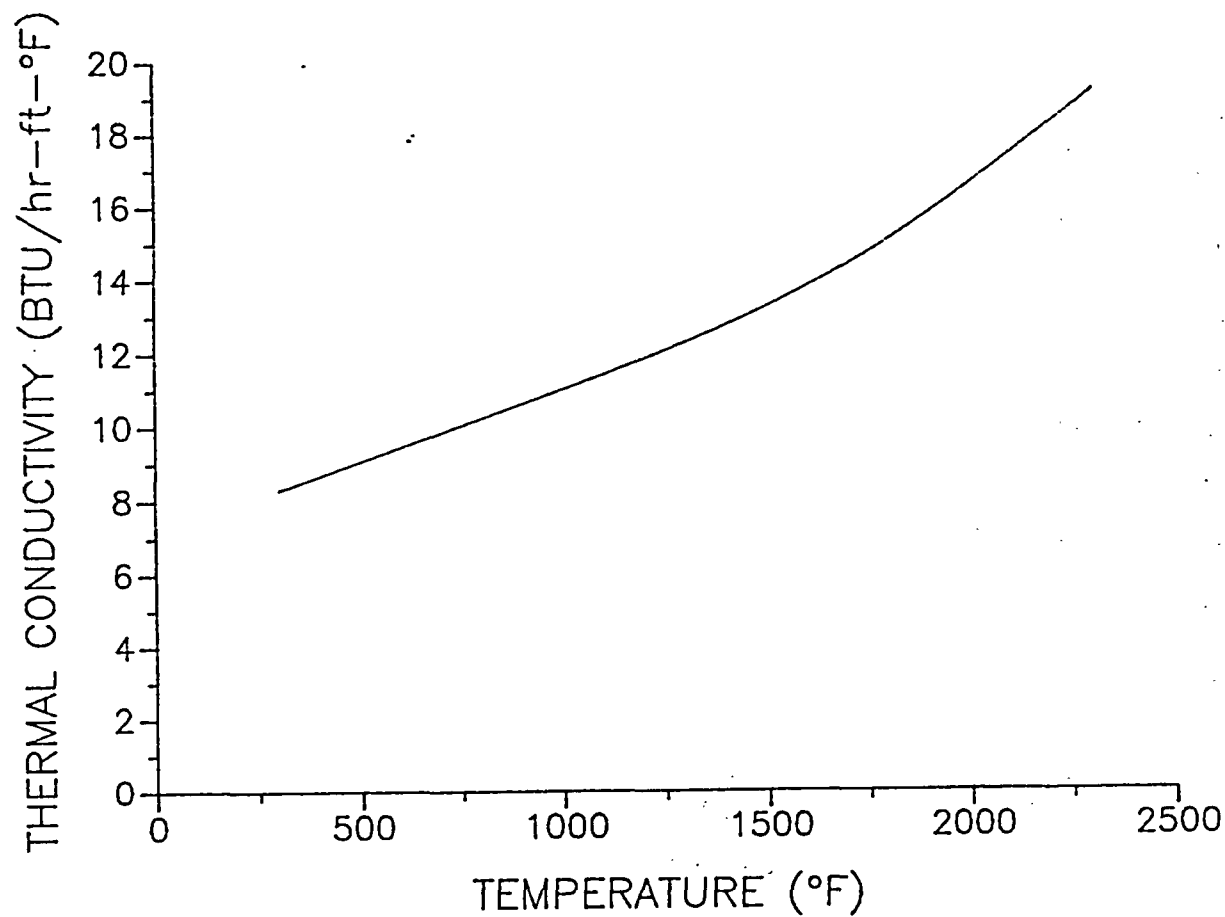


Figure 10-31. WCOBRA/TRAC Zircaloy-4 Thermal Conductivity



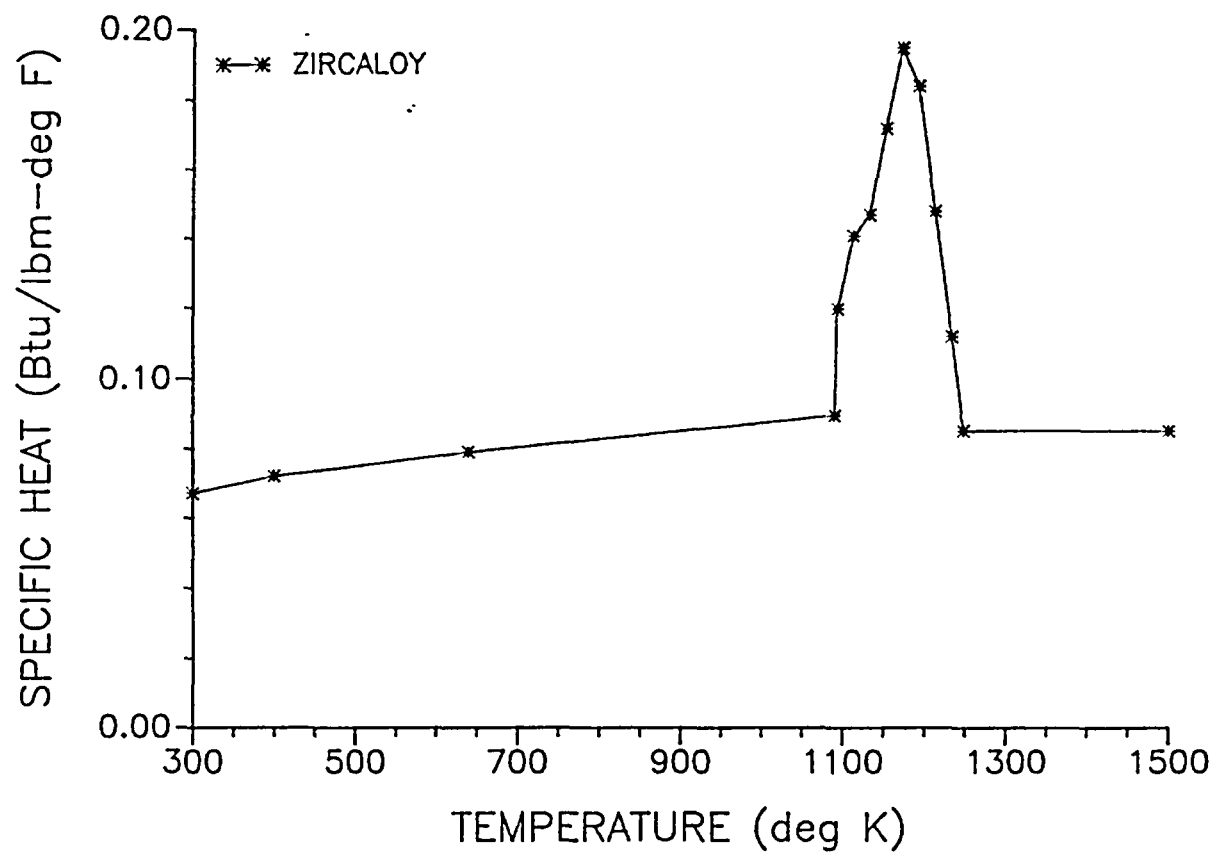


Figure 10-32. WCOBRA/TRAC Zircaloy-4 Specific Heat

a,c

**Figure 10-33. Comparison of ZIRLO™ and Zircaloy-4 Specific Heat**

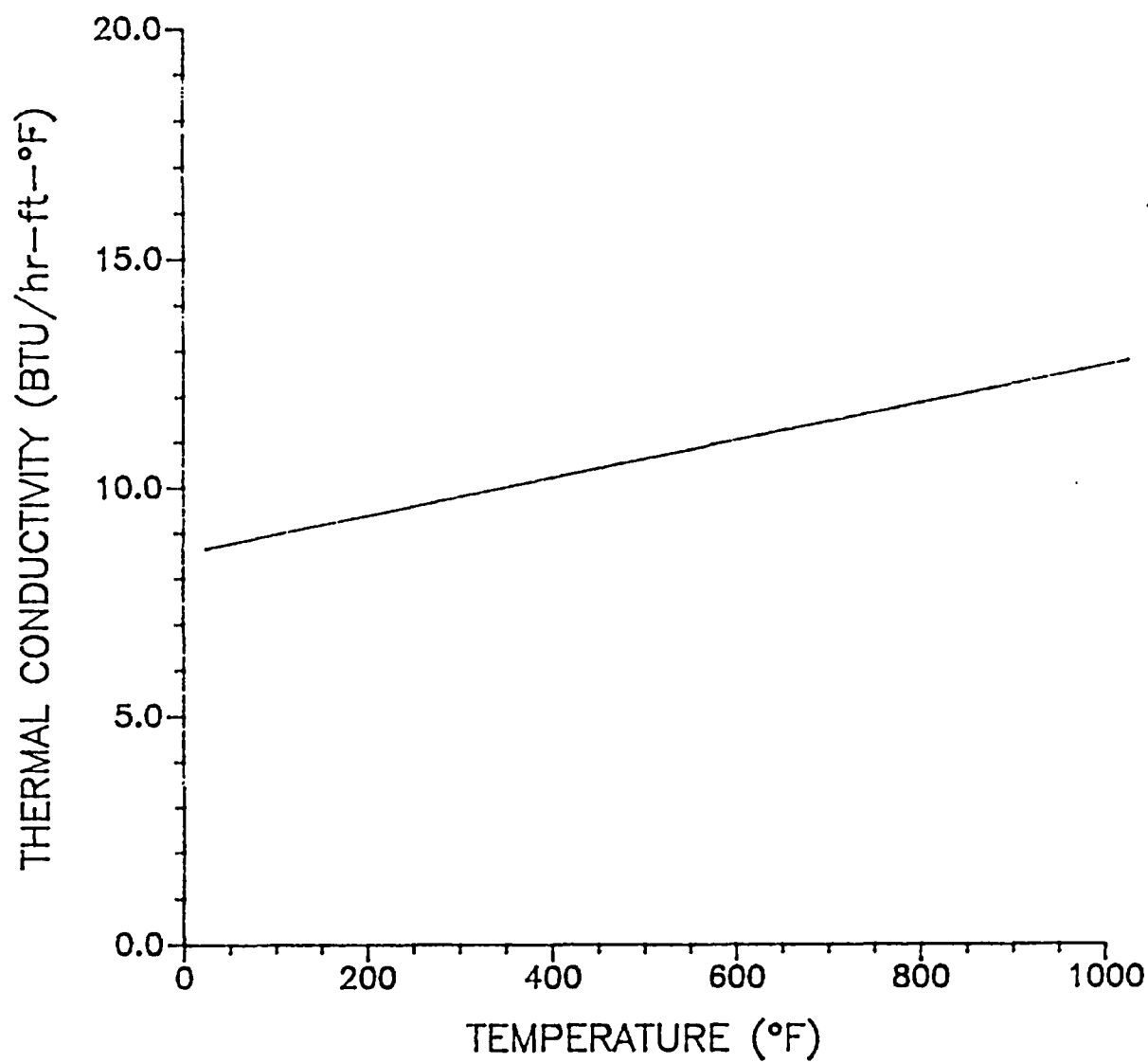


Figure 10-34. WCOBRA/TRAC 1-D Component 304 Stainless Steel Thermal Conductivity

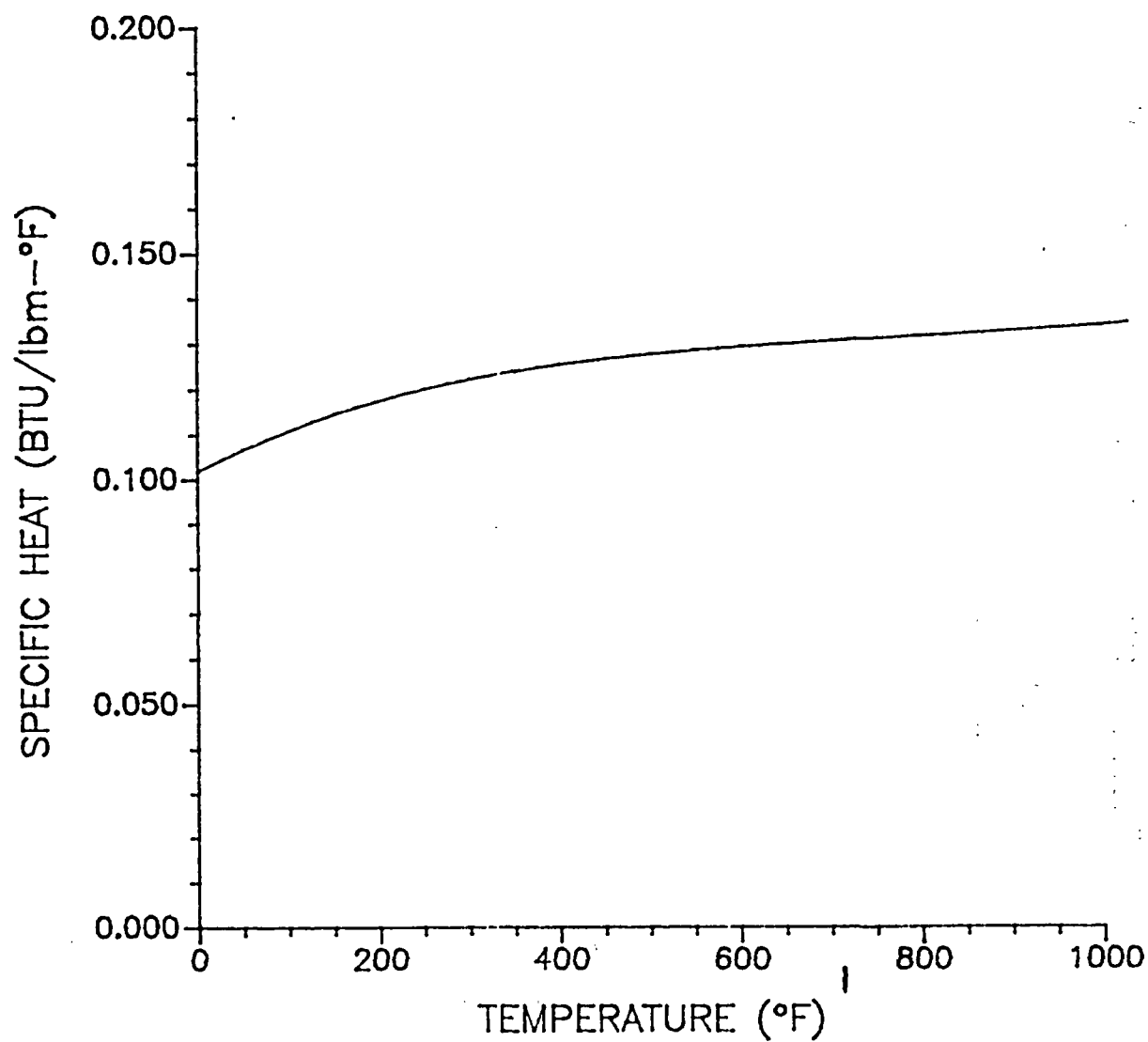


Figure 10-35. WCOBRA/TRAC 1-D Component 304 and 316 Stainless Steel Specific Heat

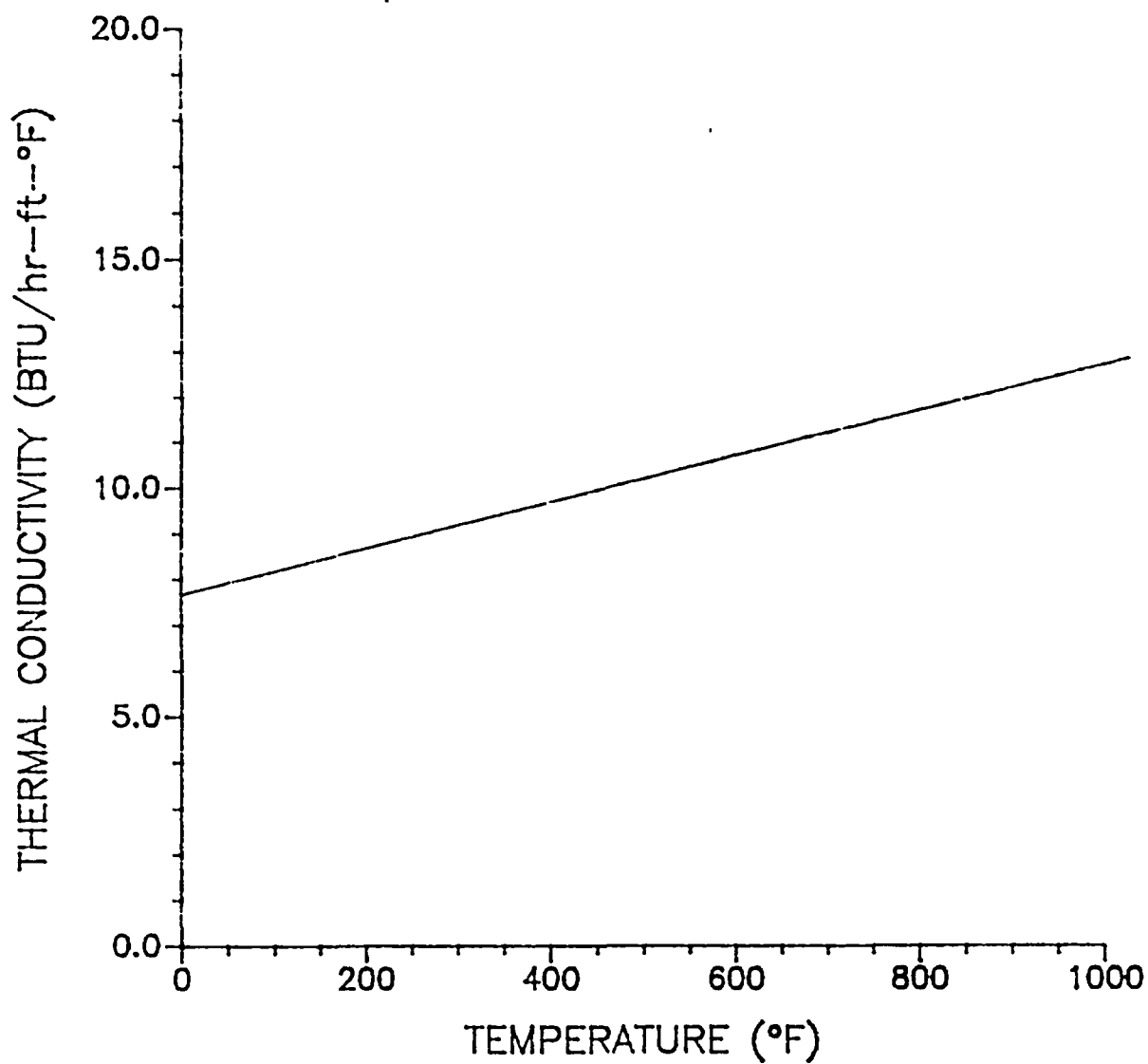


Figure 10-36. WCOBRA/TRAC 1-D Component 316 Stainless Steel Thermal Conductivity

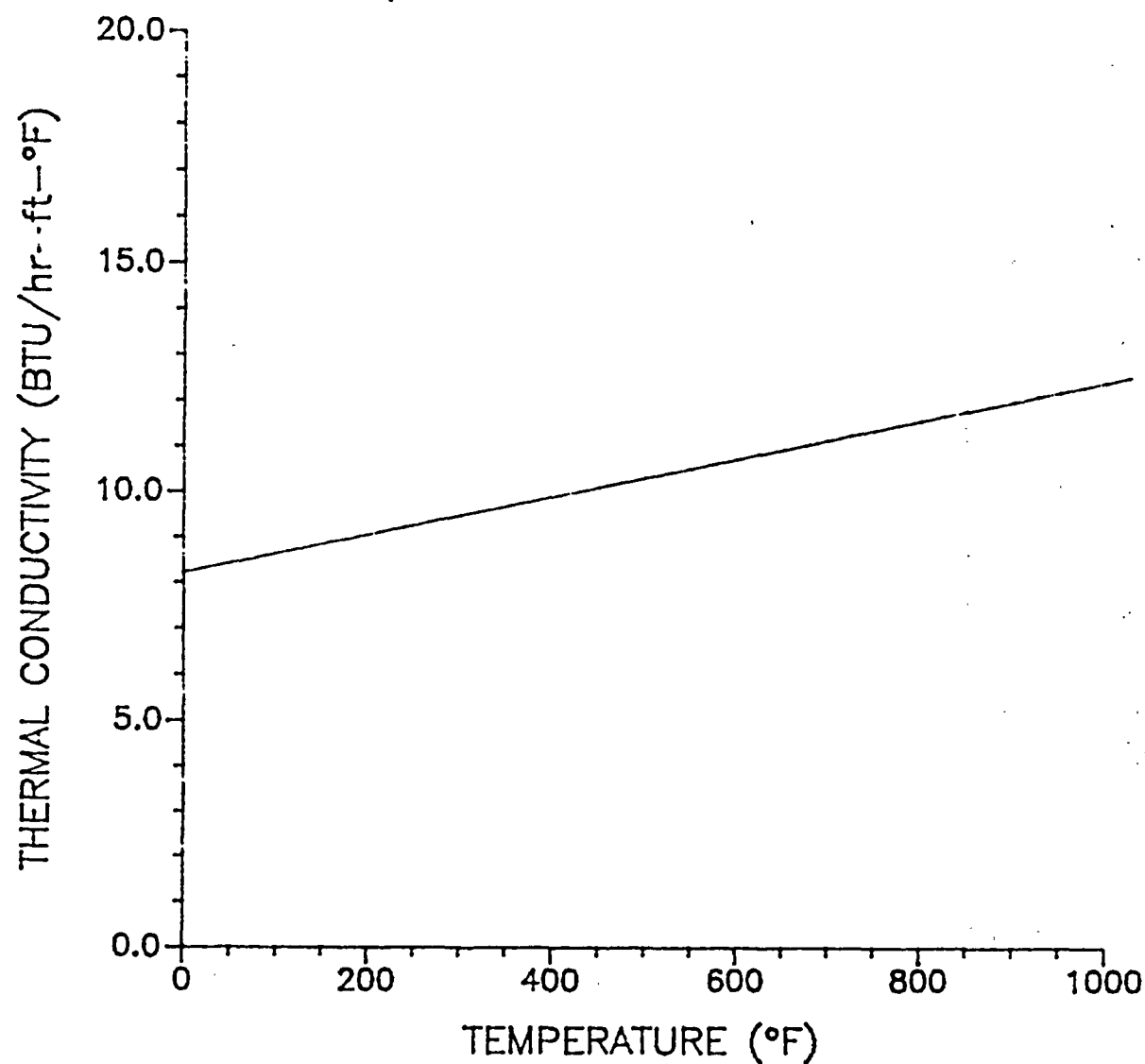


Figure 10-37. WCOBRA/TRAC 1-D Component 347 Stainless Steel Thermal Conductivity

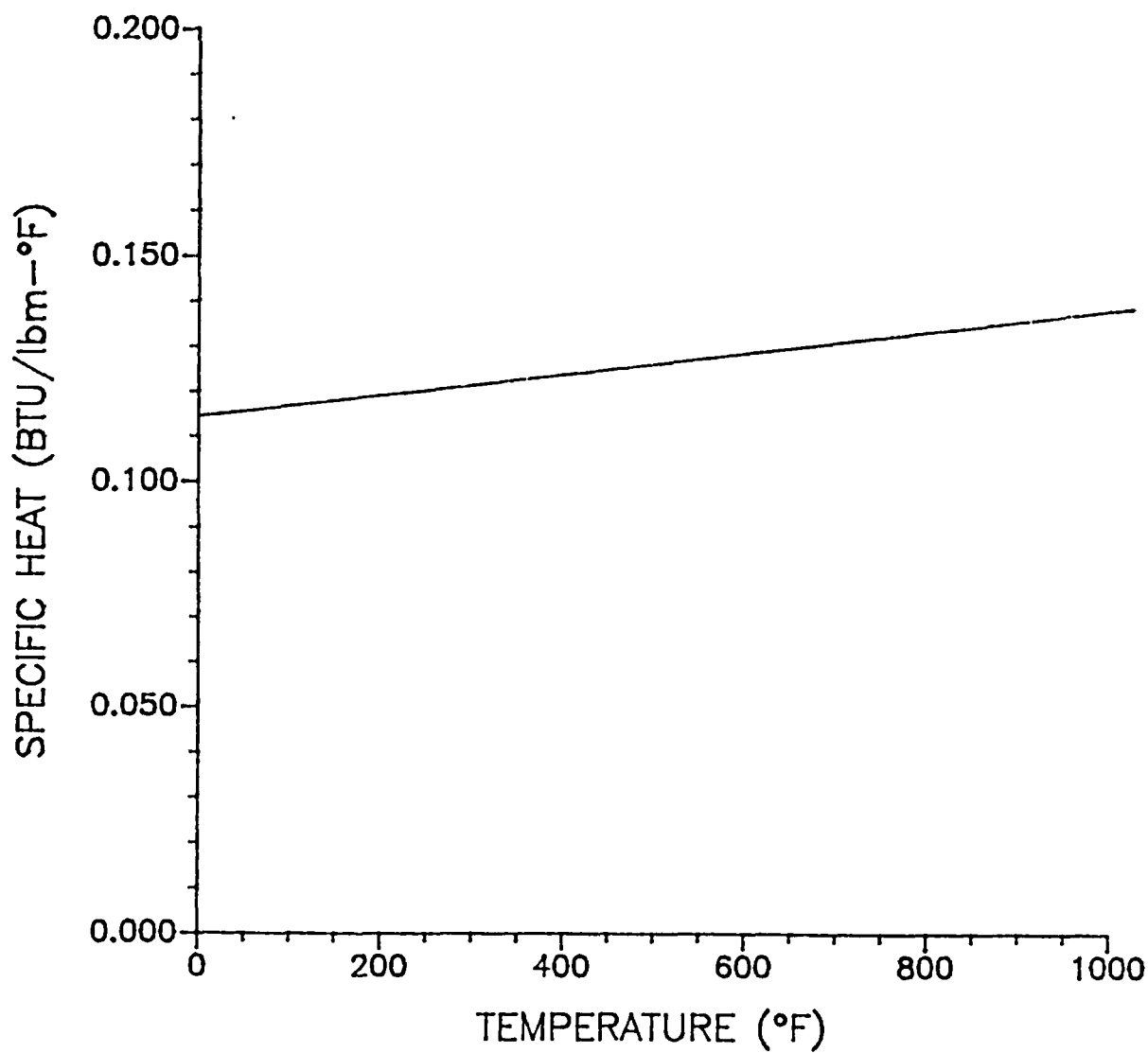


Figure 10-38. WCOBRA/TRAC 1-D Component 347 Stainless Steel Specific Heat

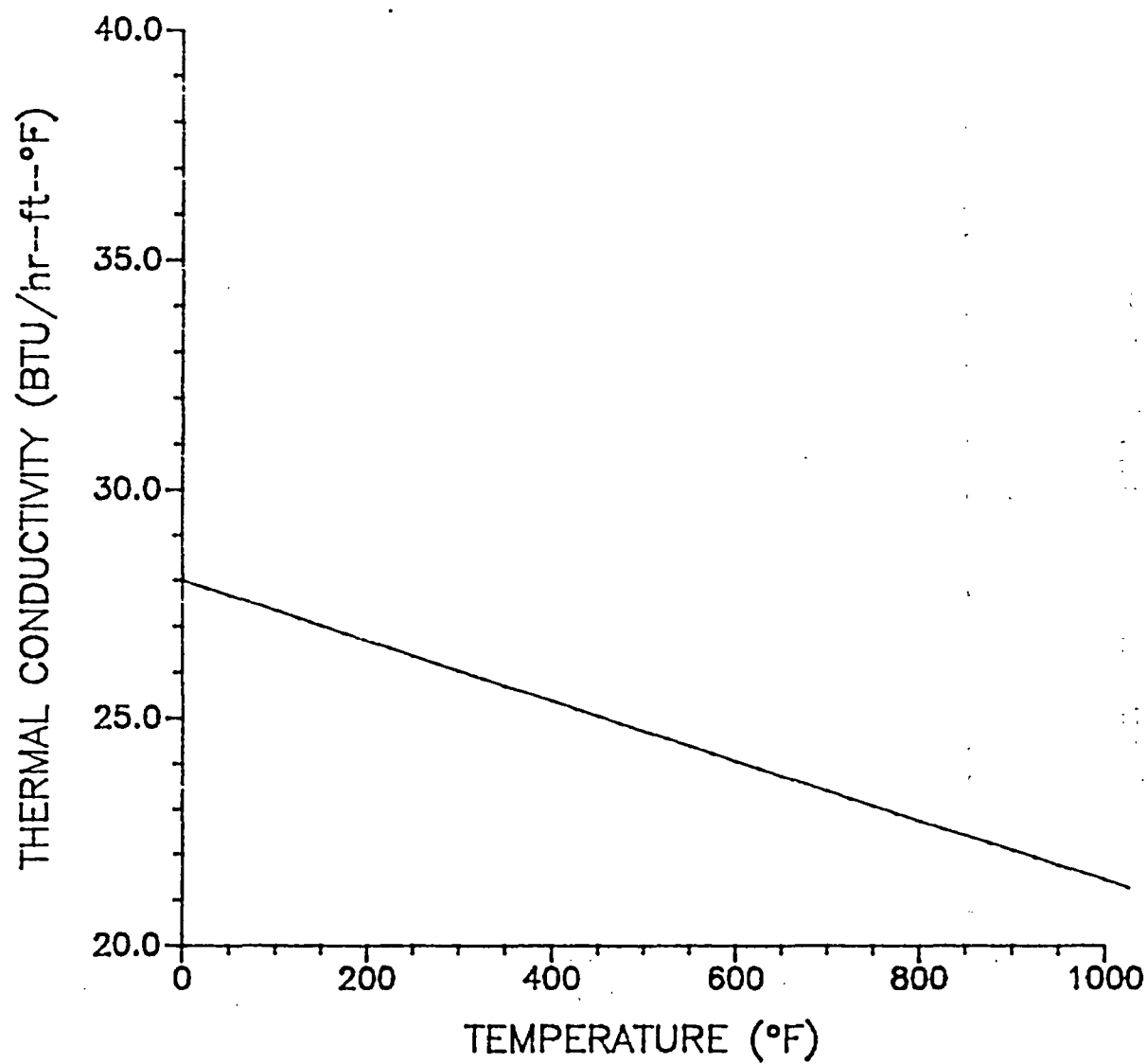


Figure 10-39. WCOBRA/TRAC 1-D Component Carbon Steel Thermal Conductivity



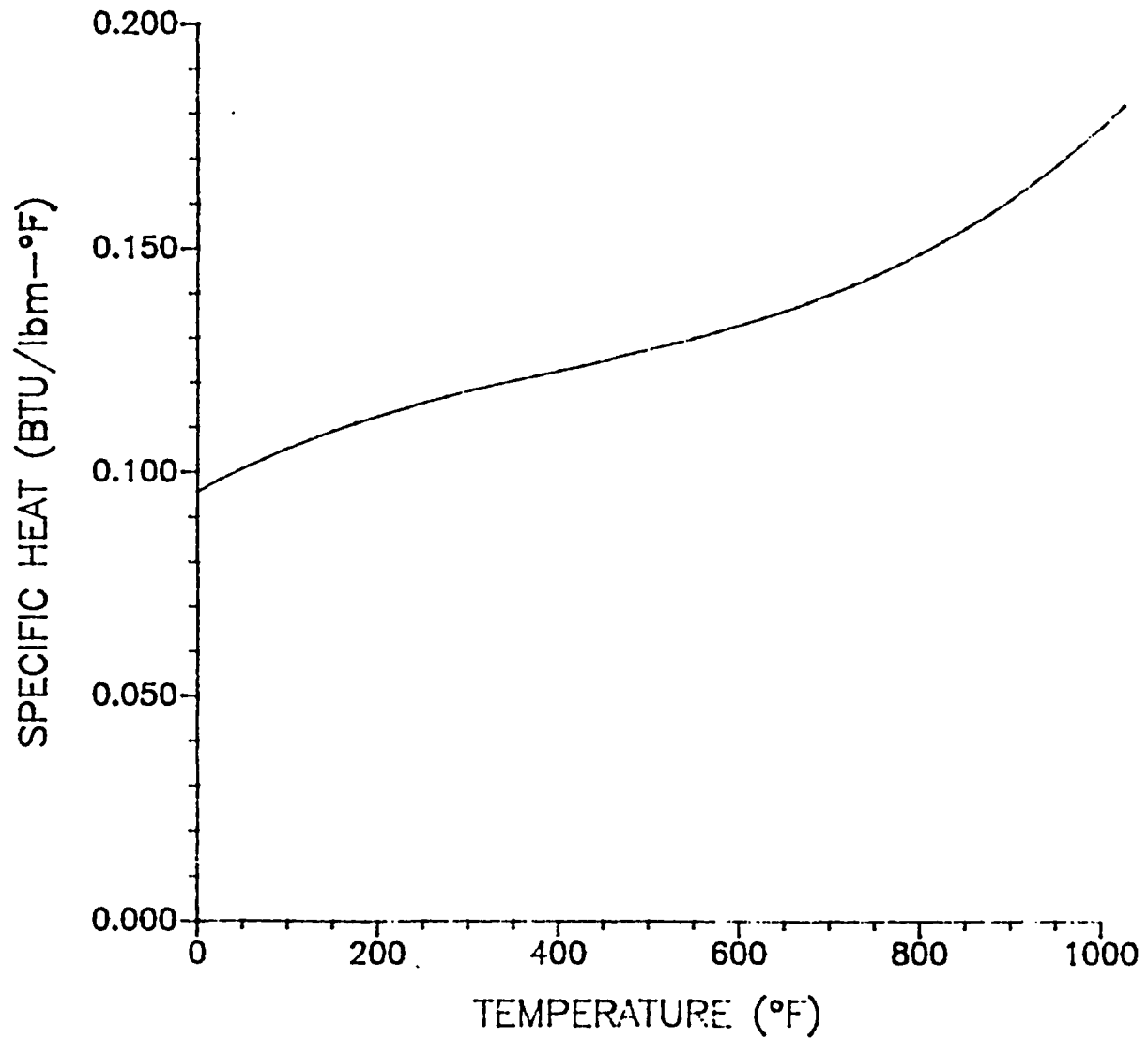


Figure 10-40. WCOBRA/TRAC 1-D Carbon Steel Specific Heat

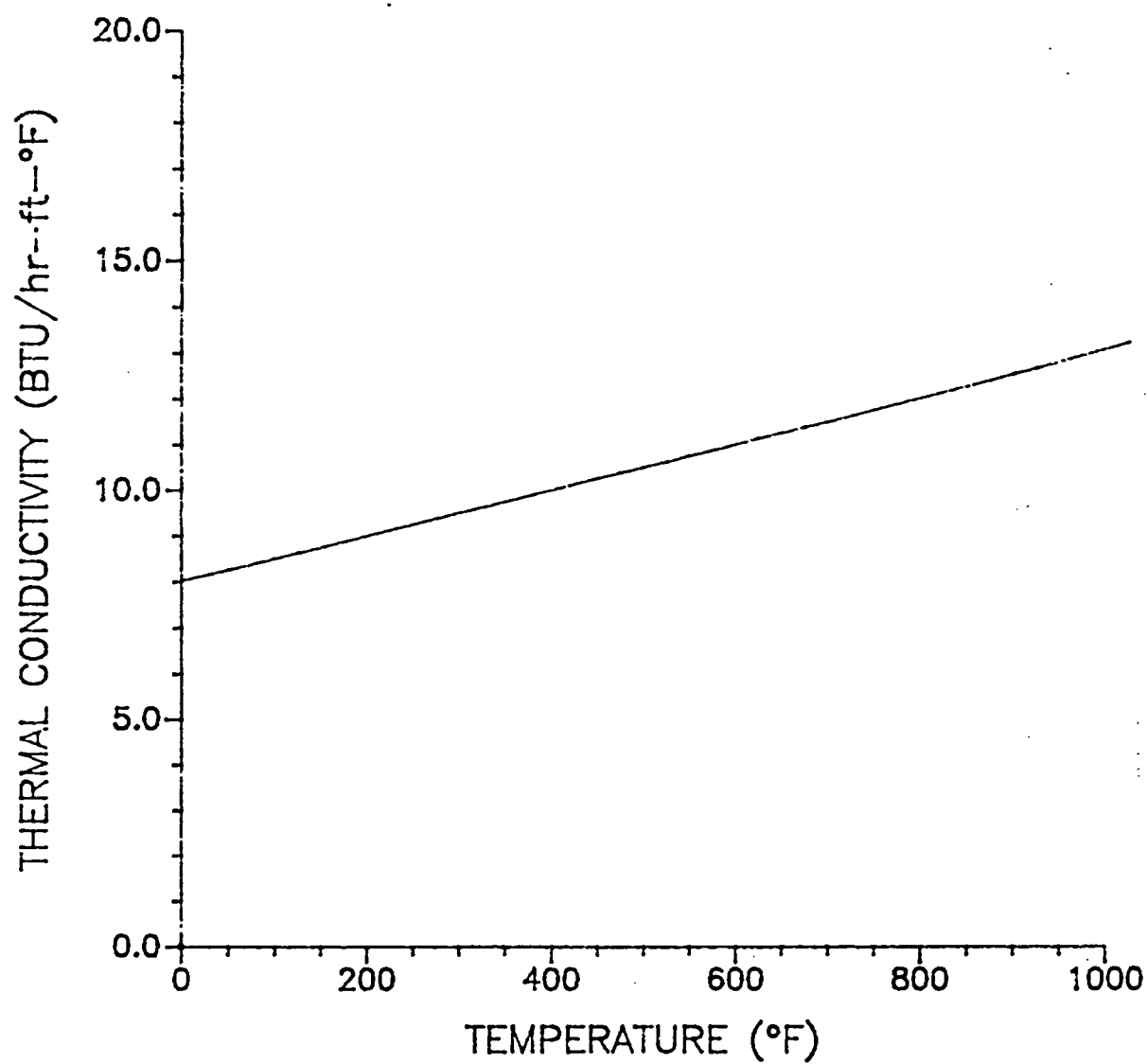


Figure 10-41. WCOBRA/TRAC 1-D Component Inconel 600 Thermal Conductivity

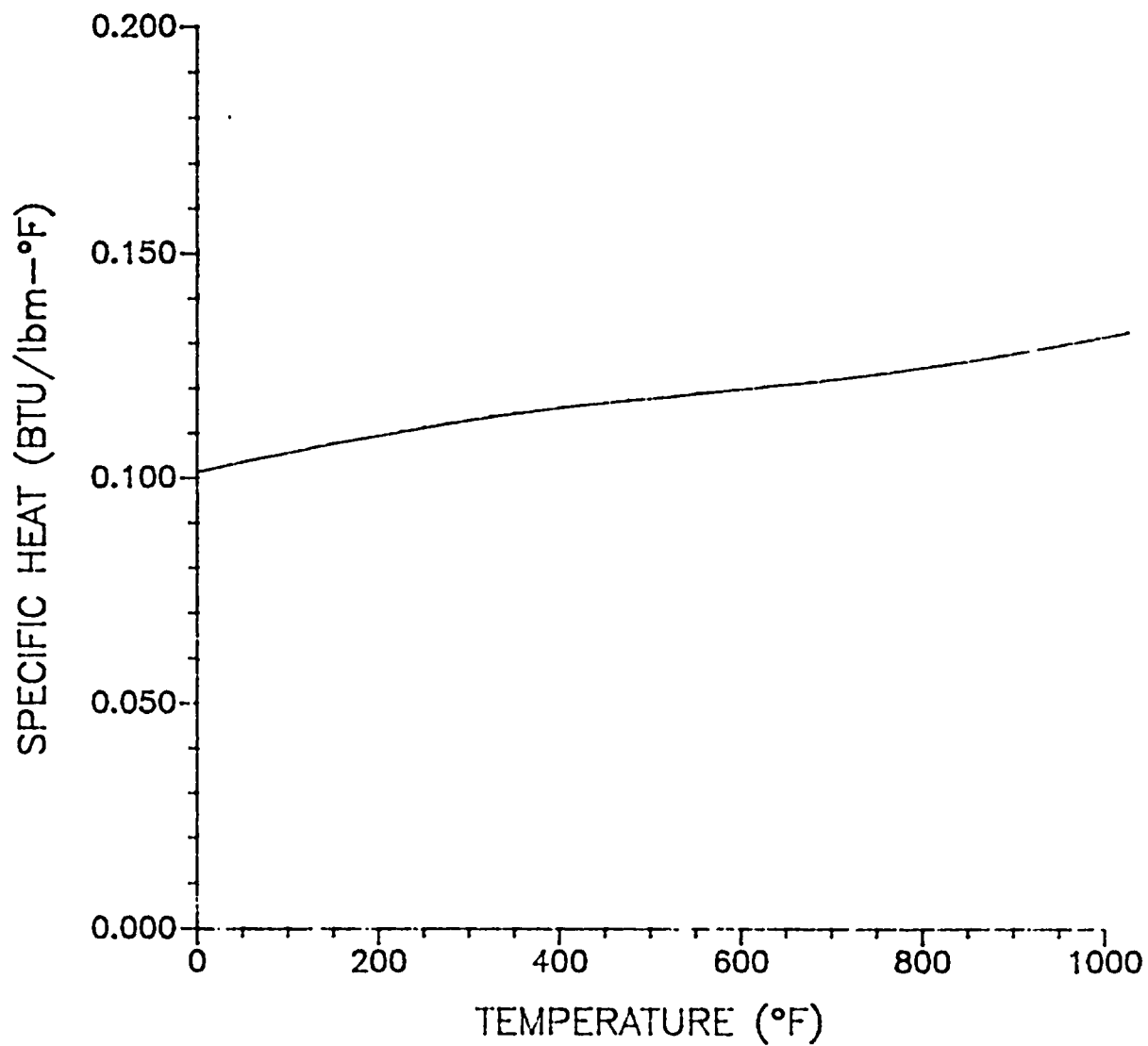


Figure 10-42. WCOBRA/TRAC 1-D Component Inconel 600 Specific Heat

## 11 SENSITIVITY AND UNCERTAINTY ANALYSIS (CSAU ELEMENT 3)

### 11-1 TECHNICAL BASIS FOR REVISED UNCERTAINTY METHODOLOGY

#### 11-1-1 Statistical Sampling Approach

Code Scaling, Applicability, and Uncertainty (CSAU) Element 3, the sensitivity and uncertainty analysis element, aims to provide a simple, singular statement of the uncertainty (Boyack, et al. 1989). To accomplish this objective, the effects of the important individual uncertainty contributors are determined. The uncertainty statement is based on the combined effect of the contributors.

To address criteria (b)(1), (b)(2) and (b)(3) of 10 CFR 50.46, the determination of peak cladding temperature (PCT), local maximum oxidation (LMO) and core wide oxidation (CWO) uncertainty in the Automated Statistical Treatment of Uncertainty Method (ASTRUM) relies on a statistical sampling technique. It is possible to determine the tolerance limits from unknown distributions by randomly sampling the characters in question (in this case, PCT, LMO, and CWO). The consideration of non-parametric tolerance limits was originally presented by Wilks (Wilks, 1941). Wilks' study showed that for continuous populations, the distribution of P, the proportion of the population between two order statistics from a random sample, is independent of the population sampled. Also, it is only a function of the particular order statistics chosen.

Derivation of non-parametric tolerance limits is presented next. This derivation is based upon the non-parametric multivariate tolerance limits formulation first proved by Wald (1943) and more recently adapted by Guba, Makai, and Pal (2003) to the problem of making safety inferences based on the output of models of complex systems. The derivation provided here of the non-parametric tolerance limits follows the formulation by Guba.

For the sake of simplicity the case with a single output variable  $y$  with a probability density function  $g(y)$  is considered first. Assume that nothing is known about the probability density function  $g(y)$  except that it is continuous. If  $N$  runs are carried out with fluctuating input(s), then a sample  $\{y_1, y_2, \dots, y_N\}$  of the random output  $y$  will be obtained.

Two functions  $L = L(y_1, y_2, \dots, y_N)$  and  $U = U(y_1, y_2, \dots, y_N)$  called tolerance limits can be defined such that:

$$P\left(\int_L^U g(y) dy > \gamma\right) = \beta \quad (11-1)$$

Where  $\beta$  represents the probability that a fraction  $\gamma$  of the random output variable  $y$  population falls within the tolerance limits  $U$  and  $L$ .

Let now arrange the values  $y_1, y_2, \dots, y_N$  in increasing order (the probability of equal values of  $y$  occurring is neglected since  $g(y)$  has been assumed to be a continuous function), and denote by  $y(k)$  the  $k^{\text{th}}$  of these ordered value.

Thus, in particular:

$$y(1) = \min_{1 \leq k \leq N} y_k \quad \text{and} \quad y(N) = \max_{1 \leq k \leq N} y_k \quad (11-2)$$

and let by definition  $y(0) = -\infty$  and  $y(N+1) = +\infty$ .

In this case for some positive  $\gamma < 1$  and  $\beta < 1$ , it can be demonstrated that there can be constructed two functions  $L = L(y_1, y_2, \dots, y_N)$  and  $U = U(y_1, y_2, \dots, y_N)$ , such that the probability  $\beta$  that

$$\int_L^U g(y) dy > \gamma \quad (11-3)$$

can be determined, as demonstrated in Guba, as:

$$\beta = 1 - I(\gamma, s-r, N-s+r+1) = \sum_{j=0}^{s-r-1} \binom{N}{j} \gamma^j (1-\gamma)^{N-j} \quad (11-4)$$

where

$$I(\gamma, j, k) = \int_0^\gamma \frac{u^{j-1} (1-u)^{k-1}}{B(j, k)} du \quad (11-5)$$

$$B(j, k) = \frac{(j-1)!(k-1)!}{(j+k-2)!} \quad (11-6)$$

$$0 \leq r < s \leq N, \text{ and } L = y(r), U = y(s)$$

Equation 11-4 can be used to provide an answer to the question “for a given  $L = y(r)$  and  $U = y(s)$ , what is the sampling size  $N$  of the output variable  $y$  that has to be collected so that there is a probability  $\beta$  that a fraction  $\gamma$  of the random output variable  $y$  population falls within the specified tolerance limits  $U$  and  $L$ .” It can be observed that the equation 11-4 does not depend on the probability density function  $g(y)$  or the number of input variables in the process (“statistics of black box model”).

In the particular case that the tolerance limits are selected such that  $r = 1$  and  $s = N$  (i.e, the maximum and minimum value of the samples  $y(k)$  of the output variable  $y$  are used to define  $L$  and  $U$ ), the two-sided tolerance level can be obtained as<sup>1</sup>:

$$\beta = 1 - \gamma^N - N(1 - \gamma)\gamma^{N-1} \quad (11-7)$$

And if the interest is limited only to an upper tolerance limits ( $r = 0$  and  $s = N$ ),

$$\beta = 1 - \gamma^N \quad (11-8)$$

Guba (2003) also provides an extension of the single output variable formulation for the case of multiple variables. For this case, some additional definitions are required. Consider an output comprised of  $p$  variables,  $y_1, y_2, \dots, y_p$ . Let  $g(y_1, \dots, y_p)$  be the joint distribution of the output variables and let  $\underline{Y}$  be defined as:

$$\underline{Y} = \begin{pmatrix} y_{11} & y_{12} & \dots & y_{1N} \\ y_{21} & y_{22} & \dots & y_{2N} \\ \dots & \dots & \dots & \dots \\ y_{p1} & y_{p2} & \dots & y_{pN} \end{pmatrix} \quad (11-9)$$

Where  $\underline{Y}$  is the sample matrix obtained in  $N \gg 2p$  independent runs. Analogous to the single output case, the problem of setting tolerance limits for  $y_1, \dots, y_p$  can be formulated as follows: for some given positive values  $\gamma < 1$  and  $\beta < 1$ , there can be constructed two random functions  $L_j = L_j(y_1, y_2, \dots, y_N)$  and  $U_j = U_j(y_1, y_2, \dots, y_N)$ , such that there is a probability  $\beta$  that:

$$\int_{L_1}^{U_1} \dots \int_{L_p}^{U_p} g(y_1, \dots, y_p) dy_1 \dots dy_p > \gamma \quad (11-10)$$

<sup>1</sup> Note that Guba (2003) equation 18 contains a typo in the definition of  $\beta$  for the two-sided case, that is corrected in equation 11-7.

If  $g(y_1, \dots, y_p)$  is continuous, it can be assumed that no two elements in  $\underline{Y}$  are equal. The sequence of rows in  $\underline{Y}$  is arbitrary, reflecting the fact that we number the output variables arbitrarily. Let us consider the first row of the sample matrix and arrange its elements in order of increasing magnitude  $y_1(1), y_1(2), \dots, y_1(N)$ . Select now between these  $y_1(r_1)$  as  $L_1$  and  $y_1(s_1) > y_1(r_1)$  as  $U_1$ . Let  $i_1, i_2, \dots, i_{s_1-r_1-1}$  stand for the original columns of the elements  $y_1(r_1+1), y_1(r_1+2), \dots, y_1(s_1-1)$ . Next, the  $N$  observed values of the output variable  $y_2$  are considered, and the part  $y_{2i_1}, y_{2i_2}, \dots, y_{2i_{s_1-r_1-1}}$  of its elements are arranged in increasing order to obtain  $y_2(1), y_2(2), \dots, y_2(s_1-r_1-1)$ . Select now between these  $y_2(r_2)$  as  $L_2$  and  $y_2(s_2) > y_2(r_2)$  as  $U_2$ , where evidently  $r_2 \geq r_1$  and  $s_2 \leq s_1-r_1-1$ . If this process is applied to the end of the sample matrix, a  $p$ -dimensional space will be defined:

$$V_p = \{[L_1, U_1] * [L_2, U_2] * \dots * [L_p, U_p]\} \quad (11-11)$$

where:

$$\begin{aligned} L_j &= y_j(r_j) \\ U_j &= y_j(s_j) \\ r_j &\geq r_{j-1} \geq \dots \geq r_1, & \text{for } j = 2, \dots, p \\ s_j &< s_{j-1} \leq s_{j-1} - r_{j-1} - 1, & \text{for } j = 2, \dots, p \end{aligned}$$

As demonstrated by Guba, in the case of  $p \geq 2$  dependent output variables with continuous joint distribution function  $g(y_1, \dots, y_p)$  it is then possible to construct  $p$ -pairs of random intervals  $[L_i, U_i]$ ,  $i = 1, \dots, p$  such that the probability of the inequality:

$$\int_{L_1}^{U_1} \dots \int_{L_p}^{U_p} g(y_1, \dots, y_p) dy_1 \dots dy_p > \gamma \quad (11-12)$$

is free of  $g(y_1, \dots, y_p)$  and is given by

$$\beta = P \left( \int_{L_1}^{U_1} \dots \int_{L_p}^{U_p} g(y_1, \dots, y_p) dy_1 \dots dy_p > \gamma \right) = 1 - I(\gamma, s_p - r_p, N - s_p + r_p + 1) \quad (11-13)$$

As demonstrated in Guba, where  $I(..., ..., ...)$  is the incomplete beta function ratio defined in equation 11-5 and

$$s_p \leq s_{p-1} - r_{p-1} - 1 \leq s_1 - \sum_{j=1}^{p-1} (r_j + 1) \quad (11-14)$$

$$r_p \geq r_{p-1} \geq r_1 \quad (11-15)$$

In several practical applications,  $r_1 = r_2 = \dots = r_p = 1$ , and  $s_p = N-2(p-1)$ , and the probability  $\beta$  from equation 11-13 can be expressed as:

$$\beta = 1 - I(\gamma, N - 2p + 1, 2p) = \sum_{j=0}^{N-2p} \binom{N}{j} \gamma^j (1-\gamma)^{N-j} \quad (11-16)$$

And for a one sided confidence level ( $r_1 = r_2 = \dots = r_p = 1$ ) and  $s_p = N-p+1$ , then<sup>2</sup>

$$\beta = 1 - I(\gamma, N - p + 1, p) = \sum_{j=0}^{N-p} \binom{N}{j} \gamma^j (1-\gamma)^{N-j} \quad (11-17)$$

For the specific application discussed herein, three output variables are considered (PCT, LMO and CWO).

Thus if  $\beta = 0.95$  and  $\gamma = 0.95$  are specified, the number of samples  $N$  can be calculated as 124. The statistical interpretation of this result is that if we observe a random sample of size  $N = 124$ , then there is a  $\beta = 95\%$  probability that the proportion of the population for the three considered output variables (PCT, LMO and CWO for the specific application presented herein) having a value below the maximum calculated values among the 124 sampled cases,  $\gamma$ , is 95%.

This formulation does not contain any consideration of the dependency between the PCT, LMO and CWO, since its derivation is based on the basis that nothing is assumed known regarding the joint density function  $g(y_1, \dots, y_p)$  except that it is a continuous function. In reality, there is a correlation between PCT, LMO and CWO, as shown for example by the sample results provided in Section 12. However, LMO and CWO cannot be considered as monotonous functions of the PCT. For example, LMO tends to

<sup>2</sup> Note that Guba (2003) equation 25 contains a typo in the definition of  $\beta$  for the single-sided case, that is corrected in equation 11-17.



be a function of the local integral over accident time of the cladding temperature. Therefore, PCT, LMO and CWO have been conservatively considered independent output variables of the same process.

### 11-1-2 Application of the Statistical Method

The run matrix is generated by using random numbers. The random numbers are obtained using a generator adapted from Press, et al. This particular generator has a period of approximately  $2.3 \times 10^{18}$ , that is, the numbers generated would not be repeated before  $2.3 \times 10^{18}$  random numbers are used. For all practical purposes, this number is quite large and period exhaustion is considered impossible.

The random number generator returns a value between 0 and 1. Sampling from a uniform distribution is quite straightforward: the random number range is linearly mapped to uniform range of interest.

$$\text{VALUE} = a + (b-a) \cdot \text{RND},$$

where a and b is the minimum and maximum of the uniform range, RND is the random number between 0 and 1 and VALUE is the sampled value from the range. Sampling of values from normal distributions is accomplished by employing the rejection type approach.

The random number generator depends on an initial *seed* to select the starting point in a random sequence. Having such algorithms allow us repeatability of results without compromising randomness. In ASTRUM, the initial seed is obtained randomly from the configuration control system. This system assigns a random identifier to each run, so that they can be uniquely identified. If the run matrix needs to be repeated or extended, by giving the same seed, repeatability is ensured.

Using the attributes corresponding to plant initial conditions, global modeling, and local uncertainty variables, the plant's response to a LOCA event is computed for each case. Then the results are tallied by ranking the PCT, LMO, and CWO from highest to lowest. Using the order statistics, the 95th percentile PCT, LMO, and CWO are determined with 95 percent confidence. Actual plant calculation employing this technique is discussed in Section 12.

## 11-2 TECHNICAL BASIS FOR ADDITIONAL PARAMETERS CONSIDERED IN UNCERTAINTY ANALYSIS

### 11-2-1 Break Type and Size

Break type and size are two of the key loss-of-coolant-accident (LOCA) parameters that are related to the postulated break. In this section, the uncertainty treatment of these parameters is discussed, in addition to the break discharge coefficient. The modeling methodology for double-ended cold-leg guillotine (DECLG) and split breaks will be described in Sections 11-2-1-1 and 11-2-1-2.

The effect of break type will be explicitly accounted for in the ASTRUM, [

] <sup>ac</sup>

### 11-2-1-1 Modeling of DECLG Breaks

#### Noding Scheme

The cold-leg double-ended guillotine break is modeled as shown in Figure 11-2. [

] <sup>ac</sup>

#### Discharge Coefficient Uncertainty Strategy

[

] <sup>ac</sup>

[

] <sup>a,c</sup>

The value of CD is sampled in the nonparametric sampling runs from a distribution determined from a comparison with Marviken tests (Figure 1-2).

### **Justification of CD Strategy**

To confirm that this modeling approach achieved the desired change in flowrate, the same changes were made to the pipe model used to simulate the Marviken experiments. In these studies, the pressure in the upstream BREAK component was reduced from 1000 to 15 psia over 10 seconds, held at 15 psia for 10 seconds, then increased again to 1000 psia over 10 seconds. The first part approximately simulated the depressurization transient that occurs in the pressurized water reactor (PWR) calculation. The results are shown in Table 11-2, and indicate that the desired increase and reduction in break flow were obtained.

#### **11-2-1-2 Modeling of Split Breaks**

A large split break is possible only if the split is longitudinal. Since there is no physical evidence that would indicate how such break types would appear, if they could in fact occur, the break geometry must be postulated.

### **Noding Scheme**

The noding scheme for a broken cold-leg pipe for a split break is shown in Figure 11-4. [

] <sup>a,c</sup>

[

] <sup>a,c</sup>

### Strategy of Varying CD and Break Size

[

] <sup>a,c</sup>

#### 11-2-1-3 Compliance to NUREG 1.157 on Break Type and Size

Regulatory Guide 1.157 states the Nuclear Regulatory Commission's (NRC's) regulatory position on the break type and size for the requirement for best-estimate LOCA (BELOCA) analysis. In this section, the compliance of the revised BELOCA sampling methodology for break type and size to NUREG 1.157 is examined. The following statements are found in NUREG 1.157:

##### Regulatory Position 3.1 – Second Paragraph

The calculations performed should be representative of the spectrum of possible break sizes from the full double-ended break of the largest pipe to a size small enough that it can be shown that smaller breaks are

of less consequence than those already considered. The analyses should also include the effects of longitudinal splits in the largest pipes, with the split area equal to twice the cross-sectional area of the pipe. The range of break sizes considered should be sufficiently broad that the system response as a function of break size is well enough defined so that interpolations between calculations, without considering unexpected behavior between the break sizes, may be made confidently.

#### **Regulatory Position 3.4.1**

In analyses of hypothetical LOCAs, a spectrum of possible break sizes should be considered, as indicated in Regulatory Position 3.1. The discharge flowrate should be calculated with a critical flowrate model that considers the fluid conditions at the break location, upstream and downstream pressures, and break geometry. The critical flow model should be justified by comparison to applicable experimental data over a range of conditions for which the model is applied. The model should be a best-estimate calculation, with uncertainty in the critical flowrate included as part of the uncertainty evaluation. Best-estimate models will be considered acceptable provided their technical basis is demonstrated with appropriate data and analyses.

The worst location of the break that results in the highest PCT was found (in WCAP-12945-P-A) to be the cold leg. The location of break was considered and analyzed, and the largest pipe to be considered in statements that appear in NUREG 1.157 was then found to be the cold-leg pipe. The critical flow modeling was qualified by comparison with a full-scale experiments applicable to large-break LOCA geometry and conditions.

In ASTRUM (revised BELOCA methodology), the uncertainty of key LOCA parameters are treated within nonparametric sampling runs. In ASTRUM, the [

] <sup>ac</sup> to the  
maximum, which is twice the cross-sectional area of the cold leg to permit the consideration of full-break spectrum. It is concluded that ASTRUM meets the intent of the NUREG 1.157 requirement for break type and size requirements.

#### **11-2-1-4 Conclusions**

Break modeling methodology for DECLG and split breaks was discussed and the CD effect is shown to be adequately captured by the break flow area variation. The size of split break is [

] <sup>ac</sup> Finally, the compliance of ASTRUM to  
NUREG 1.157 was examined and found to meet the intent of the requirement stated in its regulatory positions pertinent to break modeling.

Table 11-3 summarizes sampled items in ASTRUM relevant to the break modeling and their sampling distribution.

## **11-2-2 Time in Cycle**

### **11-2-2-1 Burnup Effects on Stored Energy and Peak Cladding Temperature**

Nuclear fuel rods are manufactured with a pellet-cladding gap on the order of 3 to 4 mils. Prior to final welding of the end plug, the rods are pressurized with helium, a gas with good heat transfer capabilities. With irradiation, several changes occur within the rods that affect the initial stored energy, and therefore, the peak cladding temperature (PCT):

- The cladding creeps down to make contact with the fuel pellets, due to the compressive stress on the cladding (system pressure greater than rod internal pressure).
- Gases generated by the fission process mix with the helium fill gas, resulting in an increase in the rod internal pressure and a decrease in the gas conductivity.

The net effect of these changes is a reduction in pellet average temperatures on the order of 300°F for high-power rods, within the first 2 cycles of operation.

Sensitivity studies illustrating the effects of the above changes due to burnup have previously been reported in Section 22-7 of WCAP-12945-P-A (Bajorek et al., 1998). Table 11-4 summarizes the observed effects of burnup on PCT. It can be seen that low burnup (first-cycle) fuel rods are consistently limiting.

### **11-2-2-2 Burnup Treatment in ASTRUM**

With ASTRUM, the LOCA is assumed to be [

] <sup>a,c</sup>

[

]a.c

### 11-3 NPP SENSITIVITY CALCULATIONS WITH ASTRUM (CSAU STEP 12)

Over 100 PWR sensitivity studies were performed in support of the original submittals for 3- and 4-loop plants with cold-leg ECCS (Bajorek et al., 1998), and 2-loop plants with upper plenum injection (UPI) (Dederer et al., 1999). The results of those studies were used to identify the treatment of each parameter identified as a potential contributor to uncertainty. This treatment falls into 3 general categories:

- **Nominal without uncertainty** – The nominal (expected or midpoint) value of the parameter is used without consideration of uncertainty when the variation in the parameter is tightly controlled, such as pressurizer level, or when the sensitivity of the transient results to the value of the parameter is negligible, such as the initial RCS boron concentration.
- **Bounded** – A conservative value of the parameter is used when the parameter varies gradually as a function of operating history, such as steam generator tube plugging, or when the value of the parameter at the time of the accident is indeterminate, such as location of the pressurizer relative to the break. A parameter may also be bounded when the sensitivity of the transient results to variations in the parameter is small, such as moderator temperature coefficient, or when the effort to develop and justify a detailed uncertainty treatment was judged to exceed the benefits of doing so, such as containment pressure response.
- **Nominal with uncertainty** – The Westinghouse methodology includes three categories of uncertainty contributors to the overall uncertainty assessment. These are the thermal-hydraulic model uncertainties, the power-related parameter uncertainties, and the initial and boundary condition uncertainties.

Values for parameters that are bounded on a plant-specific basis are established by confirmatory calculations. Those parameters that are explicitly treated in the uncertainty methodology have their effects quantified by the uncertainty propagation calculations. These two types of calculations are described below.

#### 11-3-1 Confirmatory Calculations

Prior to performing the detailed uncertainty analyses, confirmatory calculations are performed to identify the limiting settings for some parameters. The results of these cases are used to define the reference transient conditions. The confirmatory calculations performed on a plant-specific basis are as follows:

- [

]a,c



[

] <sup>a,c</sup>

### 11-3-2 NPP Uncertainty Calculations

Table 11-5 lists the physical models and plant parameters that are sampled for each case in the uncertainty analysis. The uncertainty distribution sampled for each model and parameter were given previously in Tables 1-7 through 1-11. The PCT for each case is calculated, and the results are ordered from highest to lowest. The 95/95 value of PCT is determined as described in the next section.

### 11-4 DETERMINATION OF COMBINED BIAS AND UNCERTAINTY (CSAU STEP 13)

Section 11-1 described the statistical theory used to determine the number of cases required to establish the 95th percentile PCT, LMO, and CWO at 95-percent confidence. It was shown that the highest value of each of the three parameters (PCT, LMO, and CWO) from a sample size of 124 would be a conservative estimate of the 95/95 value for that parameter.

The Westinghouse methodology for combining biases and uncertainties considers the effect of all medium- and high-ranked phenomena from the Phenomena Identification Ranking Table (PIRT), as detailed earlier in Table 1-1. The following discussion describes how each of the phenomena is considered.

#### 11-4-1 Fuel Rod

**Stored Energy** Uncertainties in the initial stored energy of the hot rod and hot assembly are large. There is a wide range of possible peaking factors and power distributions that are allowed by the Technical Specifications. For a given power distribution, the best-estimate fuel rod temperatures are a

[

] <sup>a,c</sup> Each of these factors has been considered in the uncertainty methodology, by explicitly ranging the parameters.

**Oxidation** The metal-water reaction rate is ranged based on uncertainty estimates obtained from experimental data. See Table 1-8 for the numerical values.

**Decay Heat** The decay heat uncertainties from the American National Standards Institute/American Nuclear Society (ANSI/ANS) 5.1-1979 standard are applied as described in Section 8-7. [

] <sup>a,c</sup>

## 11-4-2 Core

**Departure from Nucleate Boiling (DNB)** The core voids very quickly during a large-break LOCA, such that uncertainties in the timing of DNB are small for a given break size. Uncertainties in the timing of DNB [

] <sup>a,c</sup>

**Post-Critical Heat Flux (CHF)/Reflood Heat Transfer** Uncertainties in the post-CHF and reflood heat transfer are accounted for by ranging the blowdown heatup, blowdown cooling, refill, and reflood heat transfer multipliers. The blowdown heatup heat transfer multipliers are based on assessments of LOFT and ORNL data. The blowdown cooling heat transfer multipliers are based on ORNL and G-1 Blowdown test data. The refill heat transfer multipliers are based on G-2 Refill test data comparisons. The reflood heat transfer multipliers are based on assessments of FLECHT SEASET, FLECHT Low Flooding Rate, FLECHT Skewed, and G-2 Reflood tests. See the previous Table 1-8 and the figures referenced therein for the numerical values of the heat transfer multipliers.

**Rewet** The effects of rewet on reflood heat transfer are directly reflected in the reflood heat transfer multipliers. Assessments of the minimum film boiling temperature models used in WCOBRA/TRAC led to the conclusion that [

] <sup>a,c</sup>

**Three-Dimensional (3-D) Flow/Void Generation and Distribution** Uncertainties in these parameters are accounted for by choosing the limiting hot assembly location based on consideration of the hardware in the upper plenum, and the resulting flow distribution during the downward core flow period of blowdown. The selection of the limiting hot assembly location was supported by the responses to Requests for Additional Information (RAIs) 4-18 and 4-28 for 3- and 4-loop plants (Appendix C, Part 3, of WCAP-12945-P-A), and RAI-16 for 2-loop plants (Appendix C of WCAP-14449-P-A). Multi-dimensional effects are also captured by the core nodalization scheme, which uses 4 separate assembly groupings (hot assembly, assemblies on core periphery, interior assemblies located under guide tube assemblies, and interior assemblies located under other structures).

**Entrainment/De-entrainment** Comparisons with FLECHT, SCTF, and CCTF data indicate that WCOBRA/TRAC overpredicts the amount of entrainment from the core (Section 25-7 of WCAP-12945-P-A). For forced reflood tests, this leads to a slightly higher predicted heat transfer. For gravity reflood tests such as CCTF, however, the excess entrainment results in an over-prediction of steam binding, which reduces the flooding rate and causes an under-prediction of core heat transfer. In addition, the comparisons with Upper Plenum Test Facility (UPTF) tests showed that when the conditions at the entrance to the upper plenum are known, WCOBRA/TRAC underpredicts the mass retained in the upper plenum, therefore overpredicting the amount of water entrained into the loops. Based on the gravity reflood and UPTF test predictions, it is concluded that a conservative bias already

exists in the calculations for core entrainment/de-entrainment, and an additional bias or uncertainty is not required.

**Flow Reversal/Stagnation** Uncertainties in the blowdown flow reversal and stagnation affect the time and magnitude of the blowdown PCT, and the core-wide cooling during blowdown. Uncertainties are accounted for by varying break flowrate, via sampling of break type, split-break size, and the application of break flow multipliers based on comparisons with Marviken critical flow data. Ranging of the broken cold-leg nozzle resistance also affects the flow reversal and stagnation. The interactions between the stagnation point and the axial power distribution are accounted for by ranging the axial distribution as well.

### 11-4-3 Upper Plenum

**Hot Assembly Location** Refer to the discussion of core 3-D flow in Section 11-4-2.

**Entrainment/De-entrainment/Phase Separation** For 2-loop plants with UPI, uncertainties in these processes affect the amount of UPI water entrained out the hot legs. The associated model uncertainties are accounted for by ranging interfacial drag in the upper plenum (Section 4-7 of WCAP-14449-P-A). For 3- and 4-loop plants with cold-leg injection, refer to discussion of core entrainment/de-entrainment in Section 11-4-2.

**Condensation/Counter-Current Flow (CCF) Drain/Fallback (UPI Plants)** The amount of condensation that occurs in the upper plenum affects the temperature of the ECCS water entering the core, which in turn affects core cooling. The temperature of the ECCS water entering the upper plenum, and the amount of condensation that occurs as it falls to the upper core plate, also affects the timing of counter-current flow limitation (CCFL) breakdown at the upper core plate. The temperature of the pumped safety injection water is ranged based on historical plant data, thereby accounting for these variations. Condensation is also ranged in the upper plenum and CCFL region, as discussed in Section 4-7 of WCAP-14449-P-A.

### 11-4-4 Hot Leg

**Flow Reversal** Variations in the timing and magnitude of hot-leg flow reversal can affect blowdown cooling. Uncertainties are accounted for by varying break flowrate, via sampling of break type, split-break size, and the application of break flow multipliers based on comparisons with Marviken critical flow data. Ranging of the broken cold-leg nozzle resistance also affects the flow reversal in the hot legs.

### 11-4-5 Pressurizer

**Early Quench** There is a potential that the 2-phase discharge from the pressurizer surge line could enhance core cooling during the reverse flow period of blowdown. Sensitivity studies have shown that locating the pressurizer [

] <sup>a,c</sup>

### 11-4-6 Steam Generator

**Steam Binding** Refer to the discussion of core entrainment/de-entrainment in Section 11-4-2.

### 11-4-7 Pump

**Two-Phase Performance** Variations in the pump 2-phase performance could affect the timing of the flow reversal in the core. The intact loop pumps are in the pumping mode during the 2-phase period, and the data in this mode show little scatter (Section 16-3 of WCAP-12945-P-A). However, the broken loop pump is in the dissipative mode, where the data scatter is considerable. The uncertainty treatment, therefore, focuses on the broken loop pump resistance uncertainty in the dissipative mode.

**Delta P/Form Losses** Uncertainties in the broken loop pump resistance were found to be a significant contributor to the overall uncertainty assessment. This uncertainty is combined with the broken cold-leg nozzle resistance uncertainty, and applied as a broken loop resistance ratio uncertainty (Section 25-3 of WCAP-12945-P-A).

### 11-4-8 Cold Leg/Accumulator

**Condensation** The amount of condensation that occurs in the cold legs affects the temperature of the ECCS water entering the downcomer, which in turn, affects the amount of ECC bypass. The temperature of the ECCS water entering the downcomer also affects the timing of the onset of boiling in the downcomer-core barrel annulus.

Comparisons with experimental data showed that WCOBRA/TRAC accurately predicts heatup of the ECCS water due to condensation in the cold legs (Section 15-3-3 of WCAP-12945-P-A). The temperatures of the accumulator water and the pumped safety injection water are ranged based on historical plant data, resulting in variations in the temperature of the ECCS water entering the downcomer.

**Non-Condensable Gases** Comparisons with LOFT and ACHILLES test data indicated that WCOBRA/TRAC tends to underpredict the pressurization of the downcomer and the resulting insurge of water into the core, as discussed in Section 16-2 of WCAP-12945-P-A. The heat transfer effects during

the in-surge were examined, and it was concluded that the heat transfer coefficient should be limited to a maximum of  $[ ]^{ac}$  Btu/hr-ft<sup>2</sup>-°F during this period, due to a lack of data under these conditions (Section 25-5-5-8 of the same report). The tendency to underpredict downcomer pressurization, and the use of a maximum heat transfer limitation during the insurge, lead to the conclusion that the effects of accumulator nitrogen will be conservatively calculated.

#### 11-4-9 Downcomer

**Entrainment/De-entrainment** Uncertainties in entrainment/de-entrainment affect the amount of ECC water bypassed at the end of blowdown/beginning of refill. Code model uncertainties were assessed by comparisons with the UPTF ECC bypass test data (Test 6). Those assessments showed that there is a conservative bias, in that ECC bypass is overpredicted (Section 25-6 of WCAP-12945-P-A). The amount of water entrained from the downcomer and out of the broken loop during reflood is also effectively ranged by varying the break type, flowrate, and broken loop nozzle resistance.

Entrainment can also occur during reflood, due to the steam flow from the intact loops. Comparisons with CCTF Run 62 and UPTF Test 25 data indicated that entrainment during reflood is well predicted (Figures 14-2-26 and 14-4-161 of WCAP-12945-P-A).

**Condensation** Condensation in the downcomer affects ECC bypass and the reflood transient. Comparisons with small- and large-scale tests showed that while WCOBRA/TRAC predicted reasonable values of condensation efficiency, the range of uncertainty of the data is large. For 3- and 4-loop plants with cold-leg injection, the condensation in the downcomer is varied based on comparisons with UPTF Test 6 data (Section 25-9 of WCAP-12945-P-A). For 2-loop plants with low-pressure injection into the upper plenum, condensation in the downcomer has been shown to not be an important contributor to uncertainty (response to RAI-23b in Appendix C of WCAP-14449-P-A).

**Countercurrent/Slug/Non-equilibrium Flow** Uncertainties in the flow regimes and distributions affect the amount of ECC water bypassed at the end of blowdown/beginning of refill. Code model uncertainties were assessed by comparisons with the UPTF ECC bypass test data (Test 6). Those assessments showed that there is a conservative bias, in that ECC bypass is overpredicted (Section 25-6 of WCAP-12945-P-A).

**Hot Wall (Vessel/Barrel)** Heating of the water in the downcomer during reflood eventually causes boiling, which results in level swell, spilling of water out of the broken loop, and a reduction in reflood rate. Comparisons with CCTF Run 62 and UPTF Test 25 hot wall tests indicated that the combined effects of downcomer boiling and entrainment on downcomer level during reflood are well predicted (Figures 14-2-26 and 14-4-161 of WCAP-12945-P-A). The timing of the onset of downcomer boiling is ranged by varying the accumulator and pumped safety injection water temperatures, based on historical plant data.

**3-D Effects** Uncertainties in the downcomer flow pattern affect the amount of ECC water bypassed at the end of blowdown/beginning of refill. Code model uncertainties were assessed by comparisons with the UPTF ECC bypass test data (Test 6). Those assessments showed that there is a conservative bias, in that ECC bypass is overpredicted (Section 25-6 of WCAP-12945-P-A).

**Liquid Level Oscillations** The liquid level in the downcomer during reflood is affected by a number of parameters that are ranged, including accumulator and safety injection temperature, accumulator water volume, break type and flowrate, and broken cold-leg nozzle resistance.

#### 11-4-10 Lower Plenum

**Sweep-Out** The amount of liquid swept out of the lower plenum at the end of blowdown depends on the depressurization rate and resulting steam velocities. These parameters are varied by ranging break flowrate, via sampling of break type, split-break size, and the application of break flow multipliers based on comparisons with Marviken critical flow data. Ranging of the broken cold-leg nozzle resistance also affects the sweep-out of liquid from the lower plenum.

**Hot Wall** Heating of the water in the lower plenum during reflood eventually causes boiling, which results in level swell in the downcomer, spilling of water out of the broken loop, and a reduction in reflood rate. The timing of the onset of boiling in the lower plenum is ranged by varying the accumulator and pumped safety injection water temperatures, based on historical plant data.

#### 11-4-11 Break

**Critical Flow** The break flowrate is varied by [ ]<sup>ac</sup>. The development of the break flow multipliers is described in Section 25-2 of WCAP-12945-P-A.

**Containment Pressure** A conservatively low containment pressure is used, which eliminates the need for a detailed uncertainty treatment.

#### 11-4-12 Loop

**Flow Split** The flow split in the broken loop is ranged by varying the broken cold-leg nozzle resistance, by an amount that accounts for uncertainties in its value, and uncertainties in the broken loop pump resistance. Modeling of split break and guillotine break geometries also affects the loop flow split.

## 11-5 DETERMINATION OF TOTAL UNCERTAINTY (CSAU STEP 14)

Step 14 of the CSAU methodology has a provision to consider adding margin to the results of Step 13, if warranted, due to limitations in the code or data base. There are no significant limitations in the code or data base that require the consideration of additional margin. The results of Step 13 are, therefore, considered to be the final results for the ASTRUM.

## 11-6 APPLICATION TO OTHER 10CFR50.46 ACCEPTANCE CRITERIA

Section 11-1 described the statistical theory used to determine the number of cases required to establish the 95<sup>th</sup> percentile PCT, LMO, and CWO at 95-percent confidence. It was shown that the highest value PCT, LMO, and CWO from a sample size of 124 runs would be a conservative estimate of the 95/95 values. This assures that there is a high probability that the acceptance criteria are met, consistent with the Code of Federal Regulations (CFR) 10CFR50.46 requirements and Regulatory Guide 1.157 guidance. Details of the oxidation methodology are described below.

### 11-6-1 Local Oxidation

[

] <sup>a,c</sup>

### 11-6-2 Core-Wide Oxidation

A generic rod power census is used to calculate the core-wide oxidation for the case that yields the maximum hot assembly rod oxidation calculated by WCOBRA/TRAC. This census defines the percentage of rods in the core that are below a given relative power. The generic values are given in Table 11-6, and the resulting FdH ranges are given for an analysis that supports an FdH limit of 1.70.

The WCOBRA/TRAC code calculates the percentage of cladding volume oxidized for each rod in the core. The percentage of cladding volume oxidized for the hot assembly rod for the case that yields the

maximum value represents the Rod Group 1 contribution. A series of additional WCOBRA/TRAC calculations are performed using the same parameter settings, decreasing the hot assembly power in steps according to the generic rod power census. The percentage of cladding volume oxidized for the hot assembly (HA) rod from each of these cases is multiplied by the fraction of the core represented by that case. The results are summed to obtain the core-wide oxidation:

$$\text{Core-wide oxidation (\%)} = \sum_{i=1}^7 (\% \text{ HA cladding oxidized})_i (\text{fraction of core})_i$$

The generic rod power census is very conservative. In the unlikely event that it yields an unacceptable result, a plant-specific census would be used. It would also be checked each reload to ensure its continued applicability.

## 11-7 REFERENCES

Bajorek, S. M., et al., 1998, "Code Qualification Document for Best Estimate LOCA Analysis," WCAP-12945-P-A, Volume 1 Revision 2, and Volumes 2 through 5 Revision 1, and WCAP-14747.

Boyack, B., et al., "Quantifying Reactor Safety Margins," NUREG/CR-5249, (1989).

Dederer, S. I., et al., 1999, "Application of Best Estimate Large Break LOCA Methodology to Westinghouse PWRs with Upper Plenum Injection," WCAP-14449-PA, Revision 1 and WCAP-14450-NP-A, Revision 1 (Non-Proprietary).

Guba, A., M. Makai, and L. Pal, "Statistical Aspects of Best Estimate Method-I," Reliability Engineering and System Safety, 80, (2003), pp. 217-232.

Press, W. H., et al., Numerical Recipes in FORTRAN: the art of scientific computing, 2<sup>nd</sup> Ed., Cambridge University Press, 1992, Chapter 7.

Wald, A., "An Extension of Wilk's Method for Setting Tolerance Limits," Annals of Mathematical Statistics, Vol. 14 (1943), pp. 45-55.

Wilks, S. S., "Statistical Prediction with Special Reference to the Problem of Tolerance Limits," The Annals of Mathematical Statistics, Vol. 13 (1942), pp. 400-409.

Wilks, S. S., "Determination of Sample Sizes for Setting Tolerance Limits," The Annals of Mathematical Statistics, Vol. 12 (1941), pp. 91-96.



Table 11-1

## Break Spectrum Results (WCOBRA/TRAC MOD7)

[					
				</	

[illegible]

Table 11-3 Summary of Sampling Strategy for Break Type, Size, and CD			
[			CD
			a.c

- 3- and 4-loop plants
- 2-loop plants

Table 11-6      Generic Rod Power Census Used for Core-Wide Oxidation Assessment			
[			
			]

a.c

**Figure 11-1. Split vs. DECLG for 3- and 4-Loop PWRs**

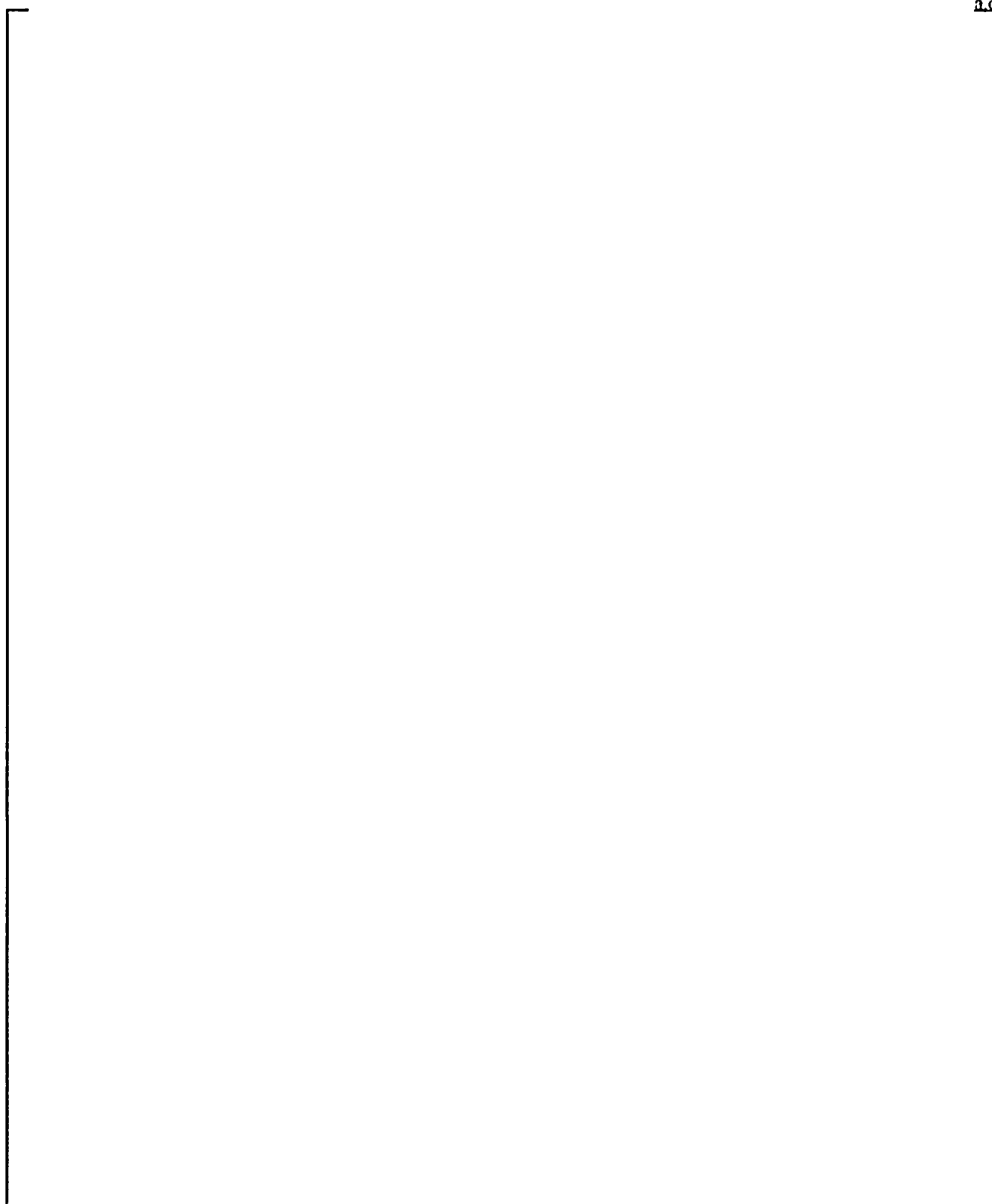


**Figure 11-2. DECLG Break Noding Scheme**

a,c

**Figure 11-3. Guillotine Break Noding Used in WCOBRA/TRAC**



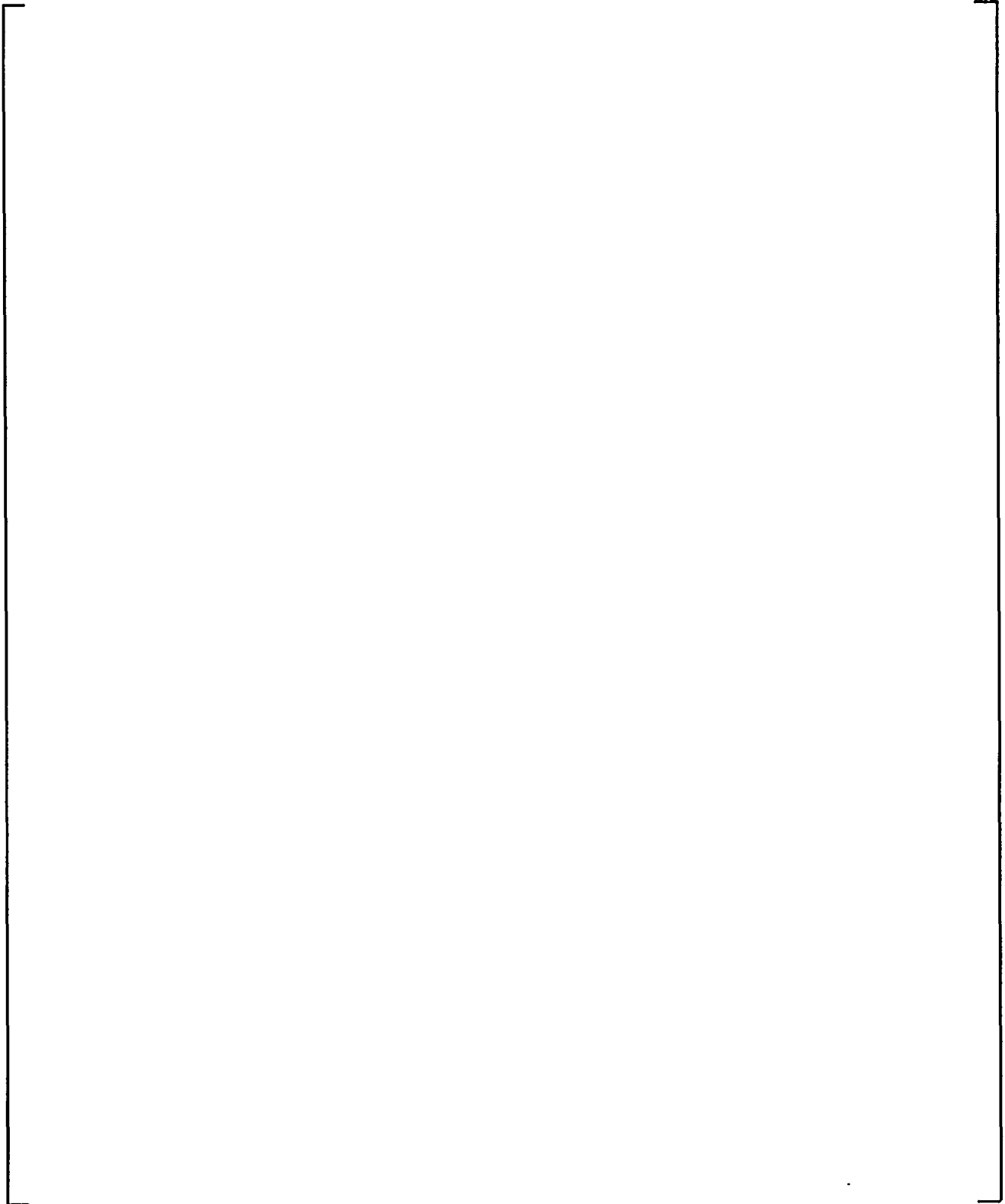


**Figure 11-4. Split Cold-Leg Break Noding Scheme**

a,c

Figure 11-5. Split Break Noding Used in WCOBRA/TRAC

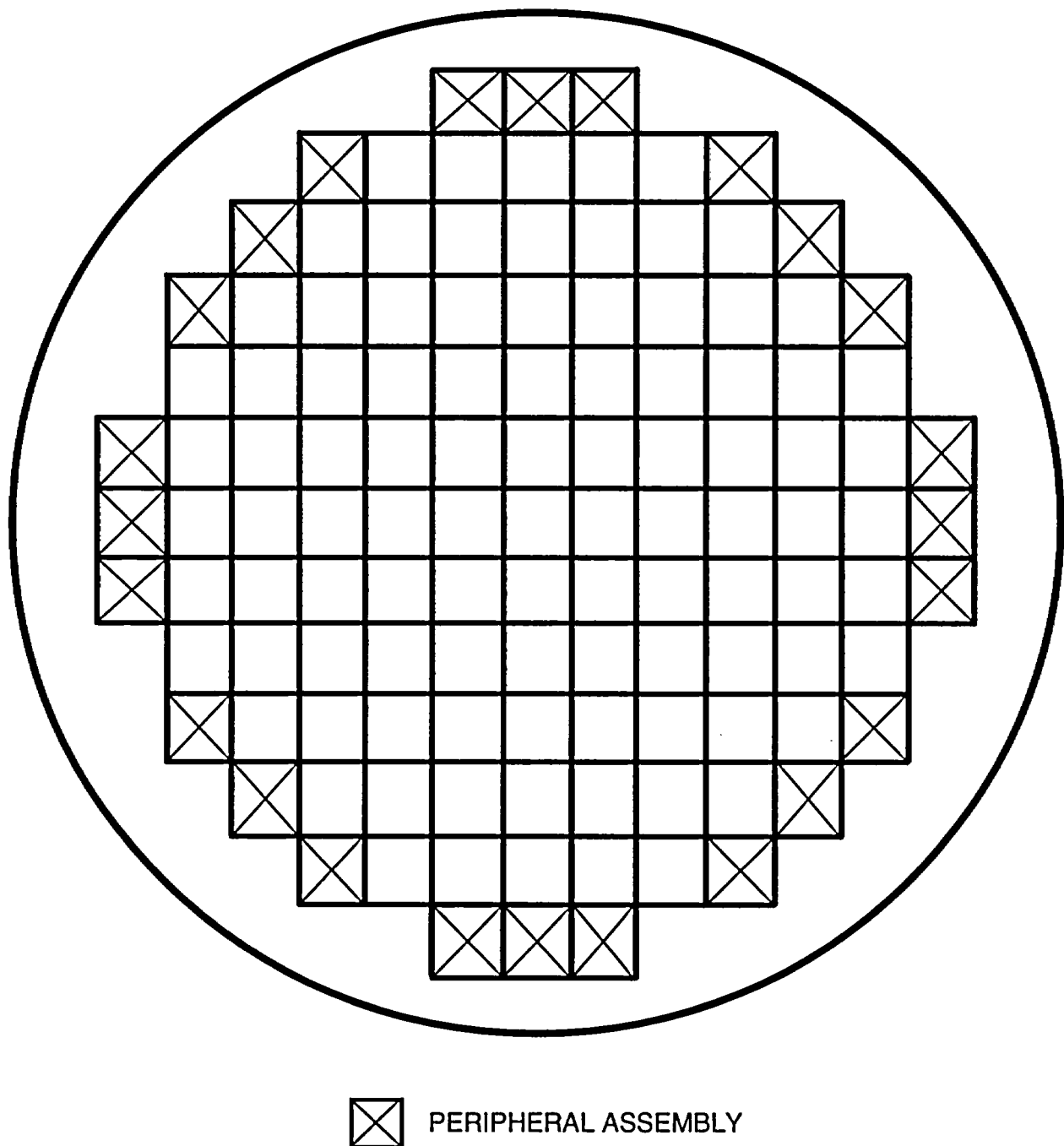


**Figure 11-6. Assemblies Included in the Peripheral (Low-Power) Assembly Channel for 2-Loop Plants**

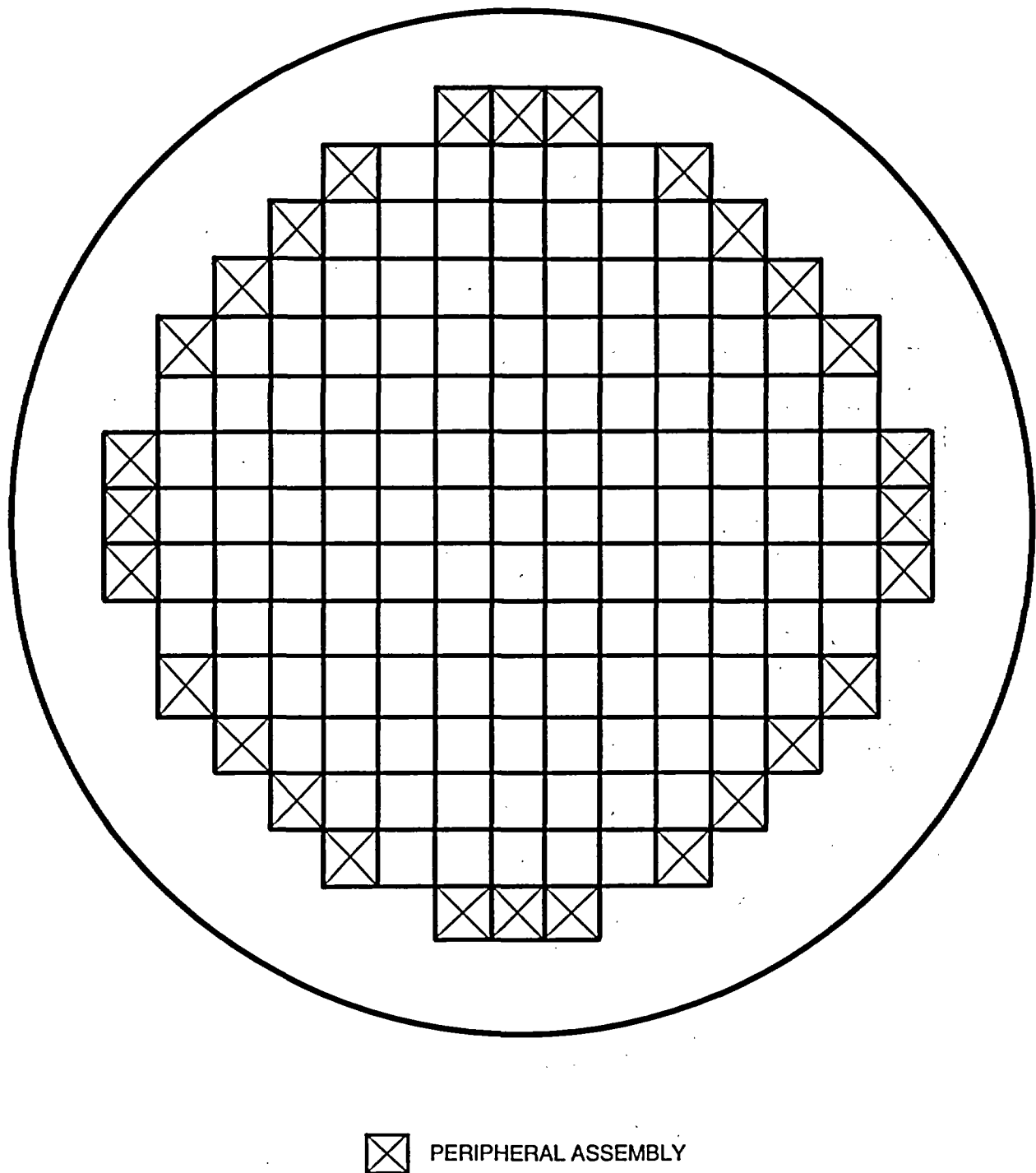


**Figure 11-7. Assemblies Included in the Peripheral (Low-Power) Assembly Channel for 3-Loop Plants**

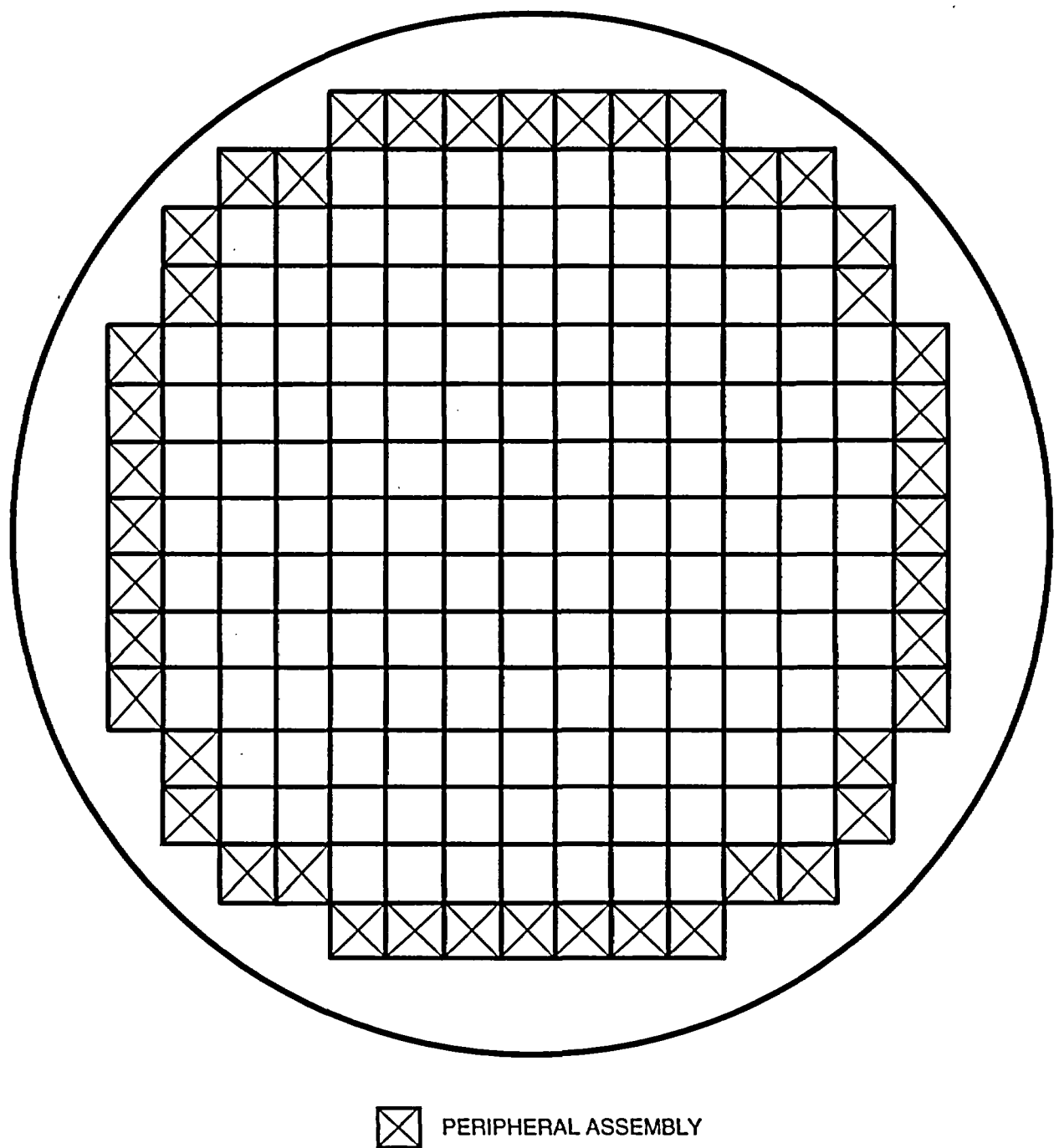


**Figure 11-8. Assemblies Included in the Peripheral (Low-Power) Assembly Channel for 4-Loop Plants**

CCTF Run62, CCTF Run63, CCTF Run64, and CCTF Run67  
Predicted quench time calculation uses Wcobra/Trac Version M7AR6

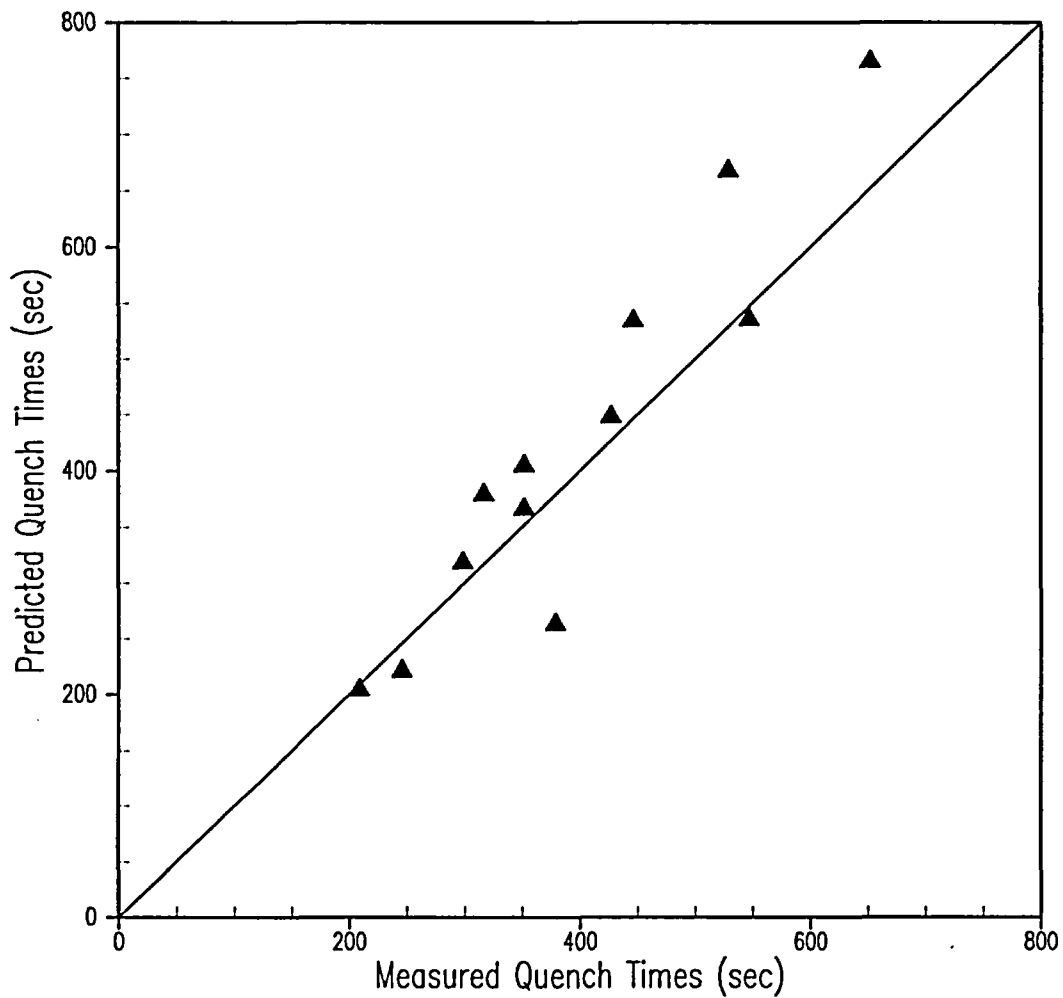


**Figure 11-9. Quench Time Predictions for CCTF Gravity Reflood Tests**

**SCTF Run604**  
**Predicted quench time calculation uses Wcobra/Trac Version M7AR6**

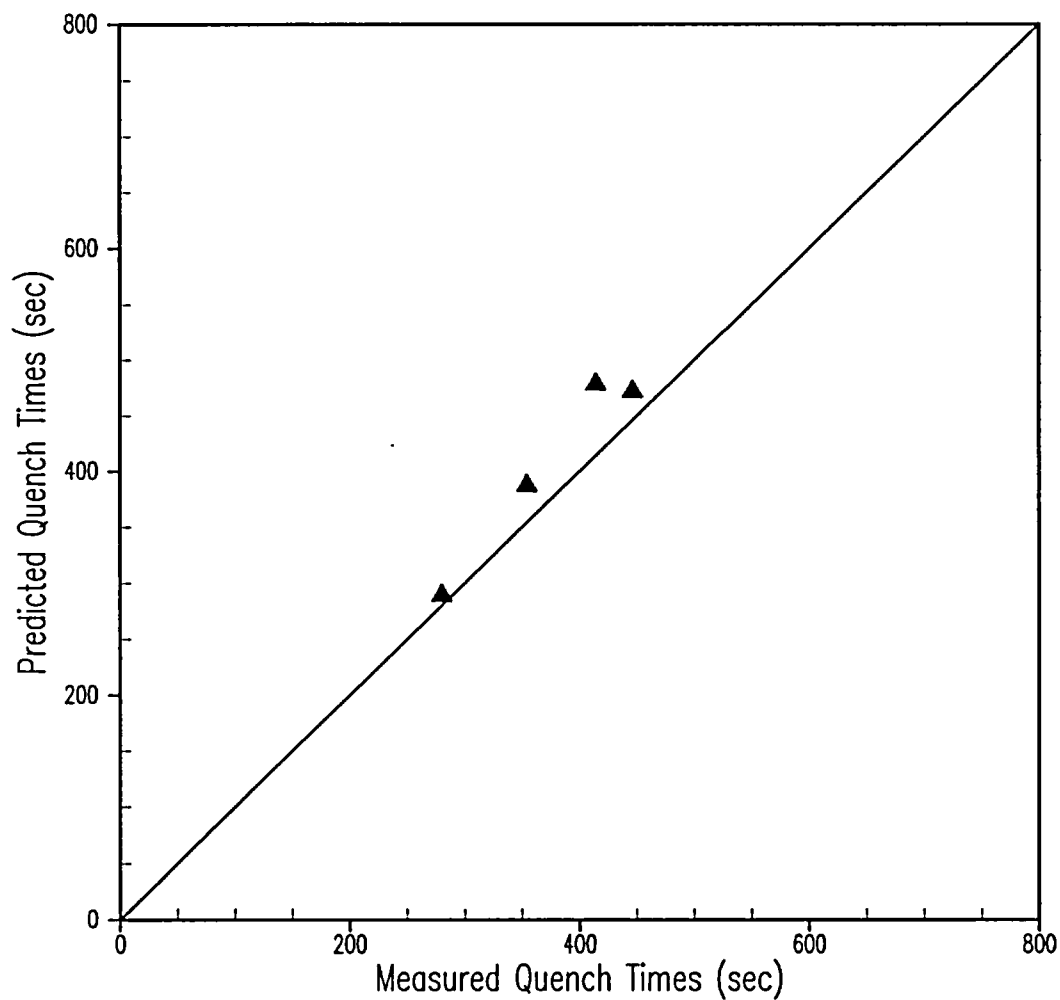


**Figure 11-10. Quench Time Predictions for SCTF Gravity Reflood Test**

## 12 EXAMPLE PWR APPLICATION

### 12-1 INTRODUCTION

All U.S. designed light-water pressurized water reactors (PWRs) have the same fundamental design. The functions of the major system components such as the reactor vessel, pressurizer, steam generators, and pumps are the same, and most have similar design features. Differences between PWR systems are primarily due to loop design and the emergency core cooling system (ECCS) configuration. Operating Westinghouse units, for example, have loop designs that are 2x2 (2-loop), 3x3 (3-loop), and 4x4 (4-loop), while Combustion Engineering units, Westinghouse advanced plants (AP600 and AP1000), and Babcock and Wilcox (B&W) units have a 2x4 loop arrangement. With the exception of size, and the B&W once-through steam generator, individual loop flow paths in each type of system are similar.

The reactor vessel internals for various PWRs are also similar. There are differences in the detailed internal structures of various regions, however. In some older Westinghouse plants, for example, the lower support plate is curved while in other plants it is flat. Within the core, there are differences in fuel design. Some plants have a thermal shield in the downcomer, while others have a neutron pad attached to the core barrel. The B&W plants include vent valves in their core barrels. The upper plenums and upper heads contain control rod guide tubes and support structures that may have slightly different designs and arrangements.

Most PWRs in the U.S. have an ECCS configuration that includes high- and low-head pumped safety injection, in addition to accumulators for passive injection. The injection location for most plants is the cold legs. The AP600 and AP1000 vessels include injection directly into the downcomer. Several 2-loop plants are equipped with an upper plenum injection (UPI) system. While the WCOBRA/TRAC models and correlations description and the existing code validation results are expected to be applicable to any of the various PWR designs, approval has been granted for Westinghouse 3- and 4-loop plant designs with ECCS injection into the cold legs (Bajorek et al., 1998). Approval has been extended to UPI plants (Dederer et al., 1999) and the AP600 design (Hochreiter et al., 1998). The justification for extending the approval to Combustion Engineering designs is provided in Appendix A.

The differences in the various PWR designs lead to differences in flow areas, volumes, and surface areas within various regions of the PWR primary system. The WCOBRA/TRAC nodalization for a PWR reactor coolant system (RCS) must model specific flow paths and regions within the system. Therefore, the PWR design itself dictates, to an extent, the specific nodalization and inputs for a plant model. However, the geometric differences do not add to the code uncertainty as long as a consistent modeling methodology is maintained while developing the nodalizations for PWRs and the test simulations used in determining the code and model uncertainties. The nodalization methodology used with WCOBRA/TRAC was established in Section 20 of WCAP-12945-P-A (Bajorek et al., 1998). Application of the methodology to a 4-loop plant is described in detail in this section.



## 12-2 SAMPLE PWR PLANT DESCRIPTION AND NODALIZATION

The sample PWR plant is the Indian Point Unit 2 (IP2). This is a 4-loop Westinghouse PWR located near New York City. It is owned and operated by Entergy. It is one of the first 4-loop PWRs completed, and has been operational for over 20 years. Figure 12-1 depicts the reactor vessel, showing the internals design.

A major portion of a WCOBRA/TRAC analysis involves generating the plant-specific vessel and loop model, and the appropriate inputs to that model, to properly describe the plant. The vessel model, in particular, requires detailed information regarding the vessel internals. Detailed engineering drawings for the plant are used to define the inputs to the plant-specific model.

### Vessel Model

Figure 12-2 shows the vessel elevation layout for IP2. The elevations shown on the right are relative to the inside bottom of the vessel. This elevation layout contained most of the information needed to divide the vessel into 9 vertical sections. Except for the elevation of the boundary between Section 1 and Section 2, all the other section boundaries were determined from Figure 12-2. Proceeding up the vessel, the bottom of Section 1 is the inside vessel bottom. The bottom of Section 3 is defined as the beginning of the active fuel. The bottom of Section 4 is the top of the active fuel. The bottom of Section 5 is the elevation at the bottom of the upper core plate (UCP). The bottom of Section 6 is the elevation of the bottom of the hot-leg inner wall. The bottom of Section 7 is the elevation of the top of the hot leg. The bottom of Section 8 is the elevation at the bottom of the upper support plate. The bottom of Section 9 is the elevation at the top of the upper guide tube in the upper head. The top of Section 9 is the inside top of the vessel upper head. The bottom of Section 2 is the only section boundary that cannot be determined by viewing Figure 12-2. The bottom of Section 2 is defined by an elevation such that the flow area of the curved lower support plate (or the lower support dome) below this elevation is approximately equal to that above this elevation. Figures 12-3 and 12-4 show the location of the section boundary between Sections 1 and 2.

After defining the elevations for each section, a noding scheme was defined following the same basic rules applied to the LOFT model. These rules include: 1) cell boundaries at all significant area changes, pressure loss locations, and changes in flow direction; 2) a minimum of two lateral subregions (channels) in each section where multi-dimensional flow is expected; 3) a hot assembly in the core section of the PWR model, as in all large-scale integral test simulations.

Figures 12-5 through 12-8 illustrate the IP2 vessel noding. Figure 12-5 is a vertical section noding diagram, and Figures 12-6 through 12-8 are horizontal views of each section. In these figures, the values within the squares are the channel numbers, and the values within the circles with arrows attached to them are the horizontal flow gap numbers. A gap is used to define a lateral flow path between channels. Positive flow is in the direction indicated by the arrow. The WCOBRA/TRAC code assumes a vertical flow path for vertically stacked channels, unless specified otherwise in the input. Upward axial flow is

considered as positive flow. As can be seen in Figures 12-5 through 12-8, 63 channels and 66 gaps are used in the IP2 model to define the vessel. Figure 12-5 also illustrates that several of the 9 sections were subdivided into 2 or more levels. For example, the active fuel region (Section 3) is divided into 16 vertical levels. By accounting for the vertical subdivision within Sections 2, 3, 5, and 7, the vessel model for IP2 has a total of 221 fluid cells.

Vessel Section 1 models the vertical section of the vessel from the inside bottom of the vessel to an elevation that splits equally (approximately) the through-flow area of the curved lower support dome above and below this elevation. This section contains 5 channels (designated 1 through 5) and 8 horizontal flow gaps (numbered 1 through 8) to model this portion of the vessel. Channels 1 to 4 represent the annulus volume continued downward from the downcomer, and Channel 5 models the center portion of this section underneath the curved dome. Because the flow in Channels 1 to 4 is expected to be parallel to the curved surfaces of the vessel wall, the area that is perpendicular to the streamlines at the top of these channels (which is at an angle of approximately 45 degrees from the vertical axis) is taken as the effective flow area at the top of these channels. The top flow area of Channel 5 represents the through-flow area in the lower support dome and has an area of about 50 percent of the total through-flow area of the lower support dome. Gaps 1 to 4 are the lateral connections between the 4 peripheral channels, and Gaps 5 to 8 are the radial connections between the peripheral channels and Channel 5. Positive flow is in the arrow direction indicated in the figure. While Channel 1 is in the vessel quadrant that connects to Loop 1 (the assumed broken loop), Channels 2, 3, and 4 are in the quadrants that connect Loops 3, 4, and 2, respectively.

Vessel Section 2 models the vertical section of the vessel from the top of Section 1 to the bottom of the active fuel region. This section contains 2 vertical sublevels. The intermediate level interface is set at the top edge of the lower support dome, which is at about the same elevation of the top surface of the radial keys. This section contains 5 channels (designated 6 through 10) and 8 horizontal flow gaps (numbered 9 to 16). Channels 6 to 9 model the annulus volume outside the curved dome, Channel 10 models the volume inside the dome. The top cell of Channel 10 contains the flow distribution plate, lower core plate, bottom fuel nozzle, non-active portion of the fuel rods, and so forth. The through-flow area in the lower core plate was used as the momentum area connecting Channel 10 to the core region. Gaps 9 to 12 model the lateral connections between the peripheral channels (Channels 6 through 9) in the extended downcomer region, and Gaps 13 to 16 model the horizontal radial connections between the peripheral channels and Channel 10. Because this section has 2 sublevels, each channel has 2 cells and each gap has 2 levels. The upper level of the radial gaps, however, is blocked since there is no flow across the core barrel extension (sometimes referred to as the flow skirt). The lower level of the radial gaps models the flow across the lower support dome in this section. The total flow area of these gaps equals about 50 percent of the through-flow area of the whole lower support dome. Area variation inputs are used to vary the axial and gap flow areas in this section to account for the area changes due to the curved walls and other structure blockages.

Vessel Section 3 models the vertical section of the vessel from the bottom to the top of the active fuel region. The modeling is accomplished using 16 vertical cells in 9 channels (designated 11 through 19),

and 12 horizontal flow gaps (17 through 28). Channels 11 to 14 each represent one-fourth of the downcomer annulus volume between the vessel inner wall and the core barrel outer wall. Channel 15 is the annulus volume between the barrel inner wall and the baffle plates (barrel/baffle region), and is designated as the B/B channel. Channels 16 through 19, combined, represent the total fluid volume within the baffle plates (minus the thimble bypass volume), that is, the entire core active fuel region for all 193 assemblies in IP2. Channel 16 includes assemblies on the periphery of the core that have relative low power. For IP2, 44 assemblies are in Channel 16, which is designated as the low-power (LP) channel. To determine the breakdown of the remaining 149 assemblies, in particular, the designation for the hot assembly, the upper plenum (vessel Section 5) structure layout was examined. Figure 12-9 shows that 4 types of internals existed in the upper plenum: guide tubes, orifice holes, support columns, and free-standing mixers. Among the 4 types of structures, the [

J<sup>ac</sup>

The active fuel length is divided into 16 axial cells. The grids are modeled within this length range at their specified elevations. The axial form loss coefficients are modeled at the appropriate momentum cell centers. The momentum area at the top of the fuel channels uses the flow area through the top fuel

nozzle, which has the limiting flow area. The momentum area at the bottom of Channels 16 through 19 uses the through-flow area of the lower core plate.

Section 4 models the vertical section of the vessel from the top of the active fuel to the bottom of the UCP. This section has 1 vertical cell and uses 9 channels (designated 20 through 28) and 8 horizontal gaps (29 to 36) to model this portion of the vessel. Channels 20 to 23 each represent one-quarter of the downcomer annulus volume between the vessel inner wall and the core barrel. Channels 24 to 28 model the vessel volume inside the baffle which is referred to as the counter-current flow limit (CCFL) region. Channels 25 to 28 represent the [

J<sup>ac</sup>

Section 5 extends vertically from the elevation of the bottom of the UCP to the elevation of the bottom of the hot leg. This section contains 2 vertical cells for 10 channels (designated 29 through 37, and 62) and 9 horizontal flow gaps (37 through 44, and 64). Channels 29 to 32 are the downcomer channels each representing one-fourth the downcomer annulus volume between the vessel wall and the barrel outer wall. Channels 34, 35, 36, and 37 model the cylindrical volumes with flow areas and wetted perimeters based on the holes in the upper plate, above the LP, SC/OH/FM, GT, and HA fuel channels, respectively. Channel 33 is the inner global channel representing the fluid volume outside of the cylindrical volumes above the fuel assemblies in the SC/OH/FM, GT, and HA channels. Channel 62 is the outer global channel representing the rest of the fluid volume in the upper plenum that is not included in the inner global channel.

Section 6 models the vertical section of the vessel from the bottom to the top of the hot leg (inner diameter). This section uses 1 vertical cell in 12 channels (designated 38 through 49) and 11 horizontal flow gaps (45 to 55) to model this section. Figures 12-5 and 12-7 provide an illustration for the vertical and radial representation of this section of the vessel model. Channels 38 to 41 each represent one-fourth of the downcomer annulus volume between the vessel inner wall and the core barrel outer wall, excluding the hot leg that passes through this region. Channel 42, the inner global channel in this section, includes the volume above the single hot assembly combined with the volume above the inner global channel in the section below. Channels 44 and 45 model the fluid volumes inside the support columns and the guide tubes in this section, respectively. Channel 43, the outer global channel, models the rest of the fluid volume in the section. Channels 46 to 49 each represents the volume of the hot leg within the vessel. Gaps 52 to 55 model the lateral flow connections between the upper plenum and the hot legs.

Section 7 extends vertically from the top of the hot leg to the bottom of the upper support plate, yielding an overall height of 82.50 inches for this section. This section is divided into 2 levels with the lower

level cell from the top of the hot legs to the bottom of the deep beam. This section contains 2 cells for 8 channels (designated 50 through 57) and 7 horizontal flow gaps (56 to 62). Channels 50 through 53 each represent one-quarter the downcomer annulus volume between the vessel inner wall and the core barrel outer wall, and are connected vertically to the upper head through the spray nozzle holes. Channel 54 is the inner global region and is a vertical extension of Channel 42. Channel 55 is the outer global region and is a vertical extension of Channel 43. Similarly, Channels 56 and 57 are the vertical extensions of Channels 44 and 45, respectively, in the section below. There are no vertical flow connections at the top of Channels 54, 55, and 56 between the upper plenum and the upper head. Channel 57 connects vertically to the upper head through the guide tube extension.

Section 8 extends vertically from the bottom of the upper support plate to the upper guide tube's top plate (elevation 444.406 inches), yielding an overall height of 19.25 inches. This section has 1 vertical cell for 4 channels (designated 58 through 60, and 63) and 3 horizontal flow gaps (63, 65, and 66). Channels 58 and 63 model the peripheral region. Channel 58 is connected vertically to the downcomer Channels 50 and 51 below, and Channel 63 is connected to the downcomer Channels 52 and 53 in Section 7. Channel 60 models the fluid volume inside the guide tube, and Channel 59 models the rest of the fluid volume in the upper head in this section. The boundary between this channel and the peripheral channels is defined by an imaginary cylindrical surface that intersects the upper head's vessel wall at an elevation of 444.406 inches.

Vessel Section 9 models the vertical section of the vessel extending from the top plate of the upper guide tube to the inside top of the vessel head, yielding an overall height of 50.531 inches for Section 9. This section is modeled by 1 channel (designated 61). There is no horizontal flow gap in this section. The flow area at the bottom of Channel 61 is equal to the sum of the flow area at the top of Channels 59 and 60 from Section 8.

Tables 12-1 and 12-2 give the channel noding and gap connection summary for the IP2 vessel model.

### Core Model

The WCOBRA/TRAC code allows for modeling of heated and unheated conductor geometries. Unheated conductors are used to model metal mass in the reactor vessel such as the vessel wall. These conductors are connected to appropriate vessel channels. For heated conductors, the code allows for detailed radial and axial noding. For the nuclear rod, other fuel related inputs (rod internal pressure, fuel rod gas molar fractions, cladding thickness, fuel theoretical density, etc.) can be specified. For the 15x15 fuel, each fuel bundle contains 204 fuel rods, 20 thimble tubes, and 1 instrumentation tube. Five fuel rod groups are modeled in the IP2 vessel model. Rod 1 represents a single fuel rod, known as the hot rod, and is located in the hot assembly (Channel 19). Rod 2 represents the remaining 203 fuel rods in the hot assembly and has a power equivalent to the hot assembly average fuel rods. Rod 3 represents the 61 average fuel assemblies contained in the guide tube channel (Channel 18). Rod 4 represents the 87 average fuel assemblies contained in the support column/open hole/free-standing mixer channel

(Channel 17). Rod 5 represents the 44 assemblies contained in the peripheral low-power channel (Channel 16).

Each fuel rod is assigned an axial power profile. The axial power profile is varied within the uncertainty analysis as discussed in Section 12-5.

### Loop Model

As with the vessel inputs, each component in the one-dimensional loop can have a number of cells to allow for changes in geometry to be modeled along the component. In the input structure, each component was identified by a module title, a unique component number, and connections to numbered junctions between components. In addition, a descriptive text title can be used to uniquely identify each component. The 4 loops for IP2 were defined using 54 components and 57 junctions in the steady-state model. To model the thimble bypass flow, 3 additional loops were used that consist of 3 pipe components and 6 junctions. A total of 57 one-dimensional components and 63 junctions were employed in the steady-state loop model. The interface junction numbers between the one-dimensional component and the vessel were defined in the vessel input. Figure 12-11 presents the IP2 WCOBRA/TRAC loop noding diagram, with component numbers indicated by rectangular boxes and junctions by circular boxes.

The loop noding convention can be illustrated using loop 4 in Figure 12-11, which contains the pressurizer. The hot leg (Component 41) was modeled as a TEE, with the pressurizer (Component 54) connected to the secondary branch line. The pressurizer was modeled using the PRIZER module. The hot-leg primary line connects to the steam generator (Component 42), which was modeled using the STGEN module. The inlet and outlet boundary conditions for the steam generator secondary side are modeled as a BREAK (Component 43) and a FILL (Component 44), respectively. The crossover leg (Component 45) connecting the steam generator outlet plenum to the pump was modeled as a PIPE, while the pump (Component 46) was modeled using the PUMP module. The cold leg was modeled using a TEE (Component 47) and a PIPE (Component 48). The components connected to the secondary branch of the cold-leg TEE represent the ECCS. The piping and valve between the cold leg and pumped safety injection (SI) location (Component 91) was modeled using the VALVE module. The SI injection connection to the accumulator injection line was modeled as a TEE (Component 92). The SI injection flow as a function of pressure was specified using a FILL (Component 93). The piping and valve between the SI TEE and the accumulator were modeled as a VALVE (Component 94). The accumulator was modeled using the ACCUM module (Component 95).

Components 55, 56, and 57 modeled the thimble bypass flow of the low-power assemblies, the support column/open hole/free-standing mixer assemblies, and the guide tube assemblies, respectively, using PIPE modules. This bypass flow, while small, must be modeled to accurately predict steady-state fluid temperatures in the core.

## Emergency Core Cooling (ECC) and Safety Injection Model

The safety injection system (SIS) for IP2 consists of 4 accumulator tanks, 3 high-head safety injection (HHSI) pumps, and 2 low-head safety injection (LHSI) pumps. All pumps are connected to injection lines that merge into either the accumulator injection lines connected to the cold legs or the cold legs. The former arrangement was modeled for all 4 loops, as can be seen in Figure 12-11. This arrangement is judged to be more conservative, because SI injection is reduced while accumulators are injecting, due to the large pressure drop through the line. The accumulators were modeled to inject at 650 psia with 795 cubic feet of borated water at 105°F. The accumulator and SI on the broken loop were assumed to spill to containment. It was assumed that 1 of the 3 HHSI pumps would fail and the other 2 remained in operation. For the LHSI, it was assumed that 1 of the 2 pumps failed (single failure) and 1 remained in operation. While the failure of 1 LHSI and 1 HHSI pump is more conservative than required, it simplifies the analysis for the following reason. The limiting single failure must take into account the effect on containment pressure. Failure of an entire safety train would result in the loss of 1 or several containment spray and fan cooling units, reducing containment cooling, and increasing containment pressure, which is expected to reduce peak cladding temperature (PCT). Failure of 1 LHSI maintains all containment cooling systems to minimize pressure. On the other hand, this failure results in slightly greater SI flow, also expected to be a benefit. Assuming loss of 1 HHSI and 1 LHSI bounds both situations. Minimum injection flows were assumed. To provide for future plant margin, only 85 percent of the resulting HHSI flow and 90 percent of the resulting LHSI flow were counted for as the available SI flow that was equally distributed among the 3 intact loops.

### 12-3 REFERENCE TRANSIENT AND ALLOWABLE PLANT OPERATING CONDITIONS

The best-estimate methodology establishes a sampling of the distribution of PCT that could occur due to changes in plant or model variables (Section 11). The following paragraphs describe the assumptions in the key LOCA parameters for IP2.

The reference case input values as well as the plant operating range for IP2 are listed in Table 12-3. The input values falls under three categories: 1) plant physical description, 2) plant initial operating conditions, and 3) accident boundary conditions. The values used for the reference case for each of these parameters is discussed in the following subsections.

For most of the parameters, the nominal value is assumed for the reference case. For others, a bounding or conservative value is assumed. The uncertainty associated with these parameters is accounted for in the uncertainty analysis, as shown in Section 12-6.

#### 12-3-1 Plant Physical Description

- a. **Dimensions:** Nominal geometry is assumed. Uncertainties in nominal geometry input are implicitly accounted for in the code assessment, since experiments were also subject to thermal

expansion and dimensional uncertainty effects. In addition, grid crushing due to seismic plus LOCA forces is not calculated to occur in the IP2 core, so the effect of distorted assembly geometry need not be analyzed.

- b. **Flow Resistance:** Best-estimate values of loop flow resistance are assumed. Uncertainty in the model used to calculate flow resistance is accounted for by ranging the broken cold-leg nozzle resistance.
- c. **Pressurizer Location:** Sensitivity studies have shown that locating the pressurizer [

]<sup>ac</sup>

- d. **Hot Assembly Location:** A conservative location for the hot assembly is assumed. For IP2, the hot assembly is located under a flow mixer.
- e. **Hot Assembly Type:** The hot assembly is a 15x15 fuel assembly design in its first cycle of irradiation.
- f. **Steam Generator Tube Plugging Level:** The highest average tube plugging likely to be present during the next several cycles is expected to be less than 25 percent. For the reference case, a tube plugging level of 25 percent is selected as the limiting value, based on prior sensitivity studies (Table 27-1-3 of WCAP-12945-P-A).

### 12-3-2 Plant Initial Operating Conditions: Reactor Power

- a. **Initial Core Average Linear Heat Rate:** The core power assumed for the reference case is 100 percent of an uprated power level (3216 MWt).
- b. **Hot Rod Peak Linear Heat Rate:** The total peaking factor (FQ) for the reference case is set to 2.215.
- c. **Hot Rod Average Linear Heat Rate ( $F_{\Delta H}$ ):** In the reference case,  $F_{\Delta H}$  is set to 1.733, which is slightly above the Technical Specification value of 1.72.
- d. **Hot Assembly Average Linear Heat Rate:** The minimum difference between the power generated in the hot rod and that in the hot assembly average rod is conservatively assumed. The hot assembly average rod is assumed to be [                      ]<sup>ac</sup> lower in power than the hot rod.



- e. **Hot Assembly Peak Linear Heat Rate:** Consistent with the average linear heat rates, the peaking factor used to calculate the peak linear heat rate generated in the hot assembly average rod is [ ]<sup>a,c</sup> lower than the value assumed in the hot rod.
- f. **Axial Power Distribution:** The power distribution represented by power shape 10 is assumed for the reference case (Figure 12-12) and corresponds to PBOT=0.2575, PMID=0.365, FQ=2.215.
- g. **Low-Power Region (PLOW):** Current and expected core designs for IP2 result in a range of PLOW from 0.4 to 0.8. A PLOW of 0.4 is selected as the limiting value for the reference case, based on prior sensitivity studies (Table 27-1-3 of WCAP-12945-P-A).
- h. **Burnup:** The burnup is selected from the [ ]<sup>a,c</sup>. For the reference case, a nominal cycle burnup equal to 2000 MWD/T is assumed.
- i. **Prior Operating History:** The power distribution assumed to exist at the time of the LOCA is conservatively assumed to have existed since plant startup when determining fission product inventories.
- j. **Moderator Temperature Coefficient (MTC):** The maximum value specified in the Technical Specifications is assumed, to conservatively estimate core reactivity and fission power.
- k. **Hot Full-Power (HFP) Boron Concentration:** A value typical of those used in current cores is assumed.

### 12-3-3 Plant Initial Operating Conditions: Fluid Conditions

- a. **Average Fluid Temperature ( $T_{av}$ ):** The maximum expected value during normal full-power operation, including uncertainties (+4°F), is used for IP2.
- b. **RCS Pressure:** The maximum value (2310 psia) is assumed for the reference transient of IP2.
- c. **Loop Flowrate:** The minimum loop flow is assumed for the reference transient.
- d. **Upper Head Temperature ( $T_{UH}$ ):** The appropriate best estimate value of  $T_{UH}$  is assumed.
- e. **Pressurizer Level:** The nominal value of pressurizer level is assumed.
- f. **Accumulator Water Temperature:** A nominal (midpoint) value within the range established for IP2 is assumed.

- g. **Accumulator Pressure:** A nominal (midpoint) value of accumulator pressure is assumed.
- h. **Accumulator Water Volume:** A nominal (midpoint) value of accumulator water volume is assumed.
- i. **Accumulator Line Resistance:** A best-estimate value of accumulator line resistance is assumed.
- j. **Accumulator Boron Concentration:** The Technical Specification minimum value is assumed.

#### 12-3-4 Accident Boundary Conditions

- a. **Break Location:** A break near the midpoint of the cold leg is assumed. Scoping studies have confirmed that the cold leg remains the limiting location for a large LOCA.
- b. **Break Type:** The guillotine break is assumed in the reference case. [  
] <sup>a,c</sup>
- c. **Break Size:** The nominal cold-leg area is assumed for the guillotine break. A nominal discharge coefficient (CD=1.0) is assumed for the reference case. The uncertainty in the discharge coefficient is accounted for within the uncertainty analysis, [  
] <sup>a,c</sup>.
- d. **Offsite Power:** No loss of offsite power is assumed, consistent with the limiting case from the prior sensitivity studies (Table 27-1-3 of WCAP-12945-P-A).
- e. **Safety Injection Flow:** Minimum SI flow is assumed, calculated using methods consistent with those currently employed for Appendix K analysis. Prior sensitivity studies indicate that increased SI flow reduces PCT. This parameter is, therefore, bounded.
- f. **Safety Injection Temperature:** Nominal (midpoint) values are assumed.
- g. **Safety Injection Delay:** Maximum values consistent with the limiting offsite-power assumption (offsite-power available) are used.
- h. **Containment Pressure:** A conservative low value calculated using currently approved containment codes and using mass and energy release from the WCOBRA/TRAC calculation is assumed.
- i. **Single-Failure Assumption:** The loss of a safety train (that is, the loss of a low-head pump and a high-head pump) will be assumed for the determination of pumped ECCS flow during the LOCA, while the train is assumed to operate in the calculation of containment backpressure.

This will result in a conservatively low containment backpressure. In other plant analyses, sensitivity studies may be performed to permit a less conservative set of assumptions.

- j. **Rod Drop Time:** Consistent with the current design basis for this plant, control rods are assumed not to drop during the LOCA.

### 12-3-5 Plant Operating Range

The PCT and its uncertainty developed by the best-estimate methodology is valid for a range of plant operating conditions. Several parameters in the reference calculation are at nominal values. The range of variation of the operating parameters is accounted for in the uncertainty analysis. This is accomplished by assuring that, in the sampling of the attributes for each run (Section 12-5), the operating range is bounded.

Table 12-3 summarizes the values that the key LOCA parameters will have in the reference case for IP2. The proposed plant operating range and limits over which the uncertainty evaluation is to be performed are also shown. The estimate of the PCT at 95-percent probability is considered to be valid over this range, with 95-percent confidence.

Table 12-4 presents the reference value of the plant variable, the nominal or midpoint operating value, and the sampling range for the initial condition and power distribution parameters. The ranges are derived from the plant operating range in Table 12-3. [

] <sup>a,c</sup>

### 12-3-6 Confirm Reference Case Limiting Assumptions

Several of the reference conditions assumed to be bounded are verified on a plant-specific basis. For IP2, the reference case assumptions were based on [

] <sup>a,c</sup> The results are shown in Table 12-5. All of the assumptions used in the reference case were confirmed.

## 12-4 REFERENCE TRANSIENT ANALYSIS

The reference transient conditions were discussed in the previous section. The transient is obtained by performing a steady-state calculation followed by the transient calculation.

### 12-4-1 Steady-State Calculation

A WCOBRA/TRAC PWR LOCA calculation is initialized from a point at which the flows, temperatures, powers, and pressures are at their specified steady-state values before the postulated break occurs. Consequently, steady-state WCOBRA/TRAC calculations are performed prior to the transient calculations to ensure that the desired steady-state reactor conditions are achieved. (See Figure 12-11 for the layout of the IP2 PWR steady-state model.)

Steady-state plant pressure drop conditions are obtained from data generated by the Westinghouse Mechanical Equipment Design group. Steam generator pressure drop and secondary-side data are obtained from data generated by the Westinghouse Steam Generator Mechanical Development group. These calculated plant conditions reflect input parameters such as reactor coolant pump flows, core power, steam generator tube plugging levels, system pressures, and fluid temperatures. The pressure drops calculated by WCOBRA/TRAC are checked against the previous design data.

Fuel parameters are obtained from the Westinghouse Fuel Division PAD code (Foster and Sidener, 2000), which provides the steady-state fuel pellet average temperatures as a function of fuel burnup and linear power, the fuel rod gas pressure, gap conductance, and so forth. The nuclear fuel rods are initialized with consistent internal gas properties and other fuel properties such that at end of the steady-state the average fuel temperatures predicted by WCOBRA/TRAC correspond to the fuel temperature obtained from the PAD code.

The calculated flowrate, pressure distribution, fluid, and fuel temperatures are adjusted to closely match the above-mentioned data. This is achieved by adjusting some of the input parameters. For example,  $T_{ave}$  is affected by the primary-to-secondary-side heat transfer. The  $T_{ave}$  can be adjusted by varying the steam generator feedwater temperature and/or the steam generator secondary-side pressure. The fuel temperature is adjusted by varying the initial cold gap widths between the pellet and the cladding. In general, there is a functional relationship between the WCOBRA/TRAC inputs and the final steady-state solution where the solution at the end of the steady state is the result of the combined effect of several input variables. An automated procedure was developed where iterative calculations are performed to determine the input value such that the calculated steady-state satisfies a pre-defined steady-state acceptance criteria.

Steady-state acceptance criteria are necessary because the above-mentioned fluid and core conditions are likely to differ somewhat from plant to plant and the degree to which these parameters are matched in the WCOBRA/TRAC simulation must be consistent. Table 12-6 shows the acceptance criteria used in WCOBRA/TRAC for acceptable simulation of plant conditions. A checklist for a number of significant parameters is given below, which utilizes this table to verify whether these variables have reached their acceptable steady-state values.

1. Core power and peak linear heat rate are matched exactly because they are input values.

2. Integrals of rod power represent the radial peaking parameter,  $F_{\Delta H}$ . Integrals of the input power are calculated and normalized by the code to give  $F_{\Delta H}$  values for the hot rod, hot assembly rod, and core average rod. These values must agree with their intended values.
3. The maximum fuel average temperatures for the hot rod, the hot assembly rod, the average rods, and the low-power rod must agree with the desired values from the PAD data, within the tolerance as indicated in Table 12-6.
4. Vessel inlet, outlet, and upper head fluid temperatures define the fluid temperature distribution in the vessel and the average RCS temperature ( $T_{ave}$ ), which is the mean value of the inlet and outlet temperatures. The  $T_{ave}$  should be within the tolerance shown in Table 12-6.
5. Pump flow must be kept within a tight tolerance to assure that the overall vessel/loop pressure drop is balanced by the pump head, and the desired flowrate through the vessel has been achieved.
6. System pressure (pressure in the top cell of the pressurizer) and the water level in the pressurizer must be kept within the tolerance shown in the table to assure that the steady-state pressurizer condition is closely simulated.
7. Pressure drops across the vessel and through the core must agree with the values provided by the mechanical design data within the tolerance shown in the table.
8. Core bypass flow (including the thimble bypass flow and the spray nozzle flow) should closely match those provided by the mechanical design data.
9. When identical loops are used to simulate the reactor system, the calculated results should be symmetrical with respect to each loop. No crossflow (lateral gap flow) is to occur in the downcomer and in the lower plenum.
10. Steam generator secondary-side water mass must closely match the value reported in the Steam Generator Thermal-Hydraulic Design Data report.

Once the fuel and fluid temperatures, vessel and loop pressure drop, and flow distributions are in agreement with the desired input parameters, and conditions are steady, a suitable initial condition has been achieved for the LOCA transient simulation.

All items in Table 12-6, with the exception of the pressure drops and bypass flowrate items (items 9, 10, 11, and 12), can differ from case to case within the Automated Statistical Treatment of Uncertainty Method (ASTRUM) run matrix. These are checked for each transient within the run matrix. Pressure drops and bypass flowrates are only adjusted for the reference conditions and can vary from case to case within the ASTRUM run matrix, due to variations in fluid conditions.

### 12-4-2 Transient Calculation

Once the steady-state calculation is achieved and found to be acceptable, the transient calculation is initialized. For the reference transient, a postulated double-ended guillotine break is assumed to occur in 1 of the cold legs as shown in Figure 12-13. Figure 12-14 shows the arrangement for the split break. The accumulator and the SI lines of the broken loop are assumed to be lost and are not modeled. Two sets of check valves are used in the intact accumulator/SI lines. Referring to Figure 12-11, check valves 71, 81, and 91 will open the SI lines when the RCS pressure drops below the maximum pressure of the HHSI pumps and the assumed SI delay time is exceeded. Check valves 74, 84, and 94 will open the accumulator lines once the RCS pressure reaches the accumulator set point. Components 73, 83, and 93 are FILL components that use flow versus pressure tables for the desired pumped emergency cooling flow. The steam generators are isolated by replacing the FILL and the BREAK components (Components 13, 14, 23, 24, 33, 34, 43, and 44) with zero-flow FILL components. Components 17 and 18 are the broken cold legs on the loop side and on the vessel side, respectively. A containment backpressure table (pressure versus time) is also provided as input to the break boundaries using results from COCO containment calculations (Bordelon and Murphy, 1974).

The steady-state calculation is restarted with the above changes to begin the transient.

### 12-4-3 Reference Transient Results

Figures 12-15 to 12-21 show results from the reference case calculated using WCOBRA/TRAC MOD7A Revision 6. Figure 12-15 shows the nominal hot rod PCT. Figure 12-16 shows the cladding temperature at several elevations. For the reference case, the blowdown and reflood PCT locations both occur at 8.8 feet. Later in reflood, the limiting location is higher in the core. Rapid flow reversal due to high break flowrates results in a relatively early blowdown PCT, which occurs 10 seconds after the LOCA begins. Core pressure (Figure 12-17) reaches containment pressure at about 25 seconds. This marks the end of blowdown heatup and cooling. The lower plenum is rapidly filled with accumulator water (Figure 12-18) after ECC bypass has ended. Refill lasts until the lower plenum collapsed liquid level reaches the bottom of the core. Reflood then begins at 40 seconds as downcomer (Figure 12-19) and core (Figure 12-20) collapsed liquid levels increase, and the first reflood PCT is reached. Shortly after reflood begins, the accumulators empty and a brief in-surge of water occurs due to nitrogen injection. During this time, heat transfer is increased and the cladding is significantly cooled. After the nitrogen flow decreases, steam generation depresses the water level in the core, and some vessel mass is lost out the break (Figure 12-21). The vessel mass again decreases for a time after 200 seconds when water in the lower plenum and downcomer becomes saturated and begins to boil. A brief late heatup occurs high in the core at about 200 seconds, until pumped SI and reduced structural heat release cause liquid levels to increase again. The hot rod is quenched entirely in the reference transient at about 500 seconds.

## 12-5 DEVELOPMENT OF RUN MATRIX

The individual uncertainty contributors are sampled with a random number generator as discussed in Section 11. The original formulation of the ASTRUM statistical treatment of uncertainties focused on the PCT, and was based on the assumption that the limiting PCT case would be used for the calculations of the LMO and CWO. Thus, only 59 runs were required to obtain the 95/95 PCT. During resolution of the USNRC Requests for Additional Information (RAIs), as documented in Appendix C-1, the ASTRUM statistical approach was modified to consider PCT, LMO, and CWO as independent variables, thus requiring 124 runs to be performed to provide the 95/95 PCT, LMO, and CWO, as documented in Section 11-1. The sample application presented in this chapter was retained from the original submittal, and therefore was performed using only 59 runs to obtain the 95/95 PCT. As noted above, LMO and CWO in this sample application were assessed using the limiting PCT case. Given the nature of the application presented herein (i.e., an example to illustrate how the methodology is applied, not a licensing basis analysis), this simplification is considered acceptable.

The list of attributes (or uncertainty contributors) can be divided into 2 main groups. The first group includes all the model uncertainty contributors. The model uncertainty contributors include global model and local model parameters. The global model parameters are varied within the WCOBRA/TRAC code whereas the local models are varied within the HOTSPOT code, which is executed once the WCOBRA/TRAC calculation is completed. The second group includes the initial condition and power distribution uncertainty contributors. These parameters are plant specific. The nominal and reference values, as well as the sampling range for IP 2, are shown in Table 12-4.

## 12-6 ASTRUM RESULTS AND DETERMINATION OF THE 95/95 PCT VALUE

The maximum PCT predicted for each run is extracted. Table 12-7 shows the value of the uncertainty contributors for the most limiting transients. The reference transient is compared to the limiting case in Figure 12-22. The most limiting transient is a double-ended cold-leg guillotine (DECLG) break. The maximum PCT is 1899°F. This corresponds to a conservative estimate of the 95-percent PCT probability with 95-percent confidence level.

The global variables listed in Table 12-7 have been defined previously, but local variable settings require some explanation. The parameter values (PVs) for most of the local variables are calculated as shown in Table 12-8. When the statistical fluctuation is expressed as a percentage of the best-estimate value, and the population is normal,  $PV$  is defined as  $I + V_n$ , where  $V_n$  is a random sample from a normal distribution with mean 0 and standard deviation  $\sigma$ . When the statistical fluctuation is expressed as a percentage of the best-estimate value and the population is uniform,  $PV$  is defined as  $I + RNG * V_n$ , where  $V_n$  is a random number between -1 and 1, and  $RNG$  is the range of the distribution. When the statistical fluctuation is a dimensional number and the population is normal,  $PV$  is defined as  $0 + V_n$ , where  $V_n$  is a random sample from a normal distribution with mean 0 and standard deviation  $\sigma$ . Finally, when the statistical fluctuation is a dimensional number and the population is uniform,  $PV$  is defined as  $RNG * V_n$ , where  $V_n$  is a random variable between -1 and 1.

The last 4 local variables shown in Table 12-7 are the heat transfer multipliers, sampled from the distributions summarized in Table 1-8.

Figure 12-23 shows the PCT transient for the 9 highest PCT cases as well as the reference transient. Of them, 2 are split break and 7 are DECLG.

In the non-parametric statistical treatment of uncertainty, all uncertainty contributors are varied simultaneously. The drawback of this method is that it is more difficult to examine the results of each individual transient, and in particular to draw conclusions about the evaluation model performance comparing one case to another. The combined effect of several parameters make this type of judgment cumbersome.

However, it is known that among all uncertainty contributors, some of them are dominant contributors. It is possible to draw some conclusions by examining different transients and looking at the single effect of the dominant factors. The effect of dominant contributors was estimated performing a parametric analysis. The base case in the parametric study was based on the reference conditions. The results from the parametric study are used to support a sanity check for the most limiting transients of the ASTRUM run matrix. The intent here is only to provide some basis to evaluate the performance of the evaluation model even though this step is not required within a non-parametric uncertainty analysis.

The selected uncertainty contributors for the parametric analysis are the power shape (essentially the peaking factor FQ), the augmented loop resistance KN, the break flow discharge coefficient (CD), the break type, and the burnup. For IP2, both the reference case and the limiting case are a double-ended guillotine break type. Therefore, the parametric studies for FQ, KN, CD, and burnup were applied to a double-ended guillotine break. The effect of the break type was analyzed using a split break with the same total break area as the double-ended guillotine break, and reference case conditions for all other attributes. Results of the parametric study are summarized in Table 12-9.

[

]ac



[

]a,c

## 12-7 OTHER 10CFR50.46 CRITERIA

The additional Code of Federal Regulations (CFR) 10CFR50.46 criteria that ASTRUM needs to address are the following:

- Verify that with high probability the maximum cladding oxidation is less than 17 percent
- Verify that with high probability the core-wide oxidation is less than 1 percent

In the approved methodology, the calculation of the local oxidation and the core-wide oxidation are based on the results from the most limiting local and core-wide oxidation transients. In the sample application, LMO and CWO were assessed with the limiting PCT transient.

The maximum local oxidation is about 2 percent, which is considerably below the 17-percent limit prescribed by the 10CFR50.46 criteria. This result includes the effects of double-sided reaction, because the limiting case had cladding burst predicted by the code.

The local oxidation is known to be a strong function of the PCT. This dependence is clearly seen in Figure 12-36.

For IP2, the whole rod volumetric oxidation fraction of the hot rod estimated from the limiting case results is 0.6 percent. Therefore, a detailed calculation of core-wide oxidation as described in Section 11-6-2 is not necessary for IP2. By definition, the core-wide oxidation fraction is less than the hot rod volumetric oxidation and the 10CFR50.46 criterion on core-wide oxidation is satisfied.

## 12-8 REFERENCES

Bajorek, S. M., et al., 1998, "Code Qualification Document for Best Estimate LOCA Analysis," WCAP-12945-P-A, Volume 1, Revision 2, and Volumes 2 through 5, Revision 1, and WCAP-14747 (Non-Proprietary).

Bordelon, F. M. and Murphy, E. T., 1974, "Containment Pressure Analysis Code (COCO)," WCAP-8327 (Proprietary), WCAP-8306 (Non-Proprietary).

Dederer, S. I., et al., 1999, "Application of Best Estimate Large Break LOCA Methodology to Westinghouse PWRs with Upper Plenum Injection," WCAP-14449-P-A, Revision 1, and WCAP-14450-NP-A, Revision 1 (Non-Proprietary).

Dederer, S. I., et al., 1988, "Westinghouse Large Break LOCA Best Estimate Methodology. Volume 2: Application to 2-loop PWRs Equipped with Upper Plenum Injection," WCAP-10924-P-A, Revision 2.

Foster, J. P. and Sidener, S., 2000, "Westinghouse Improved Performance Analysis and Design Model (PAD 4.0)," WCAP-15063-P-A, Revision 1 with Errata.

Hochreiter, L. E., et al., 1998, "WCOBRA/TRAC Applicability to AP600 Large-Break Loss-of-Coolant Accident," WCAP-14171-P, Revision 2.

Table 12-1 Channel Descriptions for WCOBRA/TRAC IP2 Vessel Model				
Section	Channel	Description	Connections to Channels	
			Above	Below
1	1	Lower Plenum – Broken Quadrant	6	–
	2	Lower Plenum – Intact Quadrant	7	–
	3	Lower Plenum – Intact Quadrant	8	–
	4	Lower Plenum – Intact Quadrant	9	–
	5	Lower Plenum – Center Portion	10	–
2	6	Lower Plenum – Broken Quadrant	11	1
	7	Lower Plenum – Intact Quadrant	12	2
	8	Lower Plenum – Intact Quadrant	13	3
	9	Lower Plenum – Intact Quadrant	14	4
	10	Lower Plenum – Core Inlet	15,16,17,18,19	5
3	11	Downcomer – Broken Quadrant	20	6
	12	Downcomer – Intact Quadrant	21	7
	13	Downcomer – Intact Quadrant	22	8
	14	Downcomer – Intact Quadrant	23	9
	15	Barrel-Baffle Region	–	10
	16	Low-Power/Periphery Assemblies	25	10
	17	Assemblies Below Support Columns/Open Holes/ Free-Standing Mixers	26	10
	18	Assemblies Below Guide Tubes	27	10
	19	Hot Assembly Under Free-Standing Mixer	28	10

**Table 12-1 Channel Descriptions for WCOBRA/TRAC IP2 Vessel Model**  
(cont.)

Section	Channel	Description	Connections to Channels	
			Above	Below
4	20	Downcomer – Broken Quadrant	29	11
	21	Downcomer – Intact Quadrant	30	12
	22	Downcomer – Intact Quadrant	31	13
	23	Downcomer – Intact Quadrant	32	14
	24	Global Volume Below UCP, Not Within Fuel Region	–	–
	25	CCFL Region Above Low-Power/Periphery Assemblies	34	16
	26	CCFL Region Below Support Columns/Open Holes/Free-Standing Mixers	35	17
	27	CCFL Region Below Guide Tubes	36	18
	28	CCFL Region Below a Free-Standing Mixer and Above Hot Assembly	37	19
5	29	Downcomer – Broken Quadrant	38	20
	30	Downcomer – Intact Quadrant	39	21
	31	Downcomer – Intact Quadrant	40	22
	32	Downcomer – Intact Quadrant	41	23
	33	Inner Global Region Above UCP	42	–
	34	Upper Plenum Support Columns/Open Holes/Free-Standing Mixers in Outer Ring Above Low-Power Assemblies	43	25
	35	Upper Plenum Support Columns/Open Holes/Free-Standing Mixers	44	26
	36	Upper Plenum Guide Tubes	45	27
	37	Upper Plenum Free-Standing Mixer Above the Hot Assembly	44	28
	62	Outer Global Region Above UCP	43	–

**Table 12-1 Channel Descriptions for WCOBRA/TRAC IP2 Vessel Model**  
(cont.)

Section	Channel	Description	Connections to Channels	
			Above	Below
6	38	Downcomer – Broken Quadrant	50	29
	39	Downcomer – Intact Quadrant	51	30
	40	Downcomer – Intact Quadrant	52	31
	41	Downcomer – Intact Quadrant	53	32
	42	Upper Plenum Inner Global Region	54	33
	43	Upper Plenum Outer Global Region	55	34, 62
	44	Upper Plenum Support Columns/Open Holes/Free-Standing Mixers	56	35, 37
	45	Upper Plenum Guide Tubes	57	36
	46	Hot Leg Inlet – Broken Quadrant	–	–
	47	Hot Leg Inlet – Intact Quadrant	–	–
	48	Hot Leg Inlet – Intact Quadrant	–	–
	49	Hot Leg Inlet – Intact Quadrant	–	–
7	50	Downcomer – Broken Quadrant	58	38
	51	Downcomer – Intact Quadrant	58	39
	52	Downcomer – Intact Quadrant	63	40
	53	Downcomer – Intact Quadrant	63	41
	54	Upper Plenum Inner Global Region	–	42
	55	Upper Plenum Outer Global Region	–	43
	56	Upper Plenum Support Columns/Open Holes/Free-Standing Mixers	–	44
	57	Upper Plenum Guide Tubes	60	45

Table 12-1 Channel Descriptions for <u>W</u> COBRA/TRAC IP2 Vessel Model (cont.)				
Section	Channel	Description	Connections to Channels	
			Above	Below
8	58	Lower Upper Head Outer Region Above Spray Nozzles – Broken/Intact Side	–	50, 51
	63	Lower Upper Head Outer Region Above Spray Nozzles – Intact/Intact Side	–	52, 53
	59	Lower Upper Head Inner Region	61	–
	60	Upper Guide Tube	61	57
9	61	Upper Head Top Region	–	59, 60

Table 12-2 Gap Connections for WCOBRA/TRAC IP2 Vessel Model			
Section	Gap	From Channel	To Channel
1	1	1	4
	2	1	2
	3	2	3
	4	3	4
	5	1	5
	6	2	5
	7	3	5
	8	4	5
2	9	6	9
	10	6	7
	11	7	8
	12	8	9
	13	6	10
	14	7	10
	15	8	10
	16	9	10
3	17	11	14
	18	11	12
	19	12	13
	20	13	14
	21	11	15
	22	12	15
	23	13	15
	24	14	15
	25	16	17
	26	16	18
	27	17	18
	28	17	19
4	29	20	23
	30	20	21
	31	21	22
	32	22	23
	33	24	25
	34	24	26
	35	24	27
	36	24	28







Table 12-3      Reference Values and Plant Operating Range-IP2 (cont.)				
Parameter		Reference		Operating Range
[				

]".c

Table 12-4 Reference, Nominal, and Range Values for Plant Initial Operating Conditions				
Parameter	Reference	Nominal	Range	Units
[				

j<sup>ac</sup>

Table 12-5 Reference Case Confirmatory Studies		
Case	Assumption	Result (Change in PCT From Reference Value)
[		

] <sup>a,c</sup>

[illegible]

**J<sup>a.c</sup>**

[illegible]

**Table 12-7 Values of the Sampled Parameters for the Top 9 Most Limiting Cases**  
(cont.)

[									

J<sup>ac</sup>



**Table 12-8      Summary of Statistical Variables in HOTSPOT**

[illegible]

<b>Table 12-9</b>	<b>Results from the Parametric Study</b>
-------------------	--

[illegible]

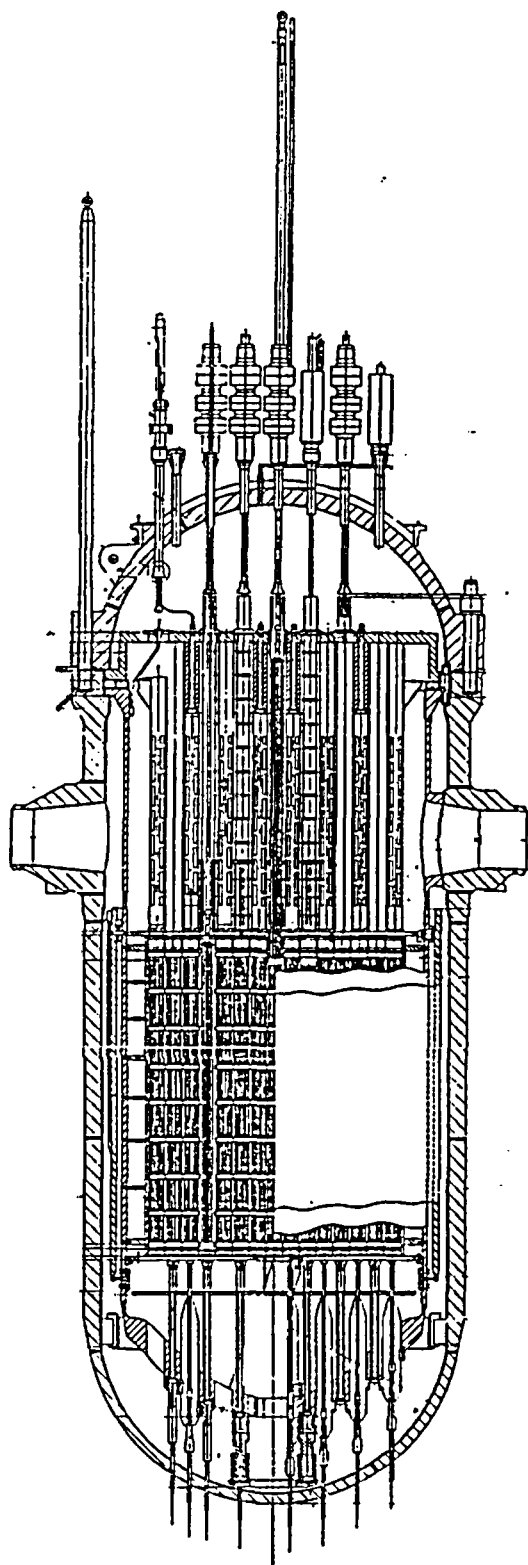
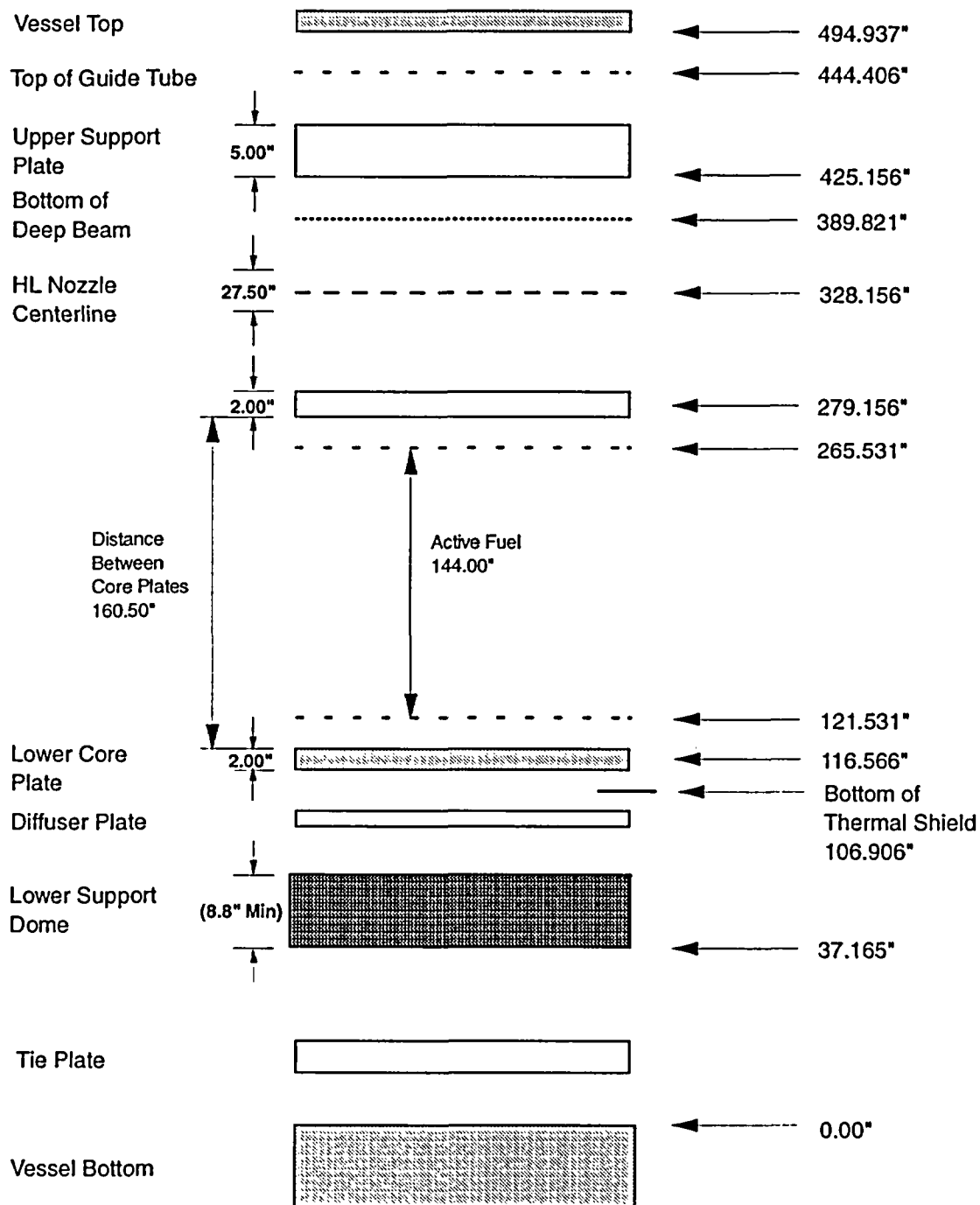


Figure 12-1. IP2 Vessel Profile



IP2

Figure 12-2. Vessel Component Elevations

January 2005  
Revision 0

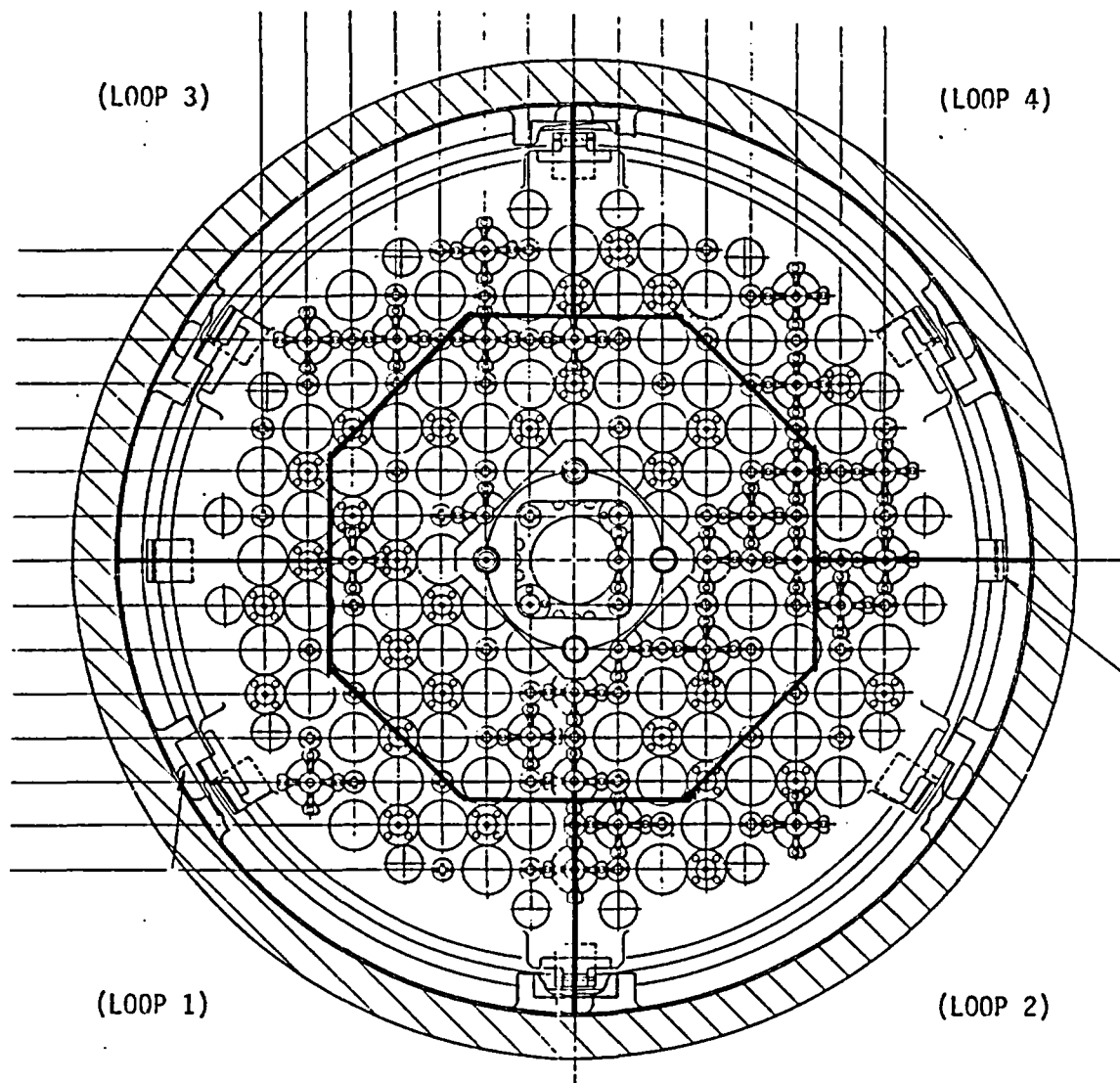


Figure 12-4. Top View of Lower Dome and Channel Divisions in Section 1



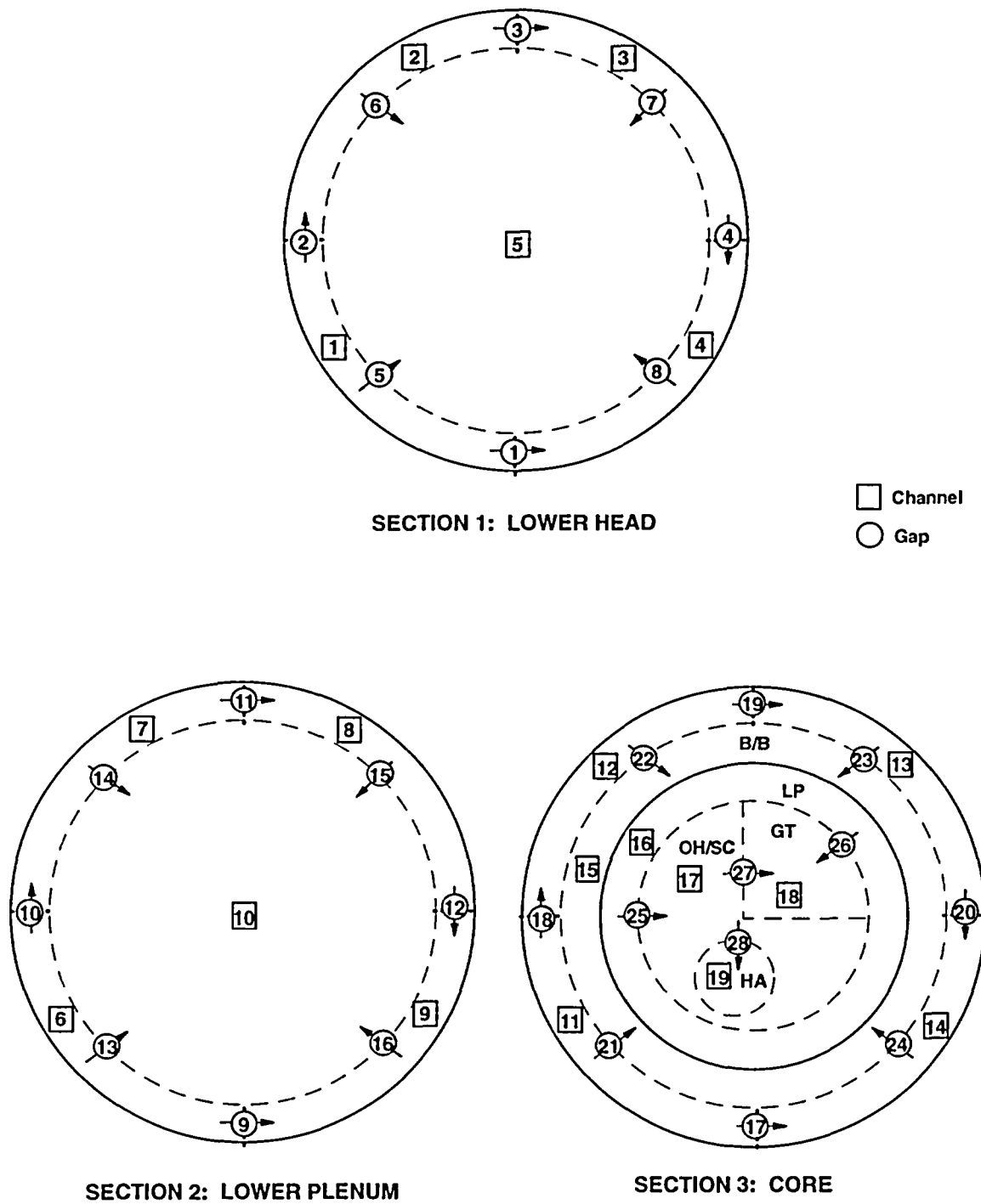


Figure 12-6. IP2 Vessel Sections 1 to 3 (Horizontal View)

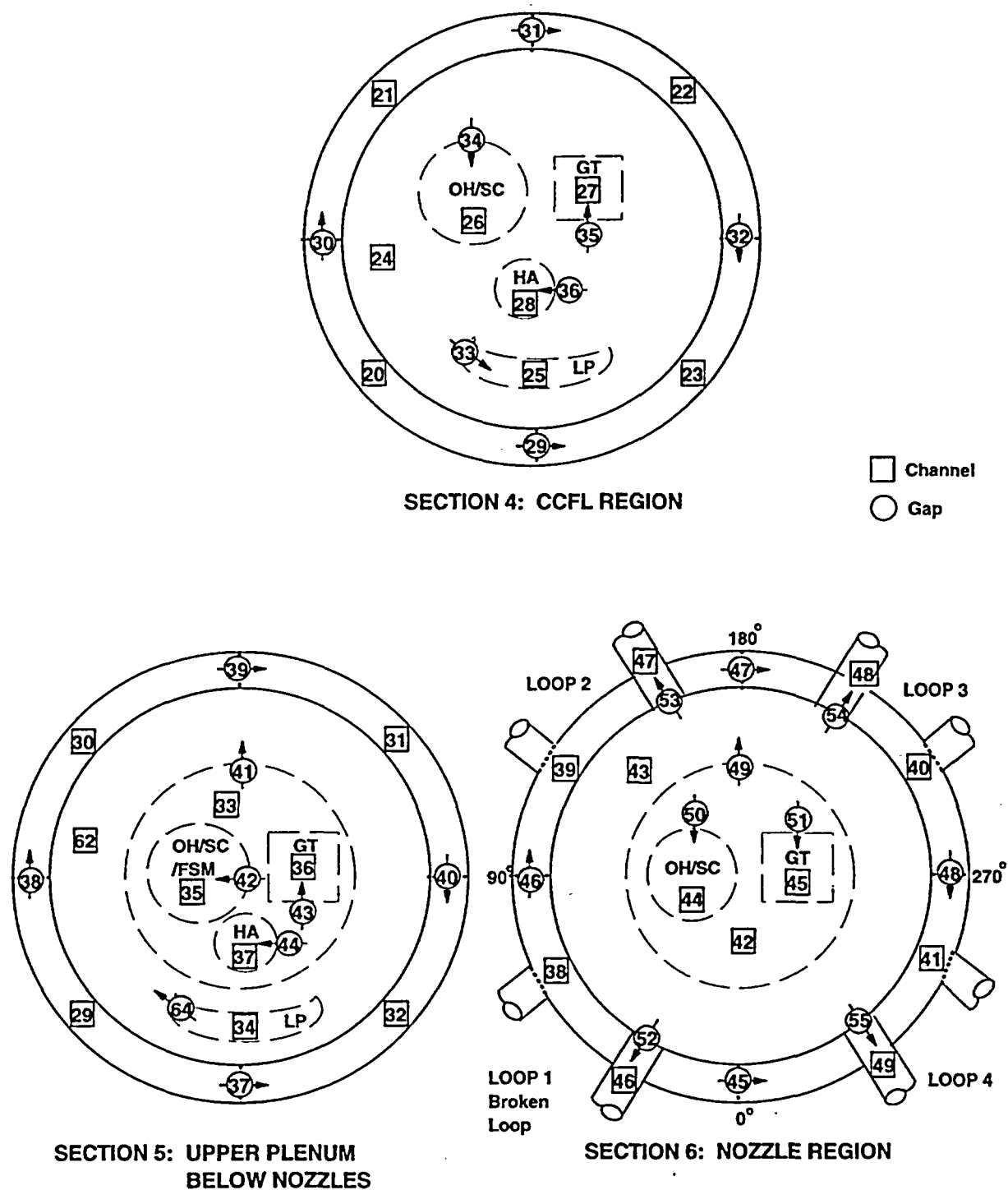
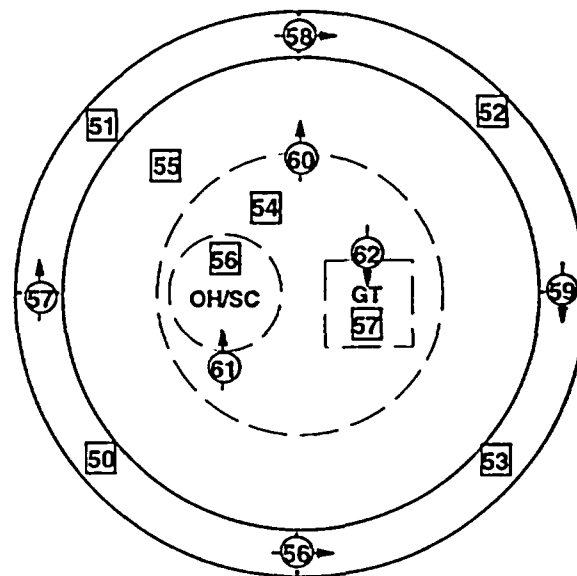


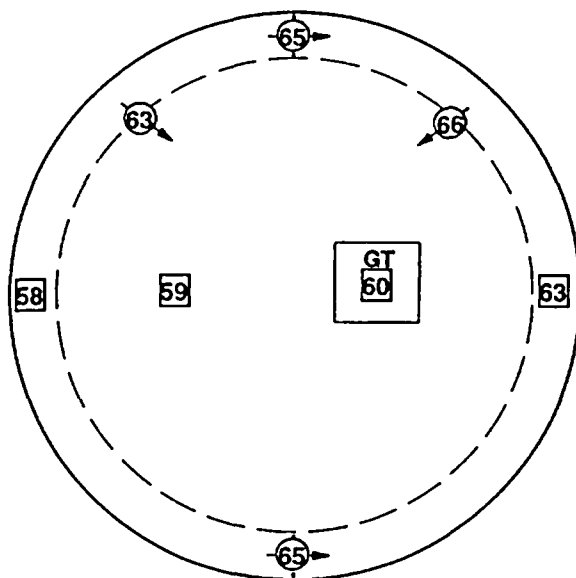
Figure 12-7. IP2 Vessel Sections 4 to 6 (Horizontal View)



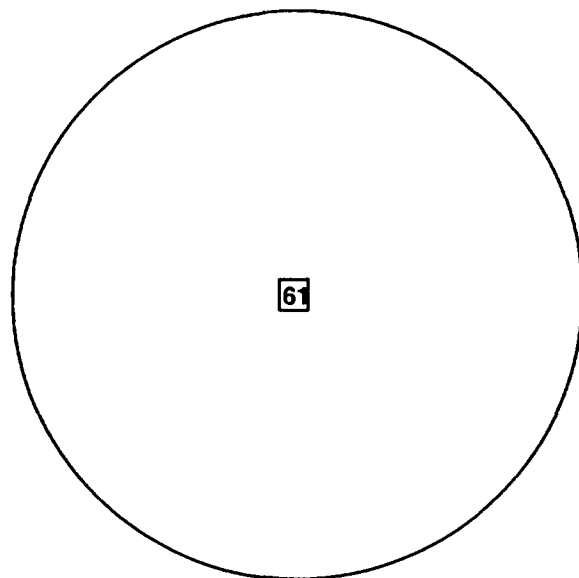


**SECTION 7: UPPER PLENUM  
ABOVE NOZZLES**

□ Channel  
○ Gap



**SECTION 8: UPPER HEAD UP TO  
TOP OF GUIDE TUBES**



**SECTION 9: UPPER HEAD ABOVE  
GUIDE TUBES**

**Figure 12-8. IP2 Vessel Sections 7 to 9 (Horizontal View)**

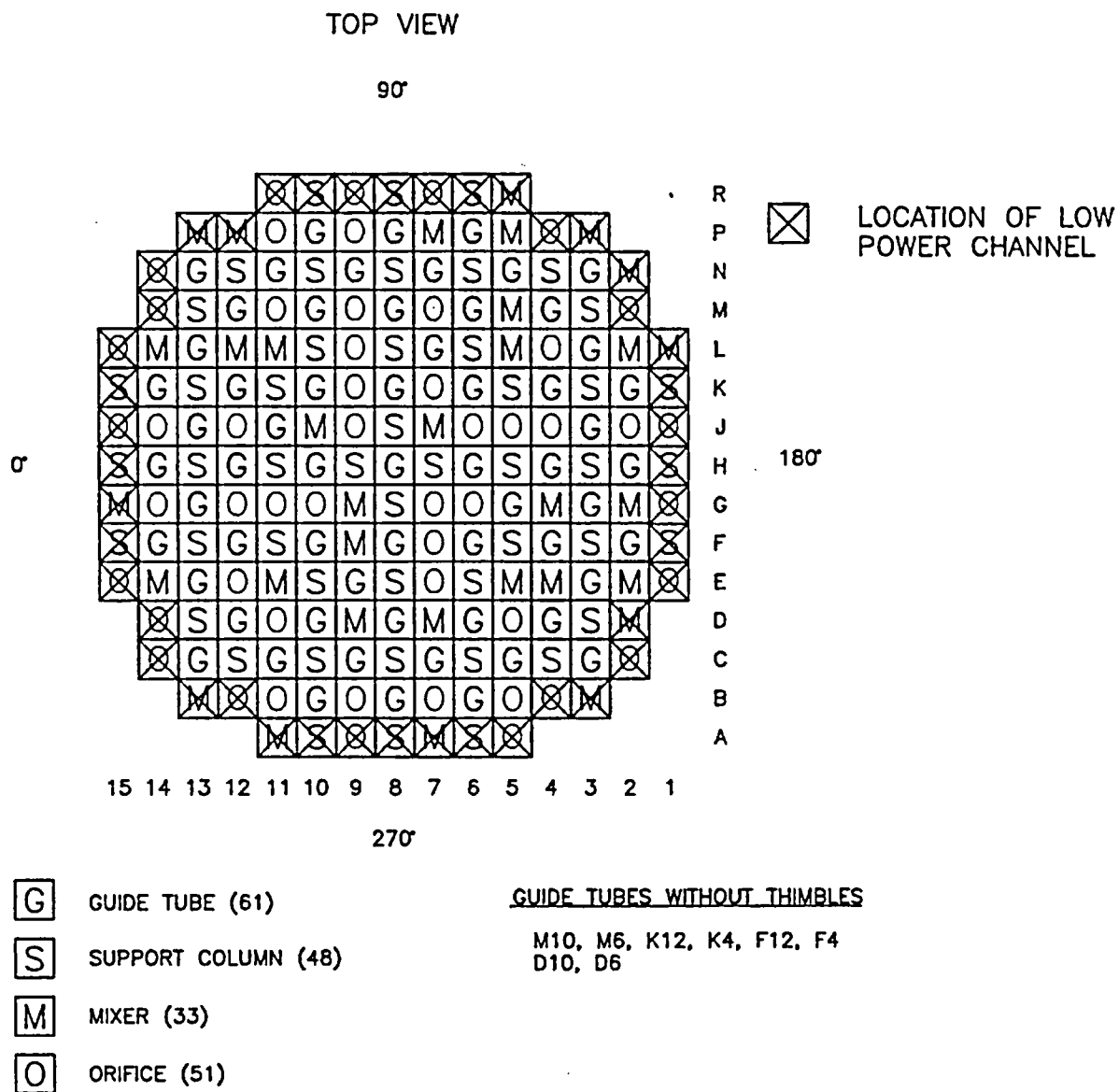


Figure 12-9. Upper Plenum Internal Distribution

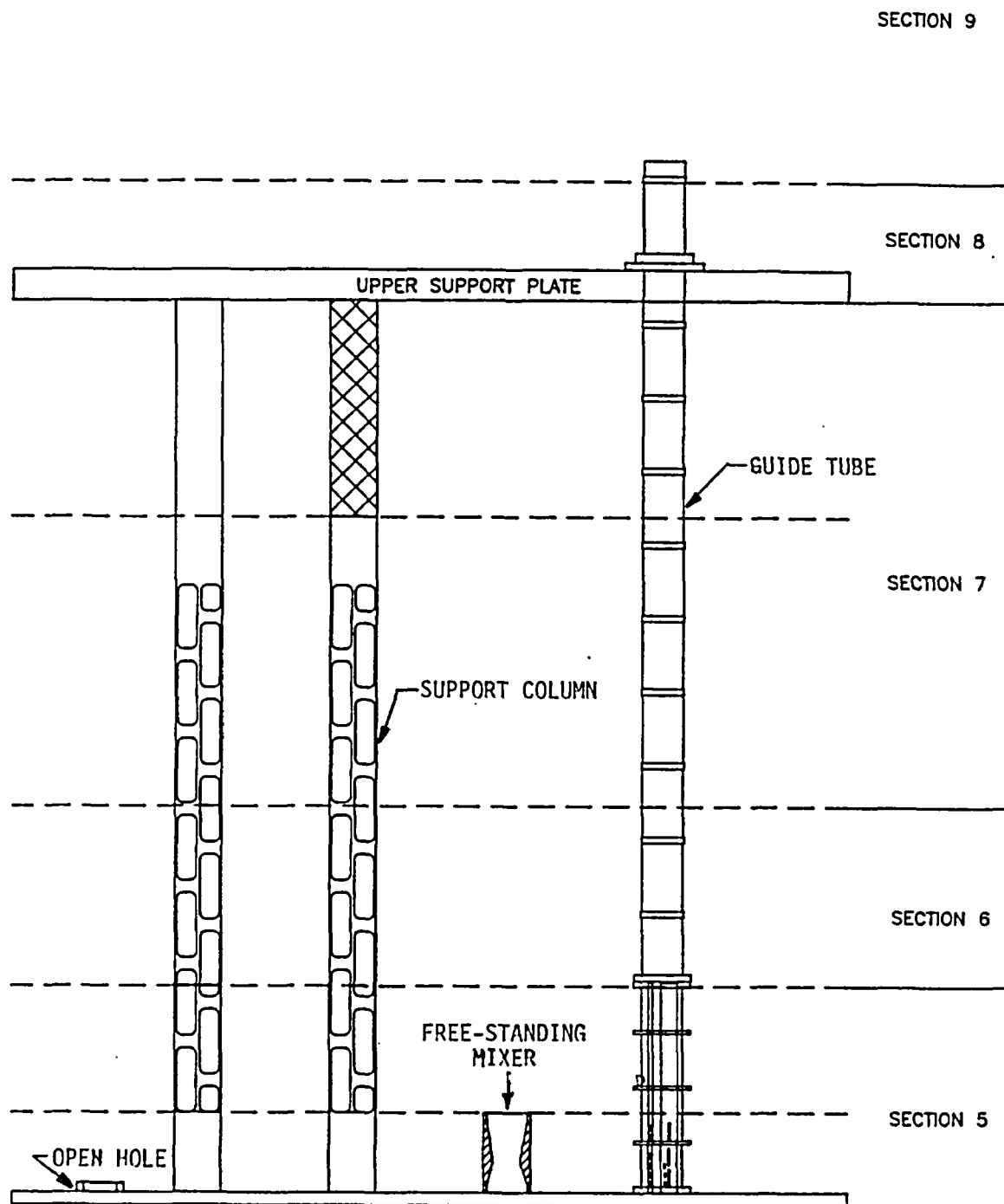


Figure 12-10. Vertical View of Open Hole, Support Column, Free-Standing Mixer, and Guide Tube in Upper Plenum

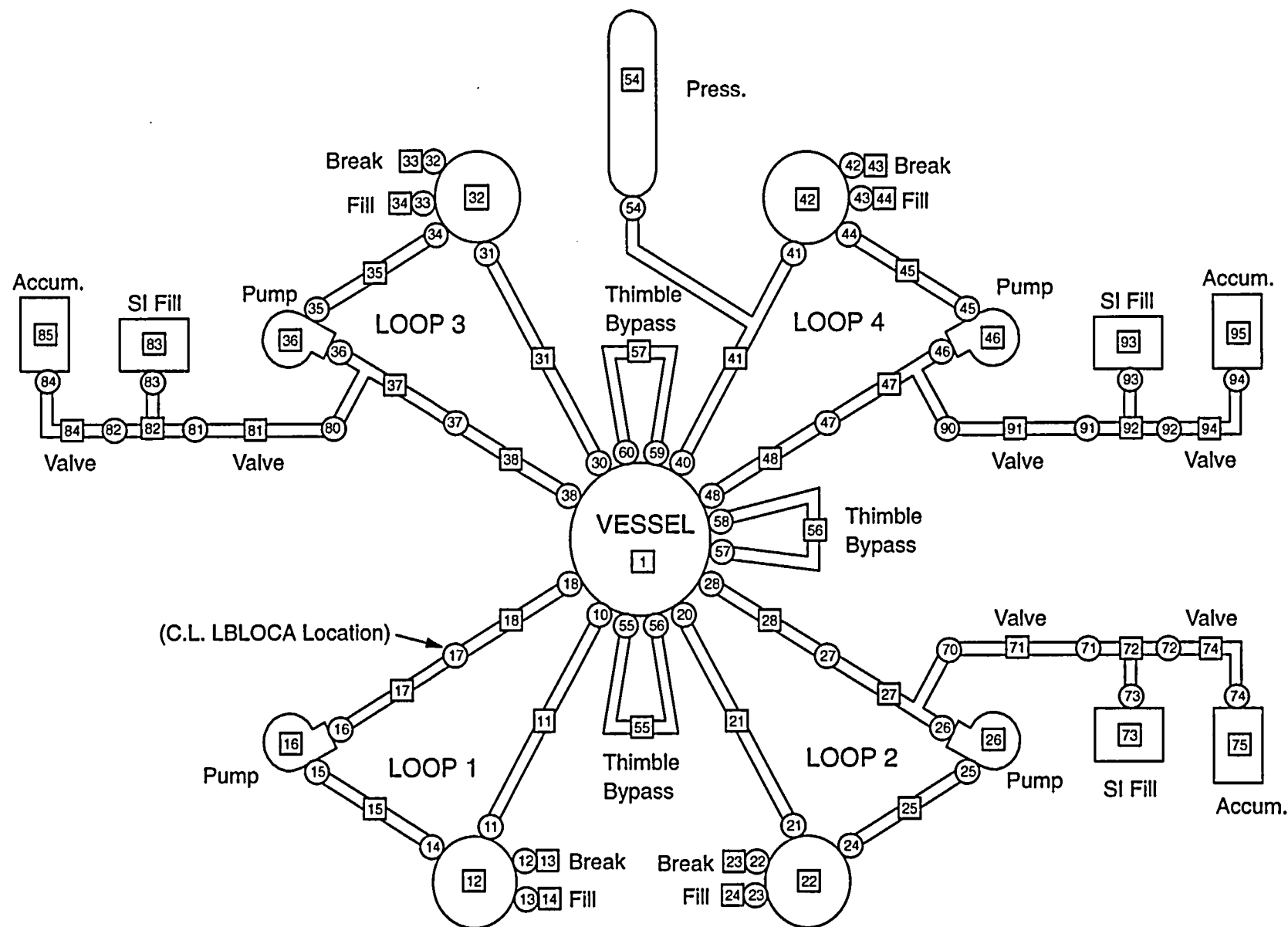
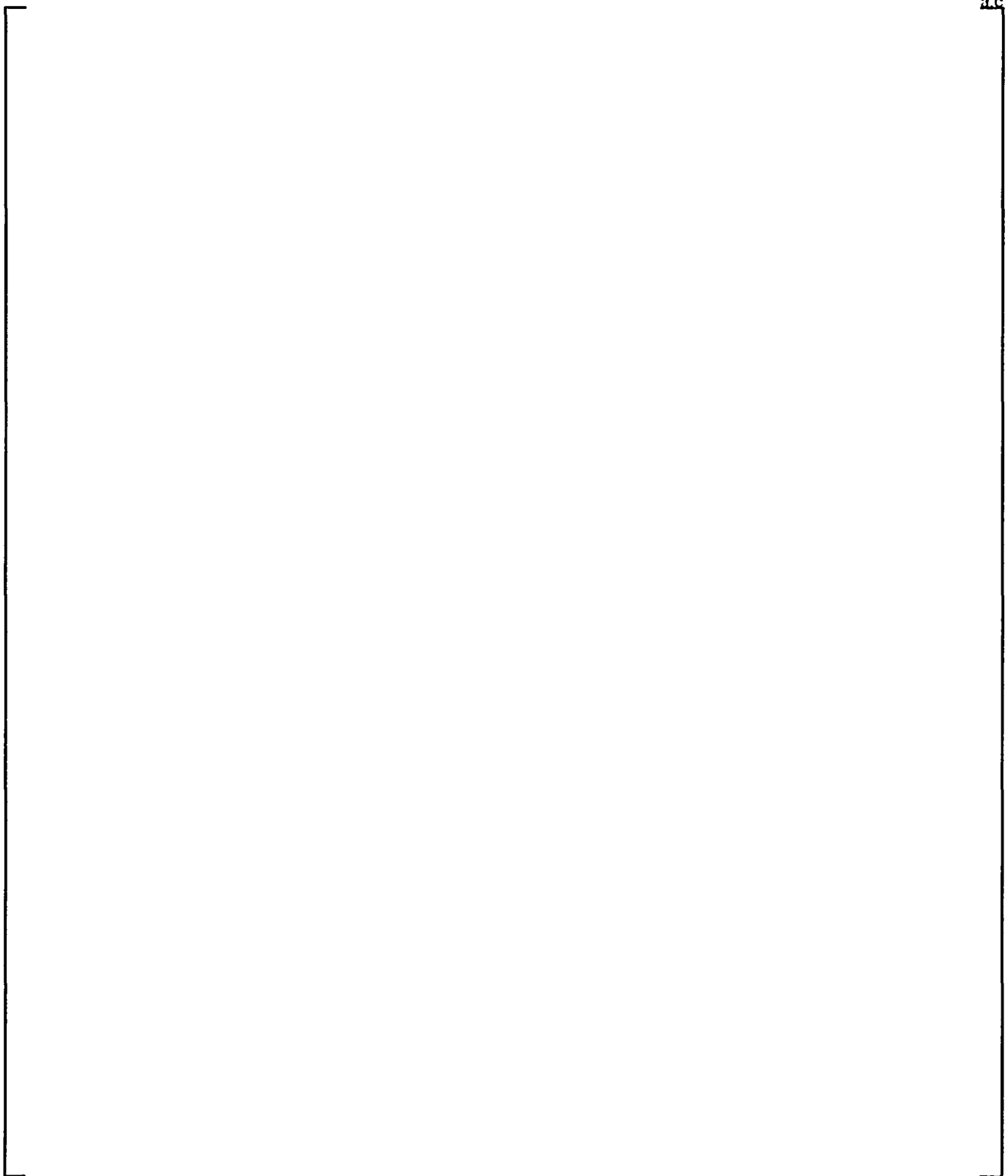


Figure 12-11. IP2 WCOBRA/TRAC Model Vessel/Loop Layout (Steady-State)



**Figure 12-12. Power Shape 10**

a,c

Figure 12-13. Broken Colde Leg 1-D Components Arrangement for DECLG Break



Figure 12-14. Broken Cold Leg 1-D Components Arrangement for Split Break

## IP2 Reference Case Peak Clad Temperature

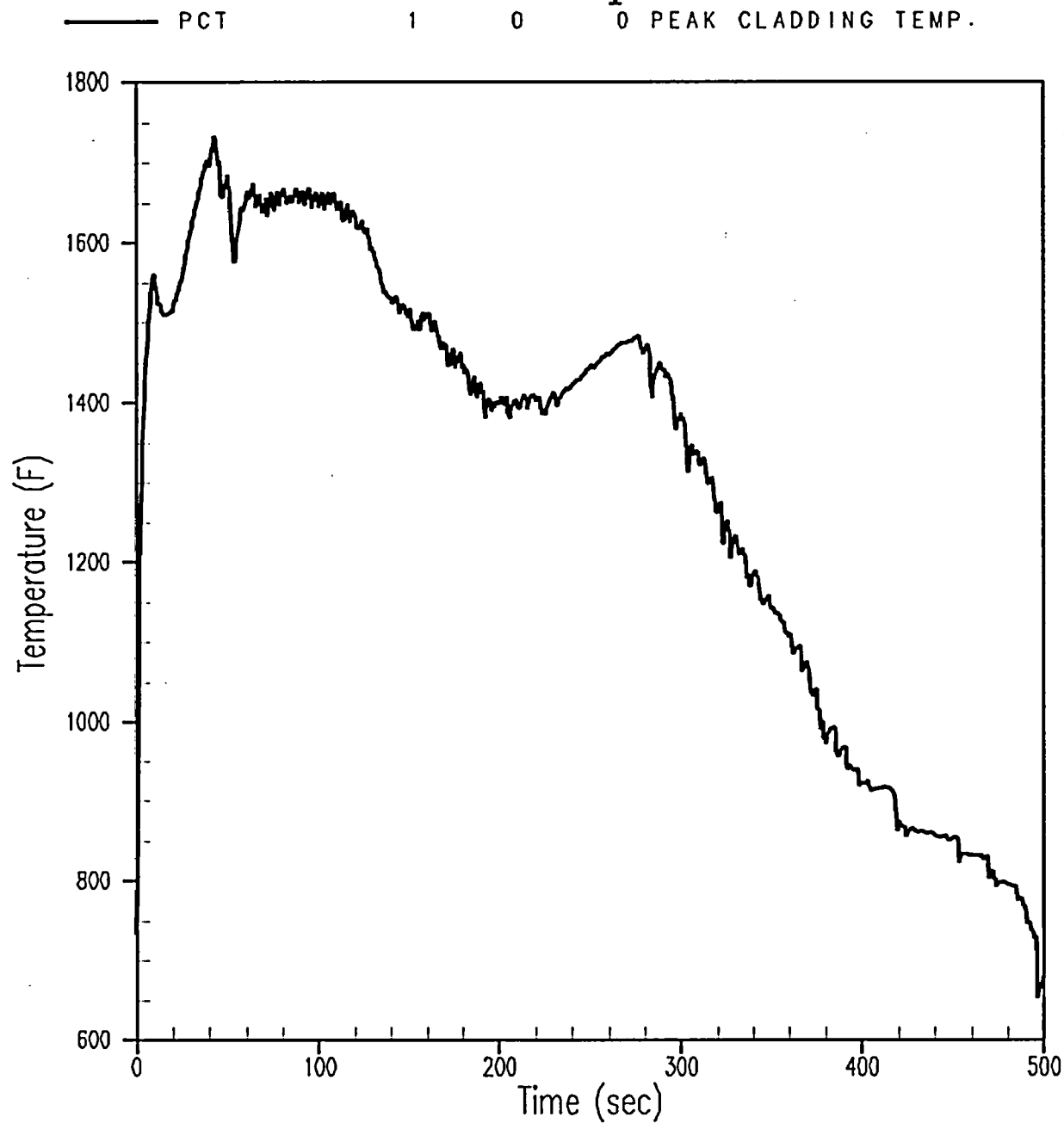


Figure 12-15. Reference Transient: Peak Cladding Temperature



## IP2 Reference Case

### PCT and Clad Temperature at Limiting Locations

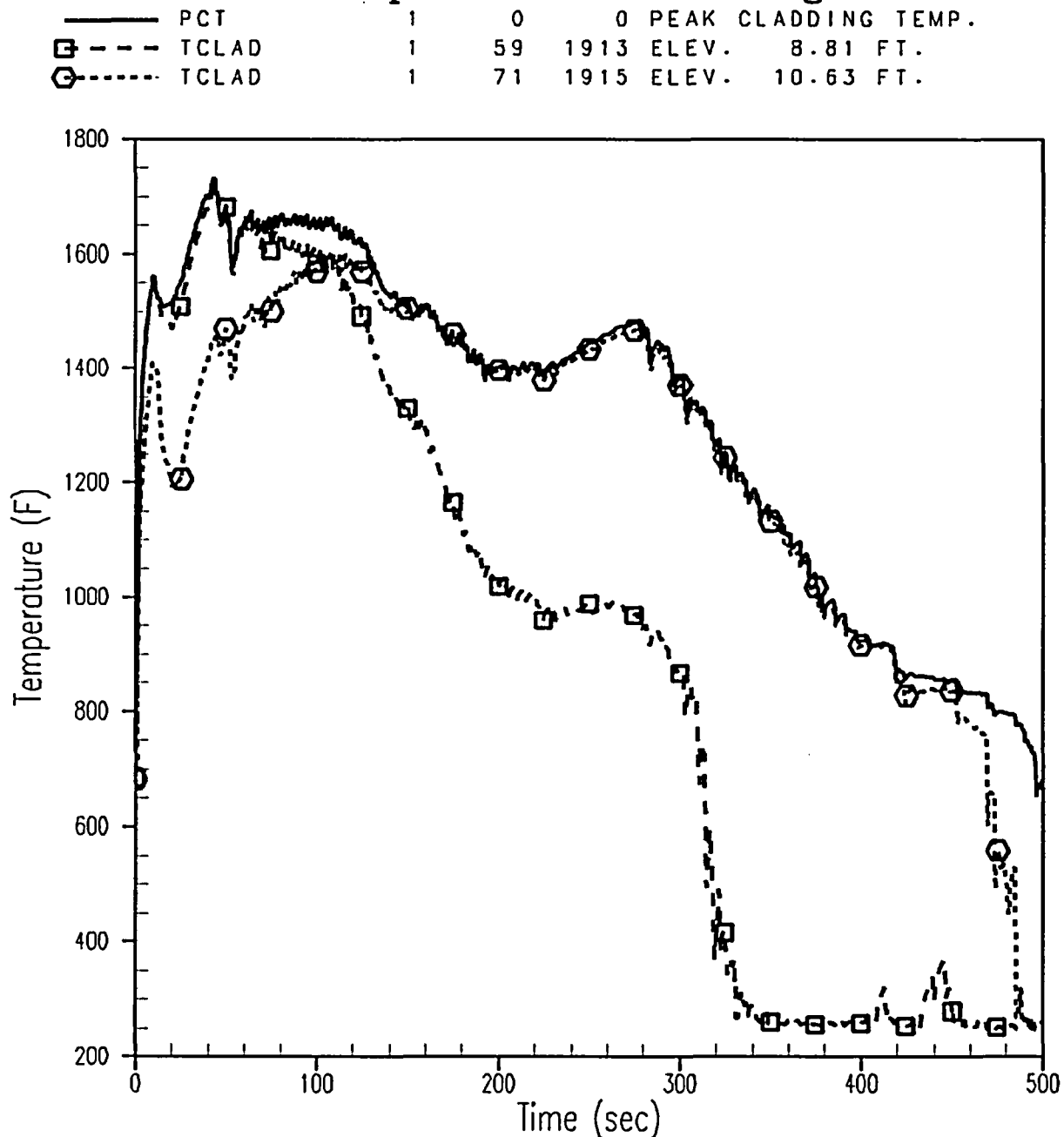


Figure 12-16. PCT and Cladding Temperature at Limiting Locations

## IP2 Reference Case Core Pressure

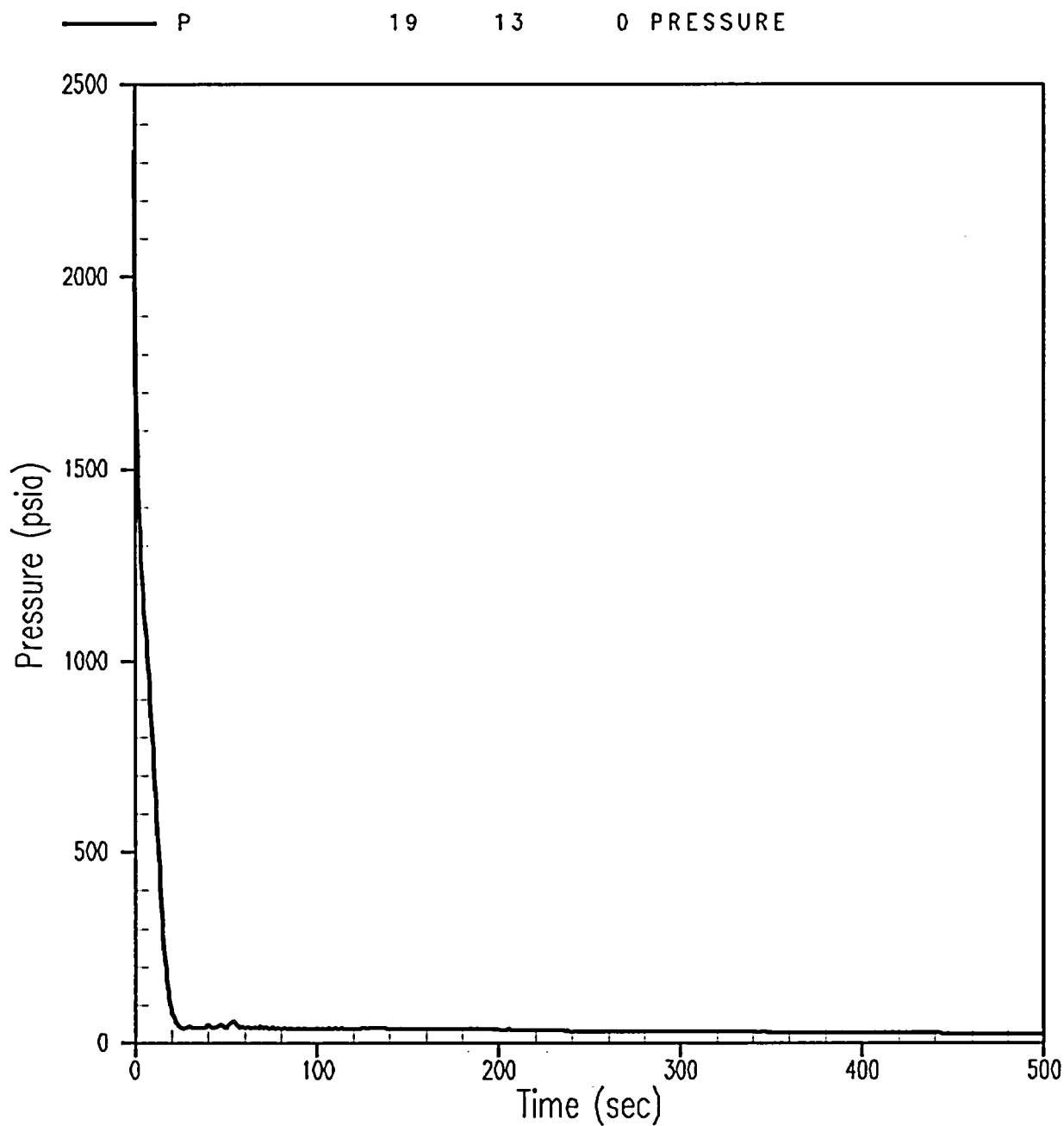


Figure 12-17. Reference Transient: Core Pressure

## IP2 Reference Case Lower Plenum Collapsed Liquid Level

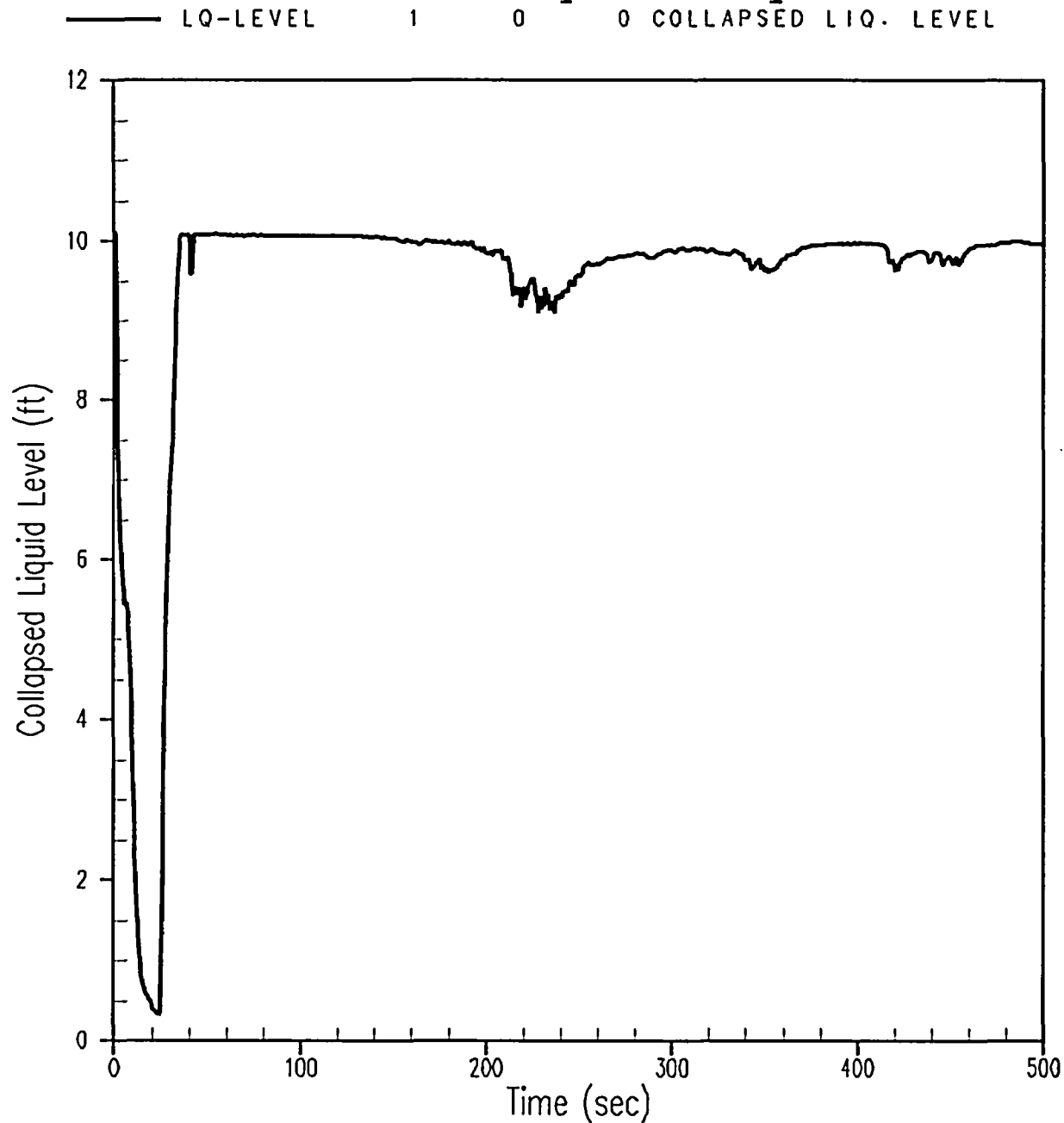


Figure 12-18. Reference Transient: Lower Plenum Collapsed Liquid Level

# IP2 Reference Case Downcomer Collapsed Liquid Level

—	LQ-LEVEL	7	0	0	COLLAPSED LIQ. LEVEL
□---	LQ-LEVEL	8	0	0	COLLAPSED LIQ. LEVEL
○---	LQ-LEVEL	9	0	0	COLLAPSED LIQ. LEVEL
△---	LQ-LEVEL	10	0	0	COLLAPSED LIQ. LEVEL

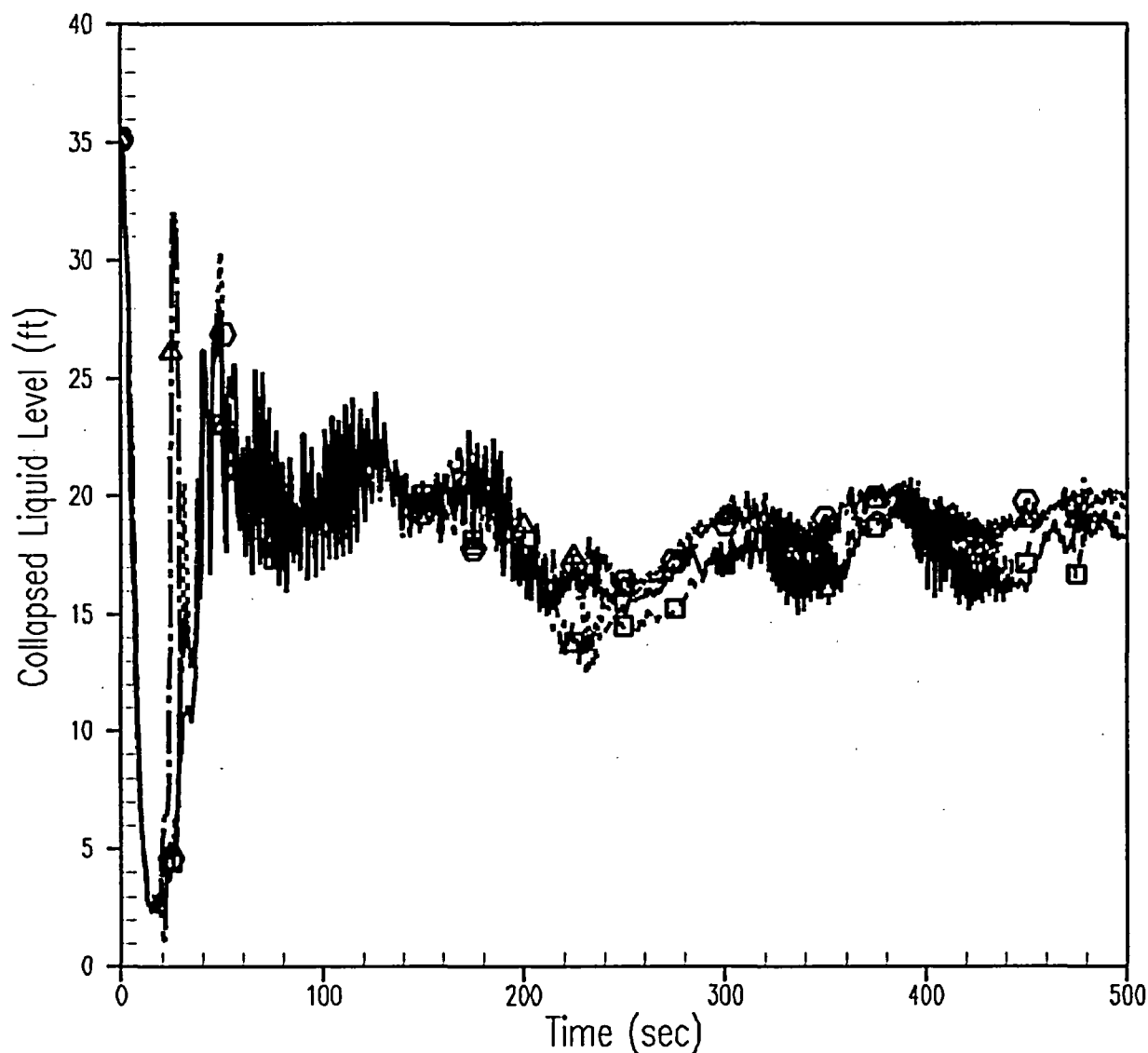
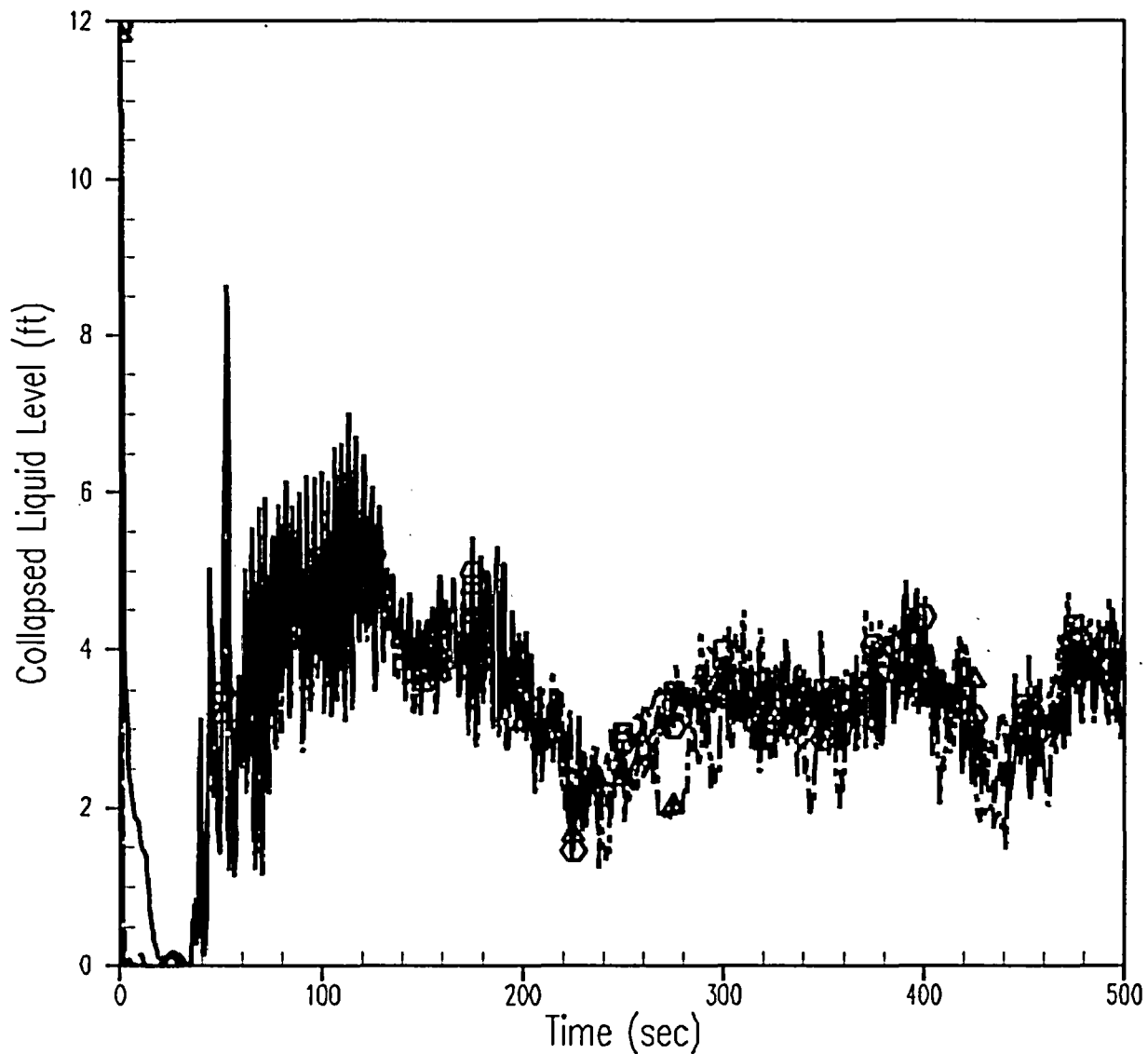


Figure 12-19. Reference Transient: Downcomer Collapsed Liquid Level

## IP2 Reference Case Core Collapsed Liquid Level

—	LQ-LEVEL	3	0	0	COLLAPSED LIQ. LEVEL
□---	LQ-LEVEL	4	0	0	COLLAPSED LIQ. LEVEL
○----	LQ-LEVEL	5	0	0	COLLAPSED LIQ. LEVEL
△---	LQ-LEVEL	6	0	0	COLLAPSED LIQ. LEVEL



**Figure 12-20. Reference Transient: Core Collapsed Liquid Level**

## IP2 Reference Case Vessel Fluid Mass

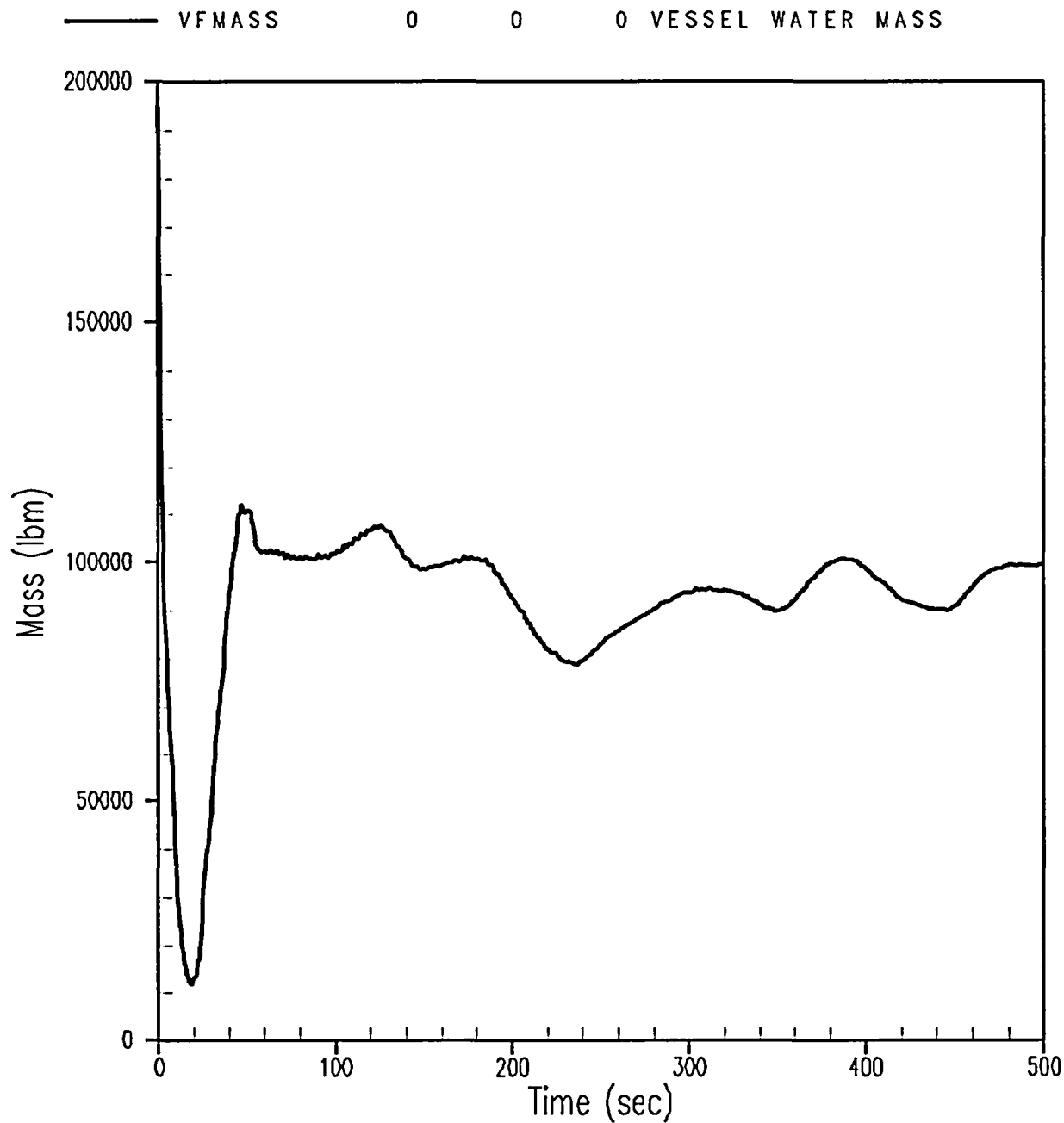


Figure 12-21. Reference Transient: Vessel Fluid Mass

a.c

**Figure 12-22. PCT for the Limiting Case and Reference Case**

a.c

**Figure 12-23. PCT for the Most Limiting Transients**



a.c

Figure 12-24. Effect of FQ

a.c

**Figure 12-25. Effect of KN**

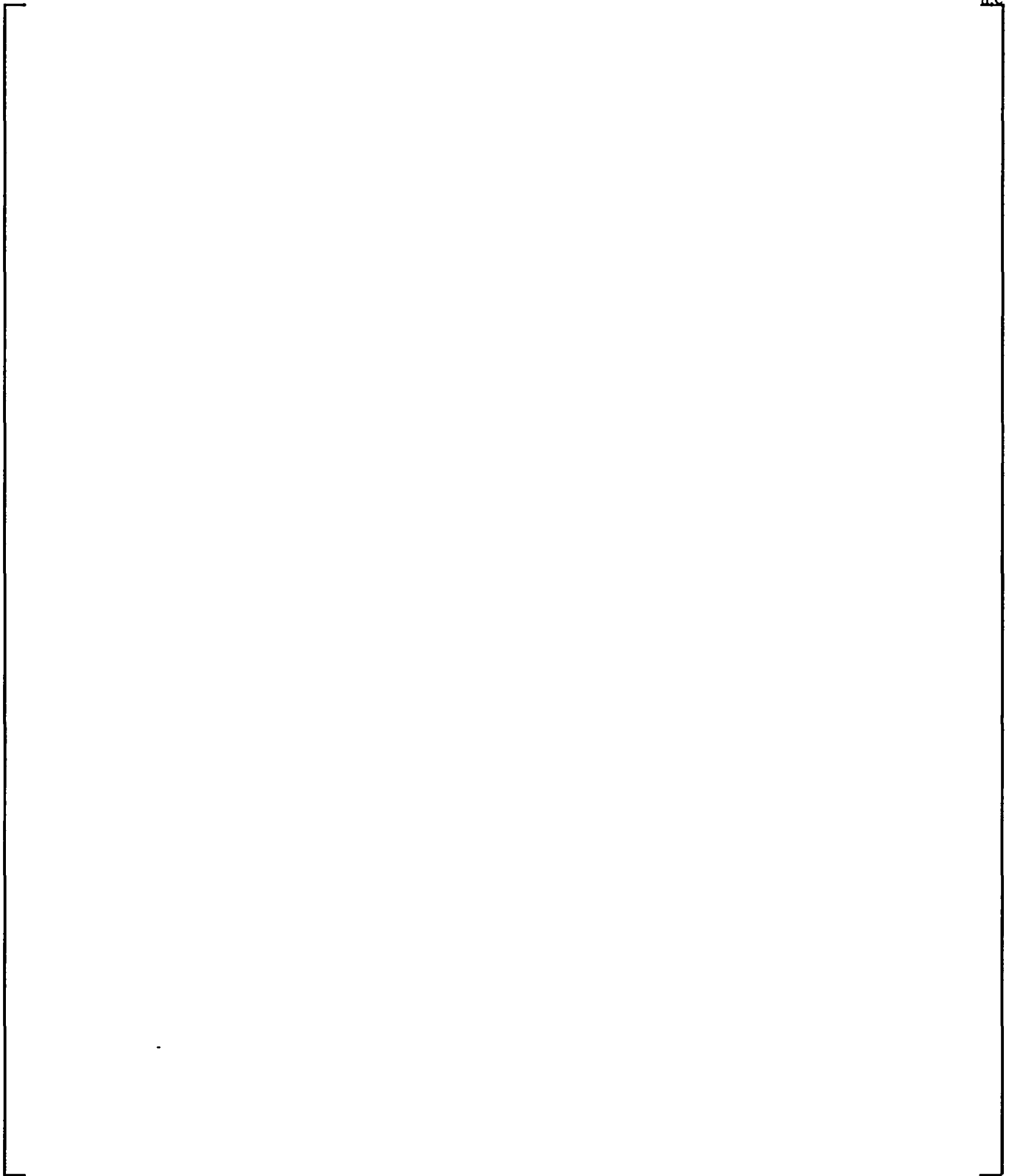


Figure 12-26. Effect of CD

a.c

**Figure 12-27. Effect of Burnup**

**Figure 12-28. Effect of Break Area for the Reference Split Break**

a,c

Figure 12-29. Final PCT vs. (CD x A)

a,c

Figure 12-30. Final PCT vs. FQ

a,c

**Figure 12-31. Final PCT vs. FQ for Most Limiting Cases**





Figure 12-32. Final PCT vs. KN

a,c

Figure 12-33. Final PCT vs. KN for Most-Limiting Cases

a,c

Figure 12-34. Final PCT vs. Burnup

a,c

**Figure 12-35. Final PCT vs. Burnup for Most-Limiting Cases**

## Local Oxidation

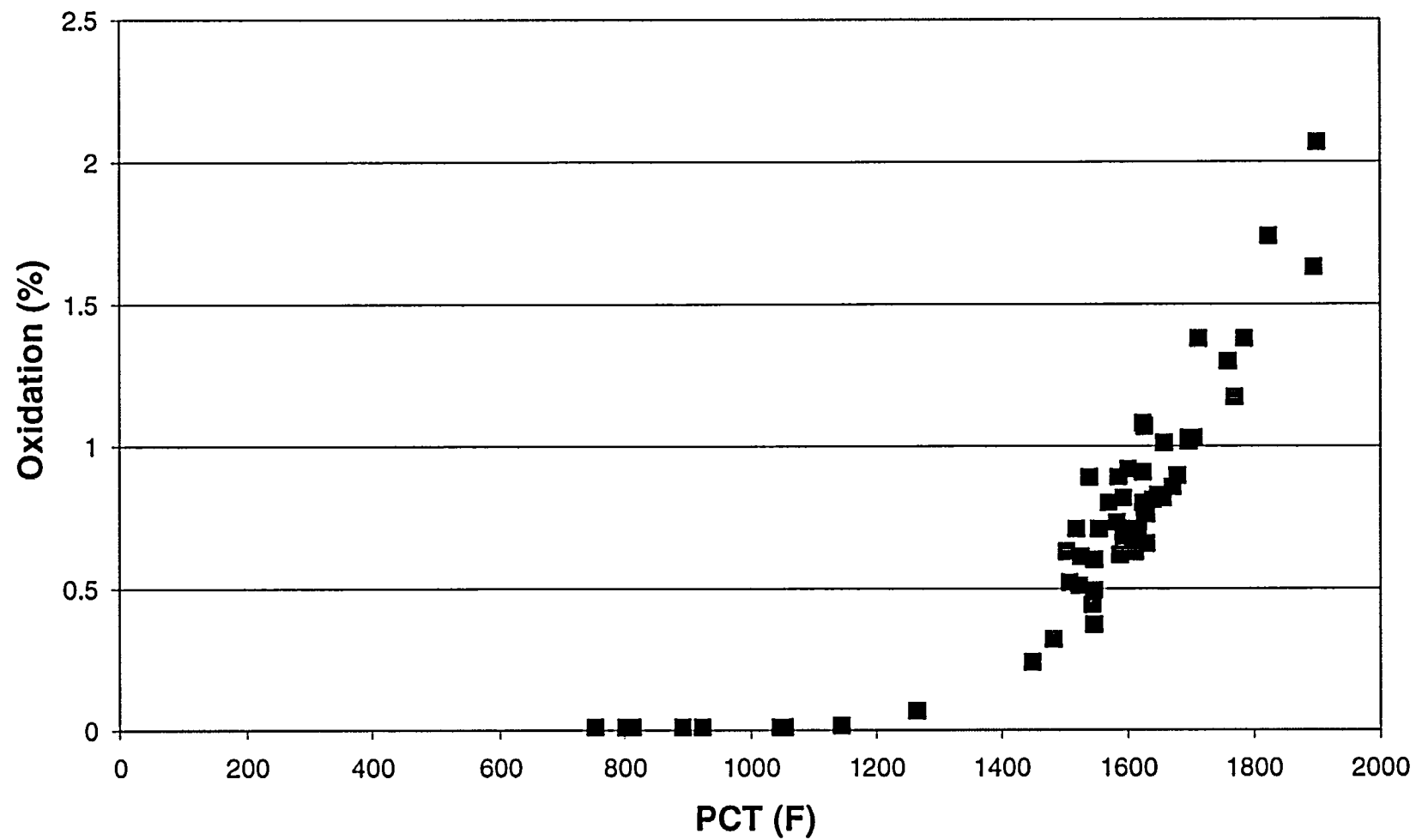


Figure 12-36. Local Oxidation vs. PCT

## 13 METHODOLOGY SUMMARY

In this section, the Automated Statistical Treatment of Uncertainty Method (ASTRUM) is compared against applicable regulatory criteria and guidance. In addition, prior Safety Evaluation Report (SER) requirements are reviewed, and their continued applicability is discussed.

### 13-1 COMPLIANCE WITH 10CFR50.46

*(a)(1)(i):* This part briefly outlines the requirements for an acceptable evaluation model, and requires that demonstration be provided that the limits of the Code of Federal Regulations (CFR) 10CFR50.46 be met with a high degree of probability. Additional details concerning these requirements are spelled out in Regulatory Guide (RG) 1.157 (US Nuclear Regulatory Commission (NRC), 1989). Compliance of the best-estimate methodology with these requirements is addressed in detail in the next section.

*(b)(1) Peak Cladding Temperature:* The peak cladding temperature (PCT) is demonstrated to remain below the limit of 2200°F for all large-break loss-of-coolant accidents (LBLOCAs), using the methods described in Sections 11-3 and 11-4. These methods result in a conservative estimate of the 95<sup>th</sup> percentile PCT at 95-percent confidence.

*(2) Maximum Cladding Oxidation:* The maximum cladding oxidation is verified to remain below the regulatory limit of 17 percent of cladding thickness, using the procedure described in Section 11-6-1.

*(3) Maximum Hydrogen Generation:* The hydrogen generated in the core, as determined by estimating the total volume of cladding oxidized for the limiting conditions, is verified to be less than the regulatory limit of 0.01 times the maximum theoretical amount, using the procedure described in Section 11-6-2.

*(4) Coolable Geometry:* Westinghouse reload cores are analyzed using plant-specific or bounding seismic and LOCA loads to confirm that the core remains coolable during the LOCA.

*(5) Long-Term Cooling:* Long-term cooling is dependent on the demonstration of continued delivery of cooling water to the core. The actions, automatic or manual, that are currently in place at these plants to maintain long-term cooling remain unchanged.

### 13-2 COMPLIANCE WITH REGULATORY GUIDE 1.157

This section contains an updated version of Section 28-2 of WCAP-12945-P-A (Bajorek et al., 1998).

The method used to identify references in this section is slightly different from the rest of this report. References for each subsection of the compliance assessment are identified by a superscript within brackets (e.g., <sup>(x)</sup>). The references may be request for additional information (RAI) responses from Appendix C of WCAP-12945-P-A, topical reports, other sections of this report, or figures from WCAP-12945-P-A. The references are then listed at the end of each subsection.

### 13-2-1 Regulatory Position 1, "Best-Estimate Calculations"

The WCOBRA/TRAC computer code used by Westinghouse for best-estimate LBLOCA calculations is an improved version of the COBRA/TRAC code<sup>(1)</sup> originally developed and assessed by the NRC and its contractor as part of the NRC's best-estimate transient code development program. The models in the code are intended to provide realistic calculations of phenomena of importance to the behavior of a pressurized water reactor (PWR) during an LBLOCA transient. These models have been assessed using comparisons of code predictions with approximately 100 experiments in a number of separate-effects and integral-effects test facilities. These assessments have been supplemented in some cases by comparisons with other available models. The applicability of the WCOBRA/TRAC models over the range of conditions expected during a PWR LBLOCA transient has been demonstrated by use of a code validation matrix that covers, to the extent practical, those ranges of conditions.

Comparisons of WCOBRA/TRAC calculations with data obtained from separate-effects and integral-effects tests have been used to determine the overall uncertainty and biases of the calculation, as recommended in Regulatory Position 1. The integral test simulations were also used to verify that important phenomena (such as, emergency core cooling (ECC) bypass or entrainment/de-entrainment in the upper plenum) are adequately predicted.

In some cases, the models used in WCOBRA/TRAC include simplifications, when a more detailed treatment is not warranted for LBLOCA calculations (such as, [ ]<sup>a.c.(3)</sup>). Assessments of model predictions of experimental data have indicated that some models that are intended to be best estimate are actually somewhat [ ]<sup>a.c.</sup>. In addition, WCOBRA/TRAC has been found to predict [ ]<sup>a.c.(6)</sup>. These simplifications, conservatism, and deficiencies have been identified. They have been corrected, accounted for in the uncertainty analysis, or determined not to result in unrealistic calculations of important phenomena.

#### References for Regulatory Position 1 Compliance Discussion

- 1) NUREG/CR-3046
- 2) RAI1-225
- 3) RAI1-134, Section 25-8 of WCAP-12945-P-A
- 4) Section 13-3, Section 25-5 of WCAP-12945-P-A
- 5) RAI1-238, Section 15-1, Section 25-6 of WCAP-12945-P-A
- 6) Section 13-5, Section 25-5 of WCAP-12945-P-A

## 13-2-2 Regulatory Position 2, "Considerations for Thermal-Hydraulic Best-Estimate Codes"

### 2.1 Basic Structure of Codes

#### 2.1.1 Numerical Methods

The overall numerical scheme used in WCOBRA/TRAC is unchanged from that used in the best-estimate COBRA/TRAC code originally developed and assessed by the NRC and its contractor. A substantial number of timestep and convergence criteria studies were performed by Westinghouse<sup>(1-6)</sup> in order to finalize acceptable values for these parameters. Noding used for code validation against experimental data, and noding used for PWR calculations, were kept consistent to the extent practical, in order to minimize the uncertainty introduced by noding. Nodalization studies of the LOFT integral-effects test facility were performed, and the variation in calculated results were included in the overall code uncertainty assessment.<sup>(7)</sup>

#### References for Regulatory Position 2.1.1 Compliance Discussion

- 1) Section 22-5 of WCAP-12945-P-A
- 2) RAI1-236
- 3) RAI1-240
- 4) RAI4-3
- 5) RAI4-50
- 6) RAIS-8
- 7) Section 19-6 of WCAP-12945-P-A

#### 2.1.2 Computational Models

WCOBRA/TRAC uses a two-fluid, three-field representation of flow in the vessel component.<sup>(1)</sup> The three fields are a vapor field, a continuous liquid field, and an entrained liquid drop field. Each field in the vessel uses a set of three-dimensional continuity, momentum, and energy equations, except that a single energy equation is used for the continuous liquid and entrained liquid drop fields.

The remainder of the reactor coolant system (RCS) is modeled using one-dimensional components. These components use a two-phase, five-equation drift flux formulation, which consists of two equations each for conservation of mass and energy and a single equation for conservation of momentum.<sup>(2)</sup> Appropriate constitutive relationships are used to obtain closure for the conservation equations.

Energy conduction equations are also used to calculate the time-dependent temperature distributions in the fuel rods,<sup>(3)</sup> vessel walls and internals,<sup>(4)</sup> and RCS piping.<sup>(5)</sup> [

] <sup>a,c</sup>



Additional discussion of noncondensable effects is contained in the discussion of Regulatory Position 3.12.2.1 given later in this section.

#### References for Regulatory Position 2.1.2 Compliance Discussion

- 1) Sections 2-2 and 2-3
- 2) Sections 2-4 and 2-5
- 3) Sections 7-2 through 7-5
- 4) Sections 7-2 and 7-6
- 5) Section 7-7

### 13-2-3 Regulatory Position 3, "Best-Estimate Code Features"

#### 3.1 Initial and Boundary Conditions and Equipment Availability

Sensitivity studies were performed to identify the most limiting initial conditions expected over the life of the plant.<sup>(1)</sup> Those studies indicated that fuel in its first cycle of irradiation is more limiting than fuel with higher burnup. [

] <sup>a,c</sup> Uncertainties in core power, peaking factors, axial power distributions, and initial fluid conditions are considered in the overall uncertainty assessment.<sup>(3)</sup>

The limiting break location was determined to be in a cold leg.<sup>(4)</sup> Double-ended guillotine breaks and split breaks in the cold leg are considered in the overall uncertainty assessment. [

] <sup>a,c</sup>

The PWR calculations consider the effect of the limiting single failure on emergency core cooling system (ECCS) performance. Scenarios with offsite power available, and onsite power only, are also considered. The minimum safety injection (SI) flowrate and maximum SI delay times are used, based on plant technical specification limits. The effect of variations in the initial conditions of the accumulators, within the ranges allowed by the plant technical specification limits, are also considered in the overall uncertainty assessment.<sup>(3)</sup>

#### References for Regulatory Position 3.1 Compliance Discussion

- 1) Section 22-7 of WCAP-12945-P-A
- 2) Section 11-2-2
- 3) Section 11-3
- 4) Section 22-6 of WCAP-12945-P-A and RAI5-53

- 5) Section 11-2-1
- 6) Section 25-2 of WCAP-12945-P-A

### 3.2 Sources of Heat During a Loss-of-Coolant Accident

#### 3.2.1 Initial Stored Energy of the Fuel

The initial stored energy in the fuel is based on calculations performed with the Westinghouse PAD code, which is a detailed fuel rod design code whose models have been developed from, and benchmarked against, appropriate in-pile and out-of-pile data. This code has been reviewed and approved by the NRC.<sup>(1)</sup>

##### 3.2.1.1 Model Evaluation Procedure for Stored Energy and Heat Transfer in Fuel Rods

The Regulatory Guide specifies that:

*"A model to be used in ECCS evaluations to calculate internal fuel rod heat transfer should:*

- a. Be checked against several sets of relevant data, and*
- b. Recognize the effects of fuel burnup, fuel pellet cracking and relocation, cladding creep, and gas mixture conductivity."*

The initial stored energy in the fuel is based on calculations performed with the NRC-approved PAD code,<sup>(1)</sup> which has been checked against relevant in-pile and out-of-pile data, and which recognizes the effects of the specified parameters. The WCOBRA/TRAC fuel rod models include explicit modeling of [

] <sup>a,c</sup>

The HOTSPOT code<sup>(4)</sup> is used to account for uncertainties in the [

] <sup>a,c</sup>

### 3.2.1.2 Experimental Data for Stored Energy in Fuel Rods and Heat Transfer

The information provided above addresses this recommendation. [

] <sup>a,c</sup>(1)

#### References for Regulatory Position 3.2.1 Compliance Discussion

- 1) WCAP-15063-P-A, Revision 1
- 2) Sections 7-3 and 7-4
- 3) RAI5-42
- 4) Section 25-4 of WCAP-12945-P-A

### 3.2.2 Fission Heat

Fission heat is calculated using a point kinetics model, which calculates shutdown reactivity on a best-estimate basis. Details of the fission heat modeling are described in Section 8-3. The modeling is consistent with RG 1.157.

No credit is taken for control rod insertion in the Westinghouse best-estimate LBLOCA methodology. Damage to some of the guide tubes in the upper plenum due to the forces generated during an LBLOCA cannot be precluded. Therefore, it is conservatively assumed that no rods insert.

### 3.2.3 Decay of Actinides

The heat from radioactive decay of U-239 and Np-239 is calculated as described in Section 8-4. [

] <sup>a,c</sup>

The treatment of the actinide decay heat source is considered to be in compliance with the regulatory guide, based on these considerations.

#### Reference for Regulatory Position 3.2.3 Compliance Discussion

- 1) RAI1-231

### 3.2.4 Fission Product Decay Heat

Fission product decay heat is calculated using the American National Standards Institute/American Nuclear Society (ANSI/ANS) 5.1-1979 model, which is consistent with the regulatory guide recommendation. Details concerning the implementation of that standard are contained in Section 8.

#### 3.2.4.1 Model Evaluation Procedure for Fission Product Decay Heat

The Q values and models for actinide decay heat are based on [

] <sup>a,c</sup>

### 3.2.5 Metal-Water Reaction Rate

The metal-water reaction rate for zircaloy cladding is calculated using the Cathcart-Pawel model. A similar model is used for the advanced ZIRLO™ cladding material developed by Westinghouse. Uncertainties in the reaction rates calculated by these correlations are considered for the hot rod. If rod burst is calculated to occur, the reaction rates on the inner surface are calculated using the same models and uncertainties.

#### 3.2.5.1 Model Evaluation Procedure for Metal-Water Reaction Rate

The Cathcart-Pawel model is used in WCOBRA/TRAC to calculate metal-water reaction for zircaloy cladding [

] <sup>a,c</sup>

Metal-water reaction rates for ZIRLO™ cladding [

] <sup>a,c</sup>

The outer surface oxide thickness at the beginning of the transient is [

] <sup>a,c</sup> Internal oxidation from

steam following burst is included in the analysis.

The WCOBRA/TRAC models for metal-water reaction [

] <sup>a,c</sup>

#### References for Regulatory Position 3.2.5 Compliance Discussion

- 1) ORNL/NUREG-17, page 67 and Figure 30
- 2) WCAP-12610, Appendix E, Figure E-4

#### 3.2.6 Heat Transfer from Reactor Internals

Heat transfer from the piping, vessel walls, and vessel internal hardware is calculated in a best-estimate manner. Heat transfer to guide tubes in the core is considered small. It is not modeled in PWR calculations or simulations of experiments.

In the simulations of experiments used to assess WCOBRA/TRAC, heat transfer between structures and fluid was also included wherever important. Illustrative examples are:

- FLECHT – test shroud
- LOFT – vessel wall, internals, loop piping

#### 3.2.7 Primary-to-Secondary Heat Transfer

Heat transfer between the primary and secondary sides is modeled using the STGEN component described in Section 9-5. [

] <sup>a,c</sup>

Simulated steam generators were used in the LOFT and CCTF integral test facilities. The WCOBRA/TRAC analyses of experiments performed in these facilities explicitly modeled the simulated steam generators using the STGEN component.

### 3.3 Reactor Core Thermal/Physical Parameters

#### 3.3.1 Thermal Parameters for Swelling and Rupture of the Cladding and Fuel Rods

WCOBRA/TRAC includes models for swelling and rupture of the cladding that are dependent on the cladding temperature and the differential pressure across the cladding. The effects of fuel rod deformation are explicitly included in the models used to calculate [

] <sup>a,c</sup>

Additional discussion of the use of swelling and burst models in WCOBRA/TRAC and HOTSPOT was previously presented in the Regulatory Position 3.2.1.1 Compliance Discussion.

#### 3.3.2 Other Core Thermal Parameters

The effect of the cladding change from alpha to beta phase is reflected in the cladding thermal and material properties. Physical changes in core geometry due to combined LOCA and safe shutdown earthquake (SSE) loads are also taken into account.<sup>(1)</sup> [

] <sup>a,c</sup>

References for Regulatory Position 3.3.2 Compliance Discussion

- 1) RAI5-53

### 3.4 Blowdown Phenomena

#### 3.4.1 Break Characteristics and Flow

Break location studies have shown the limiting location to be in the cold leg.<sup>(1)</sup> The uncertainty analysis considers double-ended guillotine and split breaks in the cold leg. [

] <sup>a,c</sup> This

methodology is considered to be in compliance with Regulatory Position 3.1.

### 3.4.1.1 Model Evaluation Procedure for Discharge Flowrate

The WCOBRA/TRAC calculation of critical flowrate considers the [

] <sup>a.c.(5)</sup> Comparisons of this model to the Marviken critical flow data have been made, to obtain uncertainties and modeling bias. In addition, a range of applicability was established. <sup>(3)</sup>

### 3.4.1.2 Experimental Data for Discharge Flowrate

The Marviken test data include a range of fluid conditions, pressures, and break nozzle geometries that are appropriate for limiting large break sizes. Comparisons with these data, and use of the resulting uncertainties and bias in the overall uncertainty methodology, result in conformance with the regulatory guide recommendations.

#### References for Regulatory Position 3.4.1 Compliance Discussion

- 1) RAI5-53
- 2) Section 11-2-1
- 3) Section 25-2 of WCAP-12945-P-A
- 4) Section 4-8-2
- 5) RAIC-5

### 3.4.2 ECC Bypass

The ECC penetration into the reactor vessel and core is calculated in WCOBRA/TRAC using the following models:

#### a. Axial and Lateral Channels in the Downcomer

To model multidimensional flow in the downcomer during the injection of ECC water, the PWR downcomer contains [ <sup>a.c.(1)</sup> The momentum equations used to model the axial areas and lateral gaps include the effects of gravity, wall shear, condensation, and convection of momentum. <sup>(2)</sup>

#### b. Wall and Interfacial Drag Models

Wall and interfacial drag models and correlations are used to calculate the interaction of upflowing steam with downflowing water. <sup>(3)</sup>

c. Entrainment Models

Entrainment models and correlations are used to calculate the steam/water interaction.<sup>(4)</sup> If steam upflow is sufficiently high, liquid films on the downcomer walls are entrained into droplets, which are more easily carried upward by the steam.

d. Condensation Models

Condensation models and correlations are used to calculate the effect of water subcooling on ECC bypass.<sup>(5)</sup>

### 3.4.2.1 Model Evaluation Procedure for ECC Bypass

The following procedure was used to evaluate the ECC bypass prediction:

1. Establish the countercurrent flow limit (CCFL) line for WCOBRA/TRAC for several geometries

A fundamental process controlling the extent of ECC bypass is the well-known CCFL. This limit has been well established over a wide range of fluid conditions by a large number of experiments in tubes, perforated plates, and annuli. WCOBRA/TRAC was used to model several different geometries,<sup>(6)</sup> using nodding similar to that employed for the PWR, and several cases were run to establish the CCFL line which would be predicted by WCOBRA/TRAC under saturated (no condensation) conditions.<sup>(6)</sup> Details of the predicted flow fields were also evaluated and explained.<sup>(11)</sup> It was found that in nearly all cases, the predicted CCFL agreed with the well-known Wallis flooding line formulation, modified as necessary for the different geometries studied.

2. Establish the CCFL line for WCOBRA/TRAC for several scales

The behavior of the CCFL as scale increased from those typical of most tests to those of the PWR was also investigated in the annulus geometry.<sup>(7)</sup> This was done to assure that the CCFL behaved consistently and conformed to established scaling principles, including those developed for the Upper Plenum Test Facility (UPTF) full-scale experiments.

3. Compare WCOBRA/TRAC to small- and full-scale subcooled ECC tests

The evaluation in steps 1 and 2 established the overall correctness of the interfacial drag and entrainment models to predict ECC phenomena. Tests at various scales with subcooled ECC were then evaluated. This approach allowed any compensating errors to be identified. Comparisons with these experiments indicated that in general the overall condensation efficiency was predicted well. [

]a,c



[

] <sup>a,c</sup>

In conclusion, it was determined that the models used to calculate ECC penetration were applied correctly, and that compensating errors did not exist, [

] <sup>a,c</sup>

### 3.4.2.2 Experimental Data for ECC Bypass

The following experiments were used in the evaluation of the ECC bypass model to establish range of applicability.<sup>(10)</sup> In some cases, correlations which were known to represent the data from these tests well were used for the comparison:

- Small diameter vertical pipes
- Perforated plates
- Horizontal pipes
- 1/15-, 1/5-scale annuli
- UPTF tests

### References for Regulatory Position 3.4.2 Compliance Discussion

- 1) Section 20 of WCAP-12945-P-A
- 2) Section 2
- 3) Sections 4-2 and 4-4
- 4) Section 4-6
- 5) Section 5
- 6) Section 15-1 of WCAP-12945-P-A
- 7) Section 15-1-5 of WCAP-12945-P-A
- 8) RAI1-238, Section 15-1 of WCAP-12945-P-A
- 9) RAI4-2
- 10) RAI1-3
- 11) RAI3-6

### 3.5 Noding Near the Break and ECCS Injection Point

Westinghouse uses node sizes in the PWR calculations that are consistent with those used in the simulations of the experiments used to validate the break flow model and the condensation behavior at

the ECCS injection point. This helps to ensure that the PWR calculations provide results with comparable accuracy as observed in the code validation. Section 16-4 of WCAP-12945-P-A includes the results of two Marviken simulations that were rerun with twice as many nodes in the nozzle region. The results indicated little effect on the critical flow predictions.

### 3.6 Frictional Pressure Drop

The frictional pressure drops calculated in WCOBRA/TRAC are Reynolds number dependent, and account for two-phase flow effects.<sup>(1)</sup>

#### 3.6.1 Model Evaluation Procedure for Frictional Pressure Drop

The frictional pressure drop models were assessed by comparing the model to other correlations,<sup>(2,3,4)</sup> and by comparing the predicted pressure drop in complex geometries with measured data.<sup>(5)</sup> [

$j_{ac}^{(10)}$

Uncertainties in the frictional pressure drop are accounted for in the overall uncertainty calculations by ranging the break flow path resistances.

#### 3.6.2 Experimental Data for Frictional Pressure Drop

The information provided above addresses this recommendation.

#### References for Regulatory Position 3.6 Compliance Discussion

- 1) Sections 4-2 and 4-7-2
- 2) Figures 4-10 through 4-13
- 3) RAI1-48
- 4) RAI1-100
- 5) RAI1-50
- 6) RAI5-52
- 7) RAI1-3
- 8) Sections 2-2 and 2-3
- 9) Sections 2-4 and 2-5
- 10) RAIC-5

### 3.7 Momentum Equation

The following effects are taken into account in the two-phase conservation of momentum equation:

- 1) Temporal change in momentum. All momentum equations applied in the thermal-hydraulic network take into account the temporal change in momentum.<sup>(1,2)</sup>
  - 2) Momentum convection. Both the vessel and one-dimensional (1-D) component momentum equations include a complete description of momentum convection.<sup>(1,2)</sup> [
- $]^{ac}$
- 3) Area change momentum flux. Both the vessel and 1-D momentum equations are formulated to account for momentum changes resulting from area changes.<sup>(1,2)</sup> The effect that the method of discretization has on these effects is recognized and taken into account.
  - 4) Momentum change due to compressibility. Both the 1-D and vessel momentum equations are formulated to account for the effects of phase compressibility on momentum flux.<sup>(1,2)</sup>
  - 5) Pressure loss resulting from wall friction. The wall friction factor models used in the 1-D and vessel momentum equations use standard approaches that compare well with other models and correlations (Regulatory Position 3.6 Compliance Discussion).
  - 6) Pressure loss resulting from area changes. These losses are taken into account, in conjunction with the area change momentum change.
  - 7) Gravitational acceleration. Both vessel and 1-D momentum equations take this effect into account.<sup>(1,2)</sup>

The validity of the [  $]^{ac}$  is demonstrated in several ways:

- Comparisons between predictions and experiments at increasing scales, where 3-D effects would be expected to become more important

- Benchmarking of the PWR model during steady-state with experimentally determined vessel and loop pressure drops<sup>(5)</sup>
- Comparison of flowrates and pressure drops in complex networks representing the PWR at various scales
- Comparison with two-phase pressure drop experiments

#### References for Regulatory Position 3.7 Compliance Discussion

- 1) Sections 2-2 and 2-3
- 2) Sections 2-4 and 2-5
- 3) Section 4-7-4
- 4) Section 25-3 of WCAP-12945-P-A
- 5) Section 20-5 of WCAP-12945-P-A

### 3.8 Critical Heat Flux

Regulatory Guide 1.157 states:

*"Best estimate models developed from appropriate steady-state or transient experimental data should be used in calculating critical heat flux (CHF) during loss-of-coolant accidents. The codes in which these models are used should contain suitable checks to ensure that the range of conditions over which these correlations are used are within those intended."*

The critical heat flux is calculated in the core using the Zuber pool boiling departure from nucleate boiling (DNB) correlation, and the Biasi correlation for forced-convection DNB. These correlations and how they are programmed into WCOBRA/TRAC are described in Section 6-2-4.<sup>(1)</sup> The Biasi correlation consists of two separate expressions, and depends on pressure, mass flux, quality, and hydraulic diameter. The Zuber correlation is applied only when the flowrate decreases to near zero, and conditions approach those of pool boiling. The mass flux is checked to ensure that the [

] <sup>a,c</sup>

[

] <sup>a,c</sup>

### References for Regulatory Position 3.8 Compliance Discussion

- 1) RAI1-166
- 2) NUREG/CR-5069
- 3) Section 11-2 of WCAP-12945-P-A
- 4) Section 14-1 of WCAP-12945-P-A
- 5) RAI3-1

### 3.9 Post-CHF Blowdown Heat Transfer

With regards to post-CHF blowdown heat transfer, RG 1.157 states:

*"Models of heat transfer from the fuel to the surrounding fluid in the post-CHF regimes of transition and film boiling should be best estimate models based on comparison to applicable steady-state or transient data. Any model should be evaluated to demonstrate that it provides acceptable results over applicable ranges. Best-estimate models will be considered acceptable provided their technical basis is demonstrated with appropriate data and analysis."*

The models for transition and film boiling are described in Sections 6-2-5 and 6-2-8, respectively. The models for each regime are formulated to be mechanistic, and are generally applicable to all phases of a LOCA transient. The models for each regime account for the effects of local void fraction and droplets, thermal radiation, thermal non-equilibrium, flowrate, wall heat flux, and liquid temperature. The models used for the phasic components of heat transfer for each of the regimes are very similar to models used in other two-fluid codes such as RELAP and TRAC-PF1, and are referenced to correlations previously proposed for these regimes.

The models for heat transfer in post-CHF blowdown flows have been checked against several sets of experimental data that are prototypical of Westinghouse and other PWR fuel assemblies. Because the blowdown transient passes through several distinct periods, tests were selected such that each period was examined. In particular, the heat transfer models were used to simulate several tests and predict cladding temperature histories in ORNL<sup>(1)</sup> (for blowdown during the upflow period), G-1<sup>(2)</sup> and G-2<sup>(3)</sup> Loop blowdown tests (for blowdown during the downflow period), and the G-2<sup>(4)</sup> Loop refill tests (for the refill period). For each test simulated, comparisons between the predicted and measured cladding

temperatures as functions of time, and axial temperature profile comparisons at select times, were reported.

[

] <sup>a,c</sup>

Sections 13-2 and 13-3 of WCAP-12945-P-A evaluate the performance of the heat transfer package during the blowdown periods. Comparisons of predicted versus measured blowdown cooling rates (G-1 and G-2 blowdown tests), PCTs (ORNL and G-2 refill tests), quench times (G-1 and G-2 blowdown tests), and heat transfer coefficients (G-1 and G-2 blowdown tests) were made in order to characterize the performance of the heat transfer models for blowdown period thermal-hydraulics. These comparisons indicated that [

] <sup>a,c(5)</sup>

In addition, Section 13-2 of WCAP-12945-P-A provides details on calculated parameters for which measurements are not available. These are provided to demonstrate that the calculated parameters are part of a consistent set of results, and that the variations in those parameters are reasonable based on engineering judgement.

Additional information regarding the effects of liquid entrainment and power density was provided in the response to RAIC (Attachment 5). The models and correlations used for post-CHF blowdown heat transfer therefore have:

- (a) Been checked against acceptable sets of relevant data, and
- (b) Recognize the effects of liquid entrainment, thermal radiation, . . .

and thus satisfy the Regulatory Guide with regards to those criteria.

Regulatory Guide 1.157 also requires that,

*"The uncertainties and bias of models or correlations used to calculate post-CHF heat transfer should be stated as well as the range of their applicability."*

The biases and uncertainties of the models and correlations used to calculate post-CHF heat transfer prior to reflood are [

] <sup>a,c</sup>

[

]a,c(7,8)

#### References for Regulatory Position 3.9 Compliance Discussion

- 1) Section 11-2 of WCAP-12945-P-A
- 2) Section 11-3 of WCAP-12945-P-A
- 3) Section 11-4 of WCAP-12945-P-A
- 4) Section 11-5 of WCAP-12945-P-A
- 5) Section 25-5 of WCAP-12945-P-A
- 6) Section 19-7, Section 25-10 of WCAP-12945-P-A
- 7) RAI2-2
- 8) RAI1-152

#### 3.9.3 Post-CHF Heat Transfer from Uncovered Bundles

The heat transfer package in WCOBRA/TRAC is described in Section 6. The models and correlations used in WCOBRA/TRAC and the techniques used to determine the phasic heat transfer contributions are very similar to, and in some cases identical to, those used in the NRC's best-estimate codes (such as, COBRA, TRAC, and RELAP).

### 3.9.3.1 Model Evaluation Procedures for Heat Transfer from Uncovered Rod Bundles

As for models and correlations used to calculate heat transfer from uncovered bundles, RG 1.157 states:

*"A correlation to be used in ECCS evaluations to calculate heat transfer from uncovered rod bundles should:*

- a. Be checked against an acceptable set of relevant data, and*
- b. Recognize the effects of radiation, and of laminar, transition, and turbulent flows.*

*Uncertainties and bias in the models and correlations used to calculate post-CHF heat transfer should be stated, as should the range of their applicability."*

The effect of [

J<sup>a.c</sup>



[

 $J_{ac}^{(9,10)}$ 

Regulatory Guide 1.157 provides some discussion on the acceptable form of correlations for turbulent convection:

*"The turbulent correlation may be of the general form:*

$$Nu = A Re^m Pr^n$$

*for higher Reynolds numbers (Re), where the coefficients A, m, and n are modifications from the basic Dittus-Boelter form and may be functions of other variables."*

The WCOBRA/TRAC relations for turbulent convection are of this form (Section 6). In addition, the distinction is made in the code between laminar and turbulent convection at low Reynolds numbers,<sup>(2)</sup> which complies with the RG 1.157 direction that:

*"A distinction from, and transition to, laminar convection (i.e.,  $Re < 2000$ ) should be made, with a value of the laminar heat transfer for rod bundles that is appropriate for the applicable bundle geometry and flow conditions."*

#### References for Regulatory Position 3.9.3 Compliance Discussion

- 1) Section 6-2-9
- 2) RAIC-5
- 3) Sections 6-2-1 and 6-2-2
- 4) Section 6-2-4
- 5) Section 6-2-7
- 6) Section 6-2-3
- 7) Section 25-5 of WCAP-12945-P-A
- 8) Section 19-7 of WCAP-12945-P-A
- 9) RAI2-2
- 10) RAI1-213
- 11) Section 25-10 of WCAP-12945-P-A

### 3.10 Pump Modeling

The pump model in WCOBRA/TRAC takes into account changes in pump rotor rotational speed as a result of changes in torque applied to the rotor from the fluid, pump rotor inertia, and resistance to

rotation, if the power to the pump is lost.<sup>(1)</sup> If power to the pump is available, the pump is assumed to continue rotating at constant speed regardless of applied torque (a characteristic of these types of motors). The interaction between the pump and the fluid is in two forms:

- Torque applied by the fluid on the pump rotor
- Energy gained or lost by the fluid (in terms of pressure rise or loss) from the pump

The torque and pressure rise are provided as empirical curves relating these quantities to pump rotational speed, fluid volumetric flow, and fluid vapor fraction. The curves are based on single- and two-phase data obtained from tests using a scaled pump with similar specific speed.

Cases in which power to the pumps continues to be supplied, and where power to the pumps is lost, are both analyzed as part of the methodology. The limiting case is used for subsequent uncertainty evaluations.

[

$J^{ac(4)}$

#### References for Regulatory Position 3.10 Compliance Discussion

- 1) Section 9-4
- 2) RAI5-47
- 3) Section 16-3 of WCAP-12945-P-A
- 4) Section 25-3 of WCAP-12945-P-A

#### 3.11 Core Flow Distribution During Blowdown

The flow through the hot assembly is calculated directly from the WCOBRA/TRAC conservation equations, and includes the effect of crossflow and cladding deformation. [

$J^{ac}$

### 3.12 Post-Blowdown Phenomena

#### 3.12.1 Containment Pressure

Containment pressure calculations are performed using the same codes as used for currently licensed evaluation models, with mass and energy rates supplied from the WCOBRA/TRAC reference transient.

#### 3.12.2 Calculation of Post-Blowdown Thermal Hydraulics for Pressurized Water Reactors

The refill and reflood phases of the transient are calculated on a best-estimate basis, taking into consideration the thermal and hydraulic characteristics of the core, the ECCS performance, and important reactor systems. The distribution of water and steam in the reactor vessel is calculated directly from the WCOBRA/TRAC conservation equations, and appropriate constitutive relations. Assessment of WCOBRA/TRAC's ability to predict processes important to refill and reflood has been performed by comparison with test data from separate-effects and integral-systems tests.

##### 3.12.2.1 Model Evaluation Procedures for Post-Blowdown Thermal-Hydraulics

**Level Swell** During the reflood phase of a PWR LOCA transient, a process similar to level swell can occur as the fuel rods rewet and substantial boiling occurs. [

] <sup>a,c</sup>

**Primary Coolant Pumps** As described in the Regulatory Position 3.10 discussion above, cases in which the pump is powered and not powered are considered in the methodology, and the limiting case is taken into account. [

] <sup>a,c</sup>

**Carryover** The total fluid flow leaving the core exit is calculated directly from the WCOBRA/TRAC conservation equations and appropriate constitutive relations. WCOBRA/TRAC predictions of carryover were assessed against FLECHT-SEASET,<sup>(4,5)</sup> Cylindrical Core Test Facility (CCTF), and Slab Core Test Facility (SCTF) tests.<sup>(2)</sup> The PWR modeling includes sufficient nodalization to capture the effects of cross-flow on carryover and the core fluid distribution during reflood.

**Upper Plenum Injection Plants** A separate phenomena identification and ranking table (PIRT) was developed for plants equipped with upper plenum injection (UPI).<sup>(6)</sup> Additional code assessment was

performed for UPI tests performed in UPTF and CCTF, as well as separate-effects tests that examined the effects of subcooling on CCFL in a rod bundle geometry. The results of those assessments were used to specify the phenomena ranging required for uncertainty analyses of UPI plants. Details of this work are reported in WCAP-14449-P-A.

**Upper Head Injection Plants** All domestic Westinghouse PWRs originally designed with upper head injection (UHI) have had these injection lines capped. These plants now rely on cold-leg injection, and are modeled as such. The PWR model described in Section 20-3 of WCAP-12945-P-A is an example of this type of plant application. There are no special post-blowdown thermal-hydraulic phenomena associated with plants that have had their UHI lines capped.

**Accumulator Nitrogen** The effects of compressed gas discharging from the accumulator are accounted for in the calculation. The discharging nitrogen has the following effects:

- Pressurization of the downcomer due to increased volumetric flow into the downcomer from the intact loops, causing a level increase in the core. This effect was assessed by comparing WCOBRA/TRAC transient predictions to data obtained in the Achilles and LOFT test facilities.<sup>(7)</sup>
  - Suppression of condensation in the intact loops and in the upper downcomer due to complete displacement of steam from these regions. This effect was assessed by [
- ] <sup>a,c</sup> (8)
- The effects of nitrogen coming out of solution [
- ] <sup>a,c</sup>.

#### References for Regulatory Position 3.12.2 Compliance Discussion

- 1) Appendix A of WCAP-12945-P-A
- 2) RAI4-37
- 3) RAI1-152
- 4) Section 15-2 of WCAP-12945-P-A
- 5) RAI3-19
- 6) Section 1-2-3
- 7) Section 16-2 of WCAP-12945-P-A
- 8) RAI1-134

#### 3.12.3 Steam Interaction with Emergency Core Cooling Water in Pressurized Water Reactors

Mixing of steam and subcooled water in the intact cold legs of a PWR is taken into account. Studies comparing predictions to small- and full-scale data indicate that the overall degree of condensation is

predicted reasonably well.<sup>(1)</sup> [

] <sup>a,c</sup>

#### References for Regulatory Position 3.12.3 Compliance Discussion

- 1) Section 15-3 of WCAP-12945-P-A
- 2) Section 25-9 of WCAP-12945-P-A

#### 3.12.4 Post Blowdown Heat Transfer for Pressurized Water Reactors

This section of RG 1.157 provides guidance on validation for heat transfer calculations, and recommends various experimental tests for that purpose. In particular, it is stated that,

*"... the heat transfer calculations should be based on a best-estimate calculation of the fluid flow through the core, accounting for unique emergency core cooling systems."*

To satisfy this requirement, validation tests are performed when a plant design has a unique cooling system. For example, because the AP600 design includes direct vessel injection, experimental tests (CCTF Run 58 and UPTF Test 21) were modeled and simulated<sup>(1)</sup> in order to demonstrate the ability of the code to calculate phenomena under those conditions. In the case of UPI plants, additional experimental tests in CCTF and UPTF were simulated<sup>(2)</sup> to show that the code can predict the necessary phenomena with those type of units.

Regulatory Guide 1.157 also states:

*"The calculations should also include the effects of any flow blockage calculated to occur as a result of cladding swelling or rupture."*

The models for swelling, rupture, and blockage are described in Section 7.<sup>(3)</sup> Additional discussion of the use of swelling and burst models in WCOBRA/TRAC and HOTSPOT was previously presented in the Regulatory Position 3.2.1.1 Compliance Discussion. The effects of hot assembly flow blockage

calculated in WCOBRA/TRAC are reflected in the local fluid conditions used in the HOTSPOT calculations.

Also, RG 1.157 states:

*"Heat transfer calculations that account for two-phase conditions in the core during refilling of the reactor vessel should be justified through comparisons with experimental data. Best estimate models will be considered acceptable provided their technical basis is demonstrated through comparison with appropriate data and analysis."*

Sections 13 and 15 of WCAP-12945-P-A contain detailed information on several test simulations. Models that originally appeared to be suspect, such as the bottom entrainment model, were clearly identified.<sup>(4)</sup> Reanalyses with the revised entrainment model have been incorporated in WCAP-12945-P-A and Appendix B of this report. Where data are available, comparisons have been made between predicted and measured parameters to show that the code predicts not only the rod PCTs well, but also other important parameters. This helps to indicate that the code does not contain any gross compensating errors. Additional assessments regarding the potential for compensating errors are contained in Appendix A of WCAP-12945-P-A.

The Westinghouse methodology ranges the overall heat transfer coefficient for the hot rod to account for uncertainties in the prediction of local fluid conditions and heat transfer coefficient. The ranges considered are based on WCOBRA/TRAC comparisons with relevant rod bundle tests.

Finally, the regulatory guide indicates several experimental tests that are useful for validation purposes:

*"The FLECHT-SEASET tests (Refs. 40, 45, and 46) should be considered when establishing an acceptable set of relevant data."*

and,

*"The results from the 2D/3D program are particularly relevant."*

The simulations used for bias and uncertainty determination included [

] <sup>a,c</sup>

[

] <sup>a,c</sup>

### References for Regulatory Position 3.12.4 Compliance Discussion

- 1) WCAP-14171-P, Rev. 2
- 2) WCAP-14449-P-A
- 3) RAI3-28, RAI4-40
- 4) RAI2-63

## 3.16 Other Features of Best-Estimate Codes

### 3.16.1 Completeness

The WCOBRA/TRAC code used by Westinghouse for best-estimate LBLOCA analyses is an improved version of the COBRA/TRAC code originally developed and assessed by the NRC and its contractor as part of the NRC's best-estimate transient code development program. The models in the code are intended to provide realistic calculations of phenomena of importance to the behavior of a PWR during an LBLOCA transient. These models have been assessed using comparisons of code predictions with approximately 100 experiments in a number of separate effects test facilities, and four integral test facilities (LOFT, CCTF, SCTF, and UPTF).<sup>(1)</sup> The code validation matrix was selected to cover the range of conditions expected during a PWR LBLOCA transient, to the extent practical.<sup>(2,3,4)</sup> Uncertainty in the experimental data was considered in the overall uncertainty assessment.<sup>(5)</sup>

### 3.16.2 Data Comparisons

The WCOBRA/TRAC validation matrix is summarized earlier in Tables 1-2 through 1-6. Comparisons of code predictions with important thermal-hydraulic parameters that were measured in these tests support the conclusion that realistic behavior is predicted and major biases do not exist in the models. The code uncertainty assessment includes the effects of uncertainties in the test data.

The methodology considers the need to range and/or bias each of the key parameters identified in the PIRT.<sup>(6)</sup> Uncertainties in the test data are reflected in the ranges over which these parameters are varied. For example, the condensation model and heat transfer coefficient ranges explicitly include variations in the test data.

### References for Regulatory Position 3.16 Compliance Discussion

- 1) Tables 1-2 through 1-6
- 2) Tables 11-1-1 through 11-1-3, Tables 12-1-1 through 12-1-3 of WCAP-12945-P-A

- 3) RAI1-3a
- 4) RAI1-152
- 5) Section 25-10
- 6) Section 1-2-3

### 13-2-4 Regulatory Position 4, "Estimation of Overall Computational Uncertainty"

#### 4.1 General

The Westinghouse approach to the overall calculational uncertainty has been to separate the uncertainty contributors into two general classifications; the code and models uncertainty contributors and the plant conditions uncertainty contributors. Each uncertainty contributor is varied simultaneously in the calculations performed for the uncertainty analysis.

The code and models uncertainty contributors account for the uncertainty in predicting the important thermal-hydraulic phenomena identified in the PIRT, and important modeling assumptions. This uncertainty was developed by performing a systematic assessment of the uncertainty associated with the prediction of break mass flowrate, break flow path resistance (nozzle and pump), stored energy and fuel rod behavior, core heat transfer, ECC bypass, steam binding, noncondensables, condensation, and upper plenum drain distribution (UPI only).<sup>(1)</sup> Estimates of the code biases and uncertainties for these parameters were based on comparisons with applicable separate-effects and integral-effects test data. Propagation of these uncertainties throughout the PWR transient was [

] <sup>a,c</sup>.

The assessment of the thermal-hydraulic models in WCOBRA/TRAC used a large number of test comparisons to ensure that estimates of the model uncertainties were well-founded, and included potential scaling effects. [

] <sup>a,c</sup>



[

]ac

The plant conditions uncertainty contributors calculations account for the different possible operating conditions and accident initial conditions that the plant could experience. Parameters such as the worst break location, worst pressurizer location relative to the break, and worst onsite power availability condition are bounded since it is not practical to treat these conditions in a statistical fashion. Parameters that are considered as plant conditions uncertainty contributors are grouped into two components. The first includes power-related parameters such as initial core power, peaking factors, axial power distributions, and decay heat. The second component includes other plant initial and boundary conditions.

#### References for Regulatory Position 4.1 Compliance Discussion

- 1) Section 25 of WCAP-12945-P-A and Section 4-7 of WCAP-14449-P-A
- 2) Sections 12-2 through 12-4 of WCAP-12945-P-A
- 3) Appendix A of WCAP-12945-P-A
- 4) RAI2-22
- 5) Section 14-1 of WCAP-12945-P-A
- 6) RAI3-1
- 7) Section 14-2 of WCAP-12945-P-A
- 8) RAI4-37
- 9) Section 14-3 of WCAP-12945-P-A

#### 4.2 Code Uncertainty

The best test of the overall accuracy of the computer code, and the accuracy of individual models, is to compare code predictions to data obtained from a wide range of experiments. Wherever possible, tests performed at full scale or large scale should be used, to eliminate or minimize uncertainties associated with scalability. WCOBRA/TRAC was used to simulate several different experiments that capture the same phenomena, such as reflood heat transfer, at different scales. The WCOBRA/TRAC validation matrix includes tests with different bundle sizes, rod arrays, lengths, power shapes, and grid types, since the computer code will have to model these effects for different plant designs and conditions. An assessment was made of the code's ability to predict PCT with [

]ac

[ ]<sup>a,c</sup> and support the conclusion that there is no additional uncertainty in applying WCOBRA/TRAC to transients in a full-scale reactor.

One measure of the accuracy of the code uses the comparisons of the predicted and measured PCTs.<sup>(2)</sup> By selecting experiments with care and by comparing to data other than the measured cladding temperatures, it can be assured that the PCT is reasonably predicted for the correct reasons. That is, the possibility of compensating errors being present can be investigated. A detailed assessment of the possibility of compensating errors in WCOBRA/TRAC has been performed, which has concluded that while compensating errors do exist, the net effect is a conservative prediction of a PWR LOCA transient.<sup>(3)</sup>

While the available integral effects tests are useful for addressing the issues of scalability and compensating errors, there are insufficient data to address the potential for propagation of uncertainties as a LOCA transient progresses. A detailed study of uncertainty propagation requires that the effects be quantified using computer code calculations of a PWR LOCA transient. Westinghouse has developed a method similar to that used in the CSAU methodology,<sup>(4)</sup> [

] <sup>a,c</sup>

#### References for Regulatory Position 4.2 Compliance Discussion

- 1) Section 18 of WCAP-12945-P-A and Section 4-6 of WCAP-14449-P-A
- 2) Section 19 of WCAP-12945-P-A
- 3) Appendix A of WCAP-12945-P-A
- 4) NUREG/CR-5249

### 4.3 Other Sources of Uncertainty

#### 4.3.1 Initial and Boundary Conditions and Equipment Availability

The treatment of important initial and boundary conditions, and assumptions of the availability of important equipment, are summarized below.

<u>Initial Condition</u>	<u>Considered in Uncertainty Evaluation?</u>
Core power level	Yes
Core power distribution	Yes
RCS fluid conditions	Yes
Accumulator conditions	Yes

Time in cycle	Yes
Hot assembly location	No (bounded)
Steam generator plugging	No (bounded)
<u>Boundary Condition</u>	
Break flow	Yes
SI temperature	Yes
SI flow and delay	No (bounded)
Containment pressure	No (bounded)
<u>Equipment Availability</u>	
Offsite power	No (bounded)
Single failure	No (bounded)
Control rod insertion	No (bounded)

#### 4.3.2 Fuel Behavior

Uncertainties in the lead fuel rod initial conditions and its behavior during the LOCA transient are explicitly accounted for. These uncertainties include hot rod peaking, gap conductance, fuel conductivity, cladding burst temperature, burst strain, fuel density after burst due to relocation, and metal-water reaction rates.<sup>(1)</sup> The treatment of fuel behavior in the Westinghouse methodology is considered to be more complete than that used in the CSAU methodology,<sup>(2)</sup> in that [

] <sup>a.c.</sup>

#### References for Regulatory Position 4.3.2 Compliance Discussion

- 1) Section 25-4 of WCAP-12945-P-A
- 2) NUREG/CR-5249

#### 4.3.3 Other Variables

Uncertainties in decay heat and break flowrate are included in the overall uncertainty assessment. The metal-water reaction rate uncertainty is also considered as one of the fuel rod uncertainty parameters, as noted in the Regulatory Position 4.3.2 Compliance Discussion.

#### 4.4 Statistical Treatment of Overall Calculational Uncertainty

The overall uncertainty in PCT, LMO, and CWO is determined using a non-parametric statistical method. Uncertainties in [

] are. The limiting case from a series of 124 PWR cases is considered to be the 95<sup>th</sup> percentile case, with 95 percent confidence.<sup>(1)</sup>

The best-estimate LBLOCA methodology used by Westinghouse addresses the PCT, maximum cladding oxidation, maximum hydrogen generation, and coolable geometry criteria defined in 10CFR50.46(b)(1) through (b)(4). The PCT at the 95th percentile level is estimated as described above. The maximum cladding oxidation criterion and the maximum hydrogen generation criterion are verified as described in Section 11-6. Coolable geometry is demonstrated by ensuring that the PCT and maximum local oxidation criteria are satisfied, including any effects of combined LOCA and SSE loads on core geometry.<sup>(2)</sup>

The Westinghouse methodology used to satisfy the long-term cooling criterion defined in 10 CFR 50.46(b)(5) is unaffected by the use of best-estimate techniques for the short-term transient calculation.

#### References for Regulatory Position 4.4 Compliance Discussion

- 1) Section 11-1
- 2) RAI5-53

#### 4.5 NRC Approach to LOCA Uncertainty Evaluation

The Westinghouse methodology is structured consistent with the CSAU methodology cited in Section 4.5 of RG 1.157.

### 13-3 EFFECT OF REVISED UNCERTAINTY METHODOLOGY ON PRIOR SER REQUIREMENTS

Page 14 of the SER regarding WCAP-12945-P-A discusses applicability limits and usage conditions regarding the prior best-estimate methodology for 3- and 4-loop plants with cold-leg ECCS injection. Pages 13 and 14 of the SER, regarding WCAP-14449-P-A, discusses applicability limits and usage conditions regarding the prior best-estimate methodology for 2-loop plants with low-head safety injection into the upper plenum. The continued applicability of these stipulations is discussed below. In each case, the stipulation is quoted from the SER, and then the continued applicability is addressed.

### 13-3-1 WCAP-12945-P-A SER Requirements

#### Applicability Limits

1. *"The use of the WCOBRA/TRAC EM for long term cooling licensing analyses is not covered in this review."*

The Westinghouse AP600 design certification review was in progress at the same time as the review of the previous WCOBRA/TRAC Evaluation Model (EM) for 3- and 4-loop plants. This applicability limit was established to ensure separation of the 2 reviews. WCOBRA/TRAC was subsequently approved for long-term cooling analyses of the AP600 review (Garner et al., 1998). It has not been approved for long-term cooling analyses of operating plant designs. Therefore, this applicability limit remains valid for operating plants.

2. *"Our review of the WCOBRA/TRAC EM has been limited to licensing application of the methodology for 3 and 4 loop non-UPI Westinghouse designs. Other designs, such as advanced designs (e.g., AP600), UPI plants, and other vendor designs were not covered."*

Subsequent to the issuance of this applicability limit, WCOBRA/TRAC-based evaluation models were approved by the USNRC for AP600 (Hochreiter et al., 1998) and UPI plants (Dederer et al., 1999). Appendix A of this report justifies the applicability of ASTRUM to Combustion Engineering plant designs. However, this applicability limit remains valid for other plant designs (e.g., AP1000 and Babcock & Wilson designs). A licensing submittal supporting the use of a WCOBRA/TRAC-based evaluation model for AP1000 design is currently under review (Westinghouse, 2001).

3. *"Our review did not cover use of the WCOBRA/TRAC EM for small break LOCA licensing analyses."*

This applicability limit remains valid at this time. A topical report supporting the use of a WCOBRA/TRAC-based evaluation model for best-estimate small-break LOCA has been submitted separately from this report (Kemper et al., 2001). The review of that report will be conducted separately from the review of this report.

#### Usage Conditions

- a. *"A recommended justification for any future time step changes (first listed item). We require that W perform this justification as recommended, and retain traceable documentation of this action in its in-house plant records."*

This usage condition remains applicable with ASTRUM. Westinghouse will retain any such documentation in our records in a traceable manner.

- b. *"Under the designation "Westinghouse agreed/committed" items are 13 additional items:*
- i. *Items 1, 3, 4.a, 4.b, 4.c, 6, and 11 are plant specific calculational requirements and W must retain traceable documentation of these actions in its in-house plant records."*

These Technical Evaluation Report (TER) items are quoted from the TER below, followed by the appropriate statement of continued applicability.

1. *"Based on the NRU results, there is some uncertainty in the transient rod internal pressure (RIP) calculation that will affect the burst temperature criterion in WCOBRA/TRAC analyses. Westinghouse's uncertainty methodology adequately accounts for the uncertainty in transient RIP for local effects. Westinghouse also calculates HA rod burst in the full WCOBRA/TRAC analyses called for in its methodology. If WCOBRA/TRAC calculates a HA rod reflood PCT greater than 1600°F but not rod burst, Westinghouse in Reference 214, List II, Item 2 committed to increasing the initial RIP in the WCOBRA/TRAC HA rod until burst is calculated and choosing the more limiting of the burst and non-burst cases. This will adequately account for transient RIP uncertainties and their effect on rod burst in the WCOBRA/TRAC runs."*

This plant-specific calculational requirement was identified to ensure that the response surfaces used in the prior methodology were based on the most conservative conditions. Response surfaces are not used in ASTRUM. Therefore, this plant-specific calculational requirement is no longer applicable.

3. *"As part of the methodology, Westinghouse agreed in Attachment 5, Reference 214, to verify the normality assumption for the initial condition uncertainty distribution on a plant specific basis."*

Initial conditions are now sampled for each run, and the initial condition uncertainty distribution is no longer used. Therefore, this requirement is no longer applicable.

4. *"In the uncertainty methodology, a number of assumptions for distribution were supported using plant specific data; therefore, in Reference 214, Attachment 5, and Reference 215, Attachments 1 and 2, Westinghouse agreed to verify the following assumptions on a plant specific basis:*
- a. *Superposition validation data points are normally distributed, with constant variance, around a straight line. The normality must be checked for each phase of the accident for each plant.*

- b. *HOTSPOT PCTs are normally distributed. This must be checked at each point where the HOTSPOT PCT is varied in a Monte Carlo sample: the points used to build the response surface for the HOTSPOT standard deviation ( $\sigma_{\alpha\beta}$ ) and the validation points.*
- c. *Response surface for  $\sigma_{\alpha\beta}$  is accurate or conservative. This should be checked by comparing the response surface estimate with the Monte Carlo standard deviation at each validation point. The response surface method should not severely underestimate any standard deviation."*

The superposition validation and correction step is not required for ASTRUM. Therefore, requirement 4.a is no longer applicable.

With the prior method, HOTSPOT was run 1000 times for each case, and the results were characterized by a mean and standard deviation. With ASTRUM, [

] <sup>a,c</sup>

Response surfaces for local models are no longer used. Therefore, requirement 4.c is no longer applicable.

- 6. *"Based on Reference 214, Attachment 7, the analysis to determine the uncertainty distributions for accumulator and SI temperatures uses plant operating data and/or plant Technical Specifications. Therefore, this analysis must be performed for each plant."*

This requirement remains applicable with ASTRUM.

- 11. *"In Reference 214, List III, Item 5, Westinghouse committed to identifying in the licensing submittal or the engineering report which of the options described in its response to Volume 2, question 62, Reference 214 (Attachment 12) were used in the calculation of cladding core wide oxidation if the 1% limit is exceeded."*

The core wide oxidation calculation has been simplified as shown in Section 11-6-2. Therefore, requirement 11 is no longer applicable.

- ii. *"Items 2, 5, and 7 are generic limits on usage of the WCOBRA/TRAC EM, which, if changed require submittal for NRC review."*

These TER items are quoted from the TER below, followed by the appropriate statement of continued applicability.

2. *"On CQD page 7-24, Westinghouse stated the fuel pellet thermal expansion model in MATPRO-11, Revision 1, Reference 176, was simplified by omitting the corrections for molten fuel and mixed oxide (Pu). In Reference 214, List II, Item 6, Westinghouse committed to resubmitting the relevant WCOBRA/TRAC models for NRC review if the code will be used to analyze US licensed plants with molten fuel or mixed oxide."*

This requirement remains applicable with ASTRUM.

- 5 *"The distributions corresponding to WCOBRA/TRAC uncertainty based on experiments ( $\sigma_{WCT}$ ) and the uncertainty due to experimental data scatter ( $\sigma_{2p}$ ) will be checked for normality if the code is modified or the assessment data base changes. See Reference 214, List III, Item 2."*

In the prior methodology,  $\sigma_{WCT}$  and  $\sigma_{2p}$  were used in the superposition validation and correction step as lower bounds on the superposition prediction uncertainty and the local HOTSPOT uncertainty. The superposition validation and correction step is not required with ASTRUM, and [

] <sup>a,c</sup>

7. *"Westinghouse, in Reference 214, List II, Item 8, committed to not changing the value and range of the broken loop cold leg nozzle loss coefficient for plant specific applications. Also, the values developed apply only to LBLOCA and must be justified for other applications."*

This requirement remains applicable for Westinghouse plants analyzed with ASTRUM. [

] <sup>a,c</sup>

- iii. *"Items 8, 9, and 10 require inclusion of specific information in the WCOBRA/TRAC EM CQD. We must implement these actions as part of providing the final updated CQD in accordance with the documentation plan identified above."*

These TER items are quoted from the TER below, followed by the appropriate statement of continued applicability.

8. *"Westinghouse, in Reference 214, Attachment 9, gave additional explanation on its use of the full Method of Characteristics model for each time step in the code implementation of choked flow. In the above reference, Westinghouse committed to include the information in the CQD."*

Westinghouse satisfied this requirement by adding the necessary text to the critical flow model description in Section 4-8-2 of WCAP-12945-P-A and this report.



9. *"Westinghouse noted that the choked flow solution is implemented in the pressure solution of the code rather than in the back substitution step after solving the pressure equation. This results in a smoother pressure and flow response in the code. In Reference 214, Attachment 9, Westinghouse committed to include this information in the CQD."*

Westinghouse satisfied this requirement by adding the necessary text to the critical flow model description in Section 4-8-2 of WCAP-12945-P-A and this report.

10. *"Westinghouse, in Reference 214, List II, Item 10, committed to use the multiplier given in Reference 214, Attachment 4, to account for rod-to-rod radiation effects in the heat transfer multiplier data base."*

Westinghouse applies a correction factor to the reflood heat transfer multipliers to account for rod-to-rod radiation effects, as described on page 25-5-26 of WCAP-12945-P-A. The same correction factor is applied with ASTRUM.

### 13-3-2 WCAP-14449-P-A SER Requirements

The WCAP-14449-P-A SER requirements are redundant with those of WCAP-12945-P-A, except for the following Applicability Limit:

4. *"Section 2.4.4 of this SER discusses that ranges and biases of parameters were based on data, including UPTF and CCTF data. Of particular concern is the ranging of interfacial drag and condensation, which is based on UPTF and CCTF data. In a letter dated April 8, 1999, to assure that the 2-loop version of the methodology would not be applied for heat generation rates higher than covered by the UPTF and CCTF data, W proposed to limit the application of the UPI methodology to nominal power levels of 1980 MWt, low power region average linear heat generation rate less than 6.9 kW/ft, and maximum analyzed linear heat generation rates of 17 kw/ft. We find the proposed limits are acceptable because they are consistent with the range of the UPTF and CCTF data. We also find that use of the methodology above these values is outside the scope of our review, and would require further justification and NRC review."*

This applicability limit remains valid for 2-loop plants analyzed with ASTRUM.

The continued applicability of other stipulations in the SER for WCAP-14449-P-A is the same as discussed in Section 13-3-1.

## 13-4 REFERENCES

Bajorek, S. M., et al., 1998, "Code Qualification Document for Best Estimate LOCA Analysis," WCAP-12945-P-A, Volume 1, Revision 2, and Volumes 2 through 5, Revision 1, and WCAP-14747 (Non-Proprietary).

Dederer, S. I., et al., 1999, "Application of Best Estimate Large Break LOCA Methodology to Westinghouse PWRs with Upper Plenum Injection," WCAP-14449-P-A, Revision 1, and WCAP-14450-NP-A (Non-Proprietary).

Garner, D. C., et al., 1998, "WCOBRA/TRAC OSU Long-Term Core Cooling Final Validation Report," WCAP-14776, Revision 4.

Hochreiter, L. E., et al., 1998, "WCOBRA/TRAC Applicability to AP600 Large-Break Loss-of-Coolant Accident," WCAP-14171-P, Revision 2.

Kemper, R. M., et al., 2001, "Code Qualification Document for Best Estimate Small Break LOCA Analysis," WCAP-14936.

Westinghouse, 2001, "AP1000 Code Applicability Report," WCAP-15644.

## APPENDIX A

### EXTENSION OF ASTRUM TO COMBUSTION ENGINEERING DESIGNS

The main body of this report described the application of the Automated Statistical Treatment of Uncertainty Method (ASTRUM) to Westinghouse-designed pressurized water reactors (PWRs). This appendix describes the application of ASTRUM to Combustion Engineering (CE) PWR designs.

The physical phenomena that would occur in a CE PWR during a large-break loss-of-coolant accident (LOCA) are the same as those which would occur in a Westinghouse PWR with cold-leg emergency core cooling system (ECCS) injection. The relative importance of the phenomena would be expected to differ somewhat, due to design differences. A review of the Code Scaling, Applicability, and Uncertainty (CSAU) methodology steps indicates that the extension of ASTRUM to CE PWR designs needs to focus on the following:

- Phenomena Identification and Ranking (CSAU Step 3) – Differences in the phenomena ranking need to be identified, and considered in the following step.
- Establishment of Assessment Matrix (CSAU Step 7) – The assessment matrix must be sufficient to address the phenomena that are more highly ranked for the CE designs. Additionally, the ranges of fluid conditions expected in the LOCA need to be examined. Any significant differences need to be addressed.
- Nodalization (CSAU Step 8) – Differences in nodalization may be required to account for differences in geometry.

These three steps are addressed in detail for CE plants in the following subsections.

#### A-1 PHENOMENA IDENTIFICATION AND RANKING

The phenomena identification and ranking table (PIRT) for Westinghouse plants with cold-leg ECCS injection was discussed in detail in Section 1-2-3. Table A-1 provides a comparison of the rankings developed for CE and Westinghouse plants. The following discussion focuses on the differences in the rankings.

**Core**

[

]ac

**Upper Plenum**

[

] <sup>a,c</sup>**Downcomer**

[

] <sup>a,c</sup>**Lower Plenum**

[

] <sup>a,c</sup>**A-2 REVIEW OF ASSESSMENT MATRIX**

This section reviews the existing assessment matrix for the WCOBRA/TRAC code and demonstrates that it adequately addresses the conditions expected to occur in a CE plants. It is organized according to the dominant phenomena previously identified for a large-break LOCA in a PWR. Those phenomena identified as being higher ranked for CE plants are also specifically addressed.

**Critical Flow** The critical flow model was assessed against 16 Marviken tests and 4 LOFT tests. Table 25-2-1 of WCAP-12945-P-A (Bajorek et al., 1998) summarizes the range of conditions examined in the tests, and the range of conditions expected for Westinghouse plants. That table is repeated herein as Table A-2, with the range of conditions expected for CE plants added. It can be seen that the range of conditions expected for CE plants are very similar to those for Westinghouse plants. The differences lie within those conditions examined in the assessment matrix.

**Break Path Resistance** The broken-loop cold-leg nozzle resistance and uncertainty distribution used for Westinghouse plants are based on Upper Plenum Test Facility (UPTF) test data, as discussed in Sections 16-3 and 25-3-3 of WCAP-12945-P-A. The uncertainty in the broken-loop pump resistance is based on scaled pump test data, and is derived in Section 25-3-2 of the same report. These resistance uncertainties are combined with other minor quantities, resulting in an overall resistance uncertainty that is then applied to the cold-leg nozzle. The uncertainty is a [

J<sup>ac</sup>

**Stored Energy/Fuel Rod** Initial stored energy for Westinghouse plants is calculated with the PAD 4.0 code (Foster and Sidener, 2000), which has been benchmarked against suitable nuclear fuel rod performance data. Initial stored energy for CE plants will be calculated with the FATES3B code (CE, 1992), which has been similarly benchmarked. This will ensure that initial stored energy for CE plants will be calculated using Nuclear Regulatory Commission (NRC)-approved codes and methods for those fuel designs.

The nuclear fuel rod models in WCOBRA/TRAC were assessed against the separate effects reflood heat transfer tests NRU MT-3 and PTH-110, and integral effects tests in LOFT. Those assessments are considered to apply to CE fuel designs as well as Westinghouse fuel designs.

**Blowdown/Reflood Heat Transfer** Section 11-1 of WCAP-12945-P-A separated the PWR blowdown/refill time phase into 4 periods. Fluid and thermal conditions predicted to occur in the PWR during each period were compared with those covered by the assessment matrix. Tables A-3 through A-5 summarize the results of that comparison, and demonstrate that the assessment matrix adequately covers the expected range of PWR conditions. There are no geometric design features in a CE plant that would significantly affect the range of fluid and thermal conditions expected during blowdown and refill. Therefore, the existing blowdown/refill heat transfer assessment matrix is adequate for application to CE plants.

Section 12-1 of the same report provided the typical conditions expected in a PWR during reflood, and reviewed the range of conditions covered by the reflood separate effects heat transfer tests. Tables A-6 through A-8 summarize the results of that comparison, and demonstrate that the assessment matrix adequately covers the expected range of PWR conditions. The PIRT discussion in Section A-1 concluded that [

J<sup>ac</sup>

[ ]<sup>ac</sup> It is concluded that the existing reflood heat transfer assessment matrix is adequate for application to CE plants.

**Delivery and Bypassing of ECC** Table A-9 compares the geometry and fluid conditions in UPTF Test 6 and other relevant Counter-Current Flow Limit (CCFL) tests with the conditions in Westinghouse and CE PWRs. This table is an expanded version of Table 25-6-1 of WCAP-12945-P-A. The CE conditions are seen to be similar to the Westinghouse conditions. Comparisons of WCOBRA/TRAC predictions of UPTF Test 6 with the data indicate that there is a conservative bias in the prediction of ECC bias. This conclusion is considered to be applicable to CE plants as well as Westinghouse plants.

**Steam Binding/Entrainment** Comparisons with FLECHT, Slab Core Test Facility (SCTF) and Cylindrical Core Test Facility (CCTF) data indicated that WCOBRA/TRAC over predicts the amount of entrainment from the core. Comparisons with UPTF Test 29B showed that, when conditions at the entrance to the upper plenum are known, WCOBRA/TRAC under predicts the mass retained in the upper plenum and over predicts the amount of water entrained into the loops. This was demonstrated in Section 15-2-3 of WCAP-12945-P-A. The results of the steam binding/entrainment assessment were that excessive liquid is predicted to be carried from the core and upper plenum to the steam generators, thereby resulting in a conservative prediction of steam binding.

The PIRT discussion in Section A-1 concluded that [

] <sup>ac</sup>

**Non-Condensable Gases/Accumulator Nitrogen** Comparisons with LOFT and ACHILLES test data indicated that WCOBRA/TRAC tends to underpredict the pressurization of the downcomer and the resulting insurge of water into the core, as discussed in Section 16-2 of WCAP-12945-P-A. The heat transfer effects during the insurge were examined, and it was concluded that the heat transfer coefficient should be limited to a maximum of [ ] <sup>ac</sup> during this period, due to a lack of data under these conditions (Section 25-5-5-8 of the same report). The tendency to underpredict downcomer pressurization, and the use of a maximum heat transfer limitation during the insurge, lead to the conclusion that the effects of accumulator nitrogen will be conservatively calculated in CE plants.

**Condensation** The condensation model was assessed against 1/3- and full-scale separate-effects tests that covered the range of conditions expected in the cold leg at the ECC injection location. As shown in Section 15-3 of WCAP-12945-P-A, the predicted condensation rate compared well with the data, and the measured condensation efficiency varied over a narrow range of [ ] <sup>ac</sup> over a wide range of test conditions. Therefore, ranging of condensation in the cold legs is not required.

The condensation model was assessed against small- and full-scale separate-effects tests using a downcomer geometry, as reported in Section 15-1 of WCAP-12945-P-A. The full-scale results indicated a wider range of condensation efficiency, depending on the method used to estimate that efficiency.

Those results were used to establish the condensation ranging used in the downcomer for PWR with cold-leg ECCS injection.

Table A-10 compares the geometry and fluid conditions in UPTF Tests 6, 8, 25 and other relevant condensation tests with the conditions in Westinghouse and CE PWRs. The similarities in test geometry and fluid conditions lead to the conclusion that the condensation assessment conclusions made for the Westinghouse design are also applicable to the CE design.

### A-3 NODALIZATION

The nodalization used for analyses of Westinghouse plants is plant-specific, and takes into account variations in vessel design, loop arrangement, and ECCS configuration. A set of guidelines has been established to ensure that the PWR nodalization is consistent with that used in analyses of test facilities. These guidelines are described in Section 20-1 of WCAP-12945-P-A. Application of the guidelines is illustrated in Sections 20-2 to 20-4 of that report, with the Section 20-2 application repeated in Section 12-1 of this report. Those same guidelines will be applied to the analyses of CE plants.

### A-4 CONCLUSIONS

The PIRT for CE designed PWRs has been constructed and compared with the PIRT for Westinghouse plants with cold-leg ECCS injection. While very similar in design, there are minor differences in some of the phenomena rankings during the reflood phase. [

] The WCOBRA/TRAC assessment matrix for the dominant large-break LOCA phenomena has been reviewed, and concluded to be applicable to CE plants. As a result, the same uncertainty methodology can be applied to CE plants.

Nodalization of CE plants will be established on a plant-specific basis, following the existing NRC-approved guidelines.

### A-5 REFERENCES

Bajorek, S. M., et al., 1998, "Code Qualification Document for Best Estimate LOCA Analysis," WCAP-12945-P-A, Volume 1 Revision 2, and Volume 2 through 5 Revision 1, and WCAP-14747 (Non-proprietary).

Combustion Engineering, 1992, "Improvements to Fuel Evaluation Model," CEN-161(B)-P, Supplement 1-P-A.

Damerell, P. S., and Simons, J. W., 1993, "Reactor Safety Issues Resolved by the 2D/3D Program," NUREG/IA-0127, MPR Associates, Inc.

Foster, J. P. and Sidener, S., 2000, "Westinghouse Improved Performance Analysis and Design Model (PAD 4.0)," WCAP-15063-P-A, Revision 1 with Errata.

Hochreiter, L. E., et al., 1998, "WCOBRA/TRAC Applicability to AP600 Large-Break Loss-of-Coolant Accident," WCAP-14171-P, Revision 2.



**Table A-1**  
**Combustion Engineering and Westinghouse PIRT for Large-Break LOCA**

[illegible]

**Table A-1 (Cont'd)**  
**Combustion Engineering and Westinghouse PIRT for Large-Break LOCA**

[illegible]

Table A-1 (Cont'd)  
Combustion Engineering and Westinghouse PIRT for Large-Break LOCA

1								
								jac

**Table A-1 (Cont'd)**  
**Combustion Engineering and Westinghouse PIRT for Large-Break LOCA**

[illegible]

**Table A-1 (Cont'd)**  
**Combustion Engineering and Westinghouse PIRT for Large-Break LOCA**

[illegible]

**Table A-2**  
**Critical Flow Model Assessment**

[				

]a,c

**Table A-3**  
**Typical Conditions in a PWR During Blowdown**

Quantity	Period	Range
Pressure (psia)	I	2250 - 1500
	II	1500 - 800
	III	800 - 100
	IV	100 - 20
Inlet Mass Velocity (lbm/ft <sup>2</sup> /s)	I	0 - 700
	II	0 - 50
	III	0 - 100
	IV	0 - 10
Inlet Subcooling (°F)	I	0 - 100
	II	0 - 0
	III	0 - 0
	IV	0 - 0
Inlet Steam Quality	I	0 - 0.1
	II	0.1 - 0.5
	III	0.5 - 0.9
	IV	0.9 - 1.0
Assembly Maximum Heat Rate (kW/ft)	I	5 - 17
	II	0.5 - 2.0
	III	0.5 - 1.0
	IV	0.5 - 1.0
Assembly Average Heat Rate (kW/ft)	I	1.0 - 5.0
	II	0.1 - 0.5
	III	0.1 - 0.5
	IV	0.1 - 0.5
Assembly PCT (°F)	I	600 - 1800
	II	1000 - 1800
	III	1000 - 1600
	IV	1000 - 1800

**Table A-4**  
**Blowdown Heat Transfer Test Conditions**

Test Series	Test Number	Pressure (psia)	Inlet Mass Velocity (lbm/ft <sup>2</sup> /s)	Peak Power (kW/ft)	Comments
ORNL	3.07.9B 3.08.6C 3.03.6AR	1850 1870-700 2031-1015	146 215-54 470-47	8.3 3.4-11 5.6-9.5-1.1	Steady-State and Transient Upflow 17x17 Rod Array
[					

jac



**Table A-5**  
**Code Validation Test Range of Conditions**

Quantity	PWR Period	Test Range
[		
		j <sup>a,c</sup>

**Table A-6**  
**Typical Conditions in a PWR During Reflood**

Quantity	Range
Pressure (psia)	15 - 50
Inlet Mass Velocity (lbm/sec/ft <sup>2</sup> )	0 - 100
Inlet Subcooling (°F)	0 - 100
Inlet Steam Quality	0 - 0.01
Assembly Maximum Heat Rate (kW/ft)	0.5 - 1.0
Assembly Average Heat Rate (kW/ft)	0.1 - 0.5
Assembly PCT (°F)	1000 - 2200

**Table A-7**  
**Reflood Heat Transfer Test Conditions**

Test Series	Test Number	Pressure (psia)	Flooding Rate (in/s)	Inlet Subcooling (°F)	Peak Power (kW/ft)	Comment
FLECHT SEASET	31805	40	0.81	143	0.7	Cosine Power Shape 17x17 Rod Array
	31203	40	1.51	141	0.7	
	31701	40	6.1	140	0.7	
	31504	40	0.97	144	0.7	
	32013	60	1.04	143	0.7	
FLECHT Low Flooding Rate	05029	40	0.85	141	0.73	Cosine Power Shape 15x15 Rod Array
	05132	40	1.0	140	0.95	
	04641	20	1.0	139	0.95	
FLECHT/Skewed	15305	40	0.8	140	0.7	Top Skewed Power Shape 15x15 Rod Array
	13812	41	1.0	83	0.7	
	15713	40	1.0	2	0.7	
	13914	21	1.0	5	0.7	
	13609	21	1.0	141	0.7	
G-2	550	40	1.0	116	0.66	14-Ft Bundle Mixing Vane Grids
	562	20	1.0	110	0.46	
	568	40	1.0	117	0.57	
FEBA	223	32	1.5	145	0.7	Flutter Power Shape Grid Effect
	234	29	1.5	145	0.7	
	216	60	1.5	185	0.7	
	229	61	1.5	185	0.7	

**Table A-8**  
**Reflood Separate Effects Test Range of Conditions**

Pressure Range (psia)	20 - 60
Initial Peak Cladding Temperature (°F)	1358 - 1640
Maximum Peak Cladding Temperature (°F)	1670 - 2184
Initial Peak Rod Power (kW/ft)	0.67 - 0.95

**Table A-9**  
**ECC Bypass/CCFL Model Assessment**



]a.c

**Table A-10**  
**Condensation Model Assessment**



]a,b,c

## APPENDIX B

### VALIDATION OF WCOBRA/TRAC MOD7A REVISION 6

The code version previously approved by the US Nuclear Regulatory Commission (USNRC) was WCOBRA/TRAC MOD7A Revision 1. The code version that Automated Statistical Treatment of Uncertainty Method (ASTRUM) is based on is WCOBRA/TRAC MOD7A Revision 6. This appendix describes the changes made to WCOBRA/TRAC since the previous USNRC review. The changes with the potential to affect any of the prior code assessment results are identified. Reanalyses of selected experiments with WCOBRA/TRAC MOD7A Revision 6 are presented to support the conclusion that the prior code assessment results remain valid.

#### B-1 REVISIONS TO WCOBRA/TRAC MOD7A REVISION 1

Changes to, or errors in, approved loss-of-coolant-accident (LOCA) evaluation models are reported to the USNRC on at least an annual basis, in accordance with the Code of Federal Regulations (CFR) 10 CFR 50.46. Table B-1 summarizes the items reported since WCOBRA/TRAC MOD7A Revision 1 was approved, and identifies where each change or error was reported to the USNRC. The table also indicates which items have the potential to affect the prior code assessment results (such as, biases and/or uncertainty distributions). Some of the reported changes or errors have no effect on any of the prior code assessment results for a number of reasons, such as:

- 1) They involve an input error that has been determined to affect certain plant-specific analyses only. "Intercell Force Gap Numbering Error," "Accumulator Line/Pressurizer Surge Line Data," "WCOBRA/TRAC Unheated Structure Multiplier," and "Broken Cold Leg Modeling Deviations" are in this category.
- 2) They involve an option, model, code, or code application that is not used for experiment simulations. "TUBE Heated Conductor Error," "Inconsistent Guidance for HOTSPOT Outputs in Best-Estimate (BE) Large-Break LOCA (LBLOCA) Methodology," "Decay Heat Uncertainty Error in Monte Carlo Calculation," "LOTIC2 Nitrogen Addition Logic Error," "LOTIC2 Time Step Logic Error," "GEDM Interface Error," "Pressure Drop Error for 1-D Connections to 3-D Vessel," "PAD 4.0 Implementation," "Enhancements to Monte Carlo Peak Cladding Temperature (PCT) Calculation," "Oxidation Thickness Index Error for Best-Estimate WCOBRA/TRAC," "1-D Condensation Ramp Error," "Potential Divide by Zero Error During Pump Rotation Reversal," "Application of Decay Heat Uncertainty to Prompt Fission Energy Error," "Monte Carlo Code Consolidation Error," "Response Surface Matrix Operation and Random Search Errors," and "User Conveniences in HOTSPOT " are in this category.
- 3) They involve enhanced input/output, or corrections to output edits that do not affect variables of interest for experiment simulations. "Miscellaneous Input/Output Revisions,"

"Drop Diameter Plot Tape Storage Error," "Cladding Oxidation Edit Error," "Output Edit Error for SI Units," and "Response Surface Plot Title Error " are in this category.

Each of the error corrections that could potentially affect the prior assessment of biases and uncertainties is discussed in more detail in the following paragraphs.

**Vessel Channel DX Error (Including Investigation of Code Uncertainties)** Calculations of the interfacial and wall drag in lateral flow use the gap flow area, which is the product of the gap width and height. See, for example, equations 4-70 (interfacial drag coefficient in small bubble regime) and 4-112 (interfacial drag coefficient in dispersed droplet flow regime). For the wall drag calculations, the gap flow area enters into the calculation of the transverse liquid and vapor mass fluxes, used as shown in equations 4-23 through 4-26, 4-28, and 4-29. The gap height used in these gap area calculations was incorrectly indexed, such that the height of all gaps in a given channel was set to be equal to the height of the top cell in the channel below.

This error potentially affected the model biases and uncertainties established for the approved methodology. After the initial correction of this error, 47 simulations of tests performed in 8 different test facilities (Upper Plenum Test Facility (UPTF), Cylindrical Core Test Facility (CCTF), FLECHT-SEASET, FLECHT Low Flooding Rate, FLECHT Skewed Power Shape, Oak Ridge National Laboratory (ORNL), G-1 Blowdown, and G-2 Refill) were repeated. A comparison of the revised and original test simulations led to the conclusion that the approved model biases and uncertainty distributions remain applicable. (The results of this study were reported in the annual report for 1998, issued in NSD-NRC-99-5839, dated July 15, 1999.)

Section B-2 of this Appendix contains reanalyses of selected experiments with WCOBRA/TRAC MOD7A Revision 6. As will be shown in Section B-2, none of the simulation results were substantially affected by this or the other error corrections.

**1-D Transition Boiling Heat Transfer Error Request for Additional Information (RAI) 1-206** questioned whether there was double accounting of the vapor phase heat transfer for 1-D components in transition boiling, based on the model description in the original Section 6-3-5. This was confirmed, and Westinghouse committed to revising the model description and the coding. The approved version of the Code Qualification Document (CQD) has the model description corrected, but the coding developed to correct the model was inadvertently not included in the configured code version.

The response to RAI1-206 illustrated that the effect of the error on the total transition boiling heat transfer was small. In addition, the time period spent in the transition boiling regime is only a few seconds, as shown in the Appendix to Attachment W of NTD-NRC-95-4399. A pressurized water reactor (PWR) calculation was performed with the error correction in order to support annual 10 CFR 50.46 reports, and it was verified that the effect on the plant transient is negligible.



This error has the potential to affect the heat transfer calculations in the steam generator tubes of the STGEN component. The only test simulations that use the STGEN component are CCTF and LOFT. Analyses of CCTF Test 62 and LOFT L2-2 with the error corrected are included later in this Appendix. Those runs demonstrate that there is no significant effect on the analysis results due to this or the other error corrections.

**Incorrect Wall Friction Factor for Convective Enhancement Term** RAID-5 questioned the formulation of the wall friction factor used in CQD Equation 6-122 (pages 6-32 and 6-33). Additional investigation indicated that the friction factor should use the Moody formulation, including a factor of 4. The as-coded model did not include the factor of 4. In response to RAID-5, Westinghouse demonstrated the effect of this error to be small, by repeating the analysis of FLECHT-SEASET Test 31805 with the error corrected. (Test 31805 was chosen because it had a low flooding rate of 0.8 in/sec, and the error was shown to have the largest effect at low vapor Reynolds numbers.) Westinghouse committed at that time to correct the error in the future, when other changes to the heat transfer model were made. The correction was made in Revision 5.

Section B-2 of this Appendix contains reanalyses of selected experiments with WCOBRA/TRAC MOD7A Revision 6. As will be shown in Section B-2, none of the simulation results were substantially affected by this or the other error corrections.

**WCOBRA/TRAC Gap Input Error in SECY Upper Plenum Injection (UPI)/Best-Estimate LOCA (BELOCA) Evaluation Model (EM)** Analyses Gap connections are to be specified from the lower numbered channel to the higher numbered channel. Slab Core Test Facility (SCTF) and UPTF Test 29B did not follow this numbering convention. After initially discovering this error, the affected cases were all reanalyzed. A comparison of the revised and original test simulations led to the conclusion that the approved model bias leading to conservative prediction of steam binding remains applicable. (The results of this study were reported in the annual report for 2000, issued in LTR-NRC-01-6, dated March 13, 2001.)

A reanalysis of SCTF Test 619 with WCOBRA/TRAC MOD7A Revision 6 is included later in this Appendix.

**Radiation Heat Transfer to Vapor Phase Error** The response to RAI1-151b indicated that radiation to steam is accounted for in the single-phase vapor regime, using the model described in Section 6-2-9. It was found that the radiation-to-steam calculation was bypassed if the void fraction exceeded 0.9999. This error was corrected, and the text in Section 6 was updated to be consistent with the correction.

Section B-2 of this Appendix contains reanalyses of selected experiments with WCOBRA/TRAC MOD7A Revision 6. As will be shown in Section B-2, none of the simulation results were substantially affected by this or the other error corrections.

**Grid Heat Transfer Error** Equation 6-130 previously applied the grid heat transfer enhancement factor to the wall-to-vapor radiation term as well as the wall-to-vapor convection term. The coding was consistent with the previous equation. Equation 6-130 and the coding have been corrected, such that the grid enhancement factor is applied to the convection term only.

Section B-2 of this Appendix contains reanalyses of selected experiments with WCOBRA/TRAC MOD7A Revision 6. As will be shown in Section B-2, none of the simulation results were substantially affected by this or the other error corrections.

**Neutronics Calculation Moderator Density Weighting Factor Error** The power used in normalization of the moderator density weighting factors for the point kinetics model was found to double-account for channels with multiple simulated rods. This error affects the initial reactivity in the core very slightly.

The Loss-of-Fluid Test (LOFT) facility tests are the only simulations the error correction could affect. Section B-2 of this Appendix contains a reanalysis of LOFT L2-2 with WCOBRA/TRAC MOD7A Revision 6. There is no substantial effect of this or the other error corrections on the LOFT L2-2 predictions.

**1-D Minimum Film Boiling Temperature Model Selection Error** Section 6-3-6 indicates that the minimum film boiling temperature calculation for 1-D components is calculated as the maximum of the homogeneous nucleation temperature and that predicted by the Iloeje correlation. The comparison of these two correlations is made if a flag (ITMIN) is set greater than zero. Otherwise, the homogeneous nucleation temperature is used. It was found that ITMIN was not initialized, resulting in the Iloeje correlation not being considered. The coding was corrected to be consistent with the description in Section 6-3-6.

This error has the potential to affect the heat transfer calculations in the steam generator tubes of the STGEN component. The only test simulations that use the STGEN component are CCTF and LOFT. Analyses of CCTF Test 62 and LOFT L2-2 with the error corrected are included later in this Appendix. Those runs demonstrate that there is no significant effect on the analysis results due to this or the other error corrections.

**Cladding Axial Thermal Expansion Error** The cladding axial thermal expansion is used in the calculation of the fuel rod internal pressure, as indicated in the gas plenum volume definition in Equation 7-46. Equation 7-39 shows how the cladding axial thermal expansion over the length of the rod is calculated. Table 7-1 shows that the cladding axial thermal expansion is based on a linear interpolation scheme over a temperature range of 1073-1273°K. The CALL statement for the interpolation subroutine had a typographical error in one of the arguments, such that the axial thermal expansion was evaluated incorrectly.

This error had the potential to affect any calculation that uses the nuclear fuel rod model and the dynamic gap conductance option. LOFT and National Research Universal (NRU) are the only test facilities that use this option. This error would be expected to have minimal effect on the LOFT and NRU PTH-11C calculations, since the rod pressures were too low to cause swelling and burst. The NRU MT-3 simulation would not be affected since cladding burst was predicted below 1073°K. Reanalysis of LOFT L2-2 was performed with WCOBRA/TRAC MOD7A Revision 6. As shown in Section B-2, there is no significant effect on the analysis results due to this or the other error corrections.

**Error in Time After Shutdown for Neutron Capture Term** Equation 8-45 shows the neutron capture correction factor specified by the American National Standards Institute/American Nuclear Society (ANSI/ANS) 5.1-1979 standard. The time after shutdown term, "t," was incorrectly programmed to use the total calculation time, including the steady-state calculation. The coding has been corrected so that "t" is defined as the time after initiation of the break.

This error could have the potential to affect the previous LOFT simulation results, since the 1979 decay heat standard was used in those analyses. The LOFT steady-state calculation was run for 30 seconds, which would be the magnitude of the error in the time after shutdown term. Evaluation of Equation 8-45 indicates that a 30-second error in time after shutdown has a negligible effect on the neutron capture term. Therefore, the effect of this error on the LOFT simulations can be considered negligible. This was confirmed by the reanalysis of LOFT L2-2 with WCOBRA/TRAC MOD7A Revision 6, as shown in Section B-2.

**Bypass of Orifice Entrainment Model in Downflow with Channel Splitting** Entrainment during downward flow is calculated as described in Section 4-6-4. An orifice entrainment model is used if the void fraction is greater than 0.8, and if there is an area expansion of greater than 5 percent in the downflow direction. There was a coding error that would result in the orifice entrainment model being bypassed if there was channel splitting (one channel above two or more channels below).

A review of the noding schemes used in the test simulations indicated that only the G-2 test predictions were potentially affected by this error. (Figure 11-4-7 of WCAP-12945-P-A, Volume 2, Revision 1, shows the noding used for G-2 blowdown test simulations). Since the G-2 test predictions were not used to establish the blowdown cooling heat transfer multipliers, there is no effect of this error on the model biases or uncertainties.

## **B-2 REANALYSIS OF SELECTED EXPERIMENTS USING WCOBRA/TRAC MOD7A REVISION 6**

Most of the experiment simulations reported in WCAP-12945-P-A (Bajorek et al., 1998) were performed with WCOBRA/TRAC MOD7A Revision 0, as discussed in Section 1-2-1 of that reference ("Step 4: Select Frozen Code"). Late in the NRC review, several minor errors were corrected which resulted in the approved code version, WCOBRA/TRAC MOD7A Revision 1. Appendix B at the end of Volume 5 of WCAP-12945-P-A provides a summary of those error corrections.

The experiment simulations performed in support of the application of the methodology to 2-loop plants with UPI used WCOBRA/TRAC MOD7A Revision 1 (WCAP-14449-P-A, Dederer et al., 1999).

In the following sections, selected experiment simulations are repeated with WCOBRA/TRAC MOD7A Revision 6, and the results are compared with the previous simulations reported in WCAP-12945-P-A and WCAP-14449-P-A. It will be shown that the prior conclusions from the code and model assessments are unaffected by the changes described earlier in Section B-1.

### **B-2-1 FLECHT-SEASET Test 31805**

In the original CQD (Bajorek et al., 1998), the WCOBRA/TRAC MOD7A Revision 0 predictions were compared against several FLECHT-SEASET tests to determine the code bias and uncertainty. The FLECHT-SEASET Test 31805 was selected here to verify that the updates included in Revision 6 of the code did not change the conclusions on the evaluation of the heat transfer coefficient uncertainties reported in the original CQD.

#### **B-2-1-1 Relevance to BELOCA Methodology**

Test 31805 was chosen because it has a lower bound flooding rate value. The reflood rate for Test 31805 was 0.81 in/sec. The test pressure was maintained at 40 psia and the injected coolant temperature was 124°F. The WCOBRA/TRAC simulation of Test 31805 was run for the first 800 seconds of the experiment, by which time all heater rod elevations had quenched in both the prediction and the test.

The comparison of the measured temperatures at different elevations (24, 48, 72, 78, 84, 96, and 120 inches) from the bottom of the heated length with the predictions obtained with WCOBRA/TRAC MOD7A Revision 0 was already discussed in Section 12-2-5 of the original CQD. At the lower elevations ( $Z < 72$  inches), the Revision 0 predictions shows generally good agreement with the data. The predicted maximum temperatures at each elevation are low at 72 inches, but otherwise approximately correct, while the predicted turn-around times are early. The predicted quench times are at about the same time as those observed in the data or slightly later. At the higher elevations ( $Z \geq 72$  inches), the WCOBRA/TRAC predictions of the peak temperatures are also lower than the peak temperatures of the data average. The time at which the peak is predicted is earlier than the data. The cooldown rate exceeds the measured rate and quench is predicted to occur earlier than the data average.

#### **B-2-1-2 Simulation Results and Comparison to Previous Results**

Figures B-1, B-3, and B-5 show the comparison of predicted and measured temperature histories at elevations 48, 78, and 120 inches from the bottom of the heated length as they were reported in the original CQD (Bajorek et al.). Figures B-2, B-4, and B-6 show the predicted temperature histories at the same elevations obtained with WCOBRA/TRAC Revision 6.

### B-2-1-3 Conclusions

Results obtained with Revision 6 are essentially unchanged from the previous predictions. Therefore, the evaluation of the heat transfer coefficient uncertainties reported in the original CQD is still valid.

### B-2-2 FLECHT-SEASET Test 31701

#### B-2-2-1 Relevance to BELOCA Methodology

Test 31701 was chosen because it has an upper bound flooding rate value. The reflood rate for Test 31701 was 6.1 in/sec. The test pressure was maintained at 40 psia and the injected coolant temperature was 127°F. The WCOBRA/TRAC simulation of Test 31701 was run for the first 100 seconds of the experiment, by which time all heater rod elevations had reached their peak temperature and had quenched. The comparison between the WCOBRA/TRAC Revision 0 code prediction and the experiment is discussed in detail in Section 12-2-9 of the original CQD. At the lower elevations (24 and 48 inches), the code temperature prediction shows good agreement with the data. The predicted maximum temperatures at each elevation are low compared to the data, and the time at which the peak temperature is predicted to occur is approximately correct. The predicted quench times are in good agreement with the data. At the higher elevations (72 inches and above), WCOBRA/TRAC's prediction of the maximum temperatures agree well with the maximum temperatures of the data average. The predicted quench times at the higher elevation are also in good agreement with data, except at 120 inches where the initial cladding temperature is below  $T_{min}$ .

#### B-2-2-2 Simulation Results and Comparison to Previous Results

Figures B-7, B-9, and B-11 show the comparison of predicted and measured temperature histories at elevations 48, 78, and 120 inches from the bottom of the heated length as they were reported in the original CQD. Figures B-8, B-10, and B-12 show the predicted temperature histories at the same elevations obtained with WCOBRA/TRAC Revision 6.

### B-2-2-3 Conclusions

Results obtained with Revision 6 are essentially unchanged from the previous predictions. Therefore, the evaluation of the heat transfer coefficient uncertainties reported in the original CQD is still valid.

### B-2-3 FLECHT Low Flooding Rate (LFR) Cosine Test 05132

#### B-2-3-1 Relevance to BELOCA Methodology

Test 05132 was one of the 3 FLECHT LFR cosine tests used in the development of the reflood heat transfer multipliers. The reflood rate for Test 05132 was 1.0 in/sec. The test pressure was maintained at 40 psia and the injected coolant temperature was 127°F. The initial peak rod power for this test was

0.95 kW/ ft. The WCOBRA/TRAC simulation of Test 05132 was run past the 500 seconds of the experiment, by which time all heater rod elevations had reached their peak temperature and had quenched. The comparison between the WCOBRA/TRAC Revision 0 code prediction and the experiment is discussed in detail in Section 12-3-6 of the original CQD. At the lower elevations (24 and 48 inches), the maximum cladding temperatures are overpredicted. The time at which the maximum temperature is predicted to occur is approximately correct. At the middle elevations (72 and 78 inches), WCOBRA/TRAC slightly underpredicts the maximum temperatures, with the predicted turn-around times ahead of the data. At the upper elevations (84 inches and above), the maximum cladding temperatures match or slightly exceed the measured values, and quench is predicted to occur late.

### **B-2-3-2 Simulation Results and Comparison to Previous Results**

Figures B-13, B-15, and B-17 show the comparison of the measured temperature histories at elevations 48, 78, and 120 inches from the bottom of the heated length and the predicted value by the Revision 0 as they were reported in the original CQD. Figures B-14, B-16, and B-18 show the predicted temperature histories at the same elevations obtained with WCOBRA/TRAC Revision 6.

### **B-2-3-3 Conclusions**

Results obtained with Revision 6 are essentially unchanged from the previous predictions. Therefore, the conclusions on the reflood heat transfer multipliers reported in the original CQD are still valid.

## **B-2-4 FLECHT Skewed Test 13812**

### **B-2-4-1 Relevance to BELOCA Methodology**

Test 13812 was one of the 5 skewed tests used in the development of the reflood heat transfer multipliers. The reflood rate for Test 13812 was 1.0 in/sec. The test pressure was maintained at 40 psia and the injected coolant temperature was 184°F. The WCOBRA/TRAC simulation of Test 13812 was run for 800 seconds of the experiment, by which time all predicted heater rod elevations had reached their peak temperature and had quenched. The comparison between the WCOBRA/ TRAC Revision 0 code prediction and the experiment is discussed in detail in Section 12-4-6 of the original CQD. At the lower elevations (24 and 48 inches), the code prediction shows good agreement with the data. The predicted maximum temperatures at each elevation are slightly overpredicted, and the time at which the peak temperature is predicted to occur is approximately correct. The predicted quench times are in reasonable agreement with the data. At the middle elevations (72 and 96 inches), WCOBRA/TRAC slightly overpredicts the maximum temperatures, but the turn-around times are underpredicted. Quench is predicted to occur ahead of the data. At the upper elevations (120, 126, and 132 inches), the maximum cladding temperatures are overpredicted, and the quench times are before the data.

### B-2-4-2 Simulation Results and Comparison to Previous Results

Figures B-19, B-21, and B-23 show the comparison of predicted and measured temperature histories at elevations 48, 72, and 132 inches from the bottom of the heated length as they were reported in the original CQD. Figures B-20, B-22, and B-24 show the predicted temperature histories at the same elevations obtained with WCOBRA/TRAC Revision 6.

### B-2-4-3 Conclusions

Results obtained with Revision 6 are essentially unchanged from the previous predictions. Therefore, the conclusions on the reflood heat transfer multipliers reported in the original CQD are still valid.

### B-2-5 G-2 Reflood Test 550

G-2 Reflood Test 550 was one of the 3 G-2 tests used in the development of the reflood heat transfer multipliers. Low pressure forced reflood tests performed at the Westinghouse G-2 test facility were simulated using the WCOBRA/TRAC computer code. The G-2 reflood bundle had a 14-foot length and typical Westinghouse mixing vane grids.

#### B-2-5-1 Relevance to BELOCA Methodology

Comparisons of the WCOBRA/TRAC results to the reflood test data can be used to help assess the capability of WCOBRA/TRAC to accurately predict rod bundle reflood heat transfer behavior including spacer grid effects on dispersed flow film boiling heat transfer. G-2 tests are also used to develop heat transfer multipliers for the reflood period.

#### B-2-5-2 Simulation Results and Comparison to Previous Results

The reflood rate for Test 550 was 1.01 in/sec. The test pressure was maintained at 40 psia and the injected coolant temperature was 150°F. The WCOBRA/TRAC simulation of Test 550 was run for the first 500 seconds of the experiment, by which time all heater rod elevations had reached their maximum temperatures and had started to decline.

Figures B-25, B-27, and B-29 show the comparison of predicted and measured temperature histories at elevations 82, 94, and 111 inches from the bottom of the heated length as they were reported in Section 12-6-5 of the original CQD. The time is after the start of reflood and start of decrease of bundle power. The code prediction is for simulated cladding temperatures in the inner channel. The data curves in these figures are based on all of the valid thermocouples located within the boundary of the WCOBRA/TRAC inner channel. These predictions were obtained by using WCOBRA/TRAC MOD7A Revision 0. Figures B-26, B-28, and B-30 show the corresponding cladding temperature results using WCOBRA/TRAC MOD7A Revision 6.

### **B-2-5-3 Conclusions**

As they are supported by the comparisons, the results obtained with Revision 6 are essentially unchanged from the previous predictions. Therefore, it is concluded that the ability of the code to predict rod bundle reflood heat transfer phenomena is essentially unchanged, and the heat transfer multipliers generated in the original methodology also apply to ASTRUM.

### **B-2-6 LOFT L2-2**

The LOFT facility (operated by EG&G, Idaho Inc. for the Department of Energy) is a 1/60 scale (by volume) 4-loop PWR, designed to provide thermal-hydraulic data during a large rupture of a main coolant pipe. The LOFT facility is the only nuclear-powered integral test available, and is therefore a required test for qualification of a best-estimate LOCA code. A large amount of thermal and hydraulic data is available for these tests, which allows the assessment of several key LOCA processes.

Four LOFT tests were simulated with WCOBRA/TRAC and documented in WCAP-12945-P-A (Bajorek et al., 1998): L2-2, L2-3, L2-5, and LB-1. The LOFT experiments L2-2, L2-3, L2-5, and LB-1 were designed to represent double-ended pipe breaks of the cold leg in a full-scale PWR. The differences between these 3 tests in the L2 series were in their power levels and whether the reactor coolant pumps were tripped or not. In addition, LB-1 was run with a lower accumulator water volume. Tests L2-2 (McCormick, 1979) and L2-3 (Prassinis, 1979) were low and intermediate power tests in which the reactor coolant pumps were allowed to continue operating. Tests L2-5 (Bayless and Divine, 1982) and LB-1 (Adams and Birchley, 1984) were intermediate- and high-power tests in which the pumps were tripped and the pump fly wheels disconnected. These 4 experiments provide good examples of the code's ability to predict the following quantities:

1. Reactor power
2. Emergency core cooling (ECC) bypass
3. Reactor coolant pump behavior
4. Break flowrate
5. Fuel rod cladding temperature
6. Core and loop flow distribution

#### **B-2-6-1 Relevance to BELOCA Methodology**

The LOFT simulations were used to supplement the WCOBRA/TRAC model validation for the 6 items listed above (Section 14-1 of WCAP-12945-P-A). The blowdown PCT predictions for the LOFT series were used in combination with the ORNL test simulation to generate the bias and uncertainty distribution for heat transfer coefficient multiplier during the blowdown heatup period. This was discussed in Section 25-5-2 of WCAP-12945-P-A.



### B-2-6-2 Simulation Results and Comparison to Previous Results

The LOFT L2-2 test simulation results are shown in Figures B-31 through B-36. The prediction with the current code version, WCOBRA/TRAC MOD7A Revision 6 and the comparison plots given in WCAP-12945-P-A, are shown. The WCOBRA/TRAC model described in Section 14-1 of WCAP-12945-P-A is unchanged with the exception of the broken cold leg. The noding for the broken cold leg was made consistent with the PWR modeling as seen in Figure B-37. The current noding recognizes that the choke plane is located at the exit of the break nozzle that has the flow area restriction (Component 970). The break component then is attached to the nozzle component (Component 970) so that the critical flow is checked at this location. As seen in comparison plot figures (Figures B-31 through B-36), the simulation results are essentially unchanged from the previous predictions. Therefore, the conclusions made in WCAP-12945-P-A including the blowdown heatup heat transfer coefficient multiplier developed with the previous code version are still valid.

### B-2-6-3 Conclusions

The LOFT L2-2 test simulation was repeated with the current code version, WCOBRA/TRAC MOD7A Revision 6. The comparison to measurements and with the previous code version (WCOBRA/TRAC MOD7A Revision 0) results indicate that the code performance is not impacted by the code version differences. In addition, the bias and uncertainty for the heat transfer coefficient multiplier for the blowdown heatup phase developed with the previous code version (WCOBRA/TRAC MOD7A) are still valid.

## B-2-7 SCTF Test 619

The WCOBRA/TRAC code was used to predict the results of tests conducted with the Japan Atomic Energy Research Institute's (JAERI) Slab Core Test Facility (SCTF). The objectives of the SCTF test program were to study two-dimensional hydrodynamics and heat transfer in the core of a simulated PWR and to determine the performance of the emergency core cooling system (ECCS) during a postulated LOCA. The specific phases of the LOCA transient investigated were the later part of blowdown, and the refill and reflood periods.

### B-2-7-1 Relevance to BELOCA Methodology

The ability of WCOBRA/TRAC to predict the cladding temperature response, mass flows, and liquid distribution was investigated using the SCTF simulations. These simulations are used to assess the code's ability to simulate steam binding/entrainment phenomena. They are also used in compensating error assessment. The original calculations for Test 619 were made using the WCOBRA/TRAC MOD7A Revision 0 and were reported in Section 14-3-7 of WCAP-12945-P-A (Bajorek et. al). These calculations were repeated using the current code versions, which includes the changes as described in this appendix.

### B-2-7-2 Simulation Results and Comparison to Previous Results

The calculations were performed as transients (that is, there was no steady-state calculation), starting at beginning of core recovery (BOCREC), when the ECC injection is initiated. The calculations were run out until the cladding temperatures in all rods at all elevations had turned over.

The cladding temperature predictions are compared with the mean of the measured data. While cladding temperature predictions are an important part of the assessment of WCOBRA/TRAC, an equally important area is the prediction of the liquid distribution in the core and upper plenum. This is directly related to the amount of water predicted by the code to be entrained out of the vessel into the hot legs. Masses in the core and upper plenum are estimated from delta-p measurements. In the SCTF, mass flows were measured outside of the vessel after the entrained liquid was separated from the steam. There was no direct measurement of liquid mass flow; an estimate was made by measuring the rate of change of water level in the steam water separator. Steam flows were measured in venturi meters or across orifice plates as the steam entered the containment vessels.

In the following comparisons, solid lines denote the WCOBRA/TRAC predictions. Figures B-38 to B-43 compare the predicted cladding temperatures at several axial locations for WCOBRA/TRAC MOD7A Revision 0 and Revision 6. Early in the transient, the predicted cladding temperature is lower than in the test. The average temperature is underpredicted for about 100 seconds, then the predicted heat transfer becomes poorer than in the test. The quench times are predicted well. Comparisons of simulations using WCOBRA/TRAC Revision 6 also supports the same findings.

The core liquid level is compared in Figures B-44 and B-45 for WCOBRA/TRAC MOD7A Revision 0 and Revision 6 simulations, respectively. As Figure B-44 indicates, WCOBRA/TRAC predicts less mass remaining in the core than is measured in the test; it was concluded in WCAP-12945-P-A that most of the under prediction occurs in the upper elevations of the bundle. The same response is also obtained from Revision 6 results, as depicted in Figure B-45.

Figures B-46 and B-47, for Revision 0 and Revision 6 respectively, compare the collapsed liquid level in the inner region of the upper plenum with the measured level at two locations: above bundle 1 and above bundle 8. In both simulations, WCOBRA/TRAC predicts a more uniform distribution. The predicted level is also higher. Importantly, WCOBRA/TRAC predicts the same relatively low liquid level during most of the test. At about 300 to 350 seconds, the discrepancy becomes larger, but this occurs after the entire core has quenched.

### B-2-7-3 Conclusions

The ability of the code to predict the cladding temperature response, mass flows, and liquid distributions has not changed. This conclusion is supported by the comparisons of code predictions using WCOBRA/TRAC MOD7A Revision 0 and Revision 6 against the data.

## B-2-8 CCTF Run 62

To assess the capability of the WCOBRA/TRAC computer code to predict the thermal-hydraulic core behavior in PWRs, specific code validation was performed using data from the CCTF (Core II). The CCTF test program was conducted by the JAERI and was used to investigate the thermal-hydraulic response of the plant during the refill and reflood phases associated with a postulated LOCA.

### B-2-8-1 Relevance to BELOCA Methodology

Using the CCTF simulations, the ability of WCOBRA/TRAC to predict the cladding temperature response, mass flows, and liquid distribution is assessed. The CCTF tests are the largest scale integral tests available to investigate the phenomena important during the reflood phase. The CCTF has a flow area scaling of 1/21.4 of a 4-loop PWR. Their large scale makes them particularly suited as verification of the code's ability to predict three-dimensional effects in the core. In addition, the full-height scaling makes these tests important indicators on the extent to which core/downcomer oscillations affect the reflood transient. The CCTF simulations are used in assessment of steam binding/entrainment phenomena and in compensating error assessment for WCOBRA/TRAC.

### B-2-8-2 Simulation Results and Comparison to Previous Results

The CCTF Run 62 is selected to benchmark WCOBRA/TRAC MOD7A Revision 6 results against Revision 0 results. These results were reported and discussed in Section 14-2-6-1 of WCAP-12945-P-A. Comparisons of key predicted variables against experimental data are presented for both the original calculations conducted with WCOBRA/TRAC MOD7A Revision 0 and the new calculations with Revision 6.

In general, PCTs and quench times in the CCTF tests were overpredicted (Figures B-48 to B-53). The WCOBRA/TRAC code also predicts a period of cooldown at about 100 seconds, followed by a second heatup, which is caused by excess entrainment into the loops. The predicted vapor temperatures (Figure B-54) are substantially higher than the data: the measurements are most likely affected by rewetting of the thermocouples (T/Cs); prior to rewet the vapor temperature measurement at 6 feet (Figure B-54) agrees well with the predicted value. This is also the case in Revision 6 results as shown in Figure B-55.

The core collapsed liquid level from Revision 0 and Revision 6 simulations are compared to experimental data in Figures B-56 and B-57, respectively. WCOBRA/TRAC underpredicts the mass in the bundle during most of the transient, except for a short time period around 150 seconds. Figures B-58 and B-59 show the collapsed level in the upper plenum prediction-to-data comparisons for MOD7A Revision 0 and Revision 6, respectively. Evidence of liquid appears soon after reflood begins in the WCOBRA/TRAC calculation. This must be due to excess entrainment from the core. There is no measured evidence of liquid until 240 seconds into the test, indicating that entrainment from the core was low prior to this time. The predicted level reaches an equilibrium value, indicating that for any liquid entrained into the upper plenum an equal amount is entrained into the hot legs.

In a gravity reflood transient, the magnitude of the inlet flow is established by two competing effects: the driving force of the column of water in the downcomer, and the resistance to steam flow in the loops. Figures B-60 to B-63 compare the pressure difference across the intact loop and broken loops. The predicted values are in good agreement with the measured values for both Revision 0 and Revision 6 results.

### **B-2-8-3 Conclusions**

The results from the 5 CCTF test simulations previously performed with WCOBRA/TRAC MOD7A Revision 0 showed the code to be giving reasonable prediction of the various phenomena involved. In summary, the ability of WCOBRA/TRAC to predict the overall thermal-hydraulics of a reflood transient properly has not changed with Revision 6. In particular, the rate of increase of mass in the core, and the steam and entrained liquid flow through the loops, are predicted the same when using WCOBRA/TRAC MOD7A Revision 6 as when using Revision 0.

### **B-2-9 ORNL Test 3.03.6AR**

The ORNL Thermal-Hydraulic Test Facility (THTF) tests were conducted to investigate heat transfer during dispersed flow film boiling. These tests simulate dryout and film boiling phenomena at high pressure. In postulated LOCA transients, the amount of heat transfer calculated to occur under these types of conditions is important in determining the initial fuel cladding temperature rise.

#### **B-2-9-1 Relevance to BELOCA Methodology**

To help validate the film boiling heat transfer models of WCOBRA/TRAC, three of the dispersed flow film boiling tests were simulated using WCOBRA/TRAC. In Section 11-2 of WCAP-12945-P-A (Bajorek et al., 1998), comparisons of WCOBRA/TRAC predictions with the experimental data were made to demonstrate the calculational capability and accuracy of WCOBRA/TRAC in predicting high-pressure film boiling heat transfer. The results were used in generation of the blowdown heat-up heat transfer multiplier, and in compensating error assessment of WCOBRA/TRAC. Here, the same comparisons are presented using Revision 6 as the prediction tool and these comparisons are contrasted against Revision 0 results.

#### **B-2-9-2 Simulation Results and Comparison to Previous Results**

Test 3.03.6AR is presented here as one of the typical ORNL tests. In this test, the pump was turned off immediately after the initiation of the transient. The bundle power was ramped to 1.65 times the initial value within 2.5 seconds, held constant for about 5 seconds, and then ramped down to a low level. The inlet flow enthalpies remained the same as the initial values over the entire transient. In the test, the axial temperature profile increases with increasing distance above the dryout point. Despite increased mixture velocity, low flowrates, increasing void fraction, and superheating of vapor decreases heat transfer.

Figures B-64 and B-65 compare the WCOBRA/TRAC predictions and experimental data at the time the PCT occurred (11 seconds from experimental data and 10 seconds from WCOBRA/TRAC predictions) for MOD7A Revision 0 and Revision 6, respectively. The WCOBRA/TRAC Revision 0 and Revision 6 predictions of the transient response of the THTF bundle are compared to data at several locations (Figures B-66 to B-71). In these figures, averaged data and individual heater rod data are shown. These comparisons indicate that WCOBRA/TRAC is generally overpredicting the heat transfer in this test, even though the peak is predicted well. These results are not significantly changed from Revision 0 to Revision 6 simulations.

### B-2-9-3 Conclusions

The WCOBRA/TRAC models and correlations provide a reasonable simulation of the ORNL dispersed flow film boiling tests. There is a reasonable prediction of temperature response both at high flowrates (film boiling downstream of the dryout point which decreases the heater rod surface temperature) and at low flowrates (low heat transfer downstream of the dryout point which causes the heater rod surface temperature to keep increasing downstream of the dryout point). In addition, the location of the dryout point is predicted well, indicating that the models and correlations for critical heat flux are also reasonable over the range covered in the tests. Comparisons against data using Revision 6 simulations indicate that the code's ability to predict the important phenomena has not changed.

### B-2-10 G-2 Refill Test 760

The Westinghouse G-2 Test Facility was designed to represent a full-length 17x17XL (14-foot length) PWR fuel assembly. The test facility's original purpose was to verify the performance of the upper head injection (UHI) ECCS, which was installed in some PWRs. This system injected subcooled water onto the top of the core during the blowdown phase of the LOCA. During the same time period, 2-phase mixture from the upper plenum and reactor coolant loops was expected to flow into the core and provide additional cooling. Both of these processes could be simulated in the test facility. For the refill tests, only the UHI flow was simulated.

#### B-2-10-1 Relevance to BELOCA Methodology

Low-pressure UHI refill tests conducted at the Westinghouse G-2 Test Facility were simulated using the WCOBRA/TRAC computer code. Comparisons of the WCOBRA/TRAC results to the refill test experimental data were used to help assess the capability of WCOBRA/TRAC to accurately predict top-down quench phenomena, low-pressure film boiling, and counter-current film boiling heat transfer. Further detail on the prior simulations and comparisons are documented in Section 11-5 of WCAP-12945-P-A (Bajorek et al., 1998). The results of those simulations were used in generation of heat transfer multipliers during the refill period (Figure 1-4).

### B-2-10-2 Simulation Results and Comparison to Previous Results

Test 760 was run with a UHI flowrate of 6.51 lb/sec, an initial peak heater rod cladding temperature of 1200°F, and a pressure of 27 psia. WCOBRA/TRAC results are in good agreement with the test data except for the 12.3-inch elevation. Figures B-72 and B-73 compare WCOBRA/TRAC MOD7A Revision 0 and Revision 6 simulation results to experimental data at the 12.3-inch elevation. At this elevation, both simulations over-predicted the cooling effect. Figures B-74 through B-81 show the comparisons for higher elevations. At these elevations, WCOBRA/TRAC results are in very good agreement with measurements. Figure B-82 is the axial profile comparison between Revision 0 simulation results and measurement average at 50 seconds. Figure B-83 shows the Revision 6 results. These results are essentially unchanged from the previous predictions.

### B-2-10-3 Conclusions

The capability of WCOBRA/TRAC to accurately predict film boiling and rewet phenomena in the simulation of G-2 refill tests is evaluated by comparisons with data of axial temperature profiles, cladding temperature transient histories at specific elevations, and the maximum cladding temperatures for the entire fuel assembly. The G-2 refill tests are unique in providing rod bundle data for both co-current downflow and counter-current flow film boiling that may exist in PWRs. Comparisons against data for Revision 0 and Revision 6 simulations indicate that the ability of the code in predicting film boiling and rewet phenomena during refill has not changed. This supports that the heat transfer multipliers currently in use are still applicable to Revision 6.

### B-2-11 UPTF

The UPTF simulated a full-scale 3900 MWt German PWR. The facility had 4 loops, each with a steam/water separator to simulate a steam generator and a variable resistance to simulate a reactor coolant pump. The upper plenum contained full-size internals in an arrangement typical of a Kraftwerk Union (KWU) PWR. The UPTF was designed to obtain experimental data relative to the multi-dimensional flows expected in a PWR during a LOCA. The UPTF was the German contribution to the 2D/3D program established by the United States (NRC), Japan (JAERI) and the Federal Republic of Germany (BMFT). Tests conducted in the UPTF gave special consideration to:

- Entrainment and de-entrainment in the upper plenum
- Co-current and counter-current two-phase flow in the upper core and tie plate region
- Co-current and counter-current flow and bypass in the downcomer
- Condensation and steam/water mixing processes caused by ECC injection in the loops

#### B-2-11-1 Relevance to BELOCA Methodology

Tests 6 and 25 were used to examine WCOBRA/TRAC's ability to predict ECC bypass in the downcomer, Test 8 was used to evaluate the code models and correlations for condensation, and Tests 10b and 29b were used to validate the models for calculating de-entrainment in the upper plenum.

The bypass tests and the previous simulations are described in Sections 14-4-3 through 14-4-6 of WCAP-12945-P-A (Bajorek et al., 1998), the steam/water mixing test in Sections 14-4-7 to 14-4-9, and the upper plenum de-entrainment tests in Sections 14-4-10 through 14-4-13.

The UPTF Test 6 simulations in particular were used to show that, for U.S. domestic PWRs, (1) the counter-current flow limitation (CCFL) in the downcomer during downcomer penetration is reasonably calculated and (2) there is a conservative bias in the WCOBRA/TRAC predicted end-of-bypass (EOB) time relative to the experiments. This was discussed in Section 25-6 of WCAP-12945-P-A. In addition, the Test 6 series was used to generate the range of the interfacial heat transfer coefficient multiplier for condensation in the downcomer. This was discussed in Section 25-9 of WCAP-12945-P-A.

### **B-2-11-2 Simulation Results and Comparison to Previous Results**

The UPTF Test 6 Run 131 test simulation results are shown in Figures B-84 through B-95. The prediction with the current code version, WCOBRA/TRAC MOD7A Revision 6 and the comparison plots (between the measurement and the MOD7A prediction) given in WCAP-12945-P-A, are shown.

The WCOBRA/TRAC simulation was run for 100 seconds, which corresponds to the test time period of 30 to 130 seconds for Run 131. Figures B-84a, B-84b, and B-84c compare the measured and predicted absolute pressures in the upper plenum and downcomer. The measured value is shown in Figure B-84a. The predicted value shown in WCAP-12945-P-A (with WCOBRA/TRAC MOD7A Revision 0) is given in Figure B-84b. The prediction with the current code version, WCOBRA/TRAC MOD7A Revision 6, is shown in Figure B-84c. The WCOBRA/TRAC prediction is seen to initially match the measured pressure, but then underestimate it after about 80 seconds. Figure B-85a shows the measured downcomer fluid temperature at downcomer Level 21, which was on the intact side of the downcomer just below the cold legs. The measured temperatures showed frequent decreases indicating that liquid frequently penetrated to this level. At the bottom of the downcomer, Level 01 (Figure B-86a), the measured temperature signal indicated only infrequent liquid penetration. The WCOBRA/TRAC prediction of fluid temperatures in the downcomer shows that the vapor phase remains constant at saturation temperature and the liquid is subcooled. A better indicator of the fluid condition, showing the frequency of liquid penetration to a given level, is the fluid mixture enthalpy shown in Figures B-85 and B-86. At Level 21, the mixture enthalpy drops rapidly to nearly the liquid enthalpy, remaining constant for most of the test simulation. This indicates that the code is predicting the frequent liquid presence at this elevation as was found in the test. At Level 01, no penetration was predicted until late in the simulation.

Delivery to the lower plenum was predicted to have occurred only on the side of the downcomer opposite the break. Liquid flow on the intact side of the downcomer (channels 8 and 9) is shown in Figure B-87 and on the broken side (channels 10 and 11) in Figure B-88. Delivery to the lower plenum occurs in discrete intervals, as "plugs" of liquid penetrate on the downcomer side opposite the broken loop. As liquid reaches the lower plenum, the vapor flow re-entrains a portion of the liquid and sweeps back up the downcomer to the break.

Differential pressures in the downcomer are compared in Figures B-89 through B-93. The WCOBRA/TRAC predictions are seen to be in good agreement with the measurements. Figures B-92a and B-93a show the measured azimuthal differential pressures in the downcomer at two elevations. Figure B-92 indicates that low in the downcomer, little if any, lateral flow occurred in the test. Lateral flow around the core barrel occurred higher in the downcomer, as shown in Figure B-93. The WCOBRA/TRAC predictions of transverse flow also indicate bypass at higher elevations in the downcomer.

The predicted and measured water levels in the UPTF vessel are compared in Figures B-94 through B-95. Figure B-94a shows the estimated water level in the vessel and lower plenum while Figure B-94c presents the calculated water level in the lower plenum. Figure B-95a shows the estimated water levels in the downcomer and Figure B-95c shows the calculated water level in each of the 4 downcomer channel stacks. The comparisons show that WCOBRA/TRAC predicts a delayed increase in vessel inventory due to a prediction of prolonged bypass.

As seen in these figures, the WCOBRA/TRAC MOD7A Revision 6 simulation results are essentially unchanged from the previous predictions. Therefore, the conclusions made in WCAP-12945-P-A are still valid.

### **B-2-11-3 Conclusions**

The simulation results with the current code version (WCOBRA/TRAC MOD7A Revision 6) are essentially identical to those shown in WCAP-12945-P-A. Therefore, it is concluded that (1) the tendency of WCOBRA/TRAC to predict the delay in end-of-bypass remains valid, and (2) the vessel condensation range calculated from UPTF Test 6 simulations is unchanged.

### **B-2-12 GE CCFL**

The General Electric (GE) CCFL tests were designed to determine the characteristics of subcooled CCFL in the upper region of a boiling water reactor (BWR) fuel bundle during safety injection. Because of the similarities in fuel bundle tie plate geometry, in terms of hydraulic diameter and thickness between BWR and UPI plants, the experimental results are also pertinent to UPI application. The tests were run at the GE's Zero Power Loop test facility. The objectives of the test program were threefold:

- Obtain CCFL data for a wide range of inlet water flowrates and subcoolings
- Obtain temperature data from the pool of water that accumulates above the tie plate during CCFL, to determine the mixing profile of the pool
- Evaluate the applicability of the existing CCFL correlations

This test program is of interest for the UPI application, because the source of water for the ECCS is significantly subcooled during the reflood of the core, following a hypothetical LOCA. A number of GE



test results were used to assess the WCOBRA/TRAC MOD7A Revision 1 prediction of the flooding characteristics. The modeling of the experiments and the results of the assessment were documented in Section 4-4 of WCAP-14449 (Dederer et al., 1999). The original simulations were prepared using Revision 1 of WCOBRA/TRAC MOD7A to support BE methodology extension for UPI plants. In ASTRUM, key tests are repeated using WCOBRA/TRAC MOD7A Revision 6.

#### **B-2-12-1 Relevance to BELOCA Methodology**

The selection of tests for simulation with WCOBRA/TRAC was intended to cover a wide range of temperatures and injection rates, in order to bound the thermal-hydraulic conditions expected during core reflood in a UPI plant. Here, one subcooled and one saturated tests are selected for comparison. The GE CCFL Test 60 is run at subcooled conditions, while Test 69 is saturated. The results from these and other CCFL tests were used to support the UPI parameter ranging. These tests in particular showed the code's ability to model the CCFL phenomena. The primary focus of the WCOBRA/TRAC simulation was on the interfacial condensation and interfacial drag, and their impact on the flooding characteristics at the tie plate.

#### **B-2-12-2 Simulation Results and Comparison to Previous Results**

Figures B-96 and B-97 show the comparison of the predicted liquid drain rate versus the steam injection rate to the test data for GE CCFL Subcooled Test 60 using WCOBRA/TRAC MOD7A Revision 1 and Revision 6, respectively. Figures B-98 and B-99 show the same comparison for Test No. 69, which is near saturation. The test data plotted in these figures read as follows: at the start of the steam increasing phase, total injected liquid drained through the tie plate. As the steam injection rate reached a certain value, the drain rate became less with increasing steam injection rate due to CCFL. Eventually, no draining took place (flooding). Then, the steam injection rate was decreased. As the steam injection rate decreased, liquid drain recovered, following the trace of steam increasing phase (no hysteresis), and eventually all the injected liquid drained.

In the analyses of Test No. 69 (Figures B-98 and B-99), it is seen that the predicted flooding during the steam increasing phase is very close to the test data for both Revision 1 and Revision 6 results. However, during the second phase, drain recovery comes later with a lower steam flow than the data. Therefore, a hysteresis is seen in the predicted Test No. 69. Note that no significant hysteresis can be seen in the predictions other than Test No. 69. However, all the predictions show the flooding takes place with less steam injection rate than the test data, except for the first phase in Test No. 69 for the near saturation flooding.

The predictions and test data in Figures B-96 to B-99 are transformed to Kutateladze numbers. The results are plotted in Figures B-100 through B-103 for each case. The test data are shown by triangles and the predictions by squares. Bankoff saturated and subcooled flooding curves obtained above are also shown by solid and dashed curves, respectively, on Figures B-100 and B-102. There are two subcooled flooding curves with condensation efficiency  $f = 0.24$  and  $0.6$ . It is interesting to observe that the test data go beyond the saturated flooding line except for the near saturated test 69 and the condensation

efficiency seems to be  $f < 0.6$ . Furthermore, the data approach the saturated flooding line as the drain rate approaches zero, because the subcooled injected water becomes saturated well above the tie plate for strong steam upflow. In fact, the measured temperature of the pooled water above the tie plate becomes saturated near flooding.

### B-2-12-3 Conclusions

The simulations results were used to show that WCOBRA/TRAC can satisfactorily simulate the counter-current flooding characteristics in the upper plenum during subcooled safety injection and the code will not overpredict the downflow from the CCFL region of the upper plenum during reflood as evidenced by the comparison of the code results to the flooding data. The same findings are also supported by Revision 6 simulations when compared to Revision 1 results.

### B-3 REFERENCES

Adams, J. P. and Birchley, J. C., "Quick Look Report on OECD LOFT Experiment LP-LB-1," OECD LOFT- TR-3504.

American Nuclear Society, 1979, "American National Standard for Decay Heat Power in Light Water Reactors," ANSI/ANS-5.1-1979.

Bajorek, S. M. et al., 1998, "Code Qualification Document for Best Estimate LOCA Analysis," WCAP-12945-P-A, Volume 1 Revision 2, and Volume 2 through 5 Revision 1, and WCAP-14747- (Non-proprietary).

Bayless, P. D. and Divine, J. M., 1982, "Experiment Data Report for LOFT Large-Break Loss-of-Coolant Experiment L2-5," NUREG/CR-2826.

Dederer, S. I., Nissley, M. E., and Takeuchi, K, "Application of Best Estimate Large Break LOCA Methodology to Westinghouse PWRs with Upper Plenum Injection," WCAP-14449-P-A, Revision 1, Westinghouse Electric Company, October 1999.

Grush, W. H., 1980, "Cold Leg Warmup Line and RABVs Flows During Experiment L3-1," Kau - 208-80.

Letter, N. J. Liparulo-(Westinghouse) to Document Control Desk-(USNRC), "Preliminary Responses to Requests for Additional Information Regarding WCAP-12945-P," NTD-NRC-95-4399, February 9, 1995.

Letter, H. A. Sepp-(Westinghouse) to T. E. Collins-(USNRC), "1997 Annual Notification of Changes to the Westinghouse Small Break LOCA and Large Break LOCA ECCS Evaluation Models, Pursuant to 10 CFR 50.46(a)(3)(ii)," NSD-NRC-98-5575, April 8, 1998.

Letter, J. S. Galembush-(Westinghouse) to J. S. Wermiel-(USNRC), "1998 Annual Notification of Changes to the Westinghouse Small Break LOCA and Large Break LOCA ECCS Evaluation Models, Pursuant to 10 CFR 50.46(a)(3)(ii)," NSD-NRC-99-5839, July 15, 1999.

Letter, H. A. Sepp-(Westinghouse) to J. S. Wermiel-(USNRC), "1999 Annual Notification of Changes to the Westinghouse Small Break LOCA and Large Break LOCA ECCS Evaluation Models, Pursuant to 10 CFR 50.46(a)(3)(ii)," NSBU-NRC-00-5970, May 12, 2000.

Letter, H. A. Sepp-(Westinghouse) to J. S. Wermiel-(USNRC), "10 CFR 50.46 Annual Notification and Reporting for 2000," LTR-NRC-01-6, March 13, 2001.

Letter, H. A. Sepp-(Westinghouse) to J. S. Wermiel-(USNRC), "10 CFR 50.46 Annual Notification and Reporting for 2001," LTR-NRC-02-10, March 13, 2002.

Letter, H. A. Sepp-(Westinghouse) to J. S. Wermiel-(USNRC), "10 CFR 50.46 Annual Notification and Reporting for 2002," LTR-NRC-03-5, March 7, 2003.

"LOFT Experiment Operating Specification" 1978, Volume 2, NE-L2 Series, EOS Vol. 2, Rev. 2.

McCormick-Barger, M., 1979, "Experiment Data Report for LOFT Power Ascension Test L2-2," NUREG/CR-0492.

Prassinis, P. G. et al., 1979, "Experiment Data Report for LOFT Power Ascension Experiment L2-3," NUREG/CR-0792.

Reeder, D. L., 1978, "LOFT System and Test Description," NUREG/CR-0247.

Russell, M. L., 1983, "Loss-of-Fluid Findings in Pressurized-Water-Reactor Core's Thermal Hydraulic Behavior," EGG-M-08882.

Young, M. Y. et al., 1998, "Code Qualification Document for Best Estimate LOCA Analysis, Volume IV: Assessment of Uncertainty," WCAP 12945-P-A, Volume 4, Revision 1.

<b>Table B-1      Changes and Errors Reported Since Approval of <u>W</u>COBRA/TRAC MOD7A Revision 1</b>		
<b>Annual Report (Reference)</b>	<b>Title of Change or Error</b>	<b>Could Biases or Uncertainties be Affected?</b>
1997 (NSD-NRC-98-5575)	Intercell Force Gap Numbering Error	No
	Vessel Channel DX Error	Yes
	1-D Transition Boiling Heat Transfer Error	Yes
	TUBE Heated Conductor Error	No
	Incorrect Wall Friction Factor for Convective Enhancement Term	Yes
	Miscellaneous Input/Output Revisions	No
1998 (NSD-NRC-99-5839)	Vessel Channel DX Error (Including Investigation of Code Uncertainties)	Yes
1999 (NSBU-NRC-00-5970)	Accumulator Line/Pressurizer Surge Line Data	No
	Inconsistent Guidance for HOTSPOT Outputs in BE LBLOCA Methodology	No
	Decay Heat Uncertainty Error in Monte Carlo Calculation	No
2000 (LTR-NRC-01-6)	LOTIC2 Nitrogen Addition Logic Error	No
	LOTIC2 Time Step Logic Error	No
	<u>W</u> COBRA/TRAC Gap Input Error in SECY UPI/BELOCA EM Analyses	Yes
	GEDM Interface Error	No
	Drop Diameter Plot Tape Storage Error	No
	Cladding Oxidation Edit Error	No
	Output Edit Error for SI Units	No
	Radiation Heat Transfer to Vapor Phase Error	Yes
	Grid Heat Transfer Error	Yes
	Pressure Drop Error for 1-D Connections to 3-D Vessel	No
	PAD 4.0 Implementation	No

<b>Table B-1                      Changes and Errors Reported Since Approval of WCOBRA/TRAC</b> <b>(cont.)                      MOD7A Revision 1</b>		
<b>Annual Report (Reference)</b>	<b>Title of Change or Error</b>	<b>Could Biases or Uncertainties be Affected?</b>
2001 (LTR-NRC-02-10)	Enhancements to Monte Carlo PCT Calculation	No
	Response Surface Plot Title Error	No
	Oxidation Thickness Index Error for Best Estimate WCOBRA/TRAC	No
	Neutronics Calculation Moderator Density Weighting Factor Error	Yes
	WCOBRA/TRAC Unheated Structure Multiplier	No
2002 (LTR-NRC-03-5)	1-D Minimum Film Boiling Temperature Model Selection Error	Yes
	1-D Condensation Ramp Error	No
	Potential Divide by Zero Error During Pump Rotation Reversal	No
	Cladding Axial Thermal Expansion Error	Yes
	Application of Decay Heat Uncertainty to Prompt Fission Energy Error	No
	Error in Time After Shutdown for Neutron Capture Term	Yes
	Bypass of Orifice Entrainment Model in Downflow with Channel Splitting	Yes
	Monte Carlo Code Consolidation Error	No
	Response Surface Matrix Operation and Random Search Errors	No
	Broken Cold Leg Modeling Deviations	No
	User Conveniences in HOTSPOT	No

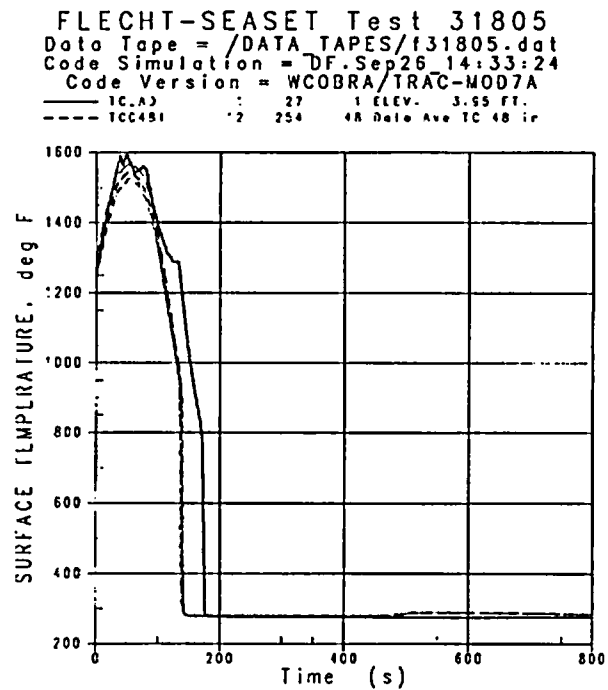


Figure B-1. FLECHT-SEASET Test 31805 Rod Temperature at 48-inch Elevation (Revision 0)

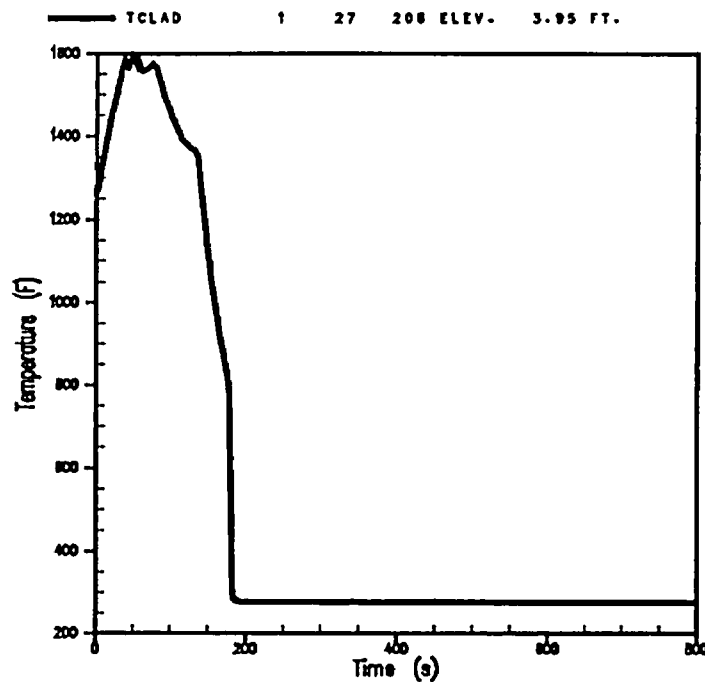


Figure B-2. FLECHT-SEASET Test 31805 Rod Temperature at 48-inch Elevation (Revision 6)

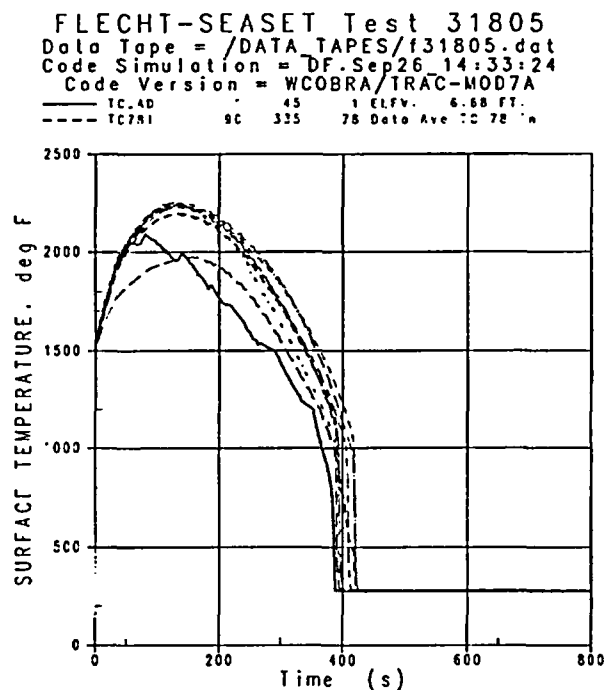


Figure B-3. FLECHT-SEASET Test 31805 Rod Temperature at 78-inch Elevation (Revision 0)

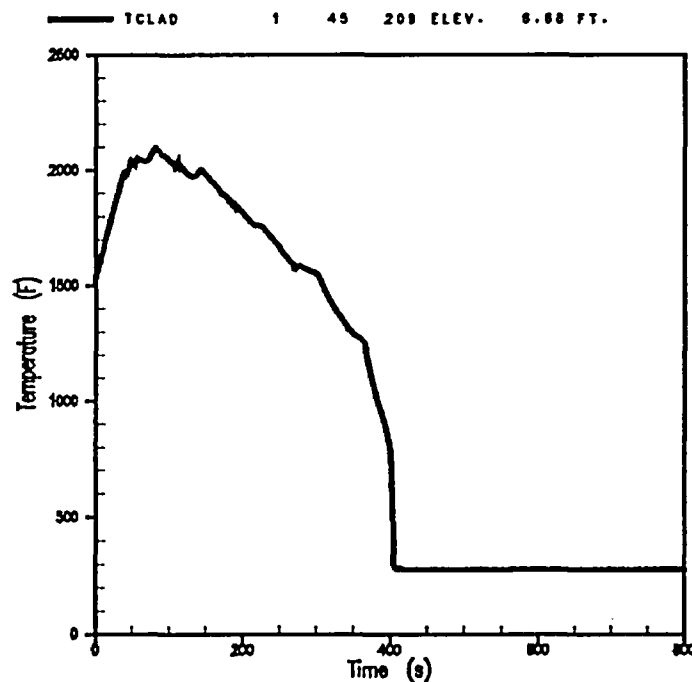


Figure B-4. FLECHT-SEASET Test 31805 Rod Temperature at 78-inch Elevation (Revision 6)

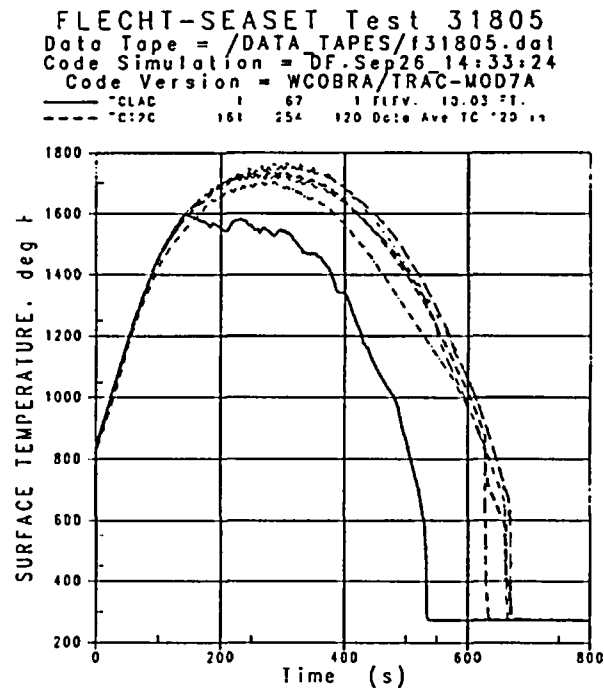


Figure B-5. FLECHT-SEASET Test 31805 Rod Temperature at 120-inch Elevation (Revision 0)

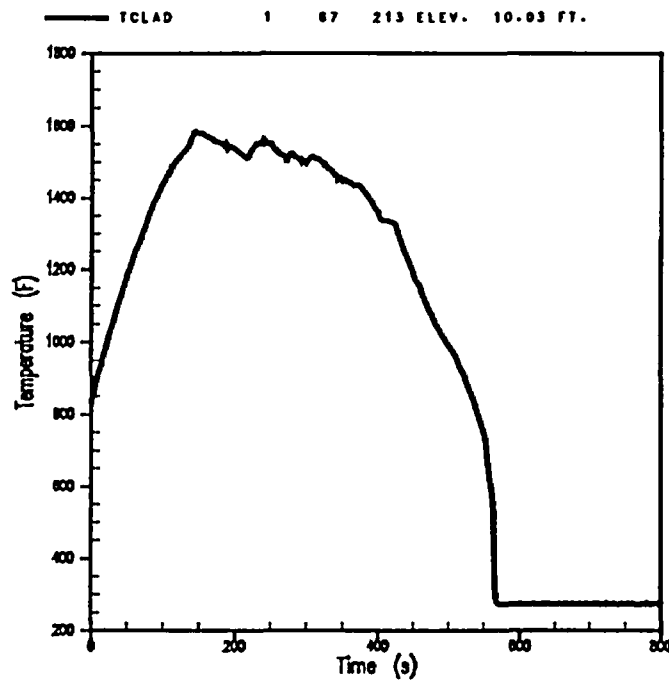


Figure B-6. FLECHT-SEASET Test 31805 Rod Temperature at 120-inch Elevation (Revision 6)



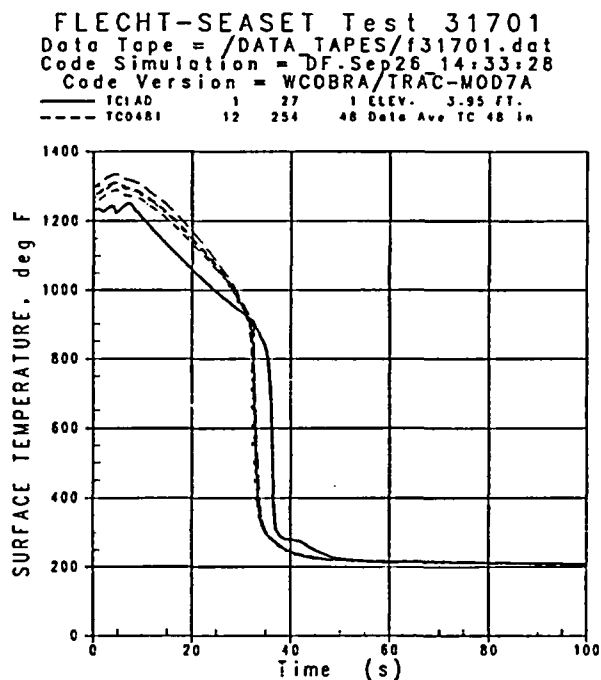


Figure B-7. FLECHT-SEASET Test 31701 Rod Temperature at 48-inch Elevation (Revision 0)

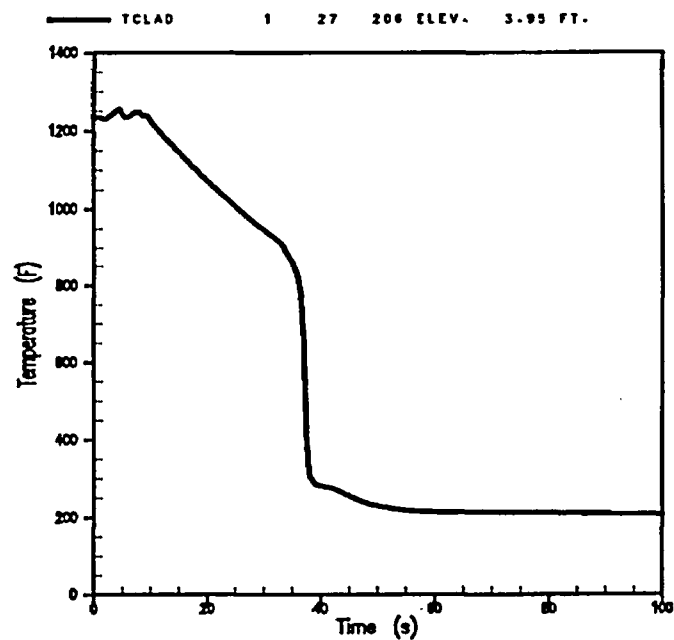


Figure B-8. FLECHT-SEASET Test 31701 Rod Temperature at 48-inch Elevation (Revision 6)

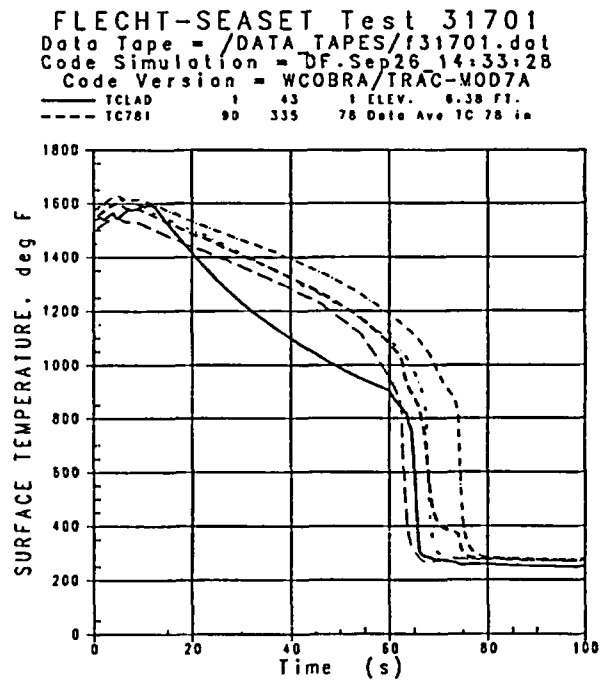


Figure B-9. FLECHT-SEASET Test 31701 Rod Temperature at 78-inch Elevation (Revision 0)

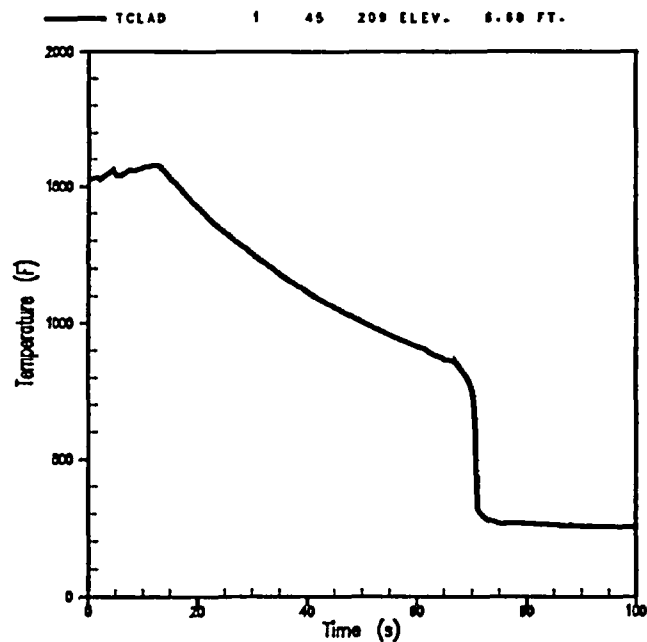


Figure B-10. FLECHT-SEASET Test 31701 Rod Temperature at 78-inch Elevation (Revision 6)

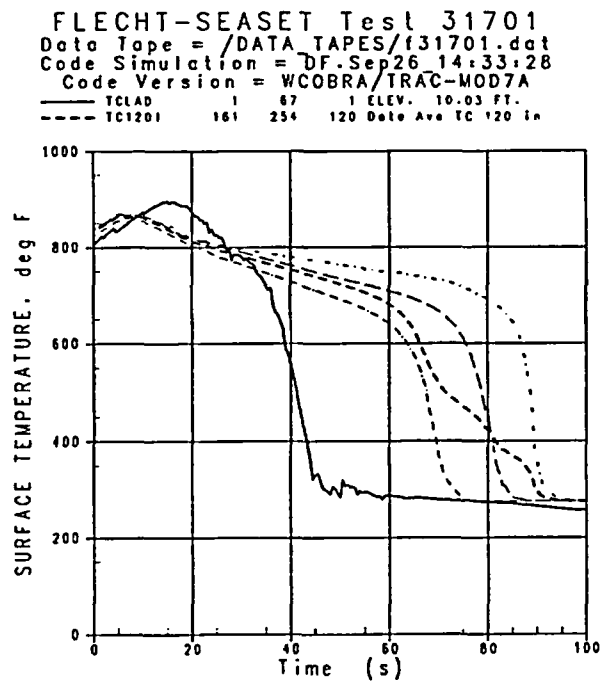


Figure B-11. FLECHT-SEASET Test 31701 Rod Temperature at 120-inch Elevation (Revision 0)

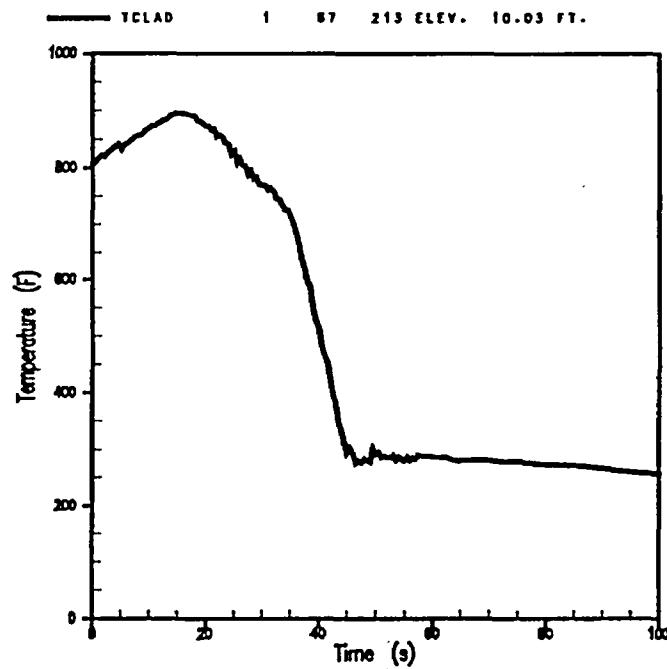


Figure B-12. FLECHT-SEASET Test 31701 Rod Temperature at 120-inch Elevation (Revision 6)

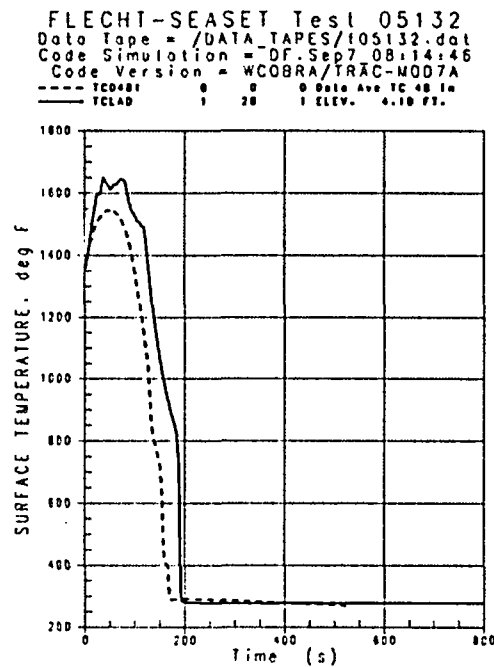


Figure B-13. FLECHT Test 05132 Rod Temperature at 48-inch Elevation (Revision 0)

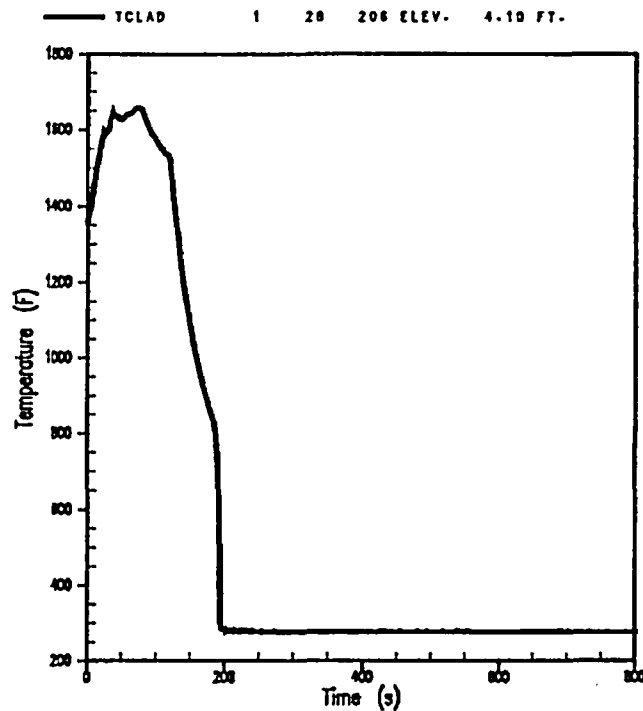


Figure B-14. FLECHT Test 05132 Rod Temperature at 48-inch Elevation (Revision 6)

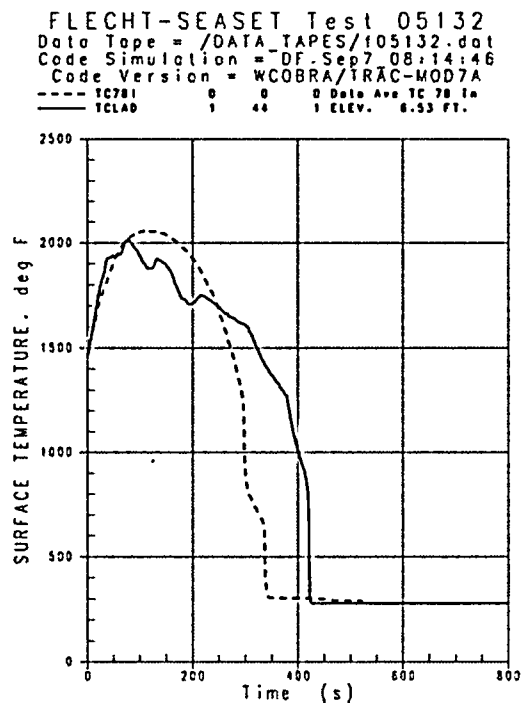


Figure B-15. FLECHT Test 05132 Rod Temperature at 78-inch Elevation (Revision 0)

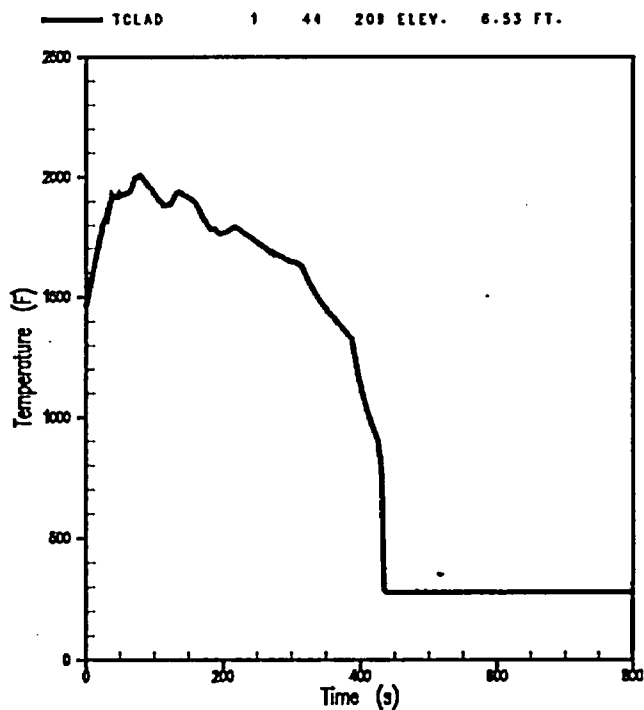


Figure B-16. FLECHT Test 05132 Rod Temperature at 78-inch Elevation (Revision 6)

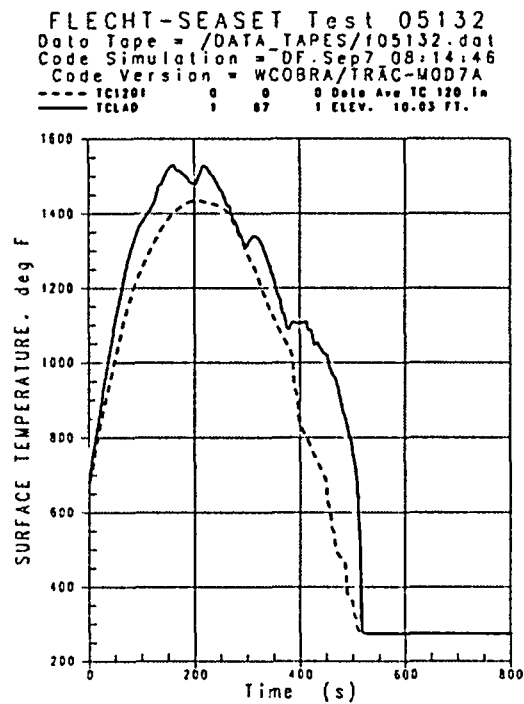


Figure B-17. FLECHT Test 05132 Rod Temperature at 120-inch Elevation (Revision 0)

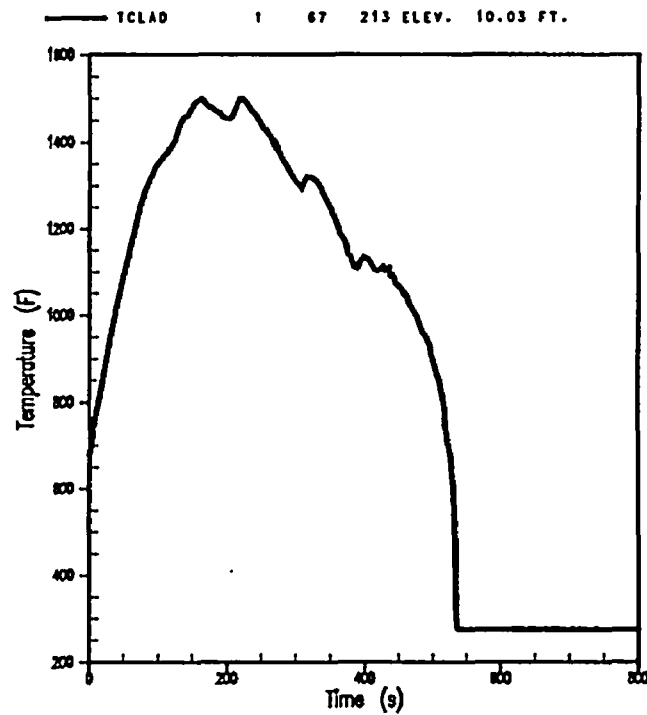


Figure B-18. FLECHT Test 05132 Rod Temperature at 120-inch Elevation (Revision 6)

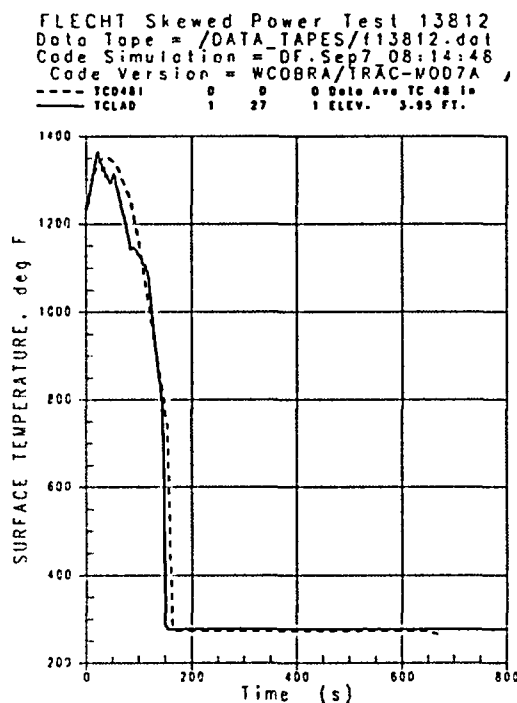


Figure B-19. FLECHT Test 13812 Rod Temperature at 48-inch Elevation (Revision 0)

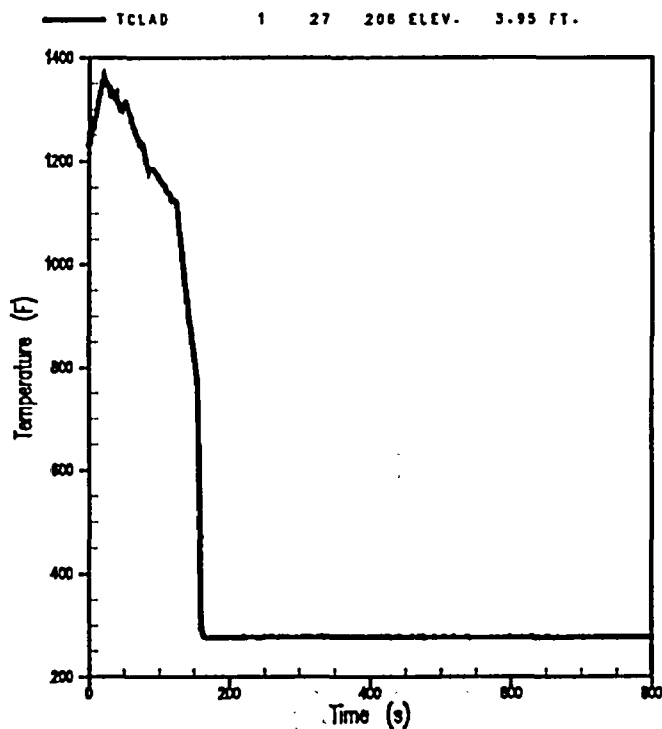


Figure B-20. FLECHT Test 13812 Rod Temperature at 48-inch Elevation (Revision 6)





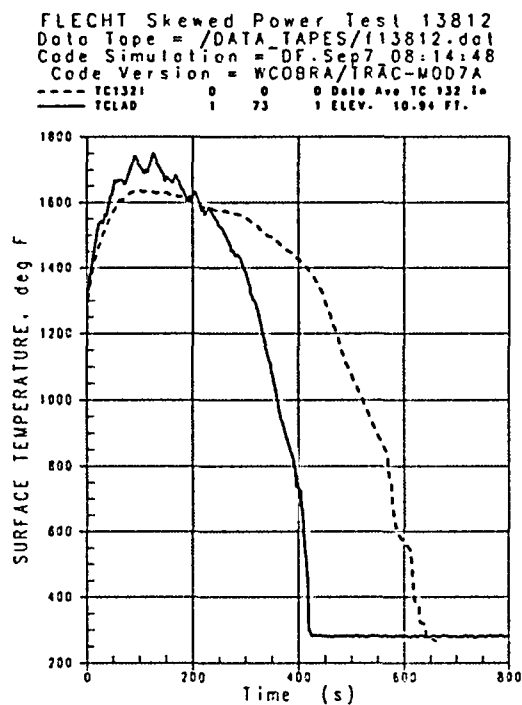


Figure B-23. FLECHT Test 13812 Rod Temperature at 132-inch Elevation (Revision 0)

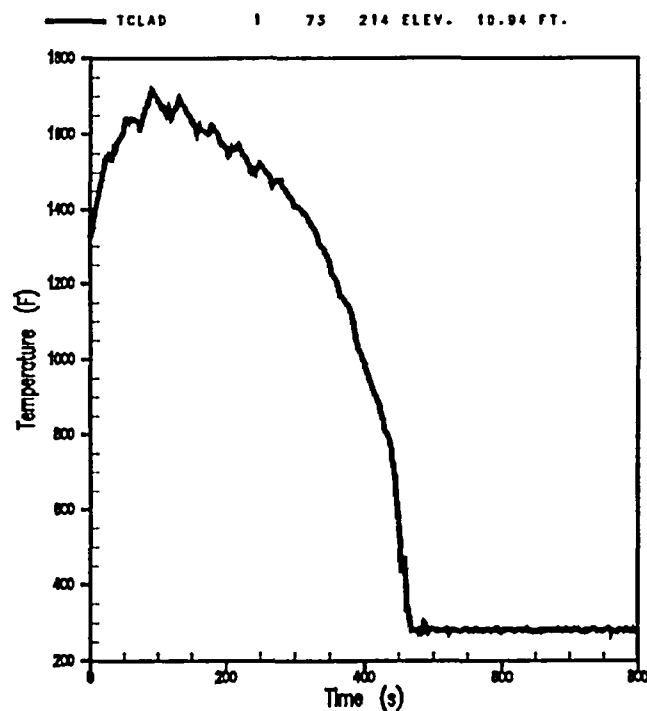


Figure B-24. FLECHT Test 13812 Rod Temperature at 132-inch Elevation (Revision 6)

Figure B-25. WCOBRA/TRAC MOD7A Rev. 0 vs. Experiment Comparison: G-2 Reflood Test 550 Rod Temperatures at 82-inch Elevation

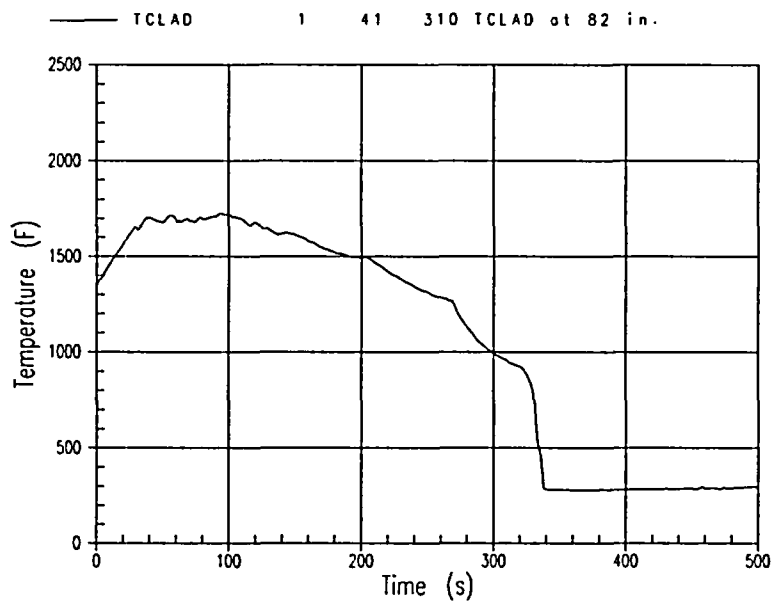


Figure B-26. WCOBRA/TRAC MOD7A Rev. 6 Prediction of G-2 Reflood Test 550 Rod Temperatures at 82-inch Elevation

b

Figure B-27. WCOBRA/TRAC MOD7A Rev. 0 vs. Experiment Comparison: G-2 Reflood Test 550 Rod Temperatures at 94-inch Elevation

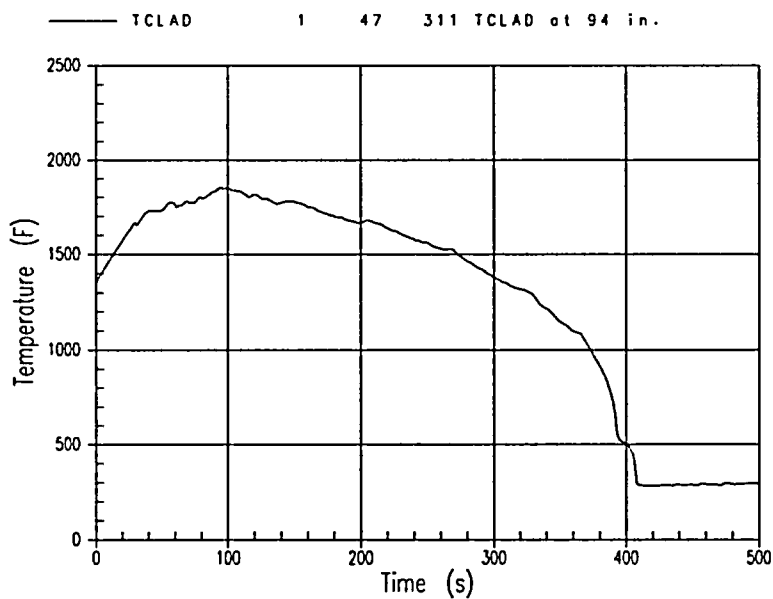


Figure B-28. WCOBRA/TRAC MOD7A Rev. 6 Prediction of G-2 Reflood Test 550 Rod Temperatures at 94-inch Elevation

Figure B-29. WCOBRA/TRAC MOD7A Rev. 0 vs. Experiment Comparison: G-2 Reflood Test 550 Rod Temperatures at 111-inch Elevation

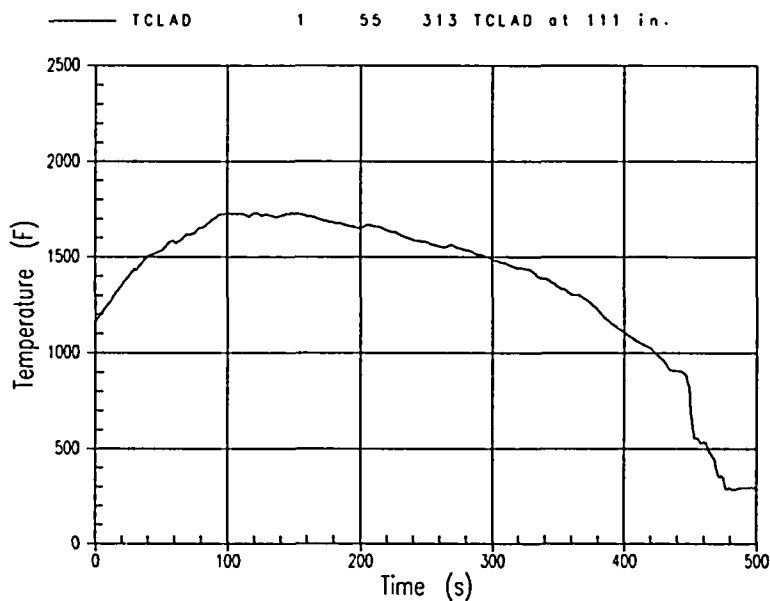


Figure B-30. WCOBRA/TRAC MOD7A Rev. 6 Prediction of G-2 Reflood Test 550 Rod Temperatures at 111-inch Elevation

# LOFT L22 MOD7A vs. DATA INTACT LOOP Pressure

—— VV-00009 810 5 0 PRESSURE  
- - - VV-00013 17 0 0 PE-PC-001

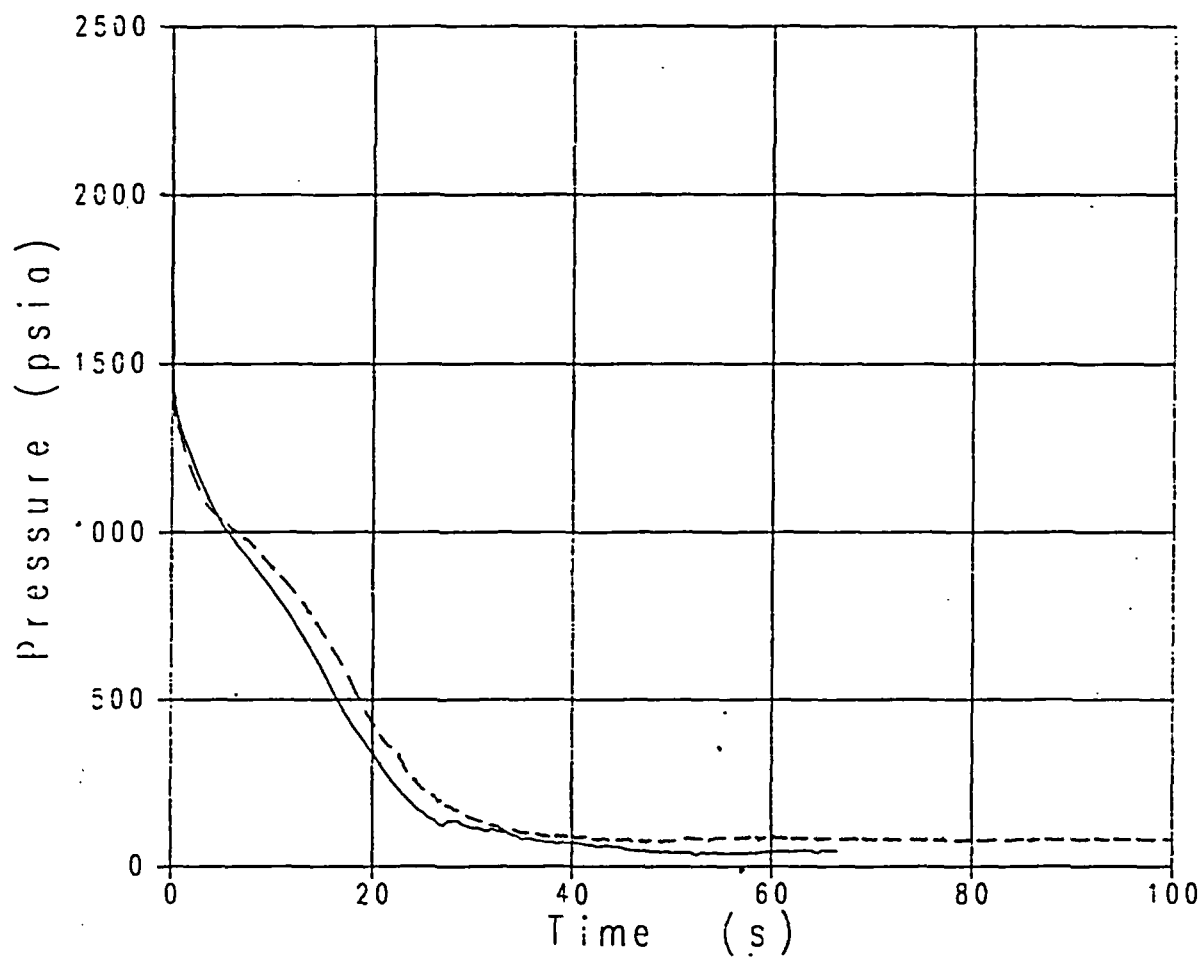


Figure B-31a. Predicted (Component 810) and Measured (PE-PC-001) Pressure, Test L2-2 with MOD7A Rev. 0

# LOFT L22 WC/T Mod7A-Rev6 Simulations INTACT LOOP Pressure

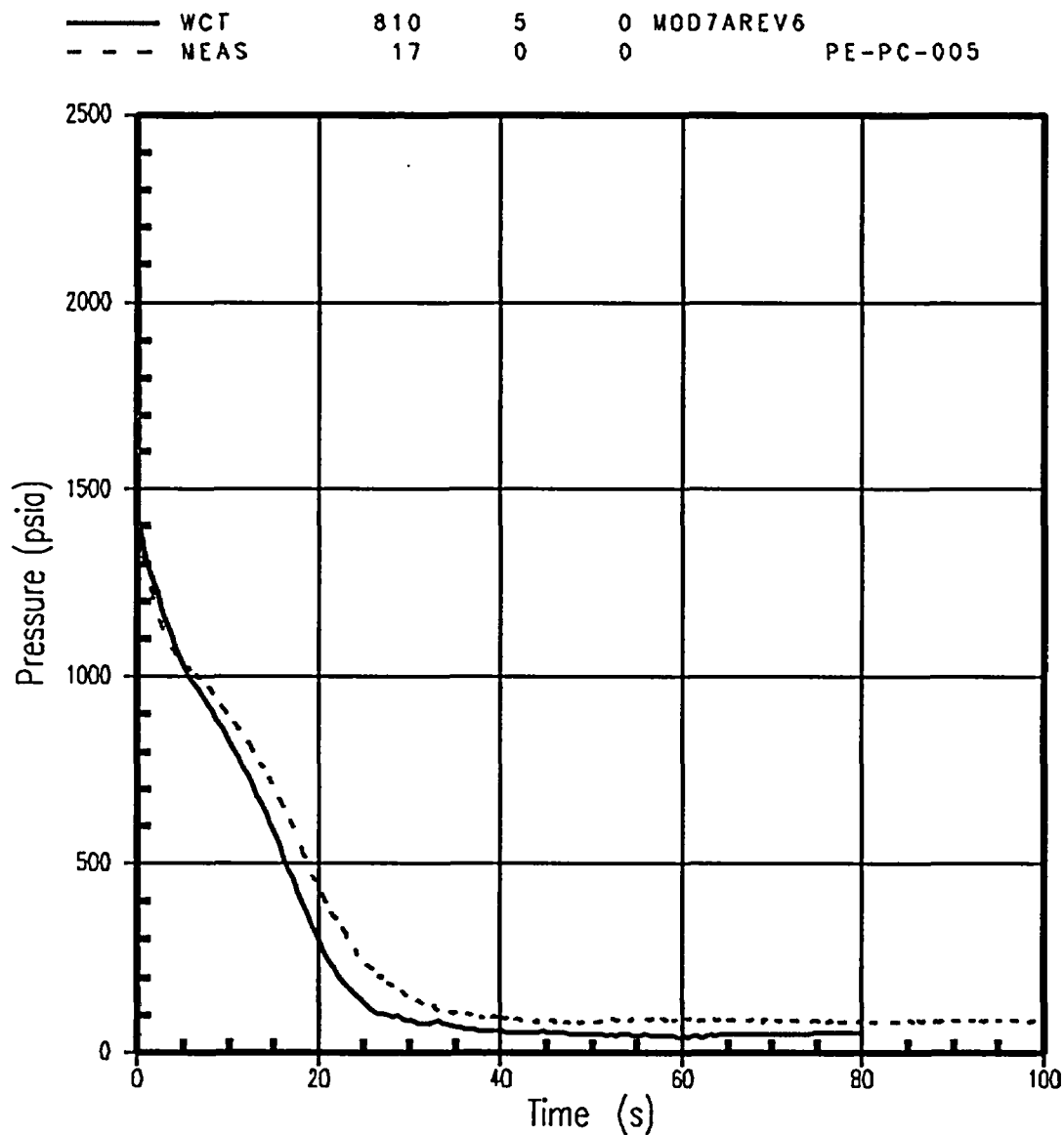


Figure B-31b. Predicted (Component 810) and Measured (PE-PC-001) Pressure, Test L2- 2 with MOD7A Rev. 6

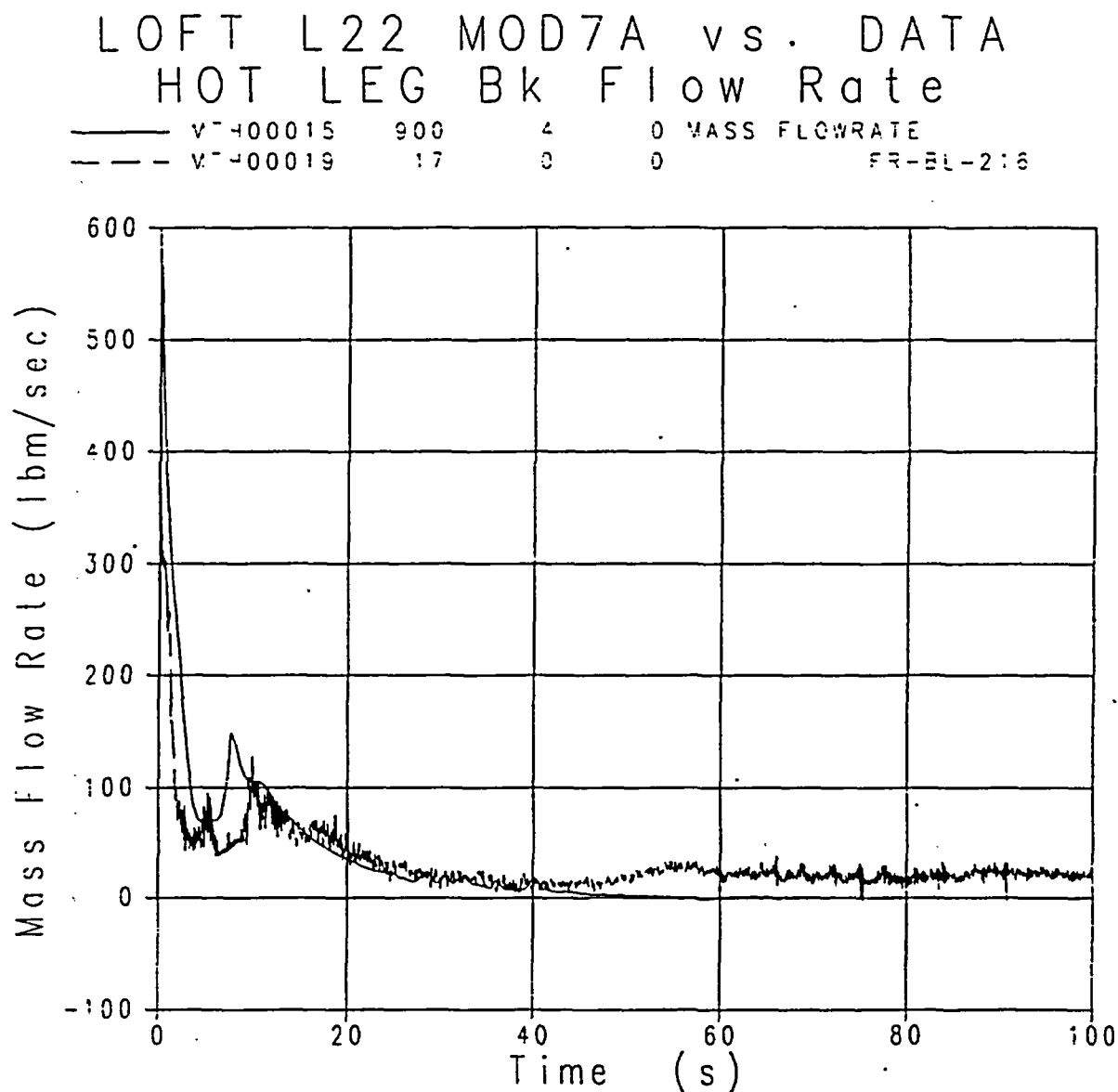


Figure B-32a. Predicted (Component 900) and Measured (FR-BL-216) Mass Flowrate in Broken Hot Leg, Test L2-2 with MOD7A Rev. 0

# LOFT L22 WC/T Mod7A-Rev6 Simulations HOT LEG Bk Flow Rate

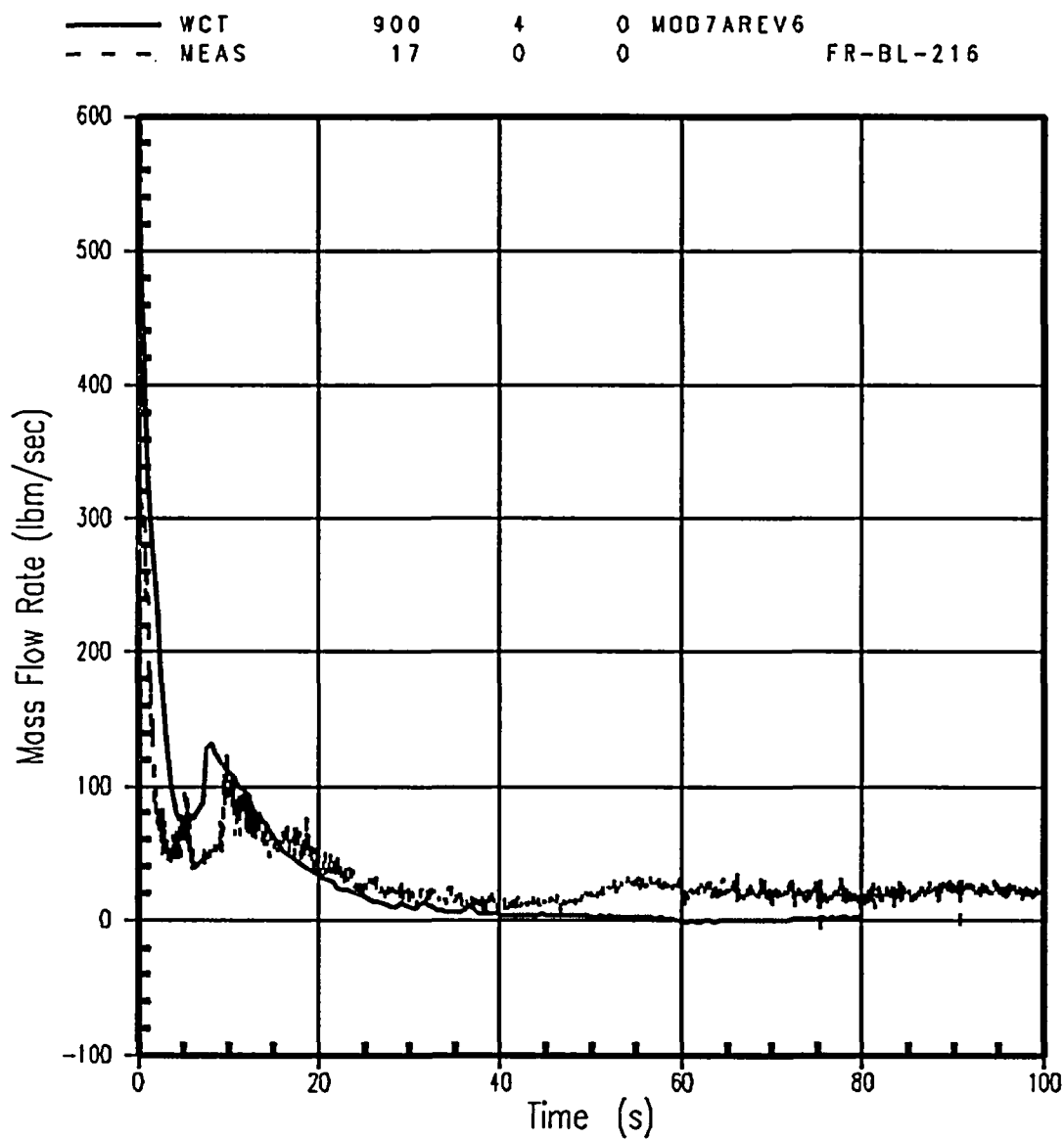


Figure B-32b. Predicted (Component 900) and Measured (FR-BL-216) Mass Flowrate in Broken Hot Leg, Test L2-2 with MOD7A Rev. 6



# LOFT L22 MOD7A vs. DATA COLD LEG Bk Flow Rate

—— V=400021 950 4 0 MASS FLOWRATE  
- - - V=400025 16 0 0 FR-BL-116

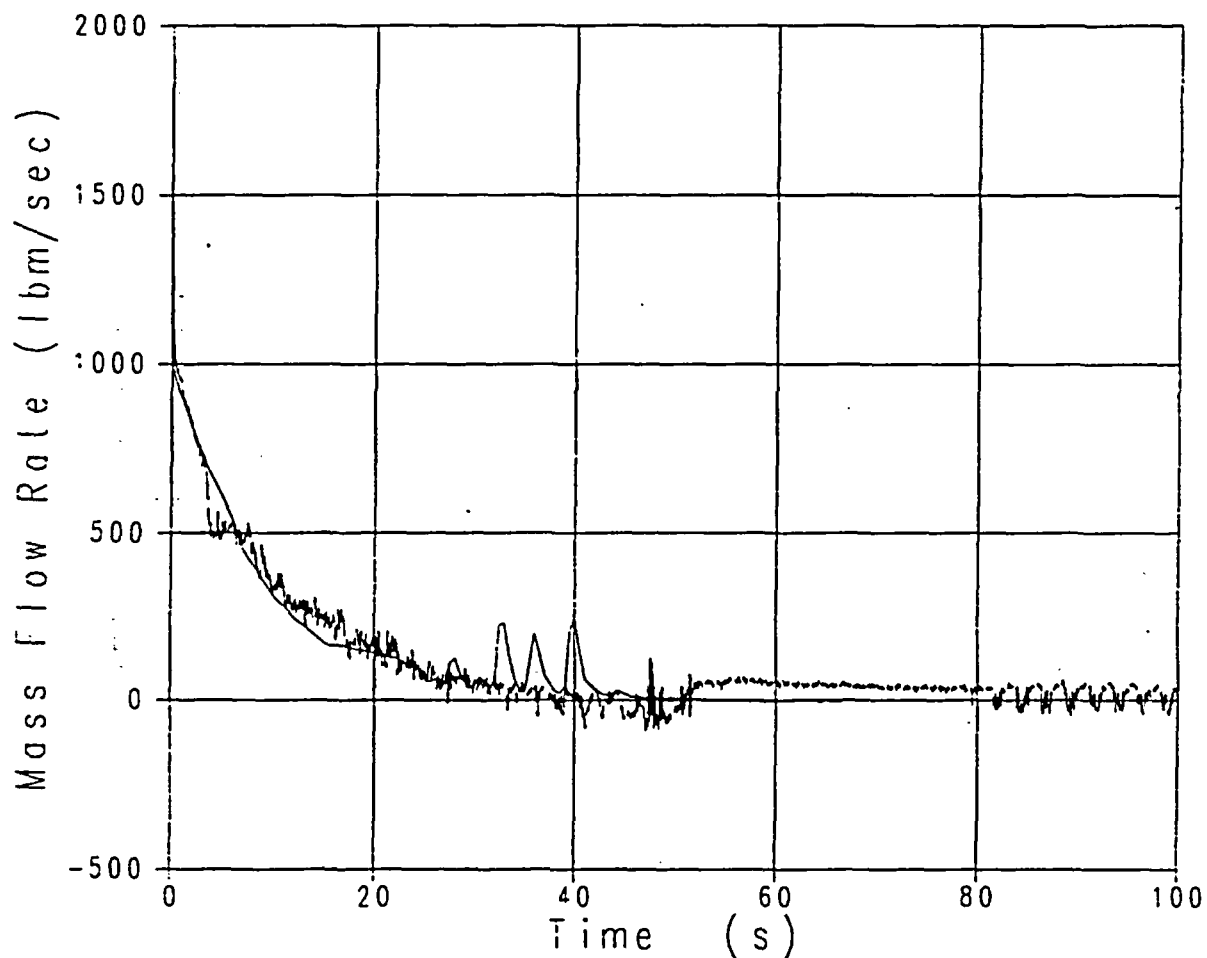


Figure B-33a. Predicted (Component 950) and Measured (FR-BL-116) Mass Flowrate in Broken Cold Leg, Test L2-2 with MOD7A Rev. 0

# LOFT L22 WC/T Mod7A-Rev6 Simulations COLD LEG Bk Flow Rate

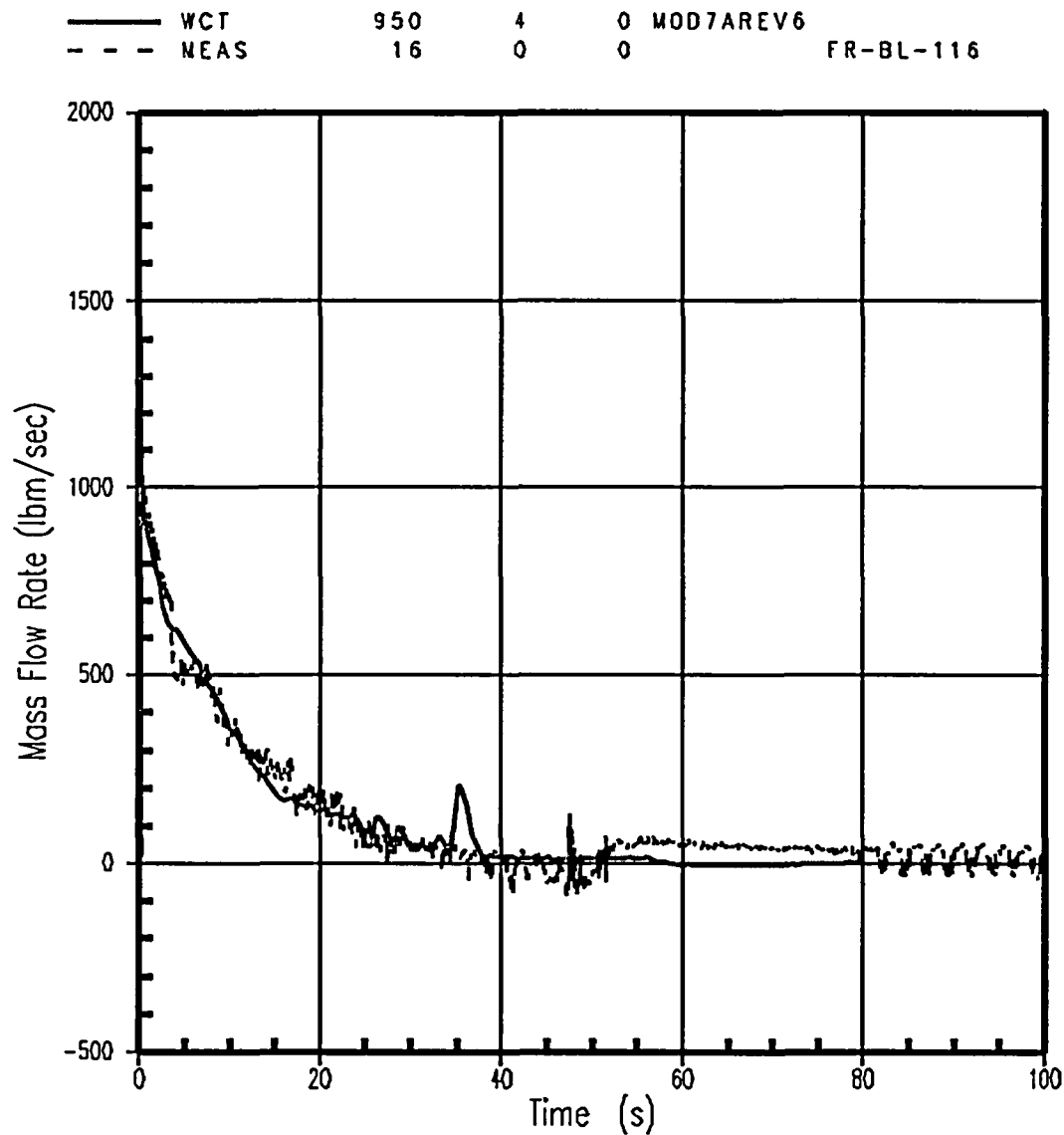


Figure B-33b. Predicted (Component 950) and Measured (FR-BL-116) Mass Flowrate in Broken Cold Leg, Test L2-2 with MOD7A Rev. 6

# LOFT L22 MOD7A vs. DATA INTACT LOOP Flow Rate

——— V-400027 300 4 0 MASS FLOWRATE  
 - - - V-400031 3 0 0 FT-P129-27

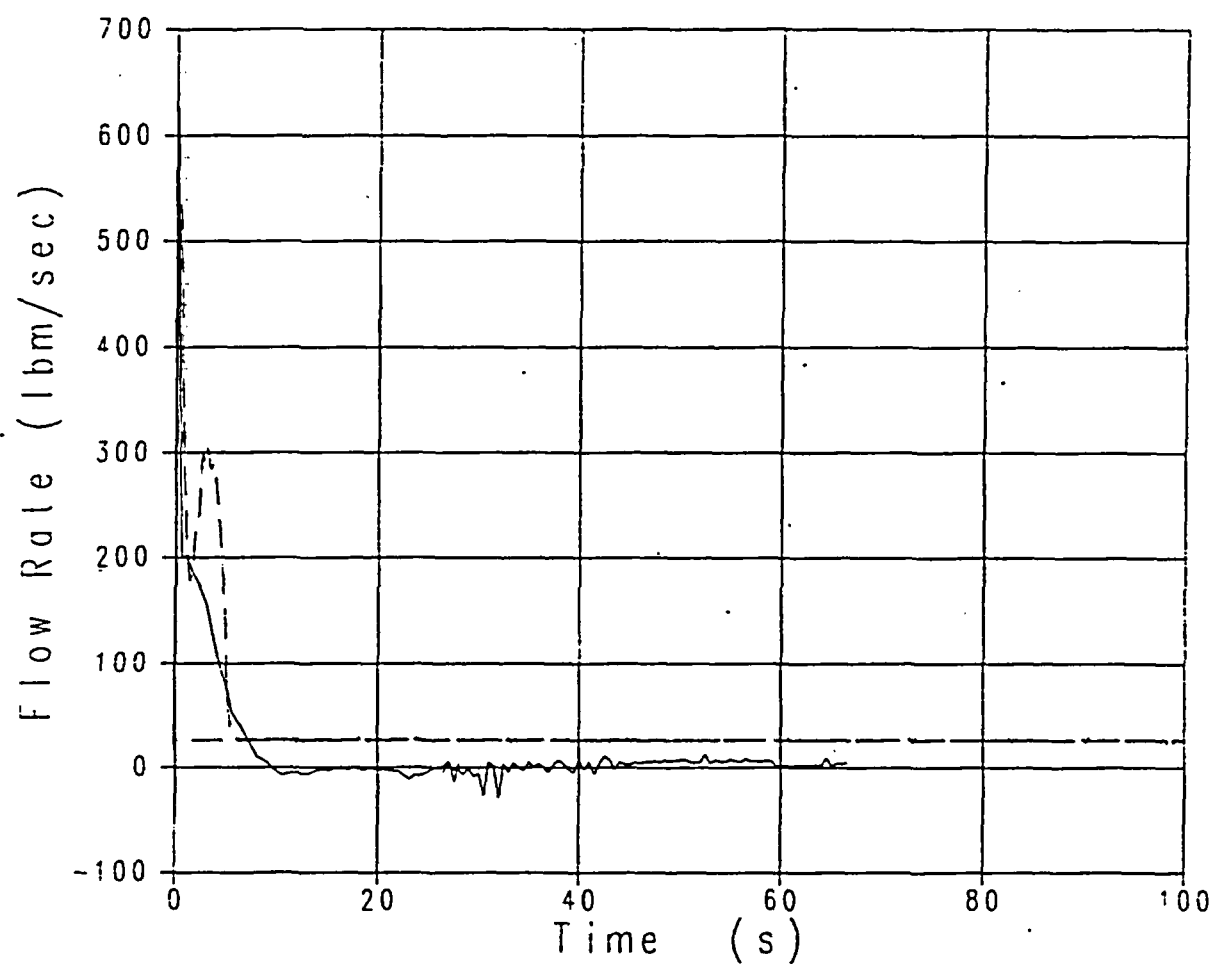


Figure B-34a. Predicted (Component 300) and Measured (FT-P129-27) Mass Flowrate in Intact Hot Leg, Test L2-2 with MOD7A Rev. 0

# LOFT L22 WC/T Mod7A-Rev6 Simulations INTACT LOOP HL Flow Rate

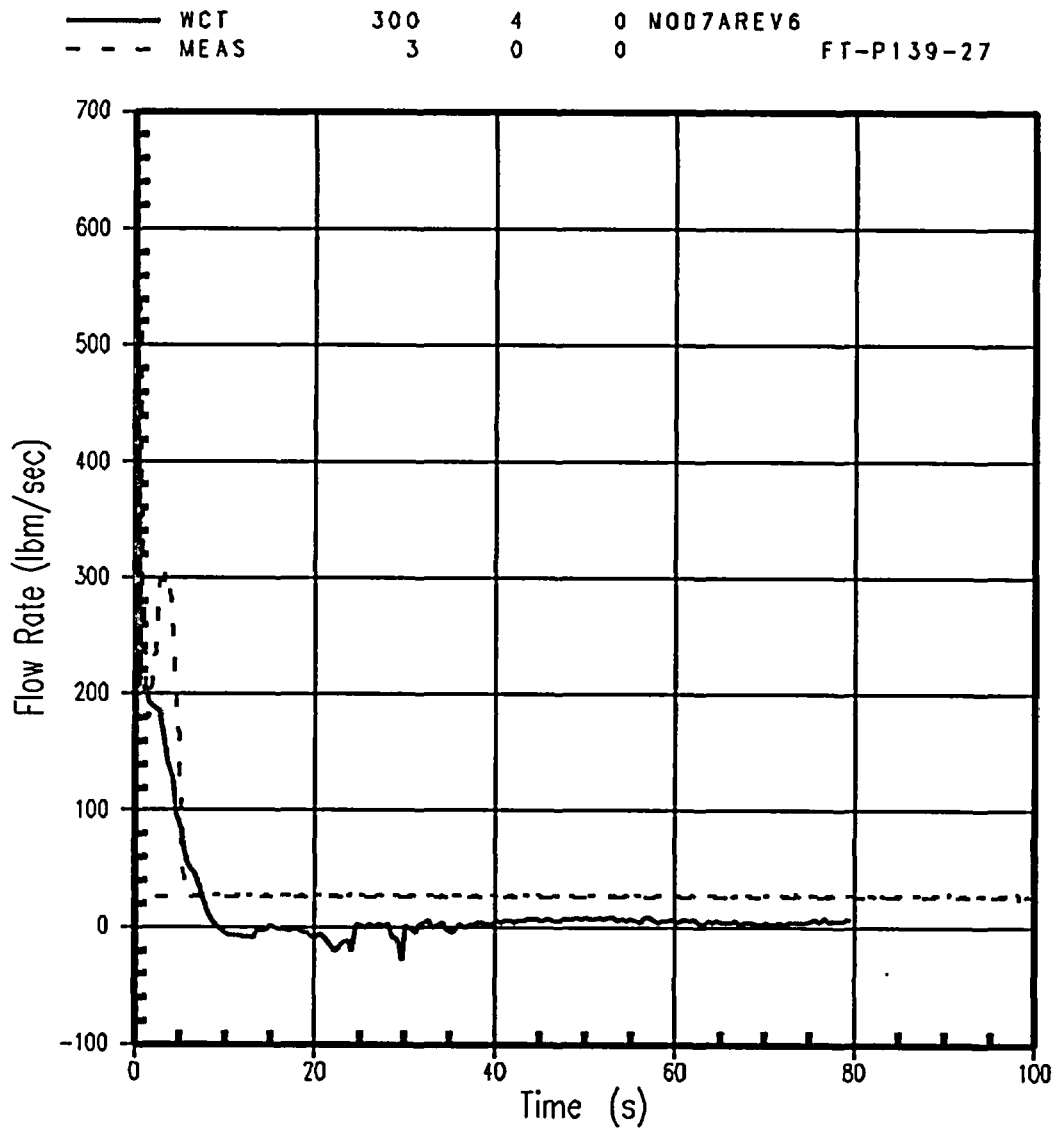


Figure B-34b. Predicted (Component 300) and Measured (FT-P129-27) Mass Flowrate in Intact Hot Leg, Test L2-2 with MOD7A Rev. 6

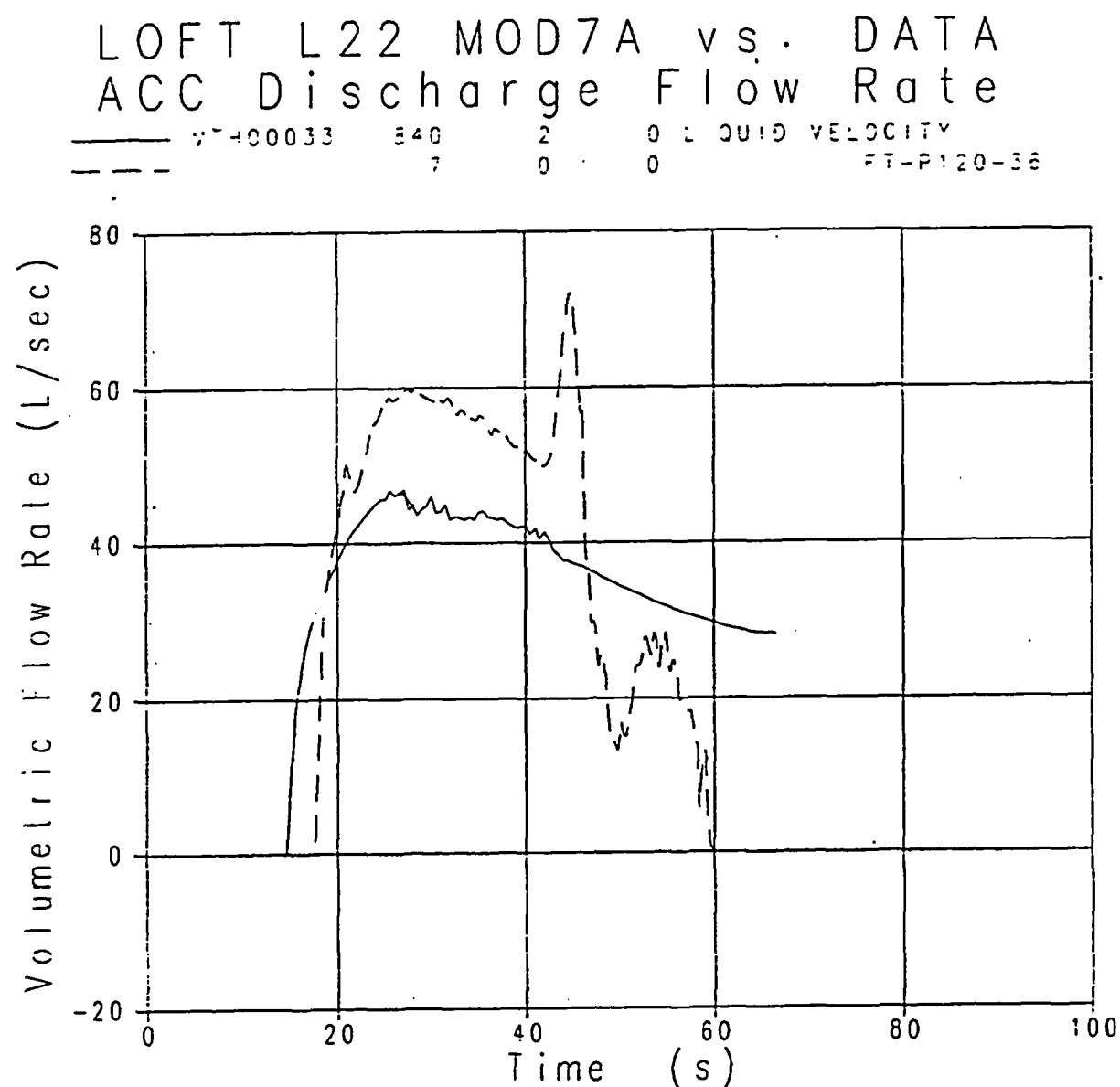


Figure B-35a. Predicted (Component 840) and Measured (FT-P120-36) Volumetric Flowrate in Accumulator, Test L2-2 with MOD7A Rev. 0

# LOFT L22 WC/T Mod7A-Rev6 Simulations ACC Discharge Flow Rate

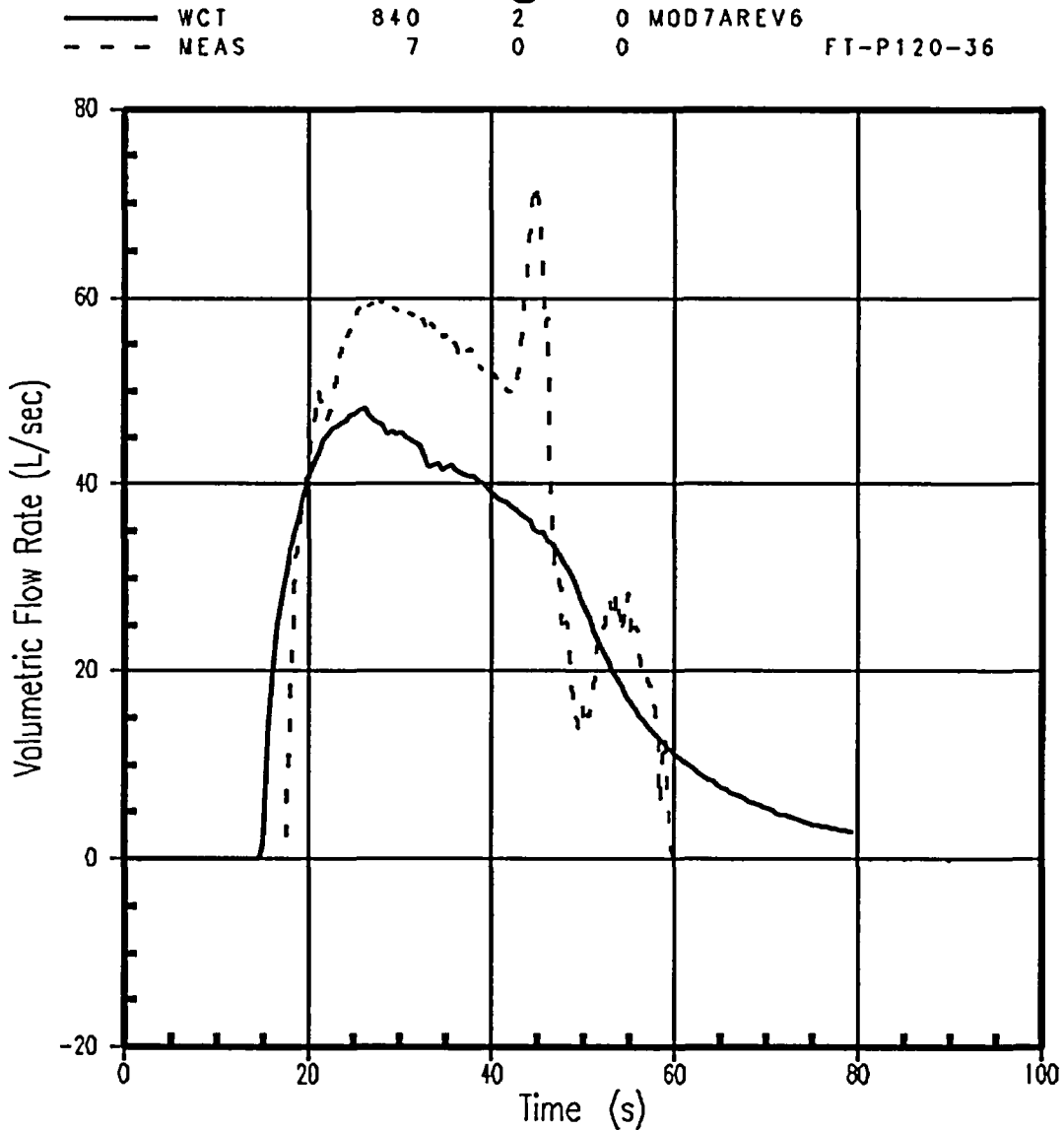


Figure B-35b. Predicted (Component 840) and Measured (FT-P120-36) Volumetric Flowrate in Accumulator, Test L2-2 with MOD7A Rev. 6

# LOFT L22 MOD7A vs. DATA HOT Rod Cladding Temperature

— T<sub>CLAD</sub> 40 ELEV. 2.87 FT  
 --- V<sub>100040</sub> 178 0 0 TE-5F4-030

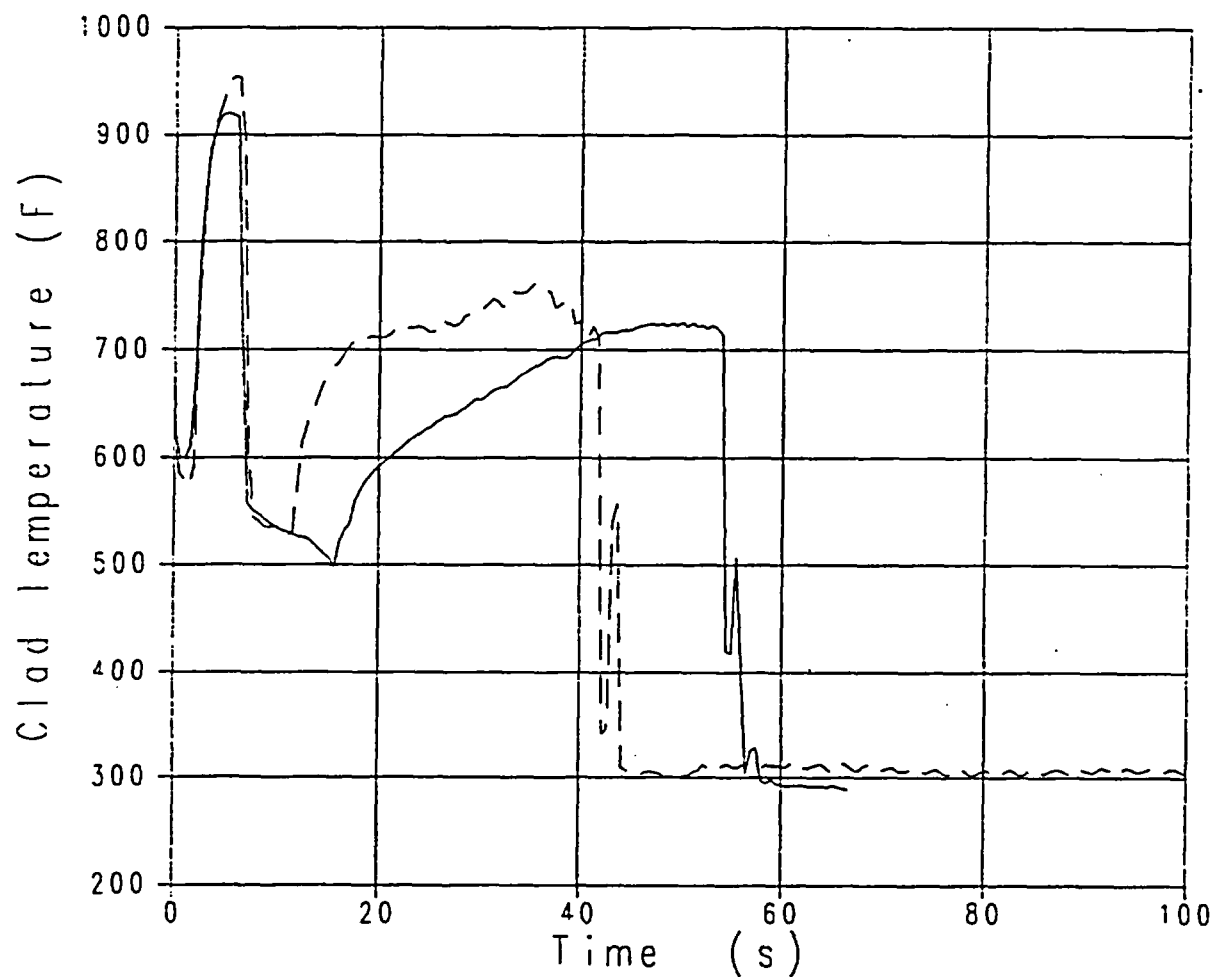


Figure B-36a. Predicted (2.87 ft) and Measured (TE-5F4-030) Cladding Temperature in the Hot Channel, Test L2-2 with MOD7A Rev. 0

# LOFT L22 WC/T Mod7A-Rev6 Simulations HOT Rod Cladding Temperature

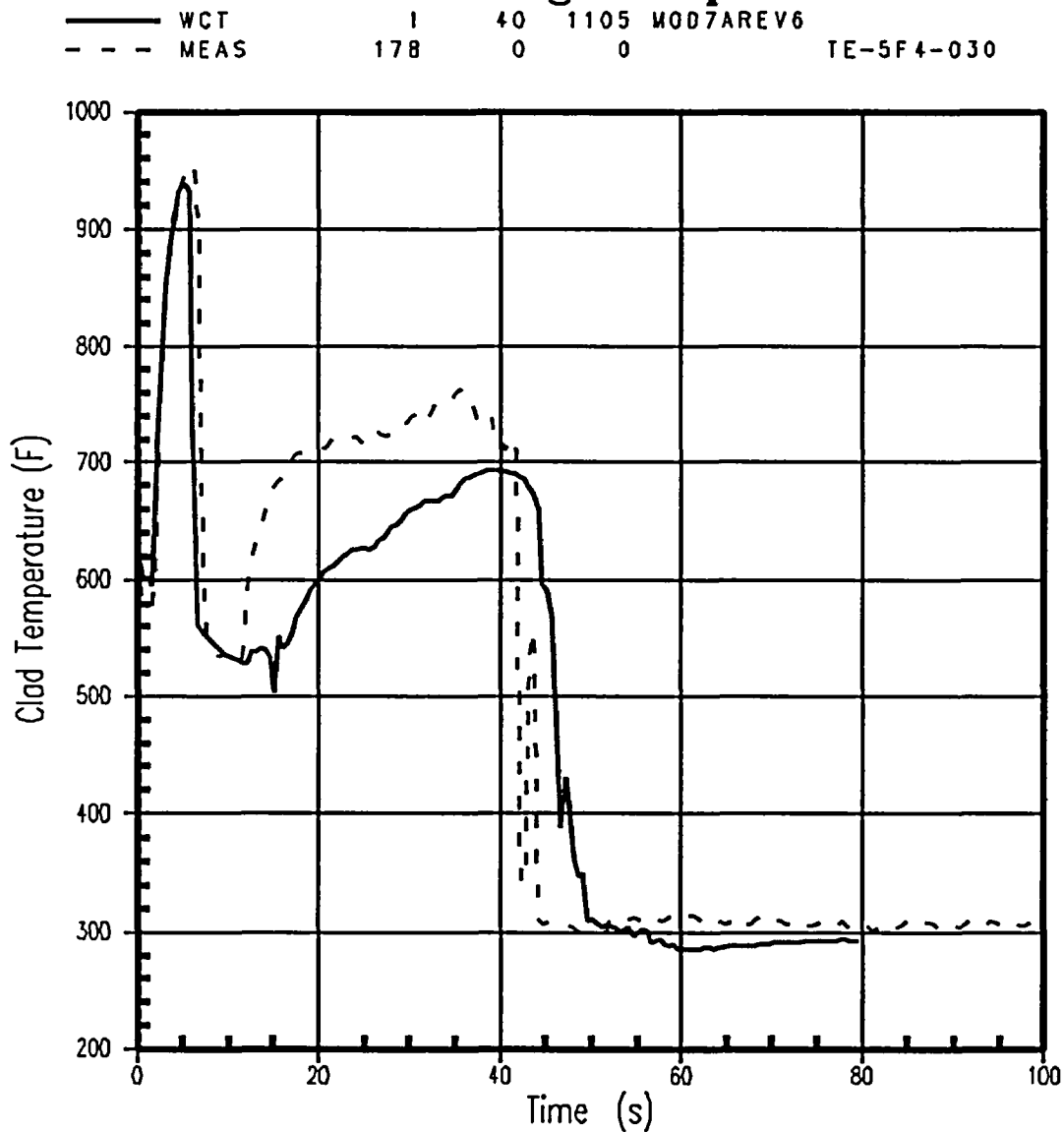


Figure B-36b. Predicted (2.87 ft) and Measured (TE-5F4-030) Cladding Temperature in the Hot Channel, Test L2-2 with MOD7A Rev. 6



a,c

**Figure B-37. Revised Broken Cold Leg Modeling**

b

**Figure B-38. SCTF Run 619 Cladding Temperature at 6.25 ft for Channel 5 (Rod 2)  
MOD7A vs. Data Comparison**

b

**Figure B-39. SCTF Run 619 Cladding Temperature at 6.25 ft for Channel 5-(Rod 2):  
MOD7A Rev. 6 vs. Data Comparison**

b

**Figure B-40. SCTF Run 619 Cladding Temperature at 8.35 ft for Channel 5-(Rod 2)  
MOD7A vs. Data Comparison**

b

**Figure B-41. SCTF Run 619 Cladding Temperature at 8.35 ft for Channel 5-(Rod 2)  
MOD7A Rev. 6 vs. Data Comparison**

b

**Figure B-42. SCTF Run 619 Cladding Temperature at 9.76 ft for Channel 5-(Rod 2)  
MOD7A vs. Data Comparison**

b

**Figure B-43. SCTF Run 619 Cladding Temperature at 9.76 ft for Channel 5-(Rod 2)  
MOD7A Rev. 6 vs. Data Comparison**

b

**Figure B-44. SCTF Run 619 Liquid Level in Core: MOD7A vs. Data Comparison**



b

**Figure B-45. SCTF Run 619 Liquid Level in Core: MOD7A Rev. 6 vs. Data Comparison**

b

**Figure B-46. SCTF Run 619 Liquid Level in Inner Global Region of Upper Plenum:  
MOD7A vs. Data Comparison**

b

**Figure B-47. SCTF Run 619 Liquid Level in Inner Global Region of Upper Plenum:  
MOD7A Rev. 6 vs. Data Comparison**

b

**Figure B-48. CCTF Run 62 Cladding Temperature at 6.0 ft: MOD7A Rev. 0 vs. Data Comparison**

b

**Figure B-49. CCTF Run 62 Cladding Temperature at 6.0 ft: MOD7A Rev. 6 vs. Data Comparison**

b

**Figure B-50. CCTF Run 62 Cladding Temperature at 8.0 ft: MOD7A Rev. 0 vs. Data Comparison**

b

**Figure B-51. CCTF Run 62 Cladding Temperature at 8.0 ft: MOD7A Rev. 6 vs. Data Comparison**

b

**Figure B-52. CCTF Run 62 Cladding Temperature at 10.0 ft: MOD7A Rev. 0 vs. Data Comparison**



b

**Figure B-53. CCTF Run 62 Cladding Temperature at 10.0 ft: MOD7A Rev. 6 vs. Data Comparison**

b

**Figure B-54. CCTF Run 62 Vapor Temperature at 6.0 ft for Channel 9**

b

**Figure B-55. CCTF Run 62 Vapor Temperature at 6.0 ft: MOD7A Rev. 6 vs. Data Comparison**

b

**Figure B-56. CCTF Run 62 Liquid Level in Core**

b

**Figure B-57. CCTF Run 62 Liquid Level in Core: MOD7A Rev. 6 vs. Data Comparison**

b

**Figure B-58. CCTF Run 62 Liquid Level in Upper Plenum**

b

**Figure B-59. CCTF Run 62 Liquid Level in Upper Plenum: MOD7A Rev. 6 vs. Data Comparison**

b

**Figure B-60. CCTF Run 62 Pressure Difference Across Intact Loop**



b

**Figure B-61. CCTF Run 62 Pressure Difference Across Intact Loop: MOD7A Rev. 6 vs.  
Data Comparison**

b

**Figure B-62. CCTF Run 62 Pressure Difference Across Broken Loop**

b

**Figure B-63. CCTF Run 62 Pressure Difference Across Broken Loop: MOD7A Rev. 6 vs. Data Comparison**

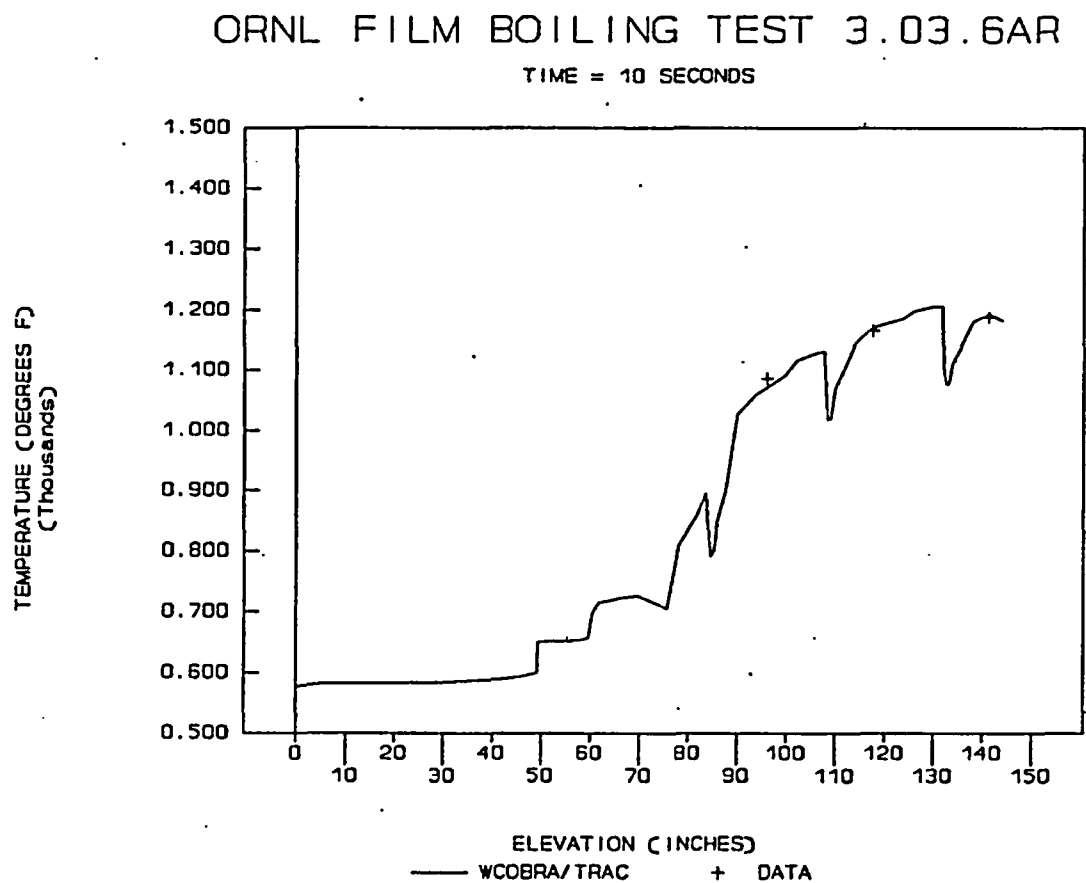


**Figure B-64. Axial Heater Rod Temperature Profile at 10 Seconds of Transient for Test 3.03.6AR: MOD7A Rev. 0 vs. Data Comparison**

# ORNL Film Boiling Test 3.03.6AR

## Cladding Temperature Axial Profile Comparison at 10 seconds

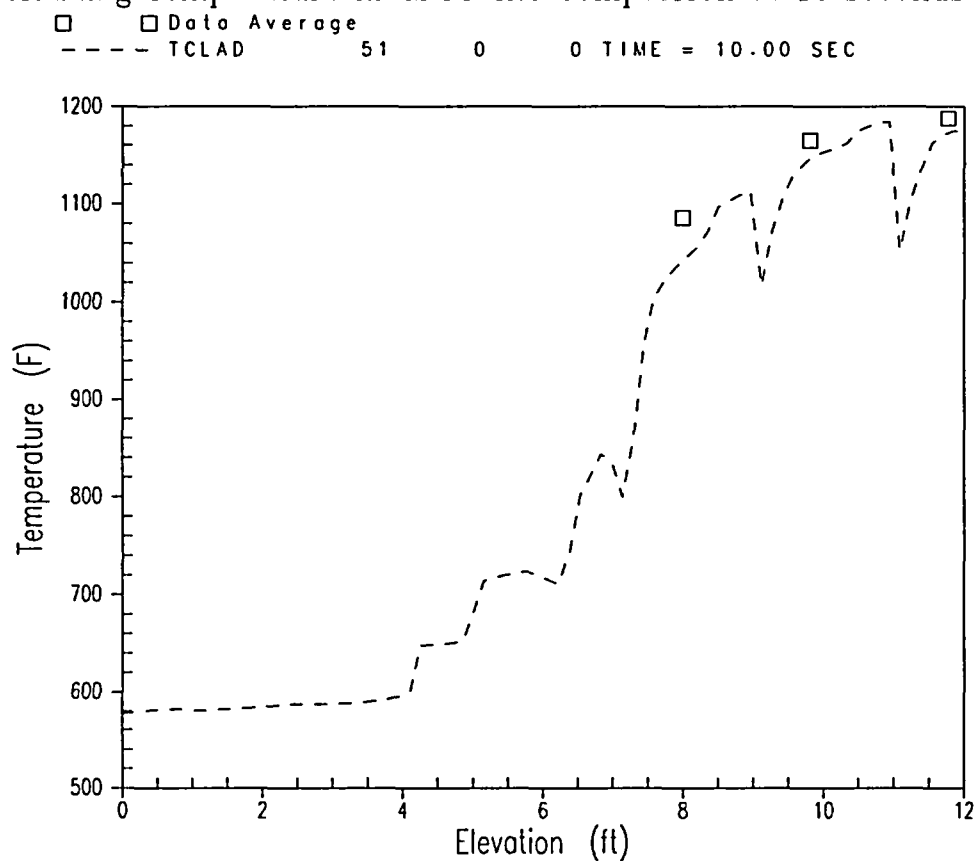


Figure B-65. Axial Heater Rod Temperature Profile at 10 Seconds of Transient for Test 3.03.6AR: MOD7A Rev. 6 vs. Data Comparison

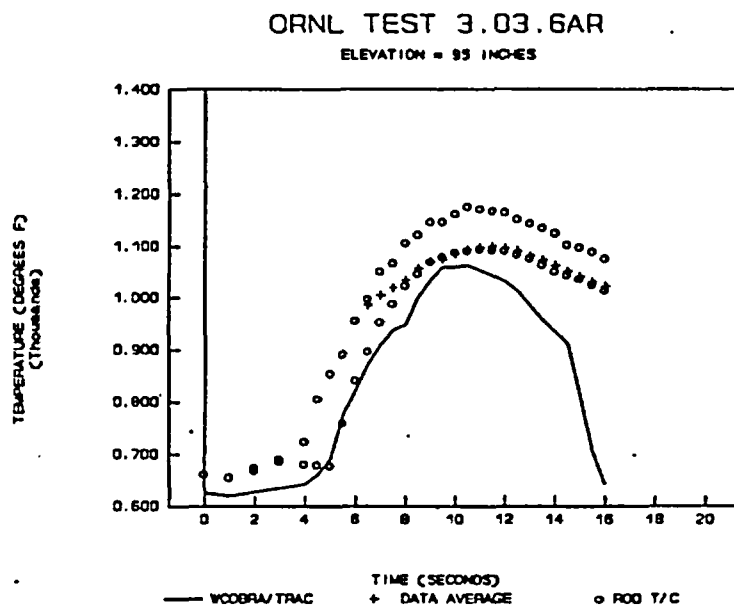


Figure B-66. Transient Heater Rod Temperature at 95 inches for Test 3.03.6AR, Nominal Inlet Flow Conditions: WCOBRA/TRAC MOD7A Rev. 0 vs. Data Comparison

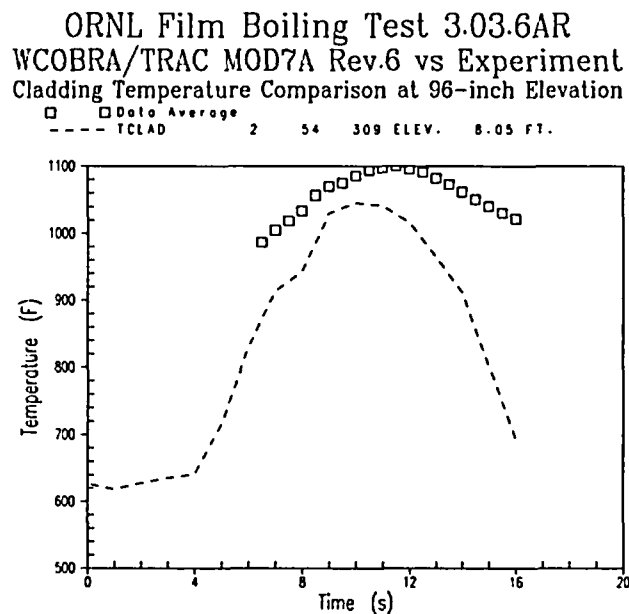
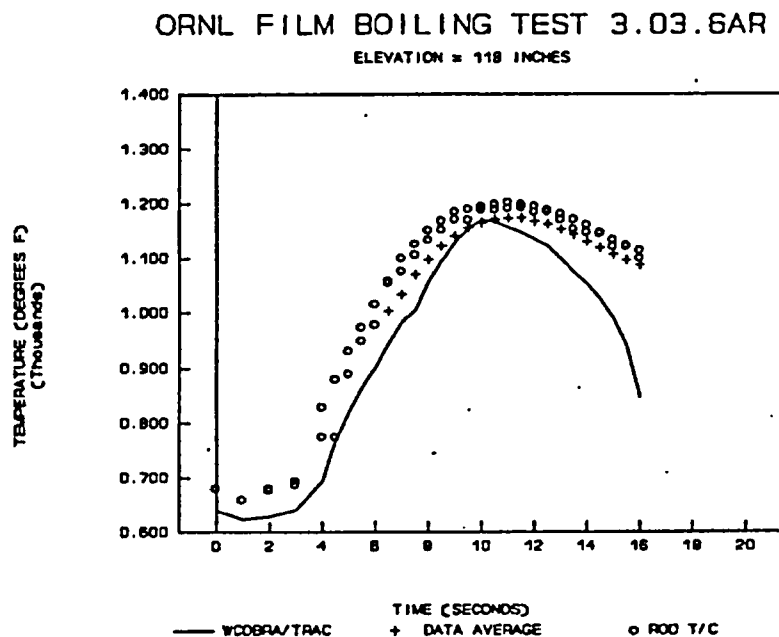
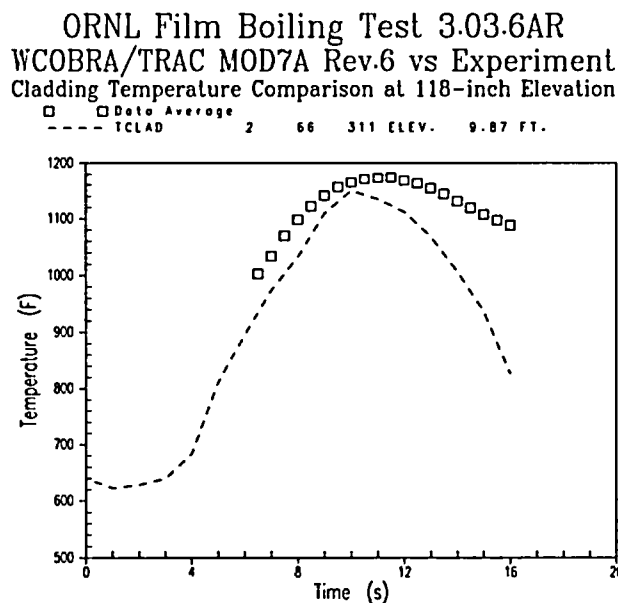


Figure B-67. Transient Heater Rod Temperature at 96-inch Elevation: WCOBRA/TRAC MOD7A Rev. 6 vs. Data Comparison



**Figure B-68. Transient Heater Rod Temperature at 118-(Near Level F) inches for Test 3.03.6AR, Nominal Inlet Flow: MOD7A Rev. 0 vs. Data Comparison**



**Figure B-69. ORNL Test 3.03.6AR Cladding Temperature Comparison at 118-inch Elevation: MOD7A Rev. 6 vs. Data Comparison**

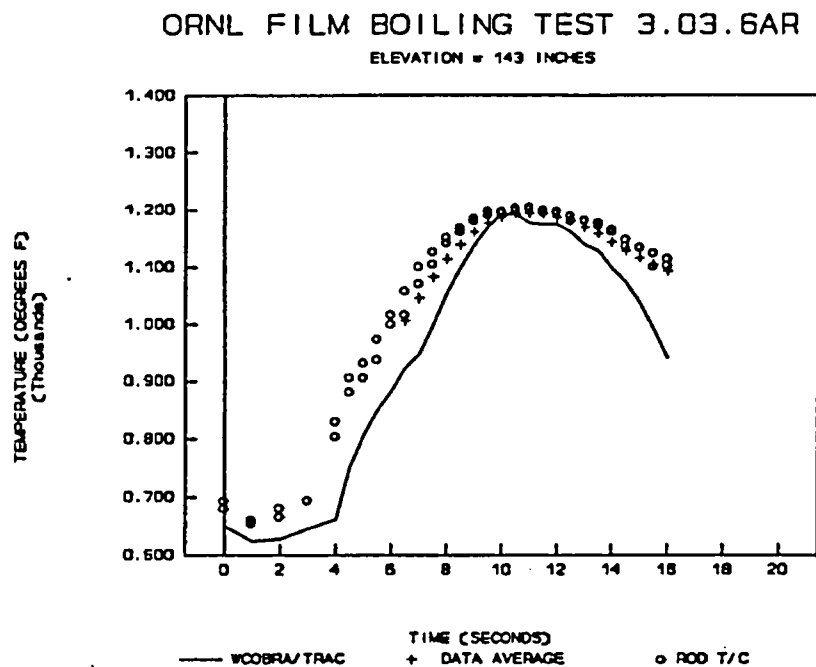


**Figure B-70. Transient Heater Rod Temperature at 143 inches for Test 3.03.6AR, Nominal Inlet Flow: MOD7A Rev. 0 vs. Data Comparison**

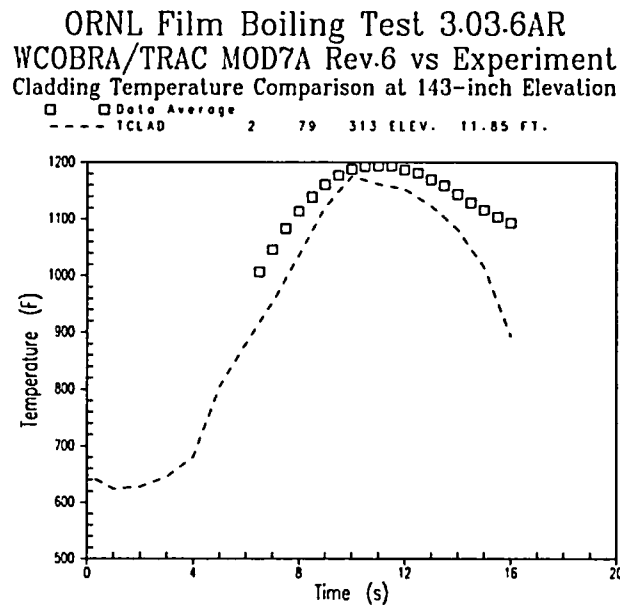


**Figure B-71. ORNL Test 3.03.6AR Cladding Temperature Comparison at 143-inch Elevation: MOD7A Rev. 6 vs. Data Comparison**



b

**Figure B-72. G-2 Refill Test 760 Cladding Temperature Time History Comparison (12.3-inch Elevation): MOD7A Rev. 0 vs. Data**

b

**Figure B-73. G-2 Refill Test 760 Cladding Temperature Comparison at 12.3-inch Elevation: MOD7A Rev. 6 vs. Data**

b

**Figure B-74. G-2 Refill Test 760 Cladding Temperature Time History Comparison (28.7-inch Elevation) MOD7A Rev. 0 vs. Data**

b

**Figure B-75. G-2 Refill Test 760 Cladding Temperature Comparison at 28.7-inch Elevation: MOD7A Rev. 6 vs. Data**

b

**Figure B-76. G-2 Refill Test 760 Cladding Temperature Time History Comparison (45.1-inch Elevation) MOD7A Rev. 0 vs. Data**

b

**Figure B-77. G-2 Refill Test 760 Cladding Temperature Comparison at 45.1-inch Elevation: MOD7A Rev. 6 vs. Data**

b

**Figure B-78. G-2 Refill Test 760 Cladding Temperature Time History Comparison (82.0-inch Elevation) MOD7A Rev. 0 vs. Data**

b

**Figure B-79. G-2 Refill Test 760 Cladding Temperature Comparison at 82.0-inch Elevation: MOD7A Rev. 6 vs. Data**

b

**Figure B-80. G-2 Refill Test 760 Cladding Temperature Time History Comparison (118.9-inch Elevation) MOD7A Rev. 0 vs. Data**

b

**Figure B-81. G-2 Refill Test 760 Cladding Temperature Comparison at 118.9-inch Elevation: MOD7A Rev. 6 vs. Data**



**Figure B-82. G-2 Refill Test 760 Axial Cladding Temperature Comparison (Time = 50 Seconds)  
MOD7A Rev. 0 vs. Data**

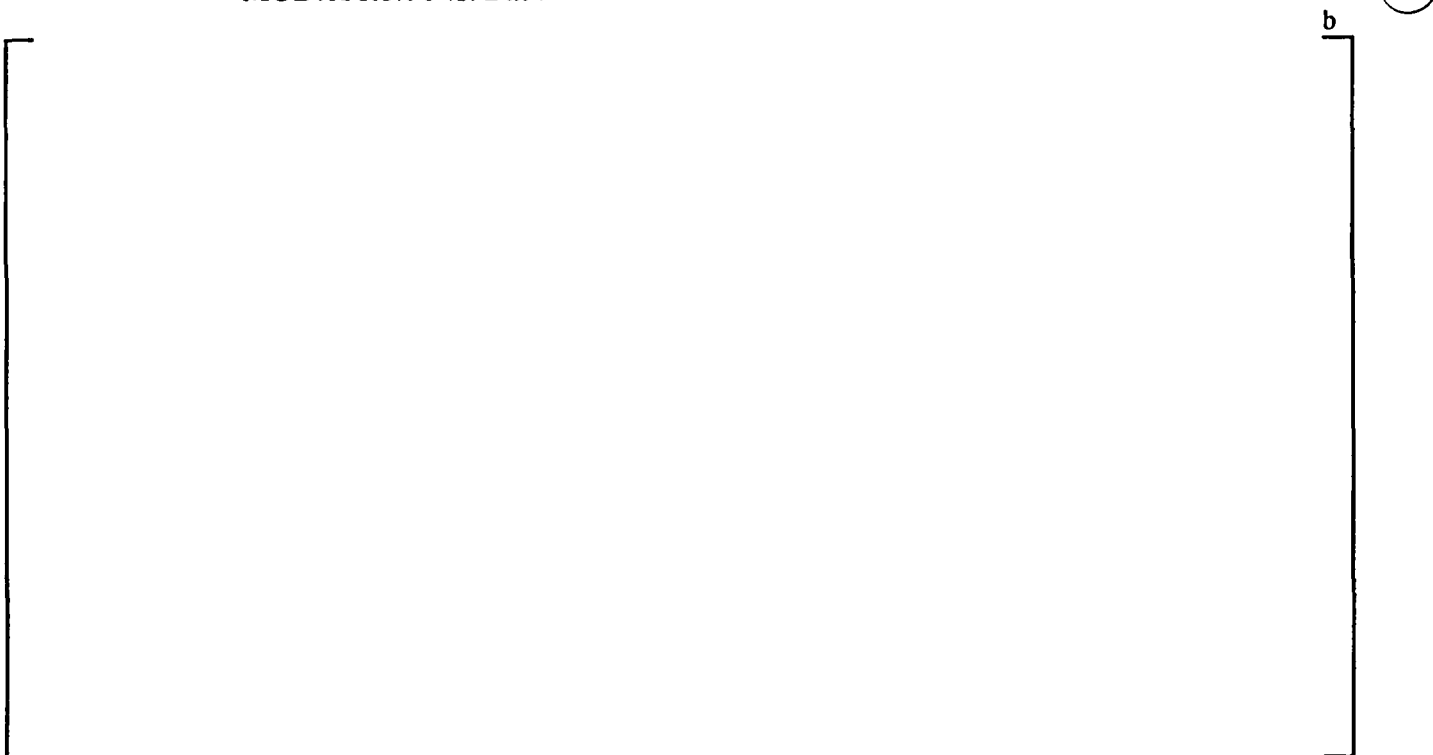


**Figure B-83. G-2 Refill Test 760 Axial Cladding Temperature at 50 Seconds, MOD7A Rev. 6  
Results**

Figure B-84a. Measured Absolute Pressure in the Upper Plenum and Downcomer, Test 6 - Run 131

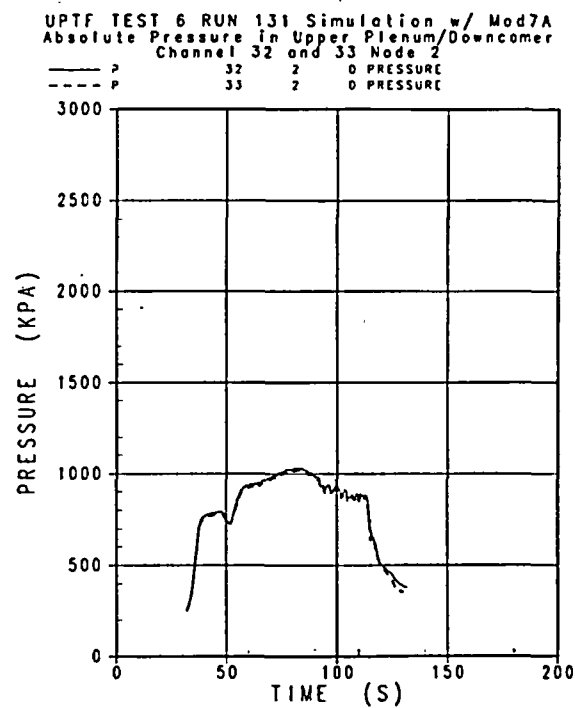


Figure B-84b. Predicted Absolute Pressure in the Upper Plenum and Downcomer, Test 6 - Run 131 with MOD7A

UPTF TEST 6 RUN 131 Simulation w/ mod7ar6  
Absolute Pressure in Upper Plenum/Downcomer  
Channel 32 and 33 Node 2

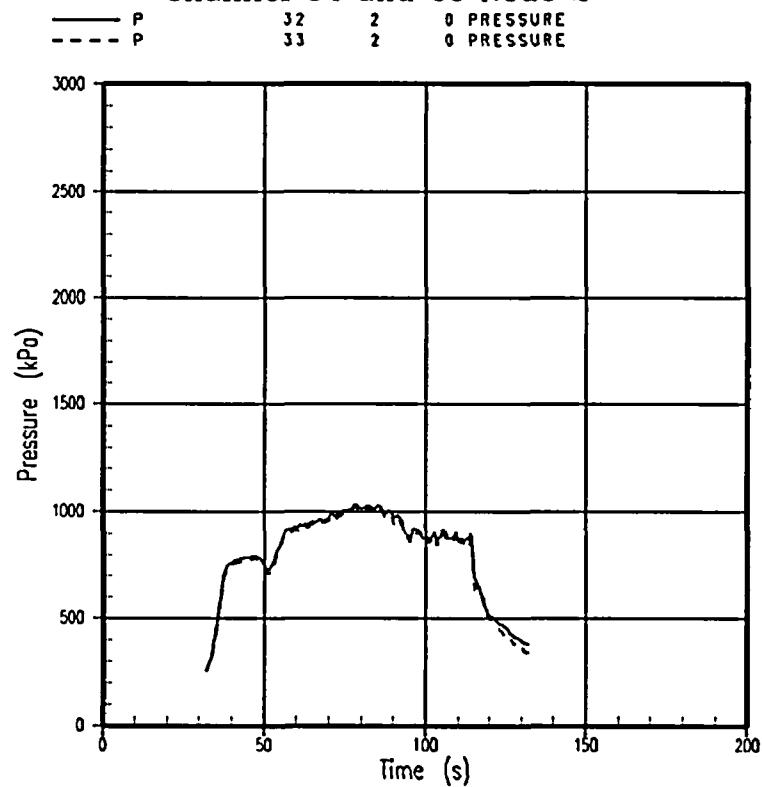


Figure B-84c. Predicted Absolute Pressure in the Upper Plenum and Downcomer,  
Test 6 -Run 131 with MOD7A Rev. 6



b

Figure B-85a. Measured Downcomer Fluid Temperature at Level 21, Test 6 - Run 131

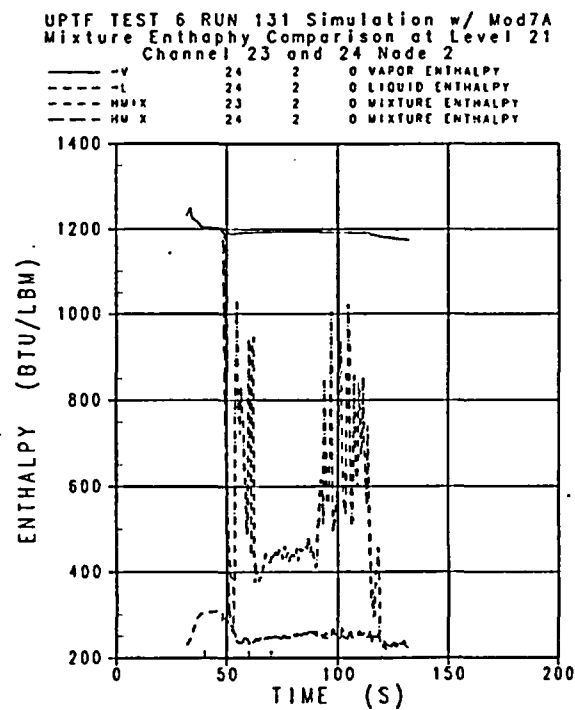


Figure B-85b. Predicted Mixture Enthalpy at Level 21, Test 6 - Run 131 with MOD7A

UPTF TEST 6 RUN 131 Simulation w/ mod7ar6  
Mixture Enthapfy Comparison at Level 21  
Channel 23 and 24 Node 2

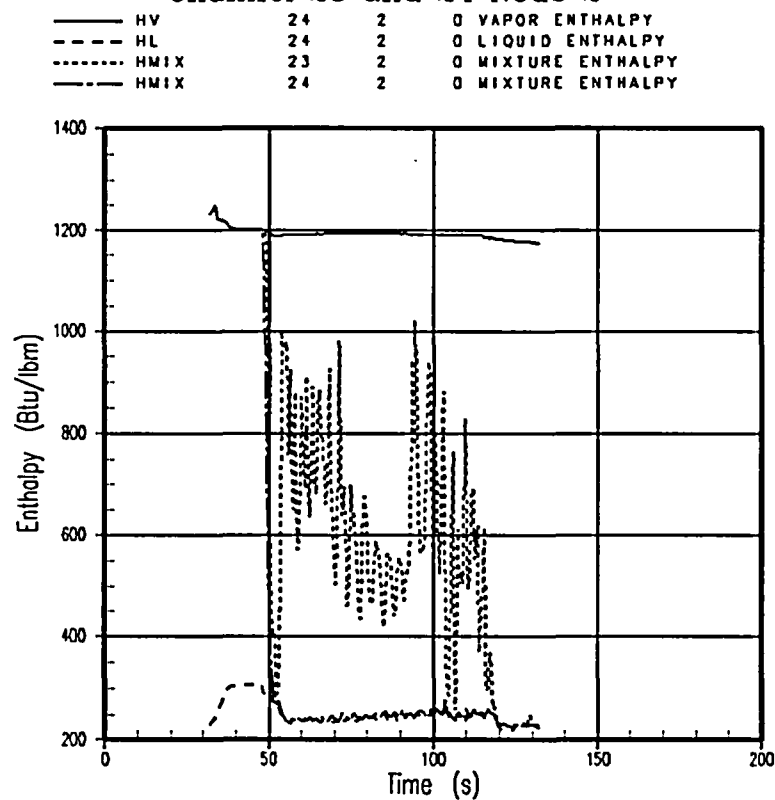


Figure B-85c. Predicted Mixture Enthalpy at Level 21, Test 6 - Run 131 with MOD7A Rev. 6

b

Figure B-86a. Measured Downcomer Fluid Temperature at Level 01, Test 6 - Run 131

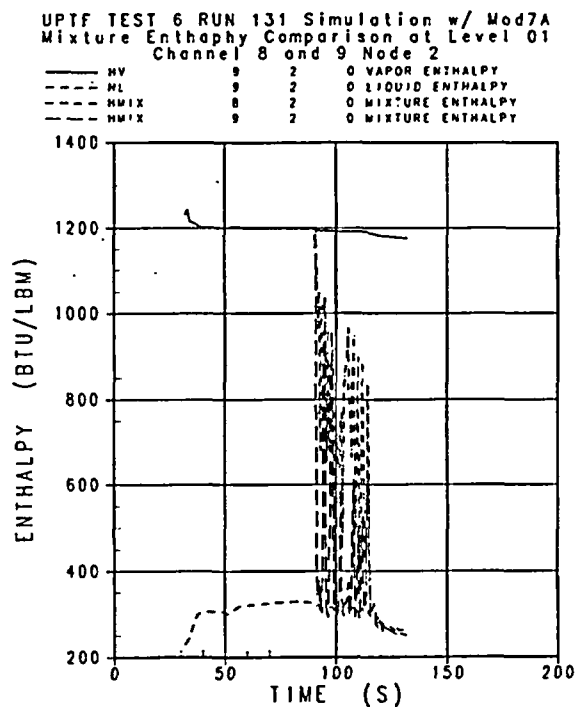


Figure B-86b. Predicted Downcomer Mixture Enthalpy at Level 01, Test 6 - Run 131 with MOD7A

UPTF TEST 6 RUN 131 Simulation w/ mod7ar6  
Mixture Enthapny Comparison at Level 01  
Channel 8 and 9 Node 2

— HV	9	2	0 VAPOR ENTHALPY
- - HL	9	2	0 LIQUID ENTHALPY
- · - HMIX	8	2	0 MIXTURE ENTHALPY
- · - HMIX	9	2	0 MIXTURE ENTHALPY

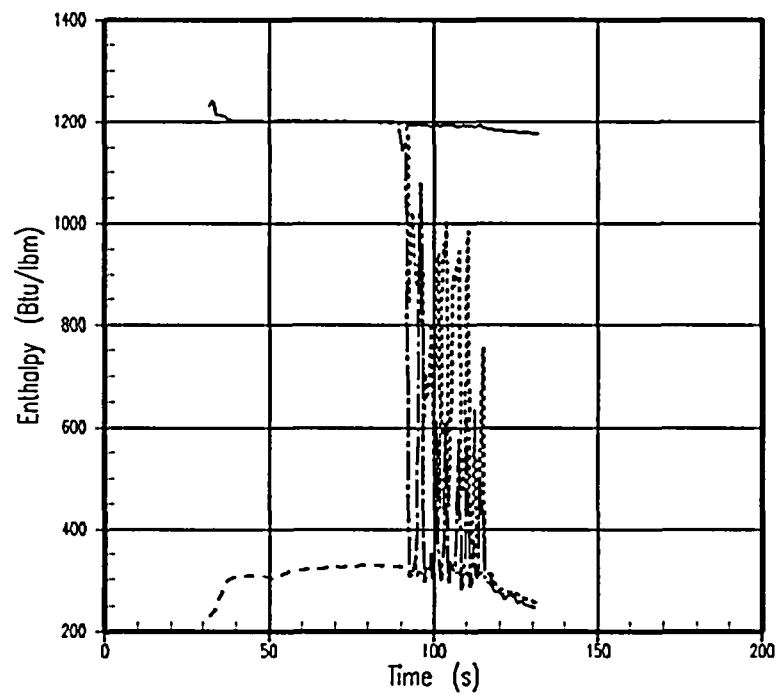


Figure B-86c. Predicted Downcomer Mixture Enthalpy at Level 01, Test 6 - Run 131 with MOD7A Rev. 6

**Figure B-87a. Predicted Liquid Flow at Bottom of Downcomer in Intact Side (Channels 8 and 9),  
Test 6 - Run 131 with MOD7A**

UPTF TEST 6 RUN 131 Simulation w/ mod7ar6  
Predicted Downcomer Liquid Flowrate at Bottom of Intact Side  
Channels 8 and 9

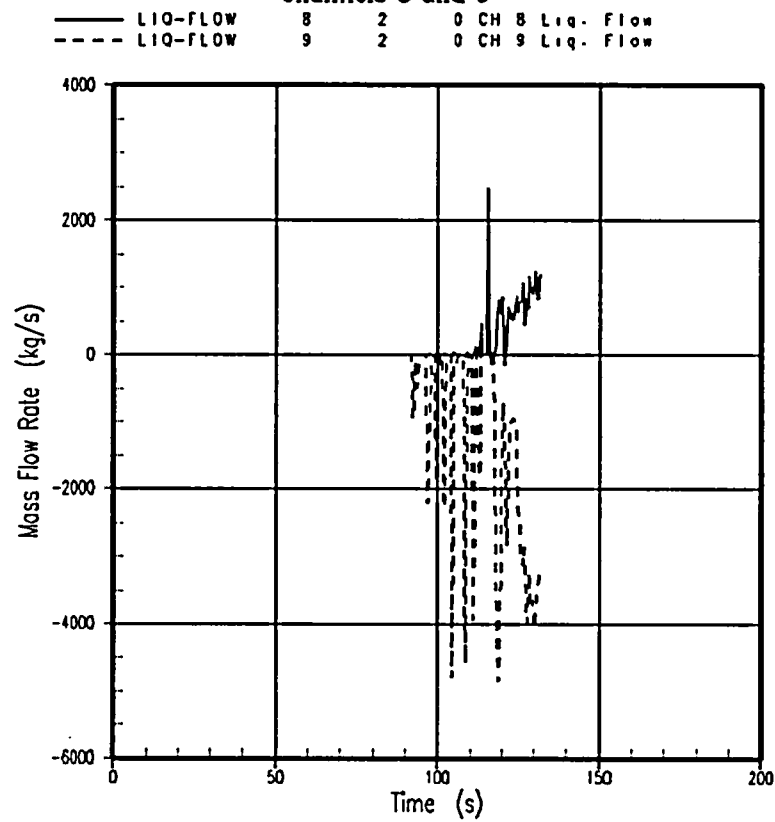


Figure B-87b. Predicted Liquid Flow at Bottom of Downcomer in Intact Side (Channels 8 and 9),  
Test 6 - Run 131 with MOD7A Rev. 6

**Figure B-88a. Predicted Liquid Flow at Bottom of Downcomer in Broken Side (Channels 10 and 11), Test 6 - Run 131 with MOD7A**

UPTF TEST 6 RUN 131 Simulation w/ mod7ar6  
Predicted Downcomer Liquid Flowrate at Bottom of Intact Side  
Channels 10 and 11

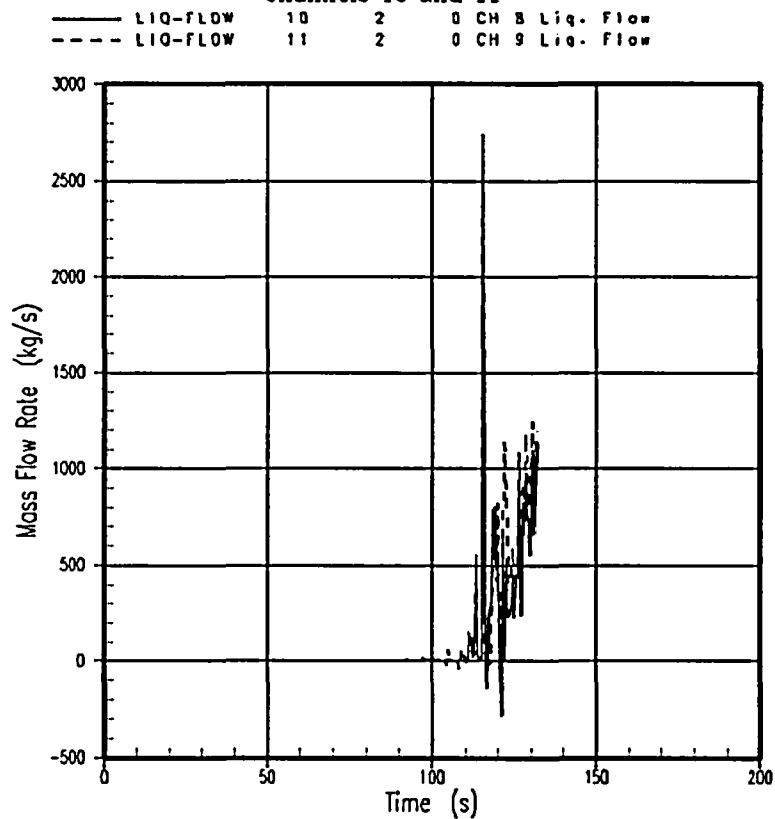


Figure B-88b. Predicted Liquid Flow at Bottom of Downcomer in Broken Side (Channels 10 and 11), Test 6 - Run 131 with MOD7A Rev. 6



b

Figure B-89a. Measured Differential Pressure Between Upper Plenum and Downcomer, Test 6 - Run 131

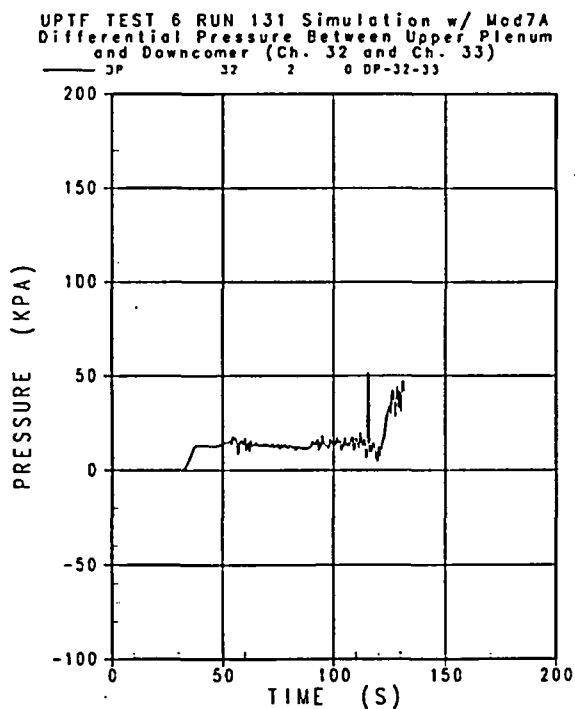


Figure B-89b. Predicted Differential Pressure Between Upper Plenum and Downcomer, Test 6 - Run 131 with MOD7A

UPTF TEST 6 RUN 131 Simulation w/ mod7ar6  
Differential Pressure Between Upper Plenum  
and Downcomer (Ch. 32 and Ch. 33)

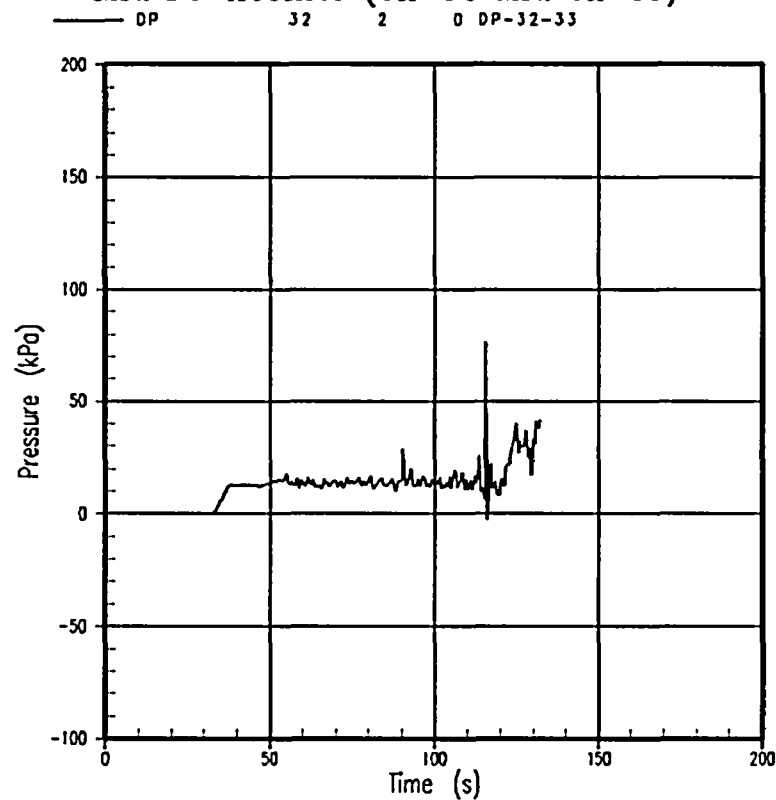


Figure B-89c. Predicted Differential Pressure Between Upper Plenum and Downcomer,  
Test 6 -Run 131 with MOD7A Rev. 6

b

Figure B-90a. Measured Axial Differential Pressure in Downcomer, Test 6 - Run 131

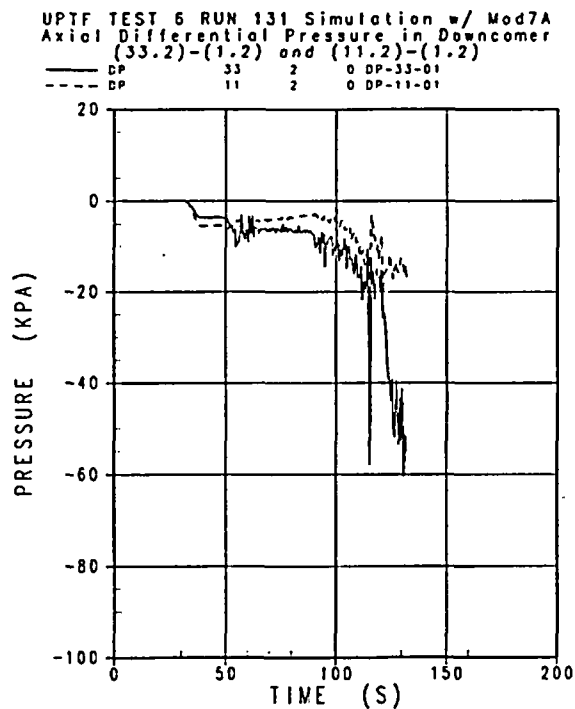


Figure B-90b. Predicted Axial Differential Pressure in Downcomer, Test 6 - Run 131 with MOD7A

UPTF TEST 6 RUN 131 Simulation w/ mod7ar6  
Axial Differential Pressure in Downcomer  
(33.2)-(1.2) and (11.2)-(1.2)

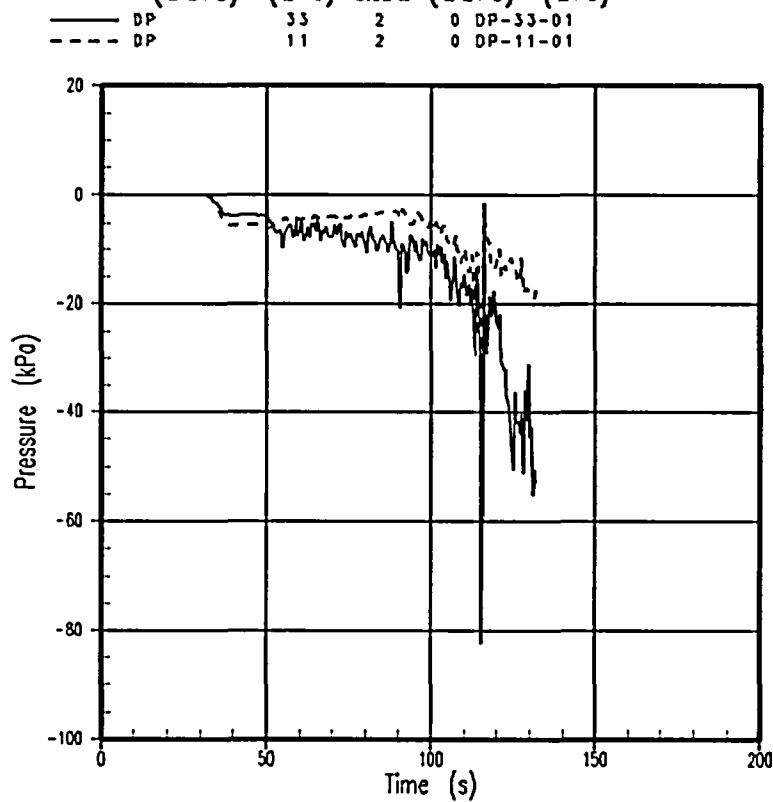


Figure B-90c. Predicted Axial Differential Pressure in Downcomer, Test 6 - Run 131 with MOD7A Rev. 6

b

Figure B-91a. Measured Axial Differential Pressure in Downcomer, Test 6 - Run 131

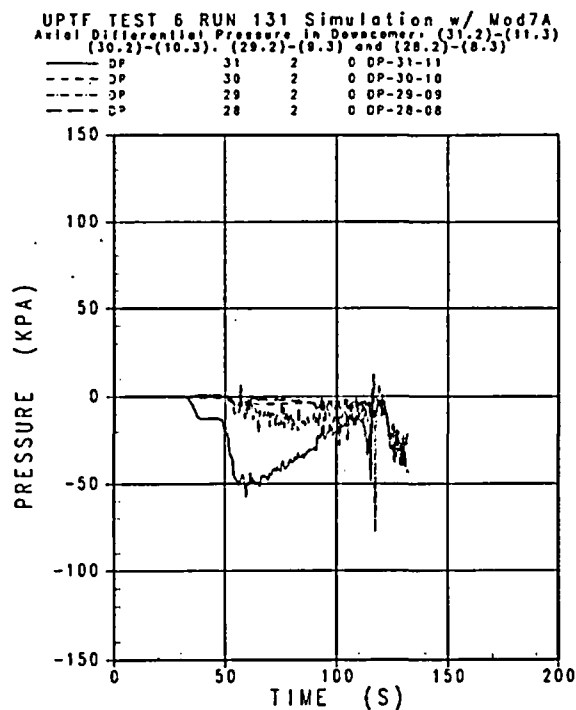


Figure B-91b. Predicted Axial Differential Pressure in Downcomer, Test 6 - Run 131 with MOD7A

UPTF TEST 6 RUN 131 Simulation w/ mod7ar6  
Axial Differential Pressure in Downcomer (31.2)-(11.3)  
(30.2)-(10.3), (29.2)-(9.3) and (28.2)-(8.3)

—	DP	31	2	0	DP-31-11
- - - -	DP	30	2	0	DP-30-10
· · · · ·	DP	29	2	0	DP-29-09
- · - · -	DP	28	2	0	DP-28-08

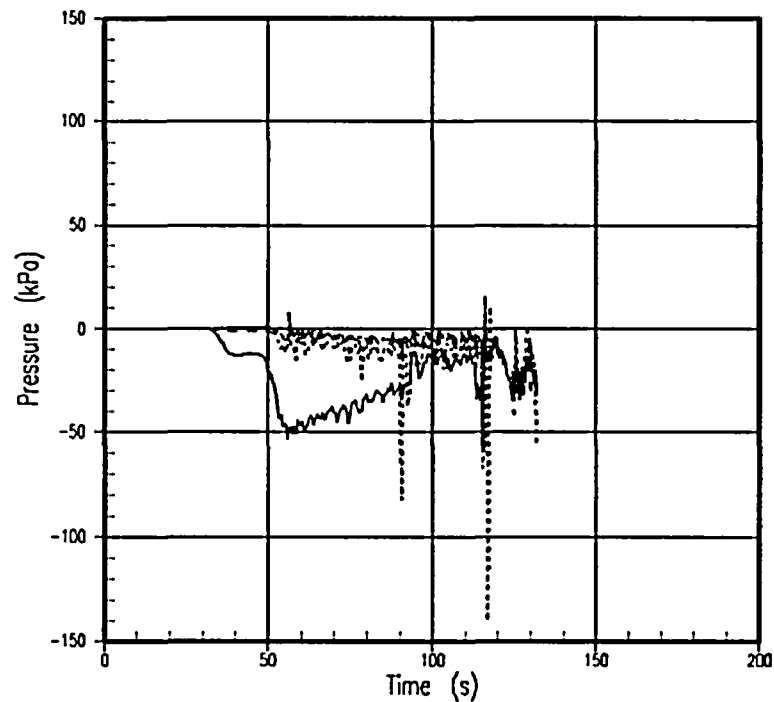


Figure B-91c. Predicted Axial Differential Pressure in Downcomer, Test 6 - Run 131 with MOD7A Rev. 6

b

Figure B-92a. Measured Azimuthal Differential Pressure in Downcomer at Level 06, Test 6 - Run 131

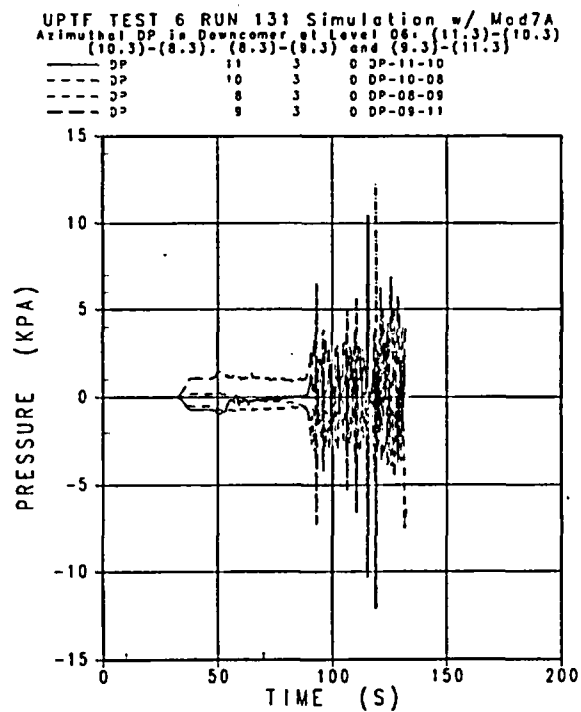


Figure B-92b. Predicted Transverse Differential Pressure in Downcomer at Level 06, Test 6 - Run 131 with MOD7A

UPTF TEST 6 RUN 131 Simulation w/ mod7ar6  
 Azimuthal DP in Downcomer at Level 06: (11.3)-(10.3)  
 (10.3)-(8.3), (8.3)-(9.3) and (9.3)-(11.3)

— DP	11	3	0 DP-11-10
- - - DP	10	3	0 DP-10-08
· · · DP	8	3	0 DP-08-09
- · - DP	9	3	0 DP-09-11

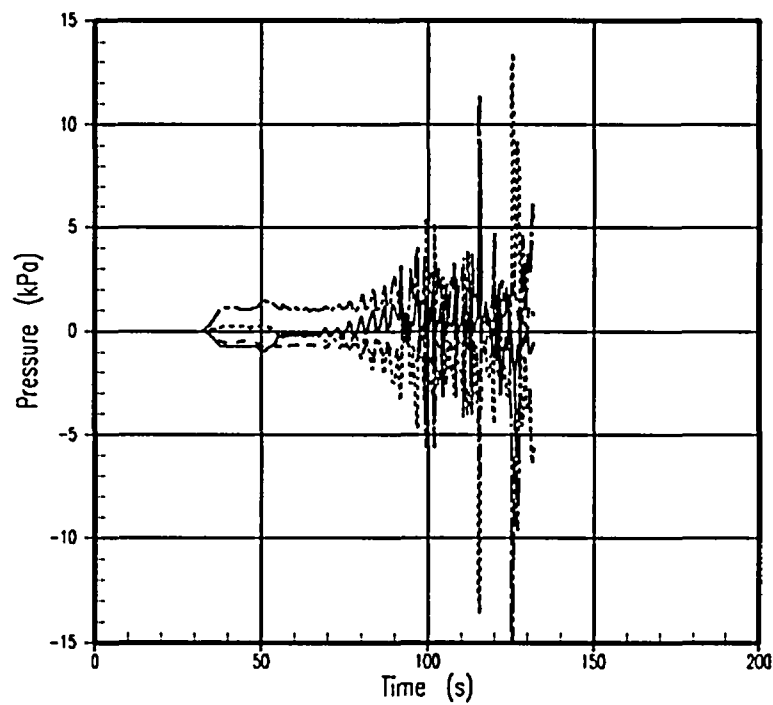


Figure B-92c. Predicted Transverse Differential Pressure in Downcomer at Level 06, Test 6 - Run 131 with MOD7A Rev. 6



b

Figure B-93a. Measured Azimuthal Differential Pressure in Downcomer at Level 22, Test 6 - Run 131

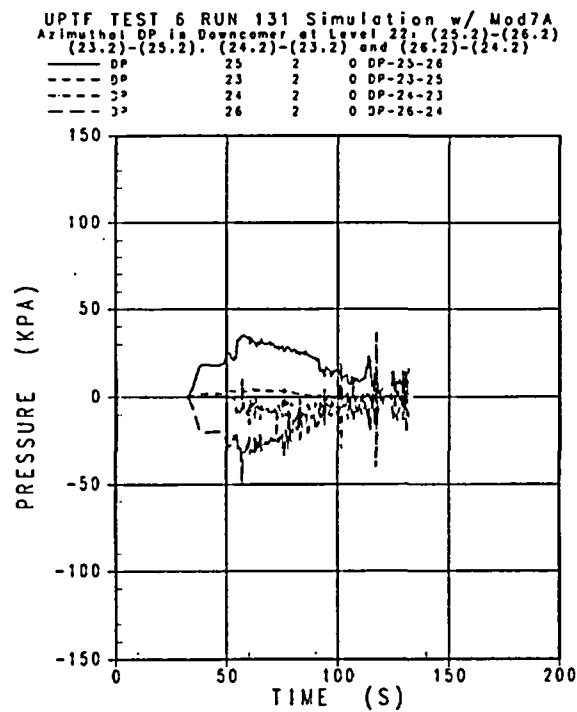


Figure B-93b. Predicted Transverse Differential Pressure in Downcomer at Level 22, Test 6 - Run 131 with MOD7A

UPTF TEST 6 RUN 131 Simulation w/ mod7ar6  
Azimuthal DP in Downcomer at Level 22: (25.2)-(26.2)  
(23.2)-(25.2), (24.2)-(23.2) and (26.2)-(24.2)

—	DP	25	2	0	DP-25-26
- - -	DP	23	2	0	DP-23-25
· · · · ·	DP	24	2	0	DP-24-23
- · - · -	DP	26	2	0	DP-26-24

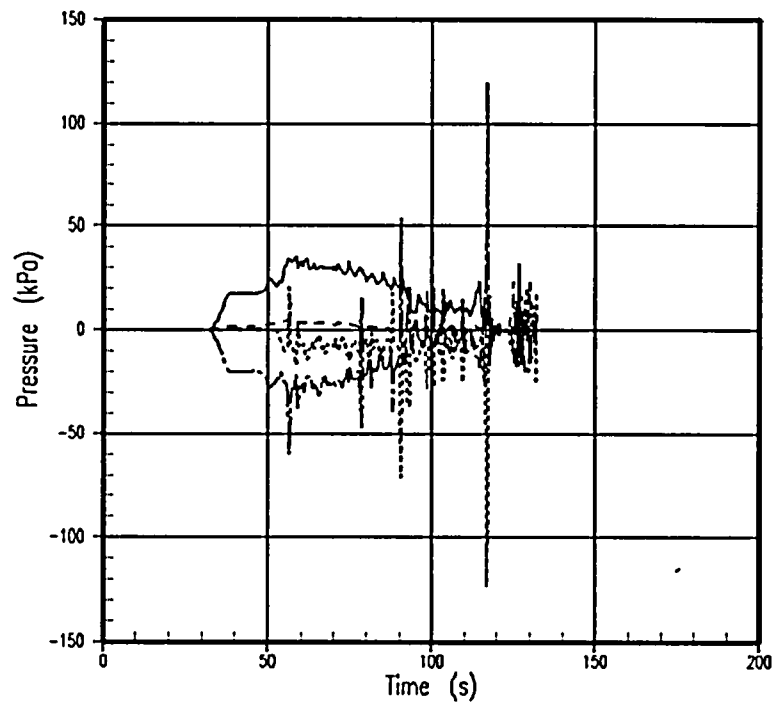


Figure B-93c. Predicted Transverse Differential Pressure in Downcomer at Level 22, Test 6 - Run 131 with MOD7A Rev. 6

b

Figure B-94a. Estimated Water Level in UPTF Vessel, Test 6 - Run 131

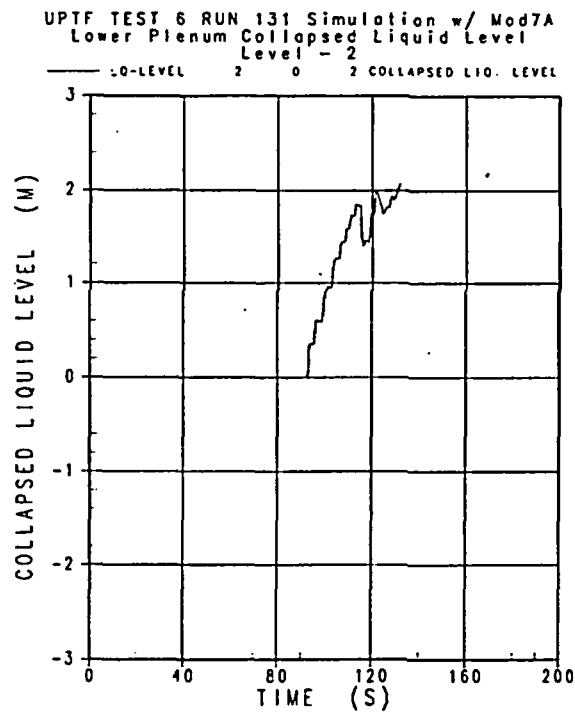


Figure B-94b. Predicted Water Level in UPTF Vessel, Test 6 - Run 131 with MOD7A

UPTF TEST 6 RUN 131 Simulation w/ mod7ar6  
Lower Plenum Collapsed Liquid Level  
Level - 2

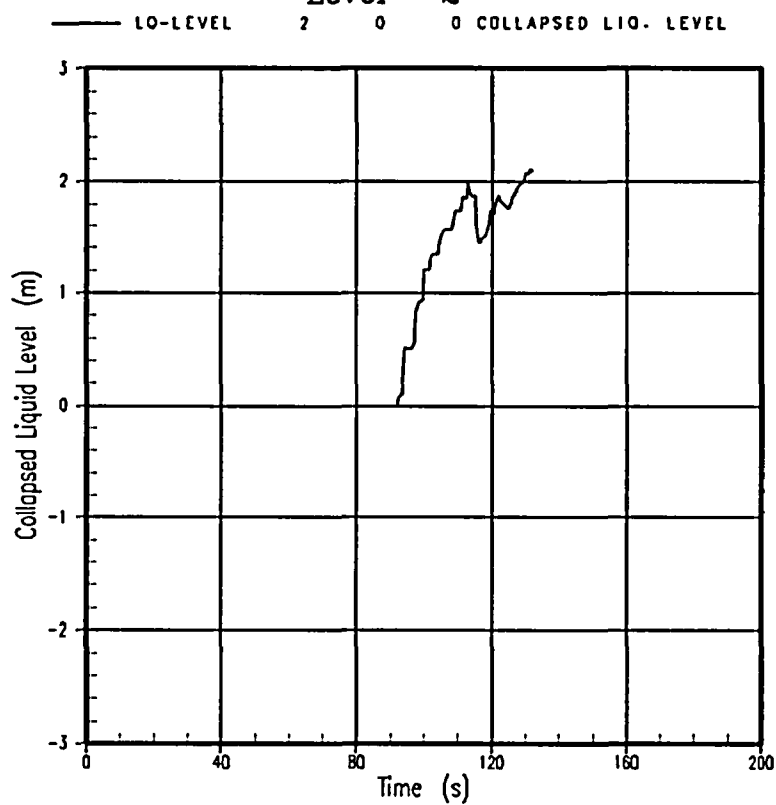


Figure B-94c. Predicted Water Level in UPTF Vessel, Test 6 - Run 131 with MOD7A Rev. 6

b

Figure B-95a. Estimated Downcomer Water Levels (Referenced to 3495 mm Elevation), Test 6 - Run 131

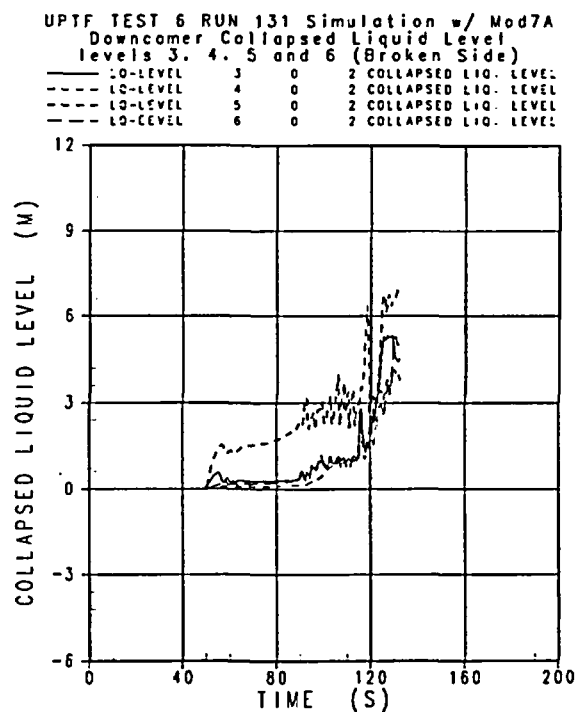


Figure B-95b. Predicted Downcomer Water Levels (Referenced to 1180 mm Elevation), Test 6 - Run 131 with MOD7A

UPTF TEST 6 RUN 131 Simulation w/ mod7ar6  
Downcomer Collapsed Liquid Level  
levels 3, 4, 5 and 6 (Broken Side)

—	LO-LEVEL	3	0	0	COLLAPSED LIQ. LEVEL
- - -	LO-LEVEL	4	0	0	COLLAPSED LIQ. LEVEL
· · · · ·	LO-LEVEL	5	0	0	COLLAPSED LIQ. LEVEL
- - -	LO-LEVEL	6	0	0	COLLAPSED LIQ. LEVEL

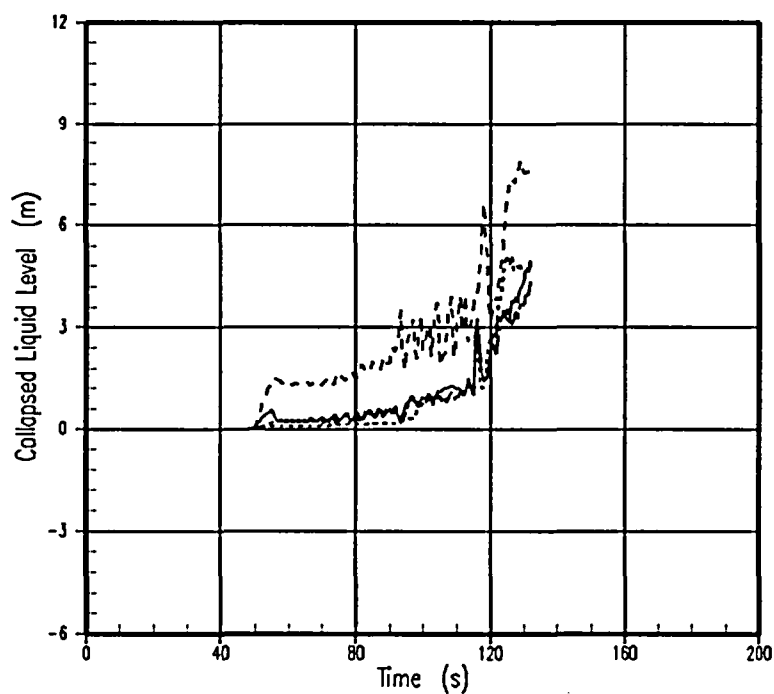


Figure B-95c. Predicted Downcomer Water Levels-(Referenced to 1180 mm Elevation), Test 6 - Run 131 with MOD7A Rev. 6

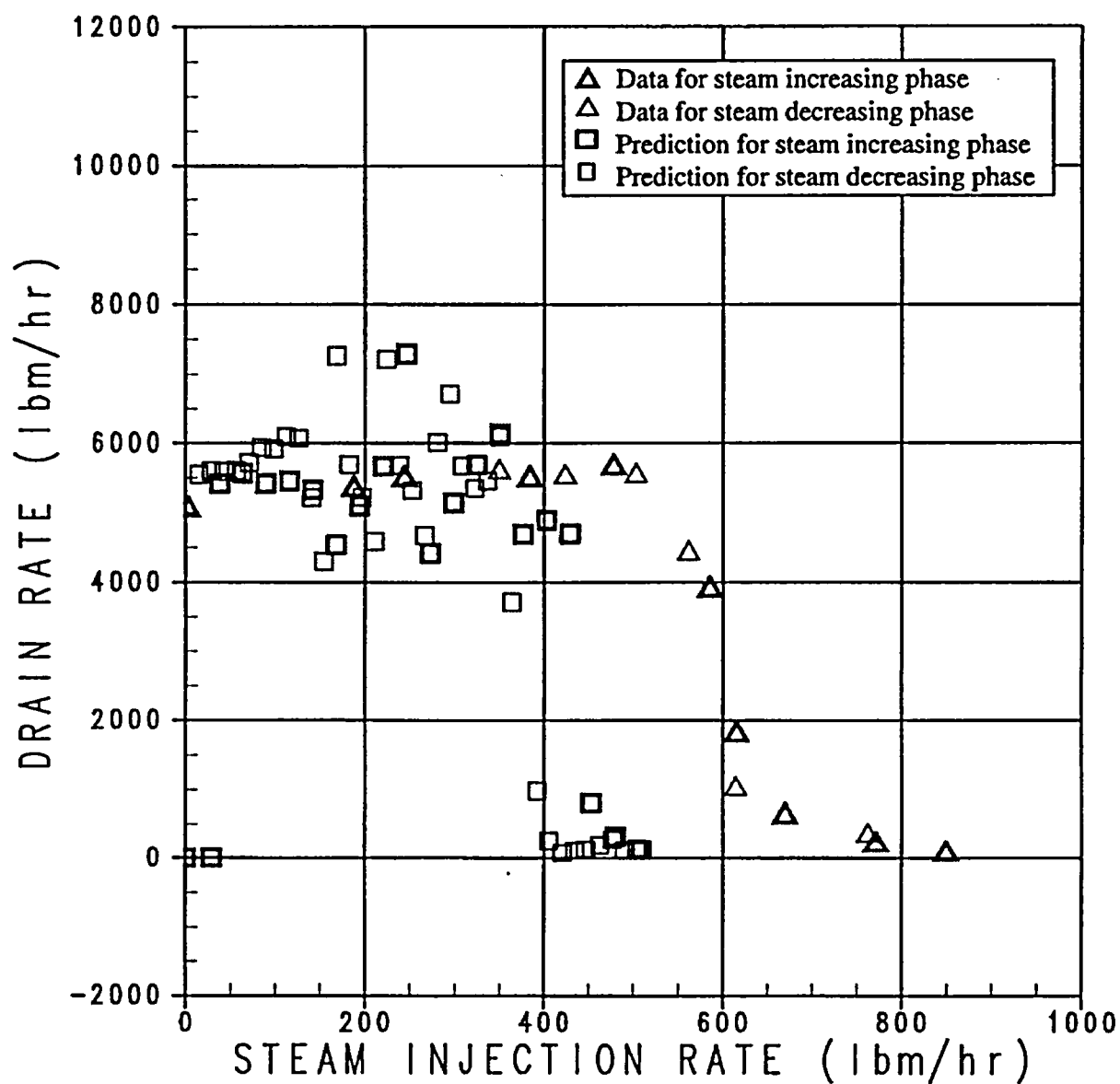


Figure B-96. GE CCFL Test No. 60. Liquid Drain Rate as a Function of Steam Injection Rate: MOD7A Revision 1 vs. Data Comparison

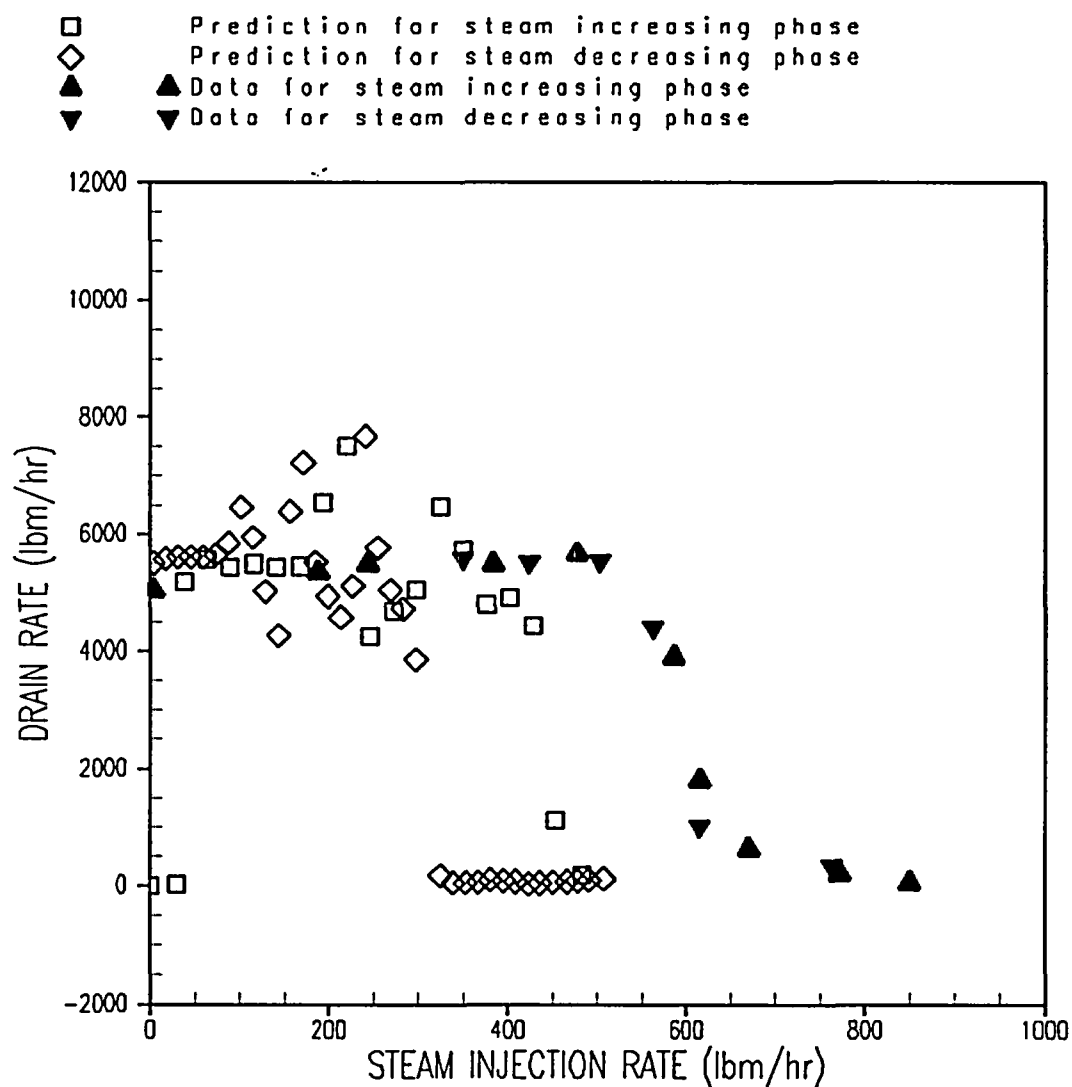


Figure B-97. GE CCFL Test No. 60. Liquid Drain Rate as a Function of Steam Injection Rate: MOD7A Revision 6 vs. Data Comparison



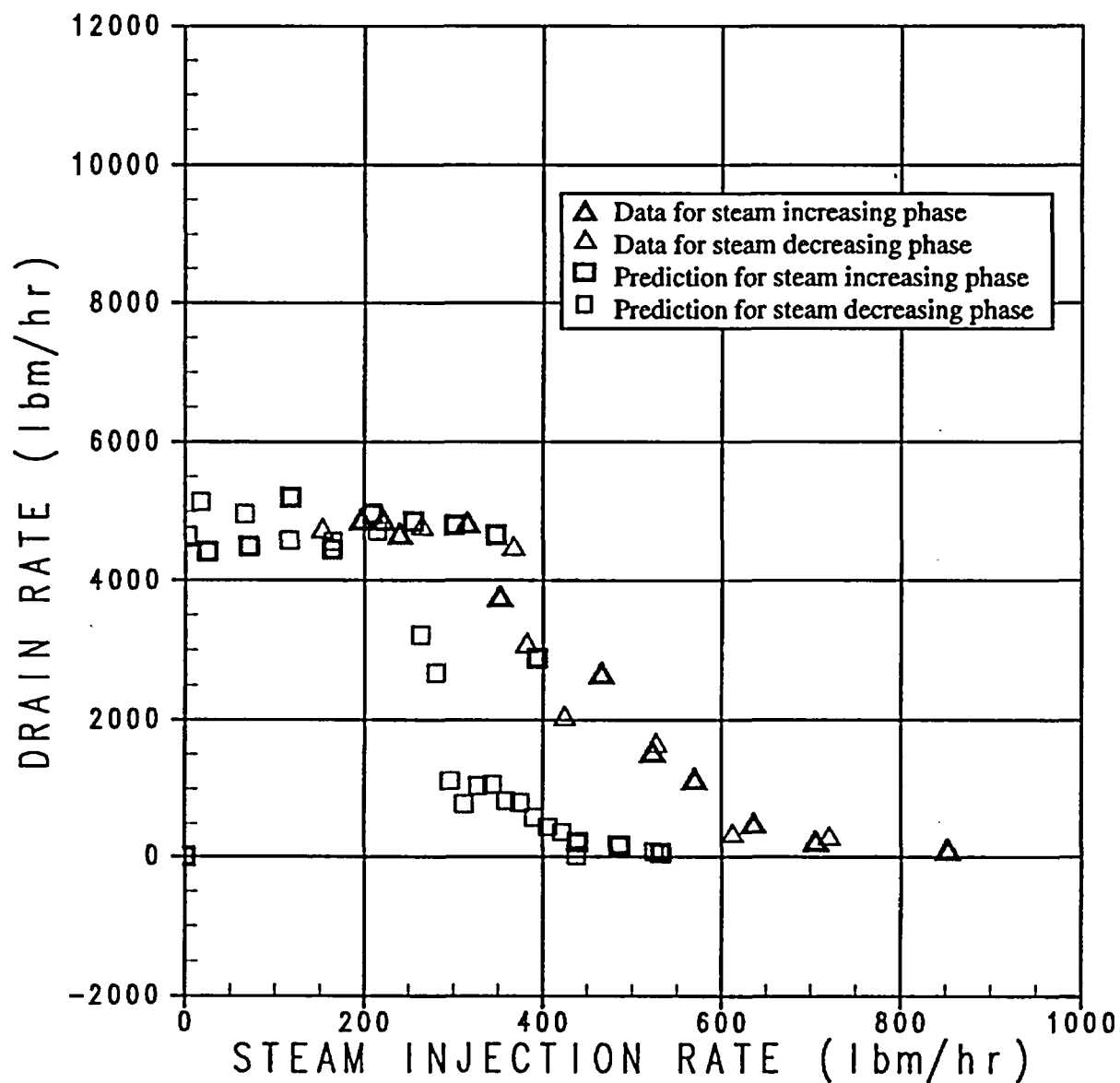


Figure B-98. GE CCFL Test No. 69. Liquid Drain Rate as a Function of Steam Injection Rate: MOD7A Revision 1 vs. Data Comparison

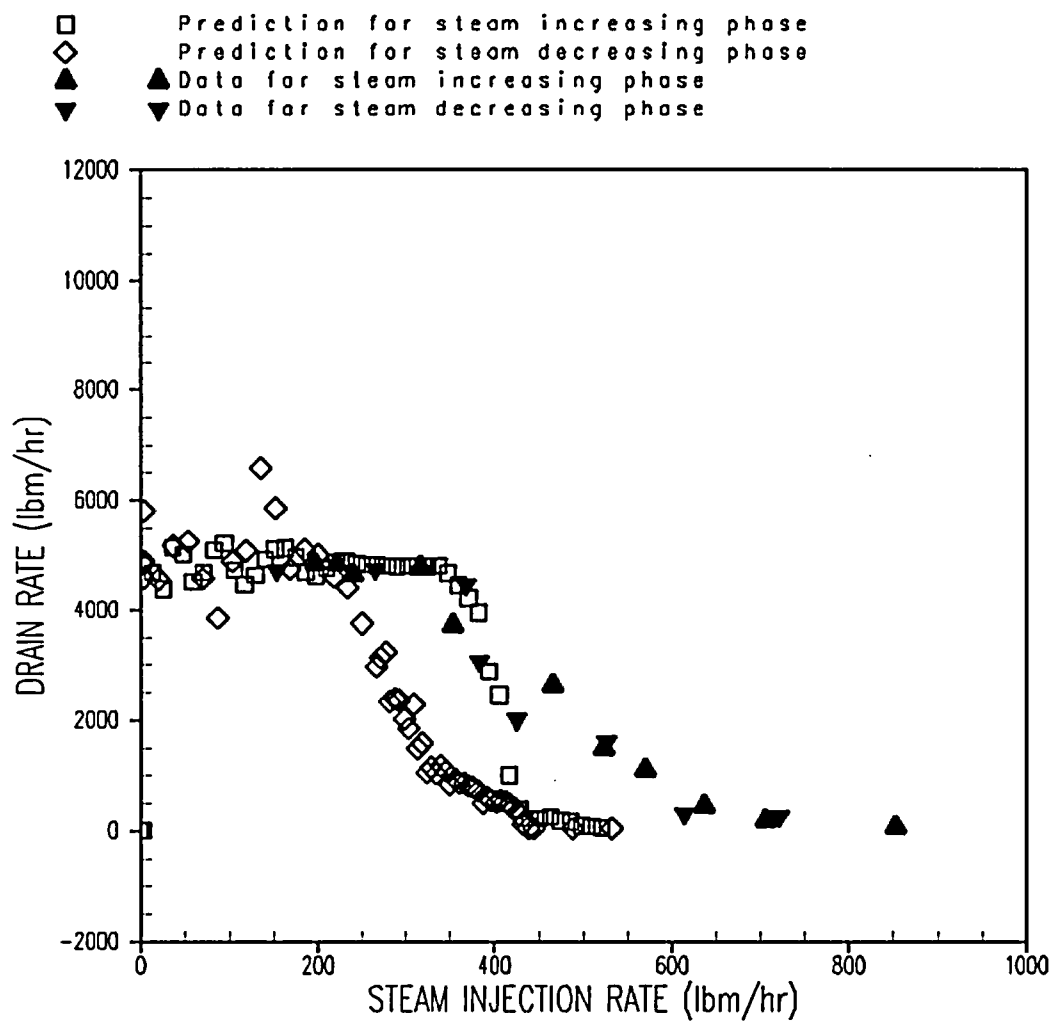
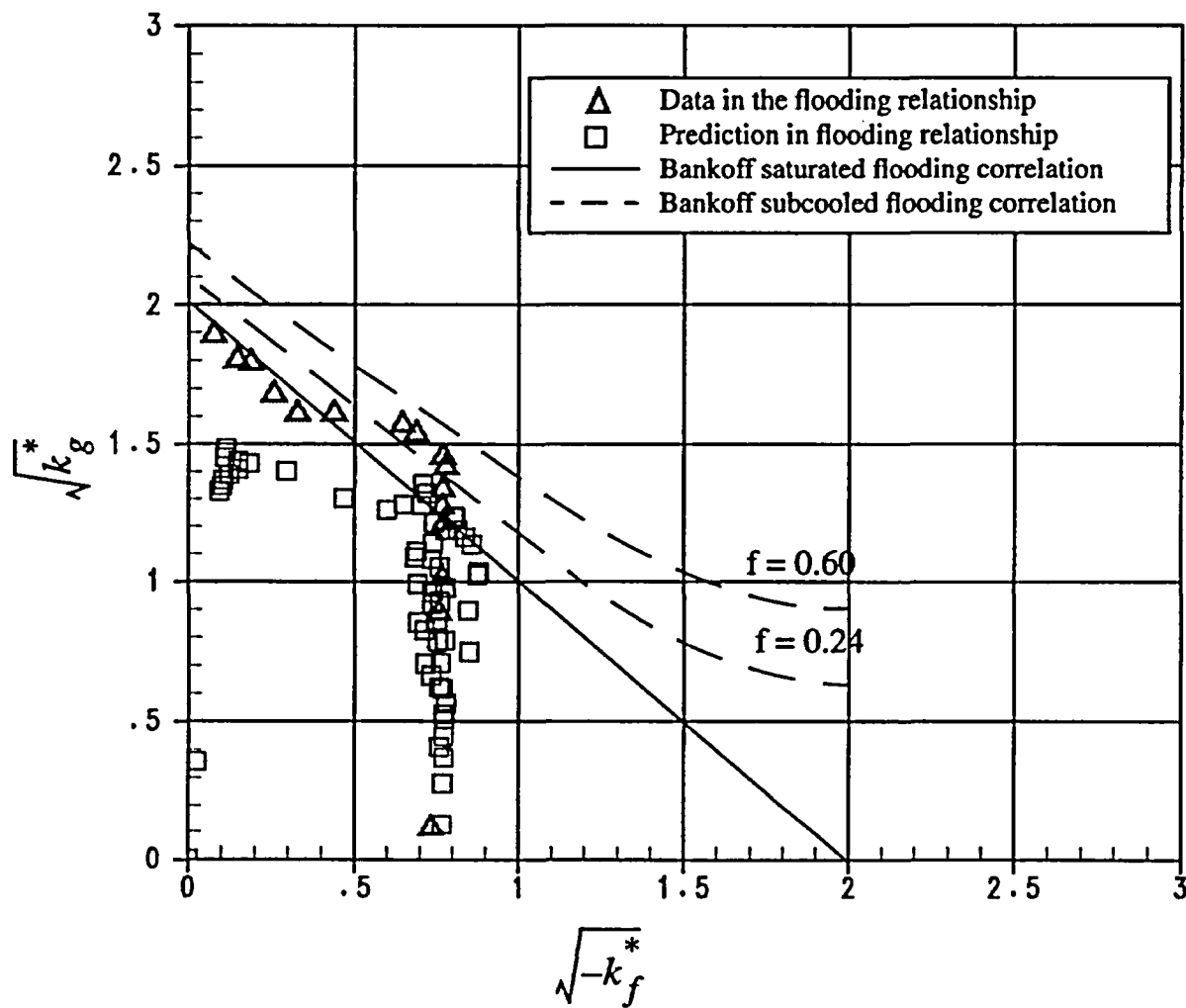


Figure B-99. GE CCFL Test No. 69. Liquid Drain Rate as a Function of Steam Injection Rate: MOD7A Revision 6 vs. Data Comparison



**Figure B-100. GE CCFL Test 60. Prediction vs. Bankoff Flooding Correlations: MOD7A**  
**Revision 1 vs. Test Data Comparison**

# Simulation of GE Subcooled CCFL Test 60 Comparison of Flooding Relation: MOD7A Rev.6 vs Data

□ Prediction of the flooding relationship  
△ Data in the flooding relationship

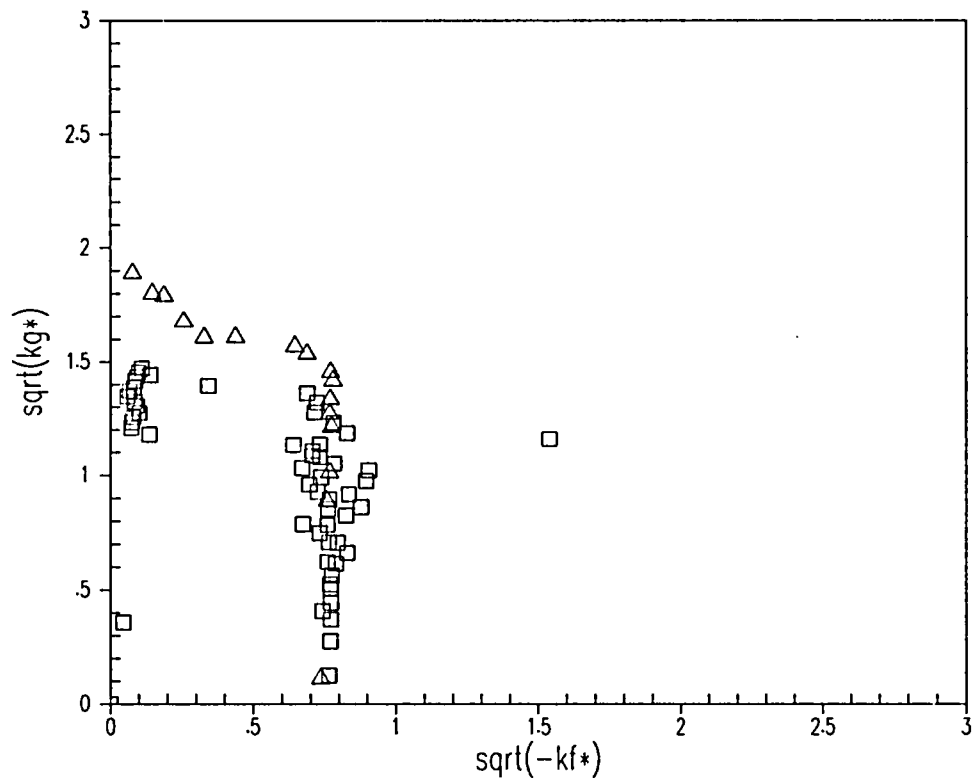


**Figure B-101. GE CCFL Test 60. Flooding Relationship Comparison: MOD7A  
Revision 6 vs. Data**

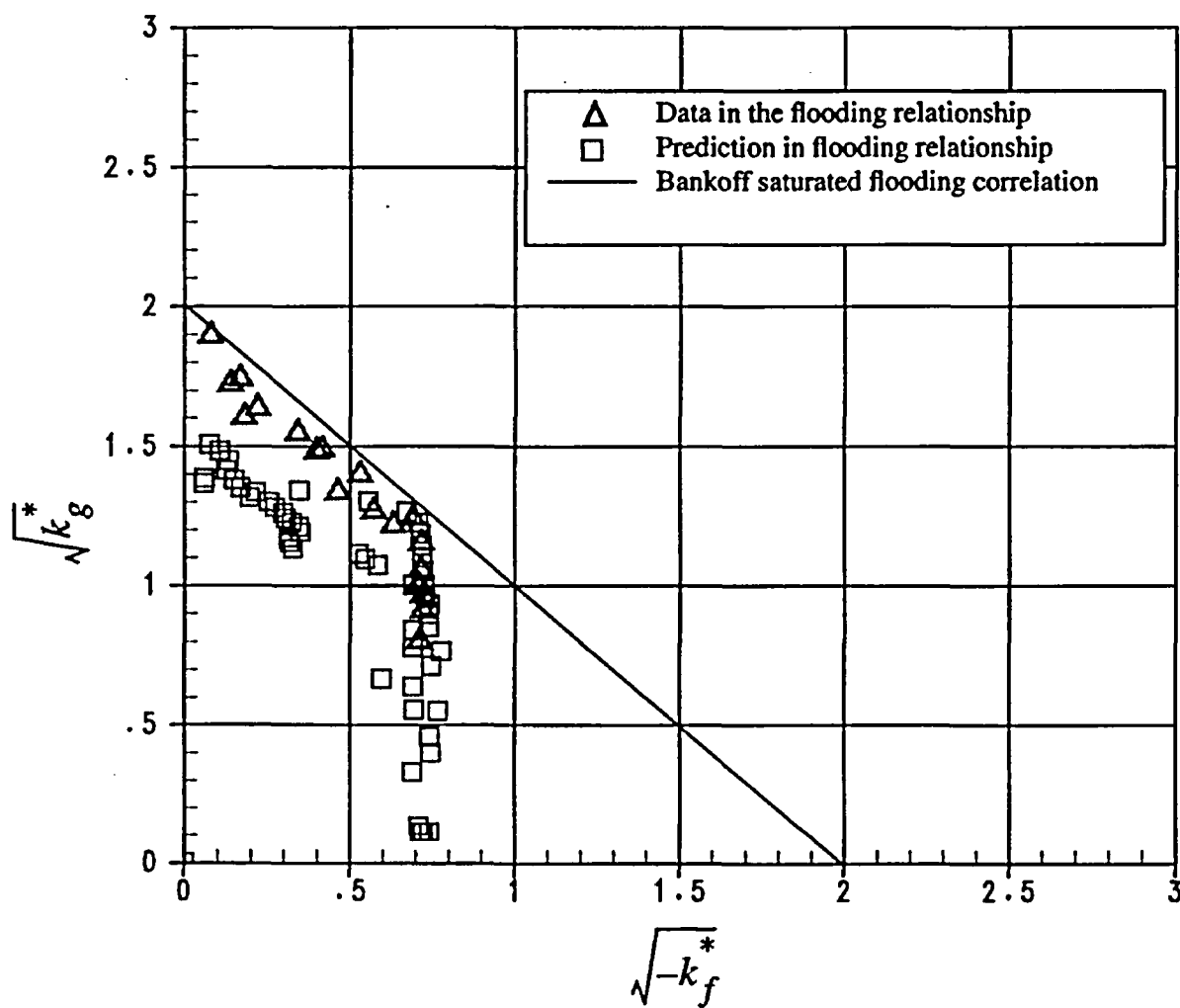


Figure B-102. GE CCFL Test 69. MOD7A Revision 1 Prediction vs. Bankoff Flooding Correlations and Test Data

# Simulation of GE Subcooled CCFL Test 69 Comparison of Flooding Relation: MOD7A Rev.6 vs Data

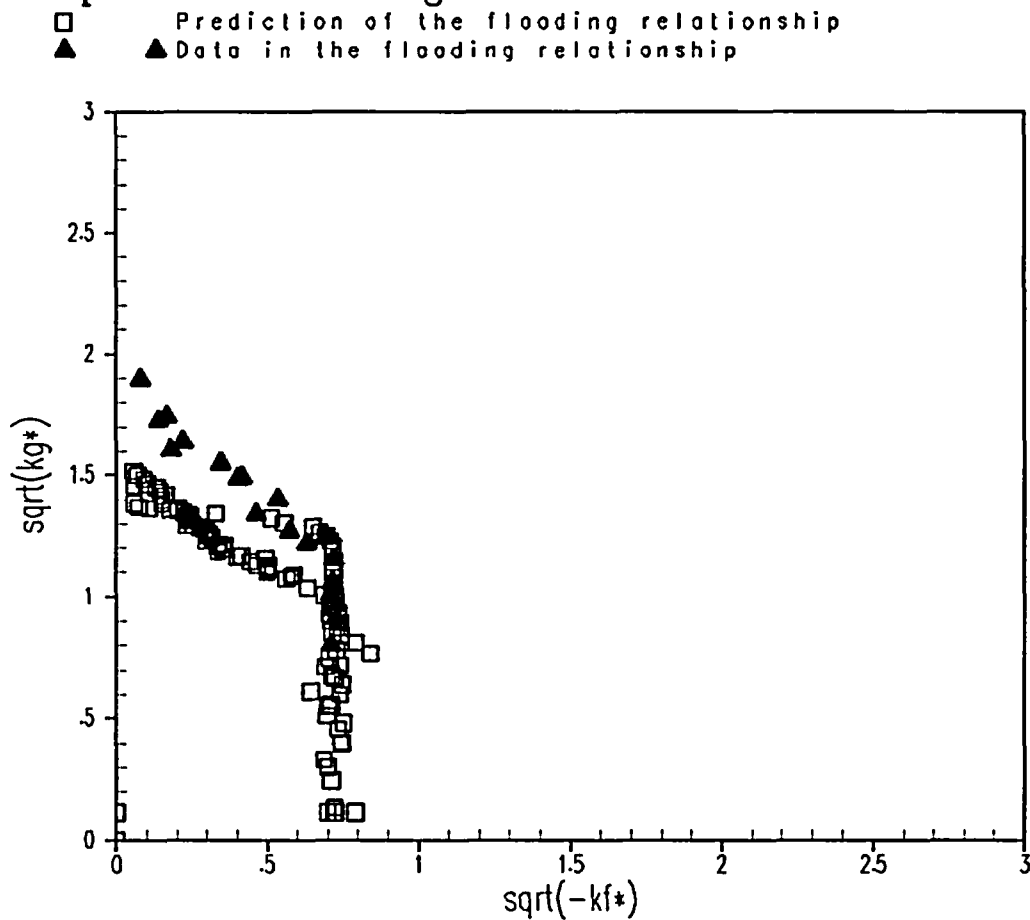


Figure B-103. GE. CCFL Test 69. Flooding Relationship Comparison: MOD7A  
Revision 6 vs. Data

## APPENDIX C

### RESOLUTION OF REQUESTS FOR ADDITIONAL INFORMATION

#### INTRODUCTION

Several Requests for Additional Information (RAIs) were generated during the USNRC review of WCAP-16009-P. Formal Resolution of the USNRC RAIs was provided in References C-1 and C-2.

Reference C-1 provided resolution for RAIs relative to the uncertainty analysis approach described in Section 11 of WCAP-16009-P. The response to these RAIs is provided in Appendix C-1.

Reference C-2 addressed radiation heat transfer issues for CE plants. The resolution of this issue is provided herein in Appendix C-2.

Table C-1 provides a summary of the USNRC RAIs for WCAP-16009-P. The questions are organized by Section of WCAP-16009-P they refer to.

#### REFERENCES

- C-1) LTR-NRC-04-30, "Westinghouse Proprietary & Nonproprietary Responses to the Requests for Additional Information on WCAP-16009-P, Realistic Large Break LOCA Evaluation Methodology Using the Automated Statistical Treatment Uncertainty Method," J. A Gresham, May 11, 2004.
- C-2) LTR-NRC-04-48, "Responses to Requests for Additional Information (RAIs) on WCAP-16009-P, Realistic Large Break LOCA Evaluation Methodology Using the Automated Statistical Treatment Uncertainty Method," J. A Gresham, August 13, 2004.

**Table C-1**  
**Requests for Additional Information: WCAP-16009-P**

Question	Reference	Page No.*	Topic
Sect. 11, Question 0	C-1	C-4	General Westinghouse response for uncertainty treatment
Sect. 11-1, Question 1	C-1	C-5	ASTRUM statement of uncertainty
Sect. 11-1, Question 2	C-1	C-6	Satisfaction of 10CFR50.46 Criteria
Sect. 11-2-1, Question 1	C-1	C-7	Break Type and Size
Sect. 11-2-1, Question 2	C-1	C-13	Modeling of Break
Sect. 11-2-2, Question 1	C-1	C-14	Time in Cycle
App. A, Question 1	C-2	C-17	Radiation Heat Transfer for CE Plants

\*Page Number refers to the page number in this Appendix where the RAI is addressed.



**APPENDIX C-1**  
**REQUESTS FOR ADDITIONAL INFORMATION (RAIs)**  
**FOR SECTION 11 OF WCAP-16009-P**

## Responses to Request for Additional Information

### General Response:

WCAP-16009-P explains the proposed revisions to the uncertainty treatment in the Westinghouse BELOCA methodology. The underlying concept of non-parametric sampling has been previously approved by the USNRC for other nuclear reactor safety calculations, including realistic large break LOCA analyses performed under the provisions of 10CFR50.46. In the original methodology described in Revision 0 of WCAP-16009-P, the maximum local oxidation (MLO) and core-wide oxidation (CWO) were calculated from the case with the limiting (highest) peak cladding temperature (PCT) from a sampling of 59 runs. Westinghouse proposes to adjust our application of the non-parametric method as follows. In order to make a unique uncertainty statement for each of the three output variables, these variables will be sampled independent of each other. Although there is a strong correlation between them, they are not exclusive functions of each other. For example, the highest maximum local oxidation among the sampled runs may not be obtained from the same case that has the highest PCT. To accommodate this, and to treat the output variables with equal weight without emphasizing one over the others, Westinghouse will report the maximum PCT, MLO and CWO values from a sampling of 124 runs. With this number of samples, we can capture a fraction of at least 0.95 of each of the three populations with a confidence of 95% [1]. [

]ac

Assuming staff concurrence, Westinghouse will provide the appropriate revisions to the affected text in WCAP-16009-P to reflect this change. This change is considered to be an improvement to the methodology, in that it reflects increased statistical rigor.

The determination of a sample size of 124 was obtained using the corrected formulation of Equation 25 of [1]. For a one-sided confidence level,  $r_1 = r_2 = \dots = r_p = 0$  and  $s_p = N - p + 1$ . The general expression for confidence level  $\beta$  is:

$$\beta = 1 - I(y, s - r, N - s + r + 1)$$

which, for this application becomes

$$\beta = 1 - I(y, N - p + 1, p)$$

NOT

$$\beta = 1 - I(y, N - p + 1, p + 2)$$

as shown in the first part of Equation 25. Note, however, that the series expression in the second part of Equation 25 is correct.)

Reference [1]:

A. Guba, M. Makai, and L. Pál, "Statistical aspects of best estimate method – I," Reliability Engineering and System Safety 80 (2003), pp.217-232.

## 11. Sensitivity and Uncertainty Analysis

### 11-1 Technical Basis for Revised Uncertainty Methodology

- 1) You state that the ASTRUM methodology will “provide a simple, singular statement of uncertainty.” Please define clearly what the “singular statement of uncertainty” is about.*

Response:

In the proposed ASTRUM methodology (revised as discussed under “General Response”), the uncertainty statement is made about the peak cladding temperature (PCT) as well as the maximum local and core-wide oxidation (MLO and CWO). In ASTRUM, we assert with a confidence of 95% that the maximum calculated PCT, MLO, and CWO from the 124 cases will capture a fraction of at least 0.95 of all possible values that could be obtained from the Code.

- i) What is/are the variable(s) about which the statement of uncertainty is made?*

Response:

The PCT, local oxidation, and core-wide oxidation are the variables about which the uncertainty statement is made.

- ii) Are they all considered random variables? What exactly is the “singular” statement?*

Response:

The computer runs are made using certain input randomly sampled from their respective distributions. PCT, MLO and CWO are each functions of these variables. Local and core-wide oxidation are closely correlated to the PCT, but the ability to satisfy the regulatory requirements is not predicated on this fact.

Variables that are functions of random variables are themselves random variables. Thus, the variables about which the uncertainty statement is made are considered random variables. The uncertainty statement is that these computed variables capture a fraction of at least 0.95 of each of the three populations at 95% confidence.

- iii) *How are you quantifying the uncertainty? That is, if you are quantifying uncertainty in terms of probability about a random variable, please give the variable and its associated probability that make up the "simple, singular statement of uncertainty."*

Response:

The revised quantification of uncertainty can be specifically stated as follows:

"We assert with 95% confidence that the maximum calculated PCT, MLO and CWO from the 124 cases will capture a fraction of at least 0.95 of all possible values that could be obtained from the Code."

- iv) *Please explain in detail how ASTRUM's "simple, singular statement of uncertainty" meets the requirements of 10CFR 50.46.*

Response:

We believe that, with the revisions described above, this question has been resolved.

- 2) *You state that "ASTRUM relies on a statistical sampling technique." We resort to sampling because of a lack of information. In light of the above discussion, what information is lacking to meet the requirements of 10CFR 50.46 without statistical sampling?*

Response:

The statistical sampling is used because of lack of information on true distribution of PCT. In other words, given the input conditions including the plant operating conditions and physical model uncertainties, one cannot claim with complete certainty a PCT answer. However, by sampling from the unknown distribution, one can ascertain with an associated confidence, that a specific percentage of the population is bracketed by the result.

The requirements of 10CFR50.46 can be met without statistical sampling by using conservative deterministic analyses.

- i) *Probability is a real number in the interval from zero to one. How does the ASTRUM methodology compute the probability (i.e., a real number in the interval from zero to one) which shows "with a high probability that none of the criteria (i.e., note plural) of paragraph 50.46(b) will be exceeded."*

Response:

We believe that, with the revisions described above, this question has been resolved.

- ii) *If the ASTRUM methodology appeals to the statement in Reg. Guide 1.157 that "since the other criteria are strongly dependent on peak cladding temperature, explicit consideration of the probability of exceeding the other criteria may not be required if it can be demonstrated that meeting the temperature criterion at the 95% probability level ensures with equal or greater probability that the other criteria will not be exceeded." How are you demonstrating this? That is, the current ASTRUM methodology is predicated on a sample of 59 runs for a 95/95 PCT one-sided tolerance limit (i.e., a single criterion); 58 runs would be insufficient; 60 runs would either increase the population fraction or level of confidence or both. Therefore, there is a limited amount of information in 59 runs. In view of this how can you claim compliance with the above statement with regard to all the criteria based on 59 runs? What is the probability (a real number between 0 and 1) that "the other criteria" will not be exceeded?*

Response:

We believe that, with the revisions described above, this question has been resolved.

## 11-2 Technical Basis for Additional Parameters Considered in Uncertainty Analysis

### 11-2-1 Break Type and Size

- 1) *The ASTRUM methodology assigns equal frequency (50%) to DECLG and split breaks based on "a series of sensitivity runs that compared split and guillotine breaks." It is concluded "that the most limiting split break and the most limiting double-ended guillotine break have comparable PCTs for both 3-loop and 4-loop plants" as justification for the 50/50 split.*
- i) *What do you mean by "most limiting?" The largest? What are the random variables in these calculations?*

Response:

The phrase "most limiting" is referring to the break with the highest peak cladding temperature (PCT). The sensitivity studies referred to in this discussion were a deterministic set of transient calculations, in which the break flow rate was varied for each break type. The break flow rate was varied for split and guillotine breaks by varying the break flow area, using the modeling shown in Figures 11-2 through 11-5. The most limiting split and guillotine transients from those sensitivity studies are summarized below (see Table 11-1 for the complete run matrix):

Plant Type	Break Type	Break Area	Break Discharge Coefficient (CD)	PCT (°F)
[				
				] <sup>a,c</sup>

The only parameters varied in these studies were break type and break flow rate. It can be seen that the limiting split and limiting guillotine breaks for the 3-loop and one of the 4-loop plants are very similar, with the split slightly higher. For the other 4-loop plant the limiting guillotine is limiting.

Had other random variables been sampled, the limiting break type and/or flow rate could be different. Therefore, it is considered appropriate to vary all of the parameters at the same time.

- ii) *Fig 11-1 is proffered as evidence for these conclusions. Please clarify the following editorial issues: The figure title refers to 3- and 4- Loop PWRs, while the labels for both figures say four-loop plant. The open and closed symbols, which distinguish split and guillotine breaks, are not distinguishable in the submitted figures.*

Response:

Enclosed are corrected Figures 11-1(a) and 11-1(b), which show the reflood (limiting) PCTs for representative 3-loop and 4-loop PWRs. We inadvertently imported the 4-loop blowdown PCT plot from Section 22-6 of WCAP-12945-P-A, instead of the 3-loop reflood PCT plot. This was noted by Westinghouse during the closed meeting held on August 5, 2003, and the correct figures were submitted as part of the proprietary presentation material [Reference: LTR-NRC-03-39, letter from H.A. Sepp (Westinghouse) to the Document Control Desk (U.S.NRC), dated July 23, 2003]. We will correct these plots in the final version of WCAP-16009-P to be consistent with this submittal.

a,c

**Figure 11-1(a). Split vs. DECLG Reflood PCT for 3-Loop PWR**



a,c

**Figure 11-1(b). Split vs. DECLG Reflood PCT for 4-Loop PWR**

- iii) *In Table 11-1 what is the difference between  $PCT_1$ ,  $PCT_2$  and  $PCT_3$ ? In this table what is meant by "Break Area Fraction Or (CD)?" In what sense are you using "Or?"*

Response:

Table 11-1 is identical to Table 22-6-2 of WCAP-12945-P-A. That methodology calculates the final PCT uncertainty distribution by a combination of response surface equations and Monte Carlo sampling. It requires that three separate time periods be considered; blowdown ( $PCT_1$ ), early reflood ( $PCT_2$ ), and late reflood ( $PCT_3$ ). Since response surfaces are not used in the ASTRUM methodology, this terminology is no longer relevant.

"Break Area Fraction" is the appropriate title for the split breaks, while "CD" is the appropriate title for the guillotine breaks. "Or" is used in this context.

- iv) *The PCT in a LOCA is a function of break flow rate which in turn in the ASTRUM methodology is dependent on the random variables – break type, size and discharge coefficient. How can you uniquely infer a density distribution for break type (i.e., probability of 0.50) from the limiting PCT? In principle, this is an inverse problem and does not have a unique solution. How would you counter my claim that the probability of a DECLG is 0.1 and a split break is 0.9?*

Response:

A large break LOCA is a hypothetical design basis accident, used for setting the ECCS performance requirements. The use of a 50/50 probability for break type is a simplifying assumption, which results in the effective break size ( $CD \cdot A$ ) being biased towards middle to high values (Figure 12-29). If the break size distribution were uniform (i.e., all break sizes are equally probable), a less conservative result might be obtained. This modest conservatism is considered acceptable, in order to avoid postulating a more complicated distribution.

The regulatory requirement for the use of realistic LOCA methods is to satisfy the ECCS acceptance criteria at a high level of probability. The most limiting split break case and the most limiting guillotine break case from a sample size of 124, with an assumed 50/50 probability on break type, will both be at a high level of probability.

- The break type sampling does affect the deterministic modeling, as noted by the reviewer. It also affects the break size, and the flow split to the break. For a double-ended guillotine break, the total flow area is, by definition, two times the pipe area. There is no direct flow communication between the two ends of the break. For a split break, the total flow area is between [ ]<sup>3c</sup>, and there is direct flow communication at the common pressure point prior to the break.

**11-2-1-1,2 Modeling of Breaks**

- 1) *In a specific application of the ASTRUM methodology is the table of the pressure in the BREAK component generated for the containment at hand or is the table a generic table?*

Response:

The pressure in the BREAK component is calculated on a plant-specific basis, for the containment at hand.

- 2) *Please show the frequency distribution of measured flow/predicted flow given by the Marviken data and on which the cumulative frequency distribution (Fig. 1-2) is based. Is there any correlation with break size (break type)? How is the "predicted flow" computed?*

Response:

The development of the cumulative frequency distribution shown in Figure 1-2 is described in detail in Section 25-2 of WCAP-12945-P-A. The histogram of measured flow/predicted flow used to develop Figure 1-2 is shown in Figure 25-2-9 of that reference.

The parameters varied in the Marviken data were nozzle length and diameter, initial subcooling, and initial pressure. The conditions for each test are shown in Table 16-4-2 of WCAP-12945-P-A. Comparisons of the predictions to the data did not show any significant differences in predictive capability for variations in nozzle geometry or test conditions.

The break flow predictions were obtained as follows (figure numbers correspond to WCAP-12945-P-A):

- Each test was modeled as shown in Figure 16-4-3.
- [

] <sup>a,c</sup>

### 11-2-2 Time in Cycle

- 1) *An ASTRUM analysis assumes that a LOCA is equally probable over the fuel residence time in a burn cycle. Thus, the time at which the LOCA occurs is distributed uniformly over the cycle length. ASTRUM samples the "cycle burnup" from a uniform distribution. What is meant by "cycle burnup?" Burnup and time-in-cycle are not the same thing; depending on reactor operation the same time-in-cycle can result in very different burnups. How do you take this variance into account in light of the basic assumption of a uniform distribution in time?*

Response:

"Cycle burnup" refers to the core average burnup accumulated during the current cycle. Typical values at end of cycle are on the order of 20,000 MWD/MTU. If a fresh fuel rod operated at an average relative power of 1.35 over that cycle, it would have accumulated a burnup of 27,000 MWD/MTU.

The most economical way to operate a PWR in the US is in "base load" mode, where 100% power is maintained throughout the cycle. In base load, burnup and time in cycle are directly related.

If a plant "load follows," or varies power based on grid demand, the two will not be as closely linked. While US PWRs have the capability to load follow, this is not a common practice due to the economics. However, the practice of doing a power coastdown at the end of cycle is fairly common. A power coastdown involves a gradual reduction in thermal and electrical power, as the core reactivity decreases. This can take place over a period of up to several weeks, and will slightly affect the relationship between time in cycle and burnup.

Mid-cycle power reductions for maintenance, scrams, etc. can also cause some differences between burnup and time in cycle. However, these are generally of limited duration.

The main parameters affected by time in cycle or burnup are initial stored energy and decay heat. For the purposes of determining initial stored energy and decay heat, we are assuming that the reactor is operating at full power throughout the cycle. With this assumption, time in cycle and burnup are equivalent. The distinction between the two to allow for those times when the reactor is not at full power does not materially affect the uncertainty analysis.

- 2) *You say "The average- and low-power rods are assumed to be at a burnup of 10,000 MWD/MTU." In principle, how can an average and a low value be the same?*

Response:

The WCOBRA/TRAC modeling of a PWR divides the core into four hydraulic channels. One is the hot assembly channel, which contains the hot rod and a hot assembly average rod. Another is the low power channel, which contains all of the fuel rods in the assemblies on the core periphery. The last two are average channels. One of these contains all of the rods in the in-board assemblies that are located under guide tube positions. The other contains all of the rods in the remaining in-board assemblies. A more detailed example of this modeling is given in the "Vessel Section 3" description starting on page 12-3.

Today's fuel management strategies include the use of low leakage, or ultra-low leakage, loading patterns. These loading patterns place depleted fuel assemblies (e.g., twice burned) on the core periphery. This reduces neutron leakage, and improves fuel utilization. Most of the assemblies on the core periphery will have a burnup of at least 40,000 MWD/MTU at the start of the cycle. Because of their depletion and their location, these assemblies operate at below average power levels.

The in-board average channels will contain a mix of fresh and burned assemblies. Typically, these assemblies will start the cycle with burnup levels of zero for the fresh assemblies, about 20,000-30,000 MWD/MTU for once-burned assemblies, and about 40,000 or so for twice-burned assemblies.

The assumption of 10,000 MWD/MTU for the burnup of the rods in the average and low power channels is based primarily on stored energy considerations. As the cladding creeps down toward the pellet, the gap conductance increases, and the fuel initial stored energy is reduced. Use of a low burnup is therefore somewhat conservative.

- 3) *Table 11-5 lists time-in-cycle as a plant parameter that is sampled in the uncertainty analysis. Where in Tables 1-7 through 1-11 is a description of the associated uncertainty distribution?*

Response:

Section 1-2 provides a comparison between the ASTRUM methodology and the methodology previously approved in WCAP-12945-P-A. Tables 1-7 through 1-11 summarize the uncertainty distributions previously approved in WCAP-12945-P-A. This can be seen in the references to these tables in the text, located on pages 1-14 and 1-16. (Note that Table 1-9 is referenced in Table 1-8, but not in the text.)

The additional parameters sampled in ASTRUM are listed at the bottom of page 1-16.

**APPENDIX C-2**  
**REQUESTS FOR ADDITIONAL INFORMATION (RAIs)**  
**ON RADIATION HEAT TRANSFER FOR CE CORES**

## Responses to Request for Additional Information

### Issue Statement

Appendix A of WCAP-16009-P provides the basis for applying the ASTRUM methodology to Combustion Engineering plants. Application of the PIRT process resulted in a higher ranking for radiation heat transfer, due to the expectation that the larger thimbles (occupying four lattice positions instead of one) would result in a larger temperature gradient in the bundle in the event of a loss of coolant accident. The USNRC has questioned whether the corner and mid-lattice side rods of the Combustion Engineering (CE) designs, which have a view factor of zero to the thimbles, might have a lower total heat transfer coefficient than reflected in the Westinghouse reflood heat transfer multipliers (including the adjustment for rod-to-rod and rod-to-thimble radiation heat transfer).

### Response

Following is the Westinghouse response to the issue. Section 1 provides the roadmap of the response and the analysis is developed in the following Sections 2 through 6. Westinghouse conclusion is that the current USNRC-approved reflood heat transfer reduction factor for rod-to-rod and rod-to-thimble radiation heat transfer in Westinghouse fuel designs is also applicable to Combustion Engineering (CE) fuel designs.

#### **1. Introduction**

- In the approved 1996 Westinghouse methodology the effect of rod-to-rod radiation heat transfer was estimated from the test data (FLECHT series), by comparing the temperature in rods which have a near zero view factor to the thimbles and the average rod temperature which was used to determine the effective reflood heat transfer. The objective of Section 2 was to perform an assessment based on the previous method, by considering a FLECHT-SEASET flow blockage reflood heat transfer test which presented severe conditions as far as thermal radiation is concerned (several rods with zero view factors to thimbles). Conclusions from this assessment are similar to the one previously obtained for other FLECHT tests (Reference 1).
- At this point, Westinghouse recognized that to fully address the effect of thermal radiation, argumentations based only on view factor considerations may not be sufficient. This leads to Section 3, which presents a detailed assessment of the effect of rod-to-rod radiation heat transfer. The purpose of the analysis was:
  1. To demonstrate that effect of rod-to-rod radiation heat transfer on the total reflood heat transfer for a hot rod is similar in both CE and Westinghouse designs.
  2. To estimate the effect of rod-to-rod radiation heat transfer under severe conditions that were observed in FLECHT-Skewed tests.



3. To demonstrate that [

] <sup>ac</sup>

- Section 4 is simply a benchmark study, to show that the radiation model utilized by Westinghouse gives exactly the same results as the USNRC model, for the same geometry and boundary conditions.
- Section 5 provides further details on the applicability of the method utilized by Westinghouse to account for the effect of the rod-to-rod radiation which is embedded in the reflood heat transfer multipliers derived from the bundle test data.

2. Assessment of Rod Bundle Data with Zero View Factor

NUREG/CR-3314 presents the FLECHT SEASET flow blockage reflood heat transfer data [2]. In this test, positions F7 and I10 were heater rods instead of the simulated thimbles used in the prior FLECHT SEASET tests. With this orientation, rods F7 and I10 had zero view factors to the thimbles (Figure 2-1). Test 61607 was selected for the following assessment, because of the low flooding rate (0.8 in/sec) and the high peak cladding temperature (2189°F), resulting in maximum radiation heat transfer effects.

Table 2-1 compares the peak cladding temperatures measured for rods with zero view factors to the unheated thimbles, with the average cladding temperatures for the instrumented rods in the central region of the bundle. The temperatures of the rods with zero view factors are slightly higher, reflecting the larger contribution of radiation heat transfer in those rods with non-zero view factors to the unheated thimbles. The rod temperatures are then converted into a total heat transfer coefficient, referenced to the saturation temperature. At each elevation the total heat transfer coefficient for the rods with zero view factors are within 3% of the average of the total heat transfer coefficients. The current methodology applies a [ ] <sup>ac</sup>, reduction to the reflood heat transfer multipliers, to account for radiation heat transfer effects. This reduction factor exceeds the observed value for the flow blockage test rods with zero view factors, providing support for the continued use of the Reference 1 methodology for both CE and Westinghouse fuel designs.

**Table 2-1**  
**Rods with Zero View Factor vs. Average Rods**

Elevation (in.)	Time (sec)	T (zero view)	T (average)	H (zero)/H (ave)*
80	165.5	2165	2144	0.99
81	198.5	2160	2103	0.97
86	157.5	2111	2064	0.97
90	159.5	2142	2097	0.98
96	230.1	2139	2087	0.97

\* calculated as  $(T(\text{zero view}) - 270^{\circ}\text{F}) / (T(\text{average}) - 270^{\circ}\text{F})$ , where  $270^{\circ}\text{F} = T_{\text{sat}}$

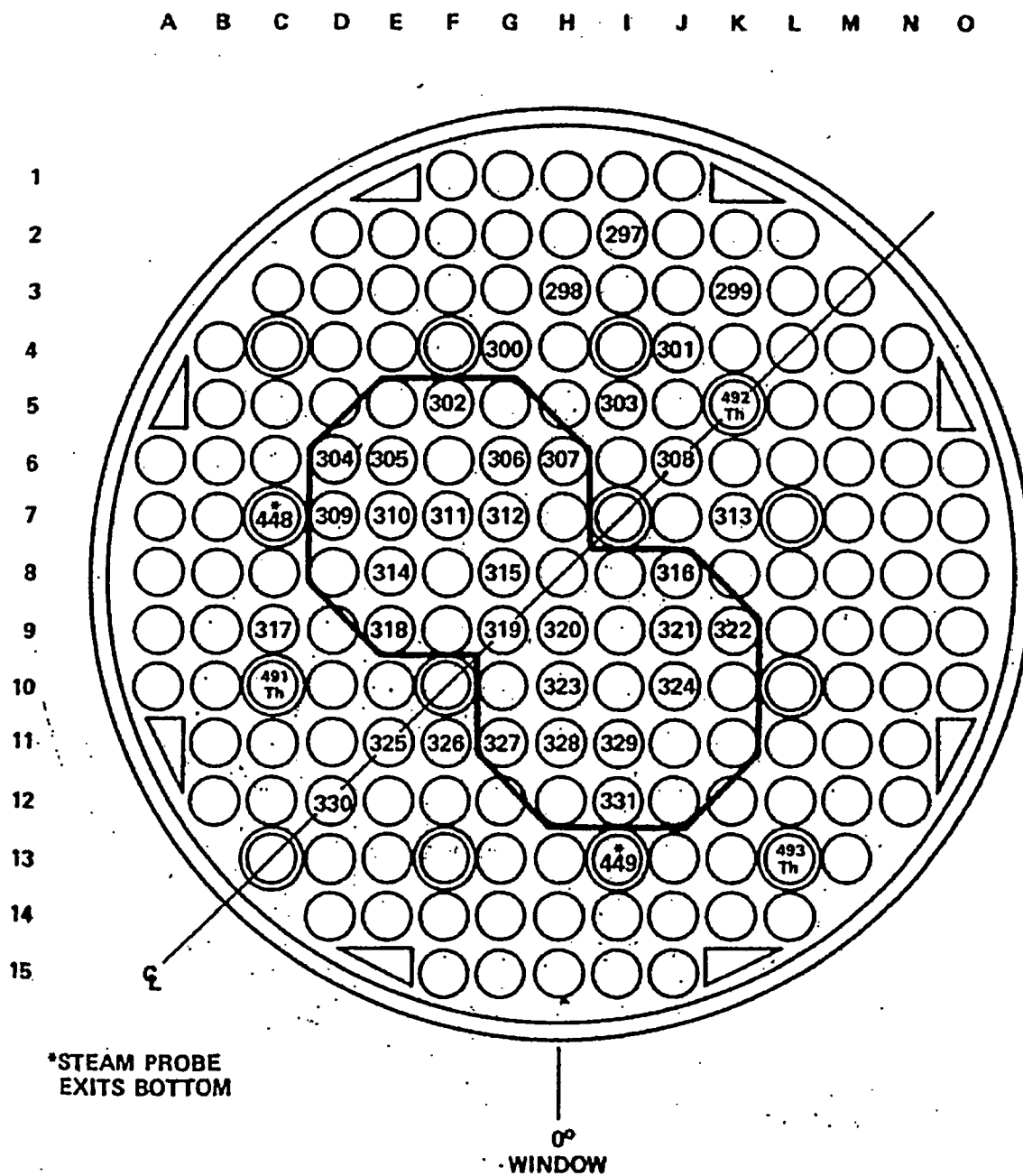


Figure 2-1. Heater Rod Instrumentation at 90 inch Elevation (from Reference 2)

### 3. Effect of the Differences in Combustion Engineering and Westinghouse Lattice Geometry

A detailed rod-to-rod radiation model was utilized to estimate the effect of the rod to rod radiation heat transfer for different bundle lattices. The model was compiled in a computer program which is described in the following. The program is a modified version of what was originally developed to support the scaling analysis for the NRC/PSU RBHT facility (Reference 3).

The equations governing the radiative heat transfer are the following:

$$J_i - (1 - \epsilon_i) \sum_{j=1}^N F_{ij} J_j = \epsilon_i E_{b,i} \quad i = 1, 2, \dots, N \quad (1)$$

where:

$$\begin{aligned} J_i &= \text{radiosity of } i\text{-th surface} \\ E_{b,i} \sigma_{SB} T_i^4 &= \text{blackbody emissive power of } i\text{-th surface} \\ F_{ij} &= \text{view factor matrix (from surface "i" to surface "j")} \\ \epsilon_i &= \text{emissivity of } i\text{-th surface} \end{aligned}$$

The emissive power for each radiating surface is calculated from the temperature field. Then equations (1) are solved for the radiosities  $J_i$  and the radiative heat fluxes are calculated from the following equations:

$$q''_{\text{rad},i} = \frac{\epsilon_i}{1 - \epsilon_i} (E_{b,i} - J_i) \quad (2)$$

The convective heat transfer is calculated from:

$$q''_{\text{conv},i} = h_v (T_{w,i} - T_v) \quad (3)$$

then the total heat flux is:

$$q''_{\text{tot},i} = q''_{\text{conv},i} + q''_{\text{rad},i} \quad (4)$$

The program can operate in either transient mode or steady-state mode. In the steady-state mode the temperature field is calculated iteratively. The temperature field is guessed initially to provide an estimate of the convective heat flux and radiation heat flux components. By solving a steady-state energy balance at the surface of the rod, a better estimate of the temperature field is obtained for the next iteration. The calculation proceeds until the error is below a prescribed tolerance (maximum update to the temperature is less than  $10^{-4}$ -F). Typically, because the combined convection and radiation heat transfer phenomenon is strongly non-linear, several hundreds of iterations may be required to achieve convergence.

The rod bundle view factor matrix is calculated for generic square lattice geometry, by specifying number of rods in the array, rod diameter and pitch. The only limitation of the program is that the rods are assumed to be geometrically identical. The power in each rod is assigned as input, therefore enabling to simulate thimbles as zero power rods.

Also, for the purpose of this assessment a 2x2 cluster of rods was assumed to be optically equivalent to the big thimble rod in the CE 16x16 assembly. The view factors from the adjacent rods to the thimble/water hole are reported in Figure 3-2. In particular for the actual geometry we have:

View Factor to Adjacent Water Hole (A->E) = 0.214

View Factor to Diagonal Water Hole (D->E) = 0.120

If the water hole is modeled with a 2x2 cluster of rods with the same diameter as the heated rods, the total view factor from the corresponding rods was estimated by adding individual view factors and results are reported in the following:

View Factor to Adjacent 2x2 Rod Cluster (equivalent to A->E) = 0.226

View Factor to Diagonal 2x2 Rod Cluster (equivalent to D->E) = 0.119

This demonstrates that the 2x2 representation of the large thimble is reasonable.

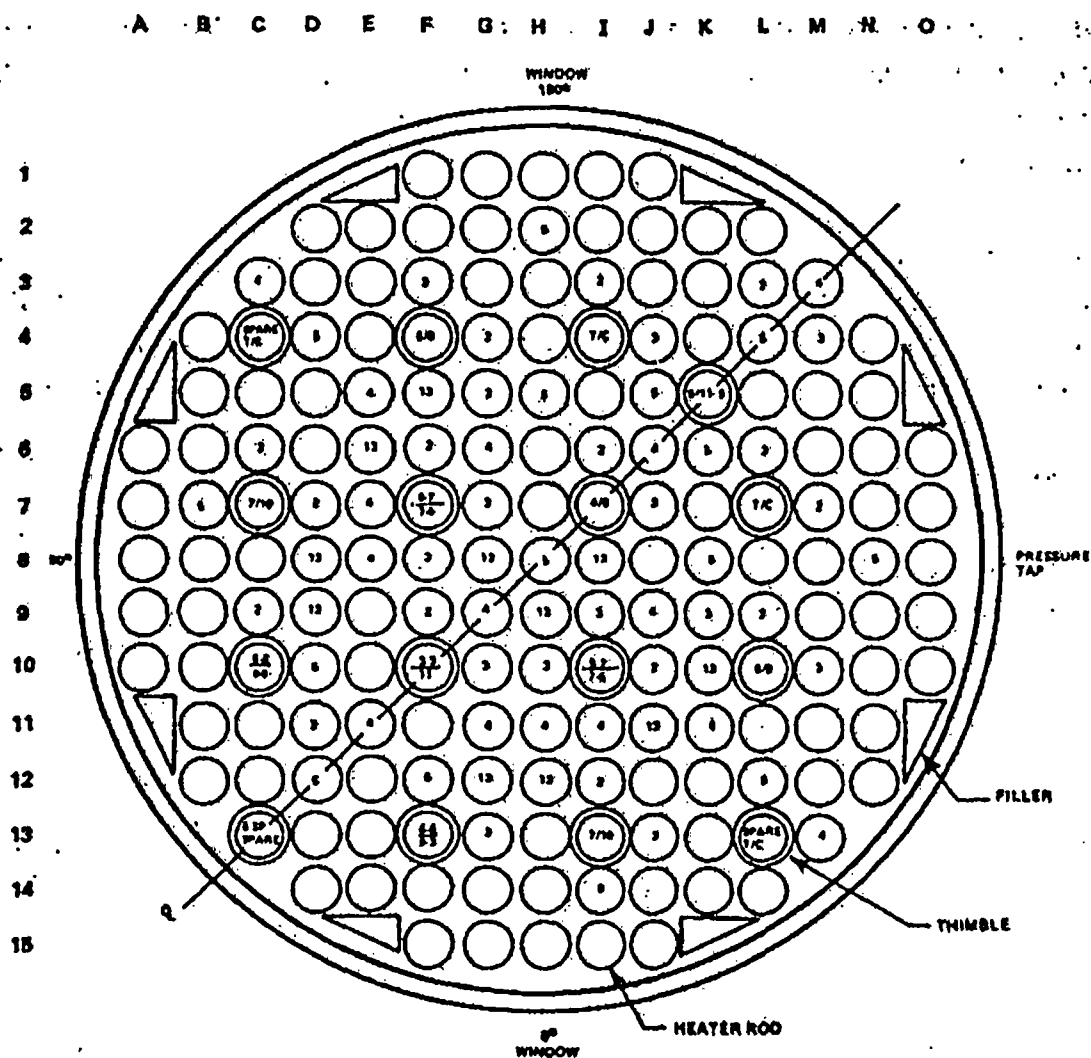
Another approximation was that the presence of a housing was implicitly modeled in the program whereas a reflective/symmetry boundary at the edge of the simulated rods array was desired for this calculation. The reflective boundary was approximated by setting the convection heat transfer from the fluid to the housing to zero and setting to zero the heat losses from the housing to the environment, resulting in a condition close to adiabatic. Also the size of the model was large enough that the temperature at the interior is basically not affected by the presence of the housing. For the purpose of this assessment these approximations were judged to be reasonable.

[

 $J^{ac}$ 

The rod-to-rod radiation heat transfer enhances the effective heat transfer coefficient by providing a heat path for the energy transfer from the surface of the fuel rod to any colder rods or thimbles, which act as a heat sink.

In order to quantify the effect of the rod-to-rod radiation for different lattice geometries, two steady state solutions were calculated for both the Westinghouse 17x17 bundle which is partially represented in the FLECHT-SEASET bundle (Figure 3-1) and the Combustion Engineering 16x16 bundle (Figure 3-2).



## BUNDLE STATISTICS

HOUSING INSIDE DIAMETER	194.0 mm (7.625 in.)
HOUSING WALL THICKNESS	5.08 mm (0.200 in.)
ROD DIAMETER	9.50 mm (0.374 in.)
THIMBLE DIAMETER	12.0 mm (0.474 in.)
ROD PITCH	12.6 mm (0.496 in.)
CROSS-SECTIONAL FLOW AREA	15571 mm <sup>2</sup> (24.136 in. <sup>2</sup> )
FILLER DIMENSIONS	18.8 x 8.43 mm (0.741 x 0.332 in.)
161 HEATER RODS	—
16 THIMBLES	—
8 FILLERS	—

Figure 3-1. FLECHT-SEASET Bundle (Westinghouse 17x17 Fuel Assembly Lattice)

Rod OD = 0.374 inch  
 Rod Pitch = 0.506 inch  
 Water Hole OD = 0.98 inches

Assembly Pitch = 8.18 inches

View Factor to Adjacent Rod (A->B) = 0.124  
 View Factor to Diagonal Rod (A->C) = 0.085  
 View Factor to Adjacent Water Hole (A->E) = 0.214  
 View Factor to Diagonal Water Hole (D->E) = 0.120

Scale Factor = 0.74

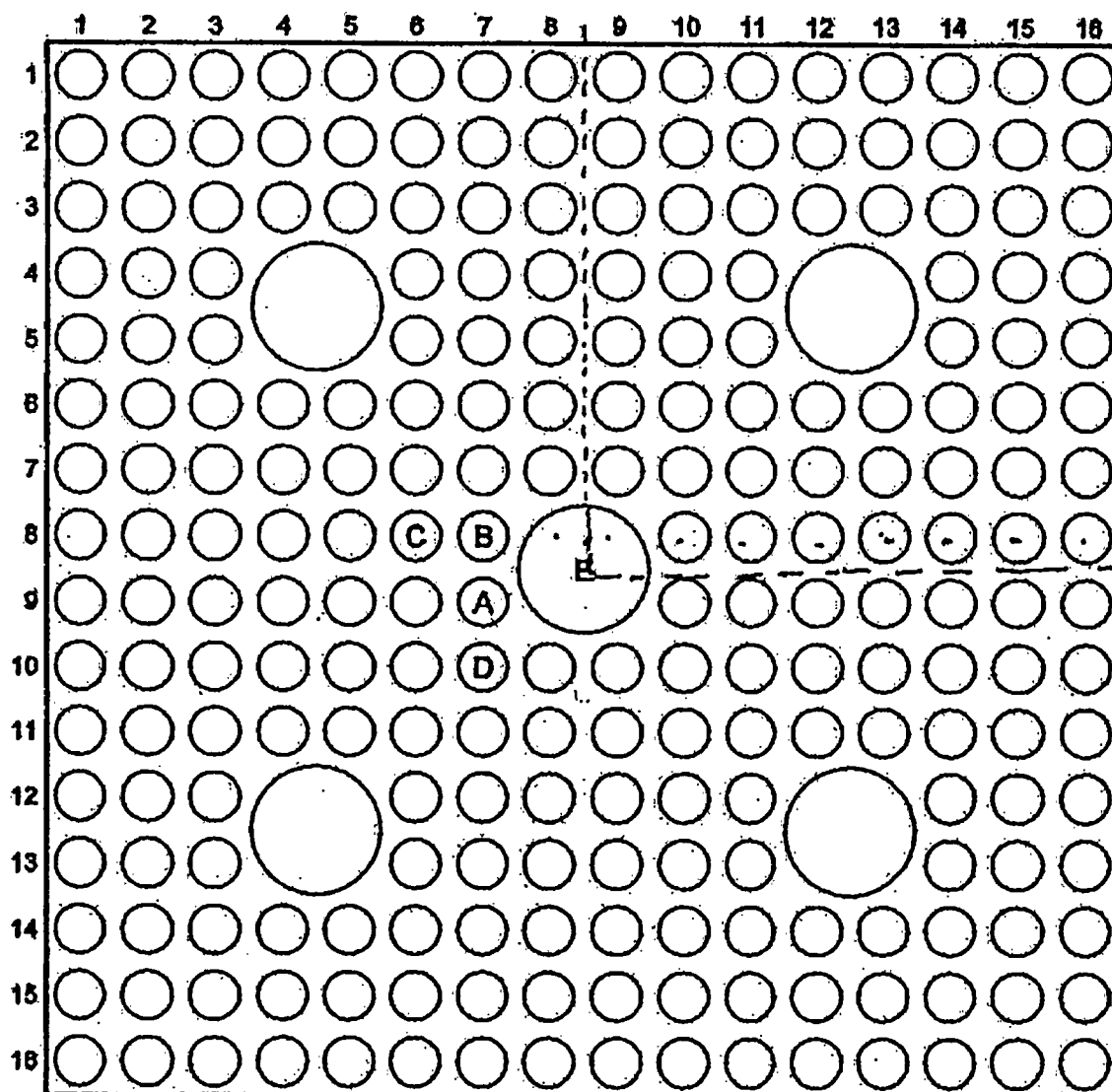


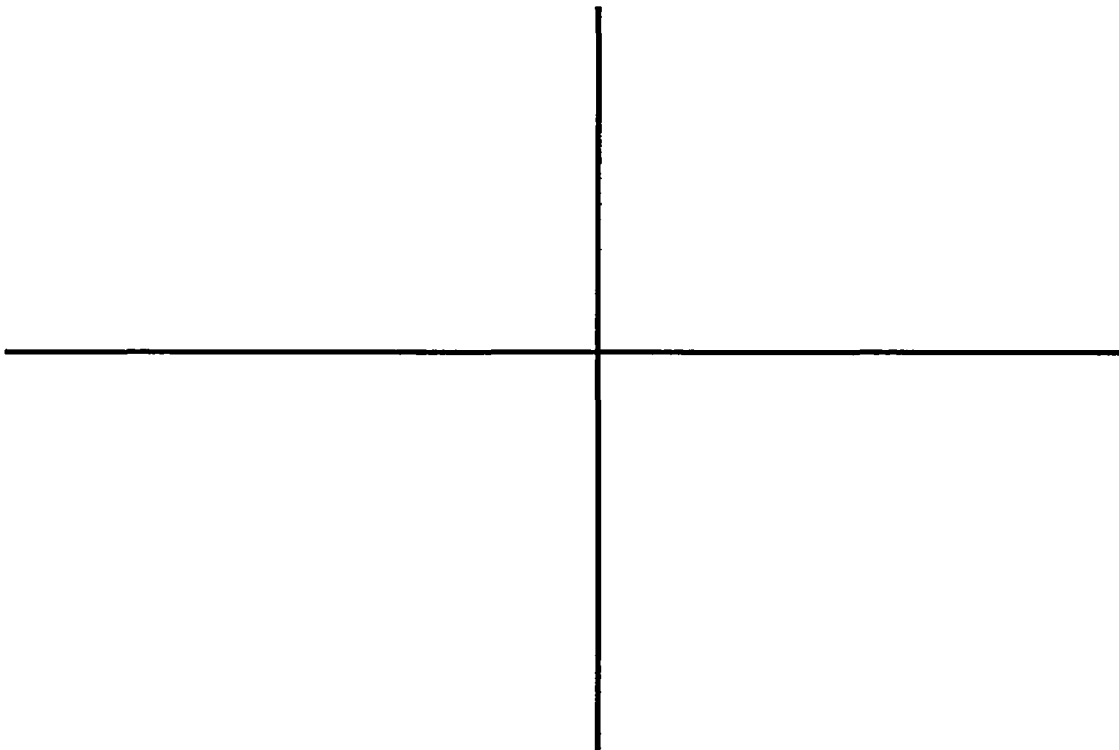
Figure 3-2. CE 16x16 Fuel Assembly Lattice

[

] <sup>a,c</sup>

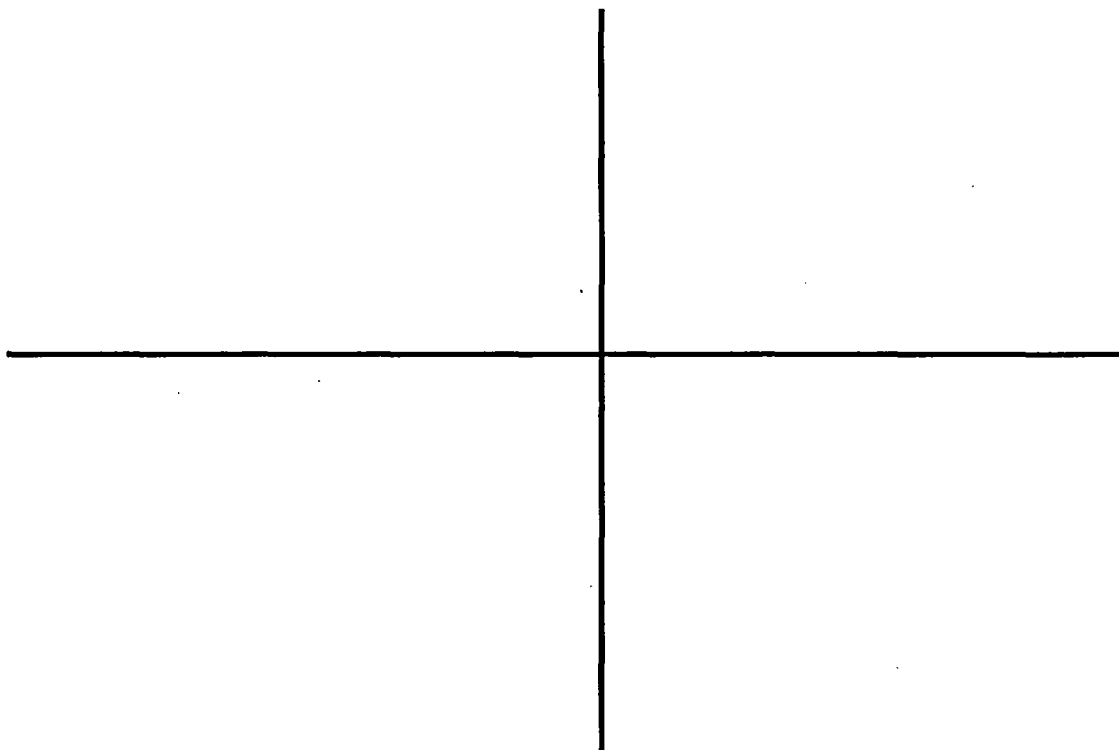
The following tables show the rod surface temperature map obtained for the CE 16x16 and Westinghouse 17x17 fuel assemblies. The assembly boundaries are identified by a thick line:

[

] <sup>a,c</sup>



[

] <sup>a,c</sup>

The following conclusions can be drawn by the previous results:

[

] <sup>a,c</sup>

The current methodology applies a [ ] <sup>a,c</sup>, reduction to the reflood heat transfer multipliers, to account for radiation heat transfer effects which were present in the reflood heat transfer test bundles. The penalty was designed to bound the rod-to-rod radiation effect which was observed in the FLECHT series of tests.

[

] <sup>a,c</sup>

In this exercise the following power distribution (normalized to the average rod power) was assumed (Table 3-3):

0.00	0.00	0.00	0.00	1.00	1.00	1.00	1.10	0.00	0.00	0.00	0.00
0.00	0.00	1.00	1.00	1.00	1.00	1.00	1.10	1.00	1.00	0.00	0.00
0.00	1.00	1.00	1.00	1.00	0.95	1.00	1.10	1.10	1.00	0.95	0.00
0.00	1.00	1.00	0.00	1.00	0.95	1.00	0.00	1.00	0.95	0.95	0.00
1.00	1.00	1.00	1.00	1.00	0.95	1.00	1.10	1.10	1.00	0.95	0.95
1.00	1.00	0.95	0.95	0.95	1.00	1.10	1.10	0.00	1.00	0.95	0.95
1.00	1.00	1.00	1.00	1.00	1.10	0.00	1.10	1.00	0.95	0.95	0.95
1.10	1.10	1.10	0.00	1.10	1.10	1.10	1.00	1.00	0.95	0.95	0.95
0.00	1.00	1.10	1.10	1.10	0.00	1.00	1.00	0.00	1.00	0.95	0.00
0.00	1.00	1.00	0.95	1.00	1.00	0.95	0.95	1.00	0.95	0.95	0.00
0.00	0.00	0.95	0.95	0.95	0.95	0.95	0.95	0.95	0.95	0.00	0.00
0.00	0.00	0.00	0.00	0.95	0.95	0.95	0.95	0.00	0.00	0.00	0.00

Table 3-3 - Power Distribution

Note that zero power rods were used to simulate the thimbles and the non-existent four corners in the test bundle.

[

] we obtain the

following temperature distribution:

I

J<sup>a,c</sup>

[

] <sup>a,c</sup>

The reflood heat transfer multipliers utilized in the HOTSPOT code, are developed from bundle tests (FLECHT series). The heat transfer multipliers are defined as the ratio between the reflood heat transfer coefficient calculated by WCOBRA/TRAC and the measured value at the same axial location. The heat transfer coefficient is defined as the ratio between the measured or calculated heat flux and the delta between the wall temperature and the fluid saturation temperature. The effect of the rod-to-rod radiation component is therefore originally embedded within the multipliers. [

] <sup>a,c</sup>

Results are shown in the following Table 3-6:

[

]<sup>ac</sup>

Similar conclusions were reached from the prior analysis of the FLECHT-Skewed test data [1]. It was observed that in each test the total heat transfer coefficient for the rods with near zero view factors are within [ ]<sup>ac</sup> of the average of the total heat transfer coefficients. To bound this effect a conservative [ ]<sup>ac</sup> penalty on the total heat transfer was applied in the USNRC-approved methodology.

This exercise shows that [ ]<sup>ac</sup> the HTC multiplier is conservative and adequate for both Westinghouse and CE fuel assembly designs.

The applicability of the Westinghouse thermal radiation model utilized in this assessment is discussed in the following Section 4, by benchmarking it against the model provided in this informal USNRC RAI. Section 5 will provide further justification on the method utilized by Westinghouse to account of the rod-to-rod thermal radiation effect in the Large Break LOCA Evaluation Model.

#### 4. Applicability of Westinghouse Surface-to-Surface Radiation Heat Transfer Model

The program utilized by Westinghouse to perform rod-to-rod radiation calculations is a modified version of what was originally developed to support the scaling analysis for the NRC/PSU RBHT facility (Reference 3). This program was benchmarked against the program provided by the NRC as part of this RAI (Reference 4 and 5).

The USNRC model considered a 5x5 rod bundle within a square enclosure (housing). The program receives in input an assumed temperature distribution and produces as output the thermal radiation heat load for each surface. On the other hand, the Westinghouse model assumes the power distribution and calculates the temperature distribution which results from the combined radiation and convection heat transfer.

The calculated view factor matrix was compared for the two models. While the rod-to-rod and rod-to-housing view factors are almost identical, we found that the housing-to-rod and housing-to-housing view factors were significantly different between the two models. The cause of the mismatch is the different assumption in the housing area. In the NRC model the housing area "A" is calculated as:

$$A = 8*(P+2*R)*L$$

where:

$P$  = rod pitch

$R$  = rod radius

$L$  = bundle vertical length

The previous assumption caused some of the view factors to be negative. In the Westinghouse model, the area is calculated as:

$$A = 4*(4*P+2*R+2*GAP)*L$$

where

$GAP$  = distance between the rod surface facing the housing and the housing

The Westinghouse equation to calculate the housing area was implemented into the NRC program and the results now indicate all view factors were identical between the two models.

The benchmark between the NRC model and Westinghouse model was then based on the following steps:

- 1) Calculate the temperature distribution for the 5x5 enclosure considered by the NRC, modified to reflect the FLECHT-Skewed geometry, using the Westinghouse model.
- 2) Input the resulting temperature distribution into the NRC model.
- 3) Compare the predicted radiation heat load and effective radiation heat transfer coefficients (based on  $T_{sat}$ ) from both models

The output file from the Westinghouse model is attached in the following:

#### SURFACE TO SURFACE RADIATION IN A ROD BUNDLE

##### INPUT DATA

Bundle Array Size	(-)	=	5x 5
Rod Diameter	(in)	=	0.422
Rods Array Pitch	(in)	=	0.563
Distance Rods-to-Housing	(in)	=	0.100
Rod Average Power	(kW/ft)	=	0.700
Rod Surface Emissivity	(-)	=	0.800
Housing Surface Emissivity	(-)	=	0.800
Bundle Convection H.T.C.	(Btu/hr-F-ft <sup>2</sup> )	=	39.290 → = 11.18 if $T_{sat}$ -based
Fluid Temperature	(F)	=	1650.000
Housing Heat Losses H.T.C.	(Btu/hr-F-ft <sup>2</sup> )	=	0.000
Environment Temperature	(F)	=	90.000
Housing Thickness	(in)	=	0.050

##### RODS POWER FACTOR

0.00	1.00	1.00	1.00	0.00
1.00	1.00	1.00	1.00	1.00
1.00	1.00	1.00	1.00	1.00
1.00	1.00	1.00	0.00	1.00
0.00	1.00	1.00	1.00	1.00

##### RESULTS STEADY STATE

##### RODS SURFACE TEMPERATURE (F)

1850.27	2050.31	2064.96	2049.85	1849.41
2050.31	2086.65	2097.53	2085.09	2047.16
2064.96	2097.53	2102.47	2088.20	2056.14
2049.85	2085.09	2088.20	1911.87	2047.91
1849.41	2047.16	2056.14	2047.91	2029.02

HOUSING TEMPERATURE (INSIDE WALL) (F) = 1873.65

Rod Surf. Temp. for Pure Convection at SS (F) = 2200.18

# RADIATION HEAT TRANSFER

I	HEAT LOAD (BTU/HR)	H.T.C. (BTU/HR-FT <sup>2</sup> -F)
1	-.108776E+05	-.497495E+01
2	0.814025E+04	0.330537E+01
3	0.734425E+04	0.295785E+01
4	0.816538E+04	0.331643E+01
5	-.108311E+05	-.495634E+01
6	0.814025E+04	0.330537E+01
7	0.616625E+04	0.245381E+01
8	0.557555E+04	0.220557E+01
9	0.625104E+04	0.248969E+01
10	0.831102E+04	0.338067E+01
11	0.734425E+04	0.295785E+01
12	0.557555E+04	0.220557E+01
13	0.530691E+04	0.209364E+01
14	0.608209E+04	0.241826E+01
15	0.782357E+04	0.316643E+01
16	0.816538E+04	0.331643E+01
17	0.625104E+04	0.248969E+01
18	0.608209E+04	0.241826E+01
19	-.142232E+05	-.626146E+01
20	0.827052E+04	0.336279E+01
21	-.108311E+05	-.495634E+01
22	0.831102E+04	0.338067E+01
23	0.782357E+04	0.316643E+01
24	0.827052E+04	0.336279E+01
25	0.929630E+04	0.382039E+01
26	-.121472E+05	-.547476E+01

The temperature distribution resulting from this analysis was input in the NRC program, with the revised equation for the housing area. The main results are summarized in the following:

## EVALUATION OF 5x5 benchmark test

ROD RADIUS (FT) = 0.0176

PITCH (FT) = 0.0469

FROM ROD I	TO ROD J	VIEW FACTOR
1	1	0.000000
1	2	0.126171

.....skipped lines.....



26	25	0.072067
26	26	0.107218

I	HEAT LOAD (BTU/HR)	H.T. COEFF. (BTU/HR-FT <sup>2</sup> -F)
1	-.108930D+05	-.499144D+01
2	0.811926D+04	0.330240D+01
3	0.732320D+04	0.295431D+01
4	0.814475D+04	0.331363D+01
5	-.108467D+05	-.497295D+01
6	0.811926D+04	0.330240D+01
7	0.614651D+04	0.245000D+01
8	0.555702D+04	0.220184D+01
9	0.623147D+04	0.248600D+01
10	0.828916D+04	0.337748D+01
11	0.732320D+04	0.295431D+01
12	0.555702D+04	0.220184D+01
13	0.528774D+04	0.208950D+01
14	0.606255D+04	0.241448D+01
15	0.780280D+04	0.316333D+01
16	0.814475D+04	0.331363D+01
17	0.623147D+04	0.248600D+01
18	0.606255D+04	0.241448D+01
19	-.142344D+05	-.627783D+01
20	0.824918D+04	0.335978D+01
21	-.108467D+05	-.497295D+01
22	0.828916D+04	0.337748D+01
23	0.780280D+04	0.316333D+01
24	0.824918D+04	0.335978D+01
25	0.927348D+04	0.381752D+01
26	-.105446D+06	-.549090D+01

.....skipped lines.....

Results from NRC model and Westinghouse model are in good agreement.

##### 5. Applicability of Westinghouse Method to Account for Rod-to-Rod Thermal Radiation Contribution Based on a Penalty to the Reflood Heat Transfer Multiplier.

As discussed in Section 1, the Westinghouse methodology applies a [ ]<sup>ac</sup> reduction to the reflood heat transfer multipliers, to account for rod-to-rod radiation heat transfer effects. The reason is that the effect of the rod-to-rod thermal radiation is "built-in" in the heat transfer multipliers obtained by assessing the code against test data where the thermal radiation is expected to be a significant factor. However there are core regions where the thermal radiation is expected to be negligible (see corners of CE 16x16 or

Westinghouse 17x17). Since the rod-to-rod radiation heat transfer is not explicitly modeled, the rod-to-rod radiation is [

]a,c

## 6. Conclusions

An evaluation of the differences between the Combustion Engineering fuel assembly design and the Westinghouse fuel assembly design has been performed, with a focus on the effects of the substantially different thimble designs on radiation heat transfer for corner rods with zero view factors to the thimbles. This evaluation considered rod bundle heat transfer data for rods with zero view factors, as well as detailed calculations of rod bundle heat transfer for the different lattices with convection only, versus convection and rod-to-rod and rod-to-thimble radiation heat transfer. This evaluation concludes that the radiation heat transfer for the corner rods of Combustion Engineering and Westinghouse fuel designs is quite comparable. Furthermore, the [ ]<sup>ac</sup> reflood heat transfer multipliers for Westinghouse fuel designs is concluded to remain conservative and applicable for Combustion Engineering fuel designs.

## References

- 1) Section 25-5-5-8 of WCAP-12475-P-A, Rev. 1, "Code Qualification Report for Large Break Loss-of-Coolant Accident Analysis," March 1998.
- 2) EPRI NP-3268/NUREG/CR-3314/WCAP-10307, "PWR FLECHT SEASET: 163-Rod Bundle Flow-Blockage Task Data Report," May 1984.
- 3) PSU ME/NE - NRC-04-98-041, Rev 1, "Dispersed Flow Heat Transfer Under Reflood Conditions in a 49 Rod Bundle: Test Plan and Design - Results From Task 1-10," February 2000.
- 4) Cox, R.L., "Radiative Heat Transfer in Arrays of Parallel Cylinders," ORNL-5239, June 1977.
- 5) Mandell, D.A., "Geometric View Factors for Radiative Heat Transfer Within Boiling Water Reactor Bundles," Nucl. Tech., Vol. 52, March 1981.

## **APPENDIX D**

### **MODIFICATIONS TO THE TOPICAL REPORT FOLLOWING FROM USNRC INTERACTION**

As a consequence of discussions, as documented by the response to the USNRC RAIs, with the USNRC during the review of the ASTRUM topical, several pages of this report were modified from the original version (WCAP-16009-P and WCAP-16009-NP) in this revision (WCAP-16009-P-A and WCAP-16009-NP-A). The following pages provide the original versions of all pages for which technical content was modified. Also, all changes to the original topical are identified with revision bars in this topical report.

Note that in the case of Section 11, the complete revision of Section 11-1 affected the page number and layout of the following pages. However, to properly identify only pages with a different technical content, only those pages that included modifications to the content of the original version are provided here.

## 11 SENSITIVITY AND UNCERTAINTY ANALYSIS (CSAU ELEMENT 3)

### 11-1 TECHNICAL BASIS FOR REVISED UNCERTAINTY METHODOLOGY

#### 11-1-1 Statistical Sampling Approach

Code Scaling, Applicability, and Uncertainty (CSAU) Element 3, the sensitivity and uncertainty analysis element, aims to provide a simple, singular statement of the uncertainty (Boyack, et al. 1989). To accomplish this objective, the effects of the important individual uncertainty contributors are determined. The uncertainty statement is based on the combined effect of the contributors.

The determination of peak cladding temperature (PCT) uncertainty in the Automated Statistical Treatment of Uncertainty Method (ASTRUM) relies on a statistical sampling technique. It is possible to determine the tolerance limits from unknown distributions by randomly sampling the character in question (in this case, PCT). The consideration of non-parametric tolerance limits was originally presented by Wilks (Wilks, 1941). Wilks' study showed that for continuous populations, the distribution of  $P$ , the proportion of the population between two order statistics from a random sample, is independent of the population sampled. Also, it is only a function of the particular order statistics chosen.

Derivation of non-parametric tolerance limits is presented next. The derivation provided here is adapted mainly from Johnson and Leone (1976).

The model appropriate to random sampling comes from an infinitely large population when a continuous character,  $X$ , is measured on each individual in the sample. The measurements obtained from a sample of size  $n$  are denoted by the random variables  $X_1, X_2, \dots, X_n$ . The  $X_i$ 's are mutually independent, and each  $X_i$  had the same probability density function, that is,

$$p_{X_i}(x_i) = f(x)_{x=x_i} \quad (11-1)$$

for  $i=1, 2, \dots, n$  where  $f(x)$  is a mathematical function of  $x$ . Also, the cumulative distribution functions are

$$F_{X_i}(x_i) = \int_{-\infty}^{x_i} f(x) dx \quad (11-2)$$

Let us introduce  $n$  new random variables  $X'_1, X'_2, \dots, X'_n$ , which are the original random variables  $X_1, X_2, \dots, X_n$  arranged in an ascending order of magnitude, so that

$$X'_1 < X'_2 < \dots < X'_n \quad (11-3)$$

## 11-2

The possibility of any two of the  $X$ 's being equal can be neglected, because they are continuous random variables.

The event  $(X'_n \leq x)$  is equivalent to the intersection of the events  $(X_1 \leq x), (X_2 \leq x), \dots, (X_n \leq x)$ . For if the greatest  $X_i$  is less than or equal to  $x$ , so are all the  $X_i$ 's; conversely, if every  $X_i$  is less than or equal to  $x$ , so is the greatest  $X_i$ . Therefore

$$Pr[X'_n \leq x] = \prod_{i=1}^n Pr[X_i \leq x] = \prod_{i=1}^n F_{X_i}(x) = [F_X(x)]^n \quad (11-4)$$

Therefore, the cumulative distribution function of  $X'_n$  is

$$F_{X'_n}(x'_n) = [F_X(x'_n)]^n \quad (11-5)$$

and the probability density function is

$$p_{X'_n}(x'_n) = n[F_X(x'_n)]^{n-1} f(x'_n) \quad (11-6)$$

The distribution of  $X'_1$ , the smallest of the  $n$   $X$ 's is investigated in exactly the same manner. The event  $(X'_1 > x)$  is equivalent to the intersection of the  $n$  events  $(X_1 > x), (X_2 > x), \dots, (X_n > x)$ . Hence

$$1 - F_{X'_1}(x) = \prod_{i=1}^n [1 - F_{X_i}(x)] = [1 - F_X(x)]^n \quad (11-7)$$

and so

$$F_{X'_1}(x'_1) = 1 - [1 - F_X(x'_1)]^n \quad (11-8)$$

and

$$p_{X'_1}(x'_1) = n[1 - F_X(x'_1)]^{n-1} f(x'_1) \quad (11-9)$$

The event  $(X'_r \leq x)$  is the logical sum of the events:

"exactly  $j$  out of  $X_1, X_2, \dots, X_n$  are less than or equal to  $x$ " for  $j = r, r+1, r+2, \dots, n$ .

These events are mutually exclusive, and so

$$Pr[X'_r \leq x] = \sum_{j=r}^n \binom{n}{j} [F_X(x)]^j [1 - F_X(x)]^{n-j} \quad (11-10)$$

The probability that the  $r$ th smallest value lies between  $x'_r - \frac{1}{2}(\delta x'_r)$  and  $x'_r + \frac{1}{2}(\delta x'_r)$  is approximately

$p_{X'_r}(x'_r)(\delta x'_r)$ . If the  $r$ th smallest  $X$  is between  $x'_r - \frac{1}{2}(\delta x'_r)$  and  $x'_r + \frac{1}{2}(\delta x'_r)$ , this is equivalent to having

$r-1$  of the  $X$ 's less than  $x_r' - \frac{1}{2}(\delta x_r')$

1 of the  $X$ 's between  $x_r' - \frac{1}{2}(\delta x_r')$  and  $x_r' + \frac{1}{2}(\delta x_r')$

and

$n-r$  of the  $X$ 's greater than  $x_r' + \frac{1}{2}(\delta x_r')$

The possibility that more than one  $X$  might be between  $x_r' - \frac{1}{2}(\delta x_r')$  and  $x_r' + \frac{1}{2}(\delta x_r')$  is neglected. The probability of this event is of the order  $(\delta x_r')^2$ .

For any one  $X$ , we have

$$Pr[X < x_r' - \frac{1}{2}(\delta x_r')] = F_X(x_r') - \frac{1}{2}f(x_r')(\delta x_r') \quad (11-11)$$

$$Pr[x_r' - \frac{1}{2}(\delta x_r') < X < x_r' + \frac{1}{2}(\delta x_r')] = f(x_r')(\delta x_r') \quad (11-12)$$

$$Pr[X > x_r' + \frac{1}{2}(\delta x_r')] = 1 - F_X(x_r') - \frac{1}{2}f(x_r')(\delta x_r') \quad (11-13)$$

Hence, applying the multinomial distribution,

$$p_{X_r'}(x_r')(\delta x_r') = \frac{n!}{(r-1)!(n-r)!} [F_X(x_r')]^{r-1} [1 - F_X(x_r')]^{n-r} f(x_r')(\delta x_r') \quad (11-14)$$

Dividing both sides by  $\delta x_r'$  and then taking limiting values as  $\delta x_r'$  tends to zero, we obtain

$$p_{X_r'}(x_r') = \frac{n!}{(r-1)!(n-r)!} [F_X(x_r')]^{r-1} [1 - F_X(x_r')]^{n-r} f(x_r') \quad (11-15)$$

11-4

For  $r < s$ 

$$p_{X_1, X_s}(x_1, x_s) = \frac{n!}{(r-1)!(s-r-1)!(n-s)!} [F_X(x_s)]^{r-1} \times [F_X(x_s) - F_X(x_1)]^{s-r-1} \times [1 - F_X(x_s)]^{n-s} f(x_s) f(x_1) \quad (11-16)$$

For the particular case  $r=1, s=n$ , we have the joint probability density function of the smallest and greatest of the  $n$   $X$ 's. This is

$$p_{X_1, X_n}(x_1, x_n) = n(n-1)[F_X(x_n) - F_X(x_1)]^{n-2} f(x_n) f(x_1) \quad (11-17)$$

For an  $X$  chosen at random, the probability density function of the probability integral  $F_X(X_i)$  is

$$p_{F_X}(X_i)[F_X(x_i)] = \frac{f(x_i)}{[dF_X(x_i)/dx_i]} = 1 \quad (0 \leq F_X(x_i) \leq 1) \quad (11-18)$$

since

$$F_X(x_i) = \int_{-\infty}^{x_i} f(x) dx \quad (11-19)$$

Thus, whatever be  $f(x)$ , provided only that  $X$  is a continuous random variable,  $F_X(X_i)$  is "rectangularly distributed" (uniformly distributed) between 0 and 1. Since  $F_X(X_r) \leq F_X(X_s)$  if  $r < s$ , the  $n$  quantities  $Y_r = F_X(X_r)$  are distributed as an ordered sample of size  $n$  from a population with the probability density function  $p_Y(y) = 1$  for  $0 \leq y \leq 1$ .

Applying Equation 11-15 with  $r, s$ , we have

$$p_{Y_r, Y_s}(y_r, y_s) = \frac{n!}{(r-1)!(s-r-1)!(n-s)!} (y_r)^{r-1} (y_s - y_r)^{s-r-1} (1 - y_s)^{n-s} \quad (0 \leq y_r \leq y_s \leq 1) \quad (11-20)$$

By making the following transformation and introducing two new variables  $Z_r$  and  $Z_n$ ,

$$z_r = y_r, \quad z_n = y_s - y_r \quad (11-21)$$

$$\frac{\partial(y_r, y_s)}{\partial(z_r, Z_n)} = \begin{vmatrix} 1 & 0 \\ 1 & 1 \end{vmatrix}$$



we have

$$p_{Z_r, Z_n}(Z_r, Z_n) = \frac{n!}{(r-1)!(s-r-1)!(n-s)!} z_r^{r-1} z_n^{s-r-1} (1-z_r-z_n)^{n-s} \quad (11-22)$$

$(0 \leq z_r, 0 \leq z_n, z_r + z_n \leq 1)$

By integrating with respect to  $Z_r$ , leaving the probability density function of  $Z_n$  in the form

$$p_{Z_n}(Z_n) = \int_0^{1-Z_n} p_{Z_r, Z_n}(Z_r, Z_n) dz_r = \frac{n!}{(r-1)!(s-r-1)!(n-s)!} z_n^{s-r-1} \times \int_0^{1-Z_n} z_r^{r-1} (1-z_r-z_n)^{n-s} dz_r \quad (11-23)$$

This reduces to

$$p_{Z_n}(Z_n) = \frac{n!}{(r-1)!(s-r-1)!(n-s)!} z_n^{s-r-1} (1-z_n)^{n-s+r} \times \int_0^{1-Z_n} u^{r-1} (1-u)^{n-s} du \quad (11-24)$$

with

$$u = \frac{z_r}{1-z_n} \quad (11-25)$$

since

$$\int_0^1 u^{r-1} (1-u)^{n-s} du = \frac{(r-1)!(n-s)!}{(n-s+r)!} \quad (11-26)$$

$$p_{Z_n}(z_n) = \frac{n!}{(s-r-1)!(n-s+r)!} z_n^{s-r-1} (1-z_n)^{n-s+r} \quad (0 \leq z_n \leq 1) \quad (11-27)$$

It is possible, therefore, to determine numbers  $z_n^{(\alpha)}(n)$  such that

$$Pr\{z_n > z_n^{(\alpha)}(n)\} = 1 - \alpha \quad (11-28)$$

These numbers are simply obtained by solving the equation

$$\int_z^1 p(z_n) dz_n = 1 - \alpha \quad (11-29)$$

To solve this equation, tables of the incomplete beta function or similar tables may be used.

## 11-6

Sample size  $n$  for non-parametric tolerance limits can be calculated using the following approximation (Conover, 1999):

$$n = \frac{1}{4} X_{1-\alpha} \frac{1+q}{1-q} + \frac{1}{2} (r+m-1) \quad (11-30)$$

where  $X_{1-\alpha}$  is the  $(1-\alpha)$  quantile of a Chi-squared random variable with  $2(r+m)$  degrees of freedom. For the one-sided (upper) tolerance limit,  $r = 0$ . From chi-squared distribution table,  $X_{1-\alpha}$  is 5.991 for  $m = 1$ , 9.488 for  $m = 2$ , with a 95-percent confidence level. Using these numbers with  $q = 0.95$  to cover 95 percent of the population, one gets  $n = 59$  for  $m = 1$  (highest) and  $n = 93$  for  $m = 2$  (second highest).

The statistical interpretation of this result is that if we observe a random sample of size  $n$ , then the probability that the proportion of the population included between  $X'$  and  $X''$  exceeds  $z_{\alpha}^{(n)}$  is  $1-\alpha$ . By choosing  $n$ ,  $r$ , and  $s$  suitably, one can be as sure as desired (that is,  $\alpha$  is as small as desired) of including at least a given proportion, say  $q$ , of the population between two specified sample values, without knowing any information about the form of  $f(x)$ .

### 11-1-2 Application of the Statistical Method

The run matrix is generated by using random numbers. The random numbers are obtained using a generator adapted from Press; et al. This particular generator has a period of approximately  $2.3 \times 10^{18}$ , that is, the numbers generated would not be repeated before  $2.3 \times 10^{18}$  random numbers are used. For all practical purposes, this number is quite large and period exhaustion is considered impossible.

The random number generator returns a value between 0 and 1. Sampling from a uniform distribution is quite straightforward: the random number range is linearly mapped to uniform range of interest.

$$\text{VALUE} = a + (b-a) \cdot \text{RND},$$

where  $a$  and  $b$  is the minimum and maximum of the uniform range,  $\text{RND}$  is the random number between 0 and 1 and  $\text{VALUE}$  is the sampled value from the range. Sampling of values from normal distributions is accomplished by employing the rejection type approach.

The random number generator depends on an initial *seed* to select the starting point in a random sequence. Having such algorithms allow us repeatability of results without compromising randomness. In ASTRUM, the initial seed is obtained randomly from the configuration control system. This system assigns a random identifier to each run, so that they can be uniquely identified. If the run matrix needs to be repeated or extended, by giving the same seed, repeatability is ensured.

Using the attributes corresponding to plant initial conditions, global modeling, and local uncertainty variables, the plant's response to a LOCA event is computed for each case. Then the results are tallied by ranking the PCT from highest to lowest. Using the order statistics, the 95th percentile PCT is determined with 95 percent confidence. Actual plant calculation employing this technique is discussed in Section 12.

11-14

• [

]™

### 11-3-2 NPP Uncertainty Calculations

Table 11-5 lists the physical models and plant parameters that are sampled for each case in the uncertainty analysis. The uncertainty distribution sampled for each model and parameter were given previously in Tables 1-7 through 1-11. The PCT for each case is calculated, and the results are ordered from highest to lowest. The 95/95 value of PCT is determined as described in the next section.

### 11-4 DETERMINATION OF COMBINED BIAS AND UNCERTAINTY (CSAU STEP 13)

Section 11-1 described the statistical theory used to determine the number of cases required to establish the 95th percentile PCT at 95-percent confidence. It was shown that the highest value PCT from a sample size of 59 would be a conservative estimate of the 95/95 value. Alternatively, the second highest value from a sample size of 93 would be a conservative 95/95 estimate.

The Westinghouse methodology for combining biases and uncertainties considers the effect of all medium- and high-ranked phenomena from the Phenomena Identification Ranking Table (PIRT), as detailed earlier in Table 1-1. The following discussion describes how each of the phenomena is considered.

#### 11-4-1 Fuel Rod

**Stored Energy** Uncertainties in the initial stored energy of the hot rod and hot assembly are large. There is a wide range of possible peaking factors and power distributions that are allowed by the Technical Specifications. For a given power distribution, the best-estimate fuel rod temperatures are a [

]™ Each of these factors has been considered in the uncertainty methodology, by explicitly ranging the parameters.

11-20

**11-4-12' Loop**

**Flow Split** The flow split in the broken loop is ranged by varying the broken cold-leg nozzle resistance, by an amount that accounts for uncertainties in its value, and uncertainties in the broken loop pump resistance. Modeling of split break and guillotine break geometries also affects the loop flow split.

**11-5 DETERMINATION OF TOTAL UNCERTAINTY (CSAU STEP 14)**

Step 14 of the CSAU methodology has a provision to consider adding margin to the results of Step 13, if warranted, due to limitations in the code or data base. There are no significant limitations in the code or data base that require the consideration of additional margin. The results of Step 13 are, therefore, considered to be the final results for the ASTRUM.

**11-6 APPLICATION TO OTHER 10CFR50.46 ACCEPTANCE CRITERIA**

The combination of conditions that result in the 95/95 PCT are also used to assess local and core-wide oxidation. This assures that there is a high probability that the acceptance criteria are met, consistent with the Code of Federal Regulations (CFR) 10CFR50.46 requirements and Regulatory Guide 1.157 guidance. Details of the oxidation methodology are described below.

**11-6-1 Local Oxidation**

I

J<sup>ac</sup>

### 11-6-2 Core-Wide Oxidation

A generic rod power census is used to calculate the core-wide oxidation for the case that yields the 95/95 PCT. This census defines the percentage of rods in the core that are below a given relative power. The generic values are given in Table 11-6, and the resulting FdH ranges are given for an analysis that supports an FdH limit of 1.70.

The WCOBRA/TRAC code calculates the percentage of cladding volume oxidized for each rod in the core. The percentage of cladding volume oxidized for the hot assembly rod for the case that yields the 95/95 PCT represents the Rod Group 1 contribution. A series of additional WCOBRA/TRAC calculations are performed using the same parameter settings, decreasing the hot assembly power in steps according to the generic rod power census. The percentage of cladding volume oxidized for the hot assembly (HA) rod from each of these cases is multiplied by the fraction of the core represented by that case. The results are summed to obtain the core-wide oxidation:

$$\text{Core-wide oxidation (\%)} = \sum_{i=1}^7 (\% \text{ HA cladding oxidized})_i (\text{fraction of core})_i$$

The generic rod power census is very conservative. In the unlikely event that it yields an unacceptable result, a plant-specific census would be used. It would also be checked each reload to ensure its continued applicability.

### 11-7 REFERENCES

- Bajorek, S. M., et al., 1998, "Code Qualification Document for Best Estimate LOCA Analysis," WCAP-12945-P-A, Volume 1 Revision 2, and Volumes 2 through 5 Revision 1, and WCAP-14747.
- Boyack, B., et al., "Quantifying Reactor Safety Margins," NUREG/CR-5249, (1989).
- Conover, W. J., "Practical Nonparametric Statistics," 3rd Ed., John Wiley & Sons, New York, 1999, Chapter 3.
- Dederer, S. I., et al., 1999, "Application of Best Estimate Large Break LOCA Methodology to Westinghouse PWRs with Upper Plenum Injection," WCAP-14449-PA, Revision 1 and WCAP-14450-NP-A, Revision 1 (Non-Proprietary).
- Johnson, N. L. and F. C. Leone, "Statistics and Experimental Design in Engineering and the Physical Sciences," Volume 1, 2nd Ed., John Wiley & Sons, New York, 1976, Chapter 6.
- Press, W. H., et al., Numerical Recipes in FORTRAN: the art of scientific computing, 2<sup>nd</sup> Ed., Cambridge University Press, 1992, Chapter 7.

---

11-22

---

Somerville, P. N., "Tables for Obtaining Non-parametric Tolerance Limits," The Annals of Mathematical Statistics, Vol. 29 (1958), pp. 599-601.

Wilks, S. S., "Statistical Prediction with Special Reference to the Problem of Tolerance Limits," The Annals of Mathematical Statistics, Vol. 13 (1942), pp. 400-409.

Wilks, S. S., "Determination of Sample Sizes for Setting Tolerance Limits," The Annals of Mathematical Statistics, Vol. 12 (1941), pp. 91-96.

11-28

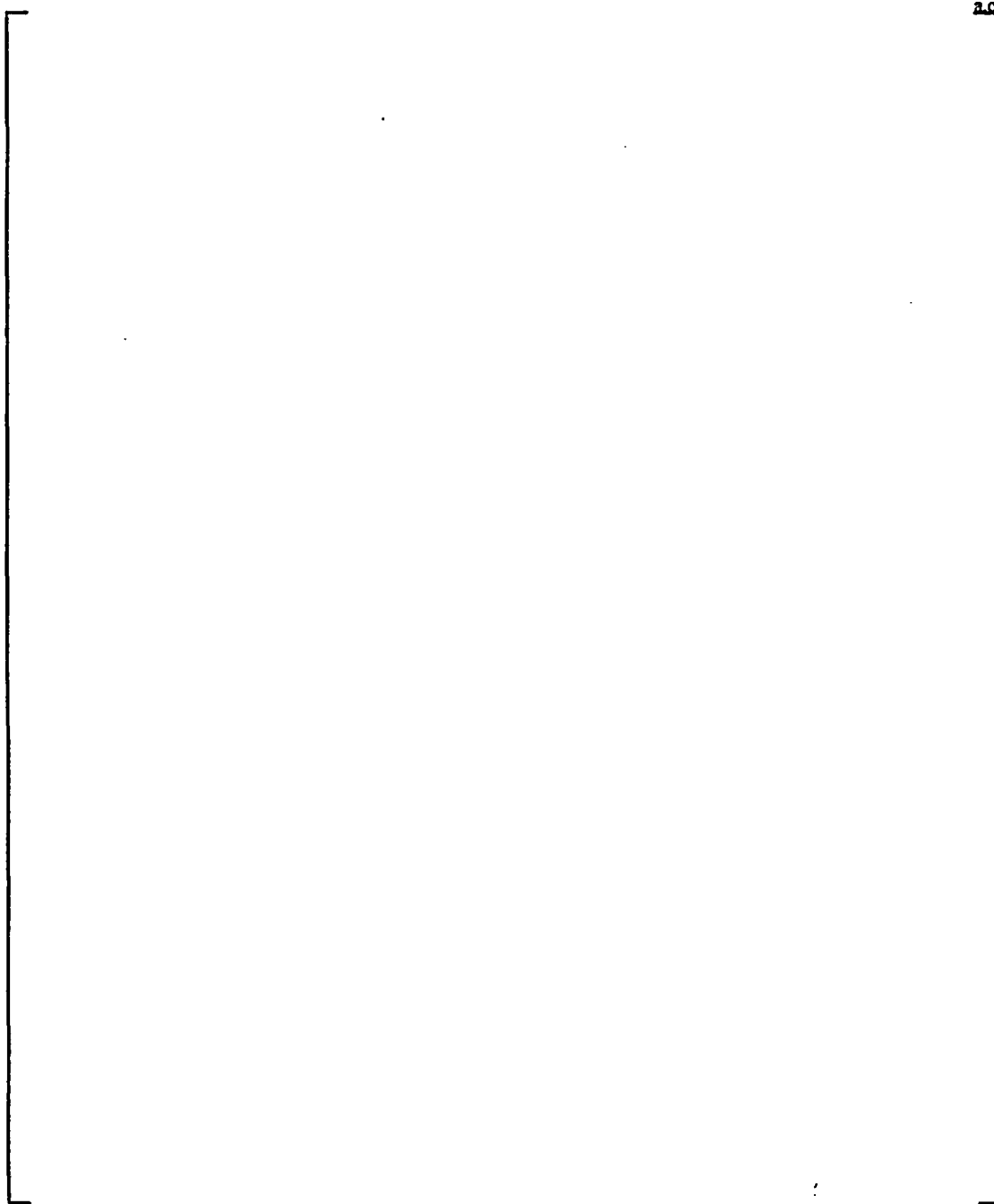


**Figure 11-1. Split vs. DECLG for 3- and 4-Loop PWRs**

Sensitivity and Uncertainty Analysis (CSAU Element 3)  
α:6155-Non-Sec11.wpd-021105

May 2003  
Rev. 0

12-16

## 12-5 DEVELOPMENT OF RUN MATRIX

The individual uncertainty contributors are sampled with a random number generator as discussed in Section 11. The random number generator generates the attributes for at least 59 WCOBRA/ TRAC runs. This is the number of runs that is required to conservatively estimate the true 95th percentile of the population of PCT.

The list of attributes (or uncertainty contributors) can be divided into 2 main groups. The first group includes all the model uncertainty contributors. The model uncertainty contributors include global model and local model parameters. The global model parameters are varied within the WCOBRA/TRAC code whereas the local models are varied within the HOTSPOT code, which is executed once the WCOBRA/TRAC calculation is completed. The second group includes the initial condition and power distribution uncertainty contributors. These parameters are plant specific. The nominal and reference values, as well as the sampling range for IP 2, are shown in Table 12-4.

## 12-6 ASTRUM RESULTS AND DETERMINATION OF THE 95/95 PCT VALUE

The maximum PCT predicted for each of the 59 runs is extracted. Table 12-7 shows the value of the uncertainty contributors for the most limiting transients. The reference transient is compared to the limiting case in Figure 12-22. The most limiting transient is a double-ended cold-leg guillotine (DECLG) break. The maximum PCT is 1899°F. This corresponds to a conservative estimate of the 95-percent PCT probability with 95-percent confidence level.

The global variables listed in Table 12-7 have been defined previously, but local variable settings require some explanation. The parameter values (PVs) for most of the local variables are calculated as shown in Table 12-8. When the statistical fluctuation is expressed as a percentage of the best-estimate value, and the population is normal,  $PV$  is defined as  $I + V_n$ , where  $V_n$  is a random sample from a normal distribution with mean 0 and standard deviation  $\sigma$ . When the statistical fluctuation is expressed as a percentage of the best-estimate value and the population is uniform,  $PV$  is defined as  $I + RNG * V_n$ , where  $V_n$  is a random number between -1 and 1, and  $RNG$  is the range of the distribution. When the statistical fluctuation is a dimensional number and the population is normal,  $PV$  is defined as  $0 + V_n$ , where  $V_n$  is a random sample from a normal distribution with mean 0 and standard deviation  $\sigma$ . Finally, when the statistical fluctuation is a dimensional number and the population is uniform,  $PV$  is defined as  $RNG * V_n$ , where  $V_n$  is a random variable between -1 and 1.

The last 4 local variables shown in Table 12-7 are the heat transfer multipliers, sampled from the distributions summarized in Table 1-8.

Figure 12-23 shows the PCT transient for the 9 highest PCT cases as well as the reference transient. Of them, 2 are split break and 7 are DECLG.



## 12-7 OTHER 10CFR50.46 CRITERIA

The additional Code of Federal Regulations (CFR) 10CFR50.46 criteria that ASTRUM needs to address are the following:

- Verify that with high probability the maximum cladding oxidation is less than 17 percent
- Verify that with high probability the core-wide oxidation is less than 1 percent

The calculation of both the local oxidation and the core-wide oxidation is based on the results from the most limiting transient.

The maximum local oxidation was calculated as described in Section 11-6-1. For IP2, the maximum local oxidation is about 2 percent, which is considerably below the 17-percent limit prescribed by the 10CFR50.46 criteria. This result includes the effects of double-sided reaction, because the limiting case had cladding burst predicted by the code.

The local oxidation is known to be a strong function of the PCT. This dependence is clearly seen in Figure 12-36.

For IP2, the whole rod volumetric oxidation fraction of the hot rod estimated from the limiting case results is 0.6 percent. Therefore, a detailed calculation of core-wide oxidation as described in Section 11-6-2 is not necessary for IP2. By definition, the core-wide oxidation fraction is less than the hot rod volumetric oxidation and the 10CFR50.46 criterion on core-wide oxidation is satisfied.

## 12.8 REFERENCES

Bajorek, S. M., et al., 1998, "Code Qualification Document for Best Estimate LOCA Analysis," WCAP-12945-P-A, Volume 1, Revision 2, and Volumes 2 through 5, Revision 1, and WCAP-14747 (Non-Proprietary).

Bordelon, F. M. and Murphy, E. T., 1974, "Containment Pressure Analysis Code (COCO)," WCAP-8327 (Proprietary), WCAP-8306 (Non-Proprietary).

Dederer, S. I., et al., 1999, "Application of Best Estimate Large Break LOCA Methodology to Westinghouse PWRs with Upper Plenum Injection," WCAP-14449-P-A, Revision 1, and WCAP-14450-NP-A, Revision 1 (Non-Proprietary).

Dederer, S. I., et al., 1988, "Westinghouse Large Break LOCA Best Estimate Methodology. Volume 2: Application to 2-loop PWRs Equipped with Upper Plenum Injection," WCAP-10924-P-A, Revision 2.

Foster, J. P. and Sidener, S., 2000, "Westinghouse Improved Performance Analysis and Design Model (PAD 4.0)," WCAP-15063-P-A, Revision 1 with Errata.

#### 4.4 Statistical Treatment of Overall Calculational Uncertainty

The overall uncertainty in PCT is determined using a non-parametric statistical method. Uncertainties in [ ]<sup>1,2</sup>. The limiting case from a series of 59 PWR cases is considered to be the 95<sup>th</sup> percentile case, with 95 percent confidence.<sup>(1)</sup>

The best-estimate LBLOCA methodology used by Westinghouse addresses the PCT, maximum cladding oxidation, maximum hydrogen generation, and coolable geometry criteria defined in 10CFR50.46(b)(1) through (b)(4). The PCT at the 95th percentile level is estimated as described above. The maximum cladding oxidation criterion and the maximum hydrogen generation criterion are verified as described in Section 11-6. Coolable geometry is demonstrated by ensuring that the PCT and maximum local oxidation criteria are satisfied, including any effects of combined LOCA and SSE loads on core geometry.<sup>(2)</sup>

The Westinghouse methodology used to satisfy the long-term cooling criterion defined in 10 CFR 50.46(b)(5) is unaffected by the use of best-estimate techniques for the short-term transient calculation.

#### References for Regulatory Position 4.4 Compliance Discussion

- 1) Section 11-1
- 2) RAIS-53

#### 4.5 NRC Approach to LOCA Uncertainty Evaluation

The Westinghouse methodology is structured consistent with the CSAU methodology cited in Section 4.5 of RG 1.157.

### 13-3 EFFECT OF REVISED UNCERTAINTY METHODOLOGY ON PRIOR SER REQUIREMENTS

Page 14 of the SER regarding WCAP-12945-P-A discusses applicability limits and usage conditions regarding the prior best-estimate methodology for 3- and 4-loop plants with cold-leg ECCS injection. Pages 13 and 14 of the SER, regarding WCAP-14449-P-A, discusses applicability limits and usage conditions regarding the prior best-estimate methodology for 2-loop plants with low-head safety injection into the upper plenum. The continued applicability of these stipulations is discussed below. In each case, the stipulation is quoted from the SER, and then the continued applicability is addressed.

## INDEX

COMBUSTION ENGINEERING DESIGNS, EXTENSION OF ASTRUM TO	A-1
COMPLIANCE WITH 10CFR50.46	13-1
COMPLIANCE WITH REGULATORY GUIDE 1.157	13-1
CONDUCTOR MODELING, VESSEL COMPONENT	7-1
Calculation of Thermal Conductance	7-6
Conduction Equation	7-3
CONDUCTOR MODELING, ONE-DIMENSIONAL COMPONENTS	7-38
CONSERVATION EQUATIONS, WCOBRA/TRAC	2-1
See ONE-DIMENSIONAL COMPONENTS, CONSERVATION EQUATIONS	2-40
See VESSEL COMPONENT, CONSERVATION EQUATIONS	2-1
CRITICAL FLOW MODEL	4-84
Critical Flow Model (TRAC-PF1)	4-85
Natural Choking Approach (TRAC-PD2)	4-84
Post Critical Flow Model	4-94
CSAU Methodology	1-1
CSAU, Step 1: Scenario Specification	1-1
CSAU, Step 2: Nuclear Power Plant Selection	1-3
CSAU, Step 3: Phenomena Identification and Ranking	1-3
Fuel Rod	1-3
Core	1-4
Upper Plenum	1-6
Hot Leg	1-7
Pressurizer	1-7
Steam Generators	1-8
Pump	1-8
Cold Leg/Accumulator	1-8
Downcomer	1-9
Lower Plenum	1-10
Break	1-10
Loop	1-10
CSAU, Step 4: Frozen Code Selection	1-11
CSAU, Step 5: Provide Complete Documentation	1-12
CSAU, Step 6: Code Applicability Determination	1-13
CSAU, Step 7: Establishment of Assessment Matrix	1-13
CSAU, Step 8: Define Nodalization	1-13
CSAU, Step 9: Determine Code and Experiment Accuracy	1-13

CSAU, Step 10: Determine Effect of Scale	1-14
CSAU, Step 11: Determine Effect of Reactor Input Parameters and State	1-15
CSAU, Step 12: Perform NPP Sensitivity Calculations	1-16
CSAU, Step 13: Combine Biases and Uncertainties	1-17
CSAU, Step 14: Calculate Total Uncertainty	1-17

## DECAY HEAT

See REACTOR KINETICS AND DECAY HEAT MODELS

## ENTRAINMENT AND DE-ENTRAINMENT MODELS

See VESSEL COMPONENT, ENTRAINMENT AND DE-ENTRAINMENT MODELS

## FLOW REGIME MAPS AND INTERFACIAL AREA

See ONE-DIMENSIONAL COMPONENT, FLOW REGIMES

See, VESSEL COMPONENT, NORMAL WALL FLOW REGIMES

See, VESSEL COMPONENT, HOT WALL FLOW REGIMES

FUEL ROD, CLADDING REACTION MODEL	7-33
-----------------------------------	------

FUEL ROD, DEFORMATION MODEL	7-16
-----------------------------	------

Deformation Mechanisms	7-17
------------------------	------

Effects of Fuel Rod Deformation on Core Thermal-Hydraulics	7-30
--	------

FUEL ROD, MODELLING	7-10
---------------------	------

Fuel Rod Quench Front Model	7-10
-----------------------------	------

Pellet-Cladding Gap Conductance Model	7-11
---------------------------------------	------

## HEAT FLUX SPLITTING IN WCOBRA/TRAC

Inverted Annular Dispersed Flow Film Boiling (IADF) and Dispersed Droplet Film Boiling	6-76
---	------

Inverted Annular Film Boiling (IAFB)	6-75
--------------------------------------	------

Saturated Nucleate Boiling	6-74
----------------------------	------

Single-Phase Liquid Forced Convection	6-73
---------------------------------------	------

Subcooled Nucleate Boiling	6-74
----------------------------	------

Transition Boiling	6-75
--------------------	------

## INTERFACIAL AREA

See FLOW REGIME MAPS AND INTERFACIAL AREA

## INTERFACIAL HEAT AND MASS TRANSFER MODELS

See ONE-DIMENSIONAL COMPONENT, INTERFACIAL HEAT AND  
MASS TRANSFER

See VESSEL COMPONENT, INTERFACIAL HEAT AND MASS TRANSFER

---

## MOMENTUM TRANSFER MODELS

See ONE-DIMENSIONAL COMPONENT, MOMENTUM TRANSFER  
See VESSEL COMPONENT, FORM LOSS  
See VESSEL COMPONENT, INTERFACIAL SHEAR MODELS  
See VESSEL COMPONENT, WALL SHEAR MODELS  
See VESSEL COMPONENT, INTERCELL DRAG

NRC REQUESTS FOR ADDITIONAL INFORMATION, RESOLUTION OF C-1

NUMERICAL SOLUTION METHOD 2-53

See ONE-DIMENSIONAL COMPONENT, NUMERICAL SOLUTION  
See TIMESTEP SIZE AND CONVERGENCE CRITERIA  
See VESSEL COMPONENT, NUMERICAL SOLUTION  
Network Matrix Equation 2-65  
Solution Routines 2-69

## ONE-DIMENSIONAL COMPONENTS, CONDUCTOR MODELING

See CONDUCTOR MODELING, ONE-DIMENSIONAL COMPONENTS

ONE-DIMENSIONAL COMPONENTS, CONSERVATION EQUATIONS 2-40

Closure of the Conservation Equations 2-45  
Conservation of Mixture Mass 2-41  
Conservation of Mixture Momentum 2-43  
Vapor and Mixture Energy Conservation Equations 2-43

ONE-DIMENSIONAL COMPONENTS, FLOW REGIMES 3-20

Annular-Mist Flow Regime 3-26  
Bubbly Flow Regime 3-21  
Churn Flow Regime 3-24  
Slug Flow Regime 3-23

## ONE-DIMENSIONAL COMPONENTS, INTERFACIAL HEAT AND MASS TRANSFER

Annular-Mist Flow Regime 5-39  
Bubbly Flow Regime 5-32  
Churn Flow Regime 5-37  
Effect of Noncondensables 5-41  
Interfacial Mass Transfer 5-42  
Slug Flow Regime 5-35

ONE-DIMENSIONAL COMPONENTS, MODEL AS CODED 2-46

Computational Mesh 2-46  
Finite Difference Formulation 2-47  
Finite Difference Formulation, Semi-Implicit Formulation 2-48  
Finite Difference Formulation, Fully Implicit Formulation 2-51

ONE-DIMENSIONAL COMPONENTS, MODEL BASIS	2-40
See VESSEL COMPONENT, CONSERVATION EQUATIONS	
ONE-DIMENSIONAL COMPONENTS, MOMENTUM TRANSFER	
Annular Flow Friction Factor Model	4-70
One-Dimensional Component Form Loss	4-78
Relative Velocity Models	4-74
ONE-DIMENSIONAL COMPONENTS, NUMERICAL SOLUTION	2-60
Solution of Momentum Equations	2-60
Solution of Mass and Energy Equations	2-61
Component Boundary Conditions	2-63
Fully Implicit One-Dimensional Components	2-64
ONE-DIMENSIONAL COMPONENTS, WALL HEAT TRANSFER	6-47
Condensation Heat Transfer	6-68
Convection to Single-Phase Vapor	6-64
Critical Heat Flux	6-54
Film Boiling Heat Transfer	6-61
Heat Transfer to Two-Phase Mixtures	6-65
Minimum Film Boiling Temperature	6-59
Nucleate Boiling	6-51
Single-Phase Liquid Natural Convection	6-48
Single-Phase Liquid Forced Convection	6-50
Transition Boiling	6-56
Wall to Fluid Heat Transfer	6-70
ONE-DIMENSIONAL COMPONENT, <u>W</u> COBRA/TRAC MODELS	9-1
Accumulator Component (ACCUM)	9-11
Break And Fill Components	9-15
Pipe Component	9-1
Pressurizer Component (PRIZER)	9-10
Pump Component	9-3
Steam Generator Component (STGEN)	9-9
Tee Component	9-2
Valve Component	9-11
PIRT, Phenomena Identification and Ranking	1-3
RAIs	
See NRC REQUESTS FOR ADDITIONAL INFORMATION	

REACTOR KINETICS AND DECAY HEAT MODELS	8-1
Actinide Decay Heat Source	8-6
Decay Heat Source	8-1
Decay Heat Uncertainty Evaluation	8-21
Energy Deposition Modeling	8-12, 8-23
Fission Heat	8-4
Interface between Neutronics and Thermal-Hydraulics Models	8-24
Reactor Point Kinetics Validation	8-21
Reactor Kinetics, Decay Heat, and Interface Models as coded	8-24
Space Dependent Heat Source Model	8-8
SAMPLE PWR PLANT, ALLOWABLE PLANT OPERATING CONDITIONS	12-8
SAMPLE PWR PLANT, DESCRIPTION AND NODALIZATION	12-2
SAMPLE PWR PLANT, REFERENCE TRANSIENT	12-12
SAMPLE PWR PLANTS, STATISTICAL ANALYSIS	12-16
Development of Run Matrix	12-16
ASTRUM Results and Determination of the 95/95 PCT Value	12-16
Other 10CFR50.46 Criteria	12-19
THERMOPHYSICAL PROPERTIES	10-1
Thermal Properties of Fuel Rod Gas Mixtures	10-34
Thermal Properties of Nuclear Fuel Rod Materials	10-30
Thermal Properties of Structural Materials, One-Dimensional Components	10-36
Thermal Properties of Structural Materials, Vessel Component	10-35
Thermal Properties of Uranium Dioxide	10-30
Thermal Properties of Zircaloy-4	10-31
Thermal Properties of ZIRLOTM	10-32
Thermophysical Properties of Air, One-Dimensional Components	10-28
Thermophysical Properties of Air, Vessel Component	10-27
Thermophysical Properties of Water, One-Dimensional Components	10-7
Thermophysical Properties of Water, Vessel Component	10-1
TIMESTEP SIZE AND CONVERGENCE CRITERIA	2-73
Coded Convergence Criteria	2-73
Numerical Stability	2-75
Timestep Size Control	2-74
UNCERTAINTY METHODOLOGY, COMBINED BIAS AND UNCERTAINTY	11-14
UNCERTAINTY METHODOLOGY, DETERMINATION OF TOTAL UNCERTAINTY	11-20

UNCERTAINTY METHODOLOGY, NON-PARAMETRIC ORDERED STATISTICS	
See UNCERTAINTY METHODOLOGY, TECHNICAL BASIS	
UNCERTAINTY METHODOLOGY, NPP SENSITIVITY CALCULATIONS	11-12
Confirmatory Calculations	11-12
NPP Uncertainty Calculations	11-14
UNCERTAINTY METHODOLOGY, TECHNICAL BASIS	11-1
Application of the Statistical Method	11-6
Break Type and Size	11-6
Statistical Sampling Approach	11-1
Time in Cycle	11-11
UNCERTAINTY METHODOLOGY, OTHER 10CFR50.46 ACCEPTANCE CRITERIA	11-20
UNHEATED CONDUCTOR MODELLING	7-37
VESSEL COMPONENT, CONDUCTOR MODELING	
See CONDUCTOR MODELING, VESSEL COMPONENT	
VESSEL COMPONENT, CONSERVATION EQUATIONS	2-1
Cartesian Coordinate Representation	2-8
Comparison of Cartesian and Subchannel Formulations	2-14
Conservation of Mass	2-6
Conservation of Momentum	2-7
Conservation of Energy	2-7
Subchannel Coordinate Formulation	2-11
Three-Field Equation Formulation	2-2
Vessel Component Three-Field Conservation Equations	2-3
VESSEL COMPONENT, ENTRAINMENT AND DE-ENTRAINMENT MODELS	4-39
Crossflow De-entrainment	4-65
De-entrainment at Area Changes	4-67
De-entrainment at Solid Surfaces and Liquid Pools	4-69
De-entrainment in Film Flow	4-63
Entrainment in Film Flow	4-39
Entrainment During Bottom Reflood	4-44
Entrainment During Top Down Reflood	4-50
Spacer Grid Droplet Breakup Model	4-57
VESSEL COMPONENT FORM LOSS	4-10



VESSEL COMPONENT, HOT WALL FLOW REGIMES	3-13
Dispersed Droplet Flow Regime	3-16
Falling Film Regime	3-16
Interfacial Area Transport Equation	3-18
Inverted Annular Flow Regime	3-13
Inverted Liquid Slug Flow Regime	3-14
Top Deluge Flow Regime	3-17
VESSEL COMPONENT, INTERCELL DRAG	4-37
VESSEL COMPONENT INTERFACIAL HEAT AND MASS TRANSFER MODELS	5-1
Churn-Turbulent Regime	5-7
Dispersed Droplet Flow Regime	5-17
Effect of Grid Spacers on Interfacial Heat Transfer	5-22
Effect of Noncondensables	5-24
Falling Film Regime	5-19
Film/Drop Regime	5-11
Interfacial Mass Transfer	5-27
Inverted Annular Regime	5-13
Inverted Liquid Slug Regime	5-15
Small Bubble Regime	5-1
Small to Large Bubble Regime	5-5
Top Deluge Flow Regime	5-21
VESSEL COMPONENT, INTERFACIAL SHEAR MODELS	4-13
Churn-Turbulent Flow Regime Interfacial Drag	4-24
Dispersed Droplet Flow Regime	4-32
Falling Film Flow Regime	4-34
Film/Drop Flow Regime	4-25
Inverted Annular Flow Regime	4-29
Inverted Liquid Slug Regime	4-30
Small Bubble Flow Regime Interfacial Drag	4-15
Small-to-Large Bubble Flow Regime Interfacial Drag	4-21
Top Deluge Flow Regime	4-35
VESSEL COMPONENT, MODEL BASIS	2-1
See VESSEL COMPONENT, CONSERVATION EQUATIONS	
VESSEL COMPONENT, MODEL AS CODED	2-15
Boundary Condition Source Terms	2-33
Computational Mesh, Vessel Component	2-16
Conservation of Mass Equations	2-17
Conservation of Momentum Equations	2-19
Conservation of Energy Equations	2-27

Finite-Difference Equations, Vessel Component	2-17
Mass, Energy, and Momentum Source Terms	2-29
Source, Viscous, and Turbulence Terms	2-29
Turbulent Shear Stress Tensors and Heat Flux Vectors	2-34
<b>VESSEL COMPONENT, NORMAL WALL FLOW REGIMES</b>	<b>3-1</b>
Churn-Turbulent Flow Regime	3-10
Film/Drop Flow Regime	3-11
Small Bubble Regime	3-3
Small to Large Bubble Regime	3-6
<b>VESSEL COMPONENT, NUMERICAL SOLUTION</b>	<b>2-53</b>
Cells Connected to One-Dimensional Components	2-59
Solution of the Momentum Equations	2-54
Linearization of the Mass and Energy Equations	2-55
Solution of the System Pressure Matrix	2-58
<b>VESSEL COMPONENT, WALL HEAT TRANSFER MODELS</b>	<b>6-1</b>
Convection to Single-Phase Vapor	6-2
Convection to Single-Phase Liquid	6-5
Critical Heat Flux and Wall Temperature at CHF	6-16
Dispersed Flow Film Boiling	6-31
Grid Rewet Model	6-42
Inverted Annular Film Boiling	6-27
Minimum Film Boiling Wall Temperature	6-25
Saturated and Subcooled Nucleate Boiling	6-7
Thermal Radiation Heat Transfer	6-36
Transition Boiling	6-20
Wall to Fluid Heat Transfer	6-44
<b>VESSEL COMPONENT, WALL SHEAR MODELS</b>	<b>4-2</b>
<b>WALL HEAT TRANSFER MODELS</b>	
See VESSEL COMPONENT WALL HEAT TRANSFER MODELS	
See ONE-DIMENSIONAL COMPONENT WALL HEAT TRANSFER	
See HEAT FLUX SPLITTING IN <u>WCOBRA/TRAC</u>	
<b><u>WCOBRA/TRAC</u> MOD7A REVISION 6, VALIDATION OF</b>	<b>B-1</b>